LEABHARLANN CHOLÁISTE NA TRÍONÓIDE, BAILE ÁTHA CLIATH | TRINITY COLLEGE LIBRARY DUBLIN
Ollscoil Átha Cliath | The University of Dublin

Terms and Conditions of Use of Digitised Theses from Trinity College Library Dublin

Copyright statement

All material supplied by Trinity College Library is protected by copyright (under the Copyright and Related Rights Act, 2000 as amended) and other relevant Intellectual Property Rights. By accessing and using a Digitised Thesis from Trinity College Library you acknowledge that all Intellectual Property Rights in any Works supplied are the sole and exclusive property of the copyright and/or other IPR holder. Specific copyright holders may not be explicitly identified. Use of materials from other sources within a thesis should not be construed as a claim over them.

A non-exclusive, non-transferable licence is hereby granted to those using or reproducing, in whole or in part, the material for valid purposes, providing the copyright owners are acknowledged using the normal conventions. Where specific permission to use material is required, this is identified and such permission must be sought from the copyright holder or agency cited.

Liability statement

By using a Digitised Thesis, I accept that Trinity College Dublin bears no legal responsibility for the accuracy, legality or comprehensiveness of materials contained within the thesis, and that Trinity College Dublin accepts no liability for indirect, consequential, or incidental, damages or losses arising from use of the thesis for whatever reason. Information located in a thesis may be subject to specific use constraints, details of which may not be explicitly described. It is the responsibility of potential and actual users to be aware of such constraints and to abide by them. By making use of material from a digitised thesis, you accept these copyright and disclaimer provisions. Where it is brought to the attention of Trinity College Library that there may be a breach of copyright or other restraint, it is the policy to withdraw or take down access to a thesis while the issue is being resolved.

Access Agreement

By using a Digitised Thesis from Trinity College Library you are bound by the following Terms & Conditions. Please read them carefully.

I have read and I understand the following statement: All material supplied via a Digitised Thesis from Trinity College Library is protected by copyright and other intellectual property rights, and duplication or sale of all or part of any of a thesis is not permitted, except that material may be duplicated by you for your research use or for educational purposes in electronic or print form providing the copyright owners are acknowledged using the normal conventions. You must obtain permission for any other use. Electronic or print copies may not be offered, whether for sale or otherwise to anyone. This copy has been supplied on the understanding that it is copyright material and that no quotation from the thesis may be published without proper acknowledgement.

TRINITY COLLEGE DUBLIN

DOCTORAL THESIS

Quantum theory of ultrafast magnetism

Author:
Jacopo SIMONI

Supervisor:
Prof. Stefano SANVITO

A thesis submitted in fulfillment of the requirements for the degree of Doctor of Philosophy

in the

Computational spintronics group
School of physics

August 16, 2017

P.hD
TRINITY COLLEGE DUBLIN
25 OCT 2017
ACADEMIC REGISTRY
School of Physics

50763102
5076310 2

THESIS
11472

TRINITY LIBRARY
05 APR 2018
DUBLIN
Thesis 11472

en submitted as an exercise for a degree at this or any other
work. I agree to deposit this thesis in the University's open access
Library to do so on my behalf, subject to Irish Copyright
y conditions of use and acknowledgement.

Signed: _____

Declaration of Authorship

I, Jacopo SIMONI, declare that this thesis titled, "Quantum theory of ultrafast magnetism" and the work presented in it are my own. I confirm that:

- This work was done wholly or mainly while in candidature for a research degree at this University.
- Where any part of this thesis has previously been submitted for a degree or any other qualification at this University or any other institution, this has been clearly stated.
- Where I have consulted the published work of others, this is always clearly attributed.
- Where I have quoted from the work of others, the source is always given. With the exception of such quotations, this thesis is entirely my own work.
- I have acknowledged all main sources of help.
- Where the thesis is based on work done by myself jointly with others, I have made clear exactly what was done by others and what I have contributed myself.

Signed: _____

Date: _____

"So it is right that in these matters you should accept the likely myth and look no further than this."

Plato, Timeus

TRINITY COLLEGE DUBLIN

Abstract

School of physics

Doctor of Philosophy

Quantum theory of ultrafast magnetism

by Jacopo SIMONI

The ultrafast demagnetization of ferromagnetic Fe based clusters, bulk transition metals and anti-ferromagnets initiated by an optical excitation is studied by making use of the time-dependent spin density functional theory. In particular after a brief introduction and the exposition of some preliminary results in Chapter 1, we proceed in Chapter 2 by describing the state of the art of the theoretical basis of the ultrafast demagnetization process. In Chapter 3 we look in more details at the time dependent spin density functional theory method that will be used in the successive chapters to simulate the ultrafast spin dynamics in the first few tens of femtoseconds. In Chapter 4 we investigate the role played by the spin-orbit interaction on the onset of the demagnetization process, it is found that the demagnetization occurs locally, in the vicinity of the atomic sites, and the initial rate of spin loss is proportional to the square of the ionic spin orbit coupling strength. A simplified quantum spin model comprising the spin-orbit interaction and an external time-dependent magnetic field is found to be the minimal model able to reproduce the *ab initio* results. In Chapter 5 the spin continuity equation is reformulated in such a way that the torque due to the spin-current divergence may be expressed in terms of a *kinetic field* that is formally equivalent to an out-of-equilibrium spin-spin interaction. This field is identified as one of the main sources of the local out-of-equilibrium spin dynamics and plays a major role in the demagnetization process. Such demagnetization is particularly strong in ''hot spots'' where the kinetic torque is maximized. In the final Chapter we analyze instead the ultrafast dynamics of the orbital momentum studying more in details its effects on the spin dynamics of the Fe_6 cluster. We find that the rate of demagnetization is strongly dependent on the direction of polarization of the applied electric field and we develop, in order to explain this effect, a model based on the interplay of the ultrafast orbital current and the electric field with the spin orbit coupling.

LIST OF PUBLICATIONS

1. M. Stamenova, J. Simoni and S. Sanvito, *Role of spin orbit interaction in the ultrafast demagnetization of small iron clusters*, Physical Review B **94**: 014423(7), (2016).
2. J. Simoni, M. Stamenova and S. Sanvito, *Ultrafast demagnetizing fields from first principles*, *Physical Review B* **95**: 024412(11), (2017).
3. J. Simoni, M. Stamenova and S. Sanvito, *Ab initio dynamical exchange interactions in frustrated anti-ferromagnets*, *Physical Review B* **96**: 054411(9), (2017).

CONTRIBUTED TALKS

1. *Ultrafast magnetism within time-dependent density functional theory*, (15 min.), *Psi K conference* San Sebastian (07/09/2015), Spain.
2. *Ultrafast demagnetization of small iron clusters from first principles*, (15 min.), *Ultrafast magnetism conference* Nijmegen (22/10/2015), Netherlands.

Acknowledgements

Firstly, I would like to express my sincere gratitude to my advisor Prof. Stefano Sanvito for the continuous support of my Ph.D study and related research. His guidance helped me in all the time of research and writing of this thesis.

Besides my advisor, I would like to thank Dr. Maria Stamenova for her insightful comments and encouragement.

I thank my collegues of the research group in Trinity College and, in particular, I express my gratitude to Mario Žic, Rajarshi Tiwari, Filiberto Rinaldi and Emanuele Bosoni for the long a stimulating discussions.

I also thank Prof. Eberhard K. U. Gross and Prof. Sangeeta Sharma from Max-Planck-Institut fur Mikrostrukturphysik, Halle, Germany for valuable discussions.

I gratefully acknowledge the DJEI/DES/SFI/HEA Irish Centre for High-End Computing (ICHEC) for the provision of computational facilities.

Last but not the least, I would like to thank my family: my mother and my brother for supporting me throughout writing this thesis and my life in general.

CONTENTS

Declaration of Authorship i

Abstract iii

Acknowledgements v

1 Introduction and some preliminary results 1
- 1.1 Introduction and motivations . . . 1
- 1.2 Brief review of classical electro-dynamics and radiation matter interaction . . . 8
- 1.3 Equation of motion for the orbital moment . . . 15
- 1.4 Equation of motion for the spin vector . . . 21
- 1.5 Local continuity equations and the Noether theorem . . . 26

2 The theory of ultrafast magnetism 34
- 2.1 Experimental methods . . . 36
- 2.2 Magneto - optical effects . . . 38
- 2.3 Spin-photons interaction . . . 40
- 2.4 Non pulse driven contributions to the spin dynamics . . . 47
  - 2.4.1 Electron - electron and electron - magnon interactions . 48
  - 2.4.2 Electron-magnon interactions . . . 53
  - 2.4.3 Electron-phonon interaction . . . 55
- 2.5 The super-diffusive mechanism . . . 57
- 2.6 Thermal processes . . . 58

3 Electronic Structure Methods 62
- 3.1 Density Functional Theory . . . 64
- 3.2 Spin Density Functional Theory . . . 70
- 3.3 Current Density Functional Theory . . . 77
  - 3.3.1 DFT and spin-orbit coupling . . . 83
- 3.4 Pseudo-potentials and spin-orbit coupling . . . 87
- 3.5 Time Dependent Density Functional Theory . . . 95
- 3.6 Time Dependent Spin Density Functional Theory . . . 99

3.7 TD-DFT in external electro-magnetic fields 102

4 The role of spin orbit in the ultrafast demagnetization of transition metals 108
4.1 Demagnetization in Fe based clusters 113
4.1.1 Fe 113
4.1.2 Fe_2 114
4.1.3 Fe_3 118
4.1.4 Fe_4 119
4.1.5 Fe_6 124
4.1.6 Comparison of cluster demagnetization 127
4.2 Minimal Demagnetizing Model 129
4.3 General law for the ultrafast demagnetization of transition metals 134

5 Dynamical Exchange Interactions 139
5.1 Exchange interactions in the adiabatic approximation 142
5.1.1 Exchange interactions from the magnetic force theorem 142
5.1.2 Exchange interactions from spin susceptibilities 145
5.2 Real time exchange coupling 147
5.3 First step towards a time-dependent exchange interaction 150
5.4 Some considerations on the spin continuity equation 152
5.5 Analysis of the ALDA spin dynamics in the Fe_6 cluster 164
5.5.1 The kinetic field and parallel transport 171
5.6 Demagnetization of bcc Fe bulk 173
5.7 Ab initio dynamical exchange interactions 176
5.8 Ultrafast spin dynamics in FeMn 178

6 The time evolution of the orbital moment 189
6.1 Center of mass and internal orbital moment 191
6.2 Analysis of the orbital moment evolution in Fe_6 204
6.3 A new model for the dynamics of the orbital moment 207
6.4 The role of the ionic potential scattering in the ultrafast dynamics of the orbital moment 215
6.5 The role of the orbital currents in the spin loss process 217
6.6 The origin of the spin non-collinearity 230
6.7 The issue of the orbital moment conservation 233

7 Conclusions 246

Bibliography 249

LIST OF FIGURES

1.1 (a) F_L shape from Eq. (1.2) with parameters $a = 1, b = 1, F_0 = 0$. (b) F_L shape from Eq. (1.2) with $a = -1, -2, b = 1, F_0 = 0$. (c) F_L shape from Eq. (1.4) with parameters $a = -2, b = 1, F_0 = 0$ and $h = 1$. (d) same F_L of (c) but with $h = 1, 2$. 4

1.2 Experimental geometry and magnetic beam employed in [8]. When the electronic beam of about 5 ps length is shot through the uniformly magnetized sample the field writes a ring-shaped magnetic pattern with an opposite magnetization direction. 6

1.3 (Color online) Ultrafast demagnetization observed in *Ni* film using Magneto-Optical Kerr Effect (MOKE) signal [9]. 7

2.1 (a) Time scales of magnetic interactions compared to different pulse duration. (From Ref. [3]). 35

2.2 (a) Scheme of a typical optical spectroscopy pump-probe experiment with pulse shaper, (from Ref. [28]). 37

2.3 (a) Simple scheme of the magneto-optical Kerr effect. 39

2.4 Different interacting energy reservoirs (electrons, spins and lattice) within the three-temperature-model ($3TM$). (From Ref. [67]). 59

4.1 Plot of the spin orbit pseudopotential component $V^l_{\mathrm{SO}}(r)$ with (a) $l = 2$ (d channel) and (b) $l = 1$ (p channel). 111

4.2 Spin dynamics of a single isolated Fe atom (a) external applied laser pulse (orthogonal to spin quantization axis) with duration of approximately 5 fs, (b) Total DFT energy evolution within the first 45 fs, (c) total $S_z(t)$ spin evolution, (d) comparison ot the z and non collinear components of the orbital moment. 113

4.3 Spin dynamics of the Fe dimer (a) external applied laser pulses, (b) Total DFT energy evolution within the first 10 fs, (c) $S_z(t)$ evolution in units of $\hbar$, (d) orbital moment $L_z(t)$ evolution also in units of $\hbar$. 115

4.4 Picture of the Fe_2 dimer with the black arrow indicating the electric field polarization direction and green arrows indicating the atomic spin direction. 115
4.5 Expectation value of the spin operator $\langle\psi_j^{KS}|\hat{\sigma}^z|\psi_j^{KS}\rangle$ over all the Kohn-Sham states between 16 and 32, the various lines represent different instants in time chosen uniformly at time intervals of 3 fs, the red line corresponds to the earliest time, the blue line is the intermediate one and the green line the latest. 116
4.6 Dynamics of the Fe dimer with and without spin orbit (a) external applied laser pulses, (b) Total DFT energy evolution within the first 10 fs, (c) $|\mathbf{S}(t)|$ evolution in units of $\hbar$, (d) orbital moment $|\mathbf{L}(t)|$ evolution also in units of $\hbar$. 117
4.7 Picture of the Fe_3 cluster with the black arrow indicating the electric field polarization direction, the green arrows represent the local moments direction in the ground state configuration. 118
4.8 Spin dynamics of the Fe_3 cluster (a) external applied laser pulses, (b) Total DFT energy evolution in the case with and without spin orbit, (c) total magnetization $S_z(t)$ of the cluster in units of $\hbar$ in the two cases, (d) total non collinear component $S_{xy}(t)$ in units of $\hbar$. 119
4.9 Spin dynamics of the Fe_3 system (a) external applied laser pulses, (b) variation of the component $\Delta S^R_{z,I}(t)$ of the magnetization over the three sites, (c) variation of the component $\Delta S^R_{x,I}(t)$, (d) variation of the component $\Delta S^R_{y,I}(t)$ in units of $\hbar$. 120
4.10 Spin dynamics of the Fe_4 cluster (a) external applied laser pulses, (b) total DFT energy evolution within the first 20 fs, (c) $S_z(t)$ evolution in units of $\hbar$, (d) non collinear component $S_{xy}(t) = \sqrt{S_x(t)^2 + S_y(t)^2}$ of the global magnetization also in units of $\hbar$. . 121
4.11 Picture of the Fe_4 with the black arrow indicating the electric field polarization direction. The green arrows represent the local spin directions in the ground state. 121
4.12 Local charge and spin dynamics of the Fe_4 cluster (a) calculation of $\Delta Q_I^R(t)/Q_I^R(t)$ where $R = 1.2$ Å and $I = 1,\ldots,4$ in units of $\hbar$, (b) calculation of $\Delta S^R_{z,I}(t)/S^R_{z,I}(t)$ over the same integration domain, (c) $S^R_{I,xy}(t) = \sqrt{S_{I,x}(t)^2 + S_{I,y}(t)^2}$, (d) evolution of $B^R_{x,zI}(t)$ z component of the exchange magnetic field. 122
4.13 Spin dynamics of the Fe_4 cluster (a) comparison of $\Delta S^R_z(t)$ for different values of the integration radius with the global magnetization loss (b) evaluation of $\Delta B^R_{x,z}(t) = \sum_I \Delta B^R_{x,zI}(t)$ for different values of R. 123

4.14 Dynamics of global and local spin quantities (a) comparison of $\Delta S^z(t)$ and $\Delta Q(t)$ in the plane of the cluster and in the region outside, (b) comparison of $\Delta S^z_{loc}(t) = \sum_I \Delta S^R_{z,I}(t)$ with the same quantity integrated over the whole volume, (c) measure of $\Delta S^{xyz}(t) = \sqrt{|\mathbf{m}(0)|^2 - |\mathbf{m}(t)|^2}$ using global values (pink curve), local measures centered on the atoms (red line) and quantities integrated over the cluster plane (blue line), (d) $\Delta S^{xy} = \sqrt{m_x^2 + m_y^2} - S^{xy}(0)$ quantity integrated over the entire simulation box and around the atoms. 124
4.15 (a) Typical electric field pulses used to excite the cluster, (b) time evolution of the total TD-DFT energy, (c) total spin and (d) total orbital moment subjected to each of the pulses in panel (a) with corresponding color code on all panels. 125
4.16 Picture of the Fe_6 with the black arrow indicating the electric field polarization direction. 125
4.17 Evolution of the different observables in the Fe_6 system (a) Evolution of global spin expectation value for different values of $\alpha = 0, 1, 2, 4$ in Eq. 4.19. (b) Plot of $S^z_{tot}(t) - S^z_{tot}(t = 0)$ multiplicated by $\eta = (\alpha_{max}/\alpha)^2$. Panels (c) and (d) show the corresponding trajectories for the exchange field $B^z_{x,loc}(t)$ of Eq. (4.20). 127
4.18 Plot of the time-dependent global spin and orbital moment of the various clusters considered for different laser pulses: (a) and (d) Fe_2; (b) and (e) Fe_4; (c) and (f) Fe_6. 128
4.19 (a) trajectories of the applied magnetic field $B(t)$; (b) and correspondent evolution of the spin component $\langle \hat{S}_z \rangle$. 132
4.20 Trajectories of $\langle \hat{S}^z \rangle$ under the action of the Hamiltonian (4.21) in the case of (a) having an initial spin-up or down state; (b) for different values of a multiplicative factor α for the spin-orbit coupling ($\lambda \rightarrow \alpha\lambda$), with an initial spin-up state; (c) similarly to Fig. 4.17 the trajectories are rescaled by a factor $1/\alpha^2$. The shaded area describes the temporal profile of the applied magnetic field $\mathbf{B}(t) = [0, 0, B(t)]$. The initial orbital state is in a linear combination of $l_z = 0, 1$ states. 133
4.21 Plot of the global spin decay of the various clusters considered up to now: (a) variation of the total magnetization with respect to its ground state value $\Delta S^z_{tot}(t)$; (b) same quantity normalized with respect to the magnetization ground state $\Delta S^z_{tot}(t)/S^z_{tot}(0)$. . 134
4.22 (a) TDSDFT trajectories of the variation of $\langle \hat{S}^z_{tot}(t) \rangle$ with respect of the ground state magnetization for three different clusters: Fe_6, Ni_6 and Co_6, all sharing the same Fe_6 geometry [121]. (b) Closer view into the coherent part of the trajectories where a parabolic decay [$y = A(t - t_0)^2 + A_0$] is fitted for each trajectory (dashed curves). (c) The fitting coefficients A from panel (b) versus the effective atomic SOC from Eq. (4.51) for each material. 136

4.23 Table of the spin orbit coefficient ξ (in mRy) for transition metal atoms. (from [131]) 137

5.1 (Color online) (a) value of the magnetization S_{1z} and S_{3z} computed on the two sites 1 and 3 within a sphere of radius R, half the lattice spacing (b) value of $\bar{\mathcal{J}}(t)$ computed according to the average of the two quantities (5.56) and (5.57), with the error bars given by $\Delta\mathcal{J} = 0.5|\mathcal{J}_1 - \mathcal{J}_3|$. 151

5.2 Fe_6 cluster dynamics: (a) typical electric field pulse used to excite the Fe_6 cluster with the black arrow indicating the direction of the field. The fluence of this pulse is $580\,mJ/cm^2$. (b) Time evolution of the z-component of $\mathbf{B}_{kin}$ and $\mathbf{B}_x$ (exchange component of the field) with respect to their values at $t = 0$ integrated over the system volume, $\mu_B\mathbf{B}^{tot}(t) = \mu_B\sum_I \mathbf{B}^I(t)$. (c) Time evolution of the variation of the total magnetization $\Delta S_z^{tot}(t) = \sum_I \Delta S_z^I(t)$ with respect to its initial value. (d) Time evolution on atomic site 6 of the magnetization variation along z, of its module and of the electron density variation with respect to its value at $t = 0$ integrated inside a sphere of radius $R = 0.9$ Å. 165

5.3 Local spin dynamics of the Fe_6 cluster: (a) Time evolution of the magnetization around the atomic centers. (b) Time evolution of the z component of $\mathbf{B}_{kin}$. All the quantities are integrated inside a sphere of radius $R = 0.9$ Å centered on the two atomic sites, where we have used $B_z^I(t) = \frac{1}{|S_R^I|}\int_{S_R^I} d^3r\, B_z(\mathbf{r},t)$. 168

5.4 Contour plots of the time- and space-averaged (in direction perpendicular to the plane spanned by atoms 1, 3, 5 and 6, as indicated on the plot) observables evaluated only within spheres of radius $R = 1.0$ Å around each atom: (a) and (b) the temporal variation of the spin density $\Delta\mathbf{m}^{(x,z)}(\mathbf{r},t)/\Delta t$ for $\Delta t = 0.1$ fs; (c) and (d) the x and z components of the first term on the right hand side of Eq. (5.130). 169

5.5 Spin non collinearity evolution in the Fe_6 cluster (a) $\Delta\theta = \theta(t) - \theta(0)$ at site 1, for the $\mathbf{B}_{xc}$ [or $\mathbf{S}(t)$] direction (black curve) and the $\mathbf{B}_{kin}$ direction (red dashed curve). (b) The same quantities of panel (a) but calculated at the atomic site 6. (c) $\sqrt{\bar{\mathcal{A}}_1^2 + \bar{\mathcal{A}}_2^2}$ where $\bar{\mathcal{A}} = \sqrt{\sum_{i=1}^3 \mathcal{A}_i^2}$ and $\mathcal{A}_i$ is introduced in Eq. (5.137), compared to $\bar{\mathcal{A}}_3$ at the atomic site 1. (d) The same quantities of panel (c) but calculated at the atomic site 6. The fields are measured within a sphere of radius $R = 0.8$ Å centered on the atom center. 170

5.6 Parallel transport on a sphere, transport of the black arrow along different directions (blue and red vectors). From ([175]). 171

5.7 The Fe bcc lattice structure with the black arrow indicating the electric field polarization direction. The green arrows represent the local moments direction in the ground state. 173

5.8 Demagnetization of bcc Fe: (a) applied external electric field; (b) local value of $\Delta B^z_{\mathrm{kin},I}$ and $\Delta B^z_{\mathrm{x,I}}$ around atom 1; (c) comparison between the value of the local magnetization $\Delta S_{z,\mathrm{I}}(t)$ around atom 1 (black curve), the total magnetization integrated around the two sites (red curve), $\sum_{\mathrm{I}} \Delta S_{z,I}(t)$, and the total magnetization integrated inside the unitary cell $\Delta S_z(t)$ (green curve). (d) Local value of $\sum_I \Delta B^{xy}_{\mathrm{kin},I}(t)$ (red curve) and of $\sum_I \Delta S_I^{xy}(t)$, non-collinear magnetization component for atom 1. All the local quantities are calculated inside a sphere of radius $R = 1.0$ Å. 174

5.9 Picture of the FeMn fcc structure with the black arrow indicating the electric field polarization direction. The green arrows represent the local moments direction in the ground state. 179

5.10 plots of the time-averaged observables evaluated in spheres of radius 0.5 Å around each atom: (a) the averaged temporal variation of the spin density module $\left|\Delta \mathbf{S}^{\mathrm{I}}(t)\right|$ for the two sites Fe and Mn under the pulses of panel (b); (b) different laser pulses employed in the dynamical simulations with shape $E_z(t) = A \cdot \sin(0.1 \cdot t) \cdot \exp\{(\} - \frac{(t-5)^2}{3})$. The amplitudes A are in units of eV /Å, the laser polarization direction is shown in Fig. 5.9. 180

5.11 Plots of the time-averaged observables evaluated in spheres of radius 0.5 Å around the atomic sites under the same type of pulses ($A = 0.7$ eV/Å): (a) the averaged temporal variation of the two on-site charge densities $\Delta Q^{\mathrm{I}}(t) = Q^{\mathrm{I}}(t) - Q^{\mathrm{I}}(t = 0)$, Fe site (black curve) and Mn site (red curve); (b) the averaged temporal variation of the magnetization along z axis $S^{\mathrm{I}}_{\mathrm{z}}(t)$ and the non collinear component $S^{\mathrm{I}}_{\mathrm{xy}}(t)$, in correspondence of the Fe site; (c) dynamical Stoner exchange parameter $I(t)$ obtained by spatial integration $I(t) = \frac{1}{\|S^{\mathrm{R}}_{\mathrm{I}}\|} \int_{S^{\mathrm{R}}_{\mathrm{I}}} d^3r\, I(\mathbf{r}, t)$, in correspondence of the Fe site (see Eq. 5.177); (d) the averaged temporal variation of $F(t) = |\langle \mathbf{S}_{\mathrm{Fe}}(t), \boldsymbol{\Xi}(t) \rangle| / (|\mathbf{S}_{\mathrm{Fe}}(t)| \cdot |\boldsymbol{\Xi}(t)|)$, where $\mathbf{S}_{\mathrm{Fe}}(t)$ is the onsite averaged magnetization calculated within a radius $R = 1.4$ Å. Here $\boldsymbol{\Xi}(t)$ represents the spin calculated within the same radius over the Mn site (solid line) and the kinetic field $\mathbf{B}^{\mathrm{I}}_{\mathrm{kin}}$ over the Fe site (dashed line). 182

5.12 Plots of the time-averaged observables evaluated in spheres of radius 1.4 Å around the atomic sites. (a) The averaged temporal evolution of $\left|\mathbf{B}^{\mathrm{Fe}}_{\mathrm{loc}}(t)\right|$ under different pulse amplitudes ($A = 0.5$ eV/Å, 0.7 eV/Å, 0.9 eV/Å); (b) comparison of $\left|\mathbf{B}^{\mathrm{Fe}}_{\mathrm{loc}}(t)\right|$ and $\left|\mathbf{B}^{\mathrm{Fe}}_{\mathrm{x}}(t)\right|$ under the pulse with amplitude ($A = 0.7$ eV/Å); (c) average value of $\cos\theta$ during the time evolution, with θ angle formed with the z axis by the $\mathbf{S}^{\mathrm{Fe}}(t)$ vector (black curve) and by the $\mathbf{B}^{\mathrm{Fe}}_{\mathrm{kin}}$ vector (red curve), same pulse of panel (b); (d) comparison between $\left|\mathbf{S}^{\mathrm{Fe}}(t)\right|$ and $S^{\mathrm{Fe}}_{\mathrm{z}}(t)$ during the temporal evolution with the same pulse of panel (b). 185

5.13 Plots of the exchange coupling evaluated inside a spheres of different radii centered on the Fe atomic site and of $S_{xy}^{Fe}(t)$ calculated inside the same spatial regions using three different type of pulses ($A = 0.7$, $A = 0.9$, $A = 0.5$) in $eV/\AA$, the dynamical exchange coupling here corresponds to the expression (5.168): (a) the averaged temporal variation of $\frac{\Delta\mathcal{J}_{mf}(t)}{|\mathcal{J}_{mf}(t=0)|} = \frac{\mathcal{J}_{mf}(t)}{|\mathcal{J}_{mf}(t=0)|} - 1$ in the first 10 fs, the quantity is integrated within a sphere of radius $R = 1.1$ Å; (b) the same averaged temporal variation $\frac{\Delta\mathcal{J}_{mf}(t)}{|\mathcal{J}_{mf}(t=0)|}$ inside a smaller sphere; (c) the averaged temporal variation of $\Delta S_{xy}^{Fe}(t)$ obtained by spatial integration inside sphere of radius $R = 1.1$ Å; (d) the averaged temporal evolution of the same quantity $S_{xy}^{Fe}(t)$. 186

5.14 Plots of the time-averaged observables evaluated in spheres of radius $R = 0.5$ Å around the Fe atomic site with three different type of pulses ($A = 1.0$, $A = 0.7$, $A = 0.5$): (a) the temporal variation of the angle $\theta(t) = \arccos(S_z^{Fe}(t)/|\mathbf{S}^{Fe}(t)|)$ with respect to its temporal averaged value $\langle\theta(t)\rangle = \frac{\sum_{n=1}^{N}\theta(t_n)}{N}$; (b) the Fourier transform $\mathfrak{F}(\theta)(\omega)$ where $\theta(t)$ is the angle previously defined. . . 187

6.1 Dynamics of the Fe_6 cluster center of mass momentum (a) Measure of the variation of the center of mass position $\Delta\mathbf{R}_{CM}(t)$ during the evolution; (b) Center of mass velocity $\mathbf{V}_{CM}(t) = \int d^3r\, \mathbf{j}_p(\mathbf{r}, t)/N$; (c) Evolution of the orbital moment center of mass component $\langle\hat{\mathbf{R}_{CM}} \times \hat{\mathbf{P}_{CM}}\rangle$ along x (red curve) and in the yz plane (black curve); (d) orbital moment $-qN\mathbf{R}_{CM} \times \mathbf{A}(t)$ evolution. 205

6.2 Dynamics of the Fe_6 cluster internal orbital moment component $\Delta\mathbf{L}_I(t)$ centered over different atomic sites and integrated within a radius $R = 1.2$ Å (a) Site 1; (b) Site 2; (c) Site 5; (d) Site 6. . . 206

6.3 Picture of the Fe_6 with the black arrow indicating the electric field polarization direction. 206

6.4 Collection of the 16 different Kohn-Sham states up and down for the Fe_2 cluster at $t = 0$ and after 4 fs. Certain states like $1\uparrow$ and $2\uparrow$ are delocalized and have the tendency to oscillate between the two atomic sites during the evolution. 209

6.5 Collection of the 16 different Kohn-Sham states up and down for the Fe_2 cluster at $t = 9$ fs and $t = 18$ fs. Certain states like $1\uparrow$ and $2\uparrow$ are delocalized and have the tendency to oscillate between the two atomic sites during the evolution. 210

6.6 Table of Slater-Koster transformations for s, p and d orbitals, with $l = d_x/|\mathbf{d}|$, $m = d_y/|\mathbf{d}|$ and $n = d_z/|\mathbf{d}|$. Here $\mathbf{d}$ is the vector distance between the two atomic centers, $(ss\sigma)$ is the irreducible integral between the s orbitals of the two sites with σ indicating the value of m_l along the bond axis (from Ref. [185]). 214

6.7 Graphical representation of one of the integrals in Eq. (6.120), with $|I, L, M\rangle$ s type orbital and $|l, l_z\rangle$ corresponding to a Υ_0^2 spherical harmonics. 214
6.8 Dynamical evolution of the model with Hamiltonian $\hat{H}(t)$ (from Eq. 6.103) and initial quantum state $|\Psi(0)\rangle = |l = 2, l_z = 1, s_z = 0.5\rangle$. (a) Amplitude of the external electric field $\mathbf{E}(t)$ and magnetic field $B_z(t)$ directed along z; (b) Evolution of the collinear $S_z(t)$ and non-collinear $S_{xy}(t)$ component of the spin vector under different ionic potentials $\hat{V}$; (c) Evolution of the total energy $E(t) = \langle \hat{H}(t) \rangle$ under different potentials $\hat{V}$; (d) Evolution of the collinear $L_z(t)$ and non-collinear component of the orbital moment $L_{xy}(t)$. 215
6.9 Dynamical evolution of the model with Hamiltonian $\hat{H}(t)$ (from Eq. 6.103) and initial quantum state $|\Psi(0)\rangle = |l = 2, l_z = 1, s_z = 0.5\rangle$. (a) Amplitude of the external electric field $\mathbf{E}(t)$ and magnetic field $B_z(t)$ directed along z; (b) Evolution of the collinear $S_z(t)$ and non-collinear $S_{xy}(t)$ component of the spin vector under different ionic potentials $\hat{V}$; (c) Evolution of the total energy $E(t) = \langle \hat{H}(t) \rangle$ under different potentials $\hat{V}$; (d) Evolution of the collinear $L_z(t)$ and non-collinear component of the orbital moment $L_{xy}(t)$. 217
6.10 Dynamics of the two angles $\theta_{\text{kin}}(t) = \text{acos}\left(\langle \Delta \mathbf{L}^{\text{I}}_{\text{kin}}(t), \hat{z} \rangle / |\Delta \mathbf{L}^{\text{I}}_{\text{kin}}(t)|\right)$ and $\phi_{\text{kin}}(t) = \text{atan}\left(\Delta L^{\text{I}}_{\text{kin},y}(t) / \Delta L^{\text{I}}_{\text{kin},x}(t)\right)$ obtained by integrating inside a radius $R = 1.4$ Å around the atoms (the sphere includes also part of the interstitial region). (a) temporal evolution of $\Delta L^{\text{I}}_{\text{kin},z}(t)$ for the in plane atoms (black curve) and the out-of-plane atoms (blue curve); (b) Evolution of $|\cos\theta_{\text{kin}}(t)|$ (thin line) together with $S^{\text{I}}_z / S^{\text{I}}_z(0)$ (thick line) for the in-plane and the out-of-plane atoms; (c) temporal evolution of $\Delta L^{\text{I}}_{\text{kin},xy}(t)$ for the in plane atoms (black curve) and the out-of-plane atoms (blue curve); (d) Evolution of $|\cos\phi_{\text{kin}}(t)|$ for in-plane (black line) and out-of-plane atoms (red line). 224
6.11 Global (a) spin and (b) energy variation in Fe_6 for two excitations differing only by the direction of polarization vector of the electric field pulse. Cartoon of the cluster with labels of the relevant atoms and the reference frame are depicted as insets. The contour plots represent the distribution of the angle (c, e) between $\mathbf{m}$ and $\mathbf{B}_{\text{kin}}$ in a plane through atoms 1, 3, 5 and 6 and the perpendicular component of $\mathbf{m}$ with respect to $\mathbf{B}_{\text{kin}}$ (d, f) averaged over the time of the simulation, for the two different excitations $\mathbf{E}\|\mathbf{x}$ and $\mathbf{E}\|\mathbf{z}$, respectively, the top and bottom panels. 226

6.12 The three columns represent the three Cartesian components of the spin-density distribution in the plane used in Fig. 6.11. Black circles are centered on all atomic sites and have a radius of 0.8 Å. The top row correspond to the ground-state properties. The next two rows show the averaged over the entire time-dependent simulation variation of the corresponding quantities with respect to their ground-state values for the two simulations only differing by the direction of the electric field of the excitation pulse. . . . 228
6.13 Evolutions of the spin around the individual atoms, defined as $S_{\mathrm{I}}^{z} = \frac{1}{|\mathcal{S}_{\mathrm{I}}^{\mathrm{R}}|} \int_{\mathcal{S}_{\mathrm{I}}^{\mathrm{R}}} \mathrm{d}^3 r \, s_z(\mathbf{r}, t)$, where $\mathcal{S}_{\mathrm{I}}^{\mathrm{R}}$ is a spherical volume of radius 0.8 Å centered at atom I, for each of the two excitations: (a) $\mathbf{E}\|\mathbf{x}$ and (b) $\mathbf{E}\|\mathbf{z}$. Comparison of the evolution of the base plane (c) and apex atoms (d) averaged spins (as in the top panels) for the two simulations. The lines are only guides to the eye connecting the data corresponding to snapshots of the TD-SDFT simulations. 229
6.14 Dynamics of the spin $\langle \hat{\mathbf{S}} \rangle$ and orbital moment $\langle \hat{\mathbf{L}} \rangle$ expectation values evolving under the time-dependent Hamiltonian (6.150) with $\mathbf{B}_{\mathrm{L}}$ directed along z and two different $\mathbf{B}(t)$. (a) and (c) temporal evolution of $B_z(t)$ (red curve) and of $B_{\mathrm{L},z}(t)$ (black curve); (b) evolution of the expectation values $\langle \hat{S}_z(t) \rangle$, $\langle S_{xy}(t) \rangle = \sqrt{\langle \hat{S}_x \rangle^2 + \langle \hat{S}_y \rangle^2}$, $\langle \hat{L}_z \rangle$ and $\langle \hat{L}_{xy} \rangle$ evolved under the fields of panel (a); (d) same quantities of panel (b) evolved under the fields of panel (c). . . . 231
6.15 Dynamics of the spin $\langle \hat{\mathbf{S}} \rangle$ and orbital moment $\langle \hat{\mathbf{L}} \rangle$ expectation values with $\mathbf{B}_{\mathrm{L}}$ lying in the $x-y$ plane. (a) temporal evolution of $B_z(t)$ (red curve), $B_{\mathrm{L},z}(t)$ (blue curve) and $B_{\mathrm{L},xy}(t)$ (black curve); (b) evolution of the expectation values $\langle \hat{S}_z(t) \rangle$ and $\langle S_{xy}(t) \rangle = \sqrt{\langle \hat{S}_x \rangle^2 + \langle \hat{S}_y \rangle^2}$; (c) temporal evolution of the Hamiltonian expectation value $\langle \hat{H}(t) \rangle$; (d) evolution of the orbital moment expectation values $\langle \hat{L}_z \rangle$ and $\langle L_{xy} \rangle$. 232
6.16 Temporal evolution of the H-H dimer. 242
6.17 Dynamics of the H-H dimer under the same field of Fig. 6.16a and same dimer orientation. (a) z component of the phononic orbital moment $L_{\mathrm{z,phon}}^{\mathrm{I}}(t)$; (b) z component of the electronic orbital moment $\langle \hat{L}_{\mathrm{z,elec}}^{\mathrm{I}}(t) \rangle$; (c) evolution of the spin expectation value at the two atomic sites $\langle \hat{S}_{\mathrm{z}}^{\mathrm{I}}(t) \rangle$; (d) global evolution of the variation of the system orbital moment with respect to its ground state value $\sum_{\mathrm{I}} (\Delta \langle \hat{L}_{\mathrm{z,elec}}^{\mathrm{I}}(t) \rangle + \Delta L_{\mathrm{z,phon}}^{\mathrm{I}}(t) + \Delta S_{\mathrm{z}}^{\mathrm{I}}(t))$. 245

LIST OF TABLES

4.1 Quantum numbers, occupations and Kohn - Sham eigenvalues of the Pseudo wavefunctions generated from the full - relativistic calculation. Looking at the occupation column we observe that the Hund rules are satisfied for the Fe atom and in the ground state configuration $L_z = 0$ and $S_z = 2\hbar$. 112

LIST OF ABBREVIATIONS

DFT	**D**ensity **F**unctional **T**heory
SDFT	**S**pin **D**ensity **F**unctional **T**heory
CDFT	**C**urrent **D**ensity **F**unctional **T**heory
TDDFT	**T**ime **D**ependent **D**ensity **F**unctional **T**heory
TDSDFT	**T**ime **D**ependent **S**pin **D**ensity **F**unctional **T**heory
TDCDFT	**T**ime **D**ependent **C**urrent **D**ensity **F**unctional **T**heory
LDA	**L**ocal **D**ensity **A**pproximation
ALDA	**A**diabatic **L**ocal **D**ensity **A**pproximation

PHYSICAL CONSTANTS

Speed of Light	$c = 2.997\,924\,58 \times 10^{8}\ \mathrm{m\,s^{-1}}$ (exact)
Electronic Charge	$e = 1.602\,176\,62 \times 10^{-19}\ \mathrm{C}$ (exact)
Planck Constant	$h = 6.626\,070\,04 \times 10^{-34}\ \mathrm{m^2 kg\,s^{-1}}$ (exact)
Electronic Mass	$m_e = 9.109\,383\,56 \times 10^{-31}\ \mathrm{kg}$ (exact)

Dedicated to my family

CHAPTER 1

INTRODUCTION AND SOME PRELIMINARY RESULTS

1.1 Introduction and motivations

In this work we are going to explore from a theoretical point of view the nature of the magnetization dynamics in metallic systems. The studies of the magnetization dynamics in mesoscopic systems could be roughly divided in two main groups [2] one is focused on the dynamics observed at times below 100 femtoseconds, while the second considers all those phenomena which become relevant after this time threshold. Since the average thermalization time of the system is of the order of 100 picoseconds [3] the laws of equilibrium thermodynamics developed in the past two centuries cannot be of much help for this problem and it is necessary, in order to deal with these out of equilibrium phenomena, to develop a new set of theoretical methods.

The greatest part of the phenomena falling into the group of the so-called fast magnetization processes have been traditionally explained within the framework of the Landau-Lifschitz or the Landau-Lifschitz-Gilbert equation [4, 5] by making use of an adiabatic extension of the equilibrium thermodynamic theory. However, the first set of phenomena are still poorly understood due to the fact that a simple adiabatic extension of the equilibrium theory cannot work in general given the complexity of the processes involved.

Due to the difficulties in providing a complete characterization of the out of equilibrium physical processes in real materials our aim is not to offer a description of all the possible different mechanisms that could play a role in the demagnetization process observed in transition metals. Instead, we want to grasp the fundamental physical mechanisms lying behind the group of ultrafast phenomena. This task requires a different set of theoretical tools with respect to those introduced in the context of the fast magnetization processes. In Chapter 3 we

will introduce the Density Functional Theory (DFT) method, that represent our basic theoretical tool for the investigation of the demagnetization process. In the successive Chapters after a detailed analysis of the DFT results we will proceed by constructing a minimal core model (M), which will be modified and enriched of new aspects at every successive step of the investigation.

The way in which this work has been structured is quite peculiar, the DFT-based calculations contribute, in fact, only to the epistemological component of the investigation. The *ab initio* DFT method is used in order to generate a set of observable quantities, namely density and magnetization, that, at least in principle, correspond to exact experimental outputs. This allows a formal replacement of experiments with numerical calculations. Based on the obtained DFT data we try to define a conceptual ontological superstructure that allows to improve our level of understanding of the ultrafast demagnetization process observed in magnetic metals in the first few hundred femtoseconds. This necessity of interpretation of the DFT data is strictly connected to the impossibility, inherent to the internal structure of quantum mechanics, of finding a direct relationship between epistemological structures and ontological concepts (which can be mathematical expressions or even simple ideas), that instead is given as a matter of fact in classical mechanics [1].

The mechanisms that we are going to analyze in this thesis constitute the core of the out of equilibrium magnetization dynamics in transition metals, but they could become not sufficient once we want to describe the entire dynamical process on a much longer time scale. In this case dissipative effects, that are neglected in our description, could become crucial and the model should be modified in order to take into account these new effects.

Up to now we have discussed the importance of the study of the far-from-equilibrium dynamics of nanostructured systems only from a pure theoretical perspective, this approach strongly underestimates its technological impact in particular in the field of information technology. At present the average access time for writes and reads in the most technologically advanced PC's is still around a few milliseconds. This is pretty low compared to the clock speed that instead is of the order of few gigahertz. The conventional way to store logical bits in a magnetic material consists in aligning the magnetization vector of a magnetic grain (bit) in one out of two possible directions, usually indicated using the numerical values 0 and 1. So, considering one of these magnetic bits, how can we reverse its magnetization direction ?

One possibility consists an increase of the average grain temperature, in this new configuration the application of a relatively small external magnetic field could lead to a reverse of the magnetization direction. This very successful procedure used in the magnetization record process is based on the equilibrium theory of phase transitions, which in its simplest and less involved version assumes the form of the phenomenological theory due to Landau [6]. In the Landau formulation the low-temperature phase of the system has a higher symmetry than its

high temperature phase. The transition between the two phases is then described by making use of an order parameter ϕ, which is different from zero in the high-symmetry phase and zero in the low-symmetry phase. Clearly in the case of a magnetic system this phenomenological parameter can be identified with the magnetization, and in the rest of the discussion we will always imply that $\phi = \mathbf{M}$. The fundamental assumption of the theory is that the Landau free energy of the system $F_L[\phi]$ is a functional of the order parameter and its minimal value corresponds to the thermodynamical free energy of the system at equilibrium

$$\min_{\phi} F_L[\phi] = F. \tag{1.1}$$

Near the transition we can expand F_{L} as follows

$$F_L[\phi] = F_0 + a\phi^2 + b\phi^4. \tag{1.2}$$

In Fig. 1.1 we show the shape of F_L using different values for a, b and F_0. By imposing $b > 0$ we observe that for $a > 0$ the solution of the minimization procedure is trivially $\phi = 0$, which means that the system has become paramagnetic and it is unable to store information. In contrast for $a < 0$ we have a double solution $\phi = \pm\sqrt{-a/2b}$ representing two states with opposite magnetization direction separated by an energy barrier. The continuous phase transition occurs, as can be clearly seen from Fig. 1.1(a) and (b), once the parameter a in F_{L} changes its sign. Making the assumption that the sign of a depends on the value of the temperature of the magnetic grain

$$a(T) = a_0(T - T_c), \tag{1.3}$$

and the Landau theory may be used to explain the phase transition occuring at the critical temperature T_c, that is also known as Curie temperature in case of ferromagnetic systems. The order parameter is now explicitly dependent on the temperature and below T_c the expression $\phi(T) = \pm\sqrt{a_0/2b}(T_c - T)^{0.5}$ becomes valid. From a pragmatic point of view the problem can be therefore restated as follows: how can we, below T_c, suppress the energy barrier and achieve magnetization reversal of the the magnetic grain of the ferromagnetic system ?

The solution, of course, requires to break the reversal symmetry $\phi \to -\phi$ of the free energy F_L. This can be translated into the following modification of the Landau expression

$$F_L[\phi] = F_0 + a\phi^2 + b\phi^4 - h\phi, \tag{1.4}$$

so that

$$F_L[\phi] \neq F_L[-\phi]. \tag{1.5}$$

Now the analytic exact expression for the minimum of F_L becomes more involved, but from Fig. 1.1 looking at panel (c) and (d) we observe that the effect of the symmetry-breaking field, h, is simply to destroy the double minimum structure of the free energy surface by introducing only one possible equilibrium value for the order parameter ϕ.

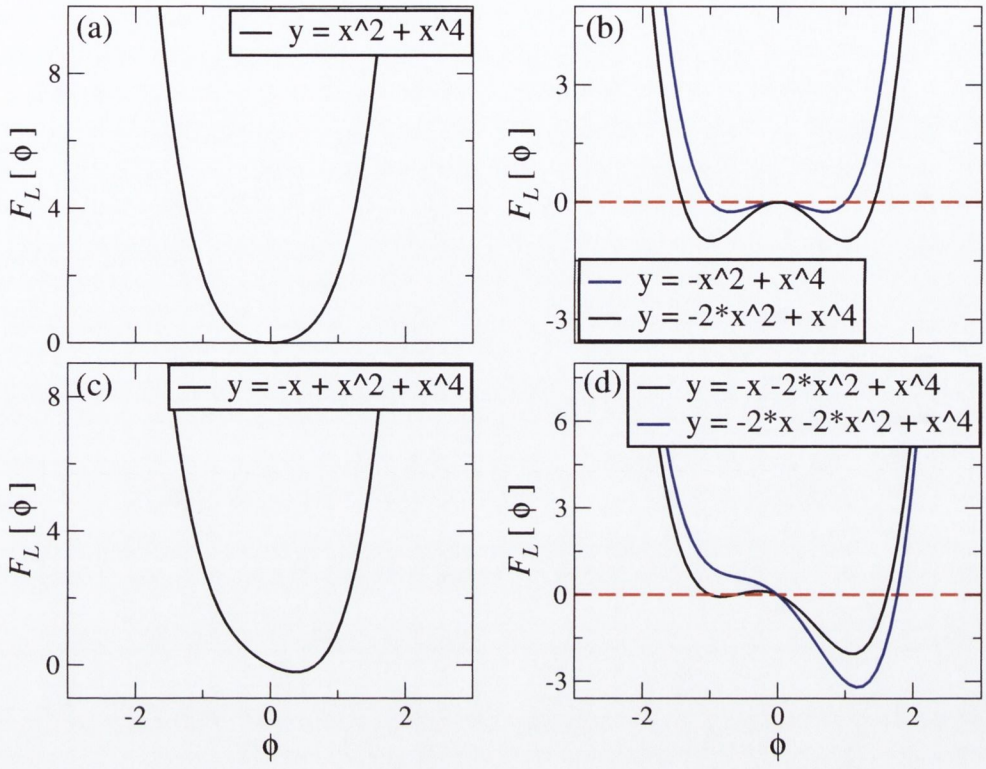


FIGURE 1.1: (a) F_L shape from Eq. (1.2) with parameters $a = 1$, $b = 1$, $F_0 = 0$. (b) F_L shape from Eq. (1.2) with $a = -1, -2$, $b = 1$, $F_0 = 0$. (c) F_L shape from Eq. (1.4) with parameters $a = -2$, $b = 1$, $F_0 = 0$ and $h = 1$. (d) same F_L of (c) but with $h = 1, 2$.

From these arguments we deduce that below T_c the reversal of the magnetization in a ferromagnetic system can be simply obtained by applying an external magnetic pulse h, which has the function to destroy the previous magnetic order of the system.

In order to achieve a deeper understanding of the problem of magnetization reversal in ferromagnetic alloys several different models have been introduced during the years. The most important one is the Stoner-Wohlfarth (SW) model [7]. The SW model of ferromagnetism is the simplest one adequate to describe the physics of magnetic grains containing single magnetic domains. Here the moment **M** of the magnetic grain is under the influence of two competing forces, the first one is due to uniaxial anisotropy and the second to an external magnetic field **H**. This means that the total energy can be written as the sum of the anisotropy and Zeeman energy ($E_z = -\mathbf{M} \cdot \mathbf{H}$), namely as

$$E = K \sin^2 \theta - HM_s \cos(\theta - \phi), \tag{1.6}$$

where K is the uniaxial anisotropy parameter, M_s is the saturation magnetization attained when all the magnetic moments are aligned along some common direction, θ represents the angle that **M** forms with the easy or anisotropy axis and ϕ

is the angle between the magnetic field and $\mathbf{M}_s$. The coercive field H_c indicates the field at which $\mathbf{M}(\mathbf{H}_c) = 0$ and H_K is the anisotropy field. For any given angle ϕ the conditions at which the magnetization $\mathbf{M}$ is reversed are obtained as

$$\left(\frac{\partial E}{\partial \theta}\right)_{\phi} = 0, \qquad \left(\frac{\partial^2 E}{\partial^2 \theta}\right)_{\phi} = 0, \tag{1.7}$$

which give an expression for the minimal, or critical field, at which the magnetization value jumps from one energy minimum to another

$$H_s(\phi) = \frac{H_K}{(\sin^{2/3}\phi + \cos^{2/3}\phi)^{3/2}}. \tag{1.8}$$

H_s represents, at this level of description, the switching magnetization field. From the previous discussion we have learnt that a possible way to reverse the magnetization direction consists in applying an external magnetic field to the magnetic domain. In the case in which the external field is directed along the spin direction of the domain the torque exerted by the field on the spin vector is exactly zero. However, thermal fluctuations can determine an effective non-zero torque causing a dynamical variation of the spin direction. This switching process is still rather slow with an effective duration of a few nanoseconds. Instead, in case of application of an external magnetic field orthogonally to the spin direction the torque exerted by the field is maximal. The spin then precesses around the direction of the applied field. However, in absence of a dissipative mechanism once the spin starts to precess it does not stop when the opposite direction is reached, i.e. the system cannot relax to the energy minimum and this constitutes a huge limitation of the method.

In a different experiment Tudosa and collaborators [8] show that by applying a very strong magnetic pulse passing through the center of a recording film at almost the speed of light the magnetic switching is obtained under the condition that the maximum angle of spin precession is reached. If the pulse duration is reduced, the condition on the angle of precession requires that the magnetic field strength must be increased in such a way that their product is still larger than the threshold value required for the switching to occur. A second necessary condition to obtain a technologically reliable switching mechanism is that the system is in an initial configuration approaching an ideal pure state in which all the spins are aligned along the same direction. If this condition is not verified, then, under the action of the pulse, some of the spins will switch while others will simply relax back to the initial state. In this way it is unlikely to obtain a final system configuration with the form of a single homogeneous magnetic bit.

Unfortunately the two conditions we have mentioned above are not compatible below a certain threshold value of the pulse duration. This is easy to understand if we consider a packet of electrons in motion with a certain average velocity $\mathbf{v}$. According to the Biot - Savart law this will produce an inhomogeneous magnetic

field $\mathbf{B}(\mathbf{r})$ that at the point P assumes the following form

$$\mathbf{B}(P) = -\frac{\mu_0 I}{4\pi} \int_\gamma \frac{d\mathbf{l} \times \mathbf{r}}{r^3}, \tag{1.9}$$

where $\mathbf{r}$ indicates the position of the point P with respect to the circuit element $d\mathbf{l}$ and I is the current flux. Clearly in case of the short and strong currents the field will be characterized by strong spatial inhomogeneities across the magnetic sample. This in turn means that in some region the field will be strong enough to cause the switching, while in others this will not occur. As a consequence after the application of the pulse the sample will be constituted by various regions characterized by different spin orientations (see Fig. 1.2).

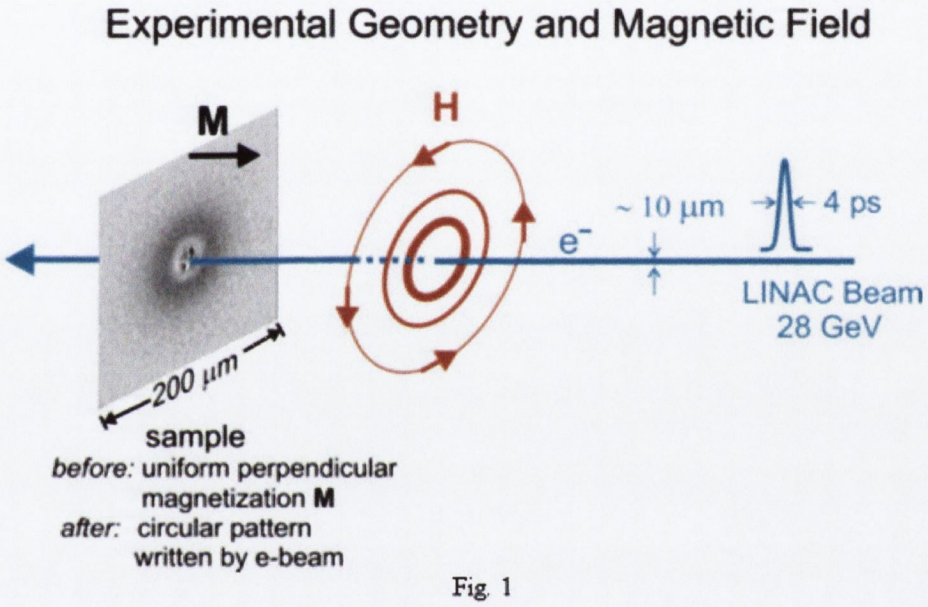


FIGURE 1.2: Experimental geometry and magnetic beam employed in [8]. When the electronic beam of about 5 ps length is shot through the uniformly magnetized sample the field writes a ring-shaped magnetic pattern with an opposite magnetization direction.

The problem is that, in order to consider the magnetic switching procedure technologically reliable, it has to be fully reversable under the repeated application of magnetic pulses, but in presence of inhomogeneous magnetic configurations, like those previously described, the successive application of magnetic pulses would lead to the formation of chaotic patterns within the sample removing any possibility for a reversible switching of the magnetic bit.

The previous experimental considerations suggest that there exists limit in the application of magnetic pulses for the switching of the magnetization direction in ferromagnetic materials, this limit is related to the evidence that shorter switching times require also stronger magnetic field and below a time interval of a few

picoseconds the process becomes not deterministic. Are there any alternatives to this approach ?

The answer is still not clear, but after the discovery of ultrafast demagnetization of a Ni film by a 60 femtosecond optical laser pulse [9] (see 1.3) the novel field of ultrafast magnetism started to attract a lot of interest. This is due also to the astonishing improvements achieved in laser technology over the past 20 years. Commercial laser sources can actually generate pulses with a duration below the 100 femtoseconds, whereas, in laboratory experiments the pulse duration can also be well below 1 femtosecond.

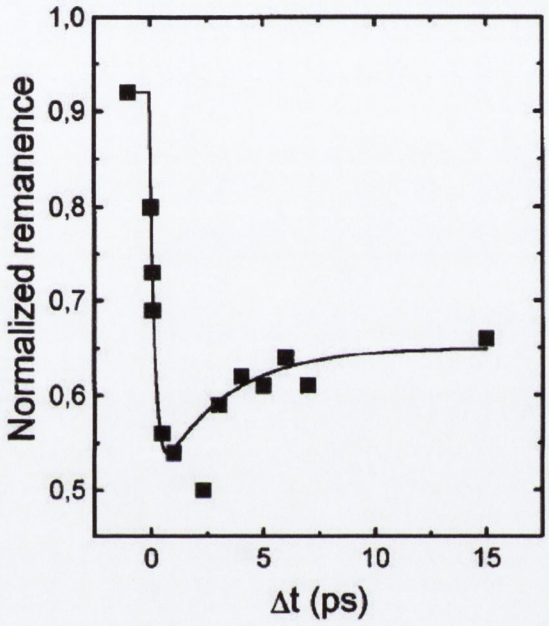


FIGURE 1.3: (Color online) Ultrafast demagnetization observed in *Ni* film using Magneto-Optical Kerr Effect (MOKE) signal [9].

It is now well known that irradiation by such ultra-short laser pulses can give rise to a wide range of magnetic effects like coherent demagnetization [10, 11], spin-reorientation [12, 13] or even a strong modification of the magnetic structure of the sample [14]. The physical origin of the variety of phenomena characterizing the field of ultrafast magnetism will be analyzed in Chapter 2, but here we want to conclude this introductory section by looking at the quantum evolution of a single particle in a central potential under the influence of an external electro - magnetic field $\mathbf{A}(t)$ purely time dependent and spatially homogeneous. The reason of this choice lies in the fact that while the magnetic field driven switching process is usually understood making use of the so-called adiabatic approximation, where only the magnetic moments of the system result affected by the application of the field, while the electronic ones are considered untouched. The same approach cannot be followed if we want to describe the femtosecond dynamics activated by the application of the laser pulse, the time scale of the magnetization dynamics requires also a complete analysis of the electronic degrees of freedom

that now play an active role in the process and cannot be considered frozen anymore.

1.2 Brief review of classical electro-dynamics and radiation matter interaction

The correct formalism to deal with when we consider the quantum mechanics of particles interacting with electro-magnetic radiation is Quantum Electro-Dynamics (QED). An extensive discussion of this theory that generalizes the standard single particle quantum mechanics approach to a purely relativistic description of both particles and fields can be found in many references [15–17]. Here we want to approach the problem from a weakly relativistic point of view and the natural starting point consists in writing down the set of Maxwell equations in vacuum (SI units)

$$\nabla \cdot \mathbf{E}(\mathbf{r},t) = \frac{\rho(\mathbf{r},t)}{\epsilon_0}, \tag{1.10}$$

$$\nabla \times \mathbf{B}(\mathbf{r},t) - \mu_0\epsilon_0\frac{\partial \mathbf{E}}{\partial t} = \mu_0\mathbf{J}(\mathbf{r},t), \tag{1.11}$$

$$\nabla \cdot \mathbf{B}(\mathbf{r},t) = 0, \tag{1.12}$$

$$\nabla \times \mathbf{E}(\mathbf{r},t) + \frac{\partial \mathbf{B}}{\partial t}(\mathbf{r},t) = 0, \tag{1.13}$$

in the previous equations $\mathbf{E}(\mathbf{r},t)$ defines the electric field, $\mathbf{B}(\mathbf{r},t)$ the magnetic field, $\rho(\mathbf{r},t)$ is the charge density and $\mathbf{J}(\mathbf{r},t)$ the current density, ϵ_0 and μ_0 are the vacuum permittivity and magnetic permeability respectively.

It can be useful to reformulate the problems in terms of a scalar, $\phi(\mathbf{r},t)$, and vector gauge potential, $\mathbf{A}(\mathbf{r},t)$, defined through the following relationships with the electro-magnetic fields

$$\mathbf{B}(\mathbf{r},t) = \nabla \times \mathbf{A}(\mathbf{r},t), \tag{1.14}$$

$$\mathbf{E}(\mathbf{r},t) = -\nabla\phi(\mathbf{r},t) - \frac{\partial \mathbf{A}}{\partial t}. \tag{1.15}$$

These fields are not physical since for a given electric and magnetic field they are not uniquely defined. We can introduce the equivalence class of the vector potentials $\mathbf{A}(\mathbf{r},t)$ and scalar potentials $\phi(\mathbf{r},t)$ which generate the same electric and magnetic field. The objects belonging to this class will be related through a gauge transformation that in its most generic form reads

$$\mathbf{A}'(\mathbf{r},t) = \mathbf{A}(\mathbf{r},t) + \nabla\Lambda(\mathbf{r},t), \tag{1.16}$$

$$\phi'(\mathbf{r},t) = \phi(\mathbf{r},t) - \frac{\partial\Lambda}{\partial t}. \tag{1.17}$$

In general this gauge freedom may be used in order to choose potentials that are easy to evaluate or they have some useful formal property that allows one to simplify the calculations. The two most common gauge choices in electrodynamics are the Lorentz and the Coulomb gauge.

The Lorentz gauge in its covariant form can be expressed by making use of the Einstein notation

$$\partial_\mu A^\mu = 0, \tag{1.18}$$

where $A^\mu = (\phi, \mathbf{A})$ is the vector potential defined over the 4-dimensional Minkowski space time $\mathscr{M}$, while in standard notation we have

$$\nabla \cdot \mathbf{A}(\mathbf{r}, t) + \frac{1}{c^2}\frac{\partial \phi}{\partial t}(\mathbf{r}, t) = 0. \tag{1.19}$$

By substituting the two potentials into the set of Maxwell equations we obtain the equations of motion for potentials ϕ and $\mathbf{A}$

$$\nabla^2\phi + \frac{\partial}{\partial t}(\nabla \cdot \mathbf{A}) = -\frac{\rho}{\epsilon_0}, \tag{1.20}$$

$$\nabla^2\mathbf{A} - \frac{1}{c^2}\frac{\partial^2 \mathbf{A}}{\partial t^2} = -\mu_0\mathbf{J} + \nabla\Big(\nabla \cdot \mathbf{A} + \frac{1}{c^2}\frac{\partial \phi}{\partial t}\Big), \tag{1.21}$$

that in Lorentz gauge is strongly simplified returning the final wave equations for the potentials

$$\nabla^2\phi + \frac{\partial}{\partial t}(\nabla \cdot \mathbf{A}) = -\frac{\rho}{\epsilon_0}, \tag{1.22}$$

$$\nabla^2\mathbf{A} - \frac{1}{c^2}\frac{\partial^2 \mathbf{A}}{\partial t^2} = -\mu_0\mathbf{J}. \tag{1.23}$$

A second way to make a simplification in the wave equations (1.20) consists in employing the following condition

$$\nabla \cdot \mathbf{A}(\mathbf{r}, t) = 0, \tag{1.24}$$

that is known as Coulomb gauge condition. The potentials now have to satisfy the following equations of motion

$$\nabla^2\phi = -\frac{\rho}{\epsilon_0}, \tag{1.25}$$

$$\nabla^2\mathbf{A} - \frac{1}{c^2}\frac{\partial^2 \mathbf{A}}{\partial t^2} = -\mu_0\mathbf{J} + \frac{1}{c^2}\nabla\frac{\partial \phi}{\partial t}. \tag{1.26}$$

The issue of the Coulomb gauge is that it cannot be written in a relativistically covariant form like the Lorentz gauge condition, however, it is widely used in the study of the interactions between radiation and matter.

After this brief, but necessary, introduction of the classical equations of electrodynamics we need also to consider the equation describing the motion of a

single particle in presence of an external electromagnetic potential. Classically we know that such particle will move according to the Lorentz force

$$m\frac{d\mathbf{v}}{dt} = q(\mathbf{E} + \mathbf{v} \times \mathbf{B}), \tag{1.27}$$

where q is the charge of the particle with mass m. The particle has a position $\mathbf{r}(t)$ at every instant in time, t, and velocity $\mathbf{v}$. We can then write the Lagrangian $\mathscr{L}(\mathbf{r}, \mathbf{v}, t)$ of a particle immersed in an electromagnetic field as

$$\mathscr{L}(\mathbf{r}, \mathbf{v}, t) = \frac{m}{2}\mathbf{v}^2 - q\phi(\mathbf{r}, t) + q\mathbf{v} \cdot \mathbf{A}(\mathbf{r}, t). \tag{1.28}$$

Through the Euler-Lagrange equation such $\mathscr{L}$ leads immediately to the Lorentz force equation for the single particle.

$\mathscr{L}(\mathbf{r}, \mathbf{v}, t)$ represents also the starting point of the quantization procedure. This requires to rewrite $\mathscr{L}$ in terms of its Legendre transform, the Hamiltonian function

$$\mathscr{H}(\mathbf{r}, \boldsymbol{\pi}, t) = \boldsymbol{\pi} \cdot \mathbf{v} - \mathscr{L}(\mathbf{r}, \mathbf{v}, t). \tag{1.29}$$

here $\boldsymbol{\pi}$ represents the conjugate momentum of the system, it is defined as $\boldsymbol{\pi} = \frac{\partial \mathscr{L}}{\partial \mathbf{v}}$ and it is equivalent to

$$\boldsymbol{\pi} = m\mathbf{v} + q\mathbf{A}(\mathbf{r}, t). \tag{1.30}$$

The previous object does not correspond to any physical momentum of the particle, since it is not gauge invariant. The appearence of these not-gauge-invariant objects within the theory is understandable in the sense that this theory is not fully relativistic. The difficulties are in fact lifted within the QED description, where it is considered the full Lagrangian of the problem that includes also the free electro-magnetic field term that here we do not take into account. By substituting the conjugate momentum expression into $\mathscr{L}$ we obtain

$$\mathscr{H}(\mathbf{r}, \boldsymbol{\pi}, t) = \frac{\boldsymbol{\pi}^2}{2m} - \frac{q}{m}\boldsymbol{\pi} \cdot \mathbf{A}(\mathbf{r}, t) + \frac{q^2}{2m}\mathbf{A}^2 + q\phi(\mathbf{r}, t). \tag{1.31}$$

That represents the Hamiltonian of the free charged particle in the external electromagnetic field.

This expression needs to be generalized in the case of a single particle with spin in an external field. The weakly-relativistic generalization leads to the Pauli Hamiltonian that we will discuss in some details in Chapter 2. Here, we limit ourselves to the case of a particle in an external ionic potential with a spin-orbit coupling term and an external magnetic field.

The reason behind this choice will become more clear in the following chapters, but we can already say that the Hamiltonian written in this specific form contains all the terms that appear to be relevant for, at least, a minimalistic description of the ultrafast demagnetization process. We start by rewriting the Hamiltonian in

the following way, with no specific choice of gauge

$$\mathscr{H}(\mathbf{r},\boldsymbol{\pi},t)=\frac{\boldsymbol{\pi}^2}{2m}-\frac{q}{m}\boldsymbol{\pi}\cdot\mathbf{A}(\mathbf{r},t)-\frac{q}{m}\mathbf{s}(\mathbf{r})\cdot\mathbf{B}(\mathbf{r},t)+V_{\mathrm{SO}}+V_{\mathrm{s}}(\mathbf{r},t), \tag{1.32}$$

where the third term on the right hand side corresponds to the interaction of an external magnetic field with the spin vector, V_{SO} defines a coupling term between the spin vector and the orbital degrees of freedom of the particle. The last term has instead the following form

$$V_{\mathrm{s}}(\mathbf{r},t)=q\phi(\mathbf{r},t)+\frac{q^2}{2m}\mathbf{A}^2. \tag{1.33}$$

By quantizing the Hamiltonian, $\mathscr{H}(\mathbf{r},\boldsymbol{\pi})$, we have

$$\hat{\mathscr{H}}(\mathbf{r},t)=\frac{\hat{\boldsymbol{\pi}}^2}{2m}-\frac{q}{m}\hat{\boldsymbol{\pi}}\cdot\mathbf{A}(\mathbf{r},t)-\mu_{\mathrm{B}}\hat{\boldsymbol{\sigma}}\cdot\mathbf{B}(\mathbf{r},t)+\hat{V}_{\mathrm{SO}}+\hat{V}_{\mathrm{s}}(\mathbf{r},t), \tag{1.34}$$

with commutation rule between position and conjugate momentum

$$[\hat{r}_i,\hat{\pi}_j]=i\hbar\delta_{i,j}. \tag{1.35}$$

The vector potential $\mathbf{A}(\mathbf{r},t)$ and the magnetic field $\mathbf{B}(\mathbf{r},t)$ are vector functions of the position operator. The spin orbit potential can be written in the following general form

$$\hat{V}_{\mathrm{SO}}=-\frac{q\hbar}{8(mc)^2}\left[\mathbf{E}(\mathbf{r},t)\times\left(\hat{\boldsymbol{\pi}}-q\mathbf{A}(\mathbf{r},t)\right)-\left(\hat{\boldsymbol{\pi}}-q\mathbf{A}(\mathbf{r},t)\right)\times\mathbf{E}(\mathbf{r},t)\right]\cdot\hat{\boldsymbol{\sigma}}. \tag{1.36}$$

The vector and scalar potentials can be subdivided into an internal and external component

$$\mathbf{A}(\mathbf{r},t) = \mathbf{A}_{\mathrm{ext}}(\mathbf{r},t)+\mathbf{A}_{\mathrm{int}}(\mathbf{r},t), \tag{1.37}$$

$$q\phi(\mathbf{r},t) = q\phi_{\mathrm{ext}}(\mathbf{r},t)+q\phi_{\mathrm{int}}(\mathbf{r},t). \tag{1.38}$$

Making use then of the electric dipole approximation according to which the wave length of the electro-magnetic field is much longer than the dimension of the physical system under study we can assume $\mathbf{E}_{\mathrm{ext}}(\mathbf{r},t)\simeq\mathbf{E}_{\mathrm{ext}}(0,t)$. The external potentials must therefore satisfy the following condition

$$\mathbf{E}_{\mathrm{ext}}(0,t)=-\nabla\phi_{\mathrm{ext}}(\mathbf{r},t)-\frac{\partial}{\partial t}\mathbf{A}_{\mathrm{ext}}(0,t). \tag{1.39}$$

Within the Coulomb gauge the two most important choices satisfying the previous condition are the length gauge

$$\mathbf{A}_{\mathrm{ext}}(0,t) = 0, \tag{1.40}$$

$$\phi_{\mathrm{ext}}(\mathbf{r},t) = -\mathbf{r}\cdot\mathbf{E}_{\mathrm{ext}}(0,t), \tag{1.41}$$

and the velocity gauge

$$\phi_{\text{ext}}(\mathbf{r},t) = 0, \tag{1.42}$$

$$\mathbf{E}_{\text{ext}}(0,t) = -\frac{\partial}{\partial t}\mathbf{A}_{\text{ext}}(0,t). \tag{1.43}$$

The internal component, $\mathbf{A}_{\text{int}}(\mathbf{r},t)$, of the vector potential is included usually in order to take into account the orbital current of the particle, which generates an internal magnetic field, but it can be neglected here. Rewriting the external potentials in the velocity gauge gives

$$\mathbf{A}(\mathbf{r},t) = \mathbf{A}_{\text{ext}}(0,t), \tag{1.44}$$

$$q\phi(\mathbf{r},t) = q\phi_{\text{int}}(\mathbf{r},t). \tag{1.45}$$

After a direct substitution into the Hamiltonian of Eq. (1.34) we obtain

$$\hat{\mathscr{H}}_{\text{vg}}(\mathbf{r},t) = \frac{\hat{\boldsymbol{\pi}}^2}{2m} - \frac{q}{m}\hat{\boldsymbol{\pi}}\cdot\mathbf{A}_{\text{ext}}(\mathbf{r},t) - \mu_{\text{B}}\hat{\boldsymbol{\sigma}}\cdot\mathbf{B}(\mathbf{r},t) + \hat{V}_{\text{SO}} + \hat{V}_{\text{s}}(\mathbf{r},t), \tag{1.46}$$

where the external potential is

$$\hat{V}_{\text{s}}(\mathbf{r},t) = q\phi_{\text{int}}(\mathbf{r},t) + \frac{q^2}{2m}\mathbf{A}^2_{\text{ext}}. \tag{1.47}$$

Here $\phi_{\text{int}}(\mathbf{r},t)$ is simply the electrostatic potential, $v_{\text{ext}}(\mathbf{r})$, acting on the particle and produced by the surrounding charges, that in our case corresponds to simply the ionic potential. The spin orbit potential, instead, becomes after a straightforward rearrangement

$$\hat{V}_{\text{SO}} = -\frac{q\hbar}{8(mc)^2}\Big[\mathbf{E}(\mathbf{r},t)\times\hat{\boldsymbol{\pi}} - \hat{\boldsymbol{\pi}}\times\mathbf{E}(\mathbf{r},t) - 2q\mathbf{E}(\mathbf{r},t)\times\mathbf{A}_{\text{ext}}(\mathbf{r},t)\Big]\cdot\hat{\boldsymbol{\sigma}}. \tag{1.48}$$

The total electric field is simply the sum of the external and internal contributions

$$\mathbf{E}(\mathbf{r},t) = \mathbf{E}_{\text{ext}}(0,t) + \frac{\nabla v_{\text{ext}}(\mathbf{r})}{q}. \tag{1.49}$$

If instead we consider the potentials into the length gauge we obtain

$$\mathbf{A}(\mathbf{r},t) = 0, \tag{1.50}$$

$$\phi(\mathbf{r},t) = -\mathbf{r}\cdot\mathbf{E}_{\text{ext}}(0,t) + v_{\text{ext}}(\mathbf{r}), \tag{1.51}$$

while the Hamiltonian becomes

$$\hat{\mathscr{H}}_{\text{lg}}(\mathbf{r},t) = \hat{\mathscr{H}}^{(1)}(\mathbf{r},t) + \hat{\mathscr{H}}^{(2)}(\mathbf{r},t) + \hat{\mathscr{H}}^{(3)}(\mathbf{r},t) + \hat{\mathscr{H}}^{(4)}(\mathbf{r},t), \tag{1.52}$$

with

$$\mathscr{H}^{(1)}(\mathbf{r},t) = \frac{\hat{\mathbf{p}}^2}{2m}, \tag{1.53}$$

$$\mathscr{H}^{(2)}(\mathbf{r},t) = -\mu_B \hat{\boldsymbol{\sigma}} \cdot \mathbf{B}(\mathbf{r},t), \tag{1.54}$$

$$\mathscr{H}^{(3)}(\mathbf{r},t) = \hat{V}_{SO}, \tag{1.55}$$

$$\mathscr{H}^{(4)}(\mathbf{r},t) = \hat{V}_s(\mathbf{r},t). \tag{1.56}$$

Where $\mathbf{p}$ here defines the physical momentum and the spin orbit and external potential are respectively

$$\hat{V}_{SO}(\mathbf{r}) = -\frac{q\hbar}{8(mc)^2}\Big[\mathbf{E}(\mathbf{r},t)\times\hat{\mathbf{p}} - \hat{\mathbf{p}}\times\mathbf{E}(\mathbf{r},t)\Big]\cdot\hat{\boldsymbol{\sigma}}, \tag{1.57}$$

$$\hat{V}_s(\mathbf{r},t) = -q\mathbf{r}\cdot\mathbf{E}_{ext}(0,t) + v_{ext}(\mathbf{r}). \tag{1.58}$$

It can be easily shown that the Hamiltonian of Eq. (1.34) does not represent a true physical quantity. In Quantum Physics, in fact, an observable is represented by a self-adjoint operator over the Hilbert space. This condition is fundamental in order to associate a set of real valued eigenvalues to the operator. At the same time this condition is verified also by the vector and the scalar potentials $(\mathbf{A}(\mathbf{r},t), \phi(\mathbf{r},t))$ which are not true physical quantities. In practice, given a certain observable $\hat{O}_g$ defined in a particular gauge g, this object will represent a true physical quantity on the Hilbert space only if the following condition is satisfied

$$\langle\psi_{g1}|\hat{O}_{g1}|\psi_{g1}\rangle = \langle\psi_{g1}|\exp\Big(-i\frac{e}{\hbar}\chi(\mathbf{r},t)\Big)\hat{O}_{g2}\exp\Big(i\frac{e}{\hbar}\chi(\mathbf{r},t)\Big)|\psi_{g1}\rangle, \tag{1.59}$$

where $|\psi_g\rangle$ represents the wave function in gauge g and $\chi(\mathbf{r},t)$ is the gauge transformation function. Passing from gauge g_2 to gauge g_1, the potentials transform as

$$\phi_{g_1}(\mathbf{r},t) = \phi_{g_2}(\mathbf{r},t) - \frac{\partial\chi}{\partial t}, \tag{1.60}$$

$$\mathbf{A}_{g_1}(\mathbf{r},t) = \mathbf{A}_{g_2}(\mathbf{r},t) + \nabla\chi, \tag{1.61}$$

and the observables must transform according to

$$\hat{O}_{g_1} = \exp\Big(-i\frac{e}{\hbar}\chi(\mathbf{r},t)\Big)\hat{O}_{g2}\exp\Big(i\frac{e}{\hbar}\chi(\mathbf{r},t)\Big). \tag{1.62}$$

Then, we may introduce the gauge invariant quantum mechanical energy operator [18]

$$\hat{\xi}(\mathbf{r},t) = \hat{\mathscr{H}}_{lg}(\mathbf{r},t) + q\mathbf{r}\cdot\mathbf{E}_{ext}(0,t), \tag{1.63}$$

where $\hat{\mathscr{H}}_{lg}(\mathbf{r},t)$ is the Hamiltonian operator in length gauge. The Heisenberg equation of motion for the quantum mechanical energy operator is

$$\frac{d}{dt}\hat{\xi} = \frac{1}{i\hbar}[\hat{\xi}, \hat{\mathscr{H}}_{lg}] + \frac{\partial}{\partial t}\hat{\xi}, \tag{1.64}$$

Where the commutator on the right-hand side may expressed as follows

$$\frac{1}{i\hbar}\langle[\hat{\xi}(t),\hat{\mathscr{H}}_{\rm lg}(t)]\rangle = \frac{q^2\hbar}{4m^2c^2}\int \mathrm{d}^3r\left[\frac{1}{q}\nabla v_{\rm ext}(\mathbf{r})\times\mathbf{E}_{\rm ext}(0,t)\right]\cdot\mathbf{m}(\mathbf{r},t) - \\ - q\int d^3r\mathbf{E}_{\rm ext}(0,t)\cdot\mathbf{j}_{\rm p}(\mathbf{r},t). \tag{1.65}$$

The first term on the right hand side arises due to the coupling of the external electric field with the internal charge sources, $\mathbf{j}_{\rm p}(\mathbf{r},t)$ is the paramagnetic current term, which can be written as

$$\mathbf{j}_{\rm p}(\mathbf{r},t) = \frac{i\hbar}{2m}\Big[\nabla\psi(\mathbf{r},t)^\dagger\psi(\mathbf{r},t) - \psi(\mathbf{r},t)^\dagger\nabla\psi(\mathbf{r},t)\Big], \tag{1.66}$$

where $\psi(\mathbf{r},t)$ is the single particle spinor wave function and $\mathbf{m}(\mathbf{r},t)$ is the magnetization density

$$\mathbf{m}(\mathbf{r},t) = \psi(\mathbf{r},t)^\dagger\hat{\sigma}\psi(\mathbf{r},t). \tag{1.67}$$

The second term appears into the description due to the fact that the commutator of the energy operator with the spin-orbit coupling term does not vanish. At the same time because of the c^{-2} dependence of the coefficient this object is expected to be very small compared to the first one and therefore negligible. The explicit time derivative of the energy operator gives instead the relation

$$\langle\frac{\hat{\xi}(t)}{\partial t}\rangle = -\frac{q\hbar}{4mc^2}\sum_{njl}\epsilon_{jln}\int \mathrm{d}^3r\,\frac{\partial E_j}{\partial t}\mathscr{J}_{\rm p}^{ln}(\mathbf{r},t). \tag{1.68}$$

In the previous expression we have introduced a second very important object called the paramagnetic spin - current tensor, defined as

$$\mathscr{J}_{\rm p}^{lk}(\mathbf{r},t) = \frac{i\hbar}{2m}\Big[\partial_l\psi(\mathbf{r},t)^\dagger\hat{\sigma}^k\psi(\mathbf{r},t) - \psi(\mathbf{r},t)^\dagger\hat{\sigma}^k\partial_l\psi(\mathbf{r},t)\Big]. \tag{1.69}$$

By summing up Eqs. (1.65) and (1.68) we arrive at the final expression for the expectation value of the power operator $\hat{\mathscr{P}}$,

$$\langle\mathscr{P}\rangle(t) = \frac{q^2\hbar}{4m^2c^2}\int \mathrm{d}^3r\left[\frac{1}{q}\nabla v_{\rm ext}(\mathbf{r})\times\mathbf{E}_{\rm ext}(0,t)\right]\cdot\mathbf{m}(\mathbf{r},t) - \\ - \frac{q\hbar}{4mc^2}\sum_{njl}\epsilon_{jln}\int \mathrm{d}^3r\,\frac{\partial E_j}{\partial t}\mathscr{J}_{\rm p}^{ln}(\mathbf{r},t) - q\int \mathrm{d}^3r\,\mathbf{E}_{\rm ext}(0,t)\cdot\mathbf{j}_{\rm p}(\mathbf{r},t). \tag{1.70}$$

The expectation value of the Hamiltonian in the length gauge is given by

$$\langle\hat{\mathscr{H}}_{\rm lg}\rangle(t) = \langle\hat{\xi}\rangle(t) + \int \mathrm{d}^3r\,\rho(\mathbf{r},t)[\mathbf{r}\cdot\mathbf{E}_{\rm ext}(0,t)], \tag{1.71}$$

where $\rho(\mathbf{r},t)$ is the electronic density. Similarly in the velocity gauge we find (neglecting terms of order c^{-3})

$$\langle \hat{\mathscr{H}}_{\mathrm{vg}} \rangle (t) = \langle \hat{\xi} \rangle (t) - q\mathbf{A}_{\mathrm{ext}}(0,t) \cdot \int \mathrm{d}^3 r\, \mathbf{j}_{\mathrm{p}}(\mathbf{r},t) + \frac{q^2}{2m}\mathbf{A}_{\mathrm{ext}}(0,t)^2 \int d^3 r \rho(\mathbf{r},t) + \\ + O(c^{-3}). \tag{1.72}$$

We are then in the position of looking at the equations of motion for the spin and the orbital moment. We will see that this simple paradigmatic case of a single particle with spin in the field of an ionic potential gives already an idea of how the ultrafast demagnetization process in metals can occur. In fact the fundamental ingredients of the spin continuity equation for a single particle will form also the basis for the description of the spin dynamics in many particle systems.

1.3 Equation of motion for the orbital moment

We first look at the orbital moment of the particle. The gauge-invariant orbital moment operator is defined as

$$\hat{\mathbf{L}} = \hat{\mathbf{r}} \times [\hat{\boldsymbol{\pi}} - q\mathbf{A}(\mathbf{r},t)], \tag{1.73}$$

where $\hat{\boldsymbol{\pi}}$ is the usual quantum mechanical momentum operator and $\mathbf{A}(\mathbf{r},t)$ is the vector potential. By Employing the length gauge we can simply write

$$\hat{\mathbf{L}}_{\mathrm{lg}} = \hat{\mathbf{r}} \times \hat{\mathbf{p}}, \tag{1.74}$$

and the Heisenberg equation of motion for the orbital moment is then

$$\frac{d}{dt}\langle \hat{\mathbf{L}}_{\mathrm{lg}} \rangle = \frac{1}{i\hbar}\langle [\hat{\mathbf{L}}_{\mathrm{lg}}, \hat{\mathscr{H}}_{\mathrm{lg}}] \rangle . \tag{1.75}$$

By looking at each component of the commutator separately we find that, by using the first term of the Hamiltonian (1.53), we can write the commutator as

$$\langle [\hat{L}^n_{\mathrm{lg}}, \hat{\mathscr{H}}^{(1)}{}_{\mathrm{lg}}] \rangle = \frac{1}{2m}\sum_{l,m} \epsilon_{nlm} \langle [\hat{r}_l, \hat{p}^2]\hat{p}_m \rangle , \tag{1.76}$$

that by using the properties of the commutator becomes

$$\langle [\hat{L}^n_{\mathrm{lg}}, \hat{\mathscr{H}}^{(1)}{}_{\mathrm{lg}}] \rangle = \frac{1}{2m}\sum_{l,m,j} \epsilon_{nlm} \langle (\hat{p}_j [\hat{r}_l, \hat{p}_j] + [\hat{r}_l, \hat{p}_j]\hat{p}_j)\hat{p}_m \rangle , \tag{1.77}$$

that is, by making use of the antisymmetric properties of the Levi-Civita tensor, automatically zero. By looking at the second term (1.54) instead we have

$$\langle [\hat{L}^n_{\rm lg}, \hat{\mathscr{H}^{(2)}}_{\rm lg}] \rangle = -\mu_B \langle [(\hat{\mathbf{r}} \times \hat{\mathbf{p}})_n, \hat{\boldsymbol{\sigma}} \cdot \mathbf{B}(\mathbf{r}, t)] \rangle , \tag{1.78}$$

which reduces to

$$\langle [\hat{L}^n_{\rm lg}, \hat{\mathscr{H}^{(2)}}_{\rm lg}] \rangle = -\mu_B \sum_{l,m} \epsilon_{nlm} \langle \hat{r}_l [\hat{p}_m, \hat{\boldsymbol{\sigma}} \cdot \mathbf{B}(\mathbf{r}, t)] \rangle , \tag{1.79}$$

$$\langle [\hat{L}^n_{\rm lg}, \hat{\mathscr{H}^{(2)}}_{\rm lg}] \rangle = i\hbar\mu_B \sum_{l,m,j} \epsilon_{nlm} \int \mathrm{d}^3 r \, r_l \, m_j(\mathbf{r}, t) \partial_m B_j(\mathbf{r}, t), \tag{1.80}$$

$$\langle [\hat{L}^n_{\rm lg}, \hat{\mathscr{H}^{(2)}}_{\rm lg}] \rangle = i\hbar\mu_B \sum_{j} \int \mathrm{d}^3 r \, (\mathbf{r} \times \nabla)_n B_j(\mathbf{r}, t) \cdot m_j(\mathbf{r}, t). \tag{1.81}$$

The third component of the Hamiltonian is the spin orbit coupling (1.55) and the evaluation of the commutator leads to

$$\langle [\hat{L}^n_{\rm lg}, \hat{\mathscr{H}^{(3)}}_{\rm lg}] \rangle = -\frac{q\hbar}{8(mc)^2} \langle [(\hat{\mathbf{r}} \times \hat{\mathbf{p}})_n, \hat{\boldsymbol{\sigma}} \cdot (\mathbf{E}(\mathbf{r}, t) \times \hat{\mathbf{p}} - \hat{\mathbf{p}} \times \mathbf{E}(\mathbf{r}, t))] \rangle . \tag{1.82}$$

This object could be rewritten as

$$\langle [\hat{L}^n_{\rm lg}, \hat{\mathscr{H}^{(3)}}_{\rm lg}] \rangle = C^n_1 + C^n_2, \tag{1.83}$$

where

$$C^n_1 = -\frac{q\hbar}{8(mc)^2} \sum_{j,l,m} \epsilon_{nlm} \left\langle \hat{r}_l \left[\hat{p}_m, \hat{\sigma}^j \left(2\mathbf{E}(0, t) \times \hat{\mathbf{p}} - \frac{\nabla v_{\rm ext}}{q} \times \hat{\mathbf{p}} + \hat{\mathbf{p}} \times \frac{\nabla v_{\rm ext}}{q} \right)_j \right] \right\rangle, \tag{1.84}$$

and

$$C^n_2 = -\frac{q\hbar}{8(mc)^2} \sum_{j,l,m} \epsilon_{nlm} \left\langle \left[\hat{r}_l, \hat{\sigma}^j \left(2\mathbf{E}(0, t) \times \hat{\mathbf{p}} - \frac{\nabla v_{\rm ext}}{q} \times \hat{\mathbf{p}} + \hat{\mathbf{p}} \times \frac{\nabla v_{\rm ext}}{q} \right)_j \right] \hat{p}_m \right\rangle. \tag{1.85}$$

By starting from the previous expression it can be useful to introduce the following Coulomb force field

$$F(\mathbf{r}) = \frac{|\nabla v_{\rm ext}|}{q|\mathbf{r}|}. \tag{1.86}$$

Our task is then to evaluate the following commutator

$$\left[(\hat{\mathbf{r}}\times\hat{\mathbf{p}})_n, \hat{\sigma}\cdot\left(\left(\mathbf{E}(0,t)-\mathbf{r}\frac{|\nabla v_{\text{ext}}|}{q|\mathbf{r}|}\right)\times\hat{\mathbf{p}}-\hat{\mathbf{p}}\times\left(\mathbf{E}(0,t)-\mathbf{r}\frac{|\nabla v_{\text{ext}}|}{q|\mathbf{r}|}\right)\right)\right]=$$

$$\begin{aligned}
&=\sum_{j=1}^{3}\hat{\sigma}^j[(\hat{\mathbf{r}}\times\hat{\mathbf{p}})_n,(\mathbf{E}(0,t)\times\hat{\mathbf{p}}-F(\mathbf{r})(\mathbf{r}\times\hat{\mathbf{p}})-\hat{\mathbf{p}}\times\mathbf{E}(0,t)+\hat{\mathbf{p}}\times\mathbf{r}F(\mathbf{r}))_j],\\
&=\sum_{j=1}^{3}\hat{\sigma}^j[(\hat{\mathbf{r}}\times\hat{\mathbf{p}})_n,2(\mathbf{E}(0,t)\times\hat{\mathbf{p}})_j]-\sum_{j=1}^{3}\hat{\sigma}^j[(\hat{\mathbf{r}}\times\hat{\mathbf{p}})_n,F(\mathbf{r})(\hat{\mathbf{r}}\times\hat{\mathbf{p}})_j]+\\
&+\sum_{j=1}^{3}\hat{\sigma}^j[(\hat{\mathbf{r}}\times\hat{\mathbf{p}})_n,(\hat{\mathbf{p}}\times\hat{\mathbf{r}})_jF(\mathbf{r})].
\end{aligned}\tag{1.87}$$

We can now evaluate the last three terms of the previous equation separately,

$$[(\hat{\mathbf{r}}\times\hat{\mathbf{p}})_n,2(\mathbf{E}(0,t)\times\hat{\mathbf{p}})_j]=2\sum_{l,m,p,q}\epsilon_{nlm}\epsilon_{jpq}E_p(0,t)[\hat{r}_l,\hat{p}_q]\hat{p}_m,\tag{1.88}$$

$$[(\hat{\mathbf{r}}\times\hat{\mathbf{p}})_n,2(\mathbf{E}(0,t)\times\hat{\mathbf{p}})_j]=-2i\hbar\sum_{l,m,s}\epsilon_{lnm}\epsilon_{ljs}E_s(0,t)\hat{p}_m.\tag{1.89}$$

By using the properties of the Levi-Civita tensor we then obtain

$$[(\hat{\mathbf{r}}\times\hat{\mathbf{p}})_n,2(\mathbf{E}(0,t)\times\hat{\mathbf{p}})_j]=-2i\hbar\delta_{nj}\sum_{m}E_m(0,t)\hat{p}_m+2i\hbar E_n(0,t)\hat{p}_j.\tag{1.90}$$

The second commutator instead may be rewritten as

$$[(\hat{\mathbf{r}}\times\hat{\mathbf{p}})_n,F(\mathbf{r})(\hat{\mathbf{r}}\times\hat{\mathbf{p}})_j]=F(\mathbf{r})[(\hat{\mathbf{r}}\times\hat{\mathbf{p}})_n,(\hat{\mathbf{r}}\times\hat{\mathbf{p}})_j]+[(\hat{\mathbf{r}}\times\hat{\mathbf{p}})_n,F(\mathbf{r})](\hat{\mathbf{r}}\times\hat{\mathbf{p}})_j,\tag{1.91}$$

and by using the commutation rules for the orbital moment operator

$$[(\hat{\mathbf{r}}\times\hat{\mathbf{p}})_n,(\hat{\mathbf{r}}\times\hat{\mathbf{p}})_j]=i\hbar\sum_{l}\epsilon_{njl}(\hat{\mathbf{r}}\times\hat{\mathbf{p}})_l,\tag{1.92}$$

and

$$[(\hat{\mathbf{r}}\times\hat{\mathbf{p}})_n,F(\mathbf{r})]=\sum_{m,l}\epsilon_{nml}\hat{r}_m[\hat{p}_l,F(\mathbf{r})],\tag{1.93}$$

that immediately becomes

$$[(\hat{\mathbf{r}}\times\hat{\mathbf{p}})_n,F(\mathbf{r})]=-i\hbar(\hat{\mathbf{r}}\times\nabla F(\mathbf{r}))_n,\tag{1.94}$$

Eq. (1.87) becomes

$$[(\hat{\mathbf{r}}\times\hat{\mathbf{p}})_n, \hat{\boldsymbol{\sigma}}\cdot(\mathbf{E}(\mathbf{r},t)\times\hat{\mathbf{p}}-\hat{\mathbf{p}}\times\mathbf{E}(\mathbf{r},t))] = -i\hbar\sum_j \hat{\sigma}_j(\hat{\mathbf{p}}\times\hat{\mathbf{r}})_j(\mathbf{r}\times\nabla F)_n -$$
$$- i\hbar F(\mathbf{r})\sum_j\hat{\sigma}^j\sum_l\epsilon_{njl}(\hat{\mathbf{r}}\times\hat{\mathbf{p}})_l - i\hbar\sum_j\hat{\sigma}^j(\mathbf{r}\times\nabla F(\mathbf{r}))_n(\hat{\mathbf{r}}\times\hat{\mathbf{p}})_j -$$
$$- i\hbar\sum_j\hat{\sigma}^j\sum_l\epsilon_{njl}(\hat{\mathbf{r}}\times\hat{\mathbf{p}})_l F(\mathbf{r}) + 2i\hbar\sum_j\hat{\sigma}^j(-\delta_{nj}\mathbf{E}(0,t)\cdot\hat{\mathbf{p}} + E_n(0,t)\hat{p}_j). \tag{1.95}$$

After some rearrangements we can finally write

$$[(\hat{\mathbf{r}}\times\hat{\mathbf{p}})_n, \hat{\boldsymbol{\sigma}}\cdot(\mathbf{E}(\mathbf{r},t)\times\hat{\mathbf{p}}-\hat{\mathbf{p}}\times\mathbf{E}(\mathbf{r},t))] = -2i\hbar\hat{\sigma}^n\sum_l E_l(0,t)\hat{p}_l -$$
$$- 2i\hbar F(\mathbf{r})\sum_j\hat{\sigma}^j\sum_l\epsilon_{njl}(\hat{\mathbf{r}}\times\hat{\mathbf{p}})_l - \hbar^2\sum_j\hat{\sigma}^j\sum_l\epsilon_{njl}(\mathbf{r}\times\nabla F(\mathbf{r}))_l +$$
$$+ i\hbar\sum_j\hat{\sigma}^j((\mathbf{r}\times\nabla F)_n(\mathbf{r}\times\hat{\mathbf{p}})_j - (\hat{\mathbf{p}}\times\mathbf{r})_j(\mathbf{r}\times\nabla F)_n) + 2i\hbar E_n(0,t)\sum_j\hat{\sigma}^j\hat{p}_j. \tag{1.96}$$

As a consequence of

$$\nabla\times(\mathbf{r}F(\mathbf{r})) = \nabla F\times\mathbf{r}, \tag{1.97}$$

we obtain, in the case of a simple centro-symmetric potential $v_{\text{ext}}(\mathbf{r})$,

$$\nabla\times(\mathbf{r}F(\mathbf{r})) = \nabla\times\left(\frac{\nabla v_{\text{ext}}}{q}\right), \tag{1.98}$$
$$\nabla\times(\mathbf{r}F(\mathbf{r})) = 0, \tag{1.99}$$

which means that the last three terms in Eq. (1.96) are exactly zero

$$[(\hat{\mathbf{r}}\times\hat{\mathbf{p}})_n, \hat{\boldsymbol{\sigma}}\cdot(\mathbf{E}(\mathbf{r},t)\times\hat{\mathbf{p}}-\hat{\mathbf{p}}\times\mathbf{E}(\mathbf{r},t))] = -2i\hbar\hat{\sigma}^n\sum_l E_l(0,t)\hat{p}_l -$$
$$- 2i\hbar F(\mathbf{r})\sum_j\hat{\sigma}^j\sum_l\epsilon_{njl}(\hat{\mathbf{r}}\times\hat{\mathbf{p}})_l + 2i\hbar E_n(0,t)\sum_j\hat{\sigma}^j\hat{p}_j. \tag{1.100}$$

From the final expression of the commutator we can now evaluate the expectation value of Eq. (1.82)

$$\langle[\hat{L}^n_{\text{lg}}, \hat{\mathscr{H}}^{(3)}{}_{\text{lg}}]\rangle = i\hbar\frac{q\hbar}{4(mc)^2}\sum_{i,\alpha,\beta}\int \mathrm{d}^3r\,\psi^*_{i\alpha}\sigma^n_{\alpha\beta}\sum_l E_l(0,t)(-i\hbar\partial_l\psi_{i\beta}) -$$
$$- i\hbar\frac{q\hbar}{4(mc)^2}\sum_{i,\alpha,\beta}\int \mathrm{d}^3r\,\psi^*_{i\alpha}E_n(0,t)\sum_j\sigma^j_{\alpha,\beta}(-i\hbar\partial_j\psi_{i\beta}) +$$
$$+ i\hbar\frac{q\hbar}{4(mc)^2}\sum_{i,\alpha,\beta}\int \mathrm{d}^3r\,\psi^*_{i\alpha}F(\mathbf{r})\sum_j\sigma^j_{\alpha,\beta}\sum_l\epsilon_{njl}[\mathbf{r}\times(-i\hbar\nabla\psi_{i\beta})]_l. \tag{1.101}$$

By making use of the definition of spin current tensor from Eq. (1.69) we can rewrite the previous expression in the form

$$\langle[\hat{L}^n_{\rm lg}, \hat{\mathscr{H}}^{(3)}{}_{\rm lg}]\rangle = i\hbar\frac{q\hbar}{4mc^2}\int \mathrm{d}^3r\left[\sum_l E_l(0,t)\mathscr{J}_{\rm p}^{ln}(\mathbf{r},t) - E_n(0,t)\sum_j \mathscr{J}_{\rm p}^{jj}(\mathbf{r},t)\right]+$$
$$+ i\hbar\frac{q\hbar}{4(mc)^2}\sum_{i,\alpha\beta}\int \mathrm{d}^3r\, F(\mathbf{r})\psi^*_{i\alpha}\sum_j[\sigma^j_{\alpha,\beta}r_n(-i\hbar\partial_j\psi_{i\beta}) - \sigma^j_{\alpha,\beta}r_j(-i\hbar\partial_n\psi_{i\beta})]. \tag{1.102}$$

By modifying the last term in the previous expression considering that

$$\partial_j(F(\mathbf{r})r_n) - \partial_n(F(\mathbf{r})r_j) = 0, \tag{1.103}$$

we arrive to the following equation

$$\langle[\hat{L}^n_{\rm lg}, \hat{\mathscr{H}}^{(3)}{}_{\rm lg}]\rangle = i\hbar\frac{q\hbar}{4mc^2}\int \mathrm{d}^3r\left[\sum_l E_l(0,t)\mathscr{J}_{\rm p}^{ln}(\mathbf{r},t) - E_n(0,t)\sum_j \mathscr{J}_{\rm p}^{jj}(\mathbf{r},t)\right]+$$
$$+ i\hbar\frac{q\hbar}{4mc^2}\int \mathrm{d}^3r\sum_j r_nF(\mathbf{r})\sum_{i,\alpha\beta}\left[\frac{i\hbar}{2m}\partial_j\psi^*_{i\alpha}\sigma^j_{\alpha\beta}\psi_{i\beta} - \psi^*_{i\alpha}\sigma^j_{\alpha\beta}\frac{i\hbar}{2m}\partial_j\psi_{i\beta}\right]-$$
$$- i\hbar\frac{q\hbar}{4mc^2}\int \mathrm{d}^3r\sum_j r_jF(\mathbf{r})\sum_{i,\alpha\beta}\left[\frac{i\hbar}{2m}\partial_n\psi^*_{i\alpha}\sigma^j_{\alpha\beta}\psi_{i\beta} - \psi^*_{i\alpha}\sigma^j_{\alpha\beta}\frac{i\hbar}{2m}\partial_n\psi_{i\beta}\right], \tag{1.104}$$

where $r_nF(\mathbf{r})$ is

$$r_nF(\mathbf{r}) = \frac{\mathbf{r}\cdot\hat{e}_n}{|\mathbf{r}|}\frac{|\nabla v_{\rm ext}|}{q}, \tag{1.105}$$

$$r_nF(\mathbf{r}) = \frac{\partial_n v_{\rm ext}}{q}. \tag{1.106}$$

By inserting this into the commutator expression we obtain the final form for the spin-orbit commutator

$$\frac{1}{i\hbar}\langle[\hat{L}^n_{\rm lg}, \hat{\mathscr{H}}^{(3)}{}_{\rm lg}]\rangle = -\frac{q\hbar}{4mc^2}\int \mathrm{d}^3r\left[\mathbf{E}(0,t) - \frac{\nabla v_{\rm ext}}{q}\right]_n\cdot\sum_j \mathscr{J}_{\rm p}^{jj}(\mathbf{r},t)+$$
$$+\frac{q\hbar}{4mc^2}\int \mathrm{d}^3r\sum_j\left[E_j(0,t)\mathscr{J}_{\rm p}^{jn}(\mathbf{r},t) - \frac{\partial_j v_{\rm ext}}{q}\mathscr{J}_{\rm p}^{nj}(\mathbf{r},t)\right]. \tag{1.107}$$

Finally we need to consider the fourth component of the Hamiltonian of Eq. (1.56) in order to complete the calculation of the time derivative of the orbital moment operator. This leads to the following term

$$\langle[\hat{L}^n_{\rm lg}, \hat{V}_{\rm s}(\mathbf{r},t)]\rangle = \langle[(\hat{\mathbf{r}}\times\hat{\mathbf{p}})_n, (v_{\rm ext}(\mathbf{r}) - q\mathbf{r}\cdot\mathbf{E}(0,t))]\rangle\,,$$

$$\langle [\hat{L}^n_{\rm lg}, \hat{V}_{\rm s}(\mathbf{r},t)]\rangle = \sum_{k,l} \epsilon_{nkl} \langle \hat{r}_k [\hat{p}_l, v_{\rm ext}(\mathbf{r}) - q\mathbf{r}\cdot\mathbf{E}(0,t)]\rangle\,,$$

$$\frac{1}{i\hbar}\langle [\hat{L}^n_{\rm lg}, \hat{V}_{\rm s}(\mathbf{r},t)]\rangle = -\sum_{k,l}\epsilon_{nkl}\int {\rm d}^3 r \sum_{i,\alpha}\left[\psi^*_{i\alpha}\psi_{i\alpha} r_k \partial_l v_{\rm ext} - \psi^*_{i\alpha}\psi_{i\alpha} r_k \cdot qE_l(0,t)\right], \tag{1.108}$$

that can be written as

$$\frac{1}{i\hbar}\langle [\hat{L}^n_{\rm lg}, \hat{V}_{\rm s}(\mathbf{r},t)]\rangle = -\int d^3 r \rho(\mathbf{r},t)[\mathbf{r}\times\nabla v_{\rm ext}(\mathbf{r})]_n + \int d^3 r \rho(\mathbf{r},t)[\mathbf{r}\times q\mathbf{E}(0,t)]_n. \tag{1.109}$$

By summing up the Eq. (1.81), (1.107) and (1.109) we finally obtain the equation of motion for the n component of the orbital moment

$$\begin{aligned}\frac{d}{dt}\langle \hat{L}^n\rangle = {}& \frac{q\hbar}{4mc^2}\int {\rm d}^3 r \sum_j \left[E_j(t)\mathscr{J}_{\rm p}^{jn}(\mathbf{r},t) - \frac{\partial_j v_{\rm ext}}{q}\mathscr{J}_{\rm p}^{nj}(\mathbf{r},t)\right] - \\ & - \frac{q\hbar}{4mc^2}\int {\rm d}^3 r \left[\mathbf{E}(t) - \frac{\nabla v_{\rm ext}}{q}\right]_n \sum_j \mathscr{J}_{\rm p}^{jj}(\mathbf{r},t) + \int {\rm d}^3 r\, \rho(\mathbf{r},t)(\mathbf{r}\times q\mathbf{E}(t))_n + \\ & + \mu_B \sum_j \int {\rm d}^3 r\, (\mathbf{r}\times\nabla)_n B_j(\mathbf{r},t) m_j(\mathbf{r},t) - \int {\rm d}^3 r\, \rho(\mathbf{r},t)[\mathbf{r}\times\nabla v_{\rm ext}(\mathbf{r})]_n + O(c^{-3}).\end{aligned} \tag{1.110}$$

Eq. (1.110) includes all the sources of variation for the orbital moment in the weakly-relativistic limit. In particular we distinguish three main contributions:

Internal sources : These represent the contribution due to the scattering of the orbital moment with the internal magnetic field $\mathbf{B}(\mathbf{r},t)$ and the electrostatic potential $v_{\rm ext}(\mathbf{r})$. We have already shown that in the case of a single pure centro - symmetric potential $\mathbf{r}\times\nabla v_{\rm ext}(\mathbf{r}) = 0$. The same is true for the magnetic field, but in the most general case we should always consider this contribution that becomes important when the rotational symmetry of the system is broken.

External sources : Here we include all the terms that are activated in the presence of an external field, that in our case is simply the homogeneous electric field $\mathbf{E}(0,t)$. The most important contribution to this group of terms is $\int d^3 r \rho(\mathbf{r},t)(\mathbf{r}\times q\mathbf{E}(0,t))_n$ that is related to the electric dipole term in the Hamiltonian. By following the same procedure in the velocity gauge this object becomes

$$\frac{d}{dt}\langle \hat{L}^n\rangle\Big|_{\rm ext} = -\frac{q}{2c}\int {\rm d}^3 r\, [\mathbf{A}_{\rm ext}(0,t)\times\mathbf{j}_{\rm p}(\mathbf{r},t)]_n,$$

showing explicitly that the coupling between the charge currents and the external electro-magnetic field represent a source of non conservation of

the orbital moment. All the other contributions due to the coupling between the system and the external field appear in the spin - orbit term and they are quite small compared to this one.

Internal spin - orbit coupling sources : In this last group we include all the remaining terms coming from the spin - orbit contribution to the Hamiltonian

$$\frac{d}{dt}\langle \hat{L}^n \rangle\Big|_{\text{s.o.c.}} = \frac{\hbar}{4mc^2}\int \mathrm{d}^3 r \left[\partial_n v_{\text{ext}} \cdot \sum_j \mathscr{J}_{\text{p}}^{jj}(\mathbf{r},t) - \partial_j v_{\text{ext}} \mathscr{J}_{\text{p}}^{nj}(\mathbf{r},t)\right],$$

which reflect the direct interaction between orbital and spin degrees of freedom.

In conclusion we can say that if the internal potentials do not break the central symmetry of the system the orbital moment equation of motion can be rewritten as follows

$$\begin{aligned}\frac{d}{dt}\langle \hat{L}^n \rangle = &-\frac{q\hbar}{4mc^2}\int \mathrm{d}^3 r \left[\mathbf{E}(0,t) - \frac{\nabla v_{\text{ext}}}{q}\right]_n \cdot \sum_j \mathscr{J}_{\text{p}}^{jj}(\mathbf{r},t) + \\ &+ \frac{q\hbar}{4mc^2}\int \mathrm{d}^3 r \sum_j \left[E_j(0,t)\mathscr{J}_{\text{p}}^{jn}(\mathbf{r},t) - \frac{\partial_j v_{\text{ext}}}{q}\mathscr{J}_{\text{p}}^{nj}(\mathbf{r},t)\right] + \\ &+ \int \mathrm{d}^3 r \rho(\mathbf{r},t)[\mathbf{r}\times q\mathbf{E}(0,t)]_n + O(c^{-3}),\end{aligned} \tag{1.111}$$

where the only contributions are due to the symmetry breaking electric field and the spin-orbit coupling term.

1.4 Equation of motion for the spin vector

We consider now the spin equation of motion for the single particle. We split, as we have done for the orbital moment, the length gauge Hamiltonian in four different parts and then look at each contribution separately. The Heisenberg equation of motion for the spin operator is then

$$\frac{d}{dt}\langle \hat{\mathbf{S}} \rangle = \frac{1}{i\hbar}\langle [\hat{\mathbf{S}}, \hat{\mathscr{H}}_{\text{lg}}] \rangle . \tag{1.112}$$

For the first Hamiltonian component we find trivially that

$$\langle [\hat{S}^n, \hat{\mathscr{H}}^{(1)}{}_{\text{lg}}] \rangle = \frac{\hbar}{4m}\langle [\hat{\sigma}^n, \hat{p}^2] \rangle , \tag{1.113}$$

$$\langle [\hat{S}^n, \hat{\mathscr{H}}^{(1)}{}_{\text{lg}}] \rangle = 0. \tag{1.114}$$

The second component instead leads to the familiar spin - magnetic field torque term

$$\langle[\hat{S}^n, \hat{\mathscr{H}^{(2)}}_{\rm lg}]\rangle = -\mu_B \frac{\hbar}{2} \langle[\hat{\sigma}^n, \hat{\sigma}^k] B_k(\mathbf{r}, t)\rangle\,, \tag{1.115}$$

and, by using the Pauli matrix commutation rules,

$$[\hat{\sigma}^i, \hat{\sigma}^j] = 2i \sum_l \epsilon_{ijl} \hat{\sigma}^l, \tag{1.116}$$

we obtain

$$\langle[\hat{S}^n, \hat{\mathscr{H}^{(2)}}_{\rm lg}]\rangle = -i\hbar\mu_B \sum_{i,\alpha,\beta} \int \mathrm{d}^3 r \sum_{k,l} \epsilon_{nkl} B_k(\mathbf{r}, t) \psi^*_{i\alpha} \sigma^l_{\alpha,\beta} \psi_{i\beta}. \tag{1.117}$$

By making use of the definition of magnetization vector the equation becomes

$$\langle[\hat{S}^n, \hat{\mathscr{H}^{(2)}}_{\rm lg}]\rangle = -i\hbar\mu_B \int \mathrm{d}^3 r\, [\mathbf{B}(\mathbf{r}, t) \times \mathbf{m}(\mathbf{r}, t)]_n. \tag{1.118}$$

The third component of the Hamiltonian involves the spin orbit coupling

$$\langle[\hat{S}^n, \hat{\mathscr{H}^{(3)}}_{\rm lg}]\rangle = -\frac{q\hbar}{8(mc)^2} \langle[(\hat{S}^n, \hat{\boldsymbol{\sigma}} \cdot (\mathbf{E}(\mathbf{r}, t) \times \hat{\mathbf{p}} - \hat{\mathbf{p}} \times \mathbf{E}(\mathbf{r}, t))]\rangle\,, \tag{1.119}$$

$$\begin{aligned}
&\langle[\hat{S}^n, \hat{\mathscr{H}^{(3)}}_{\rm lg}]\rangle = \\
&= -\frac{q\hbar^2}{16(mc)^2} \left\langle \sum_k [\hat{\sigma}^n, \hat{\sigma}^k] \left[\left(\mathbf{E}(0, t) - \frac{\nabla v_{\rm ext}}{q} \right) \times \hat{\mathbf{p}} - \hat{\mathbf{p}} \times \left(\mathbf{E}(0, t) - \frac{\nabla v_{\rm ext}}{q} \right) \right]_k \right\rangle.
\end{aligned} \tag{1.120}$$

in the following we use the following rule for the cross product of two operators

$$(\hat{\mathbf{O}} \times \hat{\mathbf{p}} - \hat{\mathbf{p}} \times \hat{\mathbf{O}})\phi = \hat{\mathbf{O}} \times (\hat{\mathbf{p}}\phi) - (\hat{\mathbf{p}}\phi) \times \hat{\mathbf{O}} - \hat{\mathbf{p}} \times \hat{\mathbf{O}}\phi, \tag{1.121}$$

where $\hat{\mathbf{p}}$ is the usual momentum operator, $\hat{\mathbf{O}}$ is a generic operator defined on the Hilbert space and ϕ is a vector

$$(\hat{\mathbf{O}} \times \hat{\mathbf{p}} - \hat{\mathbf{p}} \times \hat{\mathbf{O}})\phi = 2\hat{\mathbf{O}} \times \hat{\mathbf{p}}\phi + i\hbar\nabla \times \hat{\mathbf{O}}\phi. \tag{1.122}$$

If we now consider the single term

$$\left[\hat{\mathbf{p}} \times \left(\mathbf{E}(0, t) - \frac{\nabla v_{\rm ext}}{q} \right) \right]_j = \sum_{l,m} \epsilon_{jlm} \hat{p}_l \left(\mathbf{E}(0, t) - \frac{\nabla v_{\rm ext}}{q} \right)_m, \tag{1.123}$$

we will have

$$\left[\hat{\mathbf{p}}\times\left(\mathbf{E}(0,t)-\frac{\nabla v_{\text{ext}}}{q}\right)\right]_j=\sum_{l,m}\epsilon_{jlm}E_m(0,t)\hat{p}_l-\frac{1}{q}\sum_{l,m}\epsilon_{jlm}(-i\hbar\partial_l)\partial_m v_{\text{ext}}(\mathbf{r})-$$
$$-\frac{1}{q}\sum_{l,m}\epsilon_{jlm}\partial_m v_{\text{ext}}(\mathbf{r})\hat{p}_l, \tag{1.124}$$

and making use of the relation $\nabla\times\nabla v_{\text{ext}}(\mathbf{r})=0$

$$\left[\hat{\mathbf{p}}\times\left(\mathbf{E}(0,t)-\frac{\nabla v_{\text{ext}}}{q}\right)\right]_j=-\sum_{l,m}\epsilon_{jlm}\left(E_m(0,t)\hat{p}_l-\frac{\partial_m v_{\text{ext}}}{q}\hat{p}_l\right), \tag{1.125}$$

$$\left[\hat{\mathbf{p}}\times\left(\mathbf{E}(0,t)-\frac{\nabla v_{\text{ext}}}{q}\right)\right]_j=-\left[\left(\mathbf{E}(0,t)-\frac{\nabla v_{\text{ext}}}{q}\right)\times\hat{\mathbf{p}}\right]_j, \tag{1.126}$$

that inserted into the equation of motion gives rise to

$$\left\langle[\hat{S}^n,\hat{\mathscr{H}}^{(3)}{}_{\text{lg}}]\right\rangle=-\frac{q\hbar^2}{8(mc)^2}\left\langle\sum_k[\hat{\sigma}^n,\hat{\sigma}^k]\left[\left(\mathbf{E}(0,t)-\frac{\nabla v_{\text{ext}}}{q}\right)\times\hat{\mathbf{p}}\right]_k\right\rangle, \tag{1.127}$$

$$\left\langle[\hat{S}^n,\hat{\mathscr{H}}^{(3)}{}_{\text{lg}}]\right\rangle=-i\hbar\frac{q\hbar}{4(mc)^2}\sum_{k,l}\epsilon_{nkl}\int\mathrm{d}^3r\,\psi^\dagger\hat{\sigma}^l\left[\left(\mathbf{E}(0,t)-\frac{\nabla v_{\text{ext}}}{q}\right)\times(\hat{\mathbf{p}}\psi)\right]_k. \tag{1.128}$$

By expanding the cross product

$$\left[\left(\mathbf{E}(0,t)-\frac{\nabla v_{\text{ext}}}{q}\right)\times(-i\hbar\nabla\psi)\right]_k=\sum_{m,j}\epsilon_{kmj}\left(\mathbf{E}(0,t)-\frac{\nabla v_{\text{ext}}}{q}\right)_m(-i\hbar\partial_j\psi), \tag{1.129}$$

and by neglecting the boundary terms this leads to the following expression

$$\left\langle[\hat{S}^n,\hat{\mathscr{H}}^{(3)}{}_{\text{lg}}]\right\rangle=-\frac{iq\hbar^2}{4(mc)^2}\sum_{k,l}\epsilon_{nkl}\int\mathrm{d}^3r\,\psi^\dagger\hat{\sigma}^l\sum_{m,j}\epsilon_{kmj}\left(\frac{i\hbar}{2}\partial_j\right)\left(\mathbf{E}(0,t)-\frac{\nabla v_{\text{ext}}}{q}\right)_m\psi-$$
$$-i\hbar\frac{q\hbar}{4(mc)^2}\sum_{k,l}\epsilon_{nkl}\int\mathrm{d}^3r\,\psi^\dagger\hat{\sigma}^l\cdot\sum_{m,j}\epsilon_{kmj}\left(\mathbf{E}(0,t)-\frac{\nabla v_{\text{ext}}}{q}\right)_m\left(-\frac{i\hbar}{2}\partial_j\psi\right)-$$
$$-i\hbar\frac{q\hbar}{4(mc)^2}\sum_{k,l}\epsilon_{nkl}\int\mathrm{d}^3r\left(\frac{i\hbar}{2}\partial_j\psi^\dagger\right)\hat{\sigma}^l\cdot\sum_{m,j}\epsilon_{kmj}\left(\mathbf{E}(0,t)-\frac{\nabla v_{\text{ext}}}{q}\right)_m\psi. \tag{1.130}$$

The last term on the right hand side of the equation is precisely zero

$$\epsilon_{kmj}\partial_j\left(E_m(0,t)-\frac{\partial_m v_{\text{ext}}}{q}\right)=-\epsilon_{kmj}\frac{\partial_j\partial_m v_{\text{ext}}}{q}, \tag{1.131}$$

$$\epsilon_{kmj}\partial_j\left(E_m(0,t)-\frac{\partial_m v_{\text{ext}}}{q}\right)=0, \tag{1.132}$$

so that we can finally write

$$\begin{aligned}\left\langle[\hat{S}^n, \hat{\mathscr{H}}^{(3)}{}_{\rm lg}]\right\rangle = \\ -\frac{iq\hbar^2}{4(mc)^2}\sum_{k,l}\epsilon_{nkl}\int \mathrm{d}^3r\left(\frac{i\hbar}{2}\partial_j\psi^\dagger\right)\hat{\sigma}^l\sum_{m,j}\epsilon_{kmj}\left(\mathbf{E}(0,t)-\frac{\nabla v_{\rm ext}}{q}\right)_m\psi- \\ -i\hbar\frac{q\hbar}{4(mc)^2}\sum_{k,l}\epsilon_{nkl}\int \mathrm{d}^3r\,\psi^\dagger\hat{\sigma}^l\cdot\sum_{m,j}\epsilon_{kmj}\left(\mathbf{E}(0,t)-\frac{\nabla v_{\rm ext}}{q}\right)_m\left(-\frac{i\hbar}{2}\partial_j\psi\right).\end{aligned} \tag{1.133}$$

By making use of the definition of spin current tensor and of the properties of the Levi Civita symbol this term becomes

$$\left\langle[\hat{S}^n, \hat{\mathscr{H}}^{(3)}{}_{\rm lg}]\right\rangle = i\hbar\frac{q\hbar}{4mc^2}\sum_{m,j,l}(\delta_{n,m}\delta_{j,l}-\delta_{n,j}\delta_{l,m})\int \mathrm{d}^3r\left[\mathbf{E}(0,t)-\frac{\nabla v_{\rm ext}}{q}\right]_m\mathscr{J}_{\rm p}^{jl}(\mathbf{r},t), \tag{1.134}$$

and then

$$\begin{aligned}\left\langle[\hat{S}^n, \hat{\mathscr{H}}^{(3)}{}_{\rm lg}]\right\rangle = i\hbar\frac{q\hbar}{4mc^2}\int \mathrm{d}^3r\sum_j\left[\mathbf{E}(0,t)-\frac{\nabla v_{\rm ext}}{q}\right]_n\mathscr{J}_{\rm p}^{jj}(\mathbf{r},t)- \\ -i\hbar\frac{q\hbar}{4mc^2}\int \mathrm{d}^3r\sum_l\left[\mathbf{E}(0,t)-\frac{\nabla v_{\rm ext}}{q}\right]_l\mathscr{J}_{\rm p}^{nl}(\mathbf{r},t),\end{aligned} \tag{1.135}$$

that is our final expression for the commutator with the spin orbit coupling term. From the fact that $\hat{V}_{\rm s}(\mathbf{r})$ commutes with the spin operator we can also conclude that

$$\langle[\hat{S}^n, \hat{V}_{\rm s}]\rangle = 0, \tag{1.136}$$

and the continuity equation for the spin operator becomes finally

$$\begin{aligned}\frac{d}{dt}\langle\hat{S}^n\rangle = \frac{q\hbar}{4mc^2}\int \mathrm{d}^3r\sum_j\left[\mathbf{E}(0,t)-\frac{\nabla v_{\rm ext}}{q}\right]_n\mathscr{J}_{\rm p}^{jj}(\mathbf{r},t)- \\ -\frac{q\hbar}{4mc^2}\int \mathrm{d}^3r\sum_l\int d^3r\left[\mathbf{E}(0,t)-\frac{\nabla v_{\rm ext}}{q}\right]_l\mathscr{J}_{\rm p}^{nl}(\mathbf{r},t)- \\ -\mu_B\int d^3r\,[\mathbf{B}(\mathbf{r},t)\times\mathbf{m}(\mathbf{r},t)]_n.\end{aligned} \tag{1.137}$$

From Eq. (1.137) we see that there are only two sources of variation for the spin, the first one is due to the torque exerted by the magnetic field, while the second one is due to the spin-orbit coupling term. There is no, like for the orbital moment, a direct external source of variation due to the coupling of the spin with the external field. The electric field appears in the continuity equation only as a modification of the spin orbit coupling term and it can, in principle, modify the effective strength of the interaction.

By summing up the spin orbital components of the equation of motion for spin and orbital moment we obtain

$$\frac{d}{dt}\langle\hat{L}^n\rangle\Big|_{\text{s.o.c.}} + \frac{d}{dt}\langle\hat{S}^n\rangle\Big|_{\text{s.o.c.}} = -\frac{q\hbar}{4mc^2}\int \mathrm{d}^3r\left[\mathbf{E}(0,t) - \frac{\nabla v_{\text{ext}}}{q}\right]_n \cdot \sum_j \mathscr{J}_{\text{p}}^{jj}(\mathbf{r},t) +$$
$$+ \frac{q\hbar}{4mc^2}\int \mathrm{d}^3r \sum_j \left[E_j(0,t)\,\mathscr{J}_{\text{p}}^{jn}(\mathbf{r},t) - \frac{\partial_j v_{\text{ext}}}{q}\,\mathscr{J}_{\text{p}}^{nj}(\mathbf{r},t)\right] +$$
$$+ \frac{q\hbar}{4mc^2}\int \mathrm{d}^3r \sum_j \left[\mathbf{E}(0,t) - \frac{\nabla v_{\text{ext}}}{q}\right]_n \mathscr{J}_{\text{p}}^{jj}(\mathbf{r},t) -$$
$$- \frac{q\hbar}{4mc^2}\int \mathrm{d}^3r \sum_l \int d^3r\left[\mathbf{E}(0,t) - \frac{\nabla v_{\text{ext}}}{q}\right]_l \mathscr{J}_{\text{p}}^{nl}(\mathbf{r},t), \qquad (1.138)$$

where the first term on the right hand side exactly cancels the third one

$$\frac{d}{dt}\langle\hat{L}^n\rangle\Big|_{\text{s.o.c.}} + \frac{d}{dt}\langle\hat{S}^n\rangle\Big|_{\text{s.o.c.}} = D(t), \qquad (1.139)$$

with

$$D(t) = \frac{q\hbar}{4mc^2}\int \mathrm{d}^3r \sum_j \left[E_j(0,t)\,\mathscr{J}_{\text{p}}^{jn}(\mathbf{r},t) - E_j(0,t)\,\mathscr{J}_{\text{p}}^{nj}(\mathbf{r},t)\right]. \qquad (1.140)$$

This relation shows that, while in the absence of an external field the amount of spin lost during the dynamical evolution needs to be transfered directly into the orbital moment, this mechanism could be, in principle, broken when the laser field is not zero. It should also be noticed that while the only property of the magnetic field $\mathbf{B}(\mathbf{r},t)$ is to generate a torque of the spin direction, the spin loss mechanism requires in general the presence of spin currents.

An important point regarding the previous derivation of the continuity equations for the energy, the orbital moment and the spin of the single particle in an external applied field is that these equations describe the global evolution of the quantities, but do not take into account what happens locally. In practice changes of these quantities can occur also in a specific spatial region but with no consequences on its global dynamical evolution. In order to understand this important point we look at the symmetries of the Pauli Hamiltonian and, switching to the Lagrangian description, we make use of the Noether theorem [19] that allows a local generalization of the continuity equation for spin and orbital moment.

1.5 Local continuity equations and the Noether theorem

The Lagrangian that we use to describe the weakly-relativistic spinning particle is (in the velocity gauge)

$$\begin{aligned}\mathscr{L}(\psi,\nabla\psi) = &\frac{\hbar^2}{2m}\nabla\psi^\dagger\cdot\nabla\psi + i\frac{q\hbar}{4m}\psi^\dagger\mathbf{A}(t)\cdot\nabla\psi - 3i\frac{q\hbar}{4m}\nabla\psi^\dagger\cdot\mathbf{A}(t)\psi - \\ &- \frac{q\hbar}{2m}\psi^\dagger\hat{\boldsymbol{\sigma}}\psi\mathbf{B}(t) - i\frac{q\hbar^2}{8(mc)^2}\sum_{j,k,l}\epsilon_{jkl}\psi^\dagger\hat{\sigma}^j\partial_k v(\mathbf{r})\partial_l\psi + \frac{q^2}{2m}\psi^\dagger\mathbf{A}(t)^2\psi + \\ &+ i\frac{q\hbar^2}{8(mc)^2}\sum_{j,k,l}\epsilon_{jkl}\partial_k v(\mathbf{r})\partial_l\psi^\dagger\hat{\sigma}^j\psi + \frac{i\hbar}{2}(\partial_t\psi^\dagger\psi - \psi^\dagger\partial_t\psi),\end{aligned} \tag{1.141}$$

while the Noether theorem states that given a Lagrangian density, $\mathscr{L}(\psi,\partial\psi)$, function of the field ψ and its derivative, for each continuous symmetry of the function $\mathscr{L}$ there is a conserved quantity. Assuming that the field variation is

$$\delta\psi = \varepsilon\Delta, \tag{1.142}$$

it may be shown, by using the Euler - Lagrange equations, that the action functional S transforms as

$$\Delta S = \int_0^\infty\int \mathrm{d}^3r\left[\partial_t\Big(\frac{\delta\mathscr{L}}{\delta\partial_t\psi}\varepsilon\Delta\Big) + \nabla\cdot\Big(\frac{\delta\mathscr{L}}{\delta\nabla\psi}\varepsilon\Delta\Big)\right]. \tag{1.143}$$

We can apply this theorem for the invariance under local $U(1)$ transformations of the spinor wave function, with one free parameter. This leads to a scalar continuity equation for the electronic charge

$$\psi' = \psi e^{i\alpha(\mathbf{r},t)}, \tag{1.144}$$

for infinitesimal transformations we write

$$\psi' = \psi + i\alpha(\mathbf{r},t)\psi, \tag{1.145}$$

$$\psi'^\dagger = \psi^\dagger - i\alpha(\mathbf{r},t)\psi^\dagger. \tag{1.146}$$

The variation of the Lagrangian density under this infinitesimal transformation may be written as

$$\begin{aligned}\Delta\mathscr{L}(\psi,\nabla\psi) = &-i\nabla\alpha\psi^\dagger\cdot\frac{\hbar^2}{2m}\nabla\psi + i\nabla\alpha\cdot\nabla\psi^\dagger\frac{\hbar^2}{2m}\psi + i\frac{q\hbar}{m}\psi^\dagger\nabla(i\alpha)\cdot\mathbf{A}(t)\psi - \\ &- i\frac{q\hbar^2}{4(mc)^2}\sum_{j,k,l}\epsilon_{jkl}\psi^\dagger\hat{\sigma}^j\partial_k v(\mathbf{r})\partial_l(i\alpha)\psi + \frac{i\hbar}{2}\Big(\partial_t(-i\alpha)\psi^\dagger\psi - \psi^\dagger\partial_t(i\alpha)\psi\Big),\end{aligned} \tag{1.147}$$

then

$$\Delta S = \int_0^\infty dt \int \mathrm{d}^3 r \Big[- i\nabla\alpha\psi^\dagger \cdot \frac{\hbar^2}{2m}\nabla\psi + i\nabla\alpha \cdot \nabla\psi^\dagger \frac{\hbar^2}{2m}\psi + i\frac{q\hbar}{m}\psi^\dagger \nabla(i\alpha) \cdot \mathbf{A}(t)\psi -$$
$$- i\frac{q\hbar^2}{4(mc)^2} \sum_{j,k,l} \epsilon_{jkl}\psi^\dagger \hat{\sigma}^j \partial_k v(\mathbf{r})\partial_l(i\alpha)\psi - i\hbar\partial_t(i\alpha)\psi^\dagger\psi \Big]. \tag{1.148}$$

The Noether current can be finally computed by taking the following functional derivatives of the Lagrange density

$$\frac{\delta\mathscr{L}}{\delta\partial_t\psi^\dagger} = \frac{i\hbar}{2}\psi, \tag{1.149}$$
$$\frac{\delta\mathscr{L}}{\delta\nabla_n\psi^\dagger} = \frac{\hbar^2}{2m}\nabla_n\psi - 3i\frac{q\hbar}{4m}A_n(t)\psi + i\frac{q\hbar^2}{8(mc)^2}\sum_{j,k}\epsilon_{njk}\partial_k v(\mathbf{r})\hat{\sigma^j}\psi, \tag{1.150}$$
$$\frac{\delta\mathscr{L}}{\delta\partial_t\psi} = -\frac{i\hbar}{2}\psi^\dagger, \tag{1.151}$$
$$\frac{\delta\mathscr{L}}{\delta\nabla_n\psi} = \frac{\hbar^2}{2m}\nabla_n\psi^\dagger + i\frac{q\hbar}{4m}\psi^\dagger A^n(t) - i\frac{q\hbar^2}{8(mc)^2}\sum_{j,k}\epsilon_{njk}\psi^\dagger\hat{\sigma^j}\partial_k v(\mathbf{r}), \tag{1.152}$$

and by using the equality between (1.143) and (1.148) we find

$$\int_0^\infty dt \int \mathrm{d}^3 r\, \alpha(\mathbf{r},t)\, g(\mathbf{r},t) = 0, \tag{1.153}$$

with

$$g(\mathbf{r},t) = \partial_t(\psi^\dagger\psi) + \nabla\cdot\mathbf{j}_\mathrm{p}(\mathbf{r},t) - \frac{q}{m}\mathbf{A}(t)\cdot\nabla\rho + \frac{q\hbar}{4(mc)^2}\sum_{j,k,l}\epsilon_{jkl}\partial_l(\partial_k v(\mathbf{r})\psi^\dagger\hat{\sigma^j}\psi), \tag{1.154}$$

generating the final continuity equation for the electronic charge

$$\frac{\partial}{\partial t}\rho + \nabla\cdot\Big[\mathbf{j}_\mathrm{p}(\mathbf{r},t) - \frac{q}{m}\mathbf{A}(t)\rho + \frac{q\hbar}{4(mc)^2}\mathbf{m}(\mathbf{r},t)\times\nabla v(\mathbf{r})\Big] = 0. \tag{1.155}$$

The continuity equation for the spin may be obtained, instead, by looking at the invariance of the action functional under local $SU(2)$ group transformations. The generators of this Lie group are the set of Pauli matrices $\{\hat{\sigma^i}\}_{i=1,2,3}$, the rotation around the axis n is

$$\psi' = e^{i\lambda(\mathbf{r},t)\hat{\sigma^n}}\psi, \tag{1.156}$$

with infinitesimal transformations

$$\delta\psi = i\lambda(\mathbf{r},t)\hat{\sigma^n}\psi, \tag{1.157}$$
$$\delta\psi^\dagger = -i\lambda(\mathbf{r},t)\psi^\dagger\hat{\sigma^n}. \tag{1.158}$$

After some calculations the variation of the Lagrangian density can be written as

$$\Delta\mathscr{L} = \hbar\nabla\lambda\cdot\left[\frac{i\hbar}{2m}\nabla\psi^\dagger\hat{\sigma}^n\psi - \frac{i\hbar}{2m}\psi^\dagger\hat{\sigma}^n\nabla\psi\right] - \frac{q\hbar}{m}[\nabla\lambda\cdot\mathbf{A}(t)]\psi^\dagger\hat{\sigma}^n\psi + \\ + \frac{q\hbar}{m}\lambda\sum_{k,l}\epsilon_{nlk}\psi^\dagger\hat{\sigma}^l\psi B_k(\mathbf{r},t) - \lambda\frac{q\hbar}{2mc^2}\nabla_n v(\mathbf{r})\sum_l \mathscr{J}_{\mathrm{p}}^{ll} + \\ + \lambda\frac{q\hbar}{2mc^2}\sum_k \partial_k v(\mathbf{r})\mathscr{J}_{\mathrm{p}}^{nk} + \frac{q\hbar^2}{4(mc)^2}[\nabla v(\mathbf{r})\times\nabla\lambda]_n\psi^\dagger\psi + \hbar\partial_t\lambda\psi^\dagger\hat{\sigma}^n\psi, \tag{1.159}$$

and the action functional variation becomes instead

$$\Delta S = \int_0^\infty\int \mathrm{d}^3r\left[\partial_t(\hbar\lambda\psi^\dagger\hat{\sigma}^n\psi) + \sum_k\partial_k\left[\hbar\lambda\left(\frac{i\hbar}{2m}\partial_k\psi^\dagger\hat{\sigma}^n\psi - \psi^\dagger\hat{\sigma}^n\frac{i\hbar}{2m}\partial_k\psi\right) - \right. \\ \left. - \frac{q\hbar}{m}\lambda\psi^\dagger A^k(t)\hat{\sigma}^n\psi + \lambda\frac{q\hbar}{4(mc)^2}\sum_m\epsilon_{nmk}\partial_m v(\mathbf{r})\psi^\dagger\psi\right]\right]. \tag{1.160}$$

By subtracting the two variations (1.159) and (1.160) we find

$$\int_0^\infty dt\int \mathrm{d}^3r\, g^{(2)}(\mathbf{r},t) = 0, \tag{1.161}$$

where

$$g^{(2)}(\mathbf{r},t) = -\hbar\lambda(\mathbf{r},t)\partial_t(\psi^\dagger\hat{\sigma}^n\psi) - \hbar\lambda(\mathbf{r},t)\sum_k\partial_k\left(\frac{i\hbar}{2m}\partial_k\psi^\dagger\hat{\sigma}^n\psi - \psi^\dagger\hat{\sigma}^n\frac{i\hbar}{2m}\partial_k\psi\right) + \\ + \frac{q\hbar}{m}\lambda(\mathbf{r},t)\sum_k A^k(t)\partial_k(\psi^\dagger\hat{\sigma}^n\psi) + \frac{q\hbar}{m}\lambda(\mathbf{r},t)\sum_{k,l}\epsilon_{nlk}\psi^\dagger\hat{\sigma}^l\psi B_k(\mathbf{r},t) - \\ - \lambda(\mathbf{r},t)\frac{q\hbar}{2mc^2}\partial_n v(\mathbf{r})\sum_l\mathscr{J}_{\mathrm{p}}^{ll} + \lambda(\mathbf{r},t)\frac{q\hbar}{2mc^2}\sum_k\partial_k v(\mathbf{r})\mathscr{J}_{\mathrm{p}}^{nk} = 0. \tag{1.162}$$

From the arbitrarity of the parameter $\lambda(\mathbf{r},t)$ we have the following continuity equation for the spin vector

$$\frac{d}{dt}m^n(\mathbf{r},t) = -\nabla\cdot\left(-\frac{i\hbar}{2m}\psi^\dagger\hat{\sigma}^n\nabla\psi + \frac{i\hbar}{2m}\nabla\psi^\dagger\hat{\sigma}^n\psi\right) + \frac{q}{m}(\mathbf{A}(t)\cdot\nabla)m^n(\mathbf{r},t) + \\ + \frac{q}{m}(\mathbf{m}(\mathbf{r},t)\times\mathbf{B}(\mathbf{r},t))_n - \frac{q}{2mc^2}\partial_n v(\mathbf{r})\sum_l\mathscr{J}_{\mathrm{p}}^{ll} + \frac{q}{2mc^2}\sum_k\partial_k v(\mathbf{r})\mathscr{J}_{\mathrm{p}}^{nk}, \tag{1.163}$$

where $\mathbf{m}(\mathbf{r},t) = \psi^\dagger\hat{\boldsymbol{\sigma}}\psi$ defines the magnetization vector, while the last three terms of the previous expression are familiar and already appears in Eq. (1.137) (without external electric field that was not explicitly considered now). The first two are purely kinetic terms and can be identified with the paramagnetic component

of the spin current (1.69) and with the diamagnetic component

$$\mathscr{J}^{ij}_{\text{dia}}(\mathbf{r},t) = \frac{q}{m}A^i(t)m^j(\mathbf{r},t), \tag{1.164}$$

which leads to the final equation of motion for the spin vector field, that will be widely used in the following chapters for the description of the ultrafast demagnetization process

$$\begin{aligned}\frac{d}{dt}m^i(\mathbf{r},t) = &-\sum_k \partial_k[\mathscr{J}^{ki}_{\text{p}}(\mathbf{r},t) - \mathscr{J}^{ki}_{\text{dia}}(\mathbf{r},t)] - \frac{q}{m}[\mathbf{B}(\mathbf{r},t)\times\mathbf{m}(\mathbf{r},t)]_i + \\ &+\frac{q}{2mc^2}[-\nabla v(\mathbf{r}) + \mathbf{E}(0,t)]_i \sum_k \mathscr{J}^{kk}_{\text{p}}(\mathbf{r},t) - \frac{q}{2mc^2}\sum_k [\mathbf{E}(0,t) - \nabla v(\mathbf{r})]_k \mathscr{J}^{ik}_{\text{p}}(\mathbf{r},t).\end{aligned} \tag{1.165}$$

In the previous expression we can distinguish three terms.

Kinetic terms: The kinetic part of the continuity equation is represented by the divergence of the spin currents

$$-\sum_k \partial_k[\mathscr{J}^{ki}_{\text{p}}(\mathbf{r},t) - \mathscr{J}^{ki}_{\text{dia}}(\mathbf{r},t)].$$

This term should disappear in the limit of very large volume; the contribution of the spin currents at the boundary is in fact negligible.

Torque term: The component of the continuity equation generating a torque on the magnetization vector is

$$-\frac{q}{m}\mathbf{B}(\mathbf{r},t)\times\mathbf{m}(\mathbf{r},t),$$

with $\mathbf{B}(\mathbf{r},t)$ magnetic field acting on the system; it could be a purely externally applied field or generated by the internal motion of charges.

Internal spin - orbit coupling term: Here we include the remaining terms in the continuity equation coming from the spin - orbit part of the Hamiltonian

$$\frac{q}{2mc^2}[-\nabla v(\mathbf{r})+\mathbf{E}(0,t)]_i \sum_k \mathscr{J}^{kk}_{\text{p}}(\mathbf{r},t) - \frac{q}{2mc^2}\sum_k [\mathbf{E}(0,t)-\nabla v(\mathbf{r})]_k \mathscr{J}^{ik}_{\text{p}}(\mathbf{r},t).$$

This object describes a spin loss mechanism occuring in the system during its evolution. The spin within the Pauli approximation is not a good quantum number and it can be transferred into the orbital moment channel leading to global spin non conservation.

It is necessary at this point to spend a few more words about the concept of spin current. There is, in fact, still some debate on its exact definition, particularly in relation to the problem of spin transport in mesoscopic systems. In Ref. [20] the

authors argued that, due to the fact that the spin is a vector and it cannot be considered a locally invariant quantity, the conventionally defined spin current $\langle \hat{v}^i \hat{s}^j \rangle$ is not conservative (with $\mathbf{v}$ velocity field). The spin has not only a translational motion, but it has also a rotational motion that needs to be taken into account. Due to this rotational motion, in order to describe spin transport, it is necessary to introduce in addition to the conventional linear spin current also an angular spin current (we will see the importance of this observation in the next chapters).

In Ref. [22] it is introduced a different definition for the spin current tensor

$$\hat{\mathscr{J}}^{ij} = \frac{d}{dt}(\hat{r}^i \hat{s}^j). \tag{1.166}$$

This new formulation allows us to directly solve some of the shortcomings characterizing the previous definitions. It, in fact, vanishes identically in insulators with localized orbitals and gives rise to Onsager relations for linear response. The issue is that all these definitions are still approximated and given the relativistic nature of the spin vector, a complete definition of the spin current tensor should start directly from the Dirac equation. This was achieved in [21] where the full spin current $\mathscr{J}_s$, orbital current $\mathscr{J}_{\text{orb}}$ and the total current $\mathscr{J}_{\text{tot}}$ were derived together with the continuity equation in terms of the Dirac velocity operator $\boldsymbol{\alpha}$ and the spin operator $\boldsymbol{\Sigma}$

$$\hat{\mathscr{J}}_s^{\mu\nu} = \frac{i}{2}\hat{\alpha}^\mu \hat{\Sigma}^\nu, \tag{1.167}$$

$$\hat{\mathscr{J}}_{\text{orb}}{}^{\mu\nu} = i\hat{\alpha}^\mu \hat{L}^\nu, \tag{1.168}$$

where the orbital moment operator is written as $\hat{L}_\gamma = \epsilon_\gamma^{\alpha,\beta} x_\alpha \Pi_\beta$. The continuity equation for the full current $\mathscr{J}_{\text{tot}} = \mathscr{J}_s + \mathscr{J}_{\text{orb}}$ is

$$\partial_\mu \mathscr{J}_{\text{tot}}^{\mu\nu} = 0. \tag{1.169}$$

Eq. (1.167) and (1.168) give the most general and complete definition of spin current arising from the relativistic theory of spin 1/2 particles. However, in the following we will employ only the non relativistic quantum mechanical definition (1.69) that already includes all the informations necessary for the description of the ultrafast demagnetization process.

Finally we look at the invariance of the action functional under local rotations of the $SO(3)$ group in a three dimensional space. An infinitesimal rotation around the axis $\hat{n}$, with angle $\delta\theta(\mathbf{r}, t)$ may be expressed as

$$\mathcal{R}(\delta\theta, \mathbf{n})\psi(\mathbf{r}) = e^{-\frac{i}{\hbar}\delta\theta \mathbf{n}\cdot\hat{\mathbf{L}}}\psi(\mathbf{r}), \tag{1.170}$$

$$\delta\psi = -\frac{i}{\hbar}\delta\boldsymbol{\theta}\cdot\left[\mathbf{r}\times(-i\hbar\nabla\psi)\right], \tag{1.171}$$

$$\delta\psi^\dagger = \frac{i}{\hbar}\delta\boldsymbol{\theta}\cdot\left[\mathbf{r}\times(-i\hbar\nabla\psi^\dagger)\right]. \tag{1.172}$$

In view of the derivation of the continuity equation for the orbital moment we consider only the kinetic part of the Lagrangian, the other components are, in fact, identical to those obtained in Eq. (1.110). The variation of the kinetic part of the Lagrangian (1.141) is at the first order in $\delta\theta$,

$$\Delta\mathscr{L}_{\text{kin}}(\psi,\nabla\psi) = \frac{\hbar^2}{2m}\nabla\psi^\dagger\cdot\nabla\psi + \frac{i\hbar}{2m}\sum_k \nabla_k\delta\boldsymbol{\theta}\cdot\Big[\mathbf{r}\times(-i\hbar\nabla\psi^\dagger)\Big]\nabla_k\psi +$$
$$+\frac{i\hbar}{2m}\delta\boldsymbol{\theta}\cdot\sum_k\nabla_k\Big[\mathbf{r}\times(-i\hbar\nabla\psi^\dagger)\Big]\cdot\nabla_k\psi - \frac{i\hbar}{2m}\sum_k\nabla_k\delta\boldsymbol{\theta}\cdot\nabla_k\psi^\dagger\Big[\mathbf{r}\times(-i\hbar\nabla\psi)\Big] -$$
$$-\frac{i\hbar}{2m}\sum_k\nabla_k\psi^\dagger\delta\boldsymbol{\theta}\cdot\nabla_k\Big[\mathbf{r}\times(-i\hbar\nabla\psi)\Big] - \frac{\hbar^2}{2m}\nabla\psi^\dagger\cdot\nabla\psi. \tag{1.173}$$

We can now separate $\Delta\mathscr{L}$ in two different components

$$\Delta\mathscr{L}^{(1)}_{\text{kin}} = \frac{i\hbar}{2m}\sum_k\nabla_k\delta\boldsymbol{\theta}\cdot\Big[\mathbf{r}\times(-i\hbar\nabla\psi^\dagger)\Big]\nabla_k\psi - \frac{i\hbar}{2m}\sum_k\nabla_k\delta\boldsymbol{\theta}\cdot\nabla_k\psi^\dagger\Big[\mathbf{r}\times(-i\hbar\nabla\psi)\Big], \tag{1.174}$$

and

$$\Delta\mathscr{L}^{(2)}_{\text{kin}} = \frac{i\hbar}{2m}\delta\boldsymbol{\theta}\cdot\sum_k\Big[\nabla_k(\mathbf{r}\times(-i\hbar\nabla\psi^\dagger))\cdot\nabla_k\psi - \nabla_k\psi^\dagger\nabla_k(\mathbf{r}\times(-i\hbar\nabla\psi))\Big]. \tag{1.175}$$

By making use of $\psi^\dagger\psi = \rho(\mathbf{r},t)$ we can rewrite $\Delta\mathscr{L}^{(2)}_{\text{kin}}$ in the form

$$\Delta\mathscr{L}^{(2)}_{\text{kin}} = \frac{i\hbar}{2m}\delta\boldsymbol{\theta}\cdot\sum_k\left[\nabla_k\left(\frac{\psi^\dagger\psi}{\rho(\mathbf{r},t)}\mathbf{r}\times(-i\hbar\nabla\psi^\dagger)\right)\nabla_k\psi - \nabla_k\psi^\dagger\nabla_k\left(\frac{\psi^\dagger\psi}{\rho(\mathbf{r},t)}\mathbf{r}\times(-i\hbar\nabla\psi)\right)\right], \tag{1.176}$$

which in turn becomes

$$\Delta\mathscr{L}^{(2)}_{\text{kin}} = \frac{i\hbar}{2m}\delta\boldsymbol{\theta}\cdot\sum_k\left[\nabla_k\left(\frac{\psi^\dagger}{\rho(\mathbf{r},t)}\mathbf{L}(\mathbf{r},t)\right)\nabla_k\psi - \nabla_k\psi^\dagger\nabla_k\left(\frac{\psi}{\rho(\mathbf{r},t)}\mathbf{L}(\mathbf{r},t)\right)\right], \tag{1.177}$$

$$\Delta\mathscr{L}^{(2)}_{\text{kin}} = \frac{i\hbar}{2m}\delta\boldsymbol{\theta}\cdot\sum_k\left[\nabla_k\mathbf{L}(\mathbf{r},t)\left(\frac{\psi^\dagger\nabla_k\psi - \nabla_k\psi^\dagger\psi}{\rho(\mathbf{r},t)}\right) + \nabla_k\left(\frac{\psi^\dagger}{\rho(\mathbf{r},t)}\right)\nabla_k\psi\mathbf{L}(\mathbf{r},t) -\right.$$
$$\left. -\nabla_k\psi^\dagger\nabla_k\left(\frac{\psi}{\rho(\mathbf{r},t)}\right)\mathbf{L}(\mathbf{r},t)\right], \tag{1.178}$$

$$\Delta\mathscr{L}^{(2)}_{\text{kin}} = \delta\boldsymbol{\theta}\cdot\sum_k\left[-\nabla_k\mathbf{L}(\mathbf{r},t)v_k - \frac{i\hbar}{2m}(\psi^\dagger\nabla_k\psi - \nabla_k\psi^\dagger\psi)\frac{\nabla_k\rho}{\rho(\mathbf{r},t)^2}\mathbf{L}(\mathbf{r},t)\right], \tag{1.179}$$

$$\Delta\mathscr{L}^{(2)}_{\text{kin}} = \delta\boldsymbol{\theta}\cdot\sum_k\left[-\nabla_k\mathbf{L}(\mathbf{r},t)v_k + \frac{\nabla\rho\cdot\mathbf{v}}{\rho(\mathbf{r},t)}\mathbf{L}(\mathbf{r},t)\right], \tag{1.180}$$

where we have introduced the velocity field

$$\mathbf{v}(\mathbf{r},t)=\frac{i\hbar}{2m}\frac{\nabla\psi^{\dagger}\psi-\psi^{\dagger}\nabla\psi}{\rho(\mathbf{r},t)}. \tag{1.181}$$

The full Lagrangian variation may thus be written as

$$\Delta\mathscr{L}_{\mathrm{kin}}=\frac{i\hbar}{2m}\sum_{k}\nabla_{k}\delta\boldsymbol{\theta}\cdot\left[\mathbf{r}\times(-i\hbar\nabla\psi^{\dagger})\right]\nabla_{k}\psi-\frac{i\hbar}{2m}\sum_{k}\nabla_{k}\delta\boldsymbol{\theta}\cdot\nabla_{k}\psi^{\dagger}\left[\mathbf{r}\times(-i\hbar\nabla\psi)\right]+$$
$$+\delta\boldsymbol{\theta}\cdot\left[-\sum_{k}\nabla_{k}\mathbf{L}(\mathbf{r},t)v_{k}+\frac{\nabla\rho\cdot\mathbf{v}}{\rho(\mathbf{r},t)}\mathbf{L}(\mathbf{r},t)\right], \tag{1.182}$$

while, by making use of Eq. (1.149), we find

$$\nabla_{k}\left[\delta\psi^{\dagger}\cdot\frac{\delta\mathscr{L}_{\mathrm{kin}}}{\delta\nabla_{k}\psi^{\dagger}}+\delta\psi\cdot\frac{\delta\mathscr{L}_{\mathrm{kin}}}{\delta\nabla_{k}\psi}\right]=F_{k}(\mathbf{r},t), \tag{1.183}$$

$$F_{k}(\mathbf{r},t)=\nabla_{k}\left[\delta\boldsymbol{\theta}\cdot\left(\mathbf{r}\times(-i\hbar\nabla\psi^{\dagger})\right)\frac{i\hbar}{2m}\nabla_{k}\psi-\frac{i\hbar}{2m}\delta\boldsymbol{\theta}\cdot\left(\mathbf{r}\times(-i\hbar\nabla\psi)\right)\nabla_{k}\psi^{\dagger}\right], \tag{1.184}$$

and the kinetic part of the action functional variation becomes

$$\Delta S_{\mathrm{kin}}=\int_{t_{i}}^{t_{f}}dt\int d^{3}r\delta\boldsymbol{\theta}\cdot\mathbf{h}(\mathbf{r},t)=0, \tag{1.185}$$

where

$$\mathbf{h}(\mathbf{r},t)=\frac{i\hbar}{2m}\sum_{k}\nabla_{k}\left[(\mathbf{r}\times(-i\hbar\nabla\psi^{\dagger}))\nabla_{k}\psi-(\mathbf{r}\times(-i\hbar\nabla\psi))\nabla_{k}\psi^{\dagger}\right]+$$
$$+\sum_{k}\nabla_{k}\mathbf{L}(\mathbf{r},t)v_{k}-\frac{\nabla\rho\cdot\mathbf{v}}{\rho(\mathbf{r},t)}\mathbf{L}(\mathbf{r},t), \tag{1.186}$$

leading to the following continuity equation for the orbital moment

$$\frac{d}{dt}L^{n}(\mathbf{r},t)=\sum_{k}\nabla_{k}L^{n}(\mathbf{r},t)v_{k}-\frac{\nabla\rho\cdot\mathbf{v}}{\rho(\mathbf{r},t)}L^{n}(\mathbf{r},t)+\mu_{B}\sum_{j}(\mathbf{r}\times\nabla)_{n}B_{j}(\mathbf{r},t)m_{j}(\mathbf{r},t)-$$
$$-\rho(\mathbf{r},t)[\mathbf{r}\times\nabla v(\mathbf{r})]_{n}+\frac{i\hbar}{2m}\sum_{k}\nabla_{k}\left[(\mathbf{r}\times(-i\hbar\nabla\psi^{\dagger}))_{n}\nabla_{k}\psi-(\mathbf{r}\times(-i\hbar\nabla\psi))_{n}\nabla_{k}\psi^{\dagger}\right]+$$
$$+\frac{\hbar}{4mc^{2}}\sum_{j}\left[qE_{j}(t)\mathscr{J}_{\mathrm{p}}^{jn}(\mathbf{r},t)-\nabla_{j}v(\mathbf{r})\mathscr{J}_{\mathrm{p}}^{nj}(\mathbf{r},t)\right]+\rho(\mathbf{r},t)[\mathbf{r}\times q\mathbf{E}(t)]_{n}-$$
$$-\frac{\hbar}{4mc^{2}}[q\mathbf{E}(t)-\nabla v(\mathbf{r})]_{n}\sum_{j}\mathscr{J}_{\mathrm{p}}^{jj}(\mathbf{r},t). \tag{1.187}$$

This represents our final formulation for the continuity equation for the orbital moment. In addition to the terms appearing in Eq. (1.110) in the previous expression there are also kinetic terms that are important for a local description of the dynamics, but disappear when integrating over a large volume. They do not, in fact, generate a global torque on the angular moment.

After this discussion of the continuity equation for the spin and angular moment of a single particle under external scalar and vector fields, in the following chapters we will try to extend the formalism that we have developed here to the problem of the ultrafast magnetization dynamics in metals. After a brief review of the field in Chapter 2, given our necessity to model the ultrafast dynamics in real systems, we will look in Chapter 3 at extensions of this description to the case of many interacting particles. In Chapter 4 and 5 we will construct a basic model, based on ab initio results, of the ultrafast magnetization dynamics in transition metals, while in Chapter 6 we will focus on the ultrafast dynamics of the orbital moment by including also the interaction with the nuclei.

CHAPTER 2

THE THEORY OF ULTRAFAST MAGNETISM

In this chapter I will review the field of ultrafast magnetism, focusing in particular on metallic systems, since they will be widely studied in the following chapters. As we have already seen in the first chapter, the study of the ultrafast magnetism started after the discovery, made by E. Beaurepaire, of the quenching of the magnetic moment of a Nickel film illuminated by a 60 fs optical pulse. [23].

Later investigations not only confirm these first findings, but also suggested the possibility to coherently induce magnetic precession through the application of femtosecond laser pulses [24,26], to induce spin reorientation in anti - ferromagnets [12,25] or even modify the magnetic structure of the system. For instance it was demonstrated that ferromagnetic ordered materials can be obtained by driving an anti - ferromagnet to a new magnetic phase through the application of an optical laser pulse [14].

Clearly, after these experimental demonstrations also significant theoretical work was done with the purpose to clarify the physics behind the ultrafast demagnetization phenomenon. The main issue here is that the injection of such a large amount of energy through the laser drives the system into a highly non-equilibrium state in which the conventional macrospin approximation of the atomistic approaches does not apply anymore. In the sub-picosecond time domain we could use the quantum mechanical energy - time correlation rule to estimate the order of magnitude of the interactions responsible for the spin-relaxation dynamics.

A generic operator $\hat{A}$ in the Heisenberg representation evolves in time and its evolution is a measure of how the quantum mechanical system is changing. Denoting the standard deviation of $\hat{A}$ ($\hat{H}$) with ΔA (ΔE), from the uncertainty relation we have

$$\Delta A \cdot \Delta E \geq \frac{1}{2}\left|\langle[\hat{A},\hat{H}]\rangle\right|. \tag{2.1}$$

In the Heisenberg representation the time evolution is directly related to the expectation value of the commutator

$$\langle[\hat{A}, \hat{H}]\rangle = i\hbar \frac{d}{dt}\langle\hat{A}\rangle, \tag{2.2}$$

with the result that

$$\Delta A \cdot \Delta E \geq \frac{\hbar}{2}\left|\frac{d}{dt}\langle\hat{A}\rangle\right|. \tag{2.3}$$

In order to characterize the time scale for a significant change in the system we can compare the change rate of the observable with its initial uncertainty

$$\Delta t = \frac{\Delta A}{\left|\frac{d}{dt}\langle A\rangle\right|}. \tag{2.4}$$

This finally leads to the time-energy uncertainty relation

$$\Delta E \cdot \Delta t \geq \frac{\hbar}{2}, \tag{2.5}$$

meaning that the shortest possible time scale characterizing the dynamics of the system is given by $\Delta t \cdot \Delta E \simeq \hbar$. From this relation we could extract the time scales related to the different interaction energies at play in magnetic systems.

If we consider, for instance, typical anisotropy energies of the order of 0.01 meV, Δt will be of the order 1 picosecond, while exchange interaction energies that are of the order of 10 meV in metals will be characterized by $\Delta t \simeq 1$ fs. From

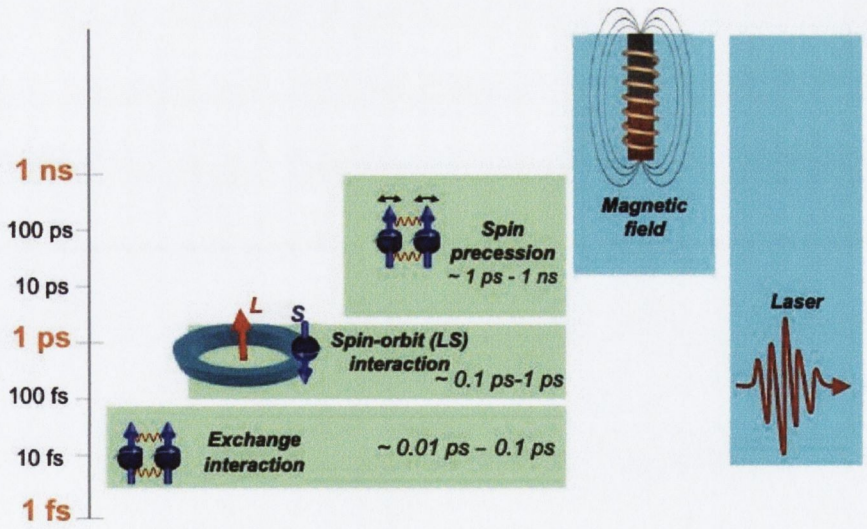


FIGURE 2.1: (a) Time scales of magnetic interactions compared to different pulse duration. (From Ref. [3]).

Fig. 2.1 we can see that the characteristic times for the spin-orbit and the exchange interaction fall below the picosecond limit. This suggests that the application of sub - picosecond laser pulses could make these interactions time

dependent, meaning that transient dynamical regime would be characterized by a completely different physics with respect to that studied in quasi equilibrium situations. The study of the physics of the ultrafast sub-picosecond dynamics in magnetic systems needs a different theoretical framework with respect to that employed in the case of longer time scales. This justifies the distinction that we also made in the Chapter 1 between fast and ultrafast dynamics in magnetic systems. In the rest of the chapter we will make this distinction more clear. However, we will first briefly review the most important experimental techniques employed in the study of the ultrafast response of solids to external laser pulses.

2.1 Experimental methods

The investgation of the sub-picosecond response of a magnetic material to the application of a laser field requires experimental methods and techniques that allow to detect magnetization changes occuring at these particular time scales. The uncertainty in time must be smaller than the relative time scale of the process considered. This requires in ultrafast processes a time resolution of the order of 1 fs. The technique generally known as pump-probe spectroscopy [27] allows the indirect observation of the process through the detection and analysis of the probe pulse.

In the most general example of pump-probe experiment a beam splitter is used to separate the incoming laser pulse into a pump and a probe pulse. The two pulses, then, approach the sample following different paths. This can be achieved in practice by orienting different mirrors in such a way that the pump and the probe pulses are directed along a predefined path.

The physical system is initially perturbed by the application of the pump pulse, which must follow a shorter path in order to reach the sample first. The delay between the pump and the probe pulse is controlled by changing the path length difference. The probe pulse is then measured by a detector after its interaction with the sample. By analysing the intensity of the probe pulse as a function of the time, we are able to describe the dynamics of the excitations in the sample (see Fig. 2.2). Clearly, the duration of the probe pulse defines the temporal resolution of the experiment, while the probe spectrum defines the set of frequencies that can be absorbed by the sample. Then, through the analysis of the intensity of the probe pulse it is possible to obtain informations about the electronic transitions activated by the interaction between the pump pulse and the sample.

Measurements in the far infrared, optical, ultraviolet or X - ray spectral ranges will determine different views of the same spectroscopy experiment. For measurements in the optical range, that is the specific case we are more interested in, it is possible to make use of the electric dipole approximation since the light wave length is much bigger than the average atomic separations.

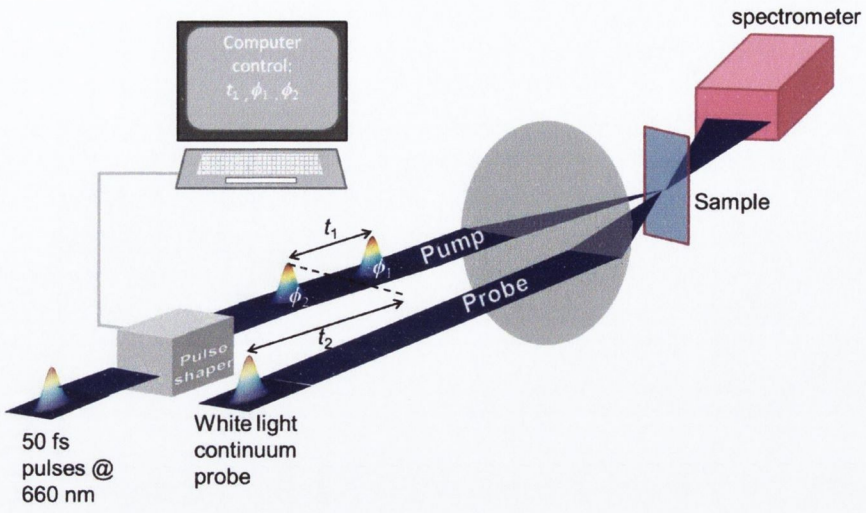


FIGURE 2.2: (a) Scheme of a typical optical spectroscopy pump-probe experiment with pulse shaper, (from Ref. [28]).

The interaction of the electro-magnetic radiation with a magnetic medium is described classically by the set of Maxwell's equations (in SI units),

$$\nabla \times \mathbf{E}(\mathbf{r},t) + \frac{\partial}{\partial t}\mathbf{B}(\mathbf{r},t) = 0, \tag{2.6}$$

$$\nabla \cdot \mathbf{B}(\mathbf{r},t) = 0, \tag{2.7}$$

$$\nabla \times \mathbf{H}(\mathbf{r},t) - \frac{\partial}{\partial t}\mathbf{D}(\mathbf{r},t) = \mathbf{j}(\mathbf{r},t), \tag{2.8}$$

$$\nabla \cdot \mathbf{D}(\mathbf{r},t) = \rho(\mathbf{r},t). \tag{2.9}$$

Here, $\mathbf{D}(\mathbf{r},t)$ represents the electric displacement, quantity that takes into account modifications of the electric field $\mathbf{E}(\mathbf{r},t)$ caused by polarization $\mathbf{P}(\mathbf{r},t)$ of the medium. $\mathbf{B}(\mathbf{r},t)$ is the magnetic induction and $\mathbf{H}(\mathbf{r},t)$ the macroscopic magnetic field. $\rho(\mathbf{r},t)$ and $\mathbf{j}(\mathbf{r},t)$ are macroscopic charge and current densities. The electric displacement and the magnetic field may be written as

$$\mathbf{D}(\mathbf{r},t) = \int \mathrm{d}^3 r' \int_{-\infty}^{t} dt' \epsilon(\mathbf{r},\mathbf{r}',t',t)\mathbf{E}(\mathbf{r}',t'), \tag{2.10}$$

$$\mathbf{B}(\mathbf{r},t) = \int \mathrm{d}^3 r' \int_{-\infty}^{t} dt' \mu(\mathbf{r},\mathbf{r}',t',t)\mathbf{H}(\mathbf{r}',t'), \tag{2.11}$$

The dielectric constant ϵ and the magnetic permeability μ are scalars only in very simple and peculiar cases. In a generic anisotropic medium these objects are tensors, while in the presence of very strong external fields the linear response theory outlined here is not applicable anymore and we need a higher order expansion in the fields. The thermodynamical potential Φ for a magnetically ordered

system with magnetization **M** is written up to the third order in the field expansion as [3]

$$\Phi = \sum_{ij} \epsilon_{ij}^{(l)} E_i(\omega)^* E_j(\omega) + \sum_{ijk} \alpha_{ijk}^{(l)} E_i(\omega)^* E_j(\omega) M_k + \sum_{ijk} \chi_{ijk}^{(nl)} E_i(2\omega)^* E_j(\omega) E_k(\omega) + \\ + \sum_{ijkl} \alpha_{ijkl}^{(nl)} E_i(2\omega)^* E_j(\omega) E_k(\omega) M_l, \tag{2.12}$$

where the superscript (l) and (nl) mean respectively linear and non linear response to the laser pulse, while $\alpha_{ijk}^{(l)}$, $\epsilon_{ij}^{(l)}$, $\chi_{ijk}^{(nl)}$, $\alpha_{ijkl}^{(nl)}$ are tensors describing the optical properties of the magnetic system. This equation includes all the possible magneto-optical effects arising from the interaction of a magnetized sample with the light.

These coefficients fully characterize the optical response of the system and together with the knowledge of the probe frequency spectrum it is possible to reconstruct the value of the magnetization vector that interacts with the probe pulse in the sample. In practice linear magneto-optical effects may be used to detect the value of the magnetization of the sample at every instant in time.

2.2 Magneto - optical effects

Magneto-optical phenomena arise when a spontaneously magnetized sample interacts with light in absence of external magnetic fields. The most important among these phenomena are the so called magneto-optical Kerr effect (MOKE) and the Faraday effect [30–32].

The MOKE describes all the situations when linear polarized light reflected at normal incidence from the surface of a magnetically ordered system becomes elliptically polarized with the major polarization axis rotated with respect to the plane of polarization of the incident beam. In particular we could distinguish between three different types of MOKE, the polar, the longitudinal and the transverse. When the magnetization **M** of the sample is directed perpendicularly to the plane of the surface and parallel to the plane of incidence of the light we have the polar Kerr effect. The transverse Kerr effect is instead observed when the magnetization is oriented perpendicularly to the plane of incidence of the light and the longitudinal effect arises when the magnetization is parallel to both the plane of incidence and to the surface (see Fig. 2.3).

In the Faraday effect, instead, the plane of polarization of the incident light rotates by an angle directly proportional to the component of the magnetization along the direction of propagation of the light pulse. Both these effects are caused by the fact that left and right circularly polarized waves propagate in a medium at slightly different velocities. Both these effects could be understood by taking

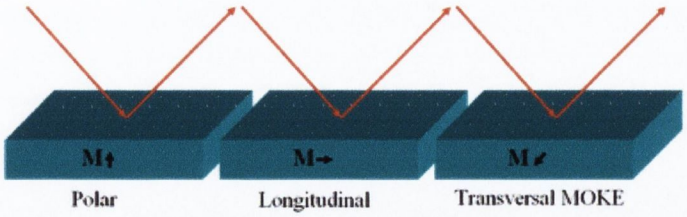


FIGURE 2.3: (a) Simple scheme of the magneto-optical Kerr effect.

the following two Maxwell equations from Eq.(2.6)

$$\nabla \times \mathbf{E}(\mathbf{r},t) = -\frac{\partial \mathbf{B}}{\partial t}, \tag{2.13}$$

$$\nabla \times \mathbf{B}(\mathbf{r},t) = \frac{\partial \mathbf{E}}{\partial t} + \mathbf{j}_{\text{tot}}(\mathbf{r},t). \tag{2.14}$$

By neglecting here the contribution of the magnetization to $\mathbf{j}_{\text{tot}}$ we can express the polarization vector through the optical susceptibility α_1. The total current becomes

$$\mathbf{j}_{\text{tot}}(\mathbf{r},t) = \sigma_1 \mathbf{E}(\mathbf{r},t) + \alpha_1 \frac{\partial \mathbf{E}}{\partial t}, \tag{2.15}$$

with

$$\nabla \times \mathbf{B}(\mathbf{r},t) = \frac{\partial \mathbf{E}}{\partial t} + \sigma_1 \mathbf{E}(\mathbf{r},t) + \alpha_1 \frac{\partial \mathbf{E}}{\partial t}. \tag{2.16}$$

By assuming a solution in the form of a monochromatic plane wave propagating along z, the electric and magnetic field may be rewritten as

$$\mathbf{E}(z,t) = \mathbf{E}_0 e^{i\omega\left(t-\frac{Nz}{c}\right)}, \tag{2.17}$$

$$\mathbf{B}(z,t) = \mathbf{B}_0 e^{i\omega\left(t-\frac{Nz}{c}\right)}. \tag{2.18}$$

Here, N is a generalized refraction index, complex in general, $\mathbf{k}$ indicates the vector along the direction of propagation. In reciprocal space the set of equations becomes

$$\frac{N}{c}(\mathbf{E}(\mathbf{k},t) \times \mathbf{k}) = -\mathbf{B}(\mathbf{k},t), \tag{2.19}$$

$$\frac{N}{c}(\mathbf{B}(\mathbf{k},t) \times \mathbf{k}) = \left(1 + \alpha_1 + \frac{1}{i\omega} \cdot \sigma_1\right) \cdot \mathbf{E}(\mathbf{k},t). \tag{2.20}$$

N can then be obtained by imposing a non trivial solution ($\mathbf{E} \neq 0$) to the following equation

$$\left(1 + \alpha_1 + \frac{1}{i\omega}\sigma_1\right) \cdot \mathbf{E}(\mathbf{k},t) = \left(\frac{N}{c}\right)^2 [\mathbf{E}(\mathbf{k},t) - \mathbf{k}(\mathbf{E}(\mathbf{k},t) \cdot \mathbf{k})]. \tag{2.21}$$

This lead to two solutions $N_\pm$ for the refraction index. The electric field propagating in the medium will be a superposition of two waves moving at different

velocities $\frac{c}{N_\pm}$

$$\mathbf{E}^{(\pm)} = \mathbf{E}_0 e^{i\omega\left(t-\frac{N_\pm}{c}z\right)}, \tag{2.22}$$

where ± denotes right- and left-handed circularly polarized light. By assuming normal incidence of the light over the sample surface, the beam then splits into refracted and reflected beams.

The refracted beam undergoes a rotation of the major axis by an angle

$$\phi_F = \frac{\omega z}{2c}\mathrm{Re}(N_+ - N_-), \tag{2.23}$$

with z indicating the distance from the boundary, while the ellipticity of the beam becomes

$$\epsilon_F = -\arctan\left(\frac{\omega z}{2c}\mathrm{Im}(N_+ - N_-)\right). \tag{2.24}$$

These two relations summarize the Farday effect in the case of normal incidence of an optical beam over the surface of the magnetically ordered system.

The reflected beam also becomes elliptically polarized with major axis rotated by an angle

$$\phi_k = -\mathrm{Im}\left(\frac{N_+ - N_-}{N_+N_- - 1}\right), \tag{2.25}$$

while the ellipticity is given by

$$\epsilon_k = -\mathrm{Re}\left(\frac{N_+ - N_-}{N_+N_- - 1}\right), \tag{2.26}$$

which describes, instead, the magneto-optical polar Kerr effect in the special case of normal incidence. Analogous relations can be obtained for the longitudinal and transversal effects.

In conclusion, the analysis of the reflected or refracted beam can provide useful informations on the nature of the magnetic field in the medium, and in the case of no external magnetic field, on the magnitude of the magnetization at any particular instant in time, only limited by the duration of the pulse.

2.3 Spin-photons interaction

In this section we consider as a first possible source of ultrafast spin modification the direct interaction between the spins and the photons carried by the electromagnetic wave. Within this context, several models, which include high orders in the interaction between the radiation and the matter have been introduced. All these models start from a fully relativistic description at the level of quantum electro-dynamics (QED) [16, 33] and they are obtained through a lower order non-relativistic expansion of the Hamiltonian, known as the Fouldy-Wouthuysen (FW) transformation [34,35]. Specifically, it can be shown that a free relativistic

1/2 spinning particle obeys the Dirac equation,

$$(i\gamma^{\mu}\partial_{\mu} - m)\Psi(x) = 0, \tag{2.27}$$

where $\{\gamma^{\mu}\}_{\mu=0}^{3}$ defines a set of Dirac matrices which satisfy the commutation rules $\{\gamma^{\mu}, \gamma^{\eta}\} = 2g^{\mu\eta}$, ($g^{\mu\eta}$ metric tensor in Minkowski space). Positive and negative energy solutions can be separately described by two-component wave functions or non relativistic spinors. In practice the fully relativistic Hamiltonian

$$\hat{H} = c\tilde{\alpha} \cdot \hat{\mathbf{p}} + \tilde{\beta}mc^2, \tag{2.28}$$

can be written into a diagonal form through the following unitary FW transformation

$$U_{\mathrm{FW}}^{\pm 1} = \frac{|\hat{H}| + mc^2 \pm c\tilde{\beta}\tilde{\alpha} \cdot \hat{\mathbf{p}}}{\sqrt{2|\hat{H}|\left(|\hat{H}| + mc^2\right)}}, \tag{2.29}$$

where $U_{\mathrm{FW}}U_{\mathrm{FW}}^{-1} = \bullet$. The transformed Hamiltonian $\hat{H}_{\mathrm{FW}} = U_{\mathrm{FW}}\hat{H}U_{\mathrm{FW}}^{-1}$ becomes diagonal in this new basis and we can write

$$\hat{H}_{\mathrm{FW}} = \tilde{\beta}|\hat{H}|, \tag{2.30}$$

where $|\hat{H}| = \sqrt{\hat{\mathbf{p}}^2c^2 + m^2c^4}$. The Hamiltonian is then diagonal in this new representation and it has separable solutions, representing positive and negative energy states

$$\Psi(x)^{(1)} = \phi(x)^{(1)} + \chi(x)^{(1)}, \tag{2.31}$$

obeying to the following Schrödinger - like equations

$$i\hbar\frac{d}{dt}\phi(x)^{(1)} = |\hat{H}|\phi(x)^{(1)}, \tag{2.32}$$

$$i\hbar\frac{d}{dt}\chi(x)^{(1)} = -|\hat{H}|\chi(x)^{(1)}, \tag{2.33}$$

while

$$i\hbar\frac{d}{dt}\Psi(x)^{(1)} = \hat{H}_{\mathrm{FW}}\Psi(x)^{(1)}. \tag{2.34}$$

In the case of non interacting Dirac particles coupled to an electro-magnetic radiation the procedure leading to the effective low-energy equations for the spinors is more involved. First of all we assume that the fields we are considering are weak, in the sense that their associated energy is small compared to $2mc^2$, so that positive and negative energy states become effectively decoupled. In the presence of an external electro-magnetic field there is no single unitary transformation that makes the Hamiltonian block diagonal. Then the separation between particle and anti-particle states can be achieved only through an infinite series of such transformations. In practice an expansion in terms of $(\frac{1}{mc^2})^n$ is usually performed. Since mc^2 is much larger than the energy scale of the problem the series converges very rapidly and we can consider only the lowest order terms in the expansion.

By separating the contributions in the Hamiltonian due to even operators (which do not connect positive and negative energy states) from the contributions due to odd operators (which do connect the two types of solutions) we can write

$$\hat{H} = \hat{\bar{\beta}}mc^2 + \hat{O}_{\text{odd}} + \hat{O}_{\text{even}}. \tag{2.35}$$

Here the first contribution is much more important than the others and we could expand around it. The unitary transformation employed in this case can be expressed as $U_{\text{FW}} = e^{iT_{\text{FW}}}$, with [35]

$$T_{\text{FW}} = -\frac{i}{2mc^2}\hat{\bar{\beta}}\hat{O}_{\text{odd}}, \tag{2.36}$$

which is a general expression for the hermitian operator $\hat{T}_{\text{FW}}$ involving all the odd operators in the Hamiltonian. This finally leads to the following expansion of the Dirac Hamiltonian

$$\hat{H}_{\text{FW}} = \hat{H} + i[\hat{T}_{\text{FW}}, \hat{H}] + \frac{i^2}{2}[\hat{T}_{\text{FW}}, [\hat{T}_{\text{FW}}, \hat{H}]] + \dots \tag{2.37}$$

The Dirac Hamiltonian in the presence of an external electro-magnetic field is written as

$$\hat{H} = \hat{\bar{\beta}}mc^2 + c\hat{\bar{\boldsymbol{\alpha}}} \cdot (\hat{\mathbf{p}} - q\mathbf{A}) + V(\mathbf{r}), \tag{2.38}$$

with $\mathbf{A}$ being the external vector potential and $V(\mathbf{r})$ scalar potential. The odd part of $\hat{H}$ is $\hat{O}_{\text{odd}} = c\hat{\bar{\boldsymbol{\alpha}}} \cdot (\hat{\mathbf{p}} - q\mathbf{A})$, while the even part is $\hat{O}_{\text{even}} = V(\mathbf{r})\hat{\bullet}$. By requiring that the new Hamiltonian $\hat{H}_{\text{FW}}$ is exact up to the order $(\frac{1}{mc^2})^3$, we can eliminate all odd operators by performing three consecutive transformations of $\hat{H}$. The final result is (in SI units)

$$\hat{H}^{(3)}_{\text{FW}} = \hat{\bar{\beta}}mc^2 + V(\mathbf{r}) + \frac{\hat{\bar{\beta}}}{2m}(\hat{\mathbf{p}} - q\mathbf{A})^2 - \mu_{\text{B}}\hat{\bar{\boldsymbol{\Sigma}}} \cdot \mathbf{B}(\mathbf{r}) - \frac{q\hbar}{4(mc)^2}\hat{\bar{\boldsymbol{\Sigma}}} \cdot \mathbf{E} \times (\hat{\mathbf{p}} - q\mathbf{A}) -$$
$$- \frac{\hat{\bar{\beta}}}{8m^3c^2}(\hat{\mathbf{p}} - q\mathbf{A})^4 + \frac{q\hbar^2}{8(mc)^2}\nabla \cdot \mathbf{E}. \tag{2.39}$$

The magnetic field arises from the vector potential $\mathbf{B} = \nabla \times \mathbf{A}$. In the previous expression all the operators are even, the 4×4 spin operator $\hat{\bar{\boldsymbol{\Sigma}}}$ is written as

$$\hat{\bar{\boldsymbol{\Sigma}}} = \begin{bmatrix} \hat{\boldsymbol{\sigma}} & 0 \\ 0 & \hat{\boldsymbol{\sigma}} \end{bmatrix}, \tag{2.40}$$

where $\hat{\boldsymbol{\sigma}}$ are the 2×2 Pauli matrices and

$$\hat{\bar{\beta}} = \begin{bmatrix} \hat{\bullet} & 0 \\ 0 & -\hat{\bullet} \end{bmatrix}. \tag{2.41}$$

This allows us to finally separate the equation for positive and negative energy states. The Hamiltonian governing the dynamics of the positive energy fermions

is

$$\hat{\mathscr{H}}_{\text{Pauli}} = mc^2 + V(\mathbf{r}) + \frac{1}{2m}(\hat{\mathbf{p}} - q\mathbf{A})^2 - \mu_{\text{B}}\hat{\boldsymbol{\sigma}} \cdot \mathbf{B} - \frac{q\hbar}{4(mc)^2}\hat{\boldsymbol{\sigma}} \cdot \mathbf{E} \times (\hat{\mathbf{p}} - q\mathbf{A}) -$$
$$- \frac{1}{8m^3c^2}(\hat{\mathbf{p}} - q\mathbf{A})^4 + \frac{q\hbar^2}{8(mc)^2}\nabla \cdot \mathbf{E}, \tag{2.42}$$

and it is known as Pauli Hamiltonian. Here $\hat{\mathbf{p}} = -i\hbar\nabla$ represents the canonical quantum mechanical momentum. In order to provide a physical interpretation for the previous expression, we can distinguish between the different terms. While the first three terms represent respectively the rest mass, the potential energy due to the presence of the scalar potential and the kinetic energy of the particle in the electro-magnetic field, the meaning of the other components is not obvious. In particular we have

1. The *Darwin* term
$$\hat{\mathscr{H}}_{\text{Darwin}} = \frac{q\hbar^2}{8(mc)^2}\nabla \cdot \mathbf{E}. \tag{2.43}$$
This object has a non negligible influence only on states with zero orbital moment, namely on the s atomic shell.

2. The spin-orbit term
$$\hat{\mathscr{H}}_{\text{SO}} = \frac{q\hbar}{4(mc)^2}\hat{\boldsymbol{\sigma}} \cdot \mathbf{E} \times (\hat{\mathbf{p}} - q\mathbf{A}), \tag{2.44}$$
which describes the coupling between spin and orbital moment operators.

3. The Zeeman term
$$\hat{\mathscr{H}}_{\text{Zeeman}} = -\mu_{\text{B}}\hat{\boldsymbol{\sigma}} \cdot \mathbf{B}, \tag{2.45}$$
which describes the direct coupling between the magnetic field and the magnetic moment of the particle $\mu_{\text{B}} = \frac{q\hbar}{2m}$.

4. The mass-velocity term
$$\hat{\mathscr{H}}_{\text{mass-vel}} = \frac{1}{8m^3c^2}(\hat{\mathbf{p}} - q\mathbf{A})^4. \tag{2.46}$$
This object is responsable for the relativistic corrections to the kinetic energy of the particle, $\frac{\mathbf{p}^2}{2m}$, due to the relativistic variation of the electron mass with the velocity.

We have seen that the Pauli Hamiltonian represents a reasonable approximation under certain conditions, but it breaks down when the magnetic system is irradiated by an electro-magnetic pulse with frequency approaching the Compton value. In this case it is necessary to include higher-order terms in the expansion of the Dirac Hamiltonian. The following extension up to the fifth order in powers

of $\frac{1}{m}$ may be obtained [39]

$$\hat{\mathscr{H}}_{\mathrm{FW}}^{(5)} = \hat{\mathscr{H}}_{\mathrm{Pauli}} - \frac{iq\hbar^2}{16m^3c^4}\hat{\boldsymbol{\sigma}}\cdot\left[\frac{\partial}{\partial t}\mathbf{E}\times(\hat{\mathbf{p}}-q\mathbf{A}) + (\hat{\mathbf{p}}-q\mathbf{A})\times\frac{\partial}{\partial t}\mathbf{E}\right] - \\ - \frac{q\hbar^2}{16m^3c^4}\left\{(\hat{\mathbf{p}}-q\mathbf{A}), \frac{\partial}{\partial t}\mathbf{E}\right\} + \frac{q\hbar}{2m}\left\{\frac{(\hat{\mathbf{p}}-q\mathbf{A})^2}{4(mc)^2}, \hat{\boldsymbol{\sigma}}\cdot\mathbf{B}\right\} - \\ - \left(\frac{q\hbar}{2m}\right)^2\frac{\mathbf{B}^2}{2mc^2} + O(m^{-4}). \tag{2.47}$$

Making use of this new expansion, the effective spin-photon interaction term becomes

$$\hat{\mathscr{H}}_{\mathrm{s-ph}} = -\frac{q\hbar}{2m}\hat{\boldsymbol{\sigma}}\cdot\mathbf{B} - \frac{iq\hbar^2}{16m^3c^4}\hat{\boldsymbol{\sigma}}\cdot\left[\frac{\partial}{\partial t}\mathbf{E}\times(\hat{\mathbf{p}}-q\mathbf{A}) + (\hat{\mathbf{p}}-q\mathbf{A})\times\frac{\partial}{\partial t}\mathbf{E}\right] - \\ - \frac{q\hbar}{8(mc)^2}\hat{\boldsymbol{\sigma}}\cdot[\mathbf{E}\times(\hat{\mathbf{p}}-q\mathbf{A}) - (\hat{\mathbf{p}}-q\mathbf{A})\times\mathbf{E}] + O(m^{-4}), \tag{2.48}$$

where the first and the last term are respectively the usual Zeeman and spin-orbit coupling interactions, the second term is instead less known and it is associated to the direct coupling between the spin and the time derivative of the external electric field.

The Pauli Hamiltonian represents the basic ingredient necessary for the understanding of any ultrafast direct coherent interaction between photons and spins. In particular there are essentially two terms, which can directly couple the electromagnetic radiation to the magnetization vector. The first one is the Zeeman term of Eq. (2.45), which can play a role in particular in the case of circularly polarized light. The second term is the spin-orbit coupling. The importance of the spin orbit-coupling in the process of ultrafast demagnetization was firstly stressed in Ref. [42], where, jointly to the standard spin-orbit coupling also a correction of the type $-i\frac{q\hbar}{8(mc)^2}\hat{\boldsymbol{\sigma}}\nabla\times\mathbf{E}$ was considered to play a role in the demagnetization process in presence of non-purely centro-symmetric potentials.

The spin-orbit interaction must be taken into account even for the prediction of the correct value of the Faraday rotation parameters in magneto-optical experiments. Its importance for the correct estimation of the Faraday rotation angle, ϕ_{F}, together with the ellipticity, ε_{F}, in experiments on ferromagnetic systems was already established in Ref. [31]. Recently it has been shown that it is possible to model these effects by directly introducing spin-orbit terms into the equations of magneto-optics [38]. The Dirac current $\hat{j}^{\mu} = \bar{\Psi}\gamma^{\mu}\Psi$ may be expanded up to order $\frac{1}{m^3}$, leading to

$$\hat{\mathbf{j}}_{\mathrm{tot}}(\mathbf{r}) = \hat{\mathbf{j}}_{\mathrm{cond}}(\mathbf{r}) + \hat{\mathbf{j}}_{\mathrm{bound}}(\mathbf{r}) + \hat{\mathbf{j}}^{(1)}(\mathbf{r}), \tag{2.49}$$

that is written in operator form, where

$$\hat{\mathbf{j}}^{(1)}(\mathbf{r}) = \frac{q\hbar}{4(mc)^2}\hat{\Psi}^{\dagger}\hat{\boldsymbol{\sigma}}\hat{\Psi}\times\mathbf{E}, \tag{2.50}$$

which represents the non linear magneto-optical effect due to the spin-orbital coupling and defines a new total current density

$$\mathbf{j}_{\text{tot}}(\mathbf{r}) = \mathbf{j}_{\text{cond}}(\mathbf{r}) + \frac{\partial}{\partial t}\mathbf{P} + c\nabla \times \mathbf{m} + \frac{e}{2mc^2}\mathbf{m} \times \mathbf{E}. \tag{2.51}$$

Finally by employing the Maxwell equations (2.13) and (2.14) it is possible to obtain non-linear corrections to the refractive index of the magnetic medium.

The accurate prediction of the magneto-optical coefficients is not the only driving force behind the necessity of improving the theoretical understanding of the laser-magnetization interaction at the femtosecond time scale. The experiments show, in fact, that also the magnetization itself is strongly affected by the application of the laser. In Ref. [36] there is an attempt in trying to explain the laser-induced demagnetization in ferromagnets, making use of a very simplified two-levels model where the states $|a\rangle$ and $|b\rangle$ are spin-mixed states. This situation may arise in presence of spin orbit coupling, when, in fact, the spin operator $\hat{S}_z$ does not commute with the Hamiltonian of the system

$$\hat{H} = E_a |a\rangle \langle a| + E_b |b\rangle \langle b| - \mu_{ab} E(t) |a\rangle \langle b| - \mu_{ba} E(t) |b\rangle \langle a| . \tag{2.52}$$

The laser field $E(t) = F(t)\cos(\omega t)$ couples, then, the states according to the electric-dipole transition rules. The solution of the time dependent Schrödinger equation is then

$$|\Psi(t)\rangle = C_a(t) e^{-i\frac{E_a}{\hbar}t} |a\rangle + C_b(t) e^{-i\frac{E_b}{\hbar}t} |b\rangle , \tag{2.53}$$

leading to the following time dependent spin expectation value

$$\langle \hat{S}_z \rangle = |C_a(t)|^2 \langle a|\hat{S}_z|a\rangle + |C_b(t)|^2 \langle b|\hat{S}_z|b\rangle + C_a^*(t) C_b(t) \langle a|\hat{S}_z|b\rangle + \text{c.c} . \tag{2.54}$$

By starting from an eigenstate of the unperturbed part of the Hamiltonian the change in the state population driven by the application of the laser pulse leads to a linear dependence between the spin and orbital expectation value, while the state interference term can lead to rapid oscillation of the orbital moment.

In Ref. [37] the authors make a step forward by employing all the relativistic contributions coming from the Pauli Hamiltonian to the study of a more involved 8–level hydrogen-like system with centro-symmetric external scalar potential. The unperturbed Hamiltonian for this single particle system reads

$$\hat{\mathscr{H}}_0 = \frac{1}{2m}(\hat{\mathbf{p}} - q\mathbf{A}_M)^2 + V(\mathbf{r}) - \frac{q\hbar}{2m}\hat{\boldsymbol{\sigma}} \cdot \mathbf{B}_M - \frac{q\hbar}{4(mc)^2}\hat{\boldsymbol{\sigma}} \cdot \mathbf{E} \times (\hat{\mathbf{p}} - q\mathbf{A}_M) + \frac{q\hbar^2}{8(mc)^2}\nabla \cdot \mathbf{E}, \tag{2.55}$$

where $\mathbf{B}_M = \nabla \times \mathbf{A}_M$ indicates the magnetic field due to the magnetization of the sample. The interaction part of the Hamiltonian is instead

$$\hat{\mathscr{H}}_1 = -\frac{q}{m}\hat{\boldsymbol{\Pi}} \cdot \mathbf{A}_L - \frac{q\hbar}{2m}\hat{\boldsymbol{\sigma}} \cdot \mathbf{B}_L - \frac{q\hbar}{4(mc)^2}(\hat{\mathbf{p}} - q\mathbf{A}_M) \times \hat{\boldsymbol{\sigma}} \cdot \mathbf{E}_L - \frac{iq\hbar}{4(mc)^2}\hat{\boldsymbol{\sigma}} \cdot \nabla \times \mathbf{E}_L. \tag{2.56}$$

Here $\hat{\mathbf{\Pi}}$ represents the conjugate momentum of the system and $\mathbf{B}_L = \nabla \times \mathbf{A}_L$ is the magnetic field of the laser in case of circularly polarized light. The dynamical evolution of the system up to the third order in the laser perturbation shows that the coherent spin-photon interaction has an influence on the magnetization dynamics at the femtosecond time scale.

The spin-orbit coupling arises, from the previous considerations, as the fundamental ingredient allowing a direct interaction between light and spin, but the way in which it affects the exchange of orbital moment between the incident laser pulse and the electronic system is still not completely clear. In order to shed some light on these issues, Ref. [40] introduces a three-levels system in which initial and final states after the transition are quasi degenerate. This paradigmatic model describes the so called Λ process in which instead of a direct transition between the two states, a third intermediate state much higher in energy, but optically addressable through electric-dipole transition rules, connects the other two during the laser induced process. In particular, through these processes at least three very different situations are permissible. If the two quasi degenerate states exhibit the same direction of the magnetization but have different magnitude, the laser transition will cause a partial demagnetization of the system. If the two states have opposite value of the spin, the process will cause a spin-flip. Finally while if the two states are located on different atoms, the result will be a direct spin transfer. The solution of the model within the rotating wave approximation shows that the process is, in general, characterized by two phases, one in which the system absorbs light with certain helicity and an emission phase when the system emits light with opposite helicity.

The last effect we should mention in this section is the so called inverse Faraday effect [41]. As we have already seen the magneto-optical Faraday effect demonstrates that a magnetically ordered medium can in principle affect the polarization of incident light. Also the inverse process is feasible. In other words it is possible for polarized photons to directly affect the magnetization of a medium. By making use of the expression (2.12) for the free energy of a magnetic system in an external electro-magnetic field, which includes also all the non linear components of the optical susceptibility, it is easy to see that the laser pulse can generate an effective magnetic field $\mathbf{H}_{\text{eff}}$ acting along its direction of propagation

$$\mathbf{H}_{\text{eff}} = -\frac{\partial \Phi}{\partial \mathbf{M}}, \tag{2.57}$$

$$H^k_{\text{eff}} = \alpha^{(I)}_{ijk} E_i(\omega) E_j(\omega)^*. \tag{2.58}$$

In isotropic media the tensor $\alpha^{(I)}$ is anti-symmetric and depends on a single parameter α, which is directly related to the strength of the spin orbit interaction in the material. This allows us to rewrite the effective magnetic field $\mathbf{H}_{\text{eff}}$ as

$$\mathbf{H}_{\text{eff}} = \alpha \mathbf{E}(\omega) \times \mathbf{E}(\omega)^*. \tag{2.59}$$

The conclusion is that circularly polarized light can affect the magnetization of

the system through the inverse Faraday effect, this effect can give rise to a magnetic field that can directly act as a torque of the magnetization vector. This expression was derived in the specific case of incident monochromatic light and under the assumption of thermal equilibrium, but in principle it can be extended to the case in which the field changes much faster than the fundamental time scales of the magnet. In fact in Ref. [43] the authors clearly show that the phenomenological term (2.59) arises in the form of an effective Hamiltonian, which includes all the perturbative terms due to the interaction of the laser field with the magnetic system in electric dipole approximation. In practice circularly polarized light constitutes an effective tool to control spins in magnetically ordered materials at the femtosecond time scale. Furthermore, the mechanism based on the inverse Faraday effect does not require annihilation of photons. The energy transfer from photons to spins occurs through an inelastic scattering process that does not require any loss of orbital moment of the photons [44].

Before proceeding further in the discussion of the ultrafast demagnetization process, it is necessary to point out that the direct coupling between photons and spins has been widely used to explain the laser driven magnetization effect. This is mainly due to the fact that even a small amount of absorbed photons per atom can induce a huge spin moment change. In Ref. [45] it has been shown that the demagnetization depends linearly on the amplitude of the applied pulse and in addition also the transition frequency of the sample may play a role in the process.

However, a complete theoretical description of the demagnetization process requires also an explanation for the magnetization dynamics occuring after the application of the pulse. This effect will be the main topic of the final part of the chapter.

2.4 Non pulse driven contributions to the spin dynamics

In the previous section we have examined how the coherent evolution of a quantum system under the application of external electro-magnetic pulses generates spin dynamics at the femtosecond time scale. In all the cases presented it is tacitly assumed that the demagnetizing system can be described, in first approximation, as a collection of independent particles. This represents a very strong simplification. At the same time it is well known that most of the demagnetization process occurs after the action of the pulse, which means that some mechanism different from the direct interaction between the spin and the laser must contribute to the process.

Below few hundred femtoseconds the spins must interact with a different subsystem in order to exchange orbital moment. After the action of the pulse, it is

known that the spin sub-system is not in thermal equilibrium with the other sub-systems. We will now consider the interaction of the spins with the electrons and with the ionic lattice. The electrons are directly excited by the action of the laser pulse through the term $-\frac{q}{2m}\mathbf{A}\cdot\hat{\mathbf{p}}$, which appears in the Pauli Hamiltonian. The difference between the masses of electrons and those at the nuclei allows to neglect, in first approximation, the motion of the nuclei from the description of the system dynamics in the first few hundred femtoseconds of the time evolution.

Electronic excitations have a direct influence on the spin dynamics. In Fig. 2.1 the time scale of modification of the exchange interaction, for instance, is of the order of hundred femtoseconds, approximately the same time scale of the observed ultrafast magnetization dynamics. Furthermore in Ref. [46] it was experimentally demonstrated that ultrafast spin dynamics occurs during the thermalization of the electronic population, after which the spins follow the electronic dynamics.

The phonons represent a second possible source of interaction for the spin systems. Several models have been proposed to take into account this effect. These are mainly based on Elliott-Yafet type of mechanism, but first we will look at the interaction between spin and electronic sub-system.

2.4.1 Electron - electron and electron - magnon interactions

The Pauli Hamiltonian employed for the study of the spin-photon interaction is of little help for understanding the interaction between electrons and spin. The reason is that the spontaneous magnetization observed in magnetically ordered systems is a many-body interaction and cannot be understood at the level of the single particle description. By writing the Coulomb interaction in second quantization and by neglecting inter-site and inter-band interaction we obtain

$$\hat{H}_{\text{coul.}} = \frac{1}{2}\sum_{\mathrm{I}}\sum_{m_1,m_2}\left[\left(K_{m_1,m_2}-\frac{1}{2}J_{m_1,m_2}\right)\hat{n}_{\mathrm{I},m_1}\hat{n}_{\mathrm{I},m_2}-2J_{m_1,m_2}\hat{\mathbf{S}}_{\mathrm{I},m_1}\cdot\hat{\mathbf{S}}_{\mathrm{I},m_2}\right]. \quad (2.60)$$

The index I labels the atomic sites, while $m_{1,2}$ is a label including all the orbital quantum numbers. The matrix elements

$$K_{m_1,m_2} = \left\langle m_1, m_2\left|\frac{e^2}{4\pi\epsilon_0|\mathbf{r}_{12}|}\right|m_2, m_1\right\rangle, \quad (2.61)$$

$$K_{m_1,m_2} = \int d^3r_1 d^3r_2 \left|\phi_{m_1}(\mathbf{r}_1)\right|^2 \frac{e^2}{4\pi\epsilon_0|\mathbf{r}_{12}|}\left|\phi_{m_2}(\mathbf{r}_2)\right|^2, \quad (2.62)$$

represent the direct Coulomb interaction between the two-particle states, while

$$J_{m_1,m_2} = \left\langle m_1, m_2 \left| \frac{e^2}{4\pi\epsilon_0 |\mathbf{r}_{12}|} \right| m_1, m_2 \right\rangle, \tag{2.63}$$

$$J_{m_1,m_2} = \int d^3 r_1 d^3 r_2 \phi_{m_1}(\mathbf{r}_1)^* \phi_{m_2}(\mathbf{r}_2)^* \frac{e^2}{4\pi\epsilon_0 |\mathbf{r}_{12}|} \phi_{m_1}(\mathbf{r}_2) \phi_{m_2}(\mathbf{r}_1), \tag{2.64}$$

is the exchange integral. The spin and density operators are expressed in second quantization as

$$\hat{n}_{\mathrm{I},m} = \sum_{\sigma} \hat{c}^{\dagger}_{\mathrm{I},m,\sigma} \hat{c}_{\mathrm{I},m,\sigma}, \tag{2.65}$$

$$\hat{\mathbf{S}}_{\mathrm{I},m} = \frac{\hbar}{2} \sum_{\sigma_1,\sigma_2} \hat{c}^{\dagger}_{\mathrm{I},m,\sigma_1} \hat{\boldsymbol{\sigma}}_{\sigma_1,\sigma_2} \hat{c}_{\mathrm{I},m,\sigma_2}, \tag{2.66}$$

where $\hat{c}_{\mathrm{I},m,\sigma}$ and $\hat{c}^{\dagger}_{\mathrm{I},m,\sigma}$ define, respectively, the fermionic annihilation and creation operators at a given site I. The Coulomb interaction has been written in the form (2.60) that explicitly involves a spin-spin interaction term. This object is therefore the fundamental ingredient for the study of the formation of permanent magnetic moments in materials [47]. Most of the magnetic properties of insulators are analyzed by making use of the so called Heisenberg model, where a collection of localized magnetic moments interact through the exchange coupling term $J_{i,j}$. In the case of N atomic sites the classical Heisenberg model Hamiltonian for spin $\mathbf{S}_i$ is generically written as

$$H_{\mathrm{Heisen.}} = \sum_{i=1}^{N} \sum_{j<i} J_{i,j} \mathbf{S}_i \cdot \mathbf{S}_j. \tag{2.67}$$

In addition to the isotropic exchange interaction, also other effects could be important, like the interaction of the magnetic moments with the dipole fields generated by the other moments

$$H_{\mathrm{D}} = \sum_{i=1}^{N} \sum_{j \neq i} D_{i,j} \left[\mathbf{S}_i \cdot \mathbf{S}_j - 3 \left(\mathbf{S}_i \cdot \frac{\mathbf{r}_i - \mathbf{r}_j}{|\mathbf{r}_i - \mathbf{r}_j|} \right) \cdot \left(\mathbf{S}_j \cdot \frac{\mathbf{r}_i - \mathbf{r}_j}{|\mathbf{r}_i - \mathbf{r}_j|} \right) \right]. \tag{2.68}$$

D_{ij} defines the anisotropic coupling constants. Other sources of anisotropy in addition to the dipole interaction can be the coupling of the electronic orbits to the crystal field and the spin-orbit coupling.

The Heisenberg model (2.67) cannot be applied to every class of magnetically ordered system. This model assumes, in fact, the existence of localized magnetic moments and it cannot be directly applied to magnetic metals where the electrons are free to move. The most widely used model in these cases is due to Hubbard [48–50] and in second quantization formalism the Hubbard Hamiltonian can be

written as follows

$$\hat{H}_{\text{Hubbard}} = \sum_{ij\sigma} t_{i,j}\hat{c}^{\dagger}_{i\sigma}\hat{c}_{j\sigma} + U\sum_{i,\sigma}\hat{n}_{i,\sigma}\hat{n}_{i,-\sigma}, \tag{2.69}$$

where the first term represents the kinetic energy part and $t_{i,j}$ is a measure of the hopping strength between two sites of the lattice. The positive parameter U is the Coulomb repulsion experienced by two electrons with opposite spin when occupying the same orbital. This particular configuration must be, in fact, energetically unfavorable. This model in its simplest form is characterized by a single band with two spin channels and by intra-site Coulomb repulsion, since the inter-site Coulomb repulsion represents only a negligible correction to $\hat{H}_{\text{Hubbard}}$.

Unfortunately the interaction term does not allow one to solve the problem exactly, with except to very peculiar case like the one-dimensional one [51]. One general approximated solution is then that obtained by a mean field treatment of the model. The final result is called the Stoner model [47], which is able to predict the existence of magnetic phase transitions in metallic systems. Within the mean-field approximation the following substitution is constructed

$$\hat{n}_{i\sigma}\hat{n}_{i-\sigma} \rightarrow \hat{n}_{i\sigma}\langle\hat{n}_{i-\sigma}\rangle + \langle\hat{n}_{i\sigma}\rangle\hat{n}_{i-\sigma} - \langle\hat{n}_{i\sigma}\rangle\langle\hat{n}_{i-\sigma}\rangle, \tag{2.70}$$

which leads to the replacement of the Hubbard Hamiltonian with following effective mean field description

$$\hat{H}_{\text{Stoner}} = \sum_{ij\sigma}[t_{ij} + U\langle\hat{n}_{i-\sigma}\rangle\delta_{ij}]\hat{c}^{\dagger}_{i\sigma}\hat{c}_{j\sigma} + E_{\text{M.F.}}. \tag{2.71}$$

Here $E_{\text{M.F.}}$ represents the mean field energy term, corresponding to $-\frac{U}{2}\sum_{i\sigma}\langle\hat{n}_{i\sigma}\rangle\cdot\langle\hat{n}_{i-\sigma}\rangle$. In the case of a magnetically ordered system, the expectation value of the occupation number operator does not depend on the particular atomic site and $\langle\hat{n}_{i\sigma}\rangle = \langle\hat{n}_{\sigma}\rangle$. The Stoner model can be rewritten in reciprocal space where the Hamiltonian becomes diagonal

$$\hat{H}_{\text{Stoner}} = \sum_{\mathbf{k}\sigma}\epsilon_{\sigma}(\mathbf{k})\hat{c}^{\dagger}_{\mathbf{k},\sigma}\hat{c}_{\mathbf{k},\sigma} + E_{\text{M.F.}}, \tag{2.72}$$

with eigenvalues

$$\epsilon_{\sigma}(\mathbf{k}) = \epsilon(\mathbf{k}) + Un_{-\sigma}. \tag{2.73}$$

By rewriting this expression in terms of magnetization $m = n_{\uparrow} - n_{\downarrow}$ and density $n = n_{\uparrow} + n_{\downarrow}$ we obtain

$$\epsilon_{\sigma}(\mathbf{k}) = \left(\epsilon(\mathbf{k}) + \frac{U}{2}n\right) - z_{\sigma}\frac{U}{2}m, \tag{2.74}$$

with $z_{\sigma} = \delta_{\sigma,\uparrow} - \delta_{\sigma,\downarrow}$. The term $Un_{-\sigma}$ in the expression of the spin dependent eigenvalue has the meaning of an effective exchange magnetic field $B^{\text{exch.}}_{\sigma} = \frac{U}{\mu_B}n_{-\sigma}$.

A finite value of the magnetization is possible only when also the eigenvalues

$\epsilon_\sigma(\mathbf{k})$ are not spin degenerate, which obviously requires a non zero value of the Coulomb repulsion parameter U. It can be demonstrated that necessary and sufficient condition for an energy band to be spin polarized is

$$1 \leq U\rho(\epsilon_F), \tag{2.75}$$

with $\rho(E) = \frac{1}{N}\sum_{\mathbf{k}} \delta(E - \epsilon_{\mathbf{k}})$ being the density of states, while ϵ_F is the Fermi level of the system. This condition is known as Stoner criterion, and it is obtained in the limit of low temperatures.

The Stoner model describes the ground state properties of magnetic metals quite well, but at finite temperature it is less adequate. For instance the Curie temperature is sensibly overestimated and electronic correlation effects are not taken into account.

Since in femto-magnetism we are mainly interested in the dynamical properties of magnetic metals and in their ultrafast response to external electro-magnetic pulses, the question about the usefulness of the Stoner model in these regimes is a very important one. The possibility to define a dynamical effective magnetic field $B_\sigma^{\text{exch.}}(t)$, which in turn implies also a dynamical $U(t)$ parameter, leads to a fully out-of-equilibrium spin dynamics driven by electron-electron interactions in the first few femtoseconds after the application of the laser pulse.

The introduction of such dynamical quantities would require to go beyond the so called rigid band approximation, where the electron dynamics is described only in terms of changes in the number of electrons occupying the different bands. A first step in this direction was made in Ref. [52] where the authors show that the photoexcitation of the system after the application of the laser pulse could induce the quenching of the exchange band splitting in transition metals. This can be simply understood by noting that in a free electron gas a sudden modification of the kinetic energy generates automatically a modification of the exchange energy [53]

$$E_{\text{exchange}} = -\frac{2e^2}{\pi} k_f \left[\frac{1}{2} + \frac{1-x^2}{4x} ln\left(\frac{1+x}{1-x}\right)\right], \tag{2.76}$$

with k_F being the Fermi wave number, $x = \frac{k}{k_F}$, while k is the electron wave number. The drop in the value of the magnetization during the laser excitation process is found to follow a quite simple empirical law

$$M_z(\Delta E) = M_z(0)\left[1 - \frac{\Delta E}{\Delta E_0}\right]^{\frac{1}{\beta}}, \tag{2.77}$$

where ΔE represents the amount of total energy absorbed by the magnetic system after the laser excitation while ΔE_0 and β are material-dependent fitting parameters. This magnetization variation is a direct consequence of the reduction of the exchange splitting between the minority and the majority energy bands.

The collapse in the exchange splitting is not the only effect produced in the electronic sub-system after a few femtoseconds from the application of the laser

pulse. In Ref. [55] a full many-body description of the spin dynamics based on a complete treatment of the Coulomb interaction shows that the the presence of the spin-orbit coupling is in principle sufficient to explain the ultrafast demagnetization in transition metal ferromagnets. Other ways to explain the demagnetization process require the introduction of an Elliott-Yafet [54, 56] type of mechanism, on which we need to spend a few words.

The Elliott-Yafet mechanism represents a source of spin loss in magnetic metals and semiconductors. It operates when the material has inversion symmetry, the spin-orbit coupling is sufficiently weak to be considered as a perturbation over the ionic scalar potential and there is a low quasi-particle scattering rate. When also the inversion symmetry is broken an equivalent spin dephasing mechanism, the so called Dýakonov-Perél effect, arises in the form of an effective **k**-dependent magnetic field.

In presence of inversion symmetry the spin-up and spin-down states remain degenerate as a result of the Kramers theorem (time reversal invariance). The degenerate admixed states may be written as

$$\left|\Psi_{n\mathbf{k}\uparrow}(\mathbf{r})\right\rangle = [a_{\mathbf{k}n}(\mathbf{r})\,|\uparrow\rangle + b_{\mathbf{k}n}(\mathbf{r})\,|\downarrow\rangle]e^{i\mathbf{k}\cdot\mathbf{r}}, \tag{2.78}$$

$$\left|\Psi_{n\mathbf{k}\downarrow}(\mathbf{r})\right\rangle = [a_{-\mathbf{k}n}(\mathbf{r})^*\,|\downarrow\rangle - b_{-\mathbf{k}n}(\mathbf{r})^*\,|\uparrow\rangle]e^{i\mathbf{k}\cdot\mathbf{r}}, \tag{2.79}$$

where $|\uparrow\rangle$ and $|\downarrow\rangle$ represent the unperturbed up and down spin states, while $\left|\Psi_{n\mathbf{k}\uparrow}\right\rangle$ and $\left|\Psi_{n\mathbf{k}\downarrow}\right\rangle$ are the perturbed admixed Bloch states. Conduction electron spins can then relax via momentum scattering by connecting two states with different k-vectors **k** and **k′**, when the scalar lattice ionic potential is perturbed by spin-orbit coupling interaction.

An example of how an Elliot-Yafet-type of scattering mechanism can affect the ultrafast spin relaxation in ferromagnetic transition metals was given in Ref. [57], where the scattering potential is simply given by the Coulomb interaction between conduction electrons. The non-equilibrium particle-momentum dynamics is then solved at the level of the Boltzmann equation for the semi-classical particle distribution, $n^{\mu}_{\mathbf{k}}$, where **k** represents the vector in momentum space and μ is the band index. The general form of the Boltzmann equation is

$$\frac{\partial}{\partial t}n^{\mu}_{\mathbf{k}} = \frac{\partial}{\partial t}n^{\mu}_{\mathbf{k}}\bigg|_{\text{optical}} + \frac{\partial}{\partial t}n^{\mu}_{\mathbf{k}}\bigg|_{e-e} + \frac{\partial}{\partial t}n^{\mu}_{\mathbf{k}}\bigg|_{\text{thermal}}, \tag{2.80}$$

with the first term on the right-hand side representing the change in electronic population of the band due to optical transitions induced by the action of the laser. The second term is more involved and represents the change in population due to electron-electron Coulomb repulsion and the last term represents the thermal relaxation effects due the interaction with the phonon bath

$$\frac{\partial}{\partial t}n^{\mu}_{\mathbf{k}} = -\frac{n^{\mu}_{\mathbf{k}} - f^{\mu}_{\mathbf{k}}}{\tau_{\text{phon.}}}, \tag{2.81}$$

where $f_{\mathbf{k}}^{\mu}$ is the Fermi distribution at finite temperature and $\tau_{\text{phon.}}$ is the relaxation time due to phonon scattering. This explains that within the general framework of the Elliott-Yafet theory also electron-electron interaction, in presence of a non negligible spin orbit coupling, can be considered as a source of spin variation.

2.4.2 Electron-magnon interactions

The last mechanism we want to consider as a source of spin change due to the electronic excitations is electron-magnon scattering. The magnon is a quantum of excitation of the localized spin subsystem. In practice the low energy excitations of a ferromagnetic system can be described in term of spin waves and the magnon is their unit of quantization. Magnon states are exact eigenstates of the quantum Heisenberg Hamiltonian (2.67), that in momentum space becomes

$$\hat{H} = -\frac{1}{N}\sum_{\mathbf{k}} J(\mathbf{k})[\hat{S}^{+}(\mathbf{k})\hat{S}^{-}(-\mathbf{k}) + \hat{S}^{z}(\mathbf{k})\hat{S}^{z}(-\mathbf{k})], \tag{2.82}$$

with the spin operators in reciprocal space given by

$$\hat{S}^{\alpha}(\mathbf{k}) = \sum_{i} \hat{S}_{i}^{\alpha} e^{-i\mathbf{k}\cdot\mathbf{R}_i}, \tag{2.83}$$

$$\hat{S}^{\pm}(\mathbf{k}) = \hat{S}^{x}(\mathbf{k}) \pm i\hat{S}^{y}(\mathbf{k}). \tag{2.84}$$

Thus the normalized one-magnon eigenstate of $\hat{H}$ can be written as

$$|\mathbf{k}\rangle = \frac{1}{\hbar\sqrt{2SN}}\hat{S}^{-}(\mathbf{k})\,|0\rangle\,. \tag{2.85}$$

This excitation corresponds to a spin deviation distributed collectively among all the localized spins of the system in the form of a wave.

While the electron-phonon scattering operator is theoretically a well defined object the same is not true for the electron-magnon scattering term that is usually expressed in the Kondo-like form [58]

$$\hat{H}_{\text{e-mag}} = \sum_{i} J(\mathbf{r} - \mathbf{R}_i)\hat{\mathbf{s}} \cdot \mathbf{S}_i, \tag{2.86}$$

where $\hat{\mathbf{s}}$ represents the spin operator of the electron at position $\mathbf{r}$, while $\mathbf{S}_i$ is the local spin moment at position $\mathbf{R}_i$. Then $\mathbf{S}_i$ can be expressed in different forms depending on the particular theoretical framework used. For instance, at the level of SDFT a natural interpretation of the localized spin moment is in terms of the exchange-correlation magnetic field (this topic will be analyzed in great detail in the Chapter 3) and the previous expression could be modified as follows

$$\hat{H}_{\text{e-mag}} = \sum_{i} \frac{g\mu_B}{\hbar}\mathbf{B}_{\text{xc}}^{i} \cdot \hat{\boldsymbol{\sigma}}, \tag{2.87}$$

where $\mathbf{B}^i_{\mathrm{xc}} = \int_{\Omega_i} d^3r \mathbf{B}_{\mathrm{xc}}(\mathbf{r})$. In the context of the Stoner model $\mathbf{B}^i_{\mathrm{xc}}$ is substituted by the local effective magnetic field responsable for the band splitting $\frac{U}{\mu_B} n_{-\sigma}$.

In Ref. [59] the electron-magnon scattering has been used also to explain the sub-picosecond spin loss in ferromagnetic thin films. In this case also the spin-orbit coupling needs to be included in the description. In fact the electron-magnon scattering alone conserves the total spin angular momentum of the system and cannot be used to explain the spin loss that is, instead, directly transferred to the electronic orbital moment. The effect of the spin orbit as we have already seen consists in mixing up and down spin states, according to the Elliott-Yafet mechanism. Electron-magnon scattering as well as the electron-phonon scattering can increase the rate of spin variation by connecting states with opposite spin polarization.

By using the Fermi golden rule for the transition between the states $|j, \mathbf{k}, m_s\rangle$ and $|j', \mathbf{k}', m'_s\rangle$, with j indicating the set of all the other quantum numbers that specify the state, the following absorbtion and emission amplitudes can be obtained

$$W^{\mathrm{A/E},\lambda}_{j\mathbf{k}m_s, j'\mathbf{k}'m'_s} = \frac{2\pi}{\hbar} \left| \langle j', \mathbf{k}', m'_s | W^{\mathrm{A/E},\lambda} | j, \mathbf{k}, m_s \rangle \right|^2 \delta[\epsilon_{j'\mathbf{k}'m'_s} - (\epsilon_{j\mathbf{k}m_s} \pm \hbar\omega_{\mathbf{q}})]. \quad (2.88)$$

The problem is therefore reduced to find the matrix elements of the transition operator $W^{\mathrm{A/E},\lambda}_{\mathbf{q}}$. In the case of electron-magnon scattering the absorbtion operator becomes

$$W^{\mathrm{A},\lambda}_{\mathbf{q}} = \begin{pmatrix} 0 & 0 \\ \hat{H}_{\uparrow\downarrow} & 0 \end{pmatrix}. \quad (2.89)$$

Where $\hat{H}_{\uparrow\downarrow}$ corresponds to the expression in Eq. (2.87)

$$\hat{H}_{\uparrow\downarrow} = \frac{g\mu_B}{\hbar} \sum_{\mathrm{I}} \frac{|\mathbf{B}^{\mathrm{I}}_{\mathrm{xc}}|}{M_{\mathrm{I}}} \hat{\mathbf{S}}_{\mathrm{I}} \cdot \hat{\boldsymbol{\sigma}}, \quad (2.90)$$

with M_{I} size of the atomic spin moment, while $\hat{\mathbf{S}}_{\mathrm{I}}$ represents its direction in space. An analogous expression is valid also for the rate of magnon emission.

By summing up over all possible states, various terms are obtained. These also can contribute to the total demagnetization rate after the action of the laser pulse

$$\frac{dM}{dt} = \frac{dM_{\mathrm{elec.}}}{dt} + \frac{dM^{\mathrm{E}}_{\mathrm{mag}}}{dt} + \frac{dM^{\mathrm{A}}_{\mathrm{mag}}}{dt}. \quad (2.91)$$

However the demagnetization rate due to electron-magnon scattering is still too low compared to the value measured in experiments. This suggests that also other mechanisms could contribute to the process, the most important one is the electron-phonon interaction.

2.4.3 Electron-phonon interaction

Considering the Hamiltonian of a system of electrons interacting with N identical ions. The total number of electrons in the system is ZN, where Z is the atomic number of the ion and the Hamiltonian reads

$$\hat{H} = -\frac{\hbar^2}{2m}\sum_i \nabla^2_{\mathbf{r}_i} - \frac{\hbar^2}{2M}\sum_I \nabla^2_{\mathbf{R}_I} + \frac{e^2}{4\pi\epsilon_0}\sum_{i,j}\frac{1}{|\mathbf{r}_i - \mathbf{r}_j|} + \hat{V}_{\text{I-I}}(\{\mathbf{R}\}) + \hat{V}_{\text{e-I}}(\mathbf{r};\{\mathbf{R}\}). \tag{2.92}$$

Here $\{\mathbf{R}\}$ represents the set of ionic centers, $\hat{V}_{\text{I-I}}(\{\mathbf{R}\})$ is the ion-ion interaction potential and $\hat{V}_{\text{e-I}}(\mathbf{r};\{\mathbf{R}\})$ is the electron-ion interaction one. The solution of the Schrödinger equation for the Hamiltonian (2.92) is in general too difficult to find and needs to be approximated. The adiabatic approximation assumes that the total wave function may be rewritten as a direct product between the electronic and the nuclear wave functions, neglecting the correlations between the two.

$$|\Psi\rangle = |\Psi_e\rangle \otimes |\Psi_I\rangle\,. \tag{2.93}$$

The Hamiltonian $\hat{H}_e$ for the electronic part is then

$$\hat{H}_e = -\frac{\hbar^2}{2m}\sum_i \nabla^2_{\mathbf{r}_i} + \frac{e^2}{4\pi\epsilon_0}\sum_{i,j}\frac{1}{|\mathbf{r}_i - \mathbf{r}_j|} + \hat{V}_{\text{e-I}}(\mathbf{r};\{\mathbf{R}\}), \tag{2.94}$$

with a stationary Schrödinger equation whose solutions depend parametrically on the ionic positions

$$\hat{H}_e(\{\mathbf{R}\})\left|\Psi^\alpha_e,\{\mathbf{R}\}\right\rangle = E_\alpha(\{\mathbf{R}\})\left|\Psi^\alpha_e,\{\mathbf{R}\}\right\rangle. \tag{2.95}$$

The parametric energy eigenvalues of the electronic system then enter as an effective potential in the Schrödinger equation for the ionic wave function [61],

$$\sum_J\Big[-\frac{\hbar^2}{2M}\nabla^2_{\mathbf{R}_J} + V_{\text{II}}(\mathbf{R}_J) + E_\alpha(\mathbf{R}_J)\Big]\left|\Psi^\beta_I\right\rangle = E\left|\Psi^\beta_I\right\rangle, \tag{2.96}$$

where E is the total energy of the system.

By considering the equation for the electronic wave function and assuming a small displacement of the ionic position $\mathbf{R}_I$, the electronic wave function will also automatically change. Its modification can be estimated, in the case of small displacements, by applying perturbation theory on the unperturbed wave function $|\Psi_e\rangle$ under a scalar potential of the form

$$\mathbf{u}_I \cdot \mathbf{W}(\mathbf{r};\mathbf{R}^0_I) = V_{\text{e-I}}(\mathbf{r};\mathbf{R}^0_I + \mathbf{u}_I) - V_{\text{e-I}}(\mathbf{r};\mathbf{R}^0_I), \tag{2.97}$$

with $\mathbf{u}_I$ representing the displacement of the ion, and $\mathbf{R}^0_I$ its equilibrium position. The interpretation of the vector field $\mathbf{W}(\mathbf{r};\mathbf{R}^0_I)$ is simple. In the context of the rigid ion approximation it is assumed that the ionic electrostatic potential $V_{\text{e-I}}(\mathbf{r};\mathbf{R}_I)$ follows rigidly the motion of the ions, with the consequence that

under small displacements we can rewrite

$$V_{\text{e-I}}(\mathbf{r};\mathbf{R}_I^0+\mathbf{u}_I)-V_{\text{e-I}}(\mathbf{r};\mathbf{R}_I^0)=\mathbf{u}_I\cdot\nabla_I V(|\mathbf{r}-\mathbf{R}_I^0|), \tag{2.98}$$

$$V_{\text{e-I}}(\mathbf{r};\mathbf{R}_I^0+\mathbf{u}_I)-V_{\text{e-I}}(\mathbf{r};\mathbf{R}_I^0)=-\mathbf{u}_I\cdot\nabla_{\mathbf{r}} V(|\mathbf{r}-\mathbf{R}_I^0|). \tag{2.99}$$

From this result we can then identify

$$\mathbf{W}(\mathbf{r};\mathbf{R}_I^0)=-\nabla_{\mathbf{r}} V(|\mathbf{r}-\mathbf{R}_I^0|), \tag{2.100}$$

which represents the standard form of the electron-phonon coupling operator. The possibility to explain the sub-picosecond demagnetization process through a phonon mediated Elliott-Yafet mechanism has received significant attention. This has been shown, for instance, in Ref. [62] where it has been argued that at least one of the channels responsable for the variation of the spin orbital moment in solids with a non negligible spin-orbit coupling could be of this type. As we have already seen in the case of magnons also the electron-phonon coupling could represent a reasonable source of scattering.

In this case the entire process can be separated in two contributions, the scattering operator $W_{\mathbf{q}}^{\lambda}$, where $\lambda=1,2,3$ defines the phonon polarization may be rewritten as

$$W_{\mathbf{q}}^{\lambda}=W_{\mathbf{q}}^{\lambda,(1)}+W_{\mathbf{q}}^{\lambda,(2)}, \tag{2.101}$$

with $W_{\mathbf{q}}^{\lambda,(1)}$ indicating the ordinary non spin polarized contribution from the ionic potential. Here $W_{\mathbf{q}}^{\lambda,(2)}$ describes the contribution coming from the spin-orbit part of the ionic potential. The first term contributes by connecting the large and the small components of the two spinors and it was the one considered in the original work of Elliott [56]. The transition amplitude of Eq. (2.101) can be, then, written in the following general form

$$W_{\mathbf{q}}^{\lambda}=\sum_I e^{i\mathbf{q}\cdot\mathbf{R}_I}(\mathbf{e}_{\mathbf{q},\lambda}\cdot\nabla_I)\left[V_{\text{e-I}}(\mathbf{r};\{\mathbf{R}\})+\frac{\hbar}{4(mc)^2}[\nabla V_{\text{e-I}}(\mathbf{r};\{\mathbf{R}\})\times\hat{\mathbf{p}}]\cdot\hat{\boldsymbol{\sigma}}\right]. \tag{2.102}$$

Significative arguments about the importance of the spin-flip phonon-mediated mechanism in the ultrafast demagnetization process where presented in Ref. [63]. Elliott-Yafet spin-flip scattering combined with a three-temperature-model have also correctly predicted the demagnetization rate of Ni, Co and Gd [63]. However, there is still not a full consensus about the role of this mechanism in the ultrafast demagnetization process mainly because of the difficulties in the prediction of the spin flip probabilities from ab initio simulations. For instance in Ref. [64] the derived spin demagnetization rate appears to be too small to account for the full demagnetization process.

2.5 The super-diffusive mechanism

All the mechanisms that we have considered in the previous sections are based, in one way or another, on the assumption that the total orbital moment of the system must be conserved during the ultrafast demagnetization process, with the obvious consequence that the spin must be transferred into the electronic orbital moment sink. These theories only differ on the choice of the particular microscopic mechanism which triggers the spin loss.

A completely different approach was undertaken in references [65, 66], where for the first time it was clearly stressed the importance of the connection between the ultrafast demagnetization process and the ultrafast femtosecond spin transport. The model is based on the solution of a set of continuity equations for the majority and minority spin carriers in a ferromagnetic metal. The different life time of the two type of carriers will then be used to explain the ultrafast demagnetization in ferromagnetic / non-magnetic metallic layered junctions (i.e. Fe / Al and Ni / Al). When the ferromagnetic layer is excited by the laser, the computed spin dynamics shows that a super-diffusive spin-current is injected into the non-magnetic Al layer. This is due to the longer lifetime of the majority carriers, that in practice, leads to a net transfer of the magnetization away from the magnetized layer surface.

The numerical simulations show that after the action of the pulse the conduction electrons move in random directions. However the transport process on the sub-picosecond time scale cannot be considered purely diffusive. Thermal diffusion processes are usually characterized by a variance $\sigma^2(t)$ of the electronic distribution, which grows linearly in time according to the following law

$$\sigma(t)^2 = K_w t^{\frac{2}{d_w}}, \tag{2.103}$$

where d_w is named anomalous diffusion exponent, and K_w is the generalized diffusion coefficient. When the regime of the diffusion process is equivalent to a pure Brownian motion, then $d_w = 2$, while in case of ballistic diffusion $d_w = 1$. The intermediate regime, characterized by $1 < d_w < 2$, is called super-diffusive and the ultrafast transport process is assumed to fall exactly in this category, even if the anomalous exponent in these case cannot be considered a constant during the evolution

$$d_w(t) = \frac{2}{t} \frac{\sigma^2(t)}{\frac{d\sigma^2}{dt}}. \tag{2.104}$$

In the super-diffusing model the demagnetization process is described by making use of a continuity equation for the first generation of electrons after the action of the laser and before any scattering event. In one dimension this reads

$$\frac{\partial}{\partial t} n^{[1]} + \frac{\partial}{\partial z} \Phi^{[1]}(z,t) = -R[n^{[1]}] + S_{\text{ext}}, \tag{2.105}$$

where $\Phi(z,t)$ represents the flux of conduction electrons through a surface z, and $R[n]$ is a reaction term, namely, the number of first generation electrons which become second generation after the scattering event. S_{ext} is the source term due to the action of the laser.

The effective source term for the second generation of electrons scattered at the surface will have, instead, the following form

$$S^{[2]} = \sum_{\sigma'} \int dE' P(\sigma, \sigma', E, E', z) R[n^{[1]}](\sigma', E'), \tag{2.106}$$

and the new continuity equation is

$$\frac{\partial}{\partial t} n^{[2]} + \frac{\partial}{\partial z} \Phi^{[2]}(z,t) = -R[n^{[2]}] + S^{[2]}. \tag{2.107}$$

An analogous procedure can be extended to all higher orders.

The rate of demagnetization in ferromagnetic transition metals predicted by the super-diffusive model is shown to be comparable to that observed in pump - probe experiments, by employing material specific energy and spin-dependent life times, suggesting a new possible interpretation of the phenomenon.

2.6 Thermal processes

A second completely different point of view to describe femto-magnetism assumes that the ultrafast demagnetization process is mainly originated due to thermal induced processes. At the sub-picosecond time scale the magnetic system cannot be considered in thermal equilibrium justifying the introduction of a simplified, very popular picture (see Fig. 2.4). The system is divided into three separated components, the electronic, the phononic and spin ones. These evolve separately towards thermal equilibrium.

Due to the initial photon absorbtion, energy is pumped into the medium. Because of the electric dipole selection rules spin-flip transitions are forbidden and the energy is not directly pumped into the spin sub-system. Instead, it is absorbed by the electronic and phononic bath. The subsequent scale of the demagnetization process, τ_{es} for electron-spin relaxation and τ_{sl} for spin-phonon relaxation is then determined by the effective strength of the interaction between the spin and the other sub-systems.

The predictive power of the $3TM$ depends essentially on the choice of the parameters representing the strength of the coupling between different sub-systems, which in turn depends on the particular microscopic theory used to to explain the ultrafast demagnetization process. As we have already seen a very popular choice consisted in connecting these couplings with the phonon-based Elliott-Yafet spin-flip probabilities [68].

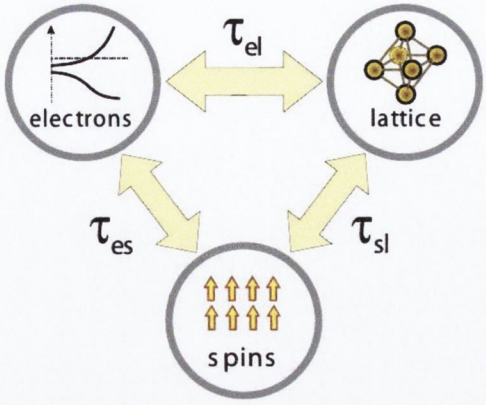


FIGURE 2.4: Different interacting energy reservoirs (electrons, spins and lattice) within the three-temperature-model ($3TM$). (From Ref. [67]).

Within the thermal model for sub-picosecond magnetization dynamics, it is generally assumed that the spin-flip processes are driven by the increased electronic temperature after the system has been invested by the external laser pulse. In these cases the spin sub-system is evolved through the Landau-Lifschitz-Gilbert (LLG) equation [69]

$$\frac{d}{dt}\mathbf{M}(\mathbf{r},t) = -\gamma(\mathbf{M}(t)\times\mathbf{H}_{\text{eff}}(\mathbf{r},t)) + \frac{1}{|\mathbf{M}(\mathbf{r},t)|}\left(\mathbf{M}(\mathbf{r},t)\times G\frac{d}{dt}\mathbf{M}(\mathbf{r},t)\right), \quad (2.108)$$

where $\mathbf{M}(\mathbf{r},t)$ is the macroscopic magnetization and γ the gyromagnetic ratio. The first term on the right-hand side indicates the effect of the precession of the magnetization vector around the axis formed by the effective magnetic field $\mathbf{H}_{\text{eff}}(\mathbf{r},t)$. By discretizing the LLG equation over the set of localized moment sites we have that the effective field at the site $\mathbf{R}$ depends on the general configuration of the atomic moments $\mathbf{H}_{\text{eff},\mathbf{R}}(\{\mathbf{e}_{\mathbf{R}'}\},t)$ and it is generally composed by a local exchange field, an anisotropy field, a dipolar field and the external magnetic field. As we have seen, under the application of strong laser fields, the inverse Faraday effect could generate, for instance, an effective external magnetic field $\alpha\mathbf{E}(\omega)^*\times\mathbf{E}(\omega)$.

$$\mathbf{H}_{\text{eff},\mathbf{R}}(t) = \mathbf{H}_{\text{exch},\mathbf{R}}(\{\mathbf{e}_{\mathbf{R}'}\}) + \mathbf{H}_{\text{anis},\mathbf{R}}(\{\mathbf{e}_{\mathbf{R}'}\}) + \mathbf{H}_{\text{dipole},\mathbf{R}}(\{\mathbf{e}_{\mathbf{R}'}\}) + \mathbf{H}_{\text{ext},\mathbf{R}}(t). \quad (2.109)$$

The anisotropy field in its most general form is written as

$$\mathbf{H}_{\text{anis},\mathbf{R}} = AM^x_{\mathbf{R}}\mathbf{n}_x + BM^y_{\mathbf{R}}\mathbf{n}_y + CM^z_{\mathbf{R}}\mathbf{n}_z, \quad (2.110)$$

while the exchange and the dipole field are defined as usual.

The second term on the right-hand side of Eq. (2.108) is the so called Gilbert damping term. In a general situation the Gilbert scalar G must be replaced by a tensor. This term is merely phenomenological and it is employed in order to account for the fact that beyond a certain critical value of the applied magnetic

field the magnetization saturates and align parallel to the field $\mathbf{H}_{\text{eff},\mathbf{R}}$. Namely, G introduces a phenomenological dissipation mechanism.

Despite its success in describing the out of equilibrium dynamics of the magnetic moments, the LLG is still a phenomenological, macroscopic equation. Significant effort has been put in trying to predict the value of the Gilbert damping coefficient and relating it to some microscopic mechanism. For instance, the ab initio theory of the damping term [70–72] was a valuable improvement. This theory is based on the atomic sphere approximation, which assumes the existence of a well defined localized magnetic moment in correspondence of the atomic site. Then, from the fact that the SDFT energy may be considered an explicit and implicit (through the electron density) functional of the magnetic moments direction $\{\mathbf{e}_\mathbf{R}\}$, the effective magnetic field acting on these moments may be computed leading to the following expression for the Gilbert tensor G_{lm}

$$G_{lm} = -\frac{\gamma}{M}\tau \sum_{j,\mathbf{k}} \frac{\partial f_{j\mathbf{k}}}{\partial \epsilon_{j\mathbf{k}}} \frac{\partial \epsilon_{j\mathbf{k}}}{\partial e_l}\bigg|_M \frac{\partial \epsilon_{j\mathbf{k}}}{\partial e_m}\bigg|_M, \tag{2.111}$$

with M magnetic moment, $\epsilon_{j\mathbf{k}}$ eigenenergy of the band j with wavevector $\mathbf{k}$, and τ the relaxation time for processes at the Fermi surface.

Even more important for the field of femto-magnetism would be the possibility to connect the damping coefficient G with the spin relaxation times, allowing to finally unify the ultrafast (sub-picosecond) and the fast regime of the magnetization dynamics describing both in terms of a generalized LLG equation, where the different types of relaxation mechanisms are included through a new definition of the Gilbert damping.

A first attempt was produced in Ref. [73] where the authors consider the fast magnetization dynamics of a homogeneously magnetized system in an external field $\mathbf{H}_{\text{eff}}$, which includes the anisotropy, the demagnetizing and the external magnetic field. Such a precession dynamics is damped at a time scale

$$\tau_p = \frac{\hbar}{g\mu_B H_{\text{eff}} G}. \tag{2.112}$$

By substituting to the effective field $\mathbf{H}_{\text{eff}}$ the Stoner exchange field $\mathbf{H}_{\text{ex}}$ which is order of magnitude larger and keeping the Gilbert damping G fixed, the typical ultrafast scale for the damping of the precession dynamics is obtained.

In references [2, 74] the authors tried to go beyond the previous partial description using the ab initio expression (2.111) for the Gilbert damping, with the relaxation time for the processes at the Fermi surface, τ, assumed to be equivalent to the relaxation time τ_c of the Drude model for the electrical resistivity. This quantity appears also in the Elliot-Yafet theory for the spin relaxation [56] and implies a strong role played by Elliott-Yafet relaxation mechanisms. The model assumes

$$\tau_M^{-1} = pb^2 \frac{1}{\tau_c}, \tag{2.113}$$

where τ_M indicates the spin relaxation time, while p is a material dependent parameter, which is usually assumed to lie between 1 and 10. In Ref. [62] b^2 has been calculated for a variety of systems by making use of SDFT. This finally leads to the following expression for the ultrafast relaxation time

$$\tau_M = \frac{M}{\gamma F_{\text{el}} p b^2} G, \tag{2.114}$$

where

$$F_{\text{el}} = -\sum_{\mathbf{k},j} \frac{\partial f_{j\mathbf{k}}}{\partial \epsilon_{j\mathbf{k}}} \left(\frac{\partial \epsilon_{j\mathbf{k}}}{\partial \mathbf{e}} \right)^2. \tag{2.115}$$

Here we conclude our overview of the different mechanisms for ultrafast demagnetization processes discussed in literature. In all these cases the theoretical predictions are based on different models, which already assume, in the majority of the cases, a particular type of spin-flip mechanism to be the relevant one for the process under discussion. Instead, a full ab initio treatment of these processes for a time scale below 100 femtoseconds has been developed only in references [75, 76]. So in Chapter 3 we will introduce the Time-Dependent-Denstity-Functional-Theory (TDDFT) and then we will explore how to apply it to the ultrafast processes.

CHAPTER 3

ELECTRONIC STRUCTURE METHODS

An ab initio theory needs always to start from some fundamental physical concept that is assumed to be undoubtedly true. In the case of condensed matter systems this starting point corresponds to the reductionist assumption that a material can be properly described by looking only at its fundamental constituents that in our case can be identified with the electrons and the nuclei.

Given these ingredients the prescription for the calculation is in principle straightforward. All you need is to solve the many body Schrödinger equation with a Hamiltonian consisting of a one-body kinetic term plus a two-body Coulomb interaction potential. In the Born-Oppenheimer non-relativistic approximation the Hamiltonian of n interacting electrons in the field of N atomic nuclei is generally written in the following form

$$\hat{\mathscr{H}} = \sum_{i=1}^{n}\Big[-\frac{\hbar^2}{2m}\nabla_i^2\Big] - \sum_{i=1}^{n}\sum_{\alpha=1}^{N}\frac{Z_\alpha}{|\mathbf{r}_i-\mathbf{R}_\alpha|} + \sum_{i<j}^{n}\frac{1}{|\mathbf{r}_i-\mathbf{r}_j|} + \sum_{\alpha<\beta}^{N}\frac{Z_\alpha Z_\beta}{|\mathbf{R}_\alpha-\mathbf{R}_\beta|}, \quad (3.1)$$

where we used $e = 1$ for the electronic charge. The issue here is that there is no exact and general solution for this kind of problem. The Schrödinger equation with Hamiltonian (3.1) is not solvable in the majority of the cases and in particular in all the cases of practical interest. This has led over the years to several alternative formulations of the electronic structure problem.

The most widely used, still today, is the so-called mean field approximation. Within this approximation each electron moves independently from the others, obeys to the exclusion principle and experiences an effective mean field potential that mimics the effect of the interaction with the other electrons. The specific nature of this potential then defines the type of approximation employed to solve the many body problem. Then, the state of the system is described in term of the eigenstates ψ_i of this effective Hamiltonian with a thermal occupation number f_i.

Even if this approach was extremily successfull in describing electrons in solids, the consequence was to eliminate almost completely the correlation effects between electrons, this is a good approximation in the case of metals, but it can predict wrong ground-state structures for strongly correlated electronic systems such as magnets, Mott insulators and high temperature superconductors [77].

The different types of most commonly used mean-field methods range from Hartree-Fock (HF) [80], that includes an exact treatment of the exchange interaction but with no correlation effects between electrons, to simple multi-configuration descriptions involving a few Slater's determinants. In general, the exact ground-state wave function of a system of many electrons is never a single determinant (like in HF theory) but a combination of several HF determinants. The correlation energy for a particular method is defined as the difference between the true ground-state energy and the energy of the mean-field ground-state. For instance in HF theory we have

$$E_{\text{corr}}^{\text{HF}} = E_{\text{GS}} - E_{\text{GS}}^{\text{HF}}. \tag{3.2}$$

The most important methods include linear mixing of many HF determinants, that is called configuration interaction [79], many-body perturbation techniques [79] and coupled cluster expansion that are mostly used in the case of finite systems. More accurate methods usually require difficult calculations, which take longer time on a computer. The need to solve ground-state electronic structure problems in an accurate enough way with no prohibitive computational costs is becoming a very important issue in modern condensed-matter theory.

The development of new theoretical and computational methods that allows us to go beyond the effective mean-field description including electron-electron correlation effects represents a bottleneck in the field. The so-called Green's function based approach consists, succinctly speaking, in solving the Dyson equation for the many-body problem. The advantage here, with respect to other methods, is due to the fact that electron-electron correlation effects enter into the equations through the self-energy function for which is easier to construct approximated functionals. At the same time the problem is usually expressed in terms of an infinite set of coupled differential equations that needs to be truncated in order to extract a solution. The computational effort required to solve these type of problems at the moment does not allow one to treat systems, which include more than a few tens of atoms. The dynamical mean-field theory is one of the most representative examples of such Green function based methods [78].

In the following sections we will review in some details the density functional theory (DFT) method, that in the last decades has become widely used to solve a variety of electronic structure problems. It has the advantage with respect to HF to include correlation effects, even if the exchange is not treated exactly. Furthermore, the computational effort required to solve the electronic structure problem, even in the case of many atoms systems, is not extremely high and it can be tackled by modern computers.

3.1 Density Functional Theory

There are several introductory works on DFT, see for example [82, 84, 85]. DFT in its standard form formulates the problem of finding the ground-state of a many-body quantum system not in terms of the state wave function, but in terms of the electronic density. The ground-state electron density, $\rho(\mathbf{r})$, substitutes the ground-state many-body wave function $\Psi(\mathbf{r}_1, \sigma_1, \ldots, \mathbf{r}_N, \sigma_N)$ as basic variable of the theory.

In order to show how this is possible in practice we start by rewriting the generic many body Hamiltonian (3.1) of the quantum system in a operator form as

$$\hat{H}_v = \hat{T} + \hat{W} + \hat{V}. \tag{3.3}$$

Here $\hat{T}$ represents the kinetic operator of the system, $\hat{W}$ is the two-body interaction potential and $\hat{V}$ is the one-body interaction potential between the electrons and the nuclei. Here we neglect the electrostatic interaction potential between the atomic nuclei that does not play any role in the following discussion

$$\hat{T} = -\sum_{i=1}^{n} \frac{\hbar^2}{2m} \nabla_i^2, \tag{3.4}$$

$$\hat{W} = \sum_{i<j}^{n} \frac{1}{|\mathbf{r}_i - \mathbf{r}_j|}, \tag{3.5}$$

$$\hat{V} = -\sum_{i=1}^{n} \sum_{\alpha=1}^{N} \frac{Z_\alpha}{|\mathbf{r}_i - \mathbf{R}_\alpha|}. \tag{3.6}$$

We can associate to every external potential operator $\hat{V}$ a function $v(\mathbf{r})$,

$$v(\mathbf{r}) \in L^{3/2}(\bullet\ ^3) \oplus L^\infty(\bullet\ ^3).$$

Then by assuming that the system has a non-degenerate ground-state and by taking the set $\mathscr{V}$ of all the equivalence classes of the external potentials $v(\mathbf{r})$ such that

$$\mathscr{V} = \bigcup_{v \in L^{3/2}+L^\infty} [v(\mathbf{r})],$$

$$v'(\mathbf{r}) \in [v(\mathbf{r})] \text{ if } v'(\mathbf{r}) = v(\mathbf{r}) + C,$$

with C arbitrary constant, the Hohenberg-Kohn theorem [86] establishes that it is possible to construct a one-to-one mapping between the set $\mathscr{V}$ and the set $\mathscr{A}$ of the non degenerate ground state densities. In other words the mapping

$$f : \mathscr{V} \to \mathscr{A} \tag{3.7}$$

is invertible.

This theorem has some important consequences. In fact, the ground-state wave function solution of the Schrödinger equation

$$\hat{H}_v \, |\Psi[v]\rangle = E[v] \, |\Psi[v]\rangle \,, \tag{3.8}$$

may be now thought as a functional of the electron density

$$|\Psi\rangle = |\Psi[n]\rangle \,. \tag{3.9}$$

This means that also the ground-state expectation value of any observable $\hat{O}$ is a functional of the density

$$O[n] = \langle \Psi[n] | O | \Psi[n] \rangle \,. \tag{3.10}$$

By substituting into the previous expression the operator $\hat{T} + \hat{W}$ we obtain the so called Hohenberg-Kohn functional

$$F_{HK}[n] = \langle \Psi[n] | \hat{T} + \hat{W} | \Psi[n] \rangle \,. \tag{3.11}$$

Finally, the expression for the ground state energy becomes

$$E[v] = \min_{n \in \mathscr{A}} \left\{ F_{HK}[n] + \int_V \mathrm{d}^3 r \, n(\mathbf{r}) v(\mathbf{r}) \right\}. \tag{3.12}$$

By assuming the differentiability of the ground state energy functional, we find [90]

$$\frac{\delta E}{\delta v(\mathbf{r})} = n(\mathbf{r}) \tag{3.13}$$

with solution of the functional equation

$$E[v] = F[n] + \int_V \mathrm{d}^3 r \, v(\mathbf{r}) n(\mathbf{r}), \tag{3.14}$$

$$\frac{\delta F}{\delta n(\mathbf{r})} = -v(\mathbf{r}). \tag{3.15}$$

The set of densities for which such a relation exists is named set of *v-representable* densities. If we consider a system of non interacting particles in the external potential $\hat{V}_\mathrm{s}$, governed by the Hamiltonian

$$\hat{H}_\mathrm{s} = \hat{T} + \hat{V}_\mathrm{s}, \tag{3.16}$$

with the non-degenerate ground-state reproduced by the many-body wave function $|\Phi_s\rangle$, we find the following relationships

$$\frac{\delta E}{\delta v_s(\mathbf{r})} = n(\mathbf{r}), \tag{3.17}$$

$$E[v_s] = T_s[n] + \int_V \mathrm{d}^3 r\, n(\mathbf{r}) v_s(\mathbf{r}), \tag{3.18}$$

$$n(\mathbf{r}) = \int_V \mathrm{d}^3 r_1 \ldots \mathrm{d}^3 r_{N-1}\, \Phi_s(\mathbf{r}, \ldots, \mathbf{r}_N)^* \Phi_s(\mathbf{r}, \ldots, \mathbf{r}_N). \tag{3.19}$$

We will call the ground-state density (3.19) *non interacting v-representable* if an equivalent non-interacting potential, which generates the same ground-state density, exists. If this is the case we can write

$$F[n] + \int_V d^3 r v(\mathbf{r}) n(\mathbf{r}) = T_s[n] + \int_V \mathrm{d}^3 r\, n(\mathbf{r}) v_s(\mathbf{r}), \tag{3.20}$$

with

$$F[n] = T_s[n] + \frac{1}{2} \int_V d^3 r \int_V \mathrm{d}^3 r' \frac{n(\mathbf{r}) n(\mathbf{r}')}{|\mathbf{r} - \mathbf{r}'|} + E_{xc}[n], \tag{3.21}$$

$$v_s(\mathbf{r}) = \frac{\delta E_{xc}}{\delta n(\mathbf{r})} + \int_V \mathrm{d}^3 r' \frac{n(\mathbf{r}')}{|\mathbf{r} - \mathbf{r}'|} + v(\mathbf{r}). \tag{3.22}$$

Finally the functional derivative becomes

$$\frac{\delta T_s}{\delta n(\mathbf{r})} = -v_s(\mathbf{r}), \tag{3.23}$$

leading to the following set of Kohn-Sham equations

$$\left[-\frac{\nabla^2}{2} + \int_V \mathrm{d}^3 r' \frac{n(\mathbf{r}')}{|\mathbf{r} - \mathbf{r}'|} + v_{xc}(\mathbf{r}) + v(\mathbf{r}) \right] \phi_i^{\mathrm{KS}}(\mathbf{r}) = \epsilon_i^{\mathrm{KS}} \phi_i^{\mathrm{KS}}(\mathbf{r}), \tag{3.24}$$

with $v_{\mathrm{xc}}(\mathbf{r}) = \frac{\delta E_{\mathrm{xc}}}{\delta n(\mathbf{r})}$, while $\{\phi_i^{\mathrm{KS}}\}$ represents the set of Kohn-Sham eigenstates and $\{\epsilon_i^{\mathrm{KS}}\}$ the set of eigenvalues. The ground-state electron density of the system is given by

$$n(\mathbf{r}) = \sum_{i=1}^{n} \left| \phi_i^{\mathrm{KS}}(\mathbf{r}) \right|^2. \tag{3.25}$$

$E_{\mathrm{xc}}[n]$ is known as the exchange correlation functional. An exact analytical expression for this functional does not exist and we only know a set of conditions that the exact functional must satisfy. In every real density functional theory calculation E_{xc} is approximated and then the set of Kohn-Sham equations are solved self consistently. $E_{\mathrm{xc}}[n]$ represents a very important ingredient of this theory, in fact it includes in principle all the many body quantum effects. Its full knowledge would lead to the exact solution of the quantum many-body problem, the issue is that only a few approximations of this functional are known.

The most important approximation for the exchange correlation functional is the *Local Density Approximation* or LDA. The LDA is exact in the special case of the uniform electron gas [82] and writes

$$E_{\rm xc}^{\rm LDA}[n] = \int_V d^3r\, n(\mathbf{r}) e_{\rm xc}[n(\mathbf{r})], \tag{3.26}$$

$$e_{\rm xc}[n(\mathbf{r})] = e_{\rm x}[n(\mathbf{r})] + e_{\rm c}[n(\mathbf{r})], \tag{3.27}$$

where we write explicitly its exchange part

$$e_{\rm x}[n(\mathbf{r})] = -\frac{3}{4}\left(\frac{3}{\pi}\right)^{1/3} n(\mathbf{r})^{1/3}. \tag{3.28}$$

Accurate numerical parametrizations of $e_{\rm c}[n(\mathbf{r})]$ are available thanks to quantum Monte Carlo calculations [93]. These have been interpolated to provide an analytic form of the correlation energy [83]. Several improvements to the LDA have been proposed over the years. More accurate energetics are usually obtained with a *Generalized Gradient Approximation* or GGA, where the exchange correlation energy is a functional of the density as well as of the gradient of the density [94]

$$E_{\rm xc}^{\rm GGA}[n(\mathbf{r}), s(\mathbf{r})] = \int_V {\rm d}^3r\, e_{\rm x}^{\rm unif}[n(\mathbf{r})] F_{\rm x}[s(\mathbf{r})], \tag{3.29}$$

where

$$s(\mathbf{r}) = \frac{|\nabla n(\mathbf{r})|}{2k_F(\mathbf{r}) n(\mathbf{r})}. \tag{3.30}$$

The third standard form of approximation is a hybrid, which mixes in a fixed fraction $E_{\rm xc}^{\rm GGA}$ with the exact exchange function, $E_{\rm X}$ that has the same form of the exchange interaction term in HF theory

$$E_{\rm xc}^{\rm hyb}[n] = a(E_{\rm X} - E_{\rm xc}^{\rm GGA}[n]) + E_{\rm xc}^{\rm GGA}[n], \tag{3.31}$$

where $E_{\rm X}$ is the exact-exchange energy

$$E_{\rm X} = -\frac{1}{2} \sum_{i,j,\sigma \in {\rm occ.}} \int {\rm d}^3r \int {\rm d}^3r' \, \frac{\phi_{i,\sigma}(\mathbf{r})^* \phi_{j,\sigma}(\mathbf{r}')^* \phi_{i,\sigma}(\mathbf{r}') \phi_{j,\sigma}(\mathbf{r})}{|\mathbf{r} - \mathbf{r}'|}, \tag{3.32}$$

and a is a universal parameter (often about $1/4$).

As we have seen, while the LDA is uniquely defined, all the other functionals can be grouped in at least two main classes. The first class includes all those functionals that have been derived by making use of a certain set of exact conditions. The second class, instead, includes all the so-called *semi-empirical* functionals obtained by means of a fitting procedure over the set of experimental data. The most important exact conditions for the first class of functionals are:

Size consistency: Consider two well separated pieces of matter with densities $n_{\rm A}(\mathbf{r})$, $n_{\rm B}(\mathbf{r})$. When The overlap between these two densities is almost negligible, the self-consistent energy of the full system needs to satisfy the

relation

$$E[n_A + n_B] = E[n_A] + E[n_B],$$

which means that the energy of the full system must be equal to the sum of the energy of the two isolated components.

One-particle limit: For any one-electron systems we need to meet the following requirement

$$\langle \hat{V}_{ee} \rangle = 0,$$

that is equivalent to

$$E_x = -U, \qquad E_c = 0,$$

where U indicates the Hartree energy, E_x the exchange, while E_c is the correlation energy. In DFT this condition is in general not satisfied, the error arising in the DFT ground-state energy due to this is called self-interaction error [92].

Self-interaction correction: The Hartree contribution to the energy functional of a many particles system

$$E_H = \frac{1}{2} \int d^3r \int d^3r' \frac{n(\mathbf{r})n(\mathbf{r}')}{|\mathbf{r} - \mathbf{r}'|},$$

contains a self-interaction term that may be expressed as follows

$$E_H^{self} = \sum_{i=1}^{N} \frac{1}{2} \int d^3r \int d^3r' \frac{|\varphi_i(\mathbf{r})|^2 |\varphi_i(\mathbf{r}')|^2}{|\mathbf{r} - \mathbf{r}'|},$$

E_H^{self} must be exactly canceled by the self-interaction contribution to the exact exchange (3.32).

Lieb-Oxford bound: This corresponds to an exact inequality for the exchange-correlation contribution to the energy

$$E_{xc}[n] \geq C_{LO} E_x^{LDA}[n],$$

providing a lower bound for the exchange-correlation energy.

Asymptotic limit: It can be shown that the exact behaviour of the exchange potential at long distance in the case of finite systems must follow the law

$$\lim_{|r| \to \infty} v_x(\mathbf{r}) = -\frac{1}{|r|},$$

where we are using for the unit of charge $e = 1$, and the exchange potential is defined as

$$v_x(\mathbf{r}) = \frac{\delta E_x}{\delta n(\mathbf{r})}.$$

The LDA exchange potential that is expressed as

$$v_{\mathrm{x}}^{\mathrm{LDA}}(\mathbf{r}) = \frac{-(3\pi^3)^{1/3}}{\pi} n(\mathbf{r})^{1/3},$$

breaks this exact condition by showing in the case of exponentially decaying densities

$$n(\mathbf{r}) \sim e^{-\alpha|\mathbf{r}|},$$

an exponential decay instead of a power law behaviour

$$v_{\mathrm{x}}(\mathbf{r}) \sim e^{-\alpha|\mathbf{r}|/3}.$$

The same issue exists also for the correlation part of the potential.

The elements of the second class of empirical functionals are usually constructed as a linear combination of the exact-exchange functional (3.32) and any number of exchange and correlation density functionals. The parameters defining the weight of each functional are usually estimated by fitting to reference data for atoms and molecules. A typical example is given by the *B3LYP* functional

$$E_{\mathrm{xc}}^{\mathrm{B3LYP}} = E_x^{\mathrm{LDA}} + a_0(E_{\mathrm{X}} - E_x^{\mathrm{LDA}}) + a_x(E_x^{\mathrm{GGA}} - E_x^{\mathrm{LDA}}) + E_c^{\mathrm{LDA}} + a_c(E_c^{\mathrm{GGA}} - E_c^{\mathrm{LDA}}), \tag{3.33}$$

where E_x^{GGA} and E_c^{GGA} are, respectively, the generalized gradient approximation for the exchange [87] and for the correlation energy [88].

The LDA has become a widely used approximation in solid-state physics yielding quite good lattice parameters. At the same time it overestimates the binding energy of about 1 eV/bond, which is not a good result in particular in the case of molecules. Usually these errors in the evaluation of the binding energy gets reduced considerably by employing the GGA or hybrid functionals. A further improvement of the previously defined functionals leads to the so-called meta-GGA functional that includes also the second derivative of the electron density, or the kinetic energy density [89].

The most important limitations of these functionals are related to the calculation of band gaps in solids. The fundamental band gap in insulators or semiconductors is defined as the difference between the binding energy of the most weakly bound electron in the ground-state and the same binding energy obtained by adding one electron to the system, namely

$$E_{\mathrm{g}} = -[(E_0^N - E_0^{N-1}) - (E_0^{N+1} - E_0^N)]. \tag{3.34}$$

The band gap can easily be evaluated for a non interacting system, namely the KS system as the difference between the lowest unoccupied and the highest occupied eigenvalue of the system

$$\Delta_{\mathrm{s}} = \epsilon_{N+1} - \epsilon_N, \tag{3.35}$$

when, in fact, ionization energies are identical to orbital energies. The issue here is that the true physical band gap Δ is not an observable of the fictitious Kohn

- Sham system and therefore Δ_s needs in principle to be corrected by adding an exchange - correlation component

$$\Delta = \Delta_s + \Delta_{xc}. \tag{3.36}$$

It can be shown [92] that, within LDA, Δ_s underestimates the true experimental band gap in semiconductors and insulators by about 40%. By employing self-interaction corrected functionals it is possible to improve the results making the KS band gap closer to the experimental one. However, in general, Δ_s should not be close to Δ even in the case of exact treatment of the exchange interaction.

3.2 Spin Density Functional Theory

The extension of density functional theory to spin-polarized systems is named *Spin Density Functional Theory* or SDFT. An important aspect of SDFT is the fact that every ground-state expectation value is not only a functional of the ground-state density but also of the magnetization, $\mathbf{m}(\mathbf{r})$. SDFT is not only a generalization of the ground-state DFT for systems immersed in an external magnetic field, it can be also useful to study systems in absence of external magnetic field.

In the simplest situation we can introduce a static magnetic field $B(\mathbf{r}) = (0, 0, B(\mathbf{r}))$ along the x_3-axis, that we identify with the spin quantization axis. This special case is called collinear-SDFT (C-SDFT), since the magnetization direction is fixed by construction, $m(\mathbf{r})$ is not a vector field but only a scalar function of the position. By introducing the spin up and down densities, respectively $\rho^{\alpha=\uparrow,\downarrow}$, the total electron density and the magnetization are defined by the following expressions

$$n(\mathbf{r}) = \rho^{\uparrow}(\mathbf{r}) + \rho^{\downarrow}(\mathbf{r}), \tag{3.37}$$

$$m(\mathbf{r}) = \rho^{\uparrow}(\mathbf{r}) - \rho^{\downarrow}(\mathbf{r}). \tag{3.38}$$

In C-SDFT it is possible to use, in an equivalent way, either the set of variables $\{\rho^{\uparrow}(\mathbf{r}), \rho^{\downarrow}(\mathbf{r})\}$ or the set $\{n(\mathbf{r}), m(\mathbf{r})\}$. In the presence of an external magnetic field $B(\mathbf{r})$ acting only on the spin degrees of freedom of the particles (the interaction of $B(\mathbf{r})$ with the electronic current is not considered at the level of C-SDFT), the Hamiltonian may be written in the following form

$$\hat{H} = -\frac{\hbar^2}{2m}\sum_{i=1}^{N}\nabla_i^2 + \hat{W} + \sum_{i=1}^{N} v(\mathbf{r}_i) + \mu_B \sum_{i=1}^{N} B(\mathbf{r}_i)\cdot\hat{\sigma}^z, \tag{3.39}$$

with N total number of particles. The first term on the right hand side is the kinetic energy operator, $\hat{W}$ indicates the full electron - electron interaction energy term, $v(\mathbf{r})$ is the external scalar potential, μ_B the Bohr magneton and $\hat{\sigma}$ is the Pauli

matrix. The electron density operator is written as

$$\hat{n}(\mathbf{r}) = \sum_{i=1}^{N} \delta^3(\mathbf{r} - \mathbf{r}_i), \tag{3.40}$$

while for the magnetization density operator we use

$$\hat{m}(\mathbf{r}) = \mu_B \sum_{i=1}^{N} \delta^3(\mathbf{r} - \mathbf{r}_i)\hat{\sigma}^z. \tag{3.41}$$

Finally, by substituting the previous two definitions into (3.39) we obtain

$$\hat{H} = \hat{T} + \hat{W} + \int d^3r \Big[\hat{n}(\mathbf{r}) \cdot v(\mathbf{r}) + B(\mathbf{r}) \cdot \hat{m}(\mathbf{r})\Big]. \tag{3.42}$$

Consider now two different C-SDFT Hamiltonians with non degenerate ground states $|\Psi_0\rangle$ and $|\Psi_0'\rangle$. These always lead to different ground state densities [85]. In other words we can always construct a one-to-one mapping between the set of non-degenerate ground-state wave functions and the densities

$$f : |\Psi_0\rangle \leftrightarrows (n_0, m_0),$$

$$|\Psi_0\rangle = |\Psi_0[n_0, m_0]\rangle .$$

The energy functional then becomes

$$E[n, m] = \langle \Psi[n, m] | \hat{T} + \hat{W} | \Psi[n, m] \rangle + \int_V d^3r \Big[v(\mathbf{r})n(\mathbf{r}) + B(\mathbf{r}) \cdot m(\mathbf{r})\Big] \tag{3.43}$$

and by construction

$$E[n_0, m_0] < E[n, m]. \tag{3.44}$$

In general it has been shown that by adding a sufficiently small and spatially uniform magnetic field, ΔB, to a field $B(\mathbf{r})$, the ground state Ψ_0 of the unperturbed system is still the ground state. In this way we break down the one-to-one mapping $(v, B) \leftrightarrows \Psi_0$, with the consequence that the extension of the Hohenberg-Kohn theorem to collinear spin systems is not valid. In Ref. [95] it was shown that for collinear magnetic systems the mapping between potentials and ground states is invertible, provided that magnetization is not saturated and that spin potentials are defined up to a spin dependent constant. By relaxing the collinearity condition the map between the ground state Ψ_0 and the new set of 4 external potentials (one scalar potential and the three components of the magnetic field) is invertible in general [96]. What makes the more general non collinear SDFT reliable is the possibility to create such a one-to-one mapping between the set of ground state densities $\mathscr{A}$ and the set of the equivalence classes of the external potentials $\mathscr{V}$

$\mathscr{A} = \{(n, \mathbf{m})$: ground state densities corresponding to external potentials $(v, \mathbf{B})\}$,

$\mathscr{V} = \{[(v, \mathbf{B})]$: equivalence class of potentials with relation $(v, \mathbf{B}) \sim (v', \mathbf{B}')$ if they have the same ground state $\Psi_0\}$.

We can therefore evaluate the expectation value of the SDFT Hamiltonian (3.42) as

$$E[n, \mathbf{m}] = \langle \Psi[n, \mathbf{m}] | \hat{T} + \hat{W} | \Psi[n, \mathbf{m}] \rangle + \int_V \mathrm{d}^3 r \left[v(\mathbf{r}) n(\mathbf{r}) + \mathbf{B}(\mathbf{r}) \cdot \mathbf{m}(\mathbf{r}) \right]. \quad (3.45)$$

By simplifying, in absence of the external magnetic field $\mathbf{B}(\mathbf{r})$, the Kohn - Hohenberg DFT approach can be generalized to the case of spin-polarized systems. The ground-state energy E_0 is written as

$$E_0 = \min_{n, \mathbf{m}} E[n, \mathbf{m}] \quad (3.46)$$

$$E_0 = \min_{n, \mathbf{m}} \left[\int_V \mathrm{d}^3 r \, v(\mathbf{r}) n(\mathbf{r}) + \min_{\Psi \to (n, \mathbf{m})} \langle \Psi | \hat{T} + \hat{W} | \Psi \rangle \right], \quad (3.47)$$

this defines the universal Kohn-Hohenberg functional in terms of density and magnetization.

$$F[n, \mathbf{m}] = \min_{\Psi \to (n, \mathbf{m})} \langle \Psi | \hat{T} + \hat{W} | \Psi \rangle . \quad (3.48)$$

In contrast to the usual universal functional, now the constrained search runs over all the wave functions corresponding to a given density pair $(n, \mathbf{m})$.

The Kohn - Sham prescription for the solution of the DFT problem requires to consider two, in principle distinct, quantum mechanical systems, the true system of interacting electrons and the fictitious Kohn-Sham system of non-interacting electrons. The condition to solve the full interacting problem requires the electron densities of the two systems to be equal, even if their wave function will be different in general. In case of open shell systems there are at least two different possibilities to introduce such an effective system. The first one requires that only the electron density of the interacting and non interacting systems coincide. This assumption leads to the so called *spin restricted* Kohn-Sham DFT formulation where the up and down Kohn-Sham states share the same potential v_s. The second possibility assumes that both density and magnetization of the non-interacting and interacting systems coincide leading to the *spin unrestricted* Kohn-Sham DFT formulation. In this second case the up states are the solution of a Kohn-Sham equation with scalar potential $v_s^{\uparrow}$ while the down states are solutions of an equation with scalar potential $v_s^{\downarrow}$.

In order to make the Kohn-Sham approach valid, it is generally required that the so-called v_s–representability for the electronic density is satisfied even though this is not always guaranteed [90, 91].

First we look at the spin restricted formulation. Considering a system of N non-interacting electrons the Hamiltonian is written as

$$\hat{H}_{\mathrm{s}} = -\frac{\hbar^2}{2m}\sum_{i=1}^{N}\nabla_i^2 + \sum_{i=1}^{N} v_{\mathrm{s}}(\mathbf{r}_i). \tag{3.49}$$

The exact many-body wave function will be an anti-symmetrized product of single particle functions obtained by solving the eigenvalue equation

$$\left[-\frac{\hbar^2}{2m}\nabla^2 + v_{\mathrm{s}}(\mathbf{r})\right]\psi_i(\mathbf{r}) = \epsilon_i\psi_i(\mathbf{r}). \tag{3.50}$$

The orbitals here are identical for the spin up and down components, since the symmetry breaking external magnetic field is missing from the description. The electron density corresponding to a spin restricted Slater determinant can be written as

$$n(\mathbf{r}) = \sum_i f_i[|\psi_i^{\uparrow}(\mathbf{r})|^2 + |\psi_i^{\downarrow}(\mathbf{r})|^2], \tag{3.51}$$

where f_i represents the occupation number for that particular spinor. The spin density is instead given by

$$m(\mathbf{r}) = \sum_i f_i[|\psi_i^{\uparrow}(\mathbf{r})|^2 - |\psi_i^{\downarrow}(\mathbf{r})|^2]. \tag{3.52}$$

The non-interacting Hamiltonian $\hat{H}_{\mathrm{s}}$ clearly commutes with both $\hat{S}^2$ and $\hat{S}_z$. This means that it is in principle possible to create linear combinations of different eigenfunctions of the spin operators, which form a degenerate ground state for the Hamiltonian $\hat{H}_{\mathrm{s}}$. The universal Hohenberg-Kohn functional for the non interacting system may be expressed as

$$T_{\mathrm{s}}[n] = \min_{\Psi_s \to n} \langle \Psi_s|\hat{T}|\Psi_s\rangle\,, \tag{3.53}$$

where T_{s} indicates the non interacting kinetic energy functional, which is independent from the spin density. The ground-state electron density is obtained by minimization of the energy functional

$$E_{\mathrm{s}}[n] = T_{\mathrm{s}}[n] + \int \mathrm{d}^3 r\, v_{\mathrm{s}}(\mathbf{r})n(\mathbf{r}), \tag{3.54}$$

under the constraint that the total number of particles into the system is conserved, leading to

$$\frac{\delta T_{\mathrm{s}}}{\delta n(\mathbf{r})} + v_{\mathrm{s}}(\mathbf{r}) = \mu, \tag{3.55}$$

where μ indicates the chemical potential. The same procedure applied to the many-particle fully interacting system shows that the Hohenberg-Kohn universal functional does not depend only on the density, but also on the magnetization.

Through its usual decomposition we have

$$F[n,m] = T_s[n] + E_H[n] + E_{xc}[n,m], \tag{3.56}$$

where its dependence on the magnetization density has been included directly into the exchange correlation part of the functional. According to this definition the energy functional becomes

$$E[n,m] = T_s[n] + E_H[n] + E_{xc}[n,m] + \int d^3r\, n(\mathbf{r}) v_{ext}(\mathbf{r}). \tag{3.57}$$

By comparing $\frac{\delta E}{\delta n(\mathbf{r})}$ from the previous expression with the one obtained for the non-interacting electronic system we find the following expression for the Kohn-Sham potential

$$v_s(\mathbf{r}) = v_H(\mathbf{r}) + v_{xc}(\mathbf{r}) + v_{ext}(\mathbf{r}). \tag{3.58}$$

As we have seen, by construction, the ground state wave function of the non interacting system $\Psi_{s,0}$ only shares the value of the electron density with the true many body ground state Ψ_0, the value of the corresponding magnetization densities $m_s(\mathbf{r})$ and $m(\mathbf{r})$ are in general not equal and cannot be identified.

In order to obtain the physical spin density in this restricted formulation we should minimize $F[n,m]$ with respect to the magnetization under the constraint that the integral of the magnetization is equal to $2m_s$ (m_s is the magnetic quantum number). The spin restricted formulation is therefore equivalent to a two steps minimization procedure, where we first minimize $E[n]$ with respect to the electron density and then with fixed ground state density we minimize $E_{xc}[n,m]$ with respect to the magnetization density.

The spin unrestricted formulation of non-collinear-SDFT is instead based on the assumption that we can introduce a reference system with the same ground-state density and magnetization of the true many-body system. In this case we start from the introduction of an effective non-interacting N-particle Hamiltonian

$$\hat{H}_s = -\frac{\hbar^2}{2m}\sum_{i=1}^{N}\nabla_i^2 + \sum_{i=1}^{N}[v_s(\mathbf{r}_i) + \hat{\sigma_z}\cdot B_s(\mathbf{r}_i)]. \tag{3.59}$$

$\hat{H}_s$, similarly to the spin-restricted case, commutes with $\hat{S}_z$, but now the different $\hat{S}_z$ eigenstates are not degenerate anymore. This leads to the set of equations for the Kohn-Sham spinors

$$\left[-\frac{\hbar^2\nabla^2}{2m} + v_s(\mathbf{r}) + \mu_B\hat{\sigma_z}\cdot B_s(\mathbf{r})\right]\psi_{i,\alpha}(\mathbf{r}) = \epsilon_{i,\alpha}\psi_{i,\alpha}(\mathbf{r}), \tag{3.60}$$

where the non interacting Kohn-Sham potential has been expressed through a component acting on the density and a component acting on the spin density

$$v_s(\mathbf{r}) = \int d^3r' \frac{n(\mathbf{r}')}{|\mathbf{r}-\mathbf{r}'|} + v_{xc}(\mathbf{r}) + v_{ext}(\mathbf{r}), \tag{3.61}$$

$$B_s(\mathbf{r}) = B_{ext}(\mathbf{r}) + B_{xc}(\mathbf{r}). \tag{3.62}$$

Here we have written the most general expression for $B_s(\mathbf{r})$ in presence of an external inhomogeneous magnetic field. The exchange - correlation potentials are then defined as usual through

$$v_{xc}[n,m](\mathbf{r}) = \frac{\delta E_{xc}}{\delta n(\mathbf{r})}, \tag{3.63}$$

$$B_{xc}[n,m](\mathbf{r}) = \frac{\delta E_{xc}}{\delta m(\mathbf{r})}. \tag{3.64}$$

In conclusion in the spin-unrestricted case both the electron density and the magnetization of the fictitious non-interacting system coincide with their physical many-body equivalents, but at the same time it is important to realize that the spin-unrestricted ground state Ψ_{s0} is not necessarily the ground state Ψ_0 of the full interacting system and other observables could be therefore different in the two cases. For instance, Ψ_0 is always an eigenstate of the $\hat{S}^2$ total spin operator, but this is not true for the spin unrestricted ground state Ψ_{s0}.

This spin unrestricted theory represents a complete extension of DFT that allows one to treat spin-polarized systems in the absence or in the presence of an external magnetic field. As in the case of standard DFT theory the difficulties arise in the choice of the exchange correlation potential that is described in terms of a 2-component or a 4-component object depending if we consider collinear or non collinear spins. The most obvious starting point is the generalization of the LDA functional to collinear spin systems. This can be easily done at least for the exchange component by making use of the expression [85]

$$E_x^{LSDA}[n_\uparrow, n_\downarrow] = \frac{1}{2}(E_x^{LDA}[2n_\uparrow] + E_x^{LDA}[2n_\downarrow]). \tag{3.65}$$

The result is usually expressed in terms of the total electron gas density $n(\mathbf{r})$ and the polarization ζ defined as follows

$$\zeta(\mathbf{r}) = \frac{n\uparrow(\mathbf{r}) - n\downarrow(\mathbf{r})}{n(\mathbf{r})}. \tag{3.66}$$

By using the scaling relations for the exchange energy functional we obtain [82]

$$e_x^{LSDA}(n,\zeta) = e_x(n,\zeta=0) + [e_x(n,\zeta=1) - e_x(n,\zeta=0)]f(\zeta), \tag{3.67}$$

$$f(\zeta) = \frac{(1+\zeta)^{4/3} + (1-\zeta)^{4/3} - 2}{2(2^{1/3}-1)}. \tag{3.68}$$

The LSDA energy functional is therefore

$$E_{xc}^{LSDA}[n,\zeta] = \int_V d^3r\, e_x^{LSDA}(n,\zeta) + E_c^{LSDA}. \tag{3.69}$$

The calculation of the correlation contribution is not straightforward, the following parametrization was suggested in [83] and it is now widely used

$$e_{\rm c}^{\rm LDA}(n,\zeta) = e_{\rm c}^{\rm LDA}(n,0) + \delta e_{\rm c}^{\rm LDA,(2)}(n,\zeta), \tag{3.70}$$

where

$$\delta e_{\rm c}^{\rm LDA(2)}(n,\zeta) = \alpha_{\rm c}(n)\frac{f(\zeta)}{\partial_\zeta^2 f(0)}(1-\zeta^4) + [e_{\rm c}^{\rm LDA}(n,\zeta=1) - e_{\rm c}^{\rm LDA}(n,\zeta=0)]f(\zeta)\zeta^4, \tag{3.71}$$

with the spin stiffness defined as

$$\alpha_{\rm c}(n) = \left.\frac{\partial^2 e_{\rm c}^{\rm LDA}(n,\zeta)}{\partial\zeta^2}\right|_{\zeta=0}. \tag{3.72}$$

From the definition of $E_{\rm xc}$ in LSDA, we can evaluate the expression for the exchange correlation magnetic field in the collinear case

$$B_{\rm xc}^{\rm LSDA}(\mathbf{r}) = \frac{\delta E_{\rm xc}^{\rm LSDA}}{\delta m(\mathbf{r})}. \tag{3.73}$$

This object is, by construction, directed along the quantization axis. Its extension to the more general non-collinear situation is harder and it is based on the idea to evaluate non-collinear functionals in a local reference frame with the local z-axis given by the magnetization direction $\mathbf{m}(\mathbf{r})$ at that particular point $\mathbf{r}$. The LSDA can be therefore immediately extended to the non collinear case by making use of the relation

$$\mathbf{B}_{\rm xc}^{\rm LSDA}(\mathbf{r}) = \frac{\delta E_{\rm xc}^{\rm NCLSDA}[n,\mathbf{m}]}{\delta\mathbf{m}(\mathbf{r})}, \tag{3.74}$$

where $E_{\rm xc}^{\rm NCLSDA}[n,\mathbf{m}]$ indicates the non-collinear functional within the LDA

$$\mathbf{B}_{\rm xc}^{\rm LSDA}(\mathbf{r}) = \frac{\delta E_{\rm xc}^{\rm LSDA}[n,|\mathbf{m}|]}{\delta|\mathbf{m}(\mathbf{r})|}\frac{\mathbf{m}(\mathbf{r})}{|\mathbf{m}(\mathbf{r})|}. \tag{3.75}$$

The result is that by construction $\mathbf{B}_{\rm xc}^{\rm LSDA}(\mathbf{r})$ is always parallel to $\mathbf{m}(\mathbf{r})$. In general since the GGA and meta-GGA functionals are semi-local, attempts were made in order to extend them to non collinear systems without invoking local reference frames. This would produce a field $\mathbf{B}_{\rm xc}$ that is locally non collinear to the magnetization. It can be demonstrated, for instance, that orbital dependent functionals generate a $\mathbf{B}_{\rm xc}$ field, which is non collinear to the local magnetization [101]. For instance, by employing the spin-spiral state of the uniform electron gas as a reference system one can write the exchange - correlation functional depending explicitly on the spin gradient, $\nabla\mathbf{m}(\mathbf{r})$. This makes $\mathbf{B}_{\rm xc}(\mathbf{r})$ clearly non-collinear to the local magnetization vector [103].

If we consider global rotations in the spin space, the set of generators for such a rotation group are the Pauli matrices $\{\hat{\sigma}_i\}_{i=1,2,3}$. These rotations transform the

spin vector $\mathbf{m}(\mathbf{r})$ according to

$$\mathbf{m}(\mathbf{r})' = \hat{\mathbf{R}}\mathbf{m}(\mathbf{r}), \tag{3.76}$$

and they are global transformations, namely the operator $\hat{\mathbf{R}}$ does not depend on the spatial coordinates. Since the kinetic operator $\hat{T}$ and the electron-electron interaction $\hat{W}$ do not change under global rotations we have that

$$E_{\mathrm{xc}}[n, \hat{\mathbf{R}}\mathbf{m}] = E_{\mathrm{xc}}[n, \mathbf{m}]. \tag{3.77}$$

Considering now an infinetesimal rotation of the magnetization vector, we have

$$\int \mathrm{d}^3 r\, \mathbf{m}(\mathbf{r}) \times \mathbf{B}_{\mathrm{xc}}(\mathbf{r}) = 0, \tag{3.78}$$

which is known as the *zero torque theorem* [95]. This theorem represents an exact condition for the exchange-correlation field and it states that $\mathbf{B}_{\mathrm{xc}}(\mathbf{r})$ cannot exert a global torque on the magnetization vector. Only the application of an external magnetic field can globally torque the magnetization vector.

3.3 Current Density Functional Theory

Simple SDFT does not provide a complete description of a system in presence of an external electromagnetic field. We have already seen that in SDFT the external magnetic field couples only to the spin through the Zeeman like term, $\mathbf{B}_{\mathrm{s}}(\mathbf{r}) \cdot \boldsymbol{\sigma}$, but it does not couple to the orbital degrees of freedom of the system. In particular, within SDFT, the Lorentz force exerted between field and electrons is neglected. The SDFT description is certainly valid at low electronic velocities but at higher velocities we need to include in the description corrections to the electronic currents induced by the action of the magnetic field.

This effect is taken into account by a density functional description of the electronic currents known as *Current Density Functional Theory* or CDFT, while the formulation that includes also the spin is known as *Spin Current Density Functional Theory* or SCDFT. In the following we will distinguish between the paramagnetic current density operator $\hat{\mathbf{j}}_{\mathrm{p}}(\mathbf{r})$ that is not invariant under transformations of the gauge potential and the physical current $\hat{\mathbf{j}}(\mathbf{r})$, which is instead gauge invariant. By making use of the single particle spinors $\hat{\psi}(\mathbf{r})$ we can write these two currents as follows

$$\hat{\mathbf{j}}_{\mathrm{p}}(\mathbf{r}) = \frac{\hbar}{2mi}[\hat{\psi}^{\dagger}(\mathbf{r})\nabla\hat{\psi}(\mathbf{r}) - \nabla\hat{\psi}^{\dagger}(\mathbf{r})\hat{\psi}(\mathbf{r})], \tag{3.79}$$

$$\hat{\mathbf{j}}(\mathbf{r}) = \hat{\mathbf{j}}_{\mathrm{p}}(\mathbf{r}) + \frac{q}{m}\hat{n}(\mathbf{r}) \cdot \mathbf{A}_{\mathrm{ext}}(\mathbf{r}) + \frac{\hbar}{2m}\nabla \times \mathbf{m}(\mathbf{r}). \tag{3.80}$$

The physical current contains three different contribution, the paramagnetic current $\hat{\mathbf{j}}_{\mathrm{p}}(\mathbf{r})$, the term due to the external vector potential and the term $\nabla \times \mathbf{m}(\mathbf{r})$, which arises from the semi-relativistic expansion of the covariant 4-current in QED [81]. In general The Hamiltonian of SCDFT may be written in terms of 4 different objects [100]

$$\hat{H} = \hat{T} + \hat{U} + \hat{W} + \hat{H}_z + \hat{V}, \tag{3.81}$$

where

$$\hat{T} = \int_V \mathrm{d}^3 r \, \hat{\Psi}^\dagger(\mathbf{r}) \Big[-\frac{\hbar^2}{2m} \nabla^2 \hat{\Psi}(\mathbf{r}) \Big], \tag{3.82}$$

is the usual kinetic operator written in second quantization form,

$$\hat{W} = \frac{1}{2} \int_V \mathrm{d}^3 r \int_V \mathrm{d}^3 r' \, \hat{\Psi}^\dagger(\mathbf{r}) \hat{\Psi}^\dagger(\mathbf{r}') w(\mathbf{r}, \mathbf{r}') \hat{\Psi}(\mathbf{r}') \hat{\Psi}(\mathbf{r}), \tag{3.83}$$

is the two-body interaction potential,

$$\hat{V} = \int_V \mathrm{d}^3 r \Big[v_{\mathrm{ext}}(\mathbf{r}) + \frac{q^2}{2m} A_{\mathrm{ext}}(\mathbf{r})^2 \Big] \hat{n}(\mathbf{r}), \tag{3.84}$$

is the scalar external potential,

$$\hat{U} = q \int_V \mathrm{d}^3 r \, \hat{\mathbf{j}}_{\mathrm{p}}(\mathbf{r}) \cdot \mathbf{A}_{\mathrm{ext}}(\mathbf{r}), \tag{3.85}$$

is the interaction term between the electrons and the external electro-magnetic field $\mathbf{A}(\mathbf{r})$ in the Coulomb-velocity gauge. The term $\hat{H}_z$ represents instead the interaction between the spin and the external magnetic field

$$\hat{H}_z = \int \mathrm{d}^3 r \, \mathbf{B}_{\mathrm{ext}}(\mathbf{r}) \cdot \hat{\mathbf{m}}(\mathbf{r}). \tag{3.86}$$

In practice the Hamiltonian $\hat{H}$ of SCDFT may be written in the form

$$\hat{H} = \frac{1}{2m} \int \mathrm{d}^3 r \, \hat{\psi}^\dagger(\mathbf{r}) [-i\hbar\nabla + q\mathbf{A}_{\mathrm{ext}}(\mathbf{r})]^2 \hat{\psi}(\mathbf{r}) + \int \mathrm{d}^3 r \, [v_{\mathrm{ext}} \hat{n}(\mathbf{r}) + \hat{\mathbf{m}}(\mathbf{r}) \cdot \mathbf{B}_{\mathrm{ext}}(\mathbf{r})] + \hat{W}, \tag{3.87}$$

where the external potential and the magnetic fields are related through

$$\mathbf{B}_{\mathrm{ext}}(\mathbf{r}) = \nabla \times \mathbf{A}_{\mathrm{ext}}(\mathbf{r}). \tag{3.88}$$

The gauge transformation of the vector potential leads to a phase correction in the expression of the ground-state wave function

$$\mathbf{A}_{\mathrm{ext}}(\mathbf{r})' = \mathbf{A}_{\mathrm{ext}}(\mathbf{r}) - \nabla \Lambda(\mathbf{r}), \tag{3.89}$$

$$|\Psi_0'\rangle = \exp\Big[\frac{iq}{\hbar} \sum_{k=1}^{N} \Lambda(\mathbf{r}_i) \Big], \tag{3.90}$$

where N is the total number of particles into the system. All the pairs $(\Psi_0, \mathbf{A}_{\text{ext}})$ differing by such a gauge transformation are in principle equivalent and should produce the same set of ground-state observables like the energy, the density, the magnetization and the physical current $\mathbf{j}_0(\mathbf{r})' = \left\langle \Psi_0' \middle| \hat{\mathbf{j}} \middle| \Psi_0' \right\rangle = \mathbf{j}_0(\mathbf{r})$. In order to set up a proper DFT scheme we need to choose the basic variables of the theory. The ground state of the system will be then determined through minimization of the energy functional with respect to this set of variables. It can be shown [100, 104] that the ground-state current density $\mathbf{j}_{g0}(\mathbf{r})$ defined as

$$\mathbf{j}_{g0}(\mathbf{r}) = \mathbf{j}_{p0}(\mathbf{r}) + \frac{\hbar}{2m} \nabla \times \mathbf{m}_0(\mathbf{r}), \tag{3.91}$$

together with the ground-state electronic density may be considered as basic variables of SCDFT. These two quantities, in fact, uniquely determine the vector potential and the ground-state wave function of the system. This connection therefore establishes the existence of a unique connection between $\left|\Psi[n, \mathbf{j}_g]\right\rangle$ and the pair $(n, \mathbf{j}_g)$. By considering the two fields $\mathbf{A}_{\text{ext}}(\mathbf{r})$ and $\mathbf{B}_{\text{ext}}(\mathbf{r})$ as independent we arrive to a different formulation of SCDFT with the basic variables of the theory being $\{n(\mathbf{r}), \mathbf{m}(\mathbf{r}), \mathbf{j}_{\text{p}}(\mathbf{r})\}$. Even in this case an extended $1-1$ correspondence between the ground-state wave function and the ground-state densities can be obtained with the wave function that can be formally rewritten as a functional of these set of variables, $\left|\Psi[n, \mathbf{m}, \mathbf{j}_{\text{p}}]\right\rangle$. At the same time if we completely neglect the coupling between the magnetic field and the spin we obtain the standard formulation of CDFT.

Making use of this extended Kohn-Hohenberg theorem it is possible to rewrite the ground-state energy functional for a set of external potentials $(v_{\text{ext}}, \mathbf{A}_{\text{ext}}, \mathbf{B}_{\text{ext}})$, as a functional of the density, magnetization and paramagnetic current. For any ground-state observable we can write

$$O[n, \mathbf{m}, \mathbf{j}_{\text{p}}] = \left\langle \Psi[n, \mathbf{m}, \mathbf{j}_{\text{p}}] \middle| \hat{O} \middle| \Psi[n, \mathbf{m}, \mathbf{j}_{\text{p}}] \right\rangle. \tag{3.92}$$

According to this the energy functional of SCDFT becomes

$$E_{v,\mathbf{B},\mathbf{A}}[n, \mathbf{m}, \mathbf{j}_{\text{p}}] = F[n, \mathbf{m}, \mathbf{j}_{\text{p}}] + E_{\text{ext}}[n, \mathbf{m}, \mathbf{j}_{\text{p}}], \tag{3.93}$$

$$F[n, \mathbf{m}, \mathbf{j}_{\text{p}}] = \left\langle \Psi[n, \mathbf{m}, \mathbf{j}_{\text{p}}] \middle| \hat{T} + \hat{W} \middle| \Psi[n, \mathbf{m}, \mathbf{j}_{\text{p}}] \right\rangle. \tag{3.94}$$

$$\begin{aligned} E_{\text{ext}}[n, \mathbf{m}, \mathbf{j}_{\text{p}}] = & \int_V \mathrm{d}^3 r \, n(\mathbf{r}) \left[v(\mathbf{r}) + \frac{q^2}{2m} A(\mathbf{r})^2 \right] + q \int_V \mathrm{d}^3 r \, \mathbf{j}_{\text{p}} \cdot \mathbf{A}(\mathbf{r}) + \\ & + \int_V \mathrm{d}^3 r \, \mathbf{m}(\mathbf{r}) \cdot \mathbf{B}(\mathbf{r}). \end{aligned} \tag{3.95}$$

The basic principle of SCDFT follows then from the fact that the energy functional (3.93) has a minimum in correspondence to the ground-state value of the

densities and the paramagnetic current, such that if $(n, \mathbf{m}, \mathbf{j}_p)$ is the set of ground-state densities for the potentials $(v, \mathbf{B}, \mathbf{A})$ then using the variational principle

$$E_{v,\mathbf{B},\mathbf{A}}[n, \mathbf{m}, \mathbf{j}_p] \leq E_{v,\mathbf{B},\mathbf{A}}[n', \mathbf{m}', \mathbf{j}'_p]. \tag{3.96}$$

The resulting set of variational equations

$$\frac{\delta E_{v,\mathbf{B},\mathbf{A}}}{\delta n(\mathbf{r})} = 0, \tag{3.97}$$

$$\frac{\delta E_{v,\mathbf{m},\mathbf{A}}}{\delta \mathbf{m}(\mathbf{r})} = 0, \tag{3.98}$$

$$\frac{\delta E_{v,\mathbf{m},\mathbf{A}}}{\delta \mathbf{j}_p(\mathbf{r})} = 0, \tag{3.99}$$

must be solved together with a set of constraints on the ground state densities.

$$\int_V d^3r\, n(\mathbf{r}) = N, \tag{3.100}$$

where N represents the total number of particles in the system. By making use of the static continuity equation we have for the physical current

$$\nabla \cdot \mathbf{j}(\mathbf{r}) = 0, \tag{3.101}$$

that translated in terms of the paramagnetic current leads to

$$\nabla \cdot \mathbf{j}_p(\mathbf{r}) = -\frac{q}{m} \nabla \cdot [n(\mathbf{r})\mathbf{A}(\mathbf{r})]. \tag{3.102}$$

As in the case of collinear-SDFT there is not, in SCDFT, a unique correspondence between the external potentials and the ground state. It is possible, in fact, to find examples of different set of potentials leading to the same ground state.

The extension of the Kohn-Sham formalism to SCDFT proceeds by assuming that an equivalent non-interacting system with the same ground-state densities exists. We can then express the universal functional as

$$F[n, \mathbf{m}, \mathbf{j}_p] = T_s[n, \mathbf{m}, \mathbf{j}_p] + E_H[n] + E_{xc}[n, \mathbf{m}, \mathbf{j}_p], \tag{3.103}$$

where $E_H[n]$ represents the usual Hartree energy functional

$$E_H[n] = \frac{1}{2} \int \mathrm{d}^3r \int \mathrm{d}^3r' \, \frac{n(\mathbf{r})n(\mathbf{r}')}{|\mathbf{r} - \mathbf{r}'|}, \tag{3.104}$$

the total energy functional becomes then

$$E[n, \mathbf{m}, \mathbf{j}_p] = T_s[n, \mathbf{m}, \mathbf{j}_p] + E_H[n] + E_{ext}[n, \mathbf{m}, \mathbf{j}_p] + E_{xc}[n, \mathbf{m}, \mathbf{j}_p]. \tag{3.105}$$

By minimizing the energy functional we arrive to the set of KS-SCDFT equations

$$\left[\frac{1}{2m}(-i\hbar\nabla + q\mathbf{A}_s(\mathbf{r}))^2 + v_s(\mathbf{r}) + \mu_B\mathbf{B}_s(\mathbf{r})\cdot\hat{\sigma}\right]\psi_i(\mathbf{r}) = \epsilon_i\psi_i(\mathbf{r}), \tag{3.106}$$

where the index s labels as usual the equivalent potentials of the non-interacting bare Kohn-Sham system

$$v_s(\mathbf{r}) = v_H(\mathbf{r}) + v_{ext}(\mathbf{r}) + v_{xc}(\mathbf{r}) - \frac{q^2}{2m}[\mathbf{A}_s(\mathbf{r})^2 - \mathbf{A}_{ext}(\mathbf{r})^2], \tag{3.107}$$

$$\mathbf{B}_s(\mathbf{r}) = \mathbf{B}_{ext}(\mathbf{r}) + \mathbf{B}_{xc}(\mathbf{r}), \tag{3.108}$$

$$\mathbf{A}_s(\mathbf{r}) = \mathbf{A}_{ext}(\mathbf{r}) + \mathbf{A}_{xc}(\mathbf{r}). \tag{3.109}$$

The set of exchange - correlation potentials are now defined as

$$v_{xc}(\mathbf{r}) = \left.\frac{\delta E_{xc}[n,\mathbf{m},\mathbf{j}_p]}{\delta n(\mathbf{r})}\right|_{\mathbf{m},\mathbf{j}_p}, \tag{3.110}$$

$$\mathbf{B}_{xc}(\mathbf{r}) = \left.\frac{\delta E_{xc}[n,\mathbf{m},\mathbf{j}_p]}{\delta \mathbf{m}(\mathbf{r})}\right|_{n,\mathbf{j}_p}, \tag{3.111}$$

$$\mathbf{A}_{xc}(\mathbf{r}) = \left.\frac{\delta E_{xc}[n,\mathbf{m},\mathbf{j}_p]}{\delta \mathbf{j}_p(\mathbf{r})}\right|_{n,\mathbf{m}}. \tag{3.112}$$

It is interesting to notice that even in the absence of an external potential $\mathbf{A}_{ext} = 0$, SCDFT predicts a different form for $\mathbf{B}_{xc}$ with respect to the one obtained from SDFT, due to the fact that now also the paramagnetic current is a basic variable of the theory. However, it has been shown in Ref. [106] that there exists, on a certain range of densities, a direct connection between the exchange-correlation functional of SDFT and the exchange-correlation functional of SCDFT that can be expressed in the form

$$\mathbf{B}_{xc}^{SDFT}[n,\mathbf{m}] = \nabla\times\mathbf{A}_{xc}(\mathbf{r}). \tag{3.113}$$

Exactly the same procedure can be followed in the SCDFT version with $(n,\mathbf{j}_g)$ as basic variables leading to an equivalent set of Kohn-Sham equations. In general these set of equations must be covariant under gauge transformations of the vector potential (3.89). At the same time the total energy functional must be invariant under gauge transformations. It has been proved [100] that in order to mantain the gauge invariance under the following transformation of the Kohn - Sham orbitals

$$\psi_i[n,\mathbf{m},\mathbf{j}_p'] = \psi_i[n,\mathbf{m},\mathbf{j}_p]\exp\left[i\frac{q}{\hbar}\Lambda(\mathbf{r})\right], \tag{3.114}$$

the exchange correlation functional must obey the following transformation rule

$$E_{xc}\left[n,\mathbf{m},\mathbf{j}_p + \frac{q}{m}\nabla\Lambda n(\mathbf{r})\right] = E_{xc}[n,\mathbf{m},\mathbf{j}_p], \tag{3.115}$$

or

$$E_{\mathrm{xc}}\left[n, \mathbf{j}_{\mathrm{g}} + \frac{q}{m}\nabla\Lambda n(\mathbf{r})\right] = E_{\mathrm{xc}}[n, \mathbf{j}_{\mathrm{g}}]. \tag{3.116}$$

The universal functional form of E_{xc}, identical for all the external potentials, requires to define its dependence from the paramagnetic current through a gauge invariant functional of $\mathbf{j}_{\mathrm{p}}$. This object is named vorticity and it has the following form

$$\nu = \nabla \times \left[\frac{\mathbf{j}_{\mathrm{p}}(\mathbf{r})}{n(\mathbf{r})}\right]. \tag{3.117}$$

It can be identified as the curl of the velocity field of the electronic gas. Of course both functionals of the two versions of SCDFT need to depend on a type of vorticity, in particular we can write

$$E_{\mathrm{xc}}[n, \mathbf{m}, \mathbf{j}_{\mathrm{p}}] = E_{\mathrm{xc}}^{(1)}[n, \mathbf{m}, \nu], \tag{3.118}$$

while

$$E_{\mathrm{xc}}[n, \mathbf{j}_{\mathrm{g}}] = E_{\mathrm{xc}}^{(2)}[n, \nu_{\mathrm{g}}], \tag{3.119}$$

where we have defined

$$\nu_{\mathrm{g}} = \nu(\mathbf{r}) + \frac{\hbar}{2m}\nabla \times \left[\frac{\nabla \times \mathbf{m}(\mathbf{r})}{n(\mathbf{r})}\right]. \tag{3.120}$$

From the equality of the other components of the energy functional in the two formalism we deduce

$$E_{\mathrm{xc}}^{(1)}[n, \mathbf{m}, \nu] = E_{\mathrm{xc}}^{(2)}[n, \nu_{\mathrm{g}}], \tag{3.121}$$

the previous equality leads to the following definition of $\mathbf{B}_{\mathrm{xc}}$ in SCDFT

$$\mathbf{B}_{\mathrm{xc}}(\mathbf{r}) = \left.\frac{\delta E_{\mathrm{xc}}^{(1)}[n, \mathbf{m}, \nu]}{\delta \mathbf{m}(\mathbf{r})}\right|_{n,\nu}, \tag{3.122}$$

which, in turn, leads to

$$\mathbf{B}_{\mathrm{xc}}(\mathbf{r}) = \frac{\hbar}{2m}\nabla \times \left.\frac{\delta E_{\mathrm{xc}}[n, \mathbf{j}_{\mathrm{g}}]}{\delta \mathbf{j}_{\mathrm{g}}(\mathbf{r})}\right|_{n}. \tag{3.123}$$

We can then conclude that $\mathbf{B}_{\mathrm{xc}}$ corresponds to the curl of $\mathbf{A}_{\mathrm{xc}}$ as we should expect.

Recently different versions of SCDFT based on the true physical current as fundamental variable have also been proposed [104]. However, these formulations are always affected by the problem that the ground-state wave function is not anymore a functional of the densities [105], justifying the need of a SCDFT theory based on the paramagnetic current.

3.3.1 DFT and spin-orbit coupling

There are, in principle, two ways to incorporate spin-orbit coupling into the DFT formalism. The first one is purely ab initio and consists in the generalization of the SCDFT set of equations to the full relativistic case or to some semi-relativistic description, while the second requires a lower level of theoretical accuracy but at the same time it allows to incorporate the spin orbit coupling into the DFT-based analysis widely used to describe real systems. A complete description of the relativistic-DFT formalism can be found in [107]. The fundamental issue is that relativistic DFT (RDFT) is not so well established like its non-relativistic counterpart. The difficulties arise from the fact that a calculation of the expectation value of the many-body observables in QED leads to divergences and therefore without a proper renormalization procedure is not even possible to prove the generalization of the Kohn - Hohenberg theorem for relativistic systems.

A reasonable way to circumvent the problem consists in modifying the SCDFT formalism in such a way to directly include the lowest order relativistic corrections coming from the Dirac equation. By following the approach used in [108], the SCDFT Hamiltonian can be rewritten in its manifestly gauge invariant form, modifying the kinetic energy term in order to include the spin-orbit coupling. The new canonical momentum can be rewritten as

$$\mathbf{\Pi} = \mathbf{p} - q\mathbf{A}_{\text{ext}}(\mathbf{r}) - \frac{q\hbar}{4mc^2}[\hat{\boldsymbol{\sigma}} \times \mathbf{E}(\mathbf{r})], \tag{3.124}$$

where $\mathbf{E}(\mathbf{r})$ represents the effective electric field experienced by the electrons and $\mathbf{A}_{\text{ext}}$ the external vector potential. This substitution yields to the following expression for the many particles Hamiltonian

$$\hat{H} = \sum_{i=1}^{N} \frac{1}{2m}\left[\mathbf{p}_i - q\mathbf{A}_{\text{ext}}(\mathbf{r}_i) - \frac{q\hbar}{4mc^2}(\hat{\boldsymbol{\sigma}} \times \mathbf{E}(\mathbf{r}))\right]^2 + \hat{W} + \hat{H}_z + \hat{V}. \tag{3.125}$$

Here $\hat{W}$ represents the electron-electron interaction, while $\hat{V}$ and $\hat{H}_z$ indicate respectively the interaction of the density and of the spin with the external potentials

$$\hat{V} = \int_V \mathrm{d}^3 r\, \hat{n}(\mathbf{r}) v_{\text{ext}}(\mathbf{r}), \tag{3.126}$$

$$\hat{H}_z = \mu_B \int_V \mathrm{d}^3 r\, \hat{\boldsymbol{\sigma}} \cdot \mathbf{B}_{\text{ext}}(\mathbf{r}). \tag{3.127}$$

Here all the relativistic terms different from the spin-orbit coupling are ignored. By following the Kohn-Sham scheme already developed for SCDFT and assuming that the true densities are reproducible from the orbitals of a non-interacting

system, we obtain the energy functional

$$E = \sum_{i=1}^{N} \frac{1}{2m} \left\langle \psi_i \left| \left[\mathbf{p}_i - q\mathbf{A}_{\text{ext}}(\mathbf{r}_i) - q\mathbf{A}_i(\mathbf{r})\hat{\sigma}_i \right]^2 \right| \psi_i \right\rangle + \int_V \mathrm{d}^3 r\, n(\mathbf{r}) v_{\text{ext}}(\mathbf{r}) + \\ + \int_V \mathrm{d}^3 r\, \mathbf{B}_{\text{ext}}(\mathbf{r}) \cdot \mathbf{m}(\mathbf{r}) + E_{\text{H}} + E_{\text{xc}}, \tag{3.128}$$

where we have used

$$\frac{e\hbar}{4mc^2}[\hat{\boldsymbol{\sigma}} \times \mathbf{E}(\mathbf{r})] = q \sum_{j=1}^{3} \mathbf{A}_j(\mathbf{r})\hat{\sigma}_j. \tag{3.129}$$

The presence of the spin-orbit coupling term requires the addition of a new basic set of variables for the theory, corresponding to the paramagnetic spin current densities

$$\hat{\mathbf{J}}_{\text{p},\lambda}(\mathbf{r}) = \frac{\hbar}{2mi} \sum_{j,\alpha,\beta} \left[\psi^*_{j\alpha}(\mathbf{r}) \sigma^{\lambda}_{\alpha,\beta} \nabla \psi_{j\beta}(\mathbf{r}) - \nabla \psi^*_{j\alpha} \sigma^{\lambda}_{\alpha,\beta} \psi_{j\beta}(\mathbf{r}) \right], \tag{3.130}$$

Therefore the energy becomes a functional of the electron density, $n(\mathbf{r})$, the magnetization density, $\mathbf{m}(\mathbf{r})$, the paramagnetic current, $\mathbf{j}_{\text{p}}(\mathbf{r})$, and the paramagnetic spin current tensor, $\mathbf{J}_{\text{p},\lambda}(\mathbf{r})$. In the context of the Kohn-Sham approach through a constraint minimization of the energy functional we have the following equations of motion

$$\left[\frac{1}{2m} \left(-i\hbar\nabla + q\mathbf{A}_{\text{s}}(\mathbf{r}) \right)^2 + U_{\text{s}} + \frac{q^2}{2m} \left(\mathbf{A}^2_{\text{ext}} + \sum_{j=1}^{3} \mathbf{A}_j^2 + 2 \sum_{j=1}^{3} \mathbf{A} \cdot \mathbf{A}_j \hat{\sigma}_j - \mathbf{A}^2_{\text{s}} \right) \right] |\psi_i\rangle = \epsilon_i |\psi_i\rangle, \tag{3.131}$$

where the U_{s} defines the effective one-particle interaction for the spin and the electron density

$$U_{\text{s}}(\mathbf{r}) = v_{\text{s}}(\mathbf{r}) + \mu_B \hat{\boldsymbol{\sigma}} \cdot \mathbf{B}_{\text{s}}(\mathbf{r}), \tag{3.132}$$

$$v_{\text{s}}(\mathbf{r}) = q^2 \int \mathrm{d}^3 r' \, \frac{n(\mathbf{r}')}{|\mathbf{r} - \mathbf{r}'|} + v_{\text{ext}}(\mathbf{r}) + v_{\text{xc}}(\mathbf{r}), \tag{3.133}$$

$$\mathbf{B}_{\text{s}}(\mathbf{r}) = \mathbf{B}_{\text{ext}}(\mathbf{r}) + \mathbf{B}_{\text{xc}}(\mathbf{r}). \tag{3.134}$$

The various exchange-correlation potentials are then defined as usual in terms of functional derivatives of the energy $E[n, \mathbf{m}, \mathbf{j}_p, \mathbf{J}_{p,\lambda}]$, namely

$$v_{xc}(\mathbf{r}) = \left.\frac{\delta E_{xc}}{\delta n(\mathbf{r})}\right|_{\mathbf{m},\mathbf{j}_p,\mathbf{J}_{p,\lambda}}, \tag{3.135}$$

$$\mathbf{B}_{xc}(\mathbf{r}) = \left.\frac{\delta E_{xc}}{\delta \mathbf{m}(\mathbf{r})}\right|_{n,\mathbf{j}_p,\mathbf{J}_{p,\lambda}}, \tag{3.136}$$

$$q\mathbf{A}_{xc} = \left.\frac{\delta E_{xc}}{\delta \mathbf{j}_p}\right|_{n,\mathbf{m},\mathbf{J}_{p,\lambda}}, \tag{3.137}$$

$$q\mathbf{A}_{xc,\lambda} = \left.\frac{\delta E_{xc}}{\delta \mathbf{J}_{p,\lambda}}\right|_{n,\mathbf{m},\mathbf{j}_p} \qquad \lambda = 1,2,3. \tag{3.138}$$

The effective vector potential $\mathbf{A}_s$ has instead the form

$$\mathbf{A}_s(\mathbf{r}) = \mathbf{A}_{ext}(\mathbf{r}) + \mathbf{A}_{xc}(\mathbf{r}) + \sum_{j=1}^{3} [\mathbf{A}_j(\mathbf{r}) + \mathbf{A}_{xc,j}(\mathbf{r})] \cdot \sigma_j. \tag{3.139}$$

In conclusion, the SCDFT extension to include the spin-orbit coupling leads to a modified DFT formalism characterized by 16 fundamental variables [98,99]

1. ground state density $n(\mathbf{r})$.
2. three magnetization densities $\mathbf{m}(\mathbf{r})$.
3. three paramagnetic currents $\mathbf{j}_p(\mathbf{r})$,
4. nine paramagnetic spin current densities $\mathbf{J}_{p,\lambda}(\mathbf{r})$, $\lambda = 1,2,3$.

The presence of so many variables clearly makes the set of equations (3.131) difficult to solve in general. In order to directly solve in a practical situation the set of Kohn-Sham equations we need to lower down the level of complexity of the theory, in particular by acting on the number of basic observables used to minimize the energy functional. Comparison of the SDFT and SCDFT, making use of an exact exchange approximation (EXX), shows that, at least in the case of spontaneous magnets like Fe, Co and Ni, there is no sensible difference in absence of external magnetic field and with spin-orbit coupling between the two approaches [102].

This suggests that, even if formally the $\mathbf{j}_p^{KS}$ paramagnetic current calculated from SDFT does not correspond to the paramagnetic current of the full interacting system, the fact that the difference between these two currents is not huge may be considered as a justification for the use of the effective Kohn-Sham current in the computation of the orbital properties of magnetic metals.

If we include the spin-orbit coupling term within the SDFT formalism and assume that the electric field acting on the electrons can be described by the gradient of a local and smooth potential $v_{\text{ext}}(\mathbf{r})$, we have

$$\hat{H} = \hat{T} + \hat{W} - \frac{q\hbar}{4mc^2}\sum_{\alpha\beta}\int \mathrm{d}^3 r\, \hat{\psi}^{\dagger}_{\alpha}(\mathbf{r})\frac{|\nabla v_{\text{ext}}|}{|\mathbf{r}|}(\hat{\sigma}_{\alpha\beta}\cdot\hat{\mathbf{L}})\hat{\psi}_{\beta}(\mathbf{r}) + \int \mathrm{d}^3 r\, v_{\text{ext}}(\mathbf{r})\hat{n}(\mathbf{r}) + \\ + \int \mathrm{d}^3 r\, \mathbf{B}_{\text{ext}}(\mathbf{r})\cdot\hat{\mathbf{m}}(\mathbf{r}), \tag{3.140}$$

$\hat{\psi}_{\alpha}$ is a single particle spinor, and $\hat{\mathbf{L}}$ is the orbital moment operator. The ground state energy within SDFT is just a functional of density and magnetization

$$E[n,\mathbf{m}] = F[n,\mathbf{m}] + \int_V \mathrm{d}^3 r\left[v_{\text{ext}}(\mathbf{r})n(\mathbf{r}) + \mathbf{B}_{\text{ext}}(\mathbf{r})\cdot\mathbf{m}(\mathbf{r})\right] - \\ - \frac{q\hbar}{4mc^2}\sum_{jkl}\int \mathrm{d}^3 r\, \epsilon_{jkl}\nabla_k v_{\text{ext}} J^{lj}_{\text{p}}(\mathbf{r}). \tag{3.141}$$

The minimization of the energy functional leads to the following set of one-particle equations

$$\left[-\frac{\hbar^2}{2m}\nabla^2 - \mu_B\mathbf{B}_{\text{s}}(\mathbf{r})\cdot\hat{\sigma} - \frac{q\hbar}{4m^2c^2}\hat{\sigma}\cdot(\nabla v_{\text{ext}}\times\hat{\mathbf{p}}) + v_{\text{s}}(\mathbf{r})\right]\psi_{i,\alpha}(\mathbf{r}) = \epsilon_{i,\alpha}\psi_{i,\alpha}(\mathbf{r}), \tag{3.142}$$

where the usual effective potentials have been introduced

$$\mathbf{B}_{\text{s}}(\mathbf{r}) = \mathbf{B}_{\text{ext}}(\mathbf{r}) - \frac{\delta E_{\text{xc}}}{\delta\mathbf{m}(\mathbf{r})}, \tag{3.143}$$

$$v_{\text{s}}(\mathbf{r}) = v_{\text{ext}}(\mathbf{r}) + q^2\int \mathrm{d}^3 r'\,\frac{n(\mathbf{r}')}{|\mathbf{r}-\mathbf{r}'|} + \frac{\delta E_{\text{xc}}}{\delta n(\mathbf{r})}. \tag{3.144}$$

Here J^{lj}_{p} indicates the Kohn-Sham spin current that must be always distinguished from the physical current of the many-body system. The previous set of equations represent just the KS-SDFT equations modified by the addition of an external term describing the interaction between orbital and spin degrees of freedom in the system. We need at this point to understand how the equations (3.142) for the Kohn - Sham spinors may be solved in practice. In general we can distinguish two major situations depending on whether or not we are explicitly considering in the calculation core electrons. In the first case the method is regarded as *all-electron* and all the electronic degrees of freedom are treated self-consistently. This, in general, allows one to perform fully relativistic calculations without conceptual complications. The drawback is that calculations are rather expensive computationally and only small systems can be considred with this method. In the case when core electrons are not trated self consistently, their contributions is cast in the form of pseudo-potentials. This approach drastically reduces the number of electrons considered in the calculation and much larger systems can

be computed. In the next section, after a concise introduction of the pseudo-potential method, we will focus on how the spin-orbit coupling may be included within this description.

3.4 Pseudo-potentials and spin-orbit coupling

There are two fundamental reasons that justify the introduction of the pseudopotentials in DFT - based calculations

1. The core states are usually not important in the description of the chemical bond.
2. There is no need for an accurate description of the valence wave functions inside the core region, where it can be replaced by a smooth, nodeless wave function that corresponds to a state of a new pseudo atomic problem.

The pseudo-potential method, in practice, allows to lower the computational effort required in a DFT ground-state calculation by creating effective potentials that reproduce the correct behaviour of the valence wave function beyond the core radius. These are fitted over a set of constraints that allow to reproduce some exact properties of the ionic potential.

One of the most used type of pseudo-potential in electronic structure calculations is the *norm-conserving*, which meets the following set of conditions

1. The eigenvalues of the pseudo and all electron wave functions are the same for a given atomic configuration.
2. The pseudo wave function R_l^{PS} is nodeless and can be expressed in the following form,
$$R_l^{\mathrm{PS}}(\epsilon, r) = \begin{cases} \widetilde{R}_l^{\mathrm{PS}} & \text{if } r < r_l^{\mathrm{cut}} \\ R_l^{\mathrm{AE}} & \text{if } r \geq r_l^{\mathrm{cut}} \end{cases} \tag{3.145}$$
where l is the orbital quantum number and r the radial distance from the nucleus. Pseudo and all electron valence wave functions coincide beyond the cut-off radius r_l^{cut} (or core radius).
3. For a given energy eigenvalue, ϵ_l, and in the vicinity of the cut-off radius, r_l^{cut}, the logarithmic derivatives of the pseudo and all electron wave functions are the same.
$$\frac{\partial}{\partial r} \ln R_l^{\mathrm{PS}}(\epsilon, r)\Big|_{r=r_l^{\mathrm{cut}}, \epsilon=\epsilon_l} = \frac{\partial}{\partial r} \ln R_l^{\mathrm{AE}}(\epsilon, r)\Big|_{r=r_l^{\mathrm{cut}}, \epsilon=\epsilon_l}. \tag{3.146}$$
The logarithmic derivative of the radial wave function, $\frac{\beta_l}{r_l^{cut}}$, is directly related to the phase shift δ_l of the wave function by means of the relation

$$\frac{\beta_l}{r_l^{\text{cut}}} = k\left[\frac{j_l'(kr_l^{\text{cut}})\cos\delta_l - n_l'(kr_l^{\text{cut}})\sin\delta_l}{j_l(kr_l^{\text{cut}})\cos\delta_l - n_l(kr_l^{\text{cut}})\sin\delta_l}\right]. \tag{3.147}$$

The phase shift that the valence pseudo wave function acquires in presence of the ionic pseudo-potential is identical to the phase shift in the all electron valence wave function under the influence of the real electrostatic potential (beyond the cut-off radius).

4. The norm conservation of the pseudo and all electron wave functions must be satisfied,

$$\int_0^{r_l^{\text{cut}}} dr\left|r\widetilde{R}_l^{\text{PS}}(\epsilon, r)\right|^2 = \int_0^{r_l^{\text{cut}}} dr\left|rR_l^{\text{AE}}(\epsilon, r)\right|^2. \tag{3.148}$$

This relation together with condition (2) produce the following equality

$$\frac{\partial}{\partial\epsilon}\frac{\partial}{\partial r}\ln R_l^{\text{PS}}(\epsilon, r)\Big|_{\epsilon=\epsilon_l, r=r_l^{\text{cut}}} = \frac{\partial}{\partial\epsilon}\frac{\partial}{\partial r}\ln R_l^{\text{AE}}(\epsilon, r)\Big|_{\epsilon=\epsilon_l, r=r_l^{\text{cut}}}, \tag{3.149}$$

which is crucial, together with the third condition for the pseudo-potential transferability. In this way scattering properties of the ion cores are reproduced with minimum error.

The pseudo valence wave function will be, in general, a linear combination of the true valence wave function and of the core states, that constitute a complete basis in the Hilbert space,

$$\left|\psi_v^{\text{PS}}\right\rangle = \alpha\left|\psi_v\right\rangle + \sum_c \alpha_c\left|\psi_c\right\rangle, \tag{3.150}$$

where $|\psi_c\rangle$ defines the core states and $|\psi_v\rangle$ the all-electron valence wave functions. The pseudo Hamiltonian $\hat{H}^{\text{PS}}$ has the property to solve the following eigenvalue equation

$$\hat{H}^{\text{PS}}\left|\psi_v^{\text{PS}}\right\rangle = \epsilon_v\left|\psi_v^{\text{PS}}\right\rangle, \tag{3.151}$$

where ϵ_v indicates the eigenvalue of the true valence wave function

$$\hat{H}_{\text{at}}\left|\psi_v\right\rangle = \epsilon_v\left|\psi_v\right\rangle. \tag{3.152}$$

By applying the atomic Hamiltonian $\hat{H}_{\text{at}}$ to the pseudo valence wave function $\left|\psi_v^{\text{PS}}\right\rangle$ we obtain the following expression

$$\left[\hat{H}_{\text{at}} + \sum_c(\varepsilon_v - \varepsilon_c)\left|\psi_c\right\rangle\left\langle\psi_c\right|\right]\left|\psi_v^{\text{PS}}\right\rangle = \epsilon_v\left|\psi_v^{\text{PS}}\right\rangle. \tag{3.153}$$

The term $\hat{H}_{\text{at}} + \sum_c(\epsilon_v - \epsilon_c)\left|\psi_c\right\rangle\left\langle\psi_c\right|$ can be thought as an effective Hamiltonian operator $\hat{H}^{PS}$, which generates the following stationary Schrodinger equation

$$\hat{H}^{\text{PS}}\left|\psi_v^{\text{PS}}\right\rangle = \epsilon_v\left|\psi_v^{\text{PS}}\right\rangle, \tag{3.154}$$

and the potential $\hat{V}^{\mathrm{PS}}$ associated to the Hamiltonian $\hat{H}^{\mathrm{PS}}$ is the pseudo-potential of the system

$$\hat{V}^{\mathrm{PS}} = \hat{V}_{\mathrm{coulomb}} + \sum_{c} (\epsilon_v - \epsilon_c) \left|\psi_c\right\rangle \left\langle\psi_c\right| . \tag{3.155}$$

It is customary to consider, in the description of atomic systems, a spherical symmetric pseudopotential. This type of potential is a function of the orbital quantum number l and of the energy eigenvalues.

$$\hat{V}_{\mathrm{PS}} = \sum_{l=0}^{\infty} v^{l}_{\mathrm{PS},\epsilon}(r)\hat{P}_l, \tag{3.156}$$

where $\hat{P}_l$ is a projection operator on the subspace spanned by the vectors $\{|l,m\rangle\}_{m=-l,\ldots,l}$.

$$\hat{P}_l = \sum_{m=-l}^{l} |l,m\rangle \langle l,m| . \tag{3.157}$$

Pseudo-potentials of the form (3.156) act differently depending on the particular angular component of the wave function. For this reason they are often called semi-local or angular dependent.

In practice we are interested only in a few angular components in the core region, and $\hat{V}_{\mathrm{PS}}$ acquires the following form

$$\hat{V}_{\mathrm{PS}} = \sum_{l=0}^{l_{\max}} v^{l}_{\mathrm{PS},\epsilon}(r)\hat{P}_l + \sum_{l=l_{\max}}^{\infty} v^{\mathrm{loc}}_{\mathrm{PS},\epsilon}(r)\hat{P}_l, \tag{3.158}$$

that becomes

$$\hat{V}_{\mathrm{PS}} = \sum_{l=0}^{\infty} v^{\mathrm{loc}}_{\mathrm{PS},\epsilon}(r)\hat{P}_l + \sum_{l=0}^{l_{\max}} [v^{l}_{\mathrm{PS},\epsilon}(r) - v^{\mathrm{loc}}_{\mathrm{PS},\epsilon}(r)]\hat{P}_l. \tag{3.159}$$

By identifying

$$v^{l}_{\mathrm{PS},\epsilon}(r) - v^{\mathrm{loc}}_{\mathrm{PS},\epsilon}(r) = \Delta v^{l}_{\mathrm{PS},\epsilon}(r) \tag{3.160}$$

we obtain

$$\hat{V}_{\mathrm{PS}} = v^{\mathrm{loc}}_{\mathrm{PS},\epsilon}(r)\bullet + \sum_{l=0}^{l_{\max}} \Delta v^{l}_{\mathrm{PS},\epsilon}(r)\hat{P}_l. \tag{3.161}$$

$\Delta v^{l}_{\mathrm{PS},\epsilon}(r)$ is confined inside the core region and $v^{\mathrm{loc}}_{\mathrm{PS},\epsilon}(r)$ is an average local potential describing the screened (by the core electrons) Coulomb interaction. The component $v^{\mathrm{loc}}_{\mathrm{PS},\epsilon}(r)$ is often associated to $v^{l_{max}+1}_{\mathrm{PS},\epsilon}(r)$. However, the energetic ordering of the atomic levels does not follow the angular momenta ordering and there is no reason to choose local pseudopotentials corresponding to a specific angular momentum.

The Kleinman-Bylander pseudo-potential (3.161) is fully non local and orbital dependent and allows one to correctly describe the scattering of an incident spherical wave with the ionic potential [109]. In this section we are specifically interested in understanding how this pseudo-potential form may be extended in order to include spin-orbit coupling effects.

The starting point is the single particle Dirac equation in a central external potential. A full treatment of this kind of problem can be found in many references, see for instance [16] (Chapter 8). The equations of motion for a single Dirac particle in an external central potential with relativistic corrections up to order α^2, with α corresponding to the fine structure constant, are given by

$$\frac{dF_{nlj}}{dr} - \frac{k}{r}F_{nlj}(r) + (\epsilon_{nlj} - V(r))\alpha G_{nlj}(r) = 0, \tag{3.162}$$

$$\frac{dG_{nlj}}{dr} + \frac{k}{r}G_{nlj}(r) - \left(\frac{2}{\alpha^2} + \epsilon_{nlj} - V(r)\right)\alpha F_{nlj}(r) = 0, \tag{3.163}$$

This represents a set of 2 coupled equations for the down and up component of the Dirac spinor, that here we indicate with $F_{nlj}(r)$ and $G_{nlj}(r)$ (the index n corresponds to the principal quantum number, l is the orbital number and j the quantum number of the total angular momentum operator). $\frac{G_{nlj}(r)}{r}$ represents the positive energy spinor, while $\frac{F_{nlj}(r)}{r}$ is the negative energy spinor that can be found mixed with positive energy states in heavy atoms within the core region. Here k is the Dirac quantum number, while ϵ_{nlj} is the energy eigenvalue and $V(r)$ the centro - symmetric potential.

Within the Kohn-Sham DFT formalism the effective equation for the spinors does not require in practice much more computational effort with respect to Eq. (3.162). The only difference is, in fact, given by the substitution of the ionic potential $V(r)$ with the effective single particle radial Kohn-Sham potential $v_s(r)$, which depends only on the radial component of the spinor wave function,

$$v_s(r) = v_{ext}(r) + v_H[n](r) + v_{xc}[n](r), \tag{3.164}$$

$$v_H[n](r) = 4\pi e^2\left[\frac{1}{r}\int_0^r dx\, x^2 n(x) + \int_r^\infty dx\, x n(x)\right], \tag{3.165}$$

$$v_{xc}[n](r) = \frac{\delta E_{xc}[n]}{\delta n(r)}, \tag{3.166}$$

$$n(r) = \sum_{n,l,j\in \text{occ.}} \frac{|F_{nlj}|^2 + |G_{nlj}|^2}{4\pi r^2}. \tag{3.167}$$

An alternative path to the complete solution of the Dirac equation is given by the so called scalar relativistic equation [110], where the last term on the left hand

side of equation

$$-\frac{1}{2M(r)}\left[\frac{d^2}{dr^2}G_{nlj}(r)+\frac{2}{r}\frac{d}{dr}G_{nlj}(r)-\frac{l(l+1)}{r^2}G_{nlj}(r)\right]-$$
$$-\frac{V(r)'}{4M(r)^2c^2}\frac{dG_{nlj}}{dr}+V(r)G_{nlj}(r)-\frac{k+1}{r}\frac{V(r)'G_{nlj}(r)}{4M(r)^2c^2}=\epsilon_{nlj}G_{nlj}(r), \quad (3.168)$$

representing the spin orbit coupling, makes the spin not a good quantum number for the radial wave functions. This term can be averaged out leading to solutions described in terms of the usual spin and orbital quantum numbers. The spin orbit coupling is usually later added to the Hamiltonian in the form of a perturbation potential.

$$\langle l,m_l,m_s\big|H\big|l',m_l',m_s'\rangle=\epsilon_{l,m_l,m_s}\langle l,m_l,m_s\big|l',m_l',m_s'\rangle+$$
$$+\delta_{l,l'}\int \mathrm{d}^3r\left[\frac{G_{nlm_l}(r)}{2M(r)c}\right]^2\frac{V(r)'}{r}\Upsilon_l^{m_l}(\Omega)^*\chi_{m_s}^*\hat{\boldsymbol{\sigma}}\cdot\hat{\mathbf{L}}\Upsilon_{l'}^{m_l'}(\Omega)\chi_{m_s'}. \quad (3.169)$$

The fully relativistic equations are expressed, instead, in terms of the Dirac quantum number k that specifies both the angular momentum, l, and the total angular momentum, j, for the spinor wave function

$$k=\begin{cases}-\left(j+\frac{1}{2}\right) & \text{if } j=\left(l+\frac{1}{2}\right)\\ j+\frac{1}{2} & \text{if } j=\left(l-\frac{1}{2}\right).\end{cases} \quad (3.170)$$

The wave function of the positive energy states will have then the following form

$$\hat{\Psi}_{njlM}(\mathbf{r})=G_{nlj}(r)\hat{\Phi}_M^j(\Omega), \quad (3.171)$$

where $\hat{\Phi}_M^j(\Omega)$ is the angular component of the wave function

$$\Phi_M^j(\Omega)=\sqrt{\frac{l+m+1}{2l+1}}\Upsilon_l^m(\Omega)\hat{\chi}_\uparrow+\sqrt{\frac{l-m}{2l+1}}\Upsilon_l^{m+1}(\Omega)\hat{\chi}_\downarrow. \quad (3.172)$$

In Eq. (3.172) $\Upsilon_l^m(\Omega)$ are the spherical harmonics, $\hat{\chi}_{\uparrow,\downarrow}$ the spinors, $j=l+\frac{1}{2}$, $M=m+\frac{1}{2}$, and

$$\Phi_M^j(\Omega)=\sqrt{\frac{l-m+1}{2l+1}}\Upsilon_l^{m-1}(\Omega)\hat{\chi}_\uparrow-\sqrt{\frac{l+m}{2l+1}}\Upsilon_l^m(\Omega)\hat{\chi}_\downarrow, \quad (3.173)$$

with $M=m-\frac{1}{2}$. It is possible now to introduce for each orbital number, l, two pseudo-potentials

$$V_{l\pm\frac{1}{2}}^{(1)}(r)=[1-f(r/r_{\mathrm{cl}})]v_{\mathrm{s}}(r)+C_{l\pm\frac{1}{2}}f(r/r_{\mathrm{cl}}). \quad (3.174)$$

Where $v_s(r)$ is the self consistent Kohn-Sham potential for the all electron calculation. The coefficients $C_{l\pm\frac{1}{2}}$ are then chosen in such a way that, when $V^{(1)}_{l\pm\frac{1}{2}}$ is used in the Kohn-Sham equation, we obtain nodeless wave functions with eigenvalues coincident with those obtained from the Dirac equation with $k = -l - 1$ and $k = l$ respectively. The cut - off function $f(x)$ is defined in the following way

$$f(x) = \begin{cases} 1 & \text{if } x \to 0, \\ 0 & \text{if } x \to \infty. \end{cases} \tag{3.175}$$

The radial wave function, solution of the all electron DFT problem, is then modified into

$$G^{(2)}_{n,l\pm\frac{1}{2}}(r) = \gamma_{l\pm\frac{1}{2}}\left[G^{(1)}_{n,l\pm\frac{1}{2}}(r) + \delta_{l\pm\frac{1}{2}} g_{l\pm\frac{1}{2}}(r/r_{\text{cl}})\right]. \tag{3.176}$$

The final pseudo-potential $V^{(2)}_{l\pm\frac{1}{2}}(r)$ is then obtained by inversion of the Kohn-Sham equation under the condition to reproduce the eigenfunction $G^{(2)}_{n,l\pm\frac{1}{2}}(r)$ with eigenvalue $\epsilon_{n,l\pm\frac{1}{2}}$ and the ionic part is obtained by subtracting the Hartree and the exchange-correlation contributions,

$$V^{\text{PS}}_{\text{ion}}(r) = \sum_{l,m}\left[\left|\Phi_{Mj}\right\rangle\left\langle\Phi_{Mj}\right| V^{\text{ion}}_{l+\frac{1}{2}}(r) + \left|\Phi_{M'j'}\right\rangle\left\langle\Phi_{M'j'}\right| V^{\text{ion}}_{l-\frac{1}{2}}(r)\right], \tag{3.177}$$

with $j = l + \frac{1}{2}$, $j' = l - \frac{1}{2}$, $M = m + \frac{1}{2}$ and $M' = m - \frac{1}{2}$. We want now to express the ionic pseudo-potential (3.177) in a form that is explicitly dependent from the spin orbit coupling. We start by rewriting the orbital function as

$$\left|\Phi_{Mj}\right\rangle = \sqrt{\frac{l+m+1}{2l+1}}\hat{\chi}_\uparrow \otimes |l, m\rangle + \sqrt{\frac{l-m}{2l+1}}\hat{\chi}_\downarrow \otimes |l, m+1\rangle\,. \tag{3.178}$$

By making use of the scaling relation for the orbital moment operator we have

$$\hat{L}_\pm |l, m\rangle = \hbar\sqrt{(l \mp m)(l \pm m + 1)}\,|l, m \pm 1\rangle\,, \tag{3.179}$$

where the operator $\hat{L}_\pm = \hat{L}_x \pm i\hat{L}_y$ has been introduced, and

$$|l, m+1\rangle = \frac{\hat{L}_+ |l, m\rangle}{\sqrt{(l-m)(l+m+1)}}, \tag{3.180}$$

$$\left|\Phi_{Mj}\right\rangle = \sqrt{\frac{l+m+1}{2l+1}}\hat{\chi}_\uparrow \otimes |l, m\rangle + \frac{\hat{L}_+}{\sqrt{(2l+1)(l+m+1)}}\hat{\chi}_\downarrow \otimes |l, m\rangle\,. \tag{3.181}$$

The projector over the state $\left|\Phi_{Mj}\right\rangle$ is given by the sum of 4 different term

$$\left|\Phi_{Mj}\right\rangle\left\langle\Phi_{Mj}\right| = \frac{l+m+1}{2l+1}\hat{P}_{l,m,m}\otimes\hat{X}_{\uparrow}\hat{X}_{\uparrow}^{\dagger} + \frac{\sqrt{(l+m+1)(l-m)}}{2l+1}\hat{P}_{l,m,m+1}\otimes\hat{X}_{\uparrow}\hat{X}_{\downarrow}^{\dagger} + \\ + \frac{\sqrt{(l-m)(l+m+1)}}{2l+1}\hat{P}_{l,m+1,m}\otimes\hat{X}_{\downarrow}\hat{X}_{\uparrow}^{\dagger} + \frac{l-m}{2l+1}\hat{P}_{l,m+1,m+1}\otimes\hat{X}_{\downarrow}\hat{X}_{\uparrow}^{\dagger}, \tag{3.182}$$

where we used the following convention for the projectors

$$\hat{P}_{l,m_1,m_2} = |l,m_1\rangle\langle l,m_2|\,. \tag{3.183}$$

The following summation now becomes

$$\sum_{l,m}\left|\Phi_{Mj}\right\rangle\left\langle\Phi_{Mj}\right|V_{l+\frac{1}{2}}^{\text{ion}}(r) = \sum_{m,l}V_{l+\frac{1}{2}}^{\text{ion}}(r)\Big[\frac{l+m+1}{2l+1}\hat{P}_{l,m,m}\otimes\hat{X}_{\uparrow}\hat{X}_{\uparrow}^{\dagger} + \\ + \frac{l-m+1}{2l+1}\hat{P}_{l,m,m}\otimes\hat{X}_{\downarrow}\hat{X}_{\downarrow}^{\dagger} + \frac{\sqrt{(l+m)(l-m+1)}}{2l+1}\hat{P}_{l,m-1,m}\otimes\hat{X}_{\uparrow}\hat{X}_{\downarrow}^{\dagger} + \\ + \frac{\sqrt{(l-m)(l+m+1)}}{2l+1}\hat{P}_{l,m+1,m}\otimes\hat{X}_{\downarrow}\hat{X}_{\uparrow}^{\dagger}\Big]. \tag{3.184}$$

By making use of the Pauli matrices and the orbital moment operators the previous expression becomes

$$\sum_{l,m}\left|\Phi_{Mj}\right\rangle\left\langle\Phi_{Mj}\right|V_{l+\frac{1}{2}}^{\text{ion}}(r) = \sum_{m,l}V_{l+\frac{1}{2}}^{\text{ion}}(r)\Big[\frac{l+m+1}{2(2l+1)}\hat{P}_{l,m,m}\otimes(\bullet + \hat{\sigma}_z) + \\ + \frac{1}{2(2l+1)}\hat{L}_{-}\hat{P}_{l,m,m}\otimes(\hat{\sigma}_x + i\hat{\sigma}_y) + \frac{1}{2(2l+1)}\hat{L}_{+}\hat{P}_{l,m,m}\otimes(\hat{\sigma}_x - i\hat{\sigma}_y) + \\ + \frac{l-m+1}{2(2l+1)}\hat{P}_{l,m,m}\otimes(\bullet - \hat{\sigma}_z)\Big], \tag{3.185}$$

$$\sum_{l,m}\left|\Phi_{Mj}\right\rangle\left\langle\Phi_{Mj}\right|V_{l+\frac{1}{2}}^{\text{ion}}(r) = \sum_{m,l}V_{l+\frac{1}{2}}^{\text{ion}}(r)\Big[\frac{l+m+1}{2(2l+1)}\bullet\otimes(\bullet + \hat{\sigma}_z) + \\ + \frac{1}{2(2l+1)}\hat{L}_{-}\otimes\hat{S}_{+} + \frac{1}{2(2l+1)}\hat{L}_{+}\otimes\hat{S}_{-} + \frac{l-m+1}{2(2l+1)}\bullet\otimes(\bullet - \hat{\sigma}_z)\Big]|l,m\rangle\langle l,m|\,, \tag{3.186}$$

$$\sum_{l,m}\left|\Phi_{Mj}\right\rangle\left\langle\Phi_{Mj}\right|V_{l+\frac{1}{2}}^{\text{ion}}(r) = \sum_{m,l}V_{l+\frac{1}{2}}^{\text{ion}}(r)\Big[\frac{l+1}{2l+1}\bullet + \frac{m}{2l+1}\bullet\otimes\hat{\sigma}_z + \\ + \frac{1}{2(2l+1)}(\hat{L}_{-}\otimes\hat{S}_{+} + \hat{L}_{+}\otimes\hat{S}_{-})\Big]|l,m\rangle\langle l,m|\,. \tag{3.187}$$

By making use of the relation between operators

$$\hat{L}_- \otimes \hat{S}_+ + \hat{L}_+ \otimes \hat{S}_- = 2\hat{\boldsymbol{S}} \otimes \hat{\boldsymbol{L}} - 2\hat{S}_z \otimes \hat{L}_z, \tag{3.188}$$

and by substituting this into (3.187) we obtain

$$\sum_{l,m} \left|\Phi_{Mj}\right\rangle \left\langle\Phi_{Mj}\right| V^{\text{ion}}_{l+\frac{1}{2}}(r) = \sum_{m,l} V^{\text{ion}}_{l+\frac{1}{2}}(r) \left[\left(\frac{1}{2} + \frac{1}{2(2l+1)}\right)\bullet + \frac{1}{2l+1}\hat{\boldsymbol{S}} \otimes \hat{\boldsymbol{L}}\right] |l,m\rangle \langle l,m| \,. \tag{3.189}$$

The second term in the expression for the ionic pseudo-potential may be also written in the form

$$\sum_{l,m} \left|\Phi_{M'j'}\right\rangle \left\langle\Phi_{M'j'}\right| V^{\text{ion}}_{l-\frac{1}{2}}(r) = \sum_{m,l} V^{\text{ion}}_{l-\frac{1}{2}}(r) \left[\left(\frac{1}{2} - \frac{1}{2(2l+1)}\right)\bullet - \frac{1}{2l+1}\hat{\boldsymbol{S}} \otimes \hat{\boldsymbol{L}}\right] |l,m\rangle \langle l,m| \,. \tag{3.190}$$

By summing up the two equations we obtain the final expression for the pseudo-potential

$$\hat{V}^{\text{PS}}_{\text{ion}}(r) = \sum_{m,l} \left[\left(\bar{V}^{\text{ion}}_l(r) + \frac{1}{2}V^{\text{SO}}_l(r)\right)\bullet + V^{\text{SO}}_l(r)\hat{\boldsymbol{S}} \cdot \hat{\boldsymbol{L}}\right] |l,m\rangle \langle l,m| \,, \tag{3.191}$$

where we have introduced the ionic orbital resolved component

$$\bar{V}^{\text{ion}}_l(r) = \frac{1}{2}\left[V^{\text{ion}}_{l+\frac{1}{2}}(r) + V^{\text{ion}}_{l-\frac{1}{2}}(r)\right], \tag{3.192}$$

and the spin orbit coupling component

$$V^{\text{SO}}_l(r) = \frac{1}{2l+1}\left[V^{\text{ion}}_{l+\frac{1}{2}}(r) - V^{\text{ion}}_{l-\frac{1}{2}}(r)\right]. \tag{3.193}$$

Eq. (3.191) represents the final form for the fully relativistic ionic pseudo-potential, its implementation in place of the full external ionic potential $v_{\text{ext}}(\mathbf{r})$ in the SDFT Kohn-Sham equations (3.60) leads to

$$\left[-\frac{\nabla^2}{2} + v_s(\mathbf{r}) + \mu_B \hat{\boldsymbol{\sigma}} \cdot \mathbf{B}_s(\mathbf{r})\right] \psi_{i,\alpha}(\mathbf{r}) = \epsilon_{i,\alpha}\psi_{i,\alpha}(\mathbf{r}), \tag{3.194}$$

where the non interacting Kohn-Sham potential is expressed as follows

$$v_s(\mathbf{r}) = \int d^3r' \frac{n(\mathbf{r}')}{|\mathbf{r} - \mathbf{r}'|} + v_{\text{xc}}(\mathbf{r}) + \hat{V}^{\text{PS}}_{\text{ion}}(\mathbf{r}). \tag{3.195}$$

Until now we have focused our discussion only on the ground-state version of the density functional formalism. Since in the next chapters we will deal with time-evolving electronic systems, it is time to look in which way this theory, in all its different flavours, may be applied to study time-dependent problems. This will be the argument of the final sections of this Chapter.

3.5 Time Dependent Density Functional Theory

The problem of studying the dynamical evolution of a system of N interacting electrons is in principle more complicated than its ground-state equivalent. In the most general case we will face the problem of finding a solution of the full time dependent many-body Schrödinger equation

$$i\hbar\frac{\partial\Psi}{\partial t} = \hat{H}(t)\Psi(t), \tag{3.196}$$

where the full many body Hamiltonian is

$$\hat{H}(t) = \hat{T} + \hat{V}_{ee} + \hat{V}_{ext}. \tag{3.197}$$

$\hat{T}$ and $\hat{V}_{ee}$ are the usual kinetic energy operator and the electron-electron interaction potential, while $\hat{V}_{ext}$ represents a generic external potential acting on the electronic gas. Obtaining a solution for this problem is an incredibly difficult task.

Time Dependent Density Functional Theory (TD-DFT) allows one to solve (3.196) within the same framework of its ground-state equivalent given that all the observables we are interested in may be calculated in terms of the one and two particle densities. The full knowledge of the many-body wave function $\Psi(t)$ is not required in order to extract informations on the dynamical evolution of the system.

Similarly to ground-state - DFT, the central theorem of TD-DFT proves the existence of a one to one correspondence between the external time-dependent potential $v_{ext}(\mathbf{r}, t)$ and the one particle electron density $n(\mathbf{r}, t)$, when the many body system evolves from a fixed initial state Ψ_0 [112]. This is the so called Runge-Gross theorem (RG)

$$\Psi_0 : v_{ext} \leftrightarrow n. \tag{3.198}$$

The backward arrow tells us that a given time-dependent electron density will be the solution of only one time-dependent external scalar potential, that is the result of the RG theorem. The forward arrow follows instead from the uniqueness of the solution of the time dependent Schrödinger equation.

For a certain initial state, Ψ_0, the time-dependent density $n(\mathbf{r}, t)$ defines the external potential $v_{ext}(\mathbf{r}, t)$ up to a purely time-dependent constant $C(t)$. As a consequence there is a gauge freedom in the definition of the time-dependent phase of the Kohn-Sham electronic wave function

$$\Psi(t) = e^{-i\alpha(t)}\Psi[n, \Psi_0](t). \tag{3.199}$$

Every observable expectation value becomes then a functional of the time-dependent density and of the initial state.

$$\langle\hat{O}(t)\rangle = O[n, \Psi_0](t). \tag{3.200}$$

It is important to notice that, in order to prove the existence of the one-to-one mapping between the density and the potential, a continuity equation is invoked. This fact has an important consequence. While in TDCDFT (time dependent extension of CDFT) the Kohn-Sham current corresponds to the true current of the interacting system, in TDDFT the current is not a fundamental variable of the theory. From the continuity equation we have in fact that the Kohn-Sham paramagnetic current,

$$\mathbf{j}_{\mathrm{KS}}(\mathbf{r},t) = \frac{\hbar}{2mi}\sum_{j\in\mathrm{occ.}}[\psi^*_{j\mathrm{KS}}(\mathbf{r},t)\nabla\psi_{j\mathrm{KS}}(\mathbf{r},t) - \nabla\psi^*_{j\mathrm{KS}}(\mathbf{r},t)\psi_{j\mathrm{KS}}(\mathbf{r},t)], \tag{3.201}$$

needs to verify the following relation

$$\frac{\partial}{\partial t}n(\mathbf{r},t) + \nabla\cdot\mathbf{j}_{\mathrm{KS}}(\mathbf{r},t) = 0. \tag{3.202}$$

For a given electron density this continuity equation is not sufficient to uniquely determine the paramagnetic current of the theory and the Kohn-Sham current does not correspond to the many body paramagnetic current. By introducing a new term $\mathbf{C}(\mathbf{r},t)$ such that

$$\mathbf{j}'_{\mathrm{KS}}(\mathbf{r},t) = \mathbf{j}_{\mathrm{KS}}(\mathbf{r},t) + \mathbf{j}_{\mathrm{xc}}(\mathbf{r},t), \tag{3.203}$$

$$\mathbf{j}_{\mathrm{xc}}(\mathbf{r},t) = \nabla\times\mathbf{C}(\mathbf{r},t), \tag{3.204}$$

the continuity equation for the electron density $n(\mathbf{r},t)$ is still valid. However, we have an infinite number of possible paramagnetic currents for a single given electron density.

Following the same procedure used in static DFT, we introduce a fictitious non-interacting system of electrons called the Kohn-Sham system, defined to exactly reproduce the density of the true interacting system. Then, like in the static case, all the properties of the interacting system can be derived by using the density of the Kohn-Sham system. The RG theorem guarantees that the one-to-one correspondence between time-dependent densities and time-dependent external potentials holds true for both the fully interacting and the non interacting system. Thus, we have two potentials corresponding to a given time-dependent density $n(\mathbf{r},t)$

1. $v_{\mathrm{ext}}[n,\Psi_0](\mathbf{r},t)$ that yields the density $n(\mathbf{r},t)$ by propagating the time dependent Schrödinger equation starting from the interacting many particles ground-state Ψ_0.
2. $v_{\mathrm{s}}[n,\Phi_0](\mathbf{r},t)$, which instead yields the same density by propagating the non-interacting TDSE starting from the non-interacting many particles ground state, Φ_0.

Furthermore we have the one to one correspondence

$$v_{\mathrm{ext}}[n,\Psi_0](\mathbf{r},t) \leftrightarrow n(\mathbf{r},t) \leftrightarrow v_{\mathrm{s}}[n,\Phi_0](\mathbf{r},t). \tag{3.205}$$

This means that the density of the interacting system can be written as

$$n(\mathbf{r},t) = \sum_{i=1}^{N} |\phi_i(\mathbf{r},t)|^2, \tag{3.206}$$

where the set of single-particle orbitals satisfies the time-dependent Kohn-Sham equations

$$i\hbar\frac{\partial}{\partial t}\phi_j^{\mathrm{KS}}(\mathbf{r},t) = \left[-\frac{\hbar^2\nabla^2}{2m} + v_{\mathrm{s}}[n,\Phi_0](\mathbf{r},t)\right]\phi_j^{\mathrm{KS}}(\mathbf{r},t). \tag{3.207}$$

As in the static case, the Kohn-Sham potential can be decomposed into three components

$$v_{\mathrm{s}}[n,\Phi_0](\mathbf{r},t) = v_{\mathrm{ext}}[n,\Psi_0](\mathbf{r},t) + \int_V \mathrm{d}^3r' \frac{n(\mathbf{r}')}{|\mathbf{r}-\mathbf{r}'|} + v_{\mathrm{xc}}[n,\Psi_0,\Phi_0](\mathbf{r},t). \tag{3.208}$$

From the knowledge of the true exchange-correlation potential, $v_{\mathrm{xc}}[n,\Phi_0,\Psi_0]$, defined as the difference between the external potential v_{ext} that generates the electron density $n(\mathbf{r},t)$ in an interacting system starting from the initial state Ψ_0 and the one-body potential that generates the same density from an initial non-interacting state Φ_0, we can propagate in time the set of Kohn-Sham equations and finally obtain the correct value of the full interacting electron density $n(\mathbf{r},t)$. The fundamental difference with respect to ground-state DFT is that now the exchange-correlation potential depends not only on the density but also on the full interacting and the non-interacting initial states. In the cases in which both Ψ_0 and Φ_0 are not degenerate ground-states, these are still functionals of the density alone and the exchange-correlation potential becomes a simple functional of the density.

Unfortunately the exact functional of the theory has *memory*, namely it depends on the history of the density as well as the interacting and non-interacting initial states.

Almost all the functionals commonly in use have no memory dependence. In contrast they are adiabatic functionals, meaning that the time-dependent functional is constructed from the ground-state one, calculated at the instantaneous density $n(t)$,

$$v_{\mathrm{xc}}^{\mathrm{adia}}[n](\mathbf{r},t) = v_{\mathrm{xc}}^{\mathrm{GS}}[n(t)](\mathbf{r}). \tag{3.209}$$

If the external time-dependence is slow and the system starts the evolution from its ground-state the approximation is in general justified.

The simplest possible approximation in TDDFT is the adiabatic local density approximation or ALDA

$$v_{\mathrm{xc}}^{\mathrm{ALDA}}[n](\mathbf{r},t) = v_{\mathrm{xc}}^{\mathrm{LDA}}[n(\mathbf{r},t)]. \tag{3.210}$$

This is used in the majority of the applications nowadays and despite its simplicity it performs quite well. This is due to the fact that it also satisfies several exact conditions. Any attempt to include memory effects in the exchange-correlation functional goes beyond the adiabatic approximation. The two most important examples of non adiabatic approximations are

Kohn - Gross approximation this is characterized by the use of the local frequency dependent kernel of the uniform electronic gas

$$f_{\mathrm{xc}}^{\mathrm{GK}}(\mathbf{r},\mathbf{r}',\omega) = \delta(\mathbf{r}-\mathbf{r}')f_{\mathrm{xc}}^{\mathrm{unif}}(n(\mathbf{r}),\omega),$$

where the exchange-correlation kernel is defined as

$$f_{\mathrm{xc}}(\mathbf{r},t,\mathbf{r}',t') = \frac{\delta v_{\mathrm{xc}}(\mathbf{r},t)}{\delta n(\mathbf{r}',t)}. \tag{3.211}$$

The causality requirement for the exchange-correlation kernel is equivalent to the condition $f_{\mathrm{xc}}(\mathbf{r},t,\mathbf{r}',t') = 0$ for $t < t'$.

Vignale - Kohn approximation this is simply the gradient expansion in the current density of the energy functional.

As in the case of ground state - DFT we show a set of exact conditions that should be met by any exchange-correlation functional in TD-DFT.

Adiabatic limit: this is the simplest exact condition for the exchange-correlation functional. It states that when the time dependence of the electronic system becomes very slow, the functionals must reduce to their adiabatic equivalents

$$v_{\mathrm{xc}}(\mathbf{r},t) \to v_{\mathrm{xc}}^{\mathrm{GS}}[n(t)](\mathbf{r}).$$

Any adiabatic approximation satisfies this condition by construction, and so does the exact exchange functional.

Zero exchange - correlation force and torque: this condition states that particle-particle interactions cannot generate a net force on the electronic system [113, 114]

$$\int \mathrm{d}^3 r\, n(\mathbf{r},t)\nabla v_{\mathrm{xc}}(\mathbf{r},t) = 0,$$

nor a net torque

$$\int \mathrm{d}^3 r\, n(\mathbf{r},t)\mathbf{r}\times\nabla v_{\mathrm{xc}}(\mathbf{r},t) = \int \mathrm{d}^3 r\, \mathbf{r}\times\frac{\partial \mathbf{j}_{\mathrm{xc}}}{\partial t},$$

where $\mathbf{j}_{\mathrm{xc}}(\mathbf{r},t)$ represents the difference between the full interacting paramagnetic current and the Kohn-Sham current (3.201). The zero-torque condition tells us that no global torque can act on the electronic gas, if Kohn-Sham current and many body current coincide. As we have already seen this is not true within TD-DFT, but it is within the time-dependent

current DFT (TD-CDFT) formalism. These conditions are met by all the previously mentioned exchange-correlation functionals.

Self interaction: The condition for one electron systems

$$v_x(\mathbf{r},t) = -\int d^3r' \frac{n(\mathbf{r}',t)}{|\mathbf{r}-\mathbf{r}'|},$$

$$v_c(\mathbf{r},t) = 0,$$

is satisfied only by the EXX approximation. ALDA violates this condition since also LDA violates it in ground state - DFT.

In the next section we will see, instead, how this general time-dependent formalism may be expanded to include also the magnetization as a fundamental variable of the theory.

3.6 Time Dependent Spin Density Functional Theory

The aim of Time Dependent Spin Density Functional Theory (TD-SDFT), in its more general non-collinear version, is to study the dynamics of the spin degrees of freedom in order to provide a proper ab initio treatment of phenomena like spin-wave excitations, Bloch wall motion, spin injection and spin filtering, which are increasingly important in the field of spintronics [116].

In this section and in the rest of the Chapter when we talk about SDFT we are considering its spin-unrestricted formulation. Its time-dependent extension will predict the value at any time of the true many-body electron density $n(\mathbf{r},t)$ and of the three magnetization components $\mathbf{m}(\mathbf{r},t)$.

Making use of the Kohn-Sham prescription, by assuming the existence of an equivalent non-interacting system with same density and magnetization at any time, as we have done in the case of TD-DFT, we obtain the set of time dependent Kohn - Sham equations

$$i\hbar\frac{\partial}{\partial t}\hat{\psi}_j^{KS}(\mathbf{r},t) = \hat{H}_{KS}(\mathbf{r},t)\hat{\psi}_j^{KS}(\mathbf{r},t), \tag{3.212}$$

where the time dependent Kohn-Sham Hamiltonian becomes

$$\hat{H}_{KS}(\mathbf{r},t) = -\frac{\hbar^2\nabla^2}{2m} + v_s[n,\Phi_0](\mathbf{r},t) + \mu_B\mathbf{B}_s[\mathbf{m},\Phi_0](\mathbf{r},t)\cdot\hat{\sigma}. \tag{3.213}$$

In Eq. (3.213) $v_s(\mathbf{r},t)$ is the time dependent version of the non interacting scalar potential

$$v_s(\mathbf{r},t) = \int d^3r' \frac{n(\mathbf{r}',t)}{|\mathbf{r}-\mathbf{r}'|} + v_{xc}(\mathbf{r},t) + v_{ext}(\mathbf{r},t), \tag{3.214}$$

where in the adiabatic approximation v_{xc} is obtained from the ground-state exchange-correlation potential by substituting the ground-state density with the density at different times during the evolution. we also assume that the initial state is completely specified by the ground state densities (this is true in the general non-collinear case)

$$v_{xc}(\mathbf{r}, t) = v_{xc}^{GS}[n(t)](\mathbf{r}). \tag{3.215}$$

The external potential $v_{ext}(\mathbf{r}, t)$ is a scalar function of the spatial coordinates and time. The non interacting magnetic field $\mathbf{B}_s(\mathbf{r}, t)$ is given by the sum of an external time-dependent magnetic field $\mathbf{B}_{ext}(\mathbf{r}, t)$ with the exchange-correlation component, $\mathbf{B}_{xc}$, in the adiabatic approximation we have

$$\mathbf{B}_s(\mathbf{r}, t) = \mathbf{B}_{ext}(\mathbf{r}, t) + \mathbf{B}_{xc}[\mathbf{m}(t)](\mathbf{r}). \tag{3.216}$$

As we have already seen in the case of static SDFT the time-dependent current $\mathbf{j}(\mathbf{r}, t)$ is not a basic variable of the theory. From the knowledge of the Kohn-Sham orbitals, $\psi_j^{KS}(\mathbf{r}, t)$, we can extract the expectation value of the current operator

$$\hat{\mathbf{j}}(\mathbf{r}) = \frac{\hbar}{2mi} \sum_{i=1}^{N} [\nabla_i \delta(\mathbf{r} - \mathbf{r}_i) + \delta(\mathbf{r} - \mathbf{r}_i)\nabla_i], \tag{3.217}$$

$$\langle \Phi_{KS}(t)|\hat{\mathbf{j}}(\mathbf{r})|\Phi_{KS}(t)\rangle = -\frac{i\hbar}{2m} \sum_{j \in occ.} [\psi_j^{KS}(\mathbf{r}, t)^* \nabla \psi_j^{KS}(\mathbf{r}, t) - \nabla \psi_j^{KS}(\mathbf{r}, t)^* \psi_j^{KS}(\mathbf{r}, t)], \tag{3.218}$$

where the expectation value of the operator is evaluated over the time dependent Kohn-Sham Slater determinant $\Phi_{KS}(t)$. This object is the time-dependent Kohn-Sham current $\mathbf{j}_{KS}(\mathbf{r}, t)$, that is formally not equivalent to the true many-body current in TD-SDFT. The same argument is also valid in the case of the more general spin current tensor $\mathbf{J}_{KS,\lambda}(\mathbf{r}, t)$. In order to shed some light on the relationship between the Kohn-Sham and the many-body currents, we consider the equation of motion for the magnetization vector $\mathbf{m}(\mathbf{r}, t)$ predicted from the true many-body system Hamiltonian and from the non-interacting Kohn-Sham system Hamiltonian [97]. Starting from the many-body Hamiltonian,

$$\hat{H}(t) = \hat{T} + \hat{W} + \int d^3r \, [\hat{\mathbf{m}}(\mathbf{r}) \cdot \mathbf{B}_{ext}(\mathbf{r}, t) + \hat{n}(\mathbf{r}) v_{ext}(\mathbf{r}, t)], \tag{3.219}$$

the continuity equation for the magnetization density can be obtained by using the Heisenberg equation of motion for the operators

$$\frac{d}{dt} m_\lambda(\mathbf{r}, t) = -\nabla \cdot \mathbf{J}_\lambda(\mathbf{r}, t) + \mu_B [\mathbf{m}(\mathbf{r}, t) \times \mathbf{B}_{ext}(\mathbf{r}, t)]_\lambda. \tag{3.220}$$

With the same procedure an analogous continuity equation can be obtained for the non interacting Kohn-Sham system

$$\frac{d}{dt} m_\lambda(\mathbf{r}, t) = -\nabla \cdot \mathbf{J}_\lambda^{\mathrm{KS}}(\mathbf{r}, t) + \mu_B [\mathbf{m}(\mathbf{r}, t) \times \mathbf{B}_{\mathrm{s}}(\mathbf{r}, t)]_\lambda. \tag{3.221}$$

The comparison of the two continuity equations gives us

$$\nabla \cdot [\mathbf{J}_\lambda^{\mathrm{KS}}(\mathbf{r}, t) - \mathbf{J}_\lambda(\mathbf{r}, t)] = \mu_B [\mathbf{m}(\mathbf{r}, t) \times (\mathbf{B}_{\mathrm{s}}(\mathbf{r}, t) - \mathbf{B}_{\mathrm{ext}}(\mathbf{r}, t))]_\lambda, \tag{3.222}$$

where we identify

$$\mathbf{J}_{\mathrm{KS}}^\lambda(\mathbf{r}, t) - \mathbf{J}^\lambda(\mathbf{r}, t) = \mathbf{J}_{\mathrm{xc}}^\lambda(\mathbf{r}, t). \tag{3.223}$$

$\mathbf{J}_{\mathrm{xc}}^\lambda(\mathbf{r}, t)$ represents the many-body correction to the Kohn-Sham spin current and satisfies the equation

$$\nabla \cdot \mathbf{J}_{\mathrm{xc}}^\lambda(\mathbf{r}, t) = \mu_B [\mathbf{m}(\mathbf{r}, t) \times \mathbf{B}_{\mathrm{xc}}(\mathbf{r}, t)]_\lambda. \tag{3.224}$$

By dividing $\mathbf{J}^\lambda(\mathbf{r}, t)$ into a longitudinal, $\mathbf{J}_L^\lambda$, and a transverse component, $\mathbf{J}_T^\lambda$, Eq. (3.224) tells us that the knowledge of $\mathbf{B}_{\mathrm{xc}}(\mathbf{r}, t)$ within TD-SDFT is sufficient to extract the longitudinal component of the many-body spin current, while the transverse component is not directly accessible from the Kohn-Sham system observables

$$\nabla \cdot \mathbf{J}_{\mathrm{xc},L}^\lambda(\mathbf{r}, t) = \mu_B [\mathbf{m}(\mathbf{r}, t) \times \mathbf{B}_{\mathrm{xc}}(\mathbf{r}, t)]_\lambda. \tag{3.225}$$

Of course a full determination of the many-body spin current requires a CDFT formalism, but it is interesting to notice that its longitudinal component is already fully determined from the knowledge of the TD-SDFT exchange-correlation functional. For a large class of systems $\mathbf{J}_{\mathrm{xc},L}$ represents the major many-body correction.

By integrating Eq. (3.224) over the entire space we obtain the zero-torque theorem that we have already established in the SDFT section starting from symmetry considerations

$$\int \mathrm{d}^3 r \, \mathbf{m}(\mathbf{r}, t) \times \mathbf{B}_{\mathrm{xc}}(\mathbf{r}, t) = 0. \tag{3.226}$$

Instead, by integrating over a finite volume we obtain the relation,

$$\mu_B \int_\Omega \mathrm{d}^3 r \, [\mathbf{m}(\mathbf{r}, t) \times \mathbf{B}_{\mathrm{xc}}(\mathbf{r}, t)]_\lambda = \int_{S_\Omega} dS \, \mathbf{J}_{\mathrm{xc}}^\lambda(\mathbf{r}, t), \tag{3.227}$$

which means that the integral over a finite volume of the magnetization torque measures the net flux of $\mathbf{J}_{\mathrm{xc}}$ through the surface associated to such volume Ω.

An important property of the ALDA exchange - correlation functional is that at every instant in time the field $\mathbf{B}_{\mathrm{xc}}(\mathbf{r}, t)$ is parallel to the magnetization vector field, $\mathbf{m}(\mathbf{r}, t)$, at every point $\mathbf{r}$ in space. As a consequence we have that

$$\mathbf{m}(\mathbf{r}, t) \times \mathbf{B}_{\mathrm{xc}}^{\mathrm{ALDA}}[\mathbf{m}(t)](\mathbf{r}) = 0, \tag{3.228}$$

which means that the relation

$$\nabla \cdot \mathbf{J}^{\lambda}_{\mathrm{xc}}(\mathbf{r}, t) = 0, \tag{3.229}$$

is valid also locally. In practice the ALDA satisfies by construction the zero-torque theorem, while the longitudinal component of the current is not modified by the exchange-correlation potential and we have $\mathbf{J}_{\mathrm{xc},L}(\mathbf{r}, t) = 0$.

In conclusion the exchange-correlation field $\mathbf{B}^{\mathrm{ALDA}}_{\mathrm{xc}}(\mathbf{r}, t)$ does not contribute to the spin dynamics. In the ALDA we expect that the only contributions to the spin dynamics originates from the spin currents and from the external magnetic field $\mathbf{B}_{\mathrm{ext}}(\mathbf{r}, t)$, while globally the magnetization vector cannot be torqued if there are no external magnetic fields acting on the system.

3.7 TD-DFT in external electro-magnetic fields

In the previous section we have proved that the DFT formalism can be extended to time-dependent problems, and used to describe the evolution of quantum systems perturbed by the action of an external scalar potential $v_{\mathrm{ext}}(\mathbf{r}, t)$. Within this description the fundamental variable of the theory is the time-dependent electron density, $n(\mathbf{r}, t)$, that is uniquely determined, through the RG theorem, by the external potential $v_{\mathrm{ext}}(\mathbf{r}, t)$ and the initial state Ψ_0. The current $\mathbf{j}(\mathbf{r}, t)$, is not an observable and it is related to the electron density through the constraint provided by the continuity equation

$$\frac{d}{dt} n(\mathbf{r}, t) = -\nabla \cdot \mathbf{j}(\mathbf{r}, t), \tag{3.230}$$

which is not sufficient to generate a one-to-one mapping between the density and the current. Of course, up to this point, we have only a partial picture of the quantum many-body evolution problem. In fact, the restriction to time-dependent scalar potentials alone excludes several other situations involving vector potentials, which arise, for instance, when we apply an external magnetic field to the system. An interesting case is also that of extended periodic systems in a uniform external electric field, that is often used to model the bulk of a crystalline solid in a laser field. Making use of periodic boundary conditions by placing the system on a ring, then the electric field cannot be generated by a scalar potential but only by a time dependent magnetic field through the Faraday's law

$$\frac{d}{dt} \mathbf{B}(\mathbf{r}, t) = -\nabla \times \mathbf{E}(\mathbf{r}, t). \tag{3.231}$$

In order to preserve periodicity, also a solid in an external electric field requires a vector potential. Standard TD-DFT cannot be applied even if $\mathbf{B} = \nabla \times \mathbf{A} = 0$ and, this is intimately connected with the fact that a general time dependent current density is not v-representable in a many-body system [115]. If we want to study

the interaction of matter with electro-magnetic radiation we need to look at the TD-DFT equations involving also vector potentials, not only scalar ones. The details of the development of a TD-DFT set of equations for matter interacting with external electro-magnetic radiation can be found in Ref. [117]. Here we look only at the most important aspects of the Time Dependent Current DFT formalism.

In a N particles system characterized by a single particle scalar potential, $\varphi(\mathbf{r},t)$, by a vector potential, $\mathbf{A}(\mathbf{r},t)$, with Coulombic two-body interactions and single-particle external ionic potential due to the nuclei $v(\mathbf{r})$, the Hamiltonian $H(t)$ can be written as

$$H(t) = \frac{1}{2m}\sum_{k=1}^{N}\Big[-i\hbar\nabla_k + \frac{e}{c}\mathbf{A}(\mathbf{r}_k,t)\Big]^2 + e\sum_{k=1}^{N}[v(\mathbf{r}_k) - \varphi(\mathbf{r}_k,t)] + V_{\mathrm{ee}}. \quad (3.232)$$

In the Coulomb gauge we have $\nabla\cdot\mathbf{A} = 0$, while the single particle densities,

$$n(\mathbf{r},t) = \langle\Psi(t)|\hat{\rho}(\mathbf{r})|\Psi(t)\rangle\,, \quad (3.233)$$

and the current density,

$$\mathbf{j}(\mathbf{r},t) = \langle\Psi(t)|\hat{\mathbf{j}}(\mathbf{r})|\Psi(t)\rangle\,, \quad (3.234)$$

form the basic set of variables of the theory. The main difference with respect to static CDFT is that now the basic variable of the theory is the true physical current, while in ground state CDFT was the paramagnetic current $\mathbf{j}_{\mathrm{p}}(\mathbf{r},t)$.

The extension of the RG theorem to TD-CDFT shows that the current density, $\mathbf{j}(\mathbf{r},t)$, determines both the potentials uniquely. In general two different sets of potentials $(\varphi,\mathbf{A})$ and $(\varphi',\mathbf{A}')$ cannot generate the same current density $\mathbf{j}(\mathbf{r},t)$. Identical densities and current densities would also result in the case that $(\varphi,\mathbf{A})$ is related to $(\varphi',\mathbf{A}')$ through a simple gauge transformation. All the properties of the system are in practice a unique functional of the current density $\mathbf{j}(\mathbf{r},t)$. In fact, from its knowledge, also the electronic density, $n(\mathbf{r},t)$, may be computed at every time through the continuity equation (3.230).

In presence of a vector potential $\mathbf{A}(\mathbf{r},t)$ we have two unique one-to-one mappings, namely

$$\mathbf{j}(\mathbf{r},t) \rightarrow \{\varphi(\mathbf{r},t),\mathbf{A}(\mathbf{r},t)\}, \quad (3.235)$$

together with

$$\mathbf{j}(\mathbf{r},t) \rightarrow n(\mathbf{r},t), \quad (3.236)$$

through the continuity equation for the density. Nevertheless, here, we will treat current and density as separate variables.

It is possible to establish a Kohn-Hohenberg theorem in TD-CDFT by introducing the following functional of the time-dependent current and density

$$\tilde{Q}[n,\mathbf{j}] = \int dt\, \langle \Psi(t)| -i\hbar\partial_t + \hat{V}_{\text{ee}} + \hat{T} + \hat{V}|\Psi(t)\rangle\,, \tag{3.237}$$

where $\hat{V}_{\text{ee}}$ represents the two particles interaction between electrons, $\hat{T}$ is the kinetic part of the Hamiltonian

$$\hat{T} = \frac{1}{2m}\sum_{k=1}^{N}\left(\hat{\mathbf{p}}_k + \frac{e}{c}\mathbf{A}(\mathbf{r}_k,t)\right)^2, \tag{3.238}$$

and $\hat{V}$ represents the scalar single-particle part of the Hamiltonian

$$\hat{V} = \sum_{k=1}^{N}[v(\mathbf{r}_k) - e\varphi(\mathbf{r}_k,t)]. \tag{3.239}$$

For a given set of external potentials $\{v,\varphi,\mathbf{A}\}$ the solution of the dynamical evolution is obtained by imposing the stationarity of the functional $\tilde{Q}_{\{v,\varphi,\mathbf{A}\}}$.

$$\delta\tilde{Q}_{\{v,\varphi,\mathbf{A}\}}[n,\mathbf{j}] = 0. \tag{3.240}$$

This stationarity condition needs to be equivalent to the continuity equations for the exact density

$$\frac{d}{dt}n(\mathbf{r},t) = -\nabla\cdot\mathbf{j}(\mathbf{r},t), \tag{3.241}$$

and the Euler equation for the current

$$\frac{d}{dt}\mathbf{j}(\mathbf{r},t) = \mathbf{P}_{\{v,\varphi,\mathbf{A}\}}[n,\mathbf{j}](\mathbf{r},t), \tag{3.242}$$

$$\mathbf{P}_{\{v,\varphi,\mathbf{A}\}}[n,\mathbf{j}](\mathbf{r},t) = -\frac{i}{\hbar}\langle\Psi(t)|[\hat{\mathbf{j}},\hat{T}_0 + \hat{V}_{\text{ee}}]|\Psi(t)\rangle - \frac{n(\mathbf{r},t)}{m}(\nabla v + e\mathbf{E}) - \frac{e}{mc}\mathbf{j}\times\mathbf{B}, \tag{3.243}$$

where $\hat{T}_0 = \frac{1}{2m}\sum_{k=1}^{N}\hat{\mathbf{p}}_k^2$ is the part of $\hat{T}$ that does not depend on the vector potential.

As in the case of its static equivalent the stationarity condition (3.240) allows the introduction of a more practical Kohn-Sham scheme for the solution of the dynamical problem. By making use of the constrained search formulation for arbitrary $(v,\mathbf{A})$-representable current densities and with the electron density obeying the continuity equation, we can rewrite the functional $\tilde{Q}_{\{v,\varphi,\mathbf{A}\}}[n,\mathbf{j}]$ in the following form

$$\tilde{Q}_{\{v,\mathbf{A},\mathbf{j}\}}[n,\mathbf{j}] = \tilde{Q}[n,\mathbf{j}] + \tilde{Q}^{(2)}[n,\mathbf{j}], \tag{3.244}$$

where

$$\tilde{Q}[n,\mathbf{j}](\mathbf{r},t) = \int dt\, \langle \Psi_s[n,\mathbf{j}]|\hat{T}_0 + \hat{V}_{ee} - i\hbar\partial_t|\Psi_s[n,\mathbf{j}]\rangle\,, \tag{3.245}$$

and

$$\tilde{Q}^{(2)}[n,\mathbf{j}] = \int dt\, \mathrm{d}^3r \left[n(\mathbf{r},t)(v(\mathbf{r}) - e\varphi(\mathbf{r},t)) + \frac{e}{c}\mathbf{A}(\mathbf{r},t)\cdot\mathbf{j}(\mathbf{r},t) - \frac{e^2}{2mc^2}\mathbf{A}(\mathbf{r},t)^2 n(\mathbf{r},t)\right]. \tag{3.246}$$

$\Psi_s[n,\mathbf{j}]$ is the stationary solution for the many-body wave function reproducing the value of $n(\mathbf{r},t)$ and $\mathbf{j}(\mathbf{r},t)$ for the electron density and current density. The stationary solution of the functional (3.244) with respect to variations in $n(\mathbf{r},t)$ and $\mathbf{j}(\mathbf{r},t)$, yields the true many body evolution of the density and current (one has to use the continuity equation as constraint). This generates the following set of TD - KS equations

$$i\hbar\frac{d}{dt}\psi_k^{\mathrm{KS}}(\mathbf{r},t) = \left[\frac{1}{2m}\left(-i\hbar\nabla + \frac{e}{c}\mathbf{A}_{\mathrm{eff}}(\mathbf{r},t)\right)^2 + v_{\mathrm{eff}}(\mathbf{r},t)\right]\psi_k^{\mathrm{KS}}(\mathbf{r},t), \tag{3.247}$$

where we have the following definition for the electron density and the current

$$n(\mathbf{r},t) = \sum_{k\in\mathrm{occ.}} \psi_k^{\mathrm{KS}}(\mathbf{r},t)^*\psi_k^{\mathrm{KS}}(\mathbf{r},t), \tag{3.248}$$

$$\mathbf{j}(\mathbf{r},t) = -\frac{i\hbar}{2m}\sum_{k\in\mathrm{occ.}} [\psi_k^{\mathrm{KS}}(\mathbf{r},t)^*\nabla\psi_k^{\mathrm{KS}}(\mathbf{r},t) - \nabla\psi_k^{\mathrm{KS}}(\mathbf{r},t)^*\psi_k^{\mathrm{KS}}(\mathbf{r},t)] + \frac{e}{mc}n(\mathbf{r},t)\mathbf{A}_{\mathrm{eff}}(\mathbf{r},t). \tag{3.249}$$

The effective potentials are instead defined according to

$$\mathbf{A}_{\mathrm{eff}}(\mathbf{r},t) = \mathbf{A}(\mathbf{r},t) + \frac{c}{e}\frac{\delta U_{\mathrm{int}}}{\delta\mathbf{j}(\mathbf{r},t)} + \frac{c}{e}\frac{\delta E_{\mathrm{xc}}}{\delta\mathbf{j}(\mathbf{r},t)}, \tag{3.250}$$

$$v_{\mathrm{eff}}(\mathbf{r},t) = v(\mathbf{r}) - e\varphi(\mathbf{r},t) + \frac{\delta U_{\mathrm{int}}}{\delta n(\mathbf{r},t)} + \frac{\delta E_{\mathrm{xc}}}{\delta n(\mathbf{r},t)}. \tag{3.251}$$

The TD-KS equations show that the true evolution of the many-body system under the effect of an external time-dependent scalar and vector potential $(\varphi(\mathbf{r},t), \mathbf{A}(\mathbf{r},t))$ is equivalent to the evolution of a non-interacting system in the field of an effective scalar and vector potential $(\varphi_{\mathrm{eff}}(\mathbf{r},t), \mathbf{A}_{\mathrm{eff}}(\mathbf{r},t))$. By looking, in particular, at $\mathbf{A}_{\mathrm{eff}}(\mathbf{r},t)$, we see that it is composed by the sum of three terms. The first term is the external vector potential, while the second one,

$$\frac{\delta U_{\mathrm{int}}}{\delta\mathbf{j}(\mathbf{r},t)} = \int \mathrm{d}^3r' \frac{\mathbf{j}(\mathbf{r},t)}{|\mathbf{r}-\mathbf{r}'|}, \tag{3.252}$$

has a relativistic nature and describes a classical current - current interaction term. This object is usually neglected from the description because its contribution is

supposed to be quite small compared to the others. We have already seen that in the context of static CDFT the exchange-correlation vector potential $\mathbf{A}_{\mathrm{xc}} = \frac{\delta E_{\mathrm{xc}}}{\delta \mathbf{j}_{\mathrm{p}}(\mathbf{r})}$ has not a strong influence on the correct description of the ground-state densities. If we neglect it from the real-time description the effective vector potential finally reduces to

$$\mathbf{A}_{\mathrm{eff}}(\mathbf{r}, t) = \mathbf{A}(\mathbf{r}, t). \tag{3.253}$$

We can now describe the interaction of a many-particle system with both electric and magnetic fields

$$\mathbf{B}(\mathbf{r}, t) = \nabla \times \mathbf{A}(\mathbf{r}, t), \tag{3.254}$$

$$\mathbf{E}(\mathbf{r}, t) = -\frac{1}{c}\frac{\partial \mathbf{A}}{\partial t} - \nabla\varphi(\mathbf{r}, t). \tag{3.255}$$

For instance, in the case of an external homogeneous electric field with no magnetic field, the scalar and vector potentials are reduced in velocity gauge to

$$\mathbf{A}(t) = -c\int_0^t dt' \mathbf{E}(0, t'), \tag{3.256}$$

$$\varphi(\mathbf{r}, t) = 0. \tag{3.257}$$

The final effective fields are given by

$$\mathbf{A}_{\mathrm{eff}}(\mathbf{0}, t) = \mathbf{A}(\mathbf{0}, t), \tag{3.258}$$

$$v_{\mathrm{eff}}(\mathbf{r}, t) = v(\mathbf{r}) + \frac{\delta U_{\mathrm{int}}}{\delta n(\mathbf{r}, t)} + \frac{\delta E_{\mathrm{xc}}}{\delta n(\mathbf{r}, t)}, \tag{3.259}$$

and can be inserted into the set of time-dependent Kohn-Sham equations.

$$i\hbar\frac{d}{dt}\psi_k^{\mathrm{KS}}(\mathbf{r}, t) = \left[\frac{1}{2m}\left(-i\hbar\nabla + \frac{e}{c}\mathbf{A}(\mathbf{0}, t)\right)^2 + v_{\mathrm{eff}}(\mathbf{r}, t)\right]\psi_k^{\mathrm{KS}}(\mathbf{r}, t). \tag{3.260}$$

These equations are equivalent, through a gauge transformation, to the electric dipole approximation, the external potential is then described in terms of a pure scalar time dependent potential and TD-SDFT is therefore suitable to describe this kind of dynamics. Of course in the context of TD-SDFT these equations could be immediately generalized by including the effective non-interacting magnetic field $\mathbf{B}_{\mathrm{s}}(\mathbf{r}, t)$

$$i\hbar\frac{d}{dt}\psi_k^{\mathrm{KS}}(\mathbf{r}, t) = \left[\frac{1}{2m}\left(-i\hbar\nabla + \frac{e}{c}\mathbf{A}(\mathbf{0}, t)\right)^2 + \mu_B\mathbf{B}_{\mathrm{s}}(\mathbf{r}, t)\cdot\hat{\sigma} + v_{\mathrm{s}}(\mathbf{r}, t)\right]\psi_k^{\mathrm{KS}}(\mathbf{r}, t), \tag{3.261}$$

where $\psi_k^{\mathrm{KS}}(\mathbf{r}, t)$ becomes a time dependent Kohn-Sham spinor. The effective non-interacting scalar potential is given by

$$v_{\mathrm{s}}(\mathbf{r}, t) = v_{\mathrm{ext}}(\mathbf{r}) + \int d^3r' \frac{n(\mathbf{r}', t)}{|\mathbf{r} - \mathbf{r}'|} + v_{\mathrm{xc}}(\mathbf{r}, t), \tag{3.262}$$

while in absence of external magnetic field $\mathbf{B}_s(\mathbf{r}, t) = \mathbf{B}_{xc}(\mathbf{r}, t)$. The external scalar potential $v_{ext}(\mathbf{r})$ includes the contributions due to the potential of the separated atoms and the spin-orbit coupling term.

Eq. (3.261) represents our final version of the Kohn-Sham equations for the description of the dynamics of a quantum many body system in an external electromagnetic field and it will be used in the following chapters to describe the ultrafast spin dynamics of magnetic atomic clusters and bulk systems.

CHAPTER 4

THE ROLE OF SPIN ORBIT IN THE ULTRAFAST DEMAGNETIZATION OF TRANSITION METALS

In this Chapter we will apply TDDFT to the problem of ultrafast magnetization dynamics in transition metal clusters. In particular we consider four different types of Fe - based clusters, Fe_2 (Fig. 4.4), Fe_3 (Fig. 4.7), Fe_4 (Fig. 4.11) and Fe_6 (Fig. 4.16). We have already introduced in Chapter 3 the mathematical formalism used to describe non-collinear, semi-relativistic, magnetic systems within the ab-initio TD-SDFT. Here we want just to mention that all these calculations are performed by adopting the adiabatic temporal extension of the local spin density approximation (ALSDA). The correlation part of the energy functional has been parametrized by Perdew and Wang [118] and implemented in the Octopus TDDFT code [119].

In all the calculations the spin dynamics is activated by a single external laser pulse described by a homogeneous time - dependent electric field. In reality every realistic electro - magnetic pulse is characterized by both an electric and a magnetic component, which are orthogonal to the direction of propagation of the pulse. The amplitude of the magnetic field is in general related to the electric field component through the Faraday law

$$\frac{\partial}{\partial t}\mathbf{B}(\mathbf{r},t) = \nabla \times \mathbf{E}(\mathbf{r},t). \tag{4.1}$$

From the assumption of spatial homogeneity of the electric field component, the external magnetic field $\mathbf{B}_{\text{ext}}$ carried by the laser should not be time - dependent, so we decide to set it to zero. In any case, its effect is assumed to be in general very small. Other opto-magnetic effects introduced in Chapter 2 are also neglected, here. In fact we are mainly interested in the study the demagnetization occuring in the system after the action of the pulse.

The Kohn - Sham ground - state of the system is evolved under the time dependent - dependent Hamiltonian $H_{\mathrm{KS}}(\mathbf{r},t)$,

$$i\hbar\frac{d}{dt}\psi_j^{\mathrm{KS}}(\mathbf{r},t) = \hat{H}_{\mathrm{KS}}[n,\mathbf{m}](\mathbf{r},t)\psi_j^{\mathrm{KS}}(\mathbf{r},t), \tag{4.2}$$

for $j = 1,\ldots,N$, where N is the total number of particles in the system. As we have already seen $\hat{H}_{\mathrm{KS}}$ is a functional of the instantaneous density and magnetization and $\psi_j^{\mathrm{KS}}(\mathbf{r},t)$ is a Kohn - Sham spinor wave function

$$n(\mathbf{r},t) = \sum_{j=1}^{N}\left|\psi_j^{\mathrm{KS}}(\mathbf{r},t)\right|^2, \tag{4.3}$$

$$\mathbf{m}(\mathbf{r},t) = \frac{1}{2}\sum_{j=1}^{N}\psi_j^{\mathrm{KS}}(\mathbf{r},t)^*\boldsymbol{\sigma}\psi_j^{\mathrm{KS}}(\mathbf{r},t), \tag{4.4}$$

where the magnetization field has been written in units of $\hbar$. The Kohn-Sham Hamiltonian that we will consider in this and in the following chapters can be written in the velocity gauge

$$\hat{H}_{\mathrm{KS}}(\mathbf{r},t) = \frac{1}{2m}\left(-i\hbar\nabla + \frac{e}{c}\mathbf{A}_{\mathrm{ext}}(\mathbf{0},t)\right)^2 + \mu_B\mathbf{B}_{\mathrm{s}}(\mathbf{r},t)\cdot\hat{\boldsymbol{\sigma}} + v_{\mathrm{s}}(\mathbf{r},t), \tag{4.5}$$

where the external vector potential is defined as

$$\mathbf{E}_{\mathrm{ext}}(\mathbf{0},t) = -\frac{1}{c}\frac{\partial}{\partial t}\mathbf{A}_{\mathrm{ext}}(\mathbf{0},t). \tag{4.6}$$

Given that there is no external applied magnetic field, we have

$$\mathbf{B}_{\mathrm{s}}(\mathbf{r},t) = \mathbf{B}_{\mathrm{xc}}^{\mathrm{ALDA}}(\mathbf{r},t). \tag{4.7}$$

The exchange correlation magnetic field in local density approximation is expressed as a sum of exchange and correlation part, where for the exchange we have

$$\mathbf{B}_{\mathrm{x}}^{\mathrm{LSDA}}(\mathbf{r},t) = -\left(\frac{3}{\pi}\right)^{1/3}\left[\left(|\mathbf{m}(\mathbf{r},t)|+n(\mathbf{r},t)\right)^{1/3} - \left(n(\mathbf{r},t)-|\mathbf{m}(\mathbf{r},t)|\right)^{1/3}\right]\cdot\frac{\mathbf{m}(\mathbf{r},t)}{|\mathbf{m}(\mathbf{r},t)|}, \tag{4.8}$$

that is locally parallel to the magnetization direction. The scalar potential $v_{\mathrm{s}}(\mathbf{r},t)$ is given by the sum of the Hartree, exchange - correlation and ionic component. The ionic component in our calculations is approximated with an effective pseudopotential, $\hat{V}_{\mathrm{ion}}^{\mathrm{PS}}$. As we have seen in Chapter 3, an atomic, relativistic, all - electron calculation may be reproduced quite accurately in terms of the following type of pseudopotential

$$\hat{V}_{\mathrm{ion}}^{\mathrm{PS}}(r) = \sum_{I}\sum_{l}\sum_{m=-l}^{l}\left[\left(\bar{V}_{I,l}^{\mathrm{ion}}(r) + \frac{1}{2}V_{I,l}^{\mathrm{SO}}(r)\right)\hat{\bullet} + V_{I,l}^{\mathrm{SO}}(r)\hat{\mathbf{L}}_I\cdot\hat{\boldsymbol{\sigma}}\right]|l,m\rangle\langle l,m|, \tag{4.9}$$

where the summation is performed over all the atomic sites I, and $\hat{\mathbf{L}}_I$ is the orbital moment operator localized on that given site. The scalar part of the pseudopotential, $\bar{V}^{\text{ion}}_{l,I}(r)$, includes also the Darwin term and the mass - velocity correction. These fully relativistic and norm - conserving pseudopotentials have been generated using the APE code (*Atomic Pseudopotential Engine*) [123]. It is well known that pseudopotentials, which depend only on the orbital quantum number (l or j in the relativistic case) and where only valence states are considered, while more localized, core states, are neglected from the description could perform quite badly in describing spin - polarized atomic configurations, in particular in the case of transition metals [124].

The applicability of the DFT - based pseudopotential technique on transition metal clusters relies, therefore, on the MRPP (Multi Reference Pseudo-Potential) method [125], that provides a tool to create from first principles fully transferable, norm - conserving pseudopotentials. These include, in addition to valence states, also semi - core states that are supposed to play a very important role in the description of the chemical bond and the magnetic properties of transition metals [126].

In this scheme it is necessary to distinguish between states of a given quantum number l for which we are going to use a single pseudo - wave function from those for which we will use more than one pseudo wave function. For the former states the Troullier - Martins (TM) recipe [127] is still valid. In general the form of the pseudo wavefunctions for the semi-core states, that in transition metal elements are the orbitals *3s* and *3p* (with l<2), will be different with respect to the form for valence states ($l \geq 2$). If $l < 2$ we have

$$R^{PP}_{0,l}(r) = \begin{cases} R^{AE}_{sc,l}(r) & \text{if } r > r_{cl} \\ r^l e^{q(r)} & \text{if } r \leq r_{cl}. \end{cases}$$

Instead for $l \geq 2$ we get

$$R^{PP}_{0,l}(r) = \begin{cases} R^{AE}_{v,l}(r) & \text{if } r > r_{cl} \\ r^l e^{p(r)} & \text{if } r \leq r_{cl}, \end{cases}$$

Where $p(r)$ is a polynomial function of order 6 in r^2 and $q(r)$ is a polynomial of order 9 in r^2. The index '0' in the expression indicates explicitly that these are nodeless wavefunctions, for which it is possible to invert the Kohn-Sham equation.

We show here the pseudopotential components obtained from the solution the relativistic two-components DFT all-electron equations for the Fe atom. The procedure has already been outlined in Chapter 3. Here, we just mention that the exchange correlation functional used to solve the DFT problem is a combination of the *Slater exchange functional* [128],

$$E_{x,\alpha}[\rho] = -\frac{9}{8}\alpha\left(\frac{3}{8\pi}\right)^{1/3} \int_0^\infty dr\rho(r)^{4/3}, \tag{4.10}$$

where α is a parameter typically between 0.7 and 0.8, and of the local spin density correlation part. Then the pseudopotential is generated by using the MRPP scheme at the level implemented in APE. The pseudo wave functions are listed in table 4.1, and the spin orbit component $V_l^{\mathrm{SO}}(r)$ for the two orbital channels $l = 1$ and $l = 2$ is shown in Fig. 4.1. In the figure we compare the calculations done for the Fe atom using different correlation functionals, the *PW* label refers to the Perdew - Wang parametrization, while *PZ* to the Perdew - Zunger one [129] and the third case represents the absence of correlations and pure Slater exchange. It is easy to observe that for both the orbital channels the support of the spin - orbit potential is a sphere centered on the atomic site with a radius of approximately $0.6\mathring{A}$. Beyond this it should not have a direct effect on the spin dynamics. For the *d* channel we see that the correlation contribution to the energy does not seem to influence the shape of the spin - orbit potential, while in the case of the *p* channel its contribution looks quite important. However, due to the fact that *p* electrons in transition metals are not so relevant for the overall magnetization (they are mostly empty), the contribution of $V_{\mathrm{SO}}^{l=1}$ to the spin dynamics is negligible compared to the one coming from the *d* states.

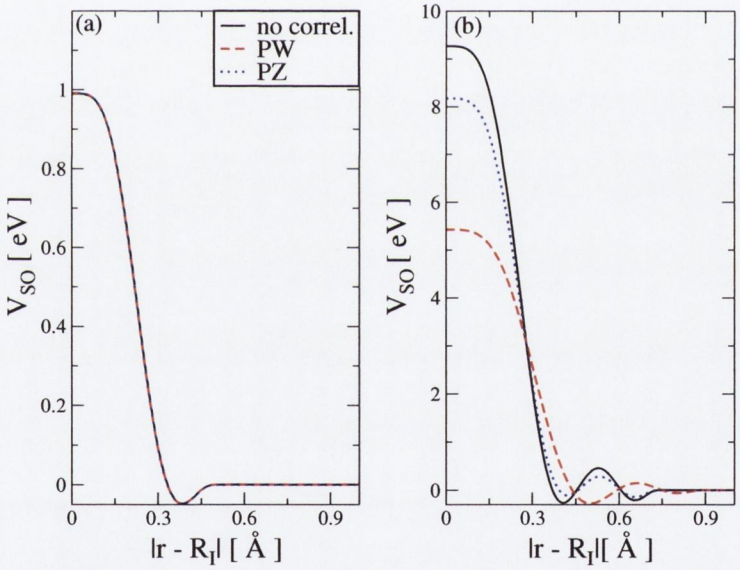


FIGURE 4.1: Plot of the spin orbit pseudopotential component $V_{\mathrm{SO}}^{l}(r)$ with (a) $l = 2$ (*d* channel) and (b) $l = 1$ (*p* channel).

Before passing to the analysis of the results of the simulations it is necessary to have a closer look at the effective equation of motion for the spins within the TD-SDFT formalism. In Chapter 1 we have derived the general form of the continuity equation for a single non-interacting spinning particle. An analogous procedure could be followed even in this case leading to the following expression valid at every point in space

$$\frac{d}{dt}\mathbf{m}(\mathbf{r},t) = -\nabla \cdot \mathbf{J}_{\mathrm{KS}}(\mathbf{r},t) + \mu_B \mathbf{m}(\mathbf{r},t) \times \mathbf{B}_{\mathrm{s}}(\mathbf{r},t) + \mathbf{T}_{\mathrm{SO}}(\mathbf{r},t). \tag{4.11}$$

State	n(quantum number)	j(orbital number)	occupations	KS eigenvalue (eV)
3s	3	0.5	2.00	-3.4358
3p	3	1.5	4.00	-2.1830
3p	3	0.5	2.00	-2.2401
3d	3	1.5	2.40	-0.2883
3d	3	2.5	3.60	-0.2827
4s	4	0.5	2.00	-0.2014
4p	4	0.5	0.00	-0.0538
4p	4	1.5	0.00	-0.0520

TABLE 4.1: Quantum numbers, occupations and Kohn - Sham eigenvalues of the Pseudo wavefunctions generated from the full - relativistic calculation. Looking at the occupation column we observe that the Hund rules are satisfied for the Fe atom and in the ground state configuration $L_z = 0$ and $S_z = 2\hbar$.

In Eq.(4.11) we have distinguished three different terms contributing to the spin dynamics, we should look at each of these terms more in detail.

Spin currents: The term

$$-\nabla \cdot \mathbf{J}_{\mathrm{KS}}(\mathbf{r}, t)$$

represents the usual spin - current divergence. $\mathbf{J}_{\mathrm{KS}}(\mathbf{r}, t)$ is the spin current tensor relative to the fictitious non interacting Kohn - Sham system. It cannot generate an overall global torque of the magnetization vector since its integral over the whole volume is automatically zero, but its contribution to the local dynamics is usually not negligible.

Magnetic torque: In absence of an external magnetic field $\mathbf{B}_{\mathrm{s}}(\mathbf{r}, t)$ is reduced to the exchange - correlation component. Within the local spin - density approximation the zero local torque theorem is valid and we have

$$\mathbf{m}(\mathbf{r}, t) \times \mathbf{B}_{\mathrm{xc}}(\mathbf{r}, t) = 0,$$

which means that the torque term is zero at every point in space and cannot contribute to a dynamical modification of the magnetization vector.

Spin orbit coupling: The spin orbit contribution, $\mathbf{T}_{\mathrm{SO}}(\mathbf{r}, t)$, within the pseudopotential approximation becomes

$$\mathbf{T}_{\mathrm{SO}}(\mathbf{r}, t) = \sum_{I,\alpha,\beta} \sum_{,m,m',l} V^{l}_{\mathrm{SO}}(|\mathbf{r} - \mathbf{R}_I|) \left\langle \Psi^{\mathrm{KS}}_{\alpha} \middle| l, m', I \right\rangle \cdot \tau^{\alpha\beta}_{I,l,m',m} \cdot \left\langle l, m, I \middle| \Psi^{\mathrm{KS}}_{\beta} \right\rangle, \tag{4.12}$$

where $\tau^{\alpha\beta}_{I,l,m',m} = \langle l, m', I | \hat{\mathbf{L}}_I | l, m, I \rangle \times \mathbf{S}_{\alpha\beta}$, and $|\Psi^{\mathrm{KS}}\rangle$ indicates the Kohn-Sham determinant wave function. $\mathbf{T}_{\mathrm{SO}}$ represents the only source of global variation for the magnetization vector.

After this brief theoretical introduction and before discussing in more details the demagnetization process observed in transition metal clusters, we will analyse

four type of magnetic systems Fe_2, Fe_3, Fe_4 and Fe_6, by discussing the role played by the spin orbit coupling in the observed demagnetization process.

4.1 Demagnetization in Fe based clusters

In this section we look at the demagnetization of the different Fe clusters under an external femtosecond laser pulse, first we consider an isolated Fe atom

4.1.1 Fe

Our starting point is to look at the ultrafast dynamics of the isolated Fe atom. As it is clearly shown in Fig. 4.2, the single atom does not demagnetize after the application of the external pulse. Panel (b) in Fig. 4.2 shows that the energy

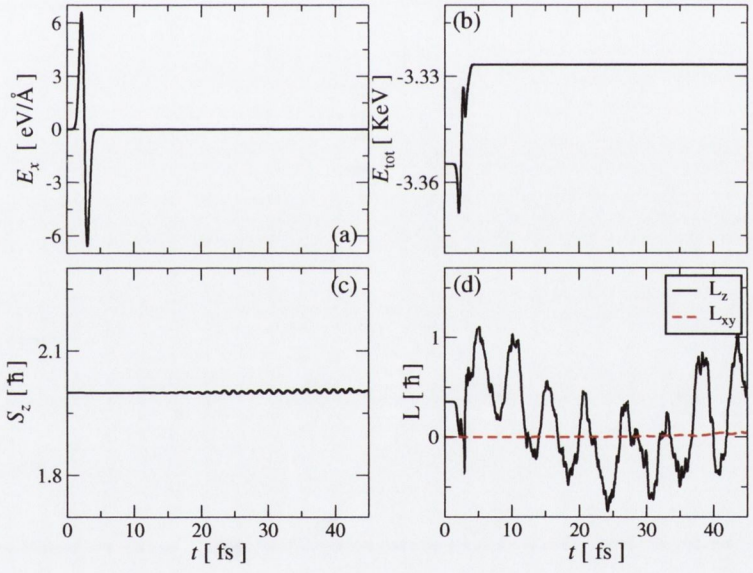


FIGURE 4.2: Spin dynamics of a single isolated Fe atom (a) external applied laser pulse (orthogonal to spin quantization axis) with duration of approximately 5 fs, (b) Total DFT energy evolution within the first 45 fs, (c) total $S_z(t)$ spin evolution, (d) comparison ot the z and non collinear components of the orbital moment.

deposited into the system by the external pulse is not released after the pulse has gone. The expression for the TD-DFT energy is given by

$$E_{\text{TDDFT}}(t) = \langle \Psi^{\text{KS}}(t) | \hat{H}_{\text{KS}}(t) | \Psi^{\text{KS}}(t) \rangle \,, \tag{4.13}$$

where $|\Psi^{\text{KS}}\rangle$ is the determinant wave function of the Kohn - Sham system in Schrodinger representation. The TD-DFT system is not isolated in the first 5 fs

during the action of the external pulse, but after its action the energy accumulated by the single atom cannot be released because at that time the electronic system is not interacting with the environment anymore.

This energy excess contained into the system leads also to an interesting long - time dynamics of the orbital moment. In panel (d) it is shown that after the initial excitation the $L_z = \langle \Psi^{KS} | \hat{L}_z | \Psi^{KS} \rangle$ component of the orbital moment renormalizes and starts to oscillate around an average value close to zero, while the non collinear component $L_{xy} = \sqrt{L_x^2 + L_y^2}$ remains almost zero for the entire duration of the simulation.

Since the spin is not affected by the application of the external laser pulse, we easily conclude that the total orbital moment $J_z = L_z + S_z$ is not conserved during the dynamics. This is valid also after the application of the laser when the Hamiltonian of the electrons in the field of a single centro - symmetric potential is invariant under rotations, allowing to J_z to be conserved. The reason for this lies in the fact that after the laser excitation the initially unoccupied p orbitals become occupied. In this new electronic configuration the spin remains constant because the gap between the up and down states proportional to $|\mathbf{B}_{xc}|$ is quite large and it does not allow for transitions, while the energy gap between orbital states in the same shell is much smaller allowing transitions between different m_l states. In conclusion the confinement potential defined by the boundaries of the simulation box breaks the rotational symmetry giving rise to the large oscillations observed between 10 and 45 fs in panel (d).

4.1.2 Fe_2

The Fe dimer represents a more interesting case with respect to the single atom. In our simulations we start from a ground state where the two atoms are at a distance of $1.96\mathring{A}$ and the total magnetic moment of the dimer is $S_z = 2.997\hbar$. In Fig. 4.3 we compare the time evolution of the dimer under two different laser pulses that are explicitly represented in panel (a). In both cases the electric field polarization is directed along the bond axis. In panel (b) we plot the evolution of the total energy of the electronic system. The second pulse has an amplitude that is approximately 10 times the amplitude of the first and the difference in the energy variation among the two cases reflects the different amount of energy injected into the dimer.

Panel (c) depicts, instead, the spin evolution. While in the case of the pulse with smaller amplitude the total spin of the system remains constant throughout the evolution, in the second case after 7 fs of evolution the dimer loses approximately 1% of its initial magnetization. This decrease appears monothonic and it starts in correspondence of the first peak of the laser field. In this picture it is clearly shown that the function of the laser in the demagnetization is to activate some spin loss mechanism, which is still present in the system also after the external pulse has disappeared. Finally in panel (d) it is considered the evolution of the

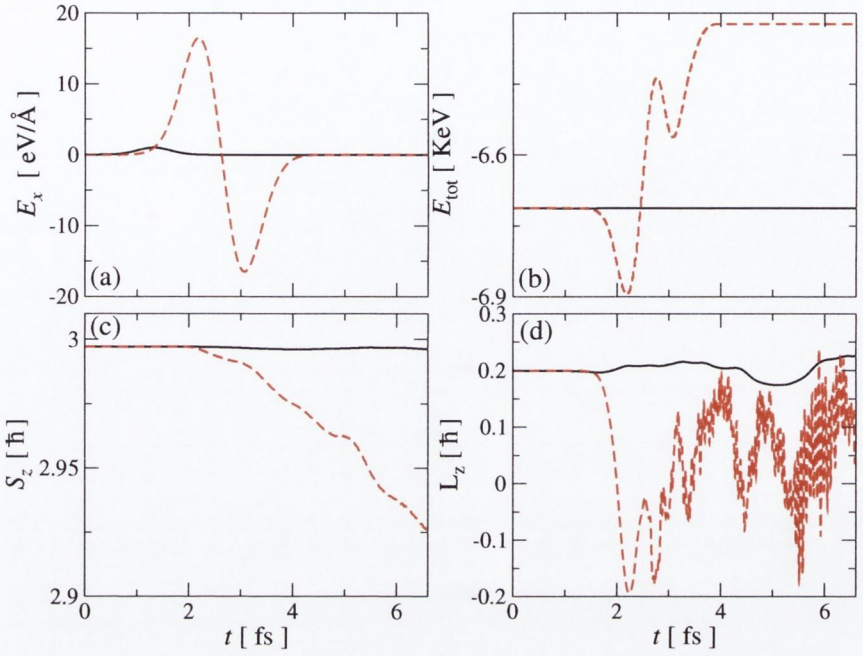


FIGURE 4.3: Spin dynamics of the Fe dimer (a) external applied laser pulses, (b) Total DFT energy evolution within the first 10 fs, (c) $S_z(t)$ evolution in units of $\hbar$, (d) orbital moment $L_z(t)$ evolution also in units of $\hbar$.

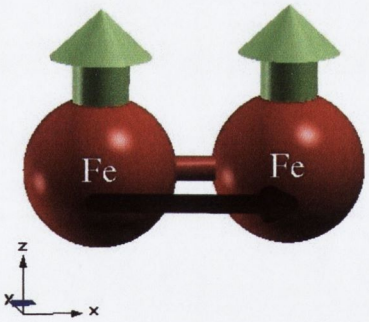


FIGURE 4.4: Picture of the Fe_2 dimer with the black arrow indicating the electric field polarization direction and green arrows indicating the atomic spin direction.

component L_z of the orbital moment of the dimer (the quantity is integrated, like the spin, over the whole simulation box). It is also evident that the energy injected by the small pulse into the system is not sufficient to excite the orbital moment. In contrast the stronger pulse excites more currents and also the orbital moment changes drastically during its action. After the pulse has disappeared the orbital moment oscillates around its new average value analogously to the case already discussed for the isolated Fe atom. The only difference with the previous situation is that at longer times the dynamics looks a superposition of waves propagating at different frequencies. After the excitation, in fact, the electrons are pushed in an out of the equilibrium configuration and are free to scatter with the crystal field produced by the two-atoms potential. The lack of coherence in the oscillations observed after the first 3 fs of evolution may be attributed to the action of the spin orbit coupling as we will see in Chapter 6.

In Fig. 4.5 we look more in details to the magnetization dynamics of the Kohn-Sham spinor states numbered from 16 to 32, representing the highest energy states, while we neglect the others, which are low in energy and not directly excited by the action of the laser pulse. We look at the results in the case of the low amplitude pulse of Fig. 4.3, as we have already mentioned a global spin loss is not visible from the picture but some dynamics may be observed by looking at the single particle states separately. It is clear that while all the states be-

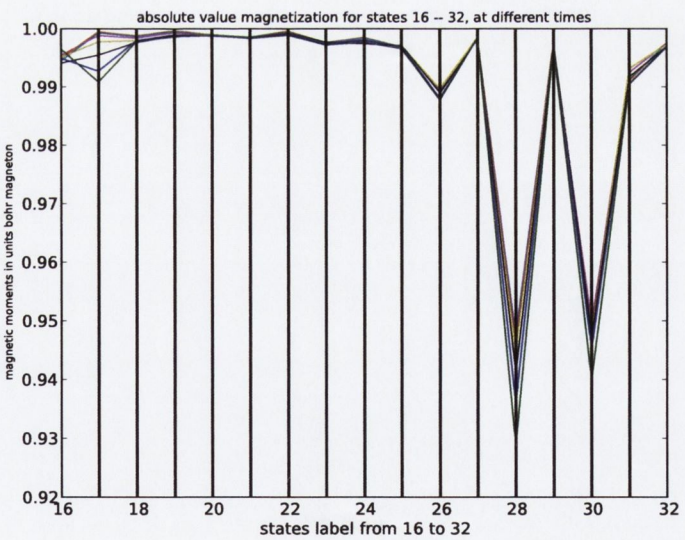


FIGURE 4.5: Expectation value of the spin operator $\langle \psi_j^{KS} | \hat{\sigma}^z | \psi_j^{KS} \rangle$ over all the Kohn-Sham states between 16 and 32, the various lines represent different instants in time chosen uniformly at time intervals of 3 fs, the red line corresponds to the earliest time, the blue line is the intermediate one and the green line the latest.

tween 16 and 25 do not change their spin expectation value during the evolution, the states 26, 28 and 30 lose more magnetization in comparison to the others.

It is interesting to observe that these states carry less magnetization even in the ground state. This can be understood by assuming that these states, due to the spin orbit coupling, are more spin mixed with respect to the others and therefore have the tendency to lose also more magnetization during the evolution. Be-

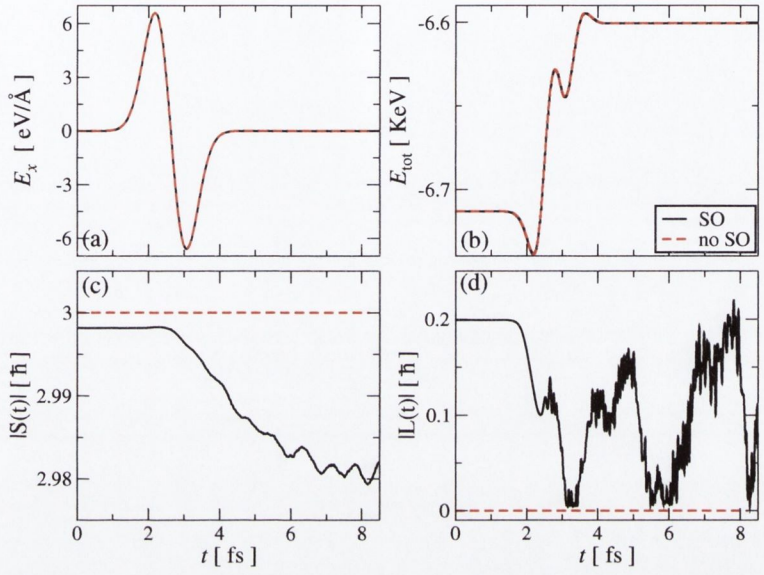


FIGURE 4.6: Dynamics of the Fe dimer with and without spin orbit (a) external applied laser pulses, (b) Total DFT energy evolution within the first 10 fs, (c) $|\mathbf{S}(t)|$ evolution in units of $\hbar$, (d) orbital moment $|\mathbf{L}(t)|$ evolution also in units of $\hbar$.

fore completing our discussion on the Fe dimer we compare also the two cases, where the system is evolved in presence and in absence of spin orbit coupling. In Fig. 4.6 the dimer in the two cases is evolved under the effect of the same external pulse, which is depicted in panel (a). In panel (b) it is shown the amount of energy injected into the system that is exactly the same in the two cases. Of more interest are the data plotted in panel (c) and (d) where the absolute value of the total magnetization $|\mathbf{S}(t)|$ remains constant to the value of 3 $\hbar$ during the entire dynamical evolution in absence of spin orbit coupling. In contrast in presence of spin-orbit we observe an evolution equivalent to that presented in Fig. 4.3. Even in this case the total momentum $\mathbf{J} = \mathbf{L} + \mathbf{S}$ is not conserved during the evolution (at least in presence of spin orbit), the variation of the orbital moment is much larger compared to the total spin variation. This behaviour will be analysed in more details in the following chapters, but here, it is already evident that while the spin orbit coupling generates a ground-state finite value of the orbital moment, in absence of spin orbit this does not happen. As a consequence, during the evolution, in the first case the application of the external pulse excites the currents present in the ground state and after its action the electronic wave functions scatter with the global crystal field potential (due to the finiteness of

the simulation box) contributing to the long-time oscillations observed in the orbital moment. In the second case, instead, nothing happen simply because the ground-state orbital moment of the system is zero and, in absence of spin orbit, the symmetry between different orbital states is not broken. In conclusion, the orbital moment is not dynamically excited by the application of the external laser pulse.

4.1.3 Fe_3

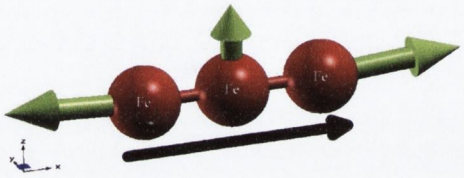


FIGURE 4.7: Picture of the Fe_3 cluster with the black arrow indicating the electric field polarization direction, the green arrows represent the local moments direction in the ground state configuration.

In this subsection we consider the linear Fe_3 cluster depicted in Fig. 4.7. The distance between the central atom and the two peripheral ones is approximately 1.97 $\AA$. The ground state results in a highly non collinear configuration with the spin of the two peripheral atoms oriented in opposite directions but equal in magnitude, and orthogonal to the spin of the central site. In Fig. 4.8 we examine

the evolution of the total magnetization vector of the system with and without spin - orbit coupling. Panel (c) and (d) show quite clearly that the effect of the spin - orbit on the magnetization dynamics of this system is not important and can be neglected compared to the dynamics of the localized spin moments. In Fig. 4.9 we compare the dynamics of the localized moments of every atomic site integrated over a sphere of radius, R, half the distance between the two neighbors. We observe that the variation of the x and y components of the spin vector over the three sites is smaller in magnitude than the variation of the z component of the local moments. At the same time, while the central atom component appears approximately constant throughout the evolution, the variation of the component over the other two sites is the same in magnitude but opposite in direction leading to an approximately constant total S_z component of the cluster magnetization.

We will analyse this interesting behaviour more in detail in Chapter 5. Here it is sufficient to observe that the spin - orbit coupling is not the main force driving the local spin evolution of the Fe_3 magnetic cluster. In particular we will see that in highly non collinear magnetic configurations the action of the external

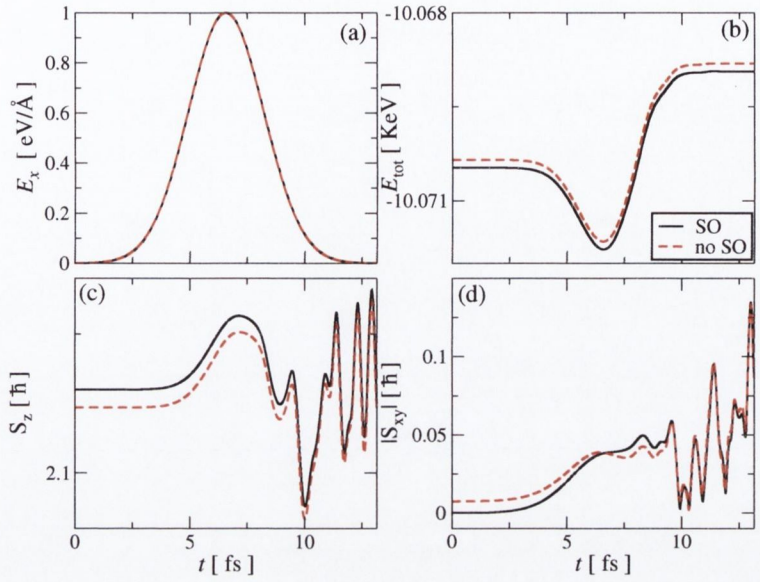


FIGURE 4.8: Spin dynamics of the Fe_3 cluster (a) external applied laser pulses, (b) Total DFT energy evolution in the case with and without spin orbit, (c) total magnetization $S_z(t)$ of the cluster in units of $\hbar$ in the two cases, (d) total non collinear component $S_{xy}(t)$ in units of $\hbar$.

laser pulse can activate very interesting dynamical effects by means of out of equilibrium potentials acting on the localized spin moments.[1]

4.1.4 Fe_4

The Fe_4 ferromagnetic cluster was already investigated theoretically in its ground - state properties in reference [121,122]. Here, we consider a ground - state ferromagnetic structure calculated within the PW - local spin density approximation. In this ground - state configuration the atoms are arranged in a square of side of 2.38 $\AA$ (see Fig. 4.11), with a total magnetization of approximately 6.996 $\hbar$.

The laser applied in this calculation is the same we used in Fig. 4.6 for Fe_2. The result is an increased magnetization loss, but the demagnetization observed per atom is in practice the same in the two cases. In panel (d) the global non collinear component $S_{xy}(t)$ of the magnetization is plotted, with no apparent variation throughout the entire dynamical evolution.

In Fig. 4.12 we consider, instead, the local demagnetization evaluated in correspondence of the four atoms of the cluster. The calculation is performed by

[1]Whenever we introduce the concept of localized magnetic moments in our discussion we always refer to the value of the magnetization density integrated within a sphere centered on a particular atomic site through Eq. (4.14). This represents a useful working definition but it can be misleading since this definition depends on the particular radius we are using for the integration procedure.

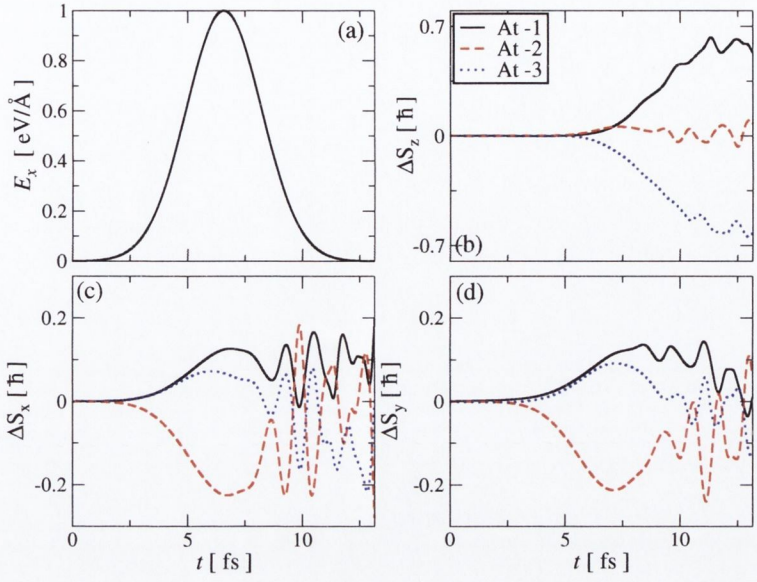


FIGURE 4.9: Spin dynamics of the Fe_3 system (a) external applied laser pulses, (b) variation of the component $\Delta S^{\mathrm{R}}_{\mathrm{z,I}}(t)$ of the magnetization over the three sites, (c) variation of the component $\Delta S^{\mathrm{R}}_{\mathrm{x,I}}(t)$, (d) variation of the component $\Delta S^{\mathrm{R}}_{\mathrm{y,I}}(t)$ in units of $\hbar$.

computing the integral of the specific quantity we are considering within a certain integration domain Ω_I^R, represented by a sphere of radius R centered on the atomic site at the position $\mathbf{R}_I$. In particular we define

$$\mathbf{S}^{\mathrm{R}}_{\mathrm{I}}(t) = \int_{\Omega_I^R} \mathrm{d}^3 r\, \mathbf{m}(\mathbf{r}, t), \tag{4.14}$$

$$Q^{\mathrm{R}}_{\mathrm{I}}(t) = \int_{\Omega^{\mathrm{R}}_{\mathrm{I}}} \mathrm{d}^3 r\, \rho(\mathbf{r}, t), \tag{4.15}$$

representing a measure of the value of the on site magnetization $\mathbf{S}^{\mathrm{R}}_{\mathrm{I}}(t)$ and of the electronic charge $Q^{\mathrm{R}}_{\mathrm{I}}(t)$, while in the case of the exchange magnetic field we can analogously define

$$\mathbf{B}^{\mathrm{R}}_{\mathrm{x,I}}(t) = \frac{1}{V_{\Omega_I^R}} \int_{\Omega_I^R} \mathrm{d}^3 r\, \mathbf{B}_{\mathrm{x}}(\mathbf{r}, t). \tag{4.16}$$

Panel (a) of Fig. 4.12 shows clearly that for all the three atomic sites there is

a sudden variation of the electronic charge that is pushed outside the integration domain region during the action of the laser pulse. After this initial phase the electron density stabilizes on a lower value that remains constant for the rest of the dynamical simulation. It is interesting also to observe that this initial variation is exactly the same for atoms 1 and 2 and for atoms 3 and 4 (see Fig. 4.11).

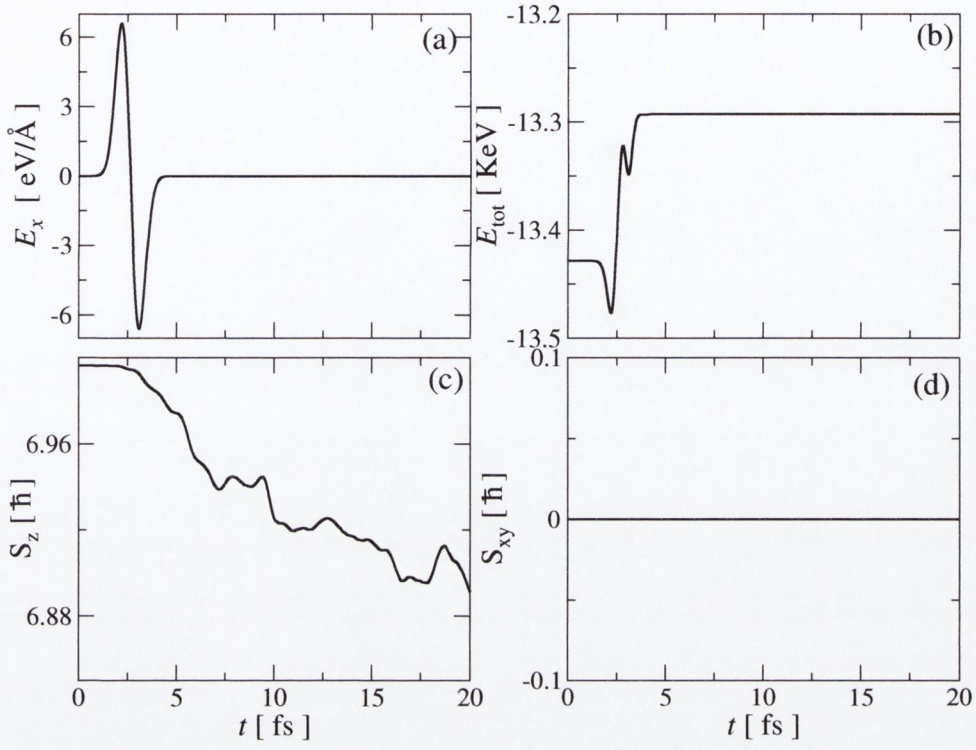


FIGURE 4.10: Spin dynamics of the Fe_4 cluster (a) external applied laser pulses, (b) total DFT energy evolution within the first 20 fs, (c) $S_z(t)$ evolution in units of $\hbar$, (d) non collinear component $S_{xy}(t) = \sqrt{S_x(t)^2 + S_y(t)^2}$ of the global magnetization also in units of $\hbar$.

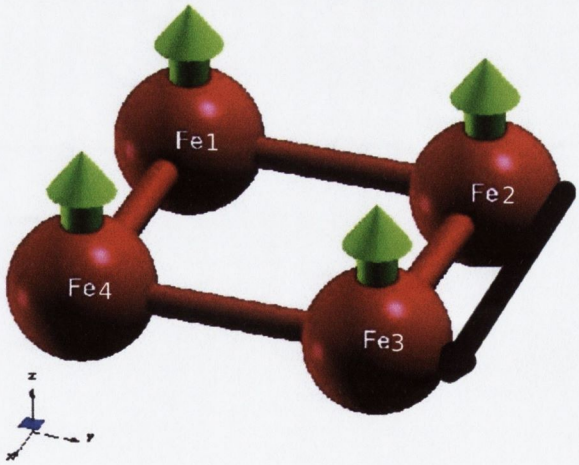


FIGURE 4.11: Picture of the Fe_4 with the black arrow indicating the electric field polarization direction. The green arrows represent the local spin directions in the ground state.

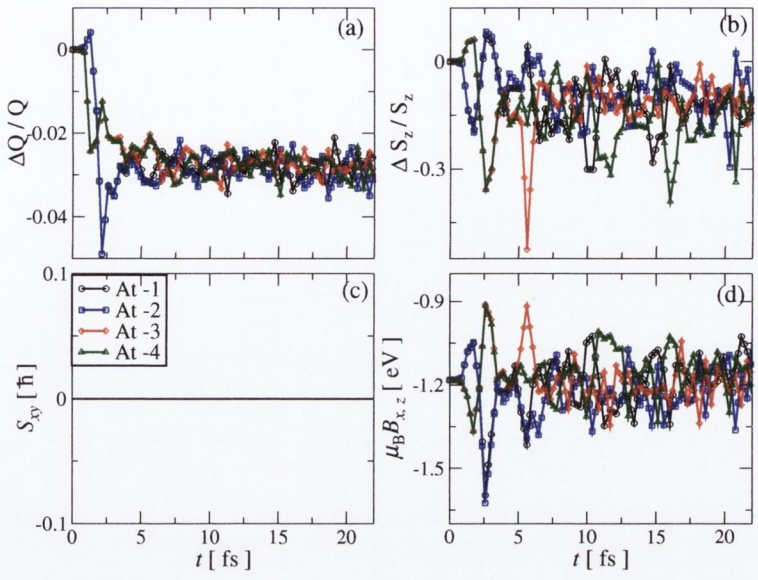


FIGURE 4.12: Local charge and spin dynamics of the Fe_4 cluster (a) calculation of $\Delta Q_I^R(t)/Q_I^R(t)$ where $R = 1.2\,\AA$ and $I = 1,\ldots,4$ in units of $\hbar$, (b) calculation of $\Delta S^R_{z,I}(t)/S^R_{z,I}(t)$ over the same integration domain, (c) $S^R_{I,xy}(t) = \sqrt{S_{I,x}(t)^2 + S_{I,y}(t)^2}$, (d) evolution of $B^R_{x,zI}(t)$ z component of the exchange magnetic field.

This is due to the fact that the application of the laser pulse breaks the symmetry only along one direction of the cluster. The evolution of the z component of the magnetization for the three atomic sites is depicted in panel (b), where the dynamics appears very similar to that of the electron density, even if the initial variation and the following oscillations are much larger in magnitude. Both quantities are characterized by an initial abrupt change leading to a stabilization around a new lower equilibrium value. In panel (c) the non collinear component $S^R_{I,xy}(t)$ for $I = 1,\ldots,4$ is seen to remain zero throughout the entire dynamical evolution, which means that if locally some non collinearity in the spin vector arises, it will be completely averaged out by the spatial integration procedure. Finally in panel (d) we consider the evolution of the z component of the exchange magnetic field of Eq. (4.8), it follows locally the same dynamics of the magnetization vector, dominant with respect to the dynamics of the electron density. As we have already mentioned in Chapter 3 in the context of the LSDA, $\mathbf{B}_{xc}$ cannot generate, by construction, a torque of the magnetization vector

$$\mathbf{m}(\mathbf{r},t) \times \mathbf{B}_{xc}(\mathbf{r},t) = 0, \tag{4.17}$$

where this relation is valid for both the exchange and correlation components separately. However it can play, in principle, an indirect role in the spin dynamics by dynamically modifying the gap between spin up and down bands and enhancing, therefore, the spin loss through the spin - orbit coupling channel. What is apparent from Fig. 4.12 (d) is that $\mathbf{B}_x(\mathbf{r},t)$ is characterized locally by strong

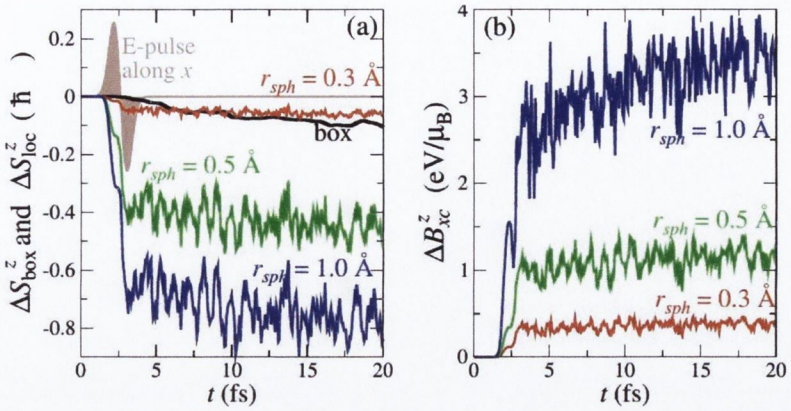


FIGURE 4.13: Spin dynamics of the Fe_4 cluster (a) comparison of $\Delta S^R_z(t)$ for different values of the integration radius with the global magnetization loss (b) evaluation of $\Delta B^R_{x,z}(t) = \sum_I \Delta B^R_{x,zI}(t)$ for different values of R.

variations in its z component, which can be justified in terms of a strong flux of spin currents from one region to another of the simulation box. How can this behaviour affect the global spin loss through the spin orbit coupling channel is still not clear up to now and it will be the main argument of the final part of this Chapter. In Fig. 4.13 instead we compare the dynamics of the localized magnetization $S^R_z(t) = \sum_I S^R_{z,I}(t)$ and exchange field $B^R_{x,z}(t)$ for different values of the radius R with the total magnetization decay. The decay and oscillations in both fields tend to increase with the radius, more density is in fact included in the integration sphere and the collapse of these quantities appears more clearly.

Before concluding our survey of the Fe_4 cluster properties it could be of some interest also to look at the evolution of the non collinear component of the spin vector. As we have seen in Fig. 4.14 (c) every non-collinear component of the spin vector must be averaged out if we consider the entire simulation box as integration domain, suggesting that the cluster remains globally ferromagnetic during the evolution. In Fig. 4.14(d) we use the quantity $S^{xy}_{loc}(t) = \sum_I \int_{\Omega^R_I} d^3r \sqrt{m_x(\mathbf{r},t)^2 + m_y(\mathbf{r},t)^2}$ to measure the amount of non collinearity present into the system. $S^{xy}_{tot}(t)$ represents the same quantity integrated over the entire volume. The picture clearly shows that the non collinear component of the spin vector grows, at least locally, during the dynamical evolution. At the same time, almost all the non collinearity present into the system is concentrated in the small regions centered around the atoms. In panel (c) we observe that the blue line, which defines the amount of non collinearity measured on the plane of the cluster, defined through the expression $\int_{z=0} d^2r \sqrt{|\mathbf{m}(\mathbf{r},t)|^2 - |\mathbf{m}(\mathbf{r},0)|^2}$, is exactly zero with the consequence that all the rotation of the spin vector must be produced out of this plane. The other curves show the same quantity integrated over different regions, with increased measure of non collinearity. In panel (a) it is measured the variation of the z component of the magnetization and of the

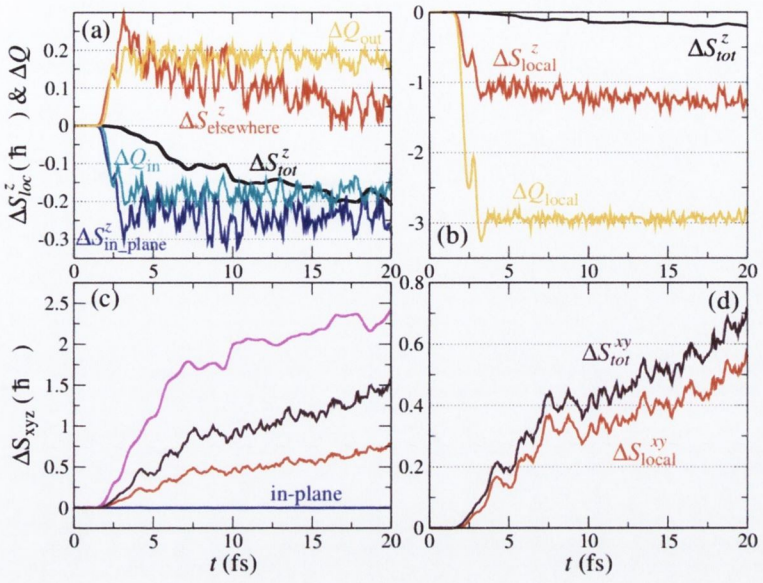


FIGURE 4.14: Dynamics of global and local spin quantities (a) comparison of $\Delta S^z(t)$ and $\Delta Q(t)$ in the plane of the cluster and in the region outside, (b) comparison of $\Delta S^z_{loc}(t) = \sum_I \Delta S^R_{z,I}(t)$ with the same quantity integrated over the whole volume, (c) measure of $\Delta S^{xyz}(t) = \sqrt{|\mathbf{m}(0)|^2 - |\mathbf{m}(t)|^2}$ using global values (pink curve), local measures centered on the atoms (red line) and quantities integrated over the cluster plane (blue line), (d) $\Delta S^{xy} = \sqrt{m_x^2 + m_y^2} - S^{xy}(0)$ quantity integrated over the entire simulation box and around the atoms.

electronic charge in plane and out of plane. Apparently the loss of the z component of the magnetization vector happens out of plane. This quantity correlates quite well also with the global magnetization loss (black line), even if they are not identical, and this is particularly true after the applied external field has gone to zero. In practice while a part of $S^z(t)$ rotates with a consequent growth of the non collinear component of the spin vector, another part is directly transfered into the orbital moment through the spin-orbit channel, this second dynamical effect is responsible for the global decay of the cluster magnetization.

4.1.5 Fe_6

The ground state geometry of the Fe_6 cluster was already predicted by LSDA [120,121] to be a compressed D_{2h} distorted octahedron (see Fig. 4.16) with bond lengths in the range 2.29 – 2.53 Å and this is the same geometry we used in our dynamical simulations. The corresponding spin ground state in LSDA for Fe_6 is $S^z_{tot} = 10\,\hbar$, with the magnetization of the two apex atoms slightly non collinear with respect to that of the in plane atoms.

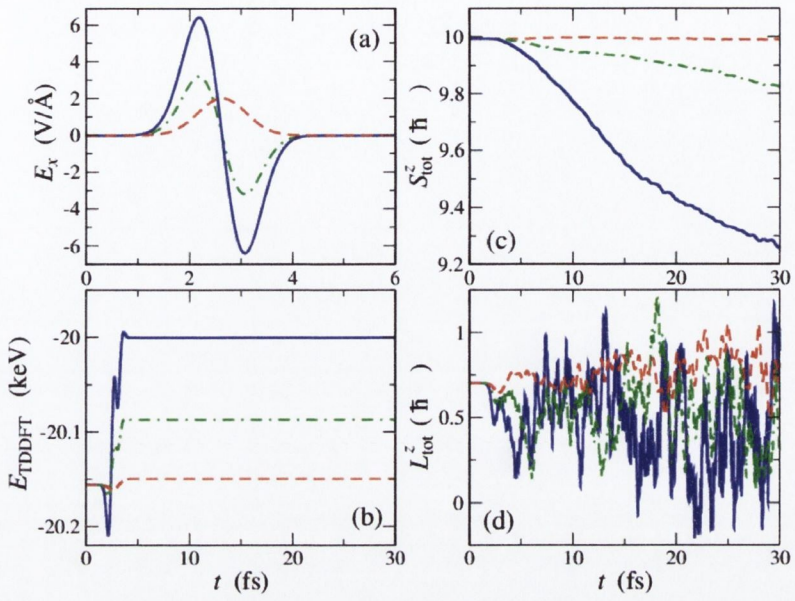


FIGURE 4.15: (a) Typical electric field pulses used to excite the cluster, (b) time evolution of the total TD-DFT energy, (c) total spin and (d) total orbital moment subjected to each of the pulses in panel (a) with corresponding color code on all panels.

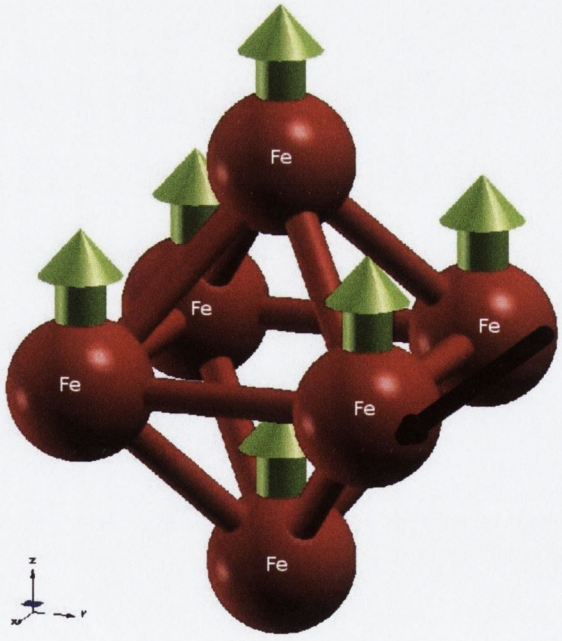


FIGURE 4.16: Picture of the Fe_6 with the black arrow indicating the electric field polarization direction.

Fig. 4.15 shows representative results from the full time-dependent simulations of the dynamics of the Fe_6 cluster. As we have already seen in the case of Fe_2 and Fe_4 clusters the magnetic response to the application of an entire range of external pulse shapes and amplitudes is a decay of the global spin expectation value $S^z_{tot}(t) = \int d^3r\, m_z(\mathbf{r}, t)$. These pulses excite the magnetic system and the rate of spin decay triggered by the excitation correlates with the total variation of the TD-SDFT total energy (4.13) before and after the action of the laser pulse. The larger is the energy deposited into the system the faster is the induced spin decay rate. In panel (d) of Fig. 4.15 it is depicted the evolution of the total Kohn-Sham orbital moment $L^z_{tot}(t)$

$$L^z_{tot}(t) = \int d^3r\, L^z(\mathbf{r}, t), \tag{4.18}$$

which shows large oscillations and a completely different dynamics with respect to that observed in the case of the total spin. As we have already observed in the case of Fe_2, even in this case the global orbital moment of the cluster is not conserved during the evolution. Fig. 4.15(d) clearly shows that the oscillations have the tendency to increase after the application of the laser, with the magnitude that appears higher in the case of stronger demagnetization and of stronger pulse amplitude. Clearly this can be explained in part as a transfer of spin into the orbital moment channel, but at the same time it suggests that the origin of this dynamical effect may be due to the scattering between the electronic wave function and the ionic potential of the cluster, as we will explore more in details in Chapter 6. Clearly, even for Fe_6, $J^z_{tot}(t) = L^z_{tot}(t) + S^z_{tot}(t)$ is not conserved during the dynamical evolution also after that the pulse has been set to zero. Analogously

to the Fe_4 case, the regions of space where the spin density decreases exhibit an increase of $\mathbf{B}_x(\mathbf{r}, t)$. Given the fact that in the same regions the exchange field is mostly negative in the ground state, we conclude that the regions of pronounced spin decay are associated with a decrease in the absolute value of the field. The spin-orbit coupling is expected to have a major role in the spin decay process. In order to extract such effect more clearly we introduce an artificial scaling factor α in front of the spin orbit coupling term of Eq. (4.9)

$$\hat{V}^{PS,(\alpha)}_{ion}(r) = \sum_I \sum_l \sum_{m=-l}^{l} \left[\left(\bar{V}^{ion}_{I,l}(r) + \frac{\alpha}{2} V^{SO}_{I,l}(r) \right) \hat{\bullet} + \alpha V^{SO}_{I,l}(r) \hat{\mathbf{L}}_I \cdot \hat{\boldsymbol{\sigma}} \right] |l, m\rangle \langle l, m| . \tag{4.19}$$

Depicted in Fig. (4.17) is the effect of the variation of α from 0 to 4 in the global spin dynamics. The rate of spin loss both during and after the pulse, is strongly affected by the spin-orbit coupling strength, with the limiting case of $\alpha = 0$ (absence of spin orbit) resulting in global spin conservation. In panel (b) we plot the same spin trajectories after having subtracted their ground state offset and by scaling them by a factor $1/\alpha^2$. The overlap of the curves demonstrates that in the initial coherent stage of the dynamics the spin decay rate scales as the square of the spin-orbit coupling strength. We then compare the global spin trajectories to

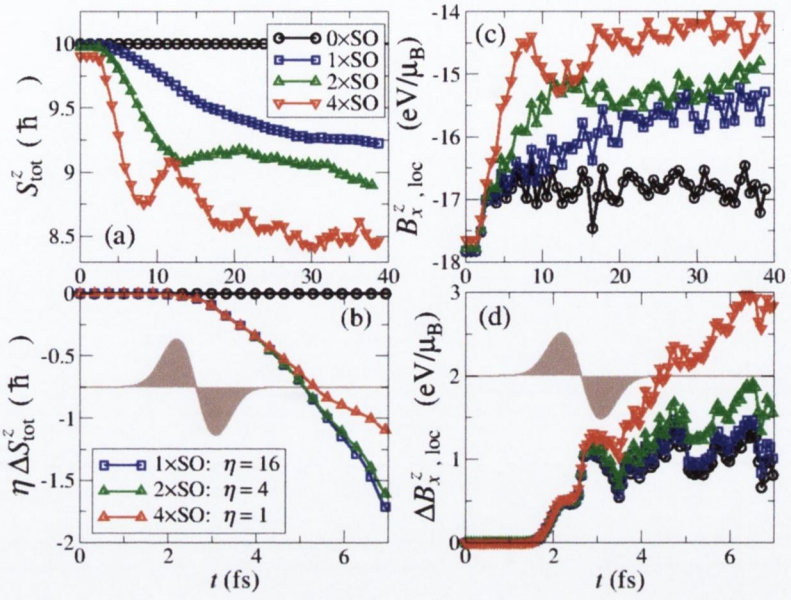


FIGURE 4.17: Evolution of the different observables in the Fe_6 system (a) Evolution of global spin expectation value for different values of $\alpha = 0, 1, 2, 4$ in Eq. 4.19. (b) Plot of $S^z_{tot}(t) - S^z_{tot}(t = 0)$ multiplicated by $\eta = (\alpha_{max}/\alpha)^2$. Panels (c) and (d) show the corresponding trajectories for the exchange field $B^z_{x,loc}(t)$ of Eq. (4.20).

those of $B^z_{x,loc}$ in the vicinity of the atomic centers

$$\mathbf{B}_{x,loc}(t) = \sum_I \frac{1}{V_{\Omega^R_I}} \int_{\Omega^R_I} d^3r\, \mathbf{B}_x(\mathbf{r}, t), \tag{4.20}$$

where Ω^R_I defines the usual sphere centered on atom I with radius $R = 0.85$ Å. Although such defined local exchange field appears noisy due to spatial grid effects, it shows the same coherent response to the external pulse that we have already observed in the case of the Fe_4 cluster, while during the initial phase of the dynamical evolution it can be considered practically independent from the strength of the spin-orbit coupling coefficient [2] [see Fig. 4.17, panels (c) and (d)]. After the pulse disappears, the decrease in the absolute value of $B^z_{x,loc}(t)$ correlates with the global spin decay in panel (a). This is particularly clear for the cases with higher value of α. All the spin loss, in practice, takes place in the vicinity of the atomic centers where also $\mathbf{B}_{x,loc}(t)$ has been computed.

4.1.6 Comparison of cluster demagnetization

In this subsection we compare the demagnetization process observed in the different clusters excited by various type of laser pulses. Fig. (4.18) briefly sum-

[2]The portion of total energy related to the spin orbit is much smaller compared to the one deposited by the pulse in the form of kinetic energy and the variation in the exchange field component is mostly due to the charge and spin motion activated by the action of the laser.

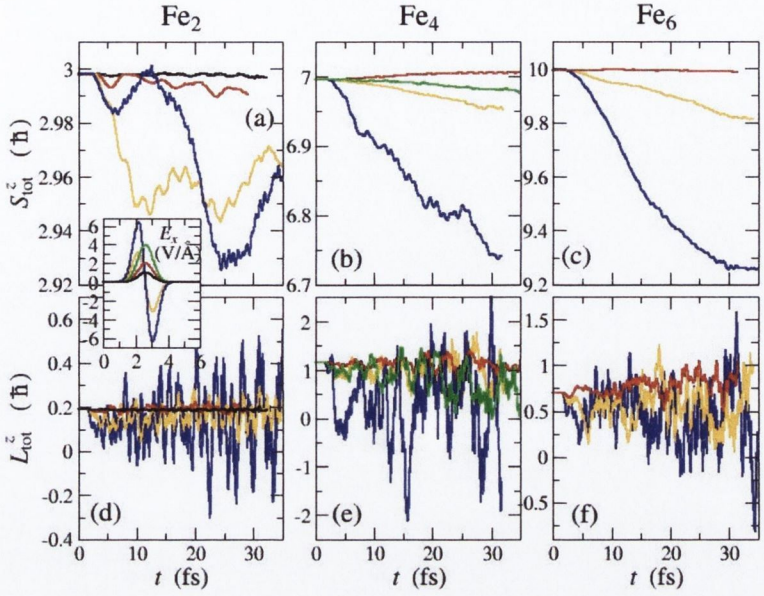


FIGURE 4.18: Plot of the time-dependent global spin and orbital moment of the various clusters considered for different laser pulses: (a) and (d) Fe_2; (b) and (e) Fe_4; (c) and (f) Fe_6.

marizes the results of the previous subsections. We observe that while all the different clusters demagnetize after the application of the laser pulse, the rate of spin loss is different in the various cases. For identical applied laser pulses we have that clusters with a higher value of the ground state magnetization (composed by a larger number of Fe atoms) demagnetize more and are characterized by a higher spin decay rate. At the same time, we observe that for every single cluster the demagnetization is faster when the pulse is more intense. Moreover the total angular momentum of the clusters, as we have already observed, is not conserved during the demagnetization process. The relationship between higher spin loss rates and higher oscillations of the orbital moment of the system is quite evident from the figure and it can be attributed to the transfer of spin into the orbital channel through the spin-orbit coupling.

In the next section we will provide a qualitative explanation of the demagnetization process in transition metal clusters through the introduction of a simplified model that involves the spin orbit and a time-dependent magnetic field. This will shed light on the intricate effects generated by the combined action of the spin-orbit coupling and of the exchange-correlation magnetic field.

4.2 Minimal Demagnetizing Model

The insights coming from the first principle spin dynamics for the Fe_2, Fe_4 and Fe_6 clusters previously examined suggest the spin orbit coupling as the key ingredient in the demagnetization process. This in fact takes place in the vicinity of the atoms where the function $V^l_{SO}(|\mathbf{r} - \mathbf{R}_I|)$ has support.

We have observed that in the same regions the local magnetic field, $\mathbf{B}_{x,loc}(t)$, decays rapidly in time, coherently with the laser field at the beginning of the simulation. This local dynamics of the exchange field may be understood mainly in terms of strong charge and spin density fluxes, which alter the local value of the field in the vicinity of the atomic centers, as we have seen in the case of both Fe_4 and Fe_6, and as will become more clear in Chapter 5 where we will discuss more in details the role played by the spin currents in the demagnetization process.

Going back to the spin continuity equation (4.11) we have three terms generating spin dynamics, namely the spin orbit coupling, the exchange correlation magnetic field $\mathbf{B}_{xc}(\mathbf{r}, t)$ and the spin currents. For the moment we neglect the influence of the spin current on the magnetization dynamics. Here we want to focus on the interplay between the spin-orbit coupling and the exchange-correlation magnetic field.

We start from a very simplified model describing a single spin immersed in an external time-dependent magnetic field. The Hamiltonian of the system is written as

$$\hat{H}(t) = \lambda \hat{\mathbf{L}} \cdot \hat{\mathbf{S}} + \mathbf{B}(t) \cdot \hat{\mathbf{S}}, \tag{4.21}$$

with $\mathbf{B}(t)$ representing the external time-dependent magnetic field, $\hat{\mathbf{S}}$ is the spin operator, while $\hat{\mathbf{L}}$ is the orbital moment operator. This model is designed to mimic the local spin dynamics at a given spatial point, resulting from the TD-SDFT simulation, but it cannot reproduce the full ab-initio dynamics. The basis set used to expand the wave function, solution of the time dependent Schrodinger equation under the Hamiltonian (4.21) is formed by the eigenstates of the operators $\hat{L}_z$ and $\hat{S}_z$. In particular, using $l = 1$ for the orbital moment quantum number we can write

$$|\Psi(t)\rangle = \sum_{l_z=-1}^{1} \sum_{s_z=-0.5}^{0.5} c_{l_z,s_z} |l_z, s_z\rangle, \tag{4.22}$$

and the Schrodinger equation becomes a 6×6 matrix equation in the $L\cdot S$ Hilbert space. In natural units ($\hbar = 1$) we have

$$\frac{d\mathbf{c}}{dt} = \mathbf{A}(t)\mathbf{c}, \tag{4.23}$$

where $\mathbf{c}$ is a 6 dimensional vector and the matrix $\mathbf{A}(t)$ has the following form, if we assume a magnetic field along z,

$$\mathbf{A}(t) = \left(\begin{array}{ccc|ccc} -\frac{i\lambda}{2} - \frac{iB(t)}{2} & 0 & 0 & & & \\ 0 & \frac{i\lambda}{2} + \frac{iB(t)}{2} & -\frac{i\lambda}{\sqrt{2}} & & \mathbf{0} & \\ 0 & -\frac{i\lambda}{\sqrt{2}} & -\frac{iB(t)}{2} & & & \\ \hline & & & \frac{iB(t)}{2} & -\frac{i\lambda}{\sqrt{2}} & 0 \\ & \mathbf{0} & & -\frac{i\lambda}{\sqrt{2}} & \frac{i\lambda}{2} - \frac{iB(t)}{2} & 0 \\ & & & 0 & 0 & -\frac{i\lambda}{2} + \frac{iB(t)}{2} \end{array}\right). \tag{4.24}$$

Given the complexity of this matrix equation, we can analyse the time-dependent evolution of the system in a subspace spanned by the two vectors $|lz = 1, sz = -1/2\rangle$ and $|lz = 0, sz = 1/2\rangle$. By assuming an initial state of the form

$$|\Psi(0)\rangle = c_1(0)\,|l_z = 1, s_z = -1/2\rangle + c_2(0)\,|l_z = 0, s_z = 1/2\rangle\,, \tag{4.25}$$

the problem may be reduced to the solution of the following two coupled first order differential equations

$$\dot{c}_1 = i\left(\frac{\lambda}{2} + \frac{B(t)}{2}\right)c_1 - \frac{i\lambda}{\sqrt{2}}c_2, \tag{4.26}$$

$$\dot{c}_2 = -\frac{i\lambda}{\sqrt{2}}c_1 - i\frac{B(t)}{2}c_2. \tag{4.27}$$

By combining the two equations we can write a single second-order differential equation for the coefficient $c_2(t)$

$$\ddot{c}_2 = \frac{i\lambda}{2}\dot{c}_2 + f(t)c_2(t), \tag{4.28}$$

where the function $f(t)$ is defined as

$$f(t) = -\frac{\lambda B(t)}{4} - \frac{B(t)^2}{4} - \frac{\lambda^2}{2} - \frac{i\dot{B}}{2}. \tag{4.29}$$

we may then consider two distinct cases:

1. Using a constant zero magnetic field $B(t) = 0$, the differential equation (4.28) becomes

$$\ddot{c}_2 = \frac{i\lambda}{2}\dot{c}_2 - \frac{\lambda^2}{2}c_2. \tag{4.30}$$

With initial conditions $c_1(0) = 0$ and $c_2(0) = 1$ the solution is

$$c_2(t) = \frac{1}{3}e^{i\lambda t} + \frac{2}{3}e^{-i\frac{\lambda}{2}t}, \tag{4.31}$$

$$|c_2(t)|^2 = \frac{5}{9} + \frac{4}{9}\cos\left(\frac{3}{2}\lambda t\right), \tag{4.32}$$

corresponding to a simple oscillatory behaviour of the probability coefficients, with a frequency proportional to the strength λ of the spin-orbit coupling. This behaviour does not directly imply a dynamical decay of the spin vector in the way obtained from the TD-SDFT calculations.

2. In the limiting case of a strongly varying magnetic field, $B(t)$, such that its time derivative is greater than the value of the field itself $\dot{B} \gg B(t)$, we could make the approximation $f(t) \simeq \frac{\dot{B}}{2}$ and the second order differential equation for the coefficient $c_2(t)$ becomes

$$\ddot{c}_2 = \frac{i\lambda}{2}\dot{c}_2 - i\frac{\dot{B}}{2}c_2, \tag{4.33}$$

for which we can find the following general solution

$$c_2(t) = Ae^{i\omega_+ t} + Be^{i\omega_- t}, \tag{4.34}$$

where the coefficients $\omega_\pm$ are given by

$$\omega_\pm = \frac{\lambda}{4} \pm \sqrt{\frac{\lambda^2}{16} + i\frac{\dot{B}}{2}}. \tag{4.35}$$

By rewriting the complex numbers $\omega_\pm$ in polar form we find

$$\omega_\pm = \frac{\lambda}{4} \pm \rho e^{i\frac{\varphi}{2}}, \tag{4.36}$$

with

$$\rho = \left[\left(\frac{\lambda}{4}\right)^4 + \left(\frac{\dot{B}}{2}\right)^2\right]^{\frac{1}{4}}. \tag{4.37}$$

In this case we can safely assume that $\frac{\dot{B}}{2} \gg \frac{\lambda^2}{16}$, such that

$$\rho \sim \sqrt{\frac{\dot{B}}{2}}, \tag{4.38}$$

$$\varphi = \operatorname{atan}\left(\frac{8\dot{B}}{\lambda^2}\right). \tag{4.39}$$

By making use of the initial condition for the wave function $c_2(0) = 1$ and $c_1(0) = 0$ we finally obtain the following solution

$$c_2(t) = \left(\frac{1}{2} - \frac{\lambda e^{-i\frac{\varphi}{2}}}{8\rho}\right)e^{i\left[\frac{\lambda}{4} + \rho\cos\left(\frac{\varphi}{2}\right)\right]t}e^{-\rho\sin\left(\frac{\varphi}{2}\right)t} + \left(\frac{1}{2} + \frac{\lambda e^{-i\frac{\varphi}{2}}}{8\rho}\right)e^{i\left[\frac{\lambda}{4} - \rho\cos\left(\frac{\varphi}{2}\right)\right]t}e^{\rho\sin\left(\frac{\varphi}{2}\right)t}, \tag{4.40}$$

while for the coefficient $c_1(t)$ we have

$$c_1(t) = -\frac{\lambda e^{i\frac{\varphi}{2}}}{2\sqrt{2}\rho}\left[e^{i\left(\frac{\lambda}{4}+\rho\cos\left(\frac{\varphi}{2}\right)\right)t}e^{\rho\sin\left(\frac{\varphi}{2}\right)t} - e^{i\left(\frac{\lambda}{4}-\rho\cos\left(\frac{\varphi}{2}\right)\right)t}e^{-\rho\sin\left(\frac{\varphi}{2}\right)t}\right]. \quad (4.41)$$

In both the expansion coefficients we find an oscillatory component coupled to a term of the form $e^{\pm\rho\sin\left(\frac{\varphi}{2}\right)t}$, that making use of the condition (4.38) becomes $e^{\pm\sqrt{|\dot{B}|}}$. This clearly shows that under strongly varying magnetic fields the variation of the probability amplitude is driven by the absolute value of $\dot{B}$. However, in absence of spin-orbit coupling ($\lambda = 0$), it is easy to see that no dynamics is possible between the two states, in fact $c_1(t) = 0$ throughout the entire evolution.

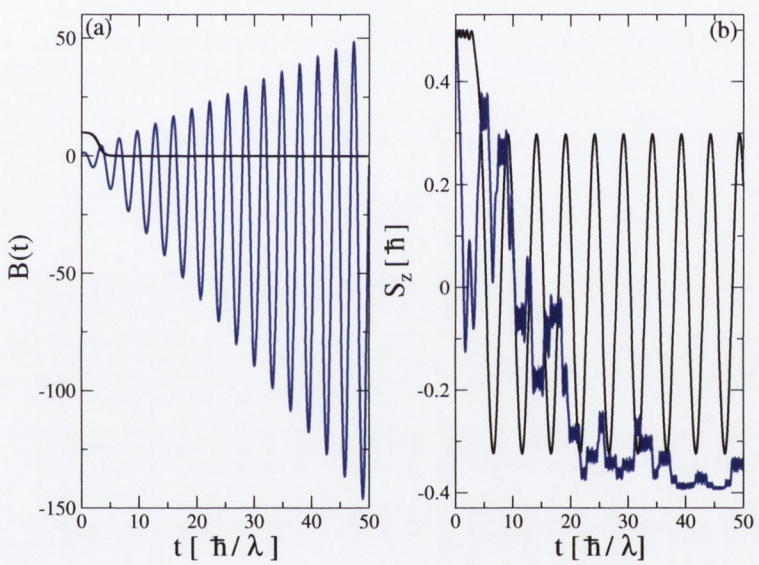


FIGURE 4.19: (a) trajectories of the applied magnetic field $B(t)$; (b) and correspondent evolution of the spin component $\langle\hat{S}_z\rangle$.

A numerical integration of the Schrodinger equation with Hamiltonian (4.21) in the case of no spin-orbit coupling ($\lambda = 0$) returns, as expected, no observable spin dynamics. $\langle\hat{S}^z\rangle$ remains constant during the evolution, if the magnetic field $\mathbf{B}(t)$ is parallel to the initial spin direction. In contrast when $\lambda \neq 0$, an initial state that is not characterized by a maximum or minimum $j_z = l_z + s_z$ value, under a step - like variation of the magnetic field $\mathbf{B}(t)$ [similar to those pictured in Fig. (4.17) (c) and (d)] produces a sharp change in the expectation value of the spin operator $\hat{S}^z$ (see Fig. 4.20). In particular, for an initial spin up state ($s_z = 1/2$) we observe a decrease of $\langle\hat{S}^z\rangle$ after the drop in the magnitude of the magnetic field, while an initially down spin state shows an increase in the expectation value $\langle\hat{S}^z\rangle$.

In other words, a change in the magnetic field $\mathbf{B}(t)$ combined with the spin-orbit coupling, leads to a transfer of part of the spin expectation value into the orbital

moment more efficiently than in the case of absence of the effective magnetic field. This will be still valid even if initially the spin state is collinear to the magnetic field direction (along the spin quantization axis). From Fig. 4.20

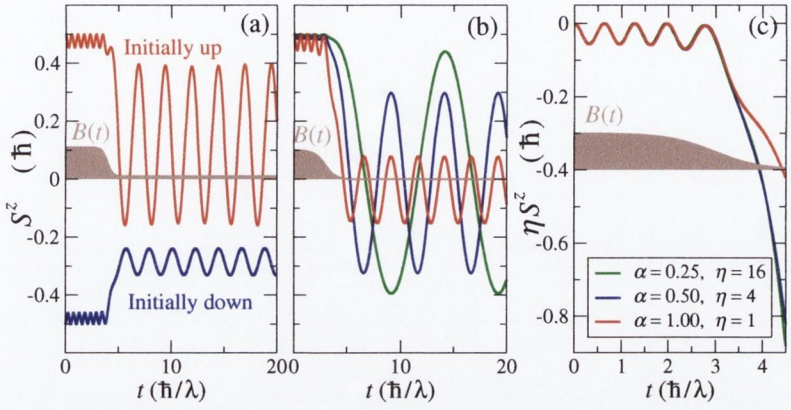


FIGURE 4.20: Trajectories of $\langle \hat{S}^z \rangle$ under the action of the Hamiltonian (4.21) in the case of (a) having an initial spin-up or down state; (b) for different values of a multiplicative factor α for the spin-orbit coupling ($\lambda \rightarrow \alpha\lambda$), with an initial spin-up state; (c) similarly to Fig. 4.17 the trajectories are rescaled by a factor $1/\alpha^2$. The shaded area describes the temporal profile of the applied magnetic field $\mathbf{B}(t) = [0, 0, B(t)]$. The initial orbital state is in a linear combination of $l_z = 0, 1$ states.

(b) it is also clear that the amount of spin lost after the action of $\mathbf{B}(t)$ is not the same for different spin-orbit coupling coefficients λ. In particular higher values of λ lead to larger spin decays. Furthermore the oscillations observed in the spin expectation value are lower in magnitude in the case of $\alpha = 1.0$ with respect to the case of $\alpha = 0.5$ and $\alpha = 0.25$.

In addition, we can see from Fig. 4.19 that for different applied magnetic fields $\mathbf{B}(t) = [0, 0, B(t)]$, and with the same spin-orbit coupling coefficient λ, the spin decay could change drastically, demonstrating the importance of the role played by the applied magnetic field into the spin dynamics of the quantum system.

In conclusion it is natural to identify the magnetic field $\mathbf{B}(t)$ with the exchange-correlation field $\mathbf{B}_{xc}(\mathbf{r}, t)$ arising from the TD-SDFT simulations. In practice the local strong variations characterizing the dynamics of this field, shown in Fig. 4.17 for Fe_6 and in Fig. 4.13 in the case of Fe_4 are approximately reproduced in our model through the time dependent $\mathbf{B}(t)$ of Fig. 4.20. This is collinear to the spin vector during the entire dynamical simulation. The loss of spin predicted by our model is qualitatively in agreement with the local dynamics of the spin vector obtained from the TD-SDFT simulations, justifying its use at least as an explanatory tool for the ultrafast demagnetization process. Of course, some of the ingredients necessary for a complete description of the spin dynamics in transition metals are still missing, and we will fill this gap in Chapter 5. In the next section we will see that the use of this simplified description does not

only provide a qualitative tool for the analysis of the ultrafast spin dynamics, but it can also make some more quantitative predictions.

4.3 General law for the ultrafast demagnetization of transition metals

We have already seen in Fig. 4.17 that the spin decay rate of the Fe_6 cluster scales, in the initial stage of the evolution, with the square of the spin-orbit coupling strength λ. Moreover, if we compare the spin decay rate of all the Fe-based clusters normalized to the ground state total magnetization we find that, under the same applied external pulse, the demagnetization rate is exactly the same in all the cases considered (see Fig. 4.21). These results confirm the validity of

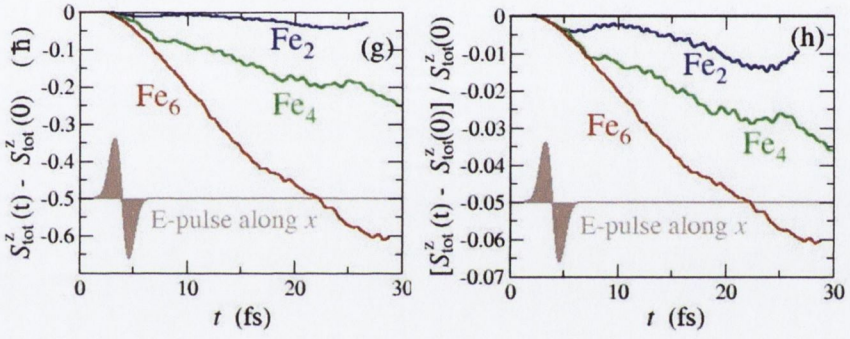


FIGURE 4.21: Plot of the global spin decay of the various clusters considered up to now: (a) variation of the total magnetization with respect to its ground state value $\Delta S^z_{tot}(t)$; (b) same quantity normalized with respect to the magnetization ground state $\Delta S^z_{tot}(t)/S^z_{tot}(0)$.

the decay rate law at least in the case of the Fe-based clusters. However, we also would like to understand whether this law can be extended to other systems. We then start from the model introduced in the previous section to see if it can predict the same decay law for the spin moment. Interestingly this is indeed the case, as it is clearly shown in Fig. 4.20(b), where we plot the results of the numerical integration of the 6–dimensional spin - orbital model for different values of the spin-orbit coupling strength, rescaled by a factor α. It is demonstrated in panel (c) of the same figure that the demagnetization curves during the variation of the magnetic pulse become steeper by a factor α^2 as the rescaled trajectories $\langle \hat{S}^z \rangle / \alpha^2$ coincide for a brief time interval.

This property may be also demonstrated analytically by deriving the lowest order terms in the perturbative expansion of the solution $|\Psi(t)\rangle$ in powers of t. For simplicity, also here, we consider the dynamics of two coupled states $|l_z = 1, s_z = -1/2\rangle$

and $|l_z = 0, s_z = 1/2\rangle$

$$|\Psi(0)\rangle = c_1 |l_z = 1, s_z = -1/2\rangle + c_2 |l_z = 0, s_z = 1/2\rangle , \tag{4.42}$$

under the time dependent Hamiltonian, $\hat{H}(t)$, that in matrix form may be expressed as

$$\hat{H}(t) = \hat{H}_0 + \hat{V}(t) = \begin{pmatrix} -\frac{\lambda}{2} & \frac{\lambda}{\sqrt{2}} \\ \frac{\lambda}{\sqrt{2}} & 0 \end{pmatrix} + \begin{pmatrix} -\frac{B(t)}{2} & 0 \\ 0 & \frac{B(t)}{2} \end{pmatrix}.$$

Here we have decomposed $\hat{H}(t)$ into a time-independent part $\hat{H}_0$ and a time-dependent part $\hat{V}(t)$. In the interaction picture representation a general operator $\hat{A}_S$ (S indicates the time independent Schrodinger representation) may be written as follows

$$\hat{A}_I(t) = e^{i\hat{H}_0 t/\hbar} \hat{A}_S e^{-i\hat{H}_0 t/\hbar}. \tag{4.43}$$

In the interaction picture the operator $\hat{V}(t)$ and the spin operator $\hat{S}^z$ are represented respectively as

$$\hat{V}_I(t) = e^{i\hat{H}_0 t/\hbar} \hat{V}(t) e^{-i\hat{H}_0 t/\hbar}, \tag{4.44}$$

$$\hat{V}_I(t) = \frac{1}{9} \begin{pmatrix} -\frac{B(t)}{2} - 4B(t)\cos\left(\frac{3}{2\hbar}\lambda t\right) & \sqrt{2}B(t)(1 + e^{\frac{3}{2\hbar}i\lambda t}) - 2\sqrt{2}B(t)e^{-\frac{3}{2\hbar}i\lambda t} \\ \sqrt{2}B(t)(1 + e^{-\frac{3}{2\hbar}i\lambda t}) - 2\sqrt{2}B(t)e^{\frac{3}{2\hbar}i\lambda t} & \frac{B(t)}{2} + 4B(t)\cos\left(\frac{3}{2\hbar}\lambda t\right) \end{pmatrix},$$

while

$$\hat{S}^z(t) = e^{i\hat{H}_0 t/\hbar} \frac{\hbar}{2} \hat{\sigma}^z e^{-i\hat{H}_0 t/\hbar}, \tag{4.45}$$

$$\hat{S}^z(t) = -\frac{\hbar}{18} \begin{pmatrix} 1 + 8\cos\left(\frac{3}{2\hbar}\lambda t\right) & -2\sqrt{2} + 4\sqrt{2}e^{-\frac{3}{2\hbar}i\lambda t} - 2\sqrt{2}e^{\frac{3}{2\hbar}i\lambda t} \\ -2\sqrt{2} + 4\sqrt{2}e^{\frac{3}{2\hbar}i\lambda t} - 2\sqrt{2}e^{-\frac{3}{2\hbar}i\lambda t} & -1 - 8\cos\left(\frac{3}{2\hbar}\lambda t\right) \end{pmatrix}.$$

where $\hat{\sigma}^z$ is the z Pauli matrix.

The wave function in the interaction representation evolves under the following dynamical equation

$$|\Psi(t)\rangle_I = e^{i\hat{H}_0 t/\hbar} |\Psi(t)\rangle_S . \tag{4.46}$$

in the $t \to 0$ limit, the equation for the time-dependent wavefunction in the interaction picture writes

$$|\Psi(t)\rangle_I = |\Psi(0)\rangle - \frac{i}{\hbar} \int_0^t dt' \hat{V}_I(t') |\Psi(t')\rangle_I , \tag{4.47}$$

and it can be expanded in powers of t as

$$|\Psi(t)\rangle_I = |\Psi(0)\rangle - \frac{i}{2\hbar} \frac{d}{dt} \hat{V}_I(t)\Big|_{t=0} t^2 |\Psi(0)\rangle + O(t^3). \tag{4.48}$$

Given the fact that $B(t = 0) = 0$, the time derivative of the operator $\mathbf{V}_I(t)$ at the time $t = 0$ is defined as follows

$$\frac{d}{dt} \hat{V}_I(t)\Big|_{t=0} = \frac{1}{2} \begin{pmatrix} -\dot{B} & 0 \\ 0 & \dot{B} \end{pmatrix}.$$

The wave function at time t then becomes

$$|\Psi(t)\rangle_{\mathrm{I}} = \begin{pmatrix} 1 + i\frac{\dot{B}t^2}{4\hbar} & 0 \\ 0 & 1 - i\frac{\dot{B}t^2}{4\hbar} \end{pmatrix} |\Psi(0)\rangle + O(t^3).$$

By restricting ourselves to terms of order t^2, the variation of the expectation value of $\hat{S}^z$ between $|\Psi(t)\rangle_{\mathrm{I}}$ and the ground state $|\Psi(0)\rangle$ then reads

$$\langle \hat{S}^z(t)\rangle - \langle \hat{S}^z(0)\rangle = -\frac{\lambda^2 t^2}{2\hbar}\Big[-\frac{\sqrt{2}}{2} c_1 c_2 - c_1^2 + c_2^2 \Big], \tag{4.49}$$

i.e. it scales as λ^2 for small times t following the initial variation of B. Note that in this approximation the early demagnetization does not depend on the strength of the field, but terms proportional to $\dot{B}$ become important at higher order, suggesting a modification of the law for strong magnetic field variations.

In practice if one starts from a spin-up configuration with $c_1 = 0$ and $c_2 = 1$, we will have that

$$\Delta \langle \hat{S}^z \rangle = -\frac{\lambda^2 t^2}{2\hbar}. \tag{4.50}$$

This shows that, according to the model, the spin decay rate at $t = 0$ is proportional to $-\lambda^2$. In order to quantitatively verify the general validity of this

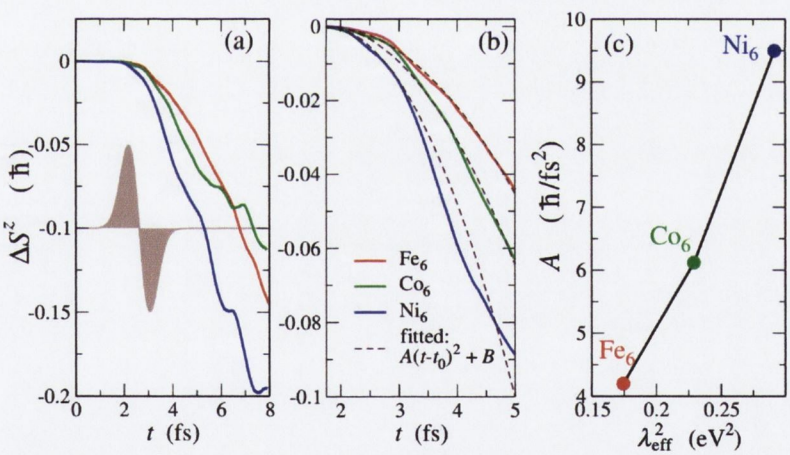


FIGURE 4.22: (a) TDSDFT trajectories of the variation of $\langle \hat{S}^z_{\mathrm{tot}}(t)\rangle$ with respect of the ground state magnetization for three different clusters: Fe_6, Ni_6 and Co_6, all sharing the same Fe_6 geometry [121]. (b) Closer view into the coherent part of the trajectories where a parabolic decay [$y = A(t - t_0)^2 + A_0$] is fitted for each trajectory (dashed curves). (c) The fitting coefficients A from panel (b) versus the effective atomic SOC from Eq. (4.51) for each material.

λ^2 dependence of the demagnetization speed, we look also at the laser-induced response of clusters geometrically identical to Fe_6 but composed of Co and Ni. Note that we keep the same frozen geometry of Fe_6 as in Ref. [130], although

this is not the ground state for Ni_6 and Co_6, in order to exclude the structural factor from the comparison. We quantify their ionic spin-orbit coupling strength through the following definition

$$\lambda_{\text{eff}} = \sum_{l \in \text{occ.}} \frac{n_l}{n_{\text{tot}}} \int_0^\infty dr V_l^{\text{SO}}(r) \left| R_{n,l}(r) \right|^2 , \tag{4.51}$$

where n_l are the KS state occupations with l spanning the valence states (in this case $3s, 3p, 3d$ and $4s$), $n_{\text{tot}} = \sum_{l \in \text{occ.}} n_l$, $R_{n,l}(r)$ the radial pseudo-atomic wave functions and $V_l^{\text{SO}}(r)$ the usual spin-orbit coupling potential of Eq. (4.9)

$$V_l^{\text{SO}}(r) = \frac{1}{2l+1} [V_{l+1/2}^{\text{ion}}(r) - V_{l-1/2}^{\text{ion}}(r)]. \tag{4.52}$$

These potentials are all obtained from LSDA calculations for isolated atoms.

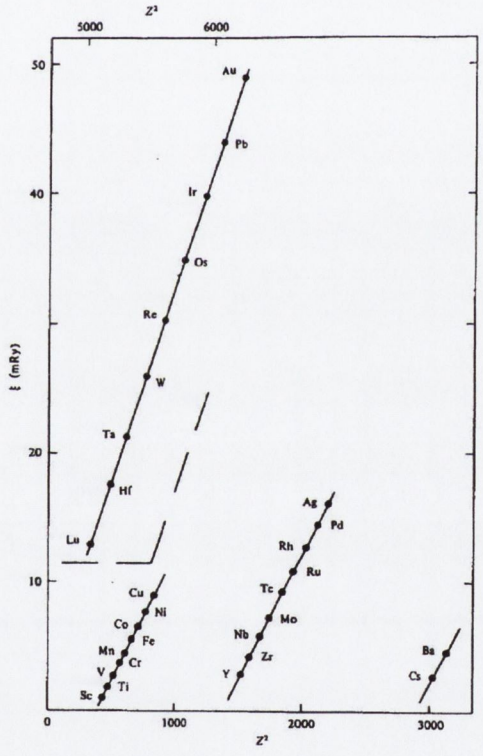


FIGURE 4.23: Table of the spin orbit coefficient ξ (in mRy) for transition metal atoms. (from [131])

By fitting the first few femtoseconds of the demagnetization curve to a quadratic time decay $\langle \hat{S}^z(t) \rangle \propto A(t - t_0)^2$ with t_0 taken during the rise of the laser pulse (around 1.5 fs), we extract the demagnetization rate A of the three different clusters. Such extracted demagnetization rates show a systematic dependence on the ionic spin-orbit coupling strength, λ_{eff}^2, of the different atoms [see Fig. 4.22(c)]. We can compare λ_{eff} for the isolated atom with the ξ coefficient appearing in the

spin orbit part of the Pauli Hamiltonian

$$H_{\mathrm{SO}} = \xi \mathbf{l} \cdot \mathbf{s}, \tag{4.53}$$

$$\xi = -\frac{e\hbar^2}{2(mc)^2} \left\langle \frac{1}{r} \frac{dV_{\mathrm{ion}}}{dr} \right\rangle, \tag{4.54}$$

with r defining the distance from the atomic center. The values of the parameter ξ extracted for different atomic systems are shown in Fig. 4.23. The difference between λ_{eff} and the coefficient ξ is due to the various approximations introduced in order to extract an effective spin orbit coupling from Eq. (4.51), but it does not pose a threat to our hypothesis of the λ^2 dependence.

From Fig. 4.22 it is evident that the onset demagnetization rate shows a strong dependence on the ionic spin-orbit coupling of the material, scaling quadratically with the strength λ. Because of the localised nature of this ultrafast demagnetization mechanism we believe that these findings are valid also beyond the cluster systems and may provide a formal backing to experimental observations. For instance, it can support the different demagnetization rates observed between Ni and $CoPt_3$ shown in Ref. [42].

In Chapter 5 we will extend our understanding of the demagnetization process to the case in which the spin vector is strongly non collinear, at least locally. This will require rethinking the entire significate of the spin continuity equation (4.11) and, in particular, the role played by the spin currents in the demagnetization process.

CHAPTER 5

DYNAMICAL EXCHANGE INTERACTIONS

In the previous chapter we have discussed the importance of the spin-orbit coupling for the femtosecond spin relaxation of transition metals. We have seen that the fundamental mechanism lying at the core of these processes is the loss of spin through the spin-orbit channel. This effect could be enhanced by the simultaneous action of a strongly varying internal magnetic field excited by the action of the external laser pulse. From now on we will call this effective spatially inhomogeneous magnetic field $\mathbf{B}_{\text{eff}}(\mathbf{r}, t)$.

In the context of the discussion started in the previous Chapter, the ultrafast demagnetization of transition metals has been studied by making use of ab initio TD-SDFT. Within this description it would be natural to identify $\mathbf{B}_{\text{eff}}(\mathbf{r}, t)$ with the exchange-correlation magnetic field $\mathbf{B}_{\text{xc}}(\mathbf{r}, t)$. That is exactly what we have done in the previous Chapter. Unfortunately there are some reasons to believe that this identification is not entirely valid.

Non-collinearity issue. In the previous chapter we have extensively shown that even for a ferromagnetic cluster like Fe_4 the amount of local non collinearity of the spin vector, measured through the quantity $S^{\text{I}}_{xy}(t) = \sqrt{S^2_{\text{Ix}} + S^2_{\text{Iy}}}$, is not negligible at least out of the cluster plane, while in the case of Fe_6 it is even more important as we will see later in chapter. A natural question to ask is then, where does all the non collinearity come from during the dynamical evolution?

We already know that within the LSD approximation the exchange-correlation magnetic field $\mathbf{B}_{\text{xc}}(\mathbf{r}, t)$ cannot exert a torque, even locally, on the magnetization vector, since we have

$$\mathbf{m}(\mathbf{r}, t) \times \mathbf{B}_{\text{xc}}(\mathbf{r}, t) = 0. \tag{5.1}$$

The only two terms in the continuity equation that can generate local non collinearity are the spin-current divergence and the spin-orbit coupling torque. Since the strength of the spin orbit torque is not so big to explain such a huge value for $S_{xy}^{loc}(t)$ the spin current must play an important role during the dynamical evolution that is, however, difficult to quantify given the tensorial nature of this object. Is it licit to ask if the spin current can really contribute to the effective field $\mathbf{B}_{eff}(\mathbf{r}, t)$?

Exchange interactions issue The second most important issue arising from the discussion of the previous chapter is directly related to the out of equilibrium nature of the exchange interactions. The exchange interaction is the most important force in magnetism and it is responsible for the magnetic ordering below the critical temperature T_c. At this level it is important to distinguish among the two most important types of exchange interactions, namely the Coulomb exchange and the direct kinetic exchange.

The coulomb type of exchange arises directly from the electrostatic interactions between electrons

$$H_C = \sum_{i<j} \frac{1}{|\mathbf{r}_i - \mathbf{r}_j|}. \tag{5.2}$$

H_C is not a spin dependent interaction, but the antisymmetry of the many-body wave function (change of sign under permutation of two electrons) makes the eigenvalues of the Hamiltonian H_C effectively spin dependent. The two fundamental matrix elements in the case of a two-particle wave function with opposite spin $|\Psi_{1\uparrow,2\downarrow}\rangle$ are

$$U_{1,2} = \left\langle \Psi_{1\uparrow,2\downarrow} \left| \frac{1}{|\mathbf{r}_1 - \mathbf{r}_2|} \right| \Psi_{1\uparrow,2\downarrow} \right\rangle, \tag{5.3}$$

which defines the amount of energy required to maintain the up / down spin configuration, and

$$J_{1,2} = \left\langle \Psi_{1\uparrow,2\downarrow} \left| \frac{1}{|\mathbf{r}_1 - \mathbf{r}_2|} \right| \Psi_{1\downarrow,2\uparrow} \right\rangle, \tag{5.4}$$

which instead represents the amount of energy required to exchange the two spins.

The Coulomb exchange is taken into account through the exchange-correlation part of the Kohn-Sham Hamiltonian (E_{xc}), and despite the fact that strong correlation effects are usually not well described in LDA [78], we have already established its importance for the ultrafast demagnetization process.

The kinetic exchange instead arises when it is the electron hopping that plays a major role. In this case anti-ferromagnetic coupling between the spins is favored, allowing the electrons to hop across neighboring sites. For parallel spin the hopping is suppressed due to the Pauli principle. This

mechanism is usually described in terms of effective Hamiltonian that in the simplest case of a two-site system acquires the form

$$\hat{H}_{\text{eff}} = \frac{4t^2}{U}\left(\hat{\mathbf{S}}_1 \cdot \hat{\mathbf{S}}_2 - \frac{1}{4}\hat{n}_1\hat{n}_2\right). \tag{5.5}$$

This is obtained from a large U expansion of the Hubbard Hamiltonian, where $\hat{n}_i$ and $\hat{\mathbf{S}}_i$ are the on-site density and spin operators

$$\hat{H}_{\text{U}} = -t(\hat{c}_1^{\dagger}\hat{c}_2 + \text{c.c}) + U\hat{n}_1\hat{n}_2. \tag{5.6}$$

The exchange coupling $4t^2/U$ in this case is proportional to the square of the hopping parameter revealing its purely kinetic nature. Such an object, however, does not appear so clearly within the SDFT continuity equation, and our purpose will be to sort out this difficulty.

The spin Hamiltonians that we have introduced are always used in the context of a pure equilibrium spin theory. The issue in the case of applications to real magnetic systems is connected to the difficulty of predicting the correct value of the various exchange parameters.

The parameters U and J for the Coulomb exchange may be estimated usually through the so called Slater integrals [132], starting from the following expression for the direct interactions between electrons on the same shell

$$U^{\text{n,l}}_{\text{m,m}'} = \iint d^3r d^3r' \left|R_{\text{n,l}}(|\mathbf{r}|)\Upsilon_{\text{m,l}}(\hat{\mathbf{r}})\right|^2 \frac{1}{|\mathbf{r}-\mathbf{r}'|}\left|R_{\text{n,l}}(|\mathbf{r}'|)\Upsilon_{\text{l,m}'}(\hat{\mathbf{r}}')\right|^2, \tag{5.7}$$

with $\Upsilon_{\text{l,m}}(\hat{\mathbf{r}})$ being spherical harmonics and the $R_{\text{n,l}}(|\mathbf{r}|)$ radial wave functions. By making use of the Klebsch - Gordon coefficients the Coulomb parameters U and J may be expressed through the so called Slater integrals [132]

$$F^k_{\text{n,l}} = e^2 \int_0^{\infty} dr r^2 \left|R_{\text{n,l}}(r)\right|^2 \int_0^{\infty} dr' (r')^2 \left|R_{\text{n,l}}(r')\right|^2 \frac{r_<^k}{r_>^{k+1}}, \tag{5.8}$$

where $r_< = r$, $r_> = r'$ ($r_> = r$, $r_< = r'$) if $r' > r$ ($r > r'$).

An alternative way to compute the Coulomb parameter, U, is through a constrained DFT calculation with fixed occupancies [133, 134], screening effects are taken into account self-consistently. If the Coulomb interaction energy contributes to the DFT energy as a function of the number n_{d} of d electrons, then according to the Hubbard expression U may be calculated as

$$U = \frac{\partial^2 E_{\text{DFT}}}{\partial n_{\text{d}}^2}. \tag{5.9}$$

This can be obtained by performing several constrained DFT calculations with a fixed value of the occupation number n_{d}. These considerations could be in principle extended with no particular difficulties also to the Coulomb exchange

parameter J.

The methods aforementioned try to extract from the DFT ground state parameters U and J necessary to construct a specific Coulomb interaction Hamiltonian $\hat{H}_{\mathrm{C}}$, which should be able, at least to a certain degree, to reproduce the DFT result. The difficulties arise, however, when we try to evolve the system dynamically. In this case constrained methods are not useful anymore and the parameters should be extracted dynamically due to their dependence on the system wave function.

5.1 Exchange interactions in the adiabatic approximation

5.1.1 Exchange interactions from the magnetic force theorem

Analogous considerations arise also in case of kinetic exchange interactions. In order to make our treatment more clear from now on we will call the kinetic exchange parameter $\mathcal{J}$. This is different from the Coulomb exchange, J. The evaluation of the static $\mathcal{J}$, from first principle has been for many years one of the desired developments in the context of material properties prediction [135–137]. This has been closely related to and motivated by the problem of theoretical predicting finite-temperature properties of magnetic systems. It is known, in fact, that the main contribution to the thermodynamical properties of itinerant electron magnets come from collective spin excitations of the Heisenberg-like Hamiltonian, generally written in the following form

$$H_{\mathrm{Heisen.}} = -\frac{1}{2N}\sum_{i\neq j}\mathcal{J}_{\mathrm{i,j}}\,\mathbf{S}_i\cdot\mathbf{S}_j, \tag{5.10}$$

where $\mathbf{S}_i$ defines the spin vector associated to the site i and $\mathcal{J}_{\mathrm{i,j}}$ represents the exchange interaction among the spins over the two atomic sites i and j (N is the number of unit cells in the macroscopic system). In the case of magnetic insulators the exchange coupling coefficient between different atomic sites $\mathcal{J}_{\mathrm{i,j}}$ is simply given by the difference in total energy among ferromagnetic and antiferromagnetic configurations of the two atomic sites. In this case the parameters are usually extracted from static DFT results through the so-called broken symmetry approach [138]. Such broken symmetry approach refers to unrestricted spin density calculations in which opposite spin directions are allowed at different atomic sites. The exchange parameters are then determined through the difference in total energy among the low spin (LS) and high spin (HS) configurations

$$\mathcal{J}_{\mathrm{i,j}} = f[\{\mathbf{S}_{\mathrm{I}}\}](E_{\mathrm{LS}} - E_{\mathrm{HS}}), \tag{5.11}$$

where $\{\mathbf{S}_{\mathrm{I}}\}$ defines the spin configuration of the system. Despite the usefulness and the applicability of the previous expression to the case of magnetic insulators,

the Heisenberg Hamiltonian (5.10) if applied to magnetic metals can describe only small spin deviations from the ground state. These difficulties are directly connected to the itinerant nature of electrons in metallic systems. When the inhomogeneities of the spin density are not small, the dependence of $\mathcal{J}_{\mathrm{i,j}}$ on the magnetic configuration cannot be neglected and one should rewrite Eq. (5.10) as

$$H_{\mathrm{Heisen.}} = -\frac{1}{2N}\sum_{i\neq j}\mathcal{J}_{\mathrm{i,j}}[\{\mathbf{S}_{\mathrm{I}}\}]\,\mathbf{S}_i\cdot\mathbf{S}_j. \tag{5.12}$$

In order to generalize the relation (5.11) in the case of metals several alternatives have been proposed. A first possibility was suggested in references [139, 140] based on the so called magnetic force theorem (MFT) [141], which states that total energy variations under local rotation angle θ of the atomic spin $\mathbf{S}_i$ coincides with the sum of one particle energy changes, for occupied states, at fixed effective ground state potential. In the context of the KKR-Green's functions method [142, 143], the spin dependent electron density $\rho_\sigma(\mathbf{r})$ is written as the sum over the non overlapping cells Ω_i

$$\rho_\sigma(\mathbf{r}) = \sum_i \rho_{i\sigma}(\mathbf{r}-\mathbf{R}_i), \tag{5.13}$$

with consequent definition of the on site magnetization M_i along the spin quantization axis

$$M_i = \int_{\Omega_i} \mathrm{d}^3 r\,[\rho_\uparrow(\mathbf{r}) - \rho_\downarrow(\mathbf{r})]. \tag{5.14}$$

The pair interaction coefficient $\mathcal{J}_{\mathrm{i,j}}$ is then related to the energy variation of two spin moments rotating at opposite angles θ,

$$\delta E'_{\mathrm{i,j}} = \delta E_{\mathrm{i,j}} - \delta E_{\mathrm{i}} - \delta E_{\mathrm{j}}, \tag{5.15}$$

where δE_{i} defines the interaction energy of the single spin moment with the rest of the system. According to this definition

$$\delta E'_{\mathrm{i,j}} \simeq \frac{1}{2}\mathcal{J}_{\mathrm{i,j}}\theta^2. \tag{5.16}$$

The possibility to extract the effective parameters $\mathcal{J}_{\mathrm{i,j}}$ relies on the availability of adiabatic total energy variations,

$$\delta E = -\int_0^{\epsilon_{\mathrm{F}}} d\epsilon\,\delta N(\epsilon), \tag{5.17}$$

with $N(\epsilon)$ being number of states available at the given energy ϵ. The Lloyd formula [144] connects $N(\epsilon)$ to the scattering path operator $\hat{T}(\epsilon)$,

$$N(\epsilon) = N_0(\epsilon) + \frac{1}{\pi}\,\mathrm{Im}\Big\{\mathrm{Tr}\Big[\ln\hat{T}(\epsilon)\Big]\Big\}, \tag{5.18}$$

formally expressed as [143]

$$(\hat{T}^{-1})_{\mathrm{i,j}}^{L\sigma,L'\sigma'} = t_{iL\sigma\sigma'}^{-1}\delta_{\mathrm{i,j}}\delta_{L,L'} - G_{\mathrm{i,j}}^{L,L'}\delta_{\sigma,\sigma'}. \tag{5.19}$$

This object defines the probability amplitude that an incoming wave at site j is scattered into an outgoing wave at site i through all possible scattering events. Here $t_i(\epsilon)$ defines the single-site scattering potential, while $G_{\mathrm{i,j}}^{L,L'}(\epsilon)$ is the two sites ground state Green's function of the system. It is convenient to rewrite the on-site scattering potential, $t_{iL\sigma\sigma'}$, which mixes the up and down spin states, in the form,

$$\hat{t}_i = \frac{1}{2}(t_{i\uparrow} + t_{i\downarrow}) + \frac{1}{2}(t_{i\uparrow} - t_{i\downarrow})(\mathbf{e}_i \cdot \hat{\boldsymbol{\sigma}}), \tag{5.20}$$

with $\mathbf{e}_i$ defining the on-site spin direction. Under infinitesimal rotation of the on-site spin direction the variation of the inverse scattering potential operator is

$$\delta\hat{t}_i^{-1} = \frac{1}{2}(t_{i\uparrow}^{-1} - t_{i\downarrow}^{-1})(\delta\mathbf{e}_i \cdot \hat{\boldsymbol{\sigma}}), \tag{5.21}$$

while the full scattering path operator in the new perturbed state is

$$\hat{T}' = \hat{T}(1 + \delta\hat{t} \cdot \hat{T})^{-1}. \tag{5.22}$$

By substituting $\hat{T}'$ into the expression for the energy variation δE between the old and the new spin configuration leads to the simplified expression

$$\delta E = \frac{1}{\pi}\int^{\epsilon_F} d\epsilon\, \mathrm{Im}\Big\{\mathrm{Tr}\Big[\ln(1 + \delta\hat{t}^{-1}\hat{T})\Big]\Big\}, \tag{5.23}$$

leading to the following result for the pair exchange coupling (by expanding it up to the lowest order in $\delta\mathbf{e}$)

$$\mathcal{J}_{\mathrm{i,j}} = \frac{1}{4\pi}\int^{\epsilon_F} d\epsilon\, \mathrm{Im}\Big\{\mathrm{Tr}_L(\Delta_i T_{\mathrm{i,j}}^{\uparrow}\Delta_j T_{\mathrm{j,i}}^{\downarrow})\Big\}, \tag{5.24}$$

where $\Delta_i = \hat{t}_{i\uparrow}^{-1} - \hat{t}_{i\downarrow}^{-1}$ and Tr_L is the trace over the orbital degrees of the scattering operator.

The elementary excitations connected to spin rotations are named spin waves. In case of small excitations the spin-wave spectrum can be mapped onto a Heisenberg Hamiltonian. For a spin spiral solution θ_i is written as $\mathbf{q}\cdot\mathbf{R}_i$, therefore small deviations imply $\mathbf{q} \to 0$ and generate the following spin wave spectrum

$$\omega_{\mathbf{q}} = \sum_j \mathcal{J}_{0\mathrm{j}}\Big[1 - \cos\big(\mathbf{q}\cdot\mathbf{R}_j\big)\Big], \tag{5.25}$$

with $\mathcal{J}_{0\mathrm{j}}$ representing the interaction with all the other crystal sites. The previous expression is formally exact in the limit of small $\mathbf{q}$ vectors. This relation provides a direct path to the estimation of the exchange coupling parameter, $\mathcal{J}_{0\mathrm{j}}$, through the knowledge of the spin-wave spectrum $\omega_{\mathbf{q}}$ of the crystal. It can also be written

in reciprocal space as

$$\omega_{\mathbf{q}} = \frac{4}{M}[\mathcal{J}(\mathbf{0}) - \mathcal{J}(\mathbf{q})], \tag{5.26}$$

which is directly used for computing the exchange coupling. The issue here is the evaluation of the spin-wave spectrum $\omega_{\mathbf{q}}$ for each value of the wave vector. It can be shown [145] that in the simplest case of a single magnetic sublattice in the crystal, the difference in total energy between the spin spiral configuration, $E(\mathbf{q}, \theta)$, and the reference ferromagnetic one, $E(\mathbf{0}, \theta)$, may be related to the magnon frequency $\omega_{\mathbf{q}}$ through

$$\omega_{\mathbf{q}} = 4\frac{E(\mathbf{q}, \theta) - E(0, \theta)}{M \sin^2 \theta}, \tag{5.27}$$

where M is the module of the onsite magnetization. By employing the magnetic force theorem, the difference in total energy between the two magnetic configurations can be directly related to the difference in the sum of the single particle energies, allowing a direct estimation of the bare exchange interaction starting from total energy of spin spiral configurations. More recently some improvements of the standard MFT have been proposed in the literature leading to the introduction of new effective exchange couplings [146] that do not completely correspond to the old bare ones of the previous version. However these corrections are assumed to be small in the adiabatic parameter $\eta = \bar{\omega}/\Delta$, where $\bar{\omega}$ is the characteristic magnon frequency, Δ is the Stoner splitting, and the mapping between the excitation spectrum of itinerant magnets with the classic Heisenberg Hamiltonian is valid only in adiabatic approximation with $\eta \to 0$ [139, 140].

The knowledge of the exchange coupling $\mathcal{J}_0 = \sum_j \mathcal{J}_{0j}$ may be also exploited to estimate the Curie temperature, T_c, of transition metals in the limit of long magnon waves lengths

$$T_c = \frac{2}{3}\mathcal{J}_0 \frac{\langle M^2 \rangle}{M_0^2}, \tag{5.28}$$

with M_0 being ferromagnetic magnetic moment at $T = 0$ and $\langle M \rangle$ indicating a thermal average at the critical temperature.

5.1.2 Exchange interactions from spin susceptibilities

A natural way to extract the spin excitation spectrum in metallic ferromagnets is based on the calculation of the spin susceptibility. It is well known that these functions are formally exactly calculated within the TD-SDFT formalism [147]. There exists in fact a direct relation between the Kohn-Sham magnetic susceptibility χ_0 and the true many-body magnetic susceptibility χ. By employing the definition of Kohn-Sham susceptibility we have in reciprocal space

$$\delta m_i(\mathbf{q}, \omega) = \sum_j \chi_0^{ij}(\mathbf{q}, \omega)\delta B_s^j(\mathbf{q}, \omega), \tag{5.29}$$

while for the true spin susceptibilty we write

$$\delta m_i(\mathbf{q},\omega) = \sum_j \chi^{ij}(\mathbf{q},\omega)\delta B^j_{\text{ext}}(\mathbf{q},\omega), \tag{5.30}$$

with $\mathbf{B}_\text{s}$ defining the effective non interacting Kohn-Sham magnetic field, and $\mathbf{B}_{\text{ext}}$ corresponding to the externally applied magnetic field. By decomposing $\mathbf{B}_\text{s} = \mathbf{B}_{\text{ext}} + \mathbf{B}_{\text{xc}}$ into the external and exchange-correlation component we obtain

$$\delta m_i(\mathbf{q},\omega) = \sum_j \chi_0^{ij}(\mathbf{q},\omega)\delta B^j_{\text{ext}}(\mathbf{q},\omega) + \sum_{jk} \chi_0^{ik}(\mathbf{q},\omega)\frac{\delta B^k_{\text{xc}}}{\delta m^j}\delta m_j(\mathbf{q},\omega), \tag{5.31}$$

which becomes by using Eq. (5.30)

$$\delta m_i(\mathbf{q},\omega) = \sum_j \chi_0^{ij}(\mathbf{q},\omega)\delta B^j_{\text{ext}}(\mathbf{q},\omega) + \sum_{jkl} \chi_0^{ik}(\mathbf{q},\omega)\frac{\delta B^k_{\text{xc}}}{\delta m^j}\chi^{jl}(\mathbf{q},\omega)\delta B^l_{\text{ext}}(\mathbf{q},\omega). \tag{5.32}$$

This leads to

$$\chi^{ij}(\mathbf{q},\omega) = \chi_0^{ij}(\mathbf{q},\omega) + \sum_{kl} \chi_0^{ik}(\mathbf{q},\omega)\frac{\delta B^k_{\text{xc}}}{\delta m^l}\chi^{lj}(\mathbf{q},\omega), \tag{5.33}$$

that is a formally exact expression in TD-SDFT. Within the LSDA we have

$$\frac{\delta B^k_{\text{xc}}}{\delta m^l} = \frac{B_{\text{xc}}}{m}\left(\delta_{kl} - \frac{m^k m^l}{m^2}\right) + \frac{m^k m^l}{m^2}\frac{\delta B_{\text{xc}}}{\delta m}. \tag{5.34}$$

we distinguish two terms in the sum. The first is purely transverse, while the second is longitudinal. In collinear magnetic systems the transverse susceptibility becomes

$$\hat{\chi^{+-}} = \hat{\chi_0^{+-}} + \hat{\chi_0^{+-}} I_{\text{xc}} \hat{\chi^{+-}}, \tag{5.35}$$

with $I_{\text{xc}} = B_{\text{xc}}/m$. It is then possible, by using the properties of B_{xc}, to express this object as follows [136]

$$\hat{\chi^{+-}} = (m + \hat{\Lambda})(\omega - I_{\text{xc}}\hat{\Lambda})^{-1} \tag{5.36}$$

where $\hat{\Lambda}$ acquires the following complicated structure in frequency space

$$\hat{\Lambda}(\mathbf{r},\mathbf{r}',\omega) = \sum_{\mu\nu} \frac{f_{\mu\uparrow} - f_{\nu\downarrow}}{\omega - \epsilon_{\mu\uparrow} + \epsilon_{\nu\downarrow}} \psi^*_{\mu\uparrow}(\mathbf{r})\psi_{\nu\downarrow}(\mathbf{r})[B_{\text{xc}}(\mathbf{r}') - \epsilon_{\nu\downarrow} + \epsilon_{\mu\uparrow}]\psi^*_{\nu\downarrow}(\mathbf{r}')\psi_{\mu\uparrow}(\mathbf{r}'), \tag{5.37}$$

with $\epsilon_{\mu\sigma}$ single-particle eigenvalues, $f_{\mu\sigma}$ is the occupation probability of the state $\psi_{\mu\sigma}$. It is necessary to note that the exchange interactions may be formally separated from the Stoner continuum only in the adiabatic approximation. Otherwise it is necessary to find the poles of the full susceptibility through the quantity

$$\hat{\Omega}(\mathbf{r},\mathbf{r}',\omega) = I_{\text{xc}}\hat{\Lambda}(\mathbf{r},\mathbf{r}',\omega), \tag{5.38}$$

corresponding to the spin excitation spectrum

$$\hat{\Omega}(\mathbf{r},\mathbf{r}',\omega) = \frac{4}{m(\mathbf{r})}\mathcal{J}(\mathbf{r},\mathbf{r}',\omega) + \\ + I_{\mathrm{xc}}(\mathbf{r})\sum_{\mu\nu}\frac{f_{\mu\uparrow}-f_{\nu\downarrow}}{\omega-\epsilon_{\mu\uparrow}+\epsilon_{\nu\downarrow}}(\epsilon_{\mu\uparrow}-\epsilon_{\nu\downarrow})\psi^*_{\mu\uparrow}(\mathbf{r})\psi_{\nu\downarrow}(\mathbf{r})\psi^*_{\nu\downarrow}(\mathbf{r}')\psi_{\mu\uparrow}(\mathbf{r}'). \tag{5.39}$$

In Eq. (5.39) the definition of frequency-dependent exchange interaction has been introduced through

$$\mathcal{J}(\mathbf{r},\mathbf{r}',\omega) = \frac{1}{4}\sum_{\mu\nu}\frac{f_{\mu\uparrow}-f_{\nu\downarrow}}{\omega-\epsilon_{\mu\uparrow}+\epsilon_{\nu\downarrow}}\psi^*_{\mu\uparrow}(\mathbf{r})B_{\mathrm{xc}}(\mathbf{r})\psi_{\nu\downarrow}(\mathbf{r})\psi^*_{\nu\downarrow}(\mathbf{r}')B_{\mathrm{xc}}(\mathbf{r}')\psi_{\mu\uparrow}(\mathbf{r}'). \tag{5.40}$$

This definition is coherent with the fact that in the adiabatic limit with $\omega \to 0$, Eq. (5.39) becomes

$$\hat{\Omega}(\mathbf{r},\mathbf{r}',0) = \frac{4}{m(\mathbf{r})}\mathcal{J}(\mathbf{r},\mathbf{r}',0) - B_{\mathrm{xc}}(\mathbf{r})\delta(\mathbf{r}-\mathbf{r}'), \tag{5.41}$$

where the Stoner contribution and the exchange term are clearly separated. These results show that at finite frequencies ω, Stoner excitations and spin waves are not completely distinguishable and both contribute to the excitation spectrum. Nevertheless, for better clarity it can be useful to introduce a frequency dependent exchange coupling $\mathcal{J}(\mathbf{r},\mathbf{r}',\omega)$ that reduces to the MFT exchange for $\omega \to 0$.

5.2 Real time exchange coupling

The methods described in the previous section rest on the adiabatic assumption that the timescales of the magnons and the electronic motion differ enough to allow for the total energy differences between two magnetic configurations to be calculated within the framework of the constrained noncollinear DFT. The latter, as it is well known, is designed to evaluate ground state properties. Therefore these methods are not necessarily adequate if we are interested in the out-of-equilibrium dynamics driven by very short (femtosecond scale) intense laser pulses. In these cases, in fact, the electronic degrees of freedom cannot be averaged out and separated from the spin ones.

The first attempt to map the spin dynamics of TDDFT into a Heisenberg Hamiltonian (5.10) was based on simple two-center molecular systems excited by very short and local in space magnetic fields [148]. It was noticed that after the extinction of the pulse excitation the two atomic spins forming an angle ϕ describe a precessional motion around the total spin axis, with angular velocity given by $\omega = 4JS\cos(\phi/2)/\hbar$. This method was later extended to more realistic magnetic molecules. However, the external pulse used to excite the system in the former

work was only an instrumental one, acting as a small perturbation with little influence on the dynamics of the electronic degrees of freedom.

In general, the external laser fields cannot be treated as perturbations. This is the case of the demagnetization process observed in metallic films excited by strong, femtosecond-long, laser pulses. There is little doubt that the exchange interaction plays a crucial role in the demagnetization observed at the femtosecond timescale and, in general, the spin dynamics in transition metals has been always explained within the framework of two different competing scenarios. In the first it is assumed that the main contribution to the spin dynamics can be attributed to collective magnonic excitations. In Ref. [149], for instance, it is shown that by analysing the ultrafast response of the conductivity tensor in the case of Fe epitaxial films, the possibility of an ultrafast modification of the electronic band structure is completely ruled out, leaving the collective spin excitations as only source of spin variation. In another experimental work [150] the authors used ultraviolet laser pulses to probe the ultrafast demagnetization in the ferromagnetic FeNi alloy. The results show that for time shorter than the characteristic time scales of the exchange interaction, the Fe localized spin collapses more quickly than the spin at the Ni site. After this initial phase the Fe moments relax in a new configuration and induce further demagnetization on the Ni site at a rate determined by the effective exchange coupling among the two magnetic sites.

The possibility to introduce some form of *dynamical exchange interaction* was considered in Ref. [151], where the authors assumed that the laser pulse induced excitation of the electronic system introduces an effective time-dependent *exchange interaction pulse*

$$\mathcal{J}(t) = \mathcal{J}_0\left[1 - Ae^{-\frac{(t-T)^2}{\tau^2}}\right]. \tag{5.42}$$

Here $\mathcal{J}_0$ is the static exchange interaction, T is the time delay of the exchange pulse and τ represents the duration. Then, the dynamics of a chain of spins coupled through the Heisenberg exchange interaction,

$$H = -\sum_{ij} \mathcal{J}_{ij}(t)\mathbf{S}_i \cdot \mathbf{S}_j, \tag{5.43}$$

was studied by assuming the spins to be classical vector. The equation of motion then becomes

$$\frac{d\mathbf{S}_i}{dt} = \mathbf{S}_i \times \sum_j \mathcal{J}_{ij}(t)\mathbf{S}_j. \tag{5.44}$$

The change in the exchange interaction is usually almost instantaneous, but its effect on the spin is delayed due to the finite spin wave velocity. In spin frustrated systems the effect of exchange coupling modification can be even more important, with the spin that can be switched from one direction to another.

A full description of out-of-equilibrium magnetic interactions in the multi-orbital

Hubbard model was proposed in Ref. [152], where expressions for the dynamical exchange interaction and three spins interaction were derived in terms of out-of-equilibrium Green functions and self energies, by assuming small deviations from the equilibrium configuration. This approach was followed in Ref. [153], where it was assumed that in a medium of arbitrary symmetry a direct ultrafast effect of the light electric field on the exchange interaction should be taken into account. The authors considered in addition to the symmetric part of the exchange interaction (5.10), responsable for the magnetic ordering of the material, also an anti-symmetric part

$$\hat{H}_{\mathrm{AS}} = \mathbf{D} \cdot \sum_{ij} \hat{\mathbf{S}}_i \times \hat{\mathbf{S}}_j, \tag{5.45}$$

called the Dzyaloshinskii-Moriya interaction [154, 155]. This gives rise to anti-ferromagnetism, chiral magnetic structures [156] and skyrmions [157]. The time dependent effective Hamiltonian is expressed in the following general form

$$\hat{H}(t) = I_{\mathrm{opt}}\alpha \sum_{ij} \hat{\mathbf{S}}_i \cdot \hat{\mathbf{S}}_j + 2I_{\mathrm{opt}}\boldsymbol{\beta} \cdot \sum_{ij} \hat{\mathbf{S}}_i \times \hat{\mathbf{S}}_j, \tag{5.46}$$

where I_{opt} is the intensity of light, while α and $\boldsymbol{\beta}$ are some scalar and vector coefficients depending on microscopic parameters. The first term describes the intensity dependent contribution to the exchange integral $\Delta\mathcal{J} = I_{\mathrm{opt}}\alpha$. In the case of the Fe-O-Fe anti-ferromagnetic cluster, characterized by a strong repulsion energy U among the d electrons of the Fe ion, an energy shift Δ between d and p electrons, and an equilibrium hopping parameter t_0 with a super-exchange coupling coefficient $\mathcal{J}$ that at the leading order in t_0/U is given by

$$\mathcal{J} = \frac{2t_0^4}{(U+\Delta)^2}\left(\frac{1}{U} + \frac{1}{U+\Delta}\right), \tag{5.47}$$

the theory developed in Ref. [152] leads to a variation, after the application of the laser, of the exchange parameter that is in good agreement with the expression obtained by making use of the Floquet theory [158] for out-of-equilibrium spin systems in presence of periodically driven laser fields,

$$\Delta\mathcal{J} = \frac{\epsilon^2 t_0^4}{2}\left[\sum_{\pm}\left(\frac{1}{U+\Delta\pm\hbar\omega} + \frac{1}{U+\Delta}\right)^2 \frac{1}{U+\Delta\pm\hbar\omega} - \frac{4}{U(U+\Delta)^2} - \frac{1}{(U+\Delta)^3}\right], \tag{5.48}$$

with $\epsilon = eaE_0/\hbar\omega$ being amplitude of the vector potential and, ω the frequency of the optical field.

In the second type of scenario, instead, single-particle Stoner excitations activated by the action of the laser pulse, are used to justify the ultrafast spin dynamics observed in itinerant magnets. This approach has lead, quite recently, to the prediction of possible ultrafast modifications of the exchange splitting directly driven by the action of the external laser pulse, We have mentioned in Chapter 2

that the possibility of a laser modification of the Stoner exchange splitting was already considered in Ref. [52], while the same approach was later applied to bulk Ni [159]. In a different work [160] similar arguments were made in order to justify the ultrafast demagnetization in ferromagnets. These use of a dynamical model based on the Elliott-Yafet spin-flip type of mechanism combined with a Stoner model for itinerant electrons, where the exchange splitting is considered as a time dependent quantity throughout the simulation

$$\Delta(t) = U_{\text{eff}} m(t). \tag{5.49}$$

Here U_{eff} is effective Coulomb interaction and $m(t)$ measures the system magnetization. The exchange splitting is therefore determined dynamically through the transient distribution of minority and majority carriers. This effect is found to strongly amplify the magnetization quenching after the action of the laser.

In summary, we have seen in this section that the ultrafast demagnetization process has been explained by making use of either dynamical band structure modification through a time dependent Stoner exchange $\Delta(t)$ (or also B_{xc} in the context of ab initio TD-SDFT), or by ultrafast spin-wave excitations driven by modification of the exchange coupling. Our aim for the remaining of the chapter will be to consider the contribution brought by these type of excitations together to the demagnetization process. As we know, away from the adiabatic approximation, the spin waves cannot be fully separated from the Stoner continuum in the excitation spectrum. Both in fact will contribute in a non trivial way to the dynamics. At the same time, the application of ultrafast laser pulses trigger an out-of-equilibrium dynamics of the magnetic system that does not allow an adiabatic treatment of the magnetic excitations. The adiabatic assumption on which the expressions for the exchange coupling (5.24) and (5.40) are based, relies on the condition that the characteristic time scale for the spin fluctuations is longer compared to the dynamics of the band electrons. This condition is not satisfied within our description of the ultrafast laser induced dynamics, where the dynamics of the spin and the electronic subsystems are strongly related. The impossibility to employ the definition of the adiabatic exchange interaction in real time automatically implies the necessity of the introduction of a new definition for the exchange interaction starting from the spin continuity equation described in the previous chapters.

5.3 First step towards a time-dependent exchange interaction

The first example we want to consider in view of the definition of a purely dynamical exchange interaction is the case of Fe_3, a cluster presenting a highly non-collinear magnetic configuration. Here we do not want to repeat the considerations that we have made in Chapter 4, but we focus in particular on the evolution of the two spins centered on the two side atoms of the cluster. We note

from Fig. 5.1(a) that the z component of the magnetization evaluated over the two opposite sites of the cluster follows quite clearly, at least in the first 10 fs of the dynamics, an opposite behaviour. This can be approximately summarized with the following equation for the time derivatives

$$\frac{d}{dt}S_{1z} = -\frac{d}{dt}S_{3z}. \tag{5.50}$$

This in turn suggests the possibility to map the spin dynamics of the two side atoms with an effective Heisenberg-type Hamiltonian

$$H_{\text{eff}}(t) = -\mathcal{J}(t)\mathbf{S}_1 \cdot \mathbf{S}_3, \tag{5.51}$$

with $\mathcal{J}(t)$ being the effective exchange coupling among the two sites and $\mathbf{S}_i$ the spin vector associated to the site $i = 1, 3$.

We intentionally neglect here the central atom from the description because at this stage our aim is not to provide a full effective description of the spin dynamics of the Fe_3 cluster, but rather some kind of simplified picture that could, at least qualitatively, describe the dynamics of the z component of the magnetization on the two opposite sites. The value of the magnetization of the central atom computed at $t = 0$ in the Fe_3 ground state is approximately half the module of the magnetization at the other two sites of the cluster. Moreover, the com-

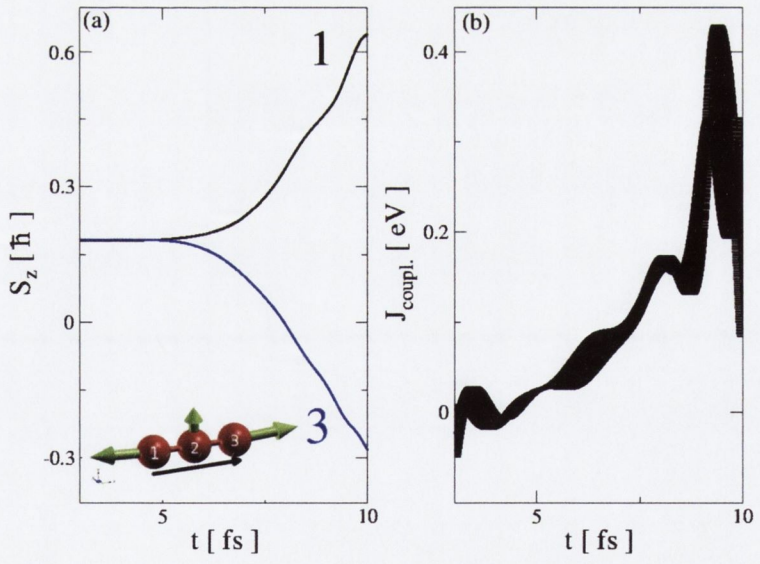


FIGURE 5.1: (Color online) (a) value of the magnetization S_{1z} and S_{3z} computed on the two sites 1 and 3 within a sphere of radius R, half the lattice spacing (b) value of $\bar{\mathcal{J}}(t)$ computed according to the average of the two quantities (5.56) and (5.57), with the error bars given by $\Delta\mathcal{J} = 0.5|\mathcal{J}_1 - \mathcal{J}_3|$.

ponent S_{2z} of the central atom magnetization does not change significantly with

respect to the magnetization of the other two sites. This considerations suggest to interpret the spin dynamics of the cluster along its z component as an effective exchange interaction between the spins on site 1 and 3, with no net charge flux and with the magnitude of the central atom spin remaining approximately fixed during the evolution. This justifies the use of Eq. (5.51) for the description of the spin dynamics

$$\dot{\mathbf{S}}_n = \frac{i}{\hbar}[H_{\text{eff}}(t), \mathbf{S}_n]. \tag{5.52}$$

For the z component of the magnetization we have

$$\dot{S}_{1,z} = \frac{i}{\hbar}\mathcal{J}(t)[\mathbf{S}_1, S_{1,z}] \cdot \mathbf{S}_3, \tag{5.53}$$

$$\dot{S}_{1,z} = \frac{i}{\hbar}\mathcal{J}(t)[S_{1,x}, S_{1,z}]S_{3,x} + \frac{i}{\hbar}\mathcal{J}(t)[S_{1,y}, S_{1,z}]S_{3,y}. \tag{5.54}$$

By using the commutation rules for the spin vector,

$$[S_i, S_j] = i\hbar \sum_k \epsilon_{ijk} S_k, \tag{5.55}$$

we obtain

$$\dot{S}_{1,z} = -\mathcal{J}(t)[S_{1,x}S_{3,y} - S_{1,y}S_{3,x}], \tag{5.56}$$

while on the opposite site we have

$$\dot{S}_{3,z} = -\mathcal{J}(t)[S_{1,y}S_{3,x} - S_{1,x}S_{3,y}]. \tag{5.57}$$

From the knowledge of the non-collinear components of the spin vector and using the two above equations we can extract two values $\mathcal{J}_1(t)$ and $\mathcal{J}_2(t)$ for the exchange coupling. In Fig. 5.1(b) the average value $\bar{\mathcal{J}}(t) = 0.5(\mathcal{J}_1(t) + \mathcal{J}_3(t))$ is plotted in time with the relative error bars. This shows that the two spin dynamics fits quite well on the effective exchange coupling, at least up to 10 fs during the application of the laser pulse. The coupling tends to grow up to almost 0.4 eV during the dynamical evolution, justifying such a huge variation of S_z in correspondence of the two atomic sites.

5.4 Some considerations on the spin continuity equation

We have already discussed the SDFT continuity equation in some details in Chapter 3 and 4,

$$\frac{d}{dt}\mathbf{m}(\mathbf{r}, t) = -\nabla \cdot \mathbf{J}_{\text{KS}}(\mathbf{r}, t) + \mu_B \mathbf{m}(\mathbf{r}, t) \times \mathbf{B}_{\text{s}}(\mathbf{r}, t) + \mathbf{T}_{\text{SO}}(\mathbf{r}, t), \tag{5.58}$$

it is now time to look in more detail into this expression. We have mentioned at the beginning of the chapter the problem of the non-collinearity. In absence of external magnetic field, $\mathbf{B}_{\text{ext}}(\mathbf{r},t) = 0$, the effective magnetic field coincides with the exchange-correlation one. In adiabatic local density approximation $\mathbf{B}_{\text{xc}}(\mathbf{r},t)$ cannot directly contribute to the spin dynamics, even locally, where it cannot exert a torque on the magnetization vector. As such the question about the origin of the local non-collinearity in the numerical simulations has still no valid answer.

The terms of Eq. (5.58) that can in principle contribute to the non collinearity of the magnetization vector are the divergence of the spin current tensor $-\nabla \cdot \mathbf{J}_{\text{KS}}(\mathbf{r},t)$, and the spin-orbit torque term $\mathbf{T}_{\text{SO}}(\mathbf{r},t)$. While the effect of the spin orbit interaction into the ultrafast magnetization dynamics was widely explored in Chapter 4, the role of the spin current tensor was totally ignored.

The reason is that it is not clear by looking at Eq. (5.58) how the term $-\nabla\cdot\mathbf{J}_{\text{KS}}(\mathbf{r},t)$ may be expressed in the form of a local torque acting on the magnetization vector. We have seen in Chapter 1 that, in principle, the spin current tensor should always give rise to two separate contributions, the first one is due to the purely translational motion of the spin vector, while the second is related to its rotational motion. What we need to do in this section is to make this separation more explicit.

This may be achieved by employing a hydrodynamical approach in order to rewrite in a more suitable form the equation of motion for the magnetization and electron density. This approach was originally based on an entirely new interpretation of the wave function in quantum mechanics, namely the so-called Bohmian interpretation [161–163].

According to the standard statistical interpretation of quantum mechanics [164], the physical state of an individual system must be completely specified in terms of a wave function which contains only informations on the actual results, obtained within a statistical ensemble of equivalent experiments. This interpretation of the quantum mechanical wave function has lead to several criticisms [165], although the internal consistency of the theory has never been under discussion. In Bohmian mechanics, instead, each individual system is conceived in terms of a precisely defined state in the classical sense, where temporal changes can be predicted by means of well defined classical equations. In practice, in Bohr's view a quantum mechanical system can be described only in terms of complementary pairs of concepts (like position and momentum). In such a way, an experimental apparatus needed to produce a precise measurement of one component of the pair, could be inadequate to measure its second component.

In Bohm version of quantum mechanics, the basic assumption is that this dualistic character of the theory is not due to the intrinsic nature of physical reality, but rather to a lack of knowledge. The quantum mechanical wave function should be conceived in the same way as a classical field, but with no sources, and the system particle + field (ψ) is, in reality, causally determined.

In order to clarify the new interpretation of the theory, Bohm starts from the time-dependent Schrodinger equation of a single particle in the presence of an external scalar potential, $V(\mathbf{r})$,

$$i\hbar\frac{d}{dt}\Psi(\mathbf{r},t) = -\frac{\hbar^2}{2m}\nabla^2\Psi + V(\mathbf{r})\Psi(\mathbf{r},t). \tag{5.59}$$

By employing the following decomposition of the wave function

$$\Psi(\mathbf{r},t) = R(\mathbf{r},t)e^{\frac{iS(\mathbf{r},t)}{\hbar}}, \tag{5.60}$$

with $S(\mathbf{r},t)$ phase of the quantum field ψ, one obtains the following two coupled equations

$$\frac{d}{dt}R(\mathbf{r},t) = -\frac{1}{2m}(R\nabla^2 S + 2\nabla R\cdot\nabla S), \tag{5.61}$$

$$\frac{d}{dt}S(\mathbf{r},t) = -\left[\frac{(\nabla S)^2}{2m} + V(\mathbf{r}) - \frac{\hbar^2}{2m}\frac{\nabla^2 R}{R}\right]. \tag{5.62}$$

By introducing the probability density distribution, $P(\mathbf{r},t) = R(\mathbf{r},t)^2$. Eq. (5.61) becomes

$$\frac{d}{dt}P(\mathbf{r},t) + \nabla\cdot\left(P(\mathbf{r},t)\frac{\nabla S}{m}\right) = 0. \tag{5.63}$$

This is a continuity equation for P, while the Hamilton-Jacobi Eq. (5.62) is

$$\frac{d}{dt}S(\mathbf{r},t) + \frac{(\nabla S)^2}{2m} + V(\mathbf{r}) - \frac{\hbar^2}{4m}\left[\frac{\nabla^2 P}{P} - \frac{1}{2}\frac{(\nabla P)^2}{P^2}\right] = 0. \tag{5.64}$$

The two equations offer a natural interpretation of $P\nabla S/m$ as probability flux, while apparently the quantum system is acted on by the classical potential $V(\mathbf{r})$ and by an effective quantum mechanical potential

$$U(\mathbf{r}) = -\frac{\hbar^2}{4m}\left[\frac{\nabla^2 P}{P} - \frac{1}{2}\frac{(\nabla P)^2}{P^2}\right]. \tag{5.65}$$

The wave function of an individual electron, regarded as a field, can exert, by interpreting ∇S as the particle momentum, a quantum mechanical force on the particle. So, the exact particle position cannot be predicted and $|\Psi|^2$ defines the probability distribution of the statistical ensemble, consequence of our ignorance on the initial conditions. A full tractation of the Bohm-causal interpretation of Quantum Mechanics can be found in Ref. [168] and it is based, in practice, on the following fundamental assumptions:

- The electron is a particle with well defined position $\mathbf{x}(t)$, which varies continuously and it is causally determined.
- The particle is not a distinct entity from the quantum field ψ that affects it. $\psi(t)$ satisfies the time-dependent Schrödinger equation and it also changes during the evolution.

- The equation of motion of the particle is

$$m\frac{d\mathbf{v}}{dt} = -\nabla V - \nabla Q, \tag{5.66}$$

  with $-\nabla V$ classical force and $-\nabla Q$ quantum force acting on the particle.

- The particle momentum is restricted to $\mathbf{p} = \nabla S$.

- In a statistical ensemble of particles selected so that all have the same quantum field ψ, the probability density, defined as $P = R^2$, is conserved.

These arguments have been applied also to the case of single spinning particles, where the field variable is the spinor wave function $\hat{\Psi}$. This was done in Ref. [166], where the entire hydrodynamical formalism for the single non-relativistic particle with spin was developed. In this type of hydrodynamics the quantum effects are separated as non-linear terms and are described through effective quantum potentials.

The formalism assumes that is possible to describe the entire dynamical process of a quantum particle immersed in an external vector potential, $\mathbf{A}(\mathbf{r}, t)$, through the so-called Madelung decomposition [168] of the system wave function, in which the amplitude is translated into probability density and the gradient of the phase determines the velocity variable. In practice one defines

$$n(\mathbf{r}, t) = \Psi^\dagger \Psi, \tag{5.67}$$

$$\mathbf{s}(\mathbf{r}, t) = \frac{\Psi^\dagger \hat{\boldsymbol{\sigma}} \Psi}{n(\mathbf{r}, t)}, \tag{5.68}$$

$$\mathbf{v}(\mathbf{r}, t) = \frac{\hbar}{2mi}\frac{\Psi^\dagger \nabla \Psi - \nabla \Psi^\dagger \Psi}{n(\mathbf{r}, t)} - \frac{e}{mc}\mathbf{A}(\mathbf{r}, t), \tag{5.69}$$

where $n(\mathbf{r}, t)$ represents the particle probability distribution, $\mathbf{s}(\mathbf{r}, t)$ is the spin vector field and $\mathbf{v}(\mathbf{r}, t)$ is the velocity vector field. An hydrodynamical model for the Schrodinger equation was also presented in Ref. [167] following directly from the ordinary interpretation of Quantum Mechanics by introducing an operator for the charge density and the current density.

The formalism was later extended also to the semi-relativistic description of a single particle in an external electro-magnetic field (Pauli approximation) in Ref. [169]. However, while in all these studies the main objective was to derive the single particle dynamics of the spin 1/2 plasma, only recently the study of the collective dynamical properties of the quantum plasma started to attract some interest [170, 171].

Here, we want to employ these methods in order to rewrite the spin continuity equation (5.58) in a form that is more suitable for our investigation. Throughout the derivation of the new equation of motion for the spin density we will need to introduce also the velocity field $\mathbf{v}(\mathbf{r}, t)$ of the Kohn-Sham system of particles. In discussing the spin dynamics this object plays the role of an auxiliary quantity for

which we do not write the equation of motion, $\mathbf{v}(\mathbf{r},t)$ will become more important in the discussion of the orbital moment dynamics, that is postponed to Chapter 6.

The electron density of the system is written in terms of the Kohn-Sham wave functions as

$$n(\mathbf{r},t) = \sum_{j\in \text{occ.}} \psi_j^{\text{KS}}(\mathbf{r},t)^\dagger \psi_j^{\text{KS}}(\mathbf{r},t)\,, \tag{5.70}$$

while the spin density is

$$\mathbf{s}(\mathbf{r},t) = \frac{\sum_{j\in \text{occ.}} \psi_j^{\text{KS}}(\mathbf{r},t)^\dagger \hat{\boldsymbol{\sigma}} \psi_j^{\text{KS}}(\mathbf{r},t)}{n(\mathbf{r},t)}\,, \tag{5.71}$$

and the covariant velocity field, from the definition of diamagnetic current, is

$$\mathbf{v}(\mathbf{r},t) = \frac{\hbar}{2mi}\cdot \frac{\sum_{j\in \text{occ.}} (\psi_j^{\text{KS}}(\mathbf{r},t)^\dagger \nabla \psi_j^{\text{KS}} - \psi_j^{\text{KS}} \nabla \psi_j^{\text{KS}}(\mathbf{r},t)^\dagger)}{n(\mathbf{r},t)} - \frac{e}{mc}\mathbf{A}(\mathbf{r},t). \tag{5.72}$$

By making use of the time-dependent Kohn-Sham equations,

$$i\hbar \frac{d}{dt}\psi_j^{\text{KS}}(\mathbf{r},t) = H_{\text{KS}}(\mathbf{r},t)\psi_j^{\text{KS}}(\mathbf{r},t), \tag{5.73}$$

the continuity equation for charge can be written straightforwardly as

$$\frac{d}{dt}n(\mathbf{r},t) = -\frac{\hbar}{2mi}\nabla \cdot \sum_{j\in \text{occ.}} \left[\psi_j^{\text{KS}}(\mathbf{r},t)^\dagger (\overrightarrow{\nabla} - \overleftarrow{\nabla})\psi_j^{\text{KS}}(\mathbf{r},t)\right] + \frac{e}{mc}\nabla \cdot [n\mathbf{A}(\mathbf{r},t)]\,, \tag{5.74}$$

while that for the spin must also include the diamagnetic contribution

$$\begin{aligned}\frac{d}{dt}\mathbf{m}(\mathbf{r},t) = &-\frac{\hbar}{2mi}\nabla \cdot \sum_{j\in \text{occ.}} \left[\psi_j^{\text{KS}}(\mathbf{r},t)^\dagger \hat{\boldsymbol{\sigma}} \nabla \psi_j^{\text{KS}} - \nabla \psi_j^{\text{KS}}(\mathbf{r},t)^\dagger \hat{\boldsymbol{\sigma}} \psi_j^{\text{KS}}\right] + \\ &+ \frac{e}{mc}\sum_j \partial_j [A^j(\mathbf{r},t) n\mathbf{s}] + \mu_B n\mathbf{s} \times \mathbf{B}_{\text{s}}(\mathbf{r},t) + \mathbf{T}_{\text{SO}}(\mathbf{r},t).\end{aligned} \tag{5.75}$$

Eq. (5.75) represents the spin continuity equation in its ordinary form. In order to rewrite the spin current divergence in a form that makes explicit the presence of a rotational component acting as a torque on the spin vector, we consider the same quantity that was introduced in Ref. [166] in the context of a single particle spinor wave function. By evaluating explicitly the partial derivative of the spin vector and by multipliying it with the component s_i we arrive to the following equality

$$s_i \partial_l s_k = s_i \left[\frac{\sum_{j\in \text{occ.}} \partial_l \psi_j^{\text{KS}}(\mathbf{r},t)^\dagger \hat{\sigma^k} \psi_j^{\text{KS}}}{n} + \frac{\sum_{j\in \text{occ.}} \psi_j^{\text{KS}}(\mathbf{r},t)^\dagger \hat{\sigma^k} \partial_l \psi_j^{\text{KS}}}{n} - \frac{\partial_l n}{n} s_k\right], \tag{5.76}$$

$$ns_i\partial_l s_k = s_i \sum_{j\in \text{occ.}} \left[\partial_l \psi_j^{\text{KS}}(\mathbf{r},t)^\dagger \hat{\sigma}^k \psi_j^{\text{KS}} + \psi_j^{\text{KS}}(\mathbf{r},t)^\dagger \hat{\sigma}^k \partial_l \psi_j^{\text{KS}}\right] - \partial_l n s_i \cdot s_k. \quad (5.77)$$

We need now to focus our attention of the first term on the right-hand side of Eq. (5.77). By using the following notation

$$\mathcal{F}_{ik}(\mathbf{r},t) = s_i \sum_{j\in \text{occ.}} \left[\nabla\psi_j^{\text{KS}}(\mathbf{r},t)^\dagger \hat{\sigma}^k \psi_j^{\text{KS}} + \psi_j^{\text{KS}}(\mathbf{r},t)^\dagger \hat{\sigma}^k \nabla\psi_j^{\text{KS}}\right], \quad (5.78)$$

we have

$$\mathcal{F}_{ik}(\mathbf{r},t) = \frac{1}{n} \sum_{j,r\in \text{occ.}} \left[\psi_r^{\text{KS}\dagger} \hat{\sigma}^i \psi_r^{\text{KS}} \nabla\psi_j^{\text{KS}\dagger} \hat{\sigma}^k \psi_j^{\text{KS}} + \psi_r^{\text{KS}\dagger} \hat{\sigma}^i \psi_r^{\text{KS}} \psi_j^{\text{KS}\dagger} \hat{\sigma}^k \nabla\psi_j^{\text{KS}}\right]. \quad (5.79)$$

By evaluating the anti-symmetric part of the tensor $\mathcal{F}_{ik}(\mathbf{r},t)$ we can write

$$\mathcal{K}_{ik}(\mathbf{r},t) = \mathcal{F}_{ik}(\mathbf{r},t) - \mathcal{F}_{ki}(\mathbf{r},t), \quad (5.80)$$

$$\mathcal{K}_{ik}(\mathbf{r},t) = \\ = \frac{1}{n} \sum_{j,r\in \text{occ.}} \sum_{\alpha\beta,\alpha'\beta'} \left[\psi_{r,\alpha}^{\text{KS}*} \psi_{r,\beta}^{\text{KS}} \sigma_{\alpha\beta}^{[i,} \sigma_{\alpha'\beta'}^{k]} \nabla\psi_{j,\alpha'}^{\text{KS}*} \psi_{j,\beta'}^{\text{KS}} + \psi_{r,\alpha}^{\text{KS}*} \psi_{r,\beta}^{\text{KS}} \sigma_{\alpha\beta}^{[i,} \sigma_{\alpha'\beta'}^{k]} \psi_{j,\alpha'}^{\text{KS}*} \nabla\psi_{j,\beta'}^{\text{KS}}\right], \quad (5.81)$$

where the matrix element $\sigma_{\alpha\beta}^{[i,} \sigma_{\alpha'\beta'}^{k]}$ is simply given by

$$\sigma_{\alpha\beta}^{[i,} \sigma_{\alpha'\beta'}^{k]} = \sigma_{\alpha\beta}^{i} \sigma_{\alpha'\beta'}^{k} - \sigma_{\alpha\beta}^{k} \sigma_{\alpha'\beta'}^{i}. \quad (5.82)$$

By making use of the following relation for the Pauli matrices (see Ref. [166])

$$\sigma_{\alpha\beta}^{[i,} \sigma_{\alpha'\beta'}^{k]} = i \sum_s \epsilon_{iks} \sigma_{\alpha\beta'}^{[s,} \sigma_{\alpha'\beta}^{0]}, \quad (5.83)$$

where $\hat{\sigma}^0 = \bullet$, we then obtain

$$\sigma_{\alpha\beta}^{[i,} \sigma_{\alpha'\beta'}^{k]} = i \sum_s \epsilon_{iks} [\sigma_{\alpha\beta'}^{s} \delta_{\alpha'\beta} - \delta_{\alpha\beta'} \sigma_{\alpha'\beta}^{s}]. \quad (5.84)$$

Now by inserting this relationship into Eq. (5.81) we have

$$\mathcal{K}_{ik}(\mathbf{r},t) = \frac{i}{n} \sum_s \epsilon_{iks} \sum_{j,r\in \text{occ.}} \sum_{\alpha\beta,\gamma} \left[\psi_{r,\alpha}^{\text{KS}*} \sigma_{\alpha,\gamma}^{s} \psi_{j,\gamma}^{\text{KS}} \psi_{r,\beta}^{\text{KS}} \nabla\psi_{j,\beta}^{\text{KS}*} - \psi_{r,\alpha}^{\text{KS}*} \psi_{j,\alpha}^{\text{KS}} \nabla\psi_{j,\gamma}^{\text{KS}*} \sigma_{\gamma\beta}^{s} \psi_{r,\beta}^{\text{KS}}\right] + \\ + \frac{i}{n} \sum_s \epsilon_{iks} \sum_{j,r\in \text{occ.}} \sum_{\alpha\beta,\gamma} \left[\psi_{j,\beta}^{\text{KS}*} \psi_{r,\beta}^{\text{KS}} \psi_{r,\alpha}^{\text{KS}*} \sigma_{\alpha,\gamma}^{s} \nabla\psi_{j,\gamma}^{\text{KS}} - \psi_{r,\alpha}^{\text{KS}*} \nabla\psi_{j,\alpha}^{\text{KS}} \psi_{j,\gamma}^{\text{KS}*} \sigma_{\gamma\beta}^{s} \psi_{r,\beta}^{\text{KS}}\right], \quad (5.85)$$

which in turn leads to the following expression

$$\mathcal{K}_{ik}(\mathbf{r},t) = \frac{i}{n}\sum_{s}\epsilon_{iks}\sum_{j,r\in\text{occ.}}\psi_r^{\text{KS}\dagger}\psi_j^{\text{KS}}\Big[\psi_j^{\text{KS}\dagger}\hat{\sigma}^s\nabla\psi_r^{\text{KS}} - \nabla\psi_j^{\text{KS}\dagger}\hat{\sigma}^s\psi_r^{\text{KS}}\Big]+$$
$$+\frac{i}{n}\sum_{s}\epsilon_{iks}\sum_{j,r\in\text{occ.}}\psi_r^{\text{KS}\dagger}\hat{\sigma}^s\psi_j^{\text{KS}}\Big[\nabla\psi_j^{\text{KS}\dagger}\psi_r^{\text{KS}} - \psi_j^{\text{KS}\dagger}\nabla\psi_r^{\text{KS}}\Big]. \tag{5.86}$$

It is convenient now to split the previous expression in two parts as follows

$$\mathcal{K}_{ik}(\mathbf{r},t) = \sum_{j,r\in\text{occ.}}\mathcal{K}_{ik}^{(\text{j,r})}(\mathbf{r},t)\delta_{j,r} + \sum_{j\in\text{occ.}}\sum_{r\neq j\in\text{occ.}}\mathcal{K}_{ik}^{(\text{j,r})}(\mathbf{r},t), \tag{5.87}$$

where the first term on the right-hand side is purely single particle and it can be rewritten as follows

$$\sum_{j\in\text{occ.}}\mathcal{K}_{ik}^{(\text{j,j})}(\mathbf{r},t) = i\sum_{s}\epsilon_{iks}\sum_{j\in\text{occ.}}\frac{\psi_j^{\text{KS}\dagger}\psi_j^{\text{KS}}}{n(\mathbf{r},t)}\Big[\psi_j^{\text{KS}\dagger}\hat{\sigma}^s\nabla\psi_j^{\text{KS}} - \nabla\psi_j^{\text{KS}\dagger}\hat{\sigma}^s\psi_j^{\text{KS}}\Big]+$$
$$+\frac{i}{n}\sum_{s}\epsilon_{iks}\sum_{j\in\text{occ.}}\psi_j^{\text{KS}\dagger}\hat{\sigma}^s\psi_j^{\text{KS}}\Big[\nabla\psi_j^{\text{KS}\dagger}\psi_j^{\text{KS}} - \psi_j^{\text{KS}\dagger}\nabla\psi_j^{\text{KS}}\Big]. \tag{5.88}$$

Up to now the procedure that we have followed is formally exact. In order to simplify the previous expression we substitute the the Kohn-Sham state dependent ratio

$$\mathscr{F}_j = \frac{\psi_j^{\text{KS}\dagger}\psi_j^{\text{KS}}}{n(\mathbf{r},t)} \tag{5.89}$$

with its average over the various occupied states

$$\mathscr{F}_j \simeq \bar{\mathscr{F}} = \frac{\langle\psi_j^{\text{KS}\dagger}\psi_j^{\text{KS}}\rangle_j}{n(\mathbf{r},t)} \tag{5.90}$$

This is formally equal to $1/N$, (N is the total number of electrons in the system) if one assumes that the coefficient $\bar{\mathscr{F}}$ is, to a good degree of approximation, spatially homogeneous and constant throughout the entire dynamical evolution. At this point we can define the following Kohn-Sham state-resolved velocity field

$$\mathbf{v}_j(\mathbf{r},t) = \frac{\hbar}{2mi}\cdot\frac{\psi_j^{\text{KS}\dagger}\nabla\psi_j^{\text{KS}} - \psi_j^{\text{KS}}\nabla\psi_j^{\text{KS}\dagger}}{\psi_j^{\text{KS}\dagger}\psi_j^{\text{KS}}} - \frac{e}{mc}\mathbf{A}(\mathbf{r},t). \tag{5.91}$$

By assuming that we can substitute $\psi_j^{\text{KS}\dagger}\psi_j^{\text{KS}}$ with its previously defined average value, Eq. (5.88) becomes

$$\bar{\mathscr{F}}^{-1}\sum_{j\in\text{occ.}}\mathcal{K}_{ik}^{(\text{j,j})}(\mathbf{r},t) = i\sum_{s}\epsilon_{iks}\sum_{j\in\text{occ.}}\Big[\psi_j^{\text{KS}\dagger}\hat{\sigma}^s\nabla\psi_j^{\text{KS}} - \nabla\psi_j^{\text{KS}\dagger}\hat{\sigma}^s\psi_j^{\text{KS}}\Big]+$$
$$+\frac{2m}{\hbar}\sum_{s}\epsilon_{iks}\sum_{j\in\text{occ.}}\psi_j^{\text{KS}\dagger}\hat{\sigma}^s\psi_j^{\text{KS}}\Big[\mathbf{v}_j(\mathbf{r},t) + \frac{e}{mc}\mathbf{A}(\mathbf{r},t)\Big]. \tag{5.92}$$

By making use of this expression, Eq. (5.87) may be finally reformulated as follows

$$\bar{\mathscr{F}}^{-1}\mathcal{K}_{ik}(\mathbf{r},t) = i\sum_s \epsilon_{iks}\sum_{j\in\text{occ.}}\left[\psi_j^{\text{KS}\dagger}\hat{\sigma}^s\nabla\psi_j^{\text{KS}} - \nabla\psi_j^{\text{KS}\dagger}\hat{\sigma}^s\psi_j^{\text{KS}}\right]+ \\ + \frac{2m}{\hbar}\sum_s \epsilon_{iks}\sum_{j\in\text{occ.}}\psi_j^{\text{KS}\dagger}\hat{\sigma}^s\psi_j^{\text{KS}}\left[\mathbf{v}_j(\mathbf{r},t) + \frac{e}{mc}\mathbf{A}(\mathbf{r},t)\right]+ \\ + \sum_{j\in\text{occ.}}\sum_{r\neq j\in\text{occ.}}\bar{\mathscr{F}}^{-1}\mathcal{K}_{ik}^{(\text{j,r})}(\mathbf{r},t). \tag{5.93}$$

In order to recover the expression of the Kohn-Sham spin current we multiply the previous equation by $\hbar/2m$

$$\frac{\hbar}{2m}\bar{\mathscr{F}}^{-1}\mathcal{K}_{ik;l}(\mathbf{r},t) = -\sum_s \epsilon_{iks}\mathbf{J}_{\text{KS}}^{sl}(\mathbf{r},t) + \sum_s \epsilon_{iks}\sum_{j\in\text{occ.}} m_j^s(\mathbf{r},t)\left[v_j^l(\mathbf{r},t) + \frac{e}{mc}A^l(\mathbf{r},t)\right]+ \\ + \frac{\hbar\bar{\mathscr{F}}^{-1}}{2m}\sum_{j\in\text{occ.}}\sum_{r\neq j\in\text{occ.}}\mathcal{K}_{ik;l}^{(\text{j,r})}(\mathbf{r},t). \tag{5.94}$$

We can now rewrite the term on the left-hand side, by making use of Eq. (5.77). We have

$$n(s_i\partial_l s_k - s_k\partial_l s_i) = \mathcal{K}_{ik;l}(\mathbf{r},t). \tag{5.95}$$

From this relation it immediately follows that

$$\frac{\hbar}{2\bar{\mathscr{F}}m}n(s_i\partial_l s_k - s_k\partial_l s_i) = \sum_s \epsilon_{iks}\sum_{j\in\text{occ.}} m_j^s(\mathbf{r},t)\left[v_j^l(\mathbf{r},t) + \frac{e}{mc}A^l(\mathbf{r},t)\right]- \\ - \sum_s \epsilon_{iks}\mathbf{J}_{\text{KS}}^{sl}(\mathbf{r},t) + \frac{\hbar}{2\bar{\mathscr{F}}m}\sum_{j\in\text{occ.}}\sum_{r\neq j\in\text{occ.}}\mathcal{K}_{ik;l}^{(\text{j,r})}(\mathbf{r},t). \tag{5.96}$$

By making use of the properties of the Levi-Civita tensor we have

$$\frac{\hbar}{2\bar{\mathscr{F}}m}n\sum_{i,k}\epsilon_{ikn}(s_i\partial_l s_k - s_k\partial_l s_i) = 2\sum_{j\in\text{occ.}} m_j^n(\mathbf{r},t)\left[v_j^l(\mathbf{r},t) + \frac{e}{mc}A^l(\mathbf{r},t)\right]- \\ - 2\mathbf{J}_{\text{KS}}^{nl}(\mathbf{r},t) + 2\mathcal{D}^{nl}(\mathbf{r},t), \tag{5.97}$$

where we have introduced a new tensor

$$\mathcal{D}^{nl}(\mathbf{r},t) = \frac{i\hbar}{2m\bar{\mathscr{F}}n}\sum_{j\in\text{occ.}}\sum_{r\neq j\in\text{occ.}}\psi_r^{\text{KS}\dagger}\psi_j^{\text{KS}}[\psi_j^{\text{KS}\dagger}\hat{\sigma}^n\partial_l\psi_r^{\text{KS}} - \partial_l\psi_j^{\text{KS}\dagger}\hat{\sigma}^n\psi_r^{\text{KS}}]+ \\ + \frac{i\hbar}{2m\bar{\mathscr{F}}n}\sum_{j\in\text{occ.}}\sum_{r\neq j\in\text{occ.}}\psi_r^{\text{KS}\dagger}\hat{\sigma}^n\psi_j^{\text{KS}}[\partial_l\psi_j^{\text{KS}\dagger}\psi_r^{\text{KS}} - \psi_j^{\text{KS}\dagger}\partial_l\psi_r^{\text{KS}}]. \tag{5.98}$$

$\mathcal{D}(\mathbf{r},t)$ is constructed by summing different occupied Kohn-Sham states. Eq. (5.97) may be finally written in the following form

$$\frac{\hbar}{2\bar{\mathcal{F}}m}n(\mathbf{s}\times\partial_l\mathbf{s})^n = -\mathbf{J}^{nl}_{\mathrm{KS}}(\mathbf{r},t) + \sum_{j\in\mathrm{occ.}} m^n_j(\mathbf{r},t)\left[v^l_j(\mathbf{r},t) + \frac{e}{mc}A^l(\mathbf{r},t)\right] + \mathcal{D}^{nl}(\mathbf{r},t). \tag{5.99}$$

From Eq. (5.99) the divergence of the spin-current tensor becomes

$$\begin{aligned}-\nabla\cdot\mathbf{J}_{\mathrm{KS}}(\mathbf{r},t) = \frac{\hbar}{2\bar{\mathcal{F}}m}\nabla\cdot(n\mathbf{s}\times\nabla\mathbf{s}) - \sum_{j\in\mathrm{occ.}}\sum_l \partial_l[\mathbf{m}_j(\mathbf{r},t)\cdot v^l_j(\mathbf{r},t)] - \\ - \frac{e}{mc}\sum_l \partial_l[n\mathbf{s}A^l(\mathbf{r},t)] - \nabla\cdot\mathcal{D}(\mathbf{r},t).\end{aligned} \tag{5.100}$$

We can now substitute the previous equation into Eq. (5.75) obtaining

$$\begin{aligned}\frac{d}{dt}\mathbf{m}(\mathbf{r},t) = -\nabla\cdot\mathcal{D}(\mathbf{r},t) - \sum_{j\in\mathrm{occ.}}\sum_l \partial_l[\mathbf{m}_j(\mathbf{r},t)\cdot v^l_j(\mathbf{r},t)] + \frac{\hbar}{2\bar{\mathcal{F}}m}\nabla\cdot(n\mathbf{s}\times\nabla\mathbf{s}) + \\ + \mu_B n\mathbf{s}\times\mathbf{B}_{\mathrm{s}}(\mathbf{r},t) + \mathbf{T}_{\mathrm{SO}}(\mathbf{r},t).\end{aligned} \tag{5.101}$$

By decomposing the system magnetization $\mathbf{m}(\mathbf{r},t)$ in its single particle components $\mathbf{m}_j$ we can introduce the following material derivative

$$\frac{D}{Dt}\mathbf{m}(\mathbf{r},t) = \frac{d}{dt}\sum_{j\in\mathrm{occ.}}\mathbf{m}_j(\mathbf{r},t) + \sum_{j\in\mathrm{occ.}}\nabla\mathbf{m}_j(\mathbf{r},t)\cdot\mathbf{v}_j(\mathbf{r},t), \tag{5.102}$$

and the spin continuity equation finally becomes

$$\begin{aligned}\frac{D}{Dt}\mathbf{m}(\mathbf{r},t) = -\nabla\cdot\mathcal{D}(\mathbf{r},t) - \sum_{j\in\mathrm{occ.}}\mathbf{m}_j(\mathbf{r},t)\nabla\cdot\mathbf{v}_j(\mathbf{r},t) + \frac{\hbar}{2\bar{\mathcal{F}}m}\nabla\cdot(n\mathbf{s}\times\nabla\mathbf{s}) + \\ + \mu_B n\mathbf{s}\times\mathbf{B}_s(\mathbf{r},t) + \mathbf{T}_{\mathrm{SO}}(\mathbf{r},t),\end{aligned} \tag{5.103}$$

or

$$\begin{aligned}\frac{D}{Dt}\mathbf{m}(\mathbf{r},t) = -\nabla\cdot\mathcal{D}(\mathbf{r},t) - \sum_{j\in\mathrm{occ.}}\mathbf{m}_j(\mathbf{r},t)\nabla\cdot\mathbf{v}_j(\mathbf{r},t) + \frac{\hbar}{2\bar{\mathcal{F}}m}\mathbf{m}\times\left[\frac{\nabla n}{n}\cdot\nabla\mathbf{s} + \nabla^2\mathbf{s}\right] + \\ + \mu_B\mathbf{m}\times\mathbf{B}_{\mathrm{s}}(\mathbf{r},t) + \mathbf{T}_{\mathrm{SO}}(\mathbf{r},t).\end{aligned} \tag{5.104}$$

At the same time the continuity equation for the density becomes

$$\frac{Dn}{Dt} = -n\nabla\cdot\mathbf{v}\,, \tag{5.105}$$

that can be expressed directly in terms of the single Kohn-Sham state densities

$$\frac{D}{Dt}n_j(\mathbf{r},t) = -n_j\nabla\cdot\mathbf{v}_j. \tag{5.106}$$

Eq. (5.104) is very important, since it will be used throughout the chapter for the discussion of the TD-SDFT results for itinerant magnets. The previous procedure has lead to the decomposition of the spin current divergence $\nabla \cdot \mathbf{J}_{\mathrm{KS}}$ into three separate terms, a linear component, a rotational component and a dissipative term. These are now analysed in detail.

Linear component $-\sum_{j\in\mathrm{occ.}} \mathbf{m}_j \nabla \cdot \mathbf{v}_j$**:** This object can be identified with the linear component of the spin current divergence. It is a local function of the state resolved magnetization vector field, $\mathbf{m}_j(\mathbf{r}, t)$, and it is directly related to the divergence of the Kohn-Sham state velocity field, $\mathbf{v}_j(\mathbf{r}, t)$. It does not contribute, during the dynamical evolution, to the variation in the global value of the system magnetization, but it describes a local magnetization loss activated by the movement of charge (that carries also spin) throughout the magnetic system. Making use of the state resolved continuity equation (5.106) for the charge density distribution, the term may be expressed as

$$-\sum_{j\in\mathrm{occ.}} \mathbf{m}_j(\mathbf{r}, t)\nabla \cdot \mathbf{v}_j = \sum_{j\in\mathrm{occ.}} \mathbf{s}_j(\mathbf{r}, t)\frac{D}{Dt} n_j(\mathbf{r}, t), \tag{5.107}$$

which provides a clear relationship with the time derivative of the electron density $\dot{n}(\mathbf{r}, t)$. By assuming that spatial inhomogeneities of the electronic distribution $n_j(\mathbf{r}, t)$ are smaller than its temporal variation $\dot{n}(\mathbf{r}, t)$, the material derivative of n_j may be approximated with its temporal derivative

$$\frac{D}{Dt} n_j(\mathbf{r}, t) \simeq \dot{n}_j(\mathbf{r}, t), \tag{5.108}$$

and we can write the continuity equation (5.104), by neglecting all the other contributions, as

$$\frac{d}{dt}\mathbf{m}_j(\mathbf{r}, t) = \mathbf{s}_j \dot{n}_j. \tag{5.109}$$

By defining $r_j = \frac{\dot{n}_j}{n_j}$ rate of density variation in a particular region of space, and by assuming that this region is small enough to consider the densities as approximately homogeneous, we can neglect the spatial dependence. With a rate $r < 0$ and constant in time the solution of the differential equation trivially becomes

$$\mathbf{m}_j(t) = \mathbf{m}_j(0)e^{-|r|t}, \tag{5.110}$$

i.e. the magnetization vector $\mathbf{m}_j$ decays exponentially in the spatial region considered. It is clear that the dynamics of the magnetization vector due to the linear component of the spin continuity equation (5.104) is directly connected to the motion of the probability density distribution. The demagnetization process is therefore purely local and connected to the loss of electronic charge experienced in the spatial region after the application of the laser pulse.

Rotational component $\frac{\hbar}{2\mathscr{F}m}\mathbf{m} \times \left(\frac{\nabla n}{n} \cdot \nabla \mathbf{s} + \nabla^2 \mathbf{s}\right)$**:** This second object plays a very

important role in our discussion. In fact, among the three terms arising from the spin-current divergence this is the only one able to generate a torque of the magnetization vector. Furthermore, it is expressed only in terms of the gradient of the electronic and the spin densities, so, its value computed in the non-interacting Kohn-Sham system is equivalent to the value computed in the physical many-body system. The cross product written in the Eq. (5.104) between the magnetization vector and the object enclosed in the brackets suggests to identify it with the source of non collinearity observed in the time-dependent simulations. A very similar expression to

$$\frac{\nabla n}{n} \cdot \nabla \mathbf{s} + \nabla^2 \mathbf{s}, \tag{5.111}$$

was already introduced in some previous work on LDA spin dynamics in Ref. [172]. This was expressed in the form $\partial_k \frac{1}{n}(\mathbf{m} \times \partial_k \mathbf{m})$, while in Ref. [173] it appears as $\frac{\nabla n \cdot \nabla \mathbf{m}}{n}$. These two expressions, although very similar, leave room for ambiguous interpretations given that they do not seem to be completely equivalent. We hope that our derivation lifts these ambiguities.

The interpretation of this contribution may look quite obscure at a first sight. However, already in Ref. [166] this object was identified with an effective spin-spin interaction potential. If we consider two spins centered around atoms located at a distance $d = |\mathbf{d}|$, we can assume naively, but reasonably, that the spin - spin interaction among the two spin distributions, computed at an arbitrary point $\mathbf{r}$ in space could be expressed in the following form

$$H_{\text{eff}}(\mathbf{r}) \simeq \mathbf{s}(\mathbf{r} - \mathbf{d}/2) \cdot \mathbf{s}(\mathbf{r} + \mathbf{d}/2), \tag{5.112}$$

where it is more convenient for us to employ a spin field, $\mathbf{s}(\mathbf{r})$, which describes the spin distribution in space, instead of an atom localized spin vector. Hence $H_{\text{eff}}(\mathbf{r})$ defines an effective single particle interaction Hamiltonian. By averaging over the number of electrons in the entire space we obtain

$$\mathbf{S}_1 \cdot \mathbf{S}_2 \simeq \int_\Omega \mathrm{d}^3 r\, n(\mathbf{r}) \mathbf{s}(\mathbf{r} - \mathbf{d}/2) \cdot \mathbf{s}(\mathbf{r} + \mathbf{d}/2). \tag{5.113}$$

By expanding the spin density in Taylor series up to second order in the distance $\mathbf{d}$ and then by neglecting the zeroth order contribution (for $\mathbf{d} = 0$) [1] after some straightforward rearrangement we arrive at

$$\mathbf{S}_1 \cdot \mathbf{S}_2 \simeq -\frac{d^2}{4} \int_\Omega \mathrm{d}^3 r\, n(\mathbf{r}) \nabla \mathbf{s}(\mathbf{r}) \cdot \nabla \mathbf{s}(\mathbf{r}), \tag{5.114}$$

[1] this choice is dictated by the fact that we seek to focus our attention on the non local term appearing into the perturbative expansion

which in turn becomes

$$\mathbf{S}_1 \cdot \mathbf{S}_2 \simeq -\frac{d^2}{4} \int_\Omega \mathrm{d}^3 r \left[\nabla \cdot \left[n(\mathbf{r}) \mathbf{s}(\mathbf{r}) \cdot \nabla \mathbf{s}(\mathbf{r}) \right] - \mathbf{m}(\mathbf{r}) \cdot \left(\frac{\nabla n(\mathbf{r}) \cdot \nabla \mathbf{s}(\mathbf{r})}{n(\mathbf{r})} + \nabla^2 \mathbf{s}(\mathbf{r}) \right) \right]. \tag{5.115}$$

Finally, by considering a sufficiently large integration volume, the use of the divergence theorem allows us to neglect all the boundary terms with consequent final expression

$$\mathbf{S}_1 \cdot \mathbf{S}_2 \simeq \int_\Omega \mathrm{d}^3 r \, \mathbf{m}(\mathbf{r}) \cdot \left[\frac{\nabla n(\mathbf{r}) \cdot \nabla \mathbf{s}(\mathbf{r})}{n(\mathbf{r})} + \nabla^2 \mathbf{s}(\mathbf{r}) \right], \tag{5.116}$$

which remarkably resembles the rotational component of the spin current divergence. Furthermore this object does not break the global spin conservation and acts only locally on the spin dynamics. We can tentatively interpret it as a mean-field internal magnetic field, even if, like $\mathbf{B}_{\mathrm{xc}}$, it has not the properties of a true magnetic field, namely

$$\nabla \cdot \left[\frac{\nabla n(\mathbf{r}) \cdot \nabla \mathbf{s}(\mathbf{r})}{n(\mathbf{r})} + \nabla^2 \mathbf{s}(\mathbf{r}) \right] \neq 0, \tag{5.117}$$

the field is not divergenceless. Nevertheless, it couples the spin vector field at different spatial locations in the same spirit of a non-local generalization of the Heisenberg spin-spin interaction.

Dissipative component $-\nabla \cdot \mathcal{D}(\mathbf{r}, t)$: The third object we need to consider is the source of spin loss in the continuity equation due to the internal motion of the spin currents. If we introduce the following generalization of the single state resolved spin-current tensor

$$\mathscr{J}^{(j,r)}(\mathbf{r}, t) = -\frac{i\hbar}{2m} \left[\psi_j^\dagger \hat{\boldsymbol{\sigma}} \nabla \psi_r - \nabla \psi_j^\dagger \hat{\boldsymbol{\sigma}} \psi_r \right], \tag{5.118}$$

and of the velocity field

$$\mathbf{v}^{(j,r)}(\mathbf{r}, t) = \frac{\hbar}{2mi} \frac{\psi_j^\dagger \nabla \psi_r - \nabla \psi_j^\dagger \psi_r}{\psi_j^\dagger \psi_r} - \frac{e}{mc} \mathbf{A}(\mathbf{r}, t), \tag{5.119}$$

the tensor field becomes

$$\mathcal{D}(\mathbf{r}, t) = - \sum_{\substack{j \in \mathrm{occ.} \\ r \neq j \in \mathrm{occ.}}} \left[\mathscr{F}_{rj} \mathscr{J}^{(j,r)} - \mathscr{F}_{jr} \mathbf{m}^{(r,j)} \otimes \left(\mathbf{v}^{(j,r)} + \frac{e}{mc} \mathbf{A} \right) \right] (\mathbf{r}, t). \tag{5.120}$$

The first component of the tensor describes the spin current due to the transitions between different Kohn-Sham states (inter-band transitions). This term is particularly relevant when, in the presence of the external field, the set of Kohn-Sham states does not form a complete and orthogonal basis of

eigenstates for the time evolved Hamiltonian and the transfer of probability density between these new states is allowed. The second term has the same meaning of the first, but here the probability transfer associated with the velocity field $\mathbf{v}^{(j,r)}(\mathbf{r},t)$ determines also an intrinsic modification of the magnetization vector through

$$\mathbf{m}^{(r,j)}(\mathbf{r},t) = \psi_r^{\mathrm{KS}\dagger}\hat{\sigma}\psi_j^{\mathrm{KS}}. \tag{5.121}$$

The charge current activated between different Kohn-Sham states by the action of the external field can also induce a change in the magnetization vector if the two states are characterized by different spin polarization directions. Clearly these terms can contribute to local changes of the magnetization vector, but they cannot affect its global behaviour.

In order to summarize the results of this section, we write the new spin continuity equation (5.104) in its final form

$$\frac{D}{Dt}\mathbf{m}(\mathbf{r},t) = -\nabla\cdot\mathcal{D}(\mathbf{r},t) - \sum_j \mathbf{m}_j(\mathbf{r},t)\nabla\cdot\mathbf{v}_j + \mu_B\mathbf{m}(\mathbf{r},t)\times\mathbf{B}_{\mathrm{eff}}(\mathbf{r},t) + \mathbf{T}_{\mathrm{SO}}(\mathbf{r},t), \tag{5.122}$$

with effective field $\mathbf{B}_{\mathrm{eff}}(\mathbf{r},t)$ that is expressed as follows

$$\mathbf{B}_{\mathrm{eff}}(\mathbf{r},t) = \mathbf{B}_{\mathrm{s}}(\mathbf{r},t) + \frac{1}{\bar{\mathscr{F}}e}\left[\frac{\nabla n(\mathbf{r},t)\cdot\nabla\mathbf{s}(\mathbf{r},t)}{n(\mathbf{r},t)} + \nabla^2\mathbf{s}(\mathbf{r},t)\right], \tag{5.123}$$

and in absence of external magnetic field $\mathbf{B}_{\mathrm{ext}}(\mathbf{r},t) = 0$ we have simply

$$\mathbf{B}_{\mathrm{eff}}(\mathbf{r},t) = \mathbf{B}_{\mathrm{xc}}(\mathbf{r},t) + \frac{1}{\bar{\mathscr{F}}e}\left[\frac{\nabla n(\mathbf{r},t)\cdot\nabla\mathbf{s}(\mathbf{r},t)}{n(\mathbf{r},t)} + \nabla^2\mathbf{s}(\mathbf{r},t)\right]. \tag{5.124}$$

In the next section we will employ the previous equation to analyse in more detail the spin dynamics of the Fe_6 cluster.

5.5 Analysis of the ALDA spin dynamics in the Fe_6 cluster

In this section we present the results of TDSDFT calculations for the Fe_6 ferromagnetic cluster. Our aim here is to study the spin dynamics by means of the new continuity equation (5.122) introduced in the previous section. As we have seen in Chapter 4, Fe_6 is the system that dynamically loses more magnetization compared to the other clusters. As we will see in Chapter 6 this effect is strongly dependent on the polarization direction of the applied electric field, however, it can be associated to the peculiar behaviour of the magnetization over the two atomic sites indicated in Fig 5.2(a, inset) with labels 5 and 6. In the remainder of the section whenever we define locally integrated quantities inside a sphere of

radius R we use

$$S_z^{\mathrm{I}}(t) = \frac{1}{|\mathcal{S}_{\mathrm{R}}^{\mathrm{I}}|} \int_{\mathcal{S}_{\mathrm{R}}^{\mathrm{I}}} \mathrm{d}^3 r \, m_z(\mathbf{r}, t), \tag{5.125}$$

with $S_z^{\mathrm{I}}(t)$ being the local spin quantity and $\mathbf{m}(\mathbf{r}, t)$ the usual magnetization density. Now, given that we have already discussed the ground state and structural properties of the Fe_6 cluster we immediately pass to discuss the dynamics. The system is excited by the application of an intense electric pulse with a duration of less than 10 fs, which initiates the dynamics (Fig. 5.2a). Then the set of time dependent Kohn-Sham equations are solved numerically with the results shown in Fig. 5.2. In Fig. 5.2(c) we plot the variation of the z and of the non-collinear

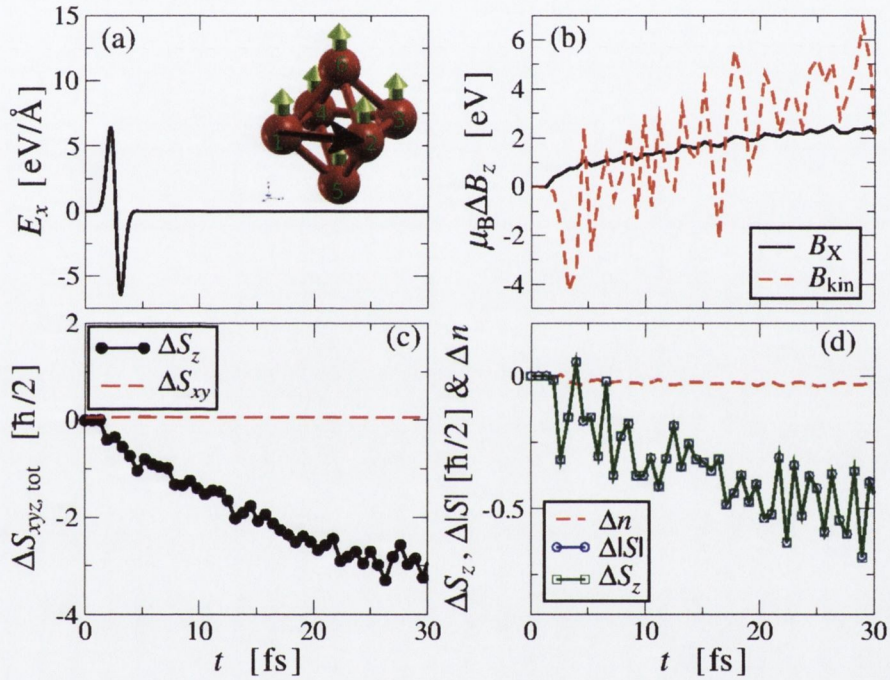


FIGURE 5.2: Fe_6 cluster dynamics: (a) typical electric field pulse used to excite the Fe_6 cluster with the black arrow indicating the direction of the field. The fluence of this pulse is 580 mJ/cm^2. (b) Time evolution of the z-component of $\mathbf{B}_{\mathrm{kin}}$ and $\mathbf{B}_{\mathrm{x}}$ (exchange component of the field) with respect to their values at $t = 0$ integrated over the system volume, $\mu_B \mathbf{B}^{\mathrm{tot}}(t) = \mu_B \sum_I \mathbf{B}^{\mathrm{I}}(t)$. (c) Time evolution of the variation of the total magnetization $\Delta S_z^{\mathrm{tot}}(t) = \sum_{\mathrm{I}} \Delta S_z^{\mathrm{I}}(t)$ with respect to its initial value. (d) Time evolution on atomic site 6 of the magnetization variation along z, of its module and of the electron density variation with respect to its value at $t = 0$ integrated inside a sphere of radius $R = 0.9$ Å.

component of the total magnetization $\Delta \mathbf{S}^{\mathrm{tot}} = \sum_{\mathrm{I}} \Delta \mathbf{S}_{\mathrm{I}}(t)$. The non-collinear component is zero during the entire dynamics, and if some non collinearity arises during the evolution, this is averaged out by the integration procedure. The total magnetization loss, therefore, coincides with the variation of the z component

$\Delta S_z^{\text{tot}}(t)$. At this stage these data do not suggest anything of conclusive because the spin loss could be due to either simple density exchange among the different components of the spin vector, or, according to Eq. (5.122), it has to be transfered into the orbital moment of the system.

In Fig. 5.2(b) we observe that the average kinetic field (over the entire simulation box), (for $\bar{\mathscr{F}} = 1$),

$$\mu_B \mathbf{B}_{\text{kin}}(\mathbf{r}, t) = \frac{\mu_B}{e}\left[\frac{\nabla n(\mathbf{r}) \cdot \nabla \mathbf{s}(\mathbf{r})}{n(\mathbf{r})} + \nabla^2 \mathbf{s}(\mathbf{r})\right], \tag{5.126}$$

is larger in magnitude than the exchange component. At the same time, $B_{\text{kin,z}}^{\text{tot}}$ shows a much more oscillatory behaviour compared to $B_{\text{x,z}}^{\text{tot}}$. In particular, while $B_{\text{x,z}}^{\text{tot}}$ evolves smoothly in time following the action of the optical excitation, $B_{\text{kin,z}}^{\text{tot}}$ presents an abrupt variation at the on-set of the electrical pulse. This is due to the fact that the laser pulse directly excites currents, through the term $-\nabla \cdot \mathcal{D}(\mathbf{r}, t)$, which, in turn, produces a modification of the gradients of the charge/spin density even on a global scale, since they are not conserved. Thus we observe huge variation of $B_{\text{kin,z}}^{\text{tot}}$. $B_{\text{x,z}}$ can also oscillate very strongly locally, following the temporal variation of the densities, but when we measure $B_{\text{x,z}}^{\text{tot}}$ these oscillations are averaged out given that the densities are approximately conserved over the entire simulation box.

During the action of the pulse we see a tendency of the two fields to compensate each other, an effect strongly resembling the Lenz law. After the pulse $B_{\text{kin,z}}^{\text{tot}}$ continues to oscillate dramatically with its average value that slowly increases during the evolution. In contrast $B_{\text{x,z}}^{\text{tot}}$ decreases (in absolute value) due to the net variation of spin angular momentum.

Moving from an analysis of global quantities to probing locally the spin dynamics, in Fig. 5.2(d) we compare the magnetization and the electron density around the atomic site 6 at the tip of the cluster [see inset of Fig. 5.2(a) for the atoms numbering]. We define the local charge $n(\mathbf{r}, t)$ associated to the particular atomic site I as

$$Q^{\text{I}}(t) = \frac{1}{|\mathcal{S}_{\text{R}}^{\text{I}}|}\int_{\mathcal{S}_{\text{R}}^{\text{I}}} d^3r\, n(\mathbf{r}, t). \tag{5.127}$$

Our results show that the loss of S_z^6 is not taking place just during the action of the external pulse, but it is rather distributed over the entire time evolution. This suggests that the spin-sink mechanism is not directly related to the coupling of the system to the laser field, but it is rather intrinsic to the electron dynamics following the pulse. Furthermore, close to the atomic site, the temporal variation of the charge, Q^6, is much smaller in magnitude and smoother than that of S_z^6. In addition for long times Q^6 settles close to an average value, while S_z^6 continues to decrease. Hence the long-term spin dynamics is not the result of a net charge displacement from the region close to the ions to the interstitial space. These observations are valid, in general, for all the atomic sites of the cluster.

The continuity equation for the electron density (5.105) may be expressed as

$$\frac{d}{dt}n(\mathbf{r},t) = -\nabla[n(\mathbf{r},t)\mathbf{v}(\mathbf{r},t)]\,, \tag{5.128}$$

where $\frac{d}{dt}n(\mathbf{r},t) = \dot{n}(\mathbf{r},t)$ is the time derivative of the electron density. From Fig. 5.2(d) we observe that during the action of the pulse the density variation in the vicinity of the atoms appears to be very small compared to the magnetization variation. We can therefore safely assume that in this spatial region $\dot{n}(\mathbf{r},t) \simeq 0$, with $n(\mathbf{r},t) \neq 0$. From these considerations we deduce that $\mathbf{v}(\mathbf{r},t) \simeq 0$ is a reasonably good approximation for the velocity field in the vicinity of the atoms (this does not imply that that the velocity field is exactly zero, but only that its effect on the spin dynamics in this particular case is negligible). The same argument is in principle valid also for the state resolved density $n_j(\mathbf{r},t)$ given that,

$$\frac{d}{dt}n(\mathbf{r},t) = \sum_j \frac{d}{dt}n_j(\mathbf{r},t), \tag{5.129}$$

the contribution of the local time derivative of the Kohn-Sham state density can be neglected. By applying the latter into Eq. (5.122) we finally obtain a relation that can be considered approximately valid in this spatial region of the simulation box,

$$\frac{d}{dt}\mathbf{m}(\mathbf{r},t) \simeq -\nabla\cdot\mathcal{D}(\mathbf{r},t) + \mu_B\mathbf{m}(\mathbf{r},t)\times\mathbf{B}_{\text{kin}}(\mathbf{r},t) + \mathbf{T}_{\text{SO}}(\mathbf{r},t)\,, \tag{5.130}$$

where the contribution to the spin dynamics due to the velocity field term has been neglected. The only surviving terms are then the spin orbit sink, $\mathbf{T}_{\text{SO}}(\mathbf{r},t)$, the spin torque term, $\mathbf{m}(\mathbf{r},t)\times\mathbf{B}_{\text{kin}}(\mathbf{r},t)$, and the spin current contribution, $\nabla\cdot\mathcal{D}(\mathbf{r},t)$, which is important during the action of the pulse, even if it cannot generate a global magnetization loss. Here we also have used the condition $\mathbf{m}(\mathbf{r},t)\times\mathbf{B}_{\text{xc}}^{\text{ALDA}}(\mathbf{r},t) = 0$, that is a consequence of the local density approximation. This does not mean that $\mathbf{B}_{\text{xc}}(\mathbf{r},t)$ does not contribute to the spin dynamics. As we have seen in Chapter 4, its ultrafast modification could, in fact, enhance the effect of the spin-orbit coupling. However, its contribution to the dynamics at longer times after the action of the laser pulse is less important than that of the kinetic field.

In Fig. 5.3 we compare the behaviour of the kinetic field and of the local magnetization at two atomic sites, respectively 1 (one of the atoms in the base plane of the bi-pyramid) and 6 (an atom at one of the apexes). It can be seen from Fig. 5.3(a) that these two sites present different rates of demagnetization. In particular, at site 6 the spin decay is considerably more prominent with respect to that observed at site 1. In contrast, the fluctuations in S_z^{I} are significantly more pronounced for site 1 than for site 6. This can be understood from the fact that we have chosen here an electric pulse with polarization vector in the basal plane of the bi-pyramid. As such, the spin fluctuations for the atoms in the basal plane

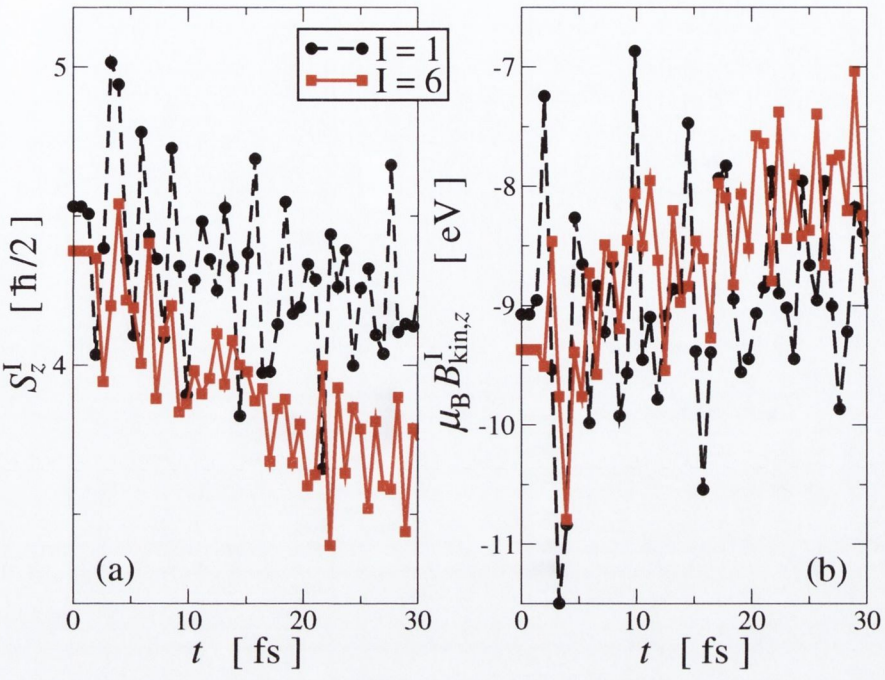


FIGURE 5.3: Local spin dynamics of the Fe_6 cluster: (a) Time evolution of the magnetization around the atomic centers. (b) Time evolution of the z component of $\mathbf{B}_{\text{kin}}$. All the quantities are integrated inside a sphere of radius $R = 0.9$ Å centered on the two atomic sites, where we have used $B_z^I(t) = \frac{1}{|S_R^I|}\int_{S_R^I} d^3r\, B_z(\mathbf{r},t)$.

are expected to be much larger than those of the apical atoms. Finally, we note that $\mathbf{B}^I_{\text{kin}}(t)$ follows similar qualitative trends as S^I_z [see Fig. 5.3(b)]. In fact, the average change following the excitation pulse is larger for site 6 (the one experiencing the larger demagnetization), but the fluctuations are more pronounced for site 1 (the one experiencing the larger fluctuations in S^I_z). The question rising naturally at this point is: why do we observe such a huge difference in the spin dynamics of the two sites? The correlations between the kinetic field and the magnetization vector are quite evident, but in order to have a more specific answer we need to look at Fig. 5.4.

In panel (a) and (c) of Fig. 5.4 we plot respectively the time-averaged variations in the x-component of the field $\mathbf{m} \times \mathbf{B}_{\text{kin}}$ and of $\dot{\mathbf{m}}(\mathbf{r},t)$. These two fields are clearly comparable in magnitude and localized over the same regions of the simulation box. This demonstrates that the kinetic field can be considered as the main force driving the non-collinearity during the spin evolution. The fact that the contrast is stronger at the apex atoms ("hot spots" for demagnetization) agrees with what we have observed in Fig. 5.3(a), while the dipole-type patterns indicate how the longitudinal spin decays preserving global collinearity. The correlation between the z components of $\mathbf{m} \times \mathbf{B}_{\text{kin}}$ and $\dot{\mathbf{m}}(\mathbf{r},t)$ is not as evident as that for the transverse components. This is due to the fact that the x and y components of the field are much smaller compared to the z one. Furthermore, the contribution to the spin dynamics along z of the SO coupling, together with

the internal dissipative term due to the spin currents, cannot be completely neglected. Summarizing we can conclude that while the dynamics of the x (and y) component of the spin vector is dominated by the action of the kinetic field $\mathbf{B}_{\text{kin}}(\mathbf{r}, t)$, the same is not true along z where instead the term $\mathbf{T}_{\text{SO}}(\mathbf{r}, t)$ of the continuity equation appears to be the dominant one together with $\nabla \cdot \mathcal{D}(\mathbf{r}, t)$, at least during the action of the pulse. An obvious way to quantify the local amount

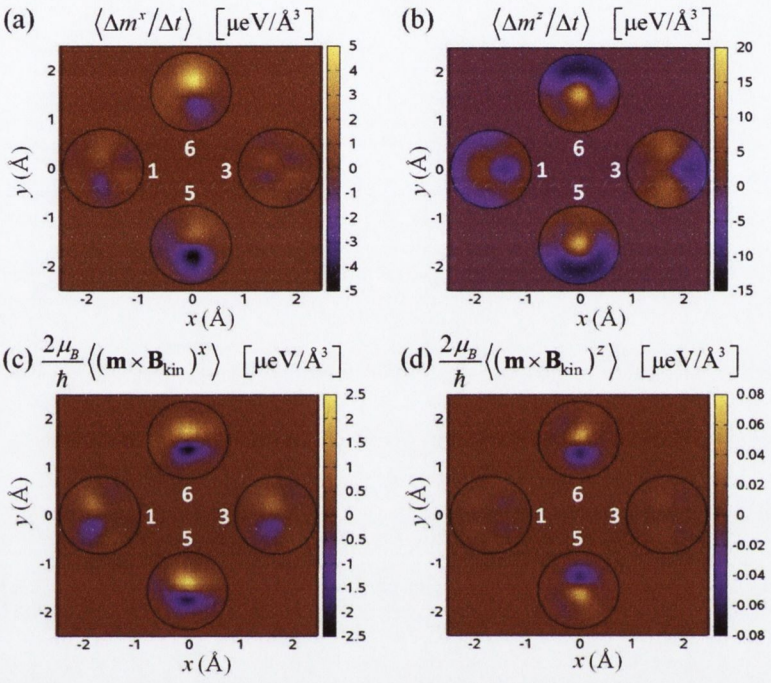


FIGURE 5.4: Contour plots of the time- and space-averaged (in direction perpendicular to the plane spanned by atoms 1, 3, 5 and 6, as indicated on the plot) observables evaluated only within spheres of radius $R = 1.0$ Å around each atom: (a) and (b) the temporal variation of the spin density $\Delta\mathbf{m}^{(x,z)}(\mathbf{r}, t)/\Delta t$ for $\Delta t = 0.1$ fs; (c) and (d) the x and z components of the first term on the right hand side of Eq. (5.130).

of non-collinearity consists in monitoring the evolution of the misalignment angle, θ, between the z-axis and the direction of the magnetic fields (averaged over spheres). It can be seen in Fig. 5.5(a) that at site 1 the averaged kinetic field and the local spin deflect very little from the quantization axis and remain rather parallel to each other. The angle that $\mathbf{B}_{\text{kin}}$ forms with the magnetization direction (the $\mathbf{m}$ direction) is substantially negligible. Instead, at site 6, $\mathbf{B}_{\text{kin}}$ shows a significant deflection from the z-axis after the first 5 fs of the time evolution and so does the spin, without the two being parallel to each other. It is important to notice that the angle between magnetization and the direction of $\mathbf{B}_{\text{kin}}$ starts to grow only after the action of the pulse. These results for atom 1 and 6 are representative for all the other sites in the base plane or outside of it, respectively. The sites located in the plane, where $\mathbf{B}_{\text{kin}}$ is mostly collinear, lose less magnetization

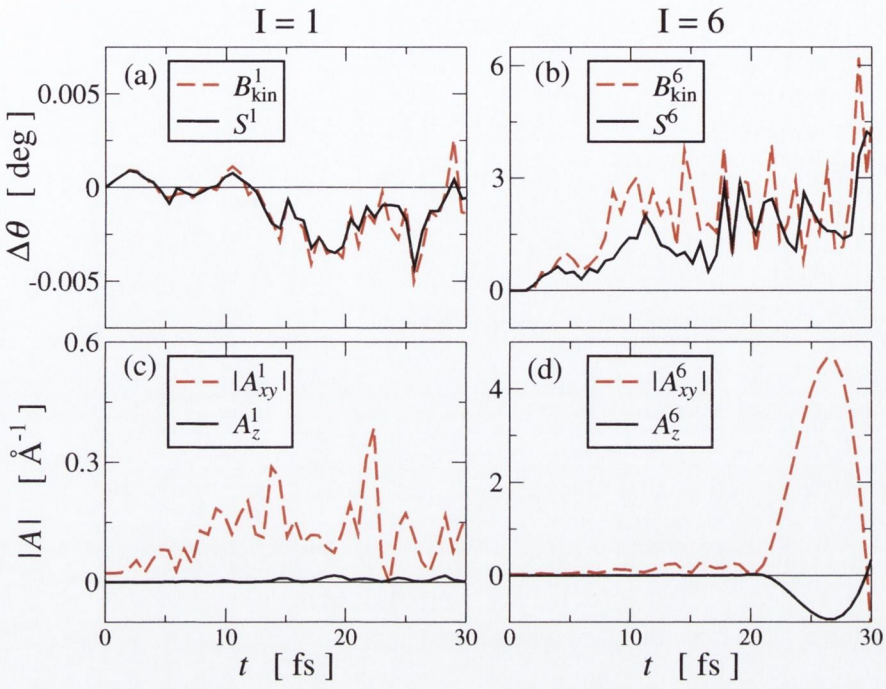


FIGURE 5.5: Spin non collinearity evolution in the Fe_6 cluster (a) $\Delta\theta = \theta(t) - \theta(0)$ at site 1, for the $\mathbf{B}_{xc}$ [or $\mathbf{S}(t)$] direction (black curve) and the $\mathbf{B}_{kin}$ direction (red dashed curve). (b) The same quantities of panel (a) but calculated at the atomic site 6. (c) $\sqrt{\bar{\mathcal{A}}_1^2 + \bar{\mathcal{A}}_2^2}$ where $\bar{\mathcal{A}} = \sqrt{\sum_{i=1}^3 \mathcal{A}_i^2}$ and $\mathcal{A}_i$ is introduced in Eq. (5.137), compared to $\bar{\mathcal{A}}_3$ at the atomic site 1. (d) The same quantities of panel (c) but calculated at the atomic site 6. The fields are measured within a sphere of radius $R = 0.8$ Å centered on the atom center.

with respect to the ones at the apices where, instead, the kinetic field shows a significant deflection from the magnetization axis and provides additional torque on the magnetization. The most obvious conclusion arising from the previous considerations is that the largest magnetization loss observed after the action of the pulse on atom 5 and 6 is connected to the rise of local non-collinearity of the spin vector. This is rotated by the kinetic field $\mathbf{B}_{kin}(\mathbf{r}, t)$ that is not parallel to the spin vector direction. However, this still does not explain the origin of the different spin dynamics observed among the base-plane atoms and those outside the plane. The problem, that represents the essence of the demagnetization process, will be faced in Chapter 6 because it requires a more complete understanding of the out-of-the equilibrium dynamics of the orbital moment. Here we want just to observe the direct correlation between the non-collinearity of the spin vector and the angle formed with the direction of the averaged kinetic field.

5.5.1 The kinetic field and parallel transport

Analogous conclusions arise from the introduction of the concept of parallel transport, widely used in the context of general relativity [174]. When we consider vector fields defined on a curved space manifold, given a certain vector at a point P_1 of the space manifold, it is not possible to give a meaning to a parallel vector located at a different point P_2. However considering a point close enough to P_1 we can define a parallel vector with an uncertainty of the first order in the distance, giving a meaning to parallel displacement of a vector (see Fig. 5.6).

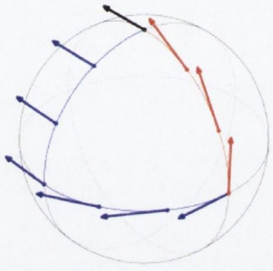


FIGURE 5.6: Parallel transport on a sphere, transport of the black arrow along different directions (blue and red vectors). From ([175]).

Considering the generic field $\phi_j(\mathbf{x})$, we need to distinguish between the spatial coordinates $\mathbf{x} \in \bullet^3$ in a euclidean, 3−dimensional, space and the internal coordinates of the field, defined by the index j. A scalar field, $\phi(\mathbf{x})$ has only one internal coordinate and it is, therefore, invariant under rotation of its internal degrees of freedom (which is the reason for the use of the term scalar). In our case we are interested in the properties of the spin vector field $\mathbf{s}(\mathbf{x})$, defined in terms of three internal components (s_x, s_y, s_z). This object is not invariant under rotations and transforms like a vector in a 3−dimensional space.

The 3−dimensional field $\boldsymbol{\phi}$ under an infinitesimal rotation of angle $|\Omega|$ around the axis $\boldsymbol{\Omega}/|\Omega|$ transforms as follows

$$\boldsymbol{\phi}' = \boldsymbol{\phi} - \boldsymbol{\Omega} \times \boldsymbol{\phi}, \tag{5.131}$$

thus the infinitesimal variation of the field is

$$\delta\boldsymbol{\phi} = -\boldsymbol{\Omega} \times \boldsymbol{\phi}. \tag{5.132}$$

The non-abelian nature of the rotation group $SO(3)$ is transfered into the non-commutativity of the cross product. In the previous expression it has been assumed that the rotation is performed in the internal $\boldsymbol{\phi}$ space (isospin space) with the same angle $|\Omega|$ at every point in space. By relaxing this condition we require that the angle of rotation depends on the spatial coordinates $\boldsymbol{\Omega} = \boldsymbol{\Omega}(\mathbf{x})$. The gradient of the field then transforms as

$$\nabla\boldsymbol{\phi}' = \nabla\boldsymbol{\phi} - \nabla\boldsymbol{\Omega} \times \boldsymbol{\phi} - \boldsymbol{\Omega} \times \nabla\boldsymbol{\phi}, \tag{5.133}$$

$$\delta\nabla\boldsymbol{\phi} = -\nabla\boldsymbol{\Omega}\times\boldsymbol{\phi} - \boldsymbol{\Omega}\times\nabla\boldsymbol{\phi}. \tag{5.134}$$

In practice $\nabla\boldsymbol{\phi}$ does not transform covariantly like $\boldsymbol{\phi}$. We can, therefore, introduce a covariant derivative equivalent to the parallel displacement of the field in a curved space,

$$D\boldsymbol{\phi} = \nabla\boldsymbol{\phi} + \mathscr{A}\times\boldsymbol{\phi}, \tag{5.135}$$

such that

$$\delta D\boldsymbol{\phi} = -\boldsymbol{\Omega}\times D\boldsymbol{\phi}. \tag{5.136}$$

The new derivative $D\boldsymbol{\phi}$ transforms covariantly like $\boldsymbol{\phi}$. Here $\mathscr{A}$ is the connection field. It is a rank 2 tensor with a set of indices corresponding to the internal vector space, and the other corresponding to the coordinates in real space. It is not a physical object, but only an instrumental gauge potential.

In our case a proper definition of the covariant derivative requires to decompose the standard derivative $\nabla\mathbf{s}(\mathbf{x})$ of the spin vector field at the position $\mathbf{x}$ into a derivative of the module of the spin vector, plus a rotation of the spin $\mathbf{s}(\mathbf{x})$. In this way the connection field $\mathcal{A}(\mathbf{x})$ acquires the meaning of the measure of the amount of non collinearity accumulated in the translation of the spin vector from $\mathbf{x}$ to $\mathbf{x}+d\mathbf{x}$. We can write the following definition of covariant derivative along the direction i

$$D_i\mathbf{s}(\mathbf{x}) = \nabla_i\mathbf{s}(\mathbf{x}) + \mathcal{A}_i(\mathbf{x})\times\mathbf{s}(\mathbf{x}). \tag{5.137}$$

The component $\mathcal{A}_i(\mathbf{x})$ of the connection tensor provides a measure of the degree of spin rotation that the system undergoes under an infinitesimal spatial translation along the direction i. By using the previous expression to rewrite the first and second order spatial derivatives, the kinetic field of Eq. (5.126) can be divided in two components

$$\mathbf{B}_{\text{kin}}(\mathbf{r},t) = \mathbf{B}^0_{\text{kin}}(\mathbf{r},t) + \delta\mathbf{B}_{\text{kin}}(\mathbf{r},t)\,. \tag{5.138}$$

Here we have introduced

$$\mathbf{B}^0_{\text{kin}}(\mathbf{r},t) = \frac{1}{\bar{\mathscr{F}}e}\left[\frac{\nabla n(\mathbf{r},t)}{n(\mathbf{r},t)}\cdot D\mathbf{s}(\mathbf{r},t) + D^2\mathbf{s}(\mathbf{r},t)\right], \tag{5.139}$$

which has no effects on the dynamics, having locally the same direction of the spin vector by construction, and

$$\begin{aligned}\delta\mathbf{B}_{\text{kin}}(\mathbf{r},t) = \frac{1}{\bar{\mathscr{F}}e}\sum_{i=1}^{3}\Big[\frac{\nabla_i n}{n}[-\mathbf{s}^2\mathcal{A}_i + (\mathbf{s}\cdot\mathcal{A}_i)\mathbf{s}] - 2[\mathbf{s}^2\nabla_i\mathcal{A}_i - \mathbf{s}(\mathbf{s}\cdot\nabla_i\mathcal{A}_i)] - \\ - 2[\mathcal{A}_i(\mathbf{s}\cdot D_i\mathbf{s}) - D_i\mathbf{s}(\mathbf{s}\cdot\mathcal{A}_i)] + 4(\mathbf{s}\times\mathcal{A}_i)(\mathbf{s}\cdot\mathcal{A}_i)\Big].\end{aligned} \tag{5.140}$$

According to Fig. 5.5(c) and (d), in the case of Fe_6, the direction in the isospin space of the connection tensor $\mathcal{A}_i$ for every i component can be considered in first approximation orthogonal to the direction of the spin vector $\mathbf{s}(\mathbf{r},t)$, since its component along z is considerably smaller than the components along x and y.

From this we could assume $\mathbf{s} \cdot \mathcal{A}_i \simeq 0$ and we obtain the following simplified expression for $\delta\mathbf{B}_{\text{kin}}(\mathbf{r}, t)$

$$\delta\mathbf{B}_{\text{kin}}(\mathbf{r}, t) = \frac{1}{\bar{\mathcal{F}}e} \sum_{i=1}^{3} \left[\left(-\frac{\nabla_i n}{n} \mathbf{s}^2 - 2\mathbf{s} \cdot D_i \mathbf{s} \right) \cdot \mathcal{A}_i - 2\mathbf{s}^2 \nabla_i \mathcal{A}_i \right]. \tag{5.141}$$

This represents the part of $\mathbf{B}_{\text{kin}}$ which effectively gives rise to a non-zero torque in Eq. (5.130), $\delta\mathbf{B}_{\text{kin}}(\mathbf{r}, t)$ goes to zero when also the connection tensor $\mathcal{A} = 0$.

5.6 Demagnetization of bcc Fe bulk

Before switching to the next topic, we briefly present results of analogous simulations for bulk materials, namely in bcc Fe, with the aim of demonstrating the universality of the spin orbit driven demagnetization process. As in the case of the Fe clusters, the role played by $\mathbf{B}_{\text{kin}}(\mathbf{r}, t)$ is also relevant in explaining the demagnetization process, which is particularly relevant at longer times. We consider bcc Fe in its ferromagnetic phase with a total spin per unit cell, $S = 4.85\hbar/2$. (2 Fe atoms per cell, see Fig. 5.7). We employ a lattice parameter $a = 2.9$ Å, and a $4 \times 4 \times 4$ k-points grid. In Fig. 5.8(c) we show the demagnetization rate for the unit cell after it has been excited with the electric field pulse [panel (a)]. The green curve represents the demagnetization calculated inside the unit cell and resembles in shape the sum of the magnetization variation, $\sum_I \Delta S_{z,I}(t)$, calculated in the vicinity of the two Fe atoms, even if it is different in magnitude. This suggests that a large amount of spin is driven outside from the atomic integration region during the evolution. Similarly to the cluster, the dynamics of the onsite magnetization can be described in terms of a two-step process with an initial fast decay during the action of the external pulse, followed by a slower and noisy decrease in magnitude. The first fast decay could be attributed, as we have seen in Chapter 4, to the effect of the spin-orbit coupling, enhanced by the collapse of the effective magnetic field $\mathbf{B}_{\text{eff}}(\mathbf{r}, t)$ (Eq. 5.124) following the action

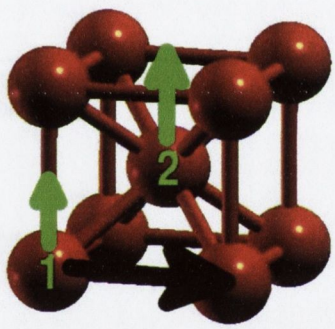


FIGURE 5.7: The Fe bcc lattice structure with the black arrow indicating the electric field polarization direction. The green arrows represent the local moments direction in the ground state.

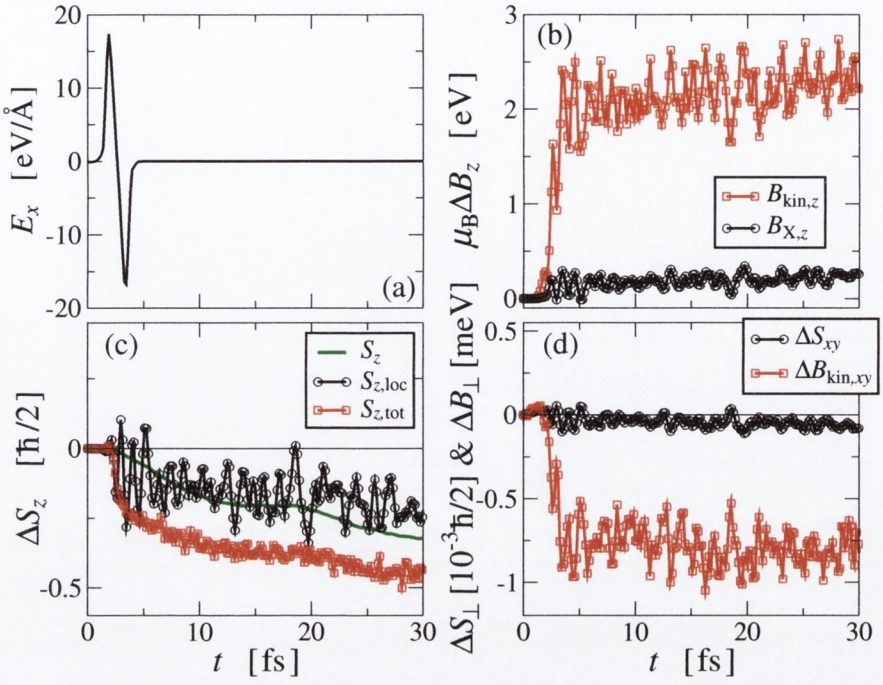


FIGURE 5.8: Demagnetization of bcc Fe: (a) applied external electric field; (b) local value of $\Delta B^z_{\mathrm{kin},I}$ and $\Delta B^z_{\mathrm{x,I}}$ around atom 1; (c) comparison between the value of the local magnetization $\Delta S_{z,\mathrm{I}}(t)$ around atom 1 (black curve), the total magnetization integrated around the two sites (red curve), $\sum_{\mathrm{I}} \Delta S_{z,I}(t)$, and the total magnetization integrated inside the unitary cell $\Delta S_z(t)$ (green curve). (d) Local value of $\sum_I \Delta B^{xy}_{\mathrm{kin},I}(t)$ (red curve) and of $\sum_I \Delta S^{xy}_I(t)$, non-collinear magnetization component for atom 1. All the local quantities are calculated inside a sphere of radius $R = 1.0$ Å.

of the laser pulse. In Fig. 5.8(b) the collapse after the first 5 fs of evolution of the z component of the effective field is quite clear, even if it appears to be more pronounced for the kinetic field $B^z_{\mathrm{kin},I}(t)$ with respect to the exchange field $B^z_{\mathrm{x,I}}(t)$. Similarly to the case of Fe_6 the role played by $\nabla \cdot \mathcal{D}(\mathbf{r}, t)$ is dominant during the action of the pulse, but after this initial phase the dynamics is dominated by intra-band transitions and the interplay between the spin-orbit coupling and the effective field $\mathbf{B}_{\mathrm{eff}}$ becomes dominant.

Fig. 5.8(d) shows the evolution of the non collinearity of the spin vector, $\sum_{\mathrm{I}} S_{xy,\mathrm{I}}(t)$, and of the kinetic field $\sum_{\mathrm{I}} B^{xy}_{\mathrm{kin,I}}$. The level of correlation between the two quantities confirms the importance of the kinetic field for the evolution of the spin non collinearity. However, the value of $S_{xy,\mathrm{I}}(t)$ looks too small to justify the loss in the S^z_{I} component [see Fig. 5.8(c)] in full. In order to interpret the origin of the spin variation at longer times, we employ an Elliott-Yafet type of mechanism, already introduced in Chapter 2, this may help in explaining the long tail of spin loss in terms of intra-band spin-up/spin-down transitions triggered by the scattering with the effective field $\mathbf{B}_{\mathrm{eff}}$. The novelty here is that the scattering potential is not identified with the ionic potential of the atoms, but with the out-of-equilibrium

magnonic fields (see Eq. 5.124).

In order to define every electronic quantum state we need three quantum numbers, the band index n, the wave vector $\mathbf{k}$ and the spin number σ. A generic wave function of the system will be expressed as $|\Psi_{n,\mathbf{k}}\rangle$, where we do not specify the spin number since, due to the presence of the spin orbit, an eigenstate of the Kohn-Sham Hamiltonian, $\hat{H}_{\mathrm{KS}}$, will not be also eigenstate of the spin operator $\hat{S}^z$. We are interested in the calculation of the scattering amplitude,

$$\mathscr{A}_{i\to f} = \langle \Psi_{n,\mathbf{k}_1} | \hat{\boldsymbol{\sigma}} \cdot \mathbf{B}_{\mathrm{eff}}(\mathbf{r},t) | \Psi_{n,\mathbf{k}_2} \rangle , \tag{5.142}$$

among two single particle states with the same band index. By making use of the following expression in reciprocal space

$$\mathbf{s}(\mathbf{r},t) = \int \frac{d^3k}{(2\pi)^3} \hat{\mathbf{s}}(\mathbf{k},t) e^{i\mathbf{k}\cdot\mathbf{r}}, \tag{5.143}$$

we obtain

$$\nabla^2 \mathbf{s}(\mathbf{r},t) = -\int \frac{d^3k}{(2\pi)^3} \mathbf{k}^2 \hat{\mathbf{s}}(\mathbf{k},t) e^{i\mathbf{k}\cdot\mathbf{r}}, \tag{5.144}$$

and

$$\nabla \log n(\mathbf{r},t) \cdot \nabla \mathbf{s}(\mathbf{r},t) = -\int \frac{d^3k}{(2\pi)^3} \int \frac{d^3q}{(2\pi)^3} \mathbf{k}\cdot\mathbf{q} \log \hat{n}(\mathbf{k},t) \hat{\mathbf{s}}(\mathbf{q},t) e^{i(\mathbf{k}+\mathbf{q})\cdot\mathbf{r}}. \tag{5.145}$$

By substituting Eq. (5.145) into the expression for $\mathbf{B}_{\mathrm{eff}}(\mathbf{r},t)$ we write

$$\begin{aligned} &\mathbf{B}_{\mathrm{eff}}(\mathbf{r},t) = \\ &= -\int \frac{d^3k}{(2\pi)^3} e^{i\mathbf{k}\cdot\mathbf{r}} \left[\frac{\mathbf{k}^2}{4e} \hat{\mathbf{s}}(\mathbf{k},t) - \hat{\mathbf{B}}_{\mathrm{xc}}(\mathbf{k},t) + \frac{1}{4e} \int \frac{d^3q}{(2\pi)^3} \mathbf{k}\cdot\mathbf{q} \log \hat{n}(\mathbf{k},t) \hat{\mathbf{s}}(\mathbf{q},t) e^{i\mathbf{q}\cdot\mathbf{r}} \right], \end{aligned} \tag{5.146}$$

that inserted into Eq. (5.142) gives

$$\begin{aligned} \mathscr{A}_{i\to f} = &- \langle \Psi_{n,\mathbf{k}_1} | \hat{\boldsymbol{\sigma}} | \Psi_{n,\mathbf{k}_2} \rangle \cdot \int d^3k \Big[\delta(\mathbf{k} - \mathbf{k}_1 + \mathbf{k}_2) \Big(\frac{\mathbf{k}^2}{4e} \hat{\mathbf{s}}(\mathbf{k},t) - \hat{\mathbf{B}}_{\mathrm{xc}}(\mathbf{k},t) \Big) + \\ &+ \frac{1}{4e} \int \frac{d^3q}{(2\pi)^3} \delta(\mathbf{k} + \mathbf{q} - \mathbf{k}_1 + \mathbf{k}_2) \mathbf{k}\cdot\mathbf{q} \log \hat{n}(\mathbf{k},t) \hat{\mathbf{s}}(\mathbf{q},t) \Big], \end{aligned} \tag{5.147}$$

or equivalently

$$\begin{aligned} \mathscr{A}_{i\to f} = &- \langle \Psi_{n,\mathbf{k}_1} | \hat{\boldsymbol{\sigma}} | \Psi_{n,\mathbf{k}_2} \rangle \cdot \Big[\Big(\frac{(\mathbf{k}_1 - \mathbf{k}_2)^2}{4e} \hat{\mathbf{s}}(\mathbf{k}_1 - \mathbf{k}_2, t) - \hat{\mathbf{B}}_{\mathrm{xc}}(\mathbf{k}_1 - \mathbf{k}_2, t) \Big) + \\ &+ \frac{1}{4e} \int \frac{d^3q}{(2\pi)^3} \mathbf{q}\cdot(\mathbf{k}_1 - \mathbf{k}_2 - \mathbf{q}) \log \hat{n}(\mathbf{k}_1 - \mathbf{k}_2 - \mathbf{q}, t) \hat{\mathbf{s}}(\mathbf{q},t) \Big]. \end{aligned} \tag{5.148}$$

We can analyse the scattering amplitude between a purely up spinor wave function $|\Psi_{n,\mathbf{k}_2}\rangle = (1,0)$ and a mixed state $|\Psi_{n,\mathbf{k}_1}\rangle = (\xi, c)$. The result is

$$\langle \Psi_{n,\mathbf{k}_1} | \hat{\sigma} | \Psi_{n,\mathbf{k}_2} \rangle = \xi^* \tag{5.149}$$

which implies a scattering amplitude $\mathscr{A}_{i\to f} \neq 0$ with consequent formation of a dynamical spin-flip scattering mechanism triggered by the effective field $\mathbf{B}_{\text{eff}}$.

5.7 Ab initio dynamical exchange interactions

In this section we want to go back for a moment to the definition of kinetic field of Eq. (5.126). This object represents the most natural candidate for an hypothetical out-of-equilibrium exchange interaction of the form

$$H_{\text{int}}(t) = -\sum_{i,j} \mathcal{J}_{ij}(t) \mathbf{S}_i \cdot \mathbf{S}_j. \tag{5.150}$$

Instead, the other terms appearing in the full out-of-equilibrium continuity equation (5.104) cannot be expressed in this form and will not be considered in the following discussion. This does not mean that the other terms do not have an influence on the spin dynamics, as we have already seen, but only that $\mathbf{B}_{\text{kin}}$, due to its structure, is the term that can in principle produce ultrafast spin wave excitations, the main argument of the final sections of the Chapter.

The kinetic field $\mathbf{B}_{\text{kin}}(\mathbf{r}, t)$ could be thought as a vector field defined on a three-dimensional space spanned by the spin vector components,

$$\mathbf{B}_{\text{kin}}(\mathbf{r}, t) = \Big(F[\mathbf{f}_1, n], F[\mathbf{f}_2, n], F[\mathbf{f}_3, n] \Big). \tag{5.151}$$

Where we have introduced the scalar functional

$$F[\mathbf{f}, n] = \frac{\nabla n}{n} \cdot \mathbf{f} + \nabla \cdot \mathbf{f}, \tag{5.152}$$

with $\mathbf{f}(\mathbf{r}, t)$ representing a generic differentiable vector field in $\bullet^3$ such that

$$\{ f_i(\mathbf{r}, t) \text{ for i} = 1, 2, 3 \in C^1(\bullet^3 \times [0, +\infty)) \}. \tag{5.153}$$

Suppose that we want to evaluate the functional from Eq. (5.152) at a certain point $x_0 \in \bullet^3 \times [0, +\infty)$. The function $\mathbf{f}(x)$ may be separated into a local and a non-local part around x_0 as follows

$$\mathbf{f}(x_0) = \mathbf{h}(x_0) + \int \mathrm{d}^3 x \, \epsilon(x_0, x) \eta(x). \tag{5.154}$$

Hence, at x_0

$$F[\mathbf{f},n](x_0) = \frac{\nabla_0 n}{n(x_0)} \cdot \left[\mathbf{h}(x_0) + \int \mathrm{d}^3x\, \boldsymbol{\epsilon}(x_0,x)\eta(x)\right] + \nabla_0 \cdot \left[\mathbf{h}(x_0) + \int \mathrm{d}^3x\, \boldsymbol{\epsilon}(x_0,x)\eta(x)\right]. \tag{5.155}$$

By separating the local from the non-local contributions in the previous expression we have

$$F[\mathbf{f},n](x_0) = \frac{\nabla_0 n}{n(x_0)} \cdot \mathbf{h}(x_0) + \nabla_0 \cdot \mathbf{h}(x_0) + \int \mathrm{d}^3x \left[\frac{\nabla_0 n}{n(x_0)} \cdot \boldsymbol{\epsilon}(x_0,x) + \nabla_0 \cdot \boldsymbol{\epsilon}(x_0,x)\right]\eta(x), \tag{5.156}$$

where we identify a local field,

$$B_{\mathrm{local}}(x_0) = \frac{\nabla_0 n}{n(x_0)} \cdot \mathbf{h}(x_0) + \nabla_0 \cdot \mathbf{h}(x_0), \tag{5.157}$$

and an effective non-local field

$$J(x,x_0) = \frac{\nabla_0 n}{n(x_0)} \cdot \boldsymbol{\epsilon}(x_0,x) + \nabla_0 \cdot \boldsymbol{\epsilon}(x_0,x). \tag{5.158}$$

We need now a proper definition for the non-local vector field $\boldsymbol{\epsilon}(x_0,x)$. This definition will depend on the choice of the scalar field $\eta(x)$ in Eq. (5.154). Here we substitute $\eta(x)$ with a given component $e_i(x)$ of the unitary magnetization vector

$$\mathbf{f}_i(x_0) = \mathbf{h}_i(x_0) + \int \mathrm{d}^3x\, \boldsymbol{\epsilon}_i(x_0,x)e_i(x). \tag{5.159}$$

By taking the average of the unitary magnetization component $e_i(x)$ over the integration region we can approximate the integral as follows

$$\mathbf{f}_i(x_0) = \mathbf{h}_i(x_0) + \bar{\boldsymbol{\epsilon}}_i(x_0)\bar{e}_i, \tag{5.160}$$

where $\mathbf{f}_i(x_0)$ has been separated into two components, the first orthogonal to the spin direction, $\bar{e}_i$, while the second parallel to it. In this form $\bar{\boldsymbol{\epsilon}}_i(x_0)$ defines simply the projection of the vector $\mathbf{f}_i(x_0)$ along the direction $\bar{e}_i$ in spin space

$$\bar{\boldsymbol{\epsilon}}_i(x_0) = \langle \mathbf{f}_i(x_0), \bar{e}_i \rangle. \tag{5.161}$$

By substituting $\mathbf{f}_i(x_0)$ with the gradient of the spin vector $\nabla s_i(x_0)$ we are now in the position to separate the local from the non-local component in the expression (5.126) of the kinetic field $\mathbf{B}_{\mathrm{kin}}(\mathbf{r},t)$. From the linearity of the functional $F[\mathbf{f},n]$ in the $\mathbf{f}$ variable we obtain

$$F[\mathbf{h}_i + \bar{\boldsymbol{\epsilon}}_i\bar{e}_i, n](x_0) = F[\mathbf{h}_i, n](x_0) + F[\bar{\boldsymbol{\epsilon}}_i, n](x_0)\bar{e}_i. \tag{5.162}$$

The first term gives rise to an effective local magnetic field with the following form

$$\hat{B}_{\mathrm{local}}(\mathbf{r},t) = \Big(F[\hat{\mathbf{h}}_1, n](\mathbf{r},t), F[\hat{\mathbf{h}}_2, n](\mathbf{r},t), F[\hat{\mathbf{h}}_3, n](\mathbf{r},t)\Big), \tag{5.163}$$

while the second term on the right hand side can be rewritten in a way that shows its explicit dependence on the spin vector $\hat{\hat{s}}$ generating a new effective mean field object[2]

$$\hat{B}_{\mathrm{mf}}(\mathbf{r},t) = \sum_{i=1}^{3} F[\bar{\boldsymbol{\epsilon}}_i, n](\mathbf{r},t)\langle \hat{\hat{e}}_i, \hat{\hat{s}}\rangle \hat{\hat{s}}. \tag{5.164}$$

The kinetic magnetic energy can be, therefore, finally separated in two contributions

$$E_{\mathrm{kin}}[n,\hat{s}] = \int \mathrm{d}^3 r\, \hat{s}(\mathbf{r},t)\cdot \hat{B}_{\mathrm{local}}(\mathbf{r},t) + \int \mathrm{d}^3 r\, \hat{s}(\mathbf{r},t)\cdot \hat{B}_{\mathrm{mf}}(\mathbf{r},t). \tag{5.165}$$

By summing up the non-interacting part of the energy with the interacting one dominated by the exchange correlation potential, we have

$$E_{\mathrm{kin+xc}}[n,\hat{s}] = \int \mathrm{d}^3 r\, \hat{s}(\mathbf{r},t)\cdot [\hat{B}_{\mathrm{local}}(\mathbf{r},t) + \hat{B}_{\mathrm{xc}}(\mathbf{r},t)] + \int \mathrm{d}^3 r\, \hat{s}(\mathbf{r},t)\cdot \hat{B}_{\mathrm{mf}}(\mathbf{r},t). \tag{5.166}$$

While the first term on the right hand side of Eq. (5.166) represents a dynamical Stoner-like field, the nature of the second term, due its spatial non-locality, is completely different and resembles the form of a Heisenberg exchange object with a mean field energy

$$E_{\mathrm{mf}}[n,\hat{s}] = \sum_{i=1}^{3} \int \mathrm{d}^3 r\, \hat{s}(\mathbf{r},t)\cdot F[\bar{\boldsymbol{\epsilon}}_i, n](\mathbf{r},t)\langle \hat{\hat{e}}_i, \hat{\hat{s}}\rangle \hat{\hat{s}}. \tag{5.167}$$

From the previous expression we can finally identify an effective dynamical exchange coupling

$$\mathcal{J}_{\mathrm{mf}}(\mathbf{r},t) = \sum_{i=1}^{3} F[\bar{\boldsymbol{\epsilon}}_i, n](\mathbf{r},t)\langle \hat{\hat{e}}_i, \hat{\hat{s}}\rangle. \tag{5.168}$$

5.8 Ultrafast spin dynamics in FeMn

In order to analyze how the previously defined objects evolve dynamically in a real magnetic system under the action of an external electric pulse we look at bulk FeMn. The ground state properties of this material have been already studied [176, 177], even though there is no full consensus on the magnetic structure of the ground state since the theoretical results often vary with the method and approximation employed. Here we consider the anti-ferromagnetic ground state in its fcc phase with lattice constant $a = 3.7$ Å [see Fig. 5.9]. This structure represents the starting point of our dynamical evolution. The ground state is characterized by two localized magnetic moments with a magnitude $|\mathbf{S}| \sim 0.57\ \hbar/2$

[2]here the $\hat{\hat{s}}$ indicates that we are considering a simple vector in spin space, the number of points used in the average depends on the definition of the gradient over the grid, usually 4 points for every direction with a total of 12.

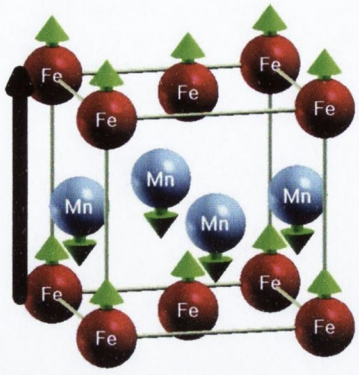


FIGURE 5.9: Picture of the FeMn fcc structure with the black arrow indicating the electric field polarization direction. The green arrows represent the local moments direction in the ground state.

computed at a distance of 0.5 Å from the respective atomic centers. The amount of non collinearity is not negligible but the ratio between m_z and m_x (or m_y) is always approximately 4 and it has the tendency to increase with the distance from the atom. The z component of the magnetization vector is thus locally dominant, even if over the entire simulation box it is approximately zero due to the anti-ferromagnetic nature of the system.

In all our calculations the system is perturbed from the initial equilibrium ground state by applying intense 7 to 10 fs long, spatially homogeneous, electric pulses (see Fig. 5.10(a) and Fig. 5.9 for the direction of polarization of the laser pulse).

In order to analyze the spin dynamics in an anti-ferromagnetic material we need to partition the spin density so to isolate the magnetic moments and the electronic charges associated with each atomic site I in the unit cell. As usual we integrate the densities inside a sphere $\mathcal{S}_R^I$ of radius R centered on the atomic site I without rescaling over the sphere volume

$$\mathbf{S}^I(t) = \int_{\mathcal{S}_R^I} d^3\mathbf{r}\ \mathbf{m}(\mathbf{r},t)\,, \quad Q^I(t) = \int_{\mathcal{S}_R^I} d^3\mathbf{r}\ n(\mathbf{r},t). \tag{5.169}$$

In Fig. 5.10(a) we show the demagnetization observed around the Fe and Mn sites in the first 20 fs under different laser pulses all polarized along the z direction, but with different amplitudes. The demagnetization process is quite pronounced since, in all the cases, the atom loses around 60% of its initial magnetization almost immediately after the action of the pulse and then it stabilizes around a different value of the magnetization vector. The demagnetization rate, instead, differs in the three cases. In particular we observe an initial decay rate proportional to the cube of the laser field amplitude

$$\left|\mathbf{S}^I(t_{\text{in}}+dt)\right| - \left|\mathbf{S}^I(t_{\text{in}})\right| \sim -A^3, \tag{5.170}$$

where t_{in} is the initial time at which the laser pulse is applied, dt is a small time

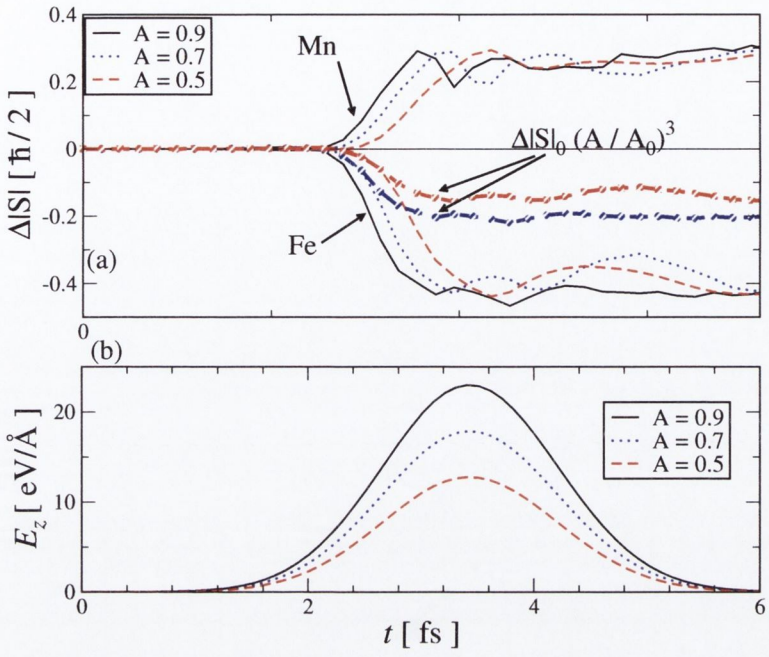


FIGURE 5.10: plots of the time-averaged observables evaluated in spheres of radius 0.5 Å around each atom: (a) the averaged temporal variation of the spin density module $|\Delta\mathbf{S}^{\mathrm{I}}(t)|$ for the two sites Fe and Mn under the pulses of panel (b); (b) different laser pulses employed in the dynamical simulations with shape $E_z(t) = A \cdot \sin(0.1 \cdot t) \cdot \exp\left(-\frac{(t-5)^2}{3}\right)$. The amplitudes A are in units of eV /Å, the laser polarization direction is shown in Fig. 5.9.

step, while A represents the amplitude of the applied laser pulse in $eV/Å$. Hence the demagnetization rate increases substantially for larger excitation amplitudes. In presence of the external laser field the initial set of Kohn-Sham eigenstates $\{\psi^{\mathrm{KS}}_{0,j}\}_{j=1,\ldots,N}$ evolve under a new time dependent Hamiltonian

$$H_{\mathrm{KS}}[n, \mathbf{m}](\mathbf{r}, t) = H^0_{\mathrm{KS}}[n_0, \mathbf{m}_0](\mathbf{r}) + H^{\mathrm{int}}_{\mathrm{KS}}(\mathbf{r}, t). \tag{5.171}$$

This means that a given initial state $\psi^{\mathrm{KS}}_{0,j}(\mathbf{r})$, eigenstate of H_0, is not eigenstate of the new time dependent Hamiltonian and it can, in principle, interfere with the other states during the dynamical evolution. This effect is clearly strongly enhanced during the action of the pulse when different states become connected through intra-site and inter-site electric dipole transitions. After the action of the laser pulse these transitions become energetically unfavourable and the new obtained Kohn-Sham states evolve independently.

The observed magnetization dynamics, localized in correspondence of the two atomic sites, suggests the existence of a charge transfer mechanism among different occupied and unoccupied Kohn-Sham states and requires the availability of a state with same global spin character above the Fermi level. Considering the full magnetization continuity equation (5.104), the terms that play a major role

during the initial phase of the dynamical evolution are the dissipative one and the magnetization transfer term due to the fact that local significative charge transfer is observed only during the initial phase of the dynamics [see Fig. 5.11(a)]. We neglect the spin-orbit coupling from the description and we find

$$\frac{D}{Dt}\mathbf{m}(\mathbf{r},t) = -\nabla\cdot\mathcal{D}(\mathbf{r},t) - \sum_{j\in\text{occ.}} \mathbf{m}_j(\mathbf{r},t)\nabla\cdot\mathbf{v}_j(\mathbf{r},t) + \mu_B\mathbf{m}\times\mathbf{B}_{\text{eff}}(\mathbf{r},t)\,. \quad (5.172)$$

From panel (a) in Fig. 5.11 we observe that in correspondence of the two atomic sites Fe (black solid line) and Mn (red dashed curve), the average temporal variation of the local electronic density is small if compared to the variation of the local on-site magnetization [see Fig. 5.11(b)]. The second term on the right-hand side of Eq. (5.172) may be therefore safely neglected in first approximation, and we are left with the following expression

$$\frac{d}{dt}\mathbf{m}(\mathbf{r},t) = -\nabla\cdot\mathcal{D}(\mathbf{r},t) + \mu_B\mathbf{m}(\mathbf{r},t)\times\mathbf{B}_{\text{eff}}(\mathbf{r},t)\,. \quad (5.173)$$

The first term on the right hand side drives the entire dynamics during the action of the laser pulse, influencing also the other fields that gets modified by the local changes in the spin density. From the previous equation, neglecting the exchange-correlation magnetic field $\mathbf{B}_{\text{xc}}(\mathbf{r},t)$ which does not contribute to the spin dynamics in ALDA and represents only an energy barrier between spin up and down states, we are left with the equation

$$\frac{d}{dt}\mathbf{m}(\mathbf{r},t) = -\nabla\cdot\mathcal{D}(\mathbf{r},t) + \mu_B\mathbf{m}(\mathbf{r},t)\times\mathbf{B}_{\text{kin}}(\mathbf{r},t). \quad (5.174)$$

Here we finally distinguish two contributions to the spin dynamics. The first one on the right-hand side of Eq. (5.174) represents a measure of the spin variation due the internal charge currents among the different Kohn-Sham states. This term is, by construction, responsible for effective Stoner-like excitations in real time. In fact, Stoner excitations by definition can be attributed to terms in the Hamiltonian of the form $\hat{c}^{\dagger}_{k,A,\uparrow}\hat{c}_{k,B,\downarrow}$, where A and B label the specific atomic site. These excitations are local in momentum space and non-local in real space and correspond to inter-site electronic excitations, which are included into the previous spin loss term.

The second contribution is given in terms of the kinetic field $\mathbf{B}_{\text{kin}}(\mathbf{r},t)$, as we have seen also in the case of Fe_6 and Fe bcc. Due to its dependence on the gradients of the electron density and magnetization it drastically changes during the action of the electric pulse, when the electronic states are excited and the dynamics is purely non adiabatic. In Fig. 5.11(b) we compare the evolution of the z component of the magnetization localized on the Fe site with its transverse component

$$S^{\text{I}}_{\text{xy}}(t) = \int_{\mathcal{S}^{\text{R}}_{\text{I}}} \mathrm{d}^3r\,\sqrt{m_{\text{x}}(\mathbf{r},t)^2 + m_{\text{y}}(\mathbf{r},t)^2}. \quad (5.175)$$

The predominant change (loss) of on-site magnetic moment during and after the action of the laser pulse is in the z component, while the magnitude of the non collinear part of the magnetization is only slightly affected. It is clear that,

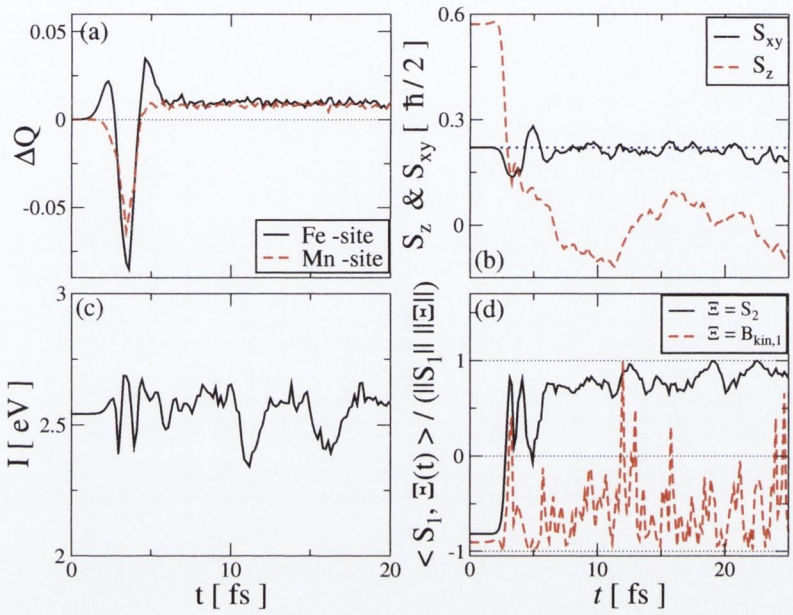


FIGURE 5.11: Plots of the time-averaged observables evaluated in spheres of radius 0.5 Å around the atomic sites under the same type of pulses ($A = 0.7\,\text{eV/Å}$): (a) the averaged temporal variation of the two on-site charge densities $\Delta Q^{\text{I}}(t) = Q^{\text{I}}(t) - Q^{\text{I}}(t=0)$, Fe site (black curve) and Mn site (red curve); (b) the averaged temporal variation of the magnetization along z axis $S^{\text{I}}_{\text{z}}(t)$ and the non collinear component $S^{\text{I}}_{\text{xy}}(t)$, in correspondence of the Fe site; (c) dynamical Stoner exchange parameter $I(t)$ obtained by spatial integration $I(t) = \frac{1}{\|S^{\text{R}}_{\text{I}}\|}\int_{S^{\text{R}}_{\text{I}}} d^3r\, I(\mathbf{r},t)$, in correspondence of the Fe site (see Eq. 5.177); (d) the averaged temporal variation of $F(t) = |\langle \mathbf{S}_{\text{Fe}}(t), \Xi(t)\rangle|/(|\mathbf{S}_{\text{Fe}}(t)| \cdot |\Xi(t)|)$, where $\mathbf{S}_{\text{Fe}}(t)$ is the on-site averaged magnetization calculated within a radius $R = 1.4$ Å. Here $\Xi(t)$ represents the spin calculated within the same radius over the Mn site (solid line) and the kinetic field $\mathbf{B}^{\text{I}}_{\text{kin}}$ over the Fe site (dashed line).

while the component $S^{\text{I}}_{z}(t)$ collapses during the action of the electric field, after that it starts to oscillate around a new averaged value [3]. The behavior of the non-collinear component of the magnetization is instead different. After an initial bump during the action of the pulse, $S^{\text{I}}_{xy}(t)$ returns to a value which is approximately equal to its initial one and then it remains substantially constant for the rest of the temporal evolution. This kind of dynamical behavior suggests the existence of different effective equations of motion for the two magnetization components. The reason for this very different dynamical behavior observed in the S^{I}_{z} and S^{I}_{xy} components lies in the fact that the Stoner excitations connect

[3]Note that in Fig. 5.11(b) only the first period of the oscillation is shown.

only up and down states along the quantization axis. In the initial ($t = 0$) state the magnetic configuration of the system is, to a good level of accuracy, aligned along the z axis. Hence, we would expect a pulse-driven Stoner-like excitation to mainly affect the component $S^{\mathrm{I}}_{\mathrm{z}}$ and to a lesser degree the non-collinear $S^{\mathrm{I}}_{\mathrm{xy}}$ magnetization component.

In Fig. 5.11 we introduce also a time-dependent effective Stoner parameter $\mathrm{I}(t)$. Typically within the DFT formalism I is a measure of the drag in transfering charge density between the spin-up and spin-down bands in the solid. At the level of the ground-state collinear spin DFT it is therefore commonly associated with the ratio between the exchange-correlation magnetic field $\mathbf{B}_{\mathrm{xc}}(\mathbf{r}, t)$ and the local value of the magnetization density. In order to generalize this concept to the case of a non-collinear magnetic system evolving in time we note that the effective local Hamiltonian, corresponding to the magnetic energy in Eq. (5.166), contains together with the exchange-correlation field $\mathbf{B}_{\mathrm{xc}}(\mathbf{r}, t)$ also a second local contribution so that we can define the following effective total magnetic field

$$\mathbf{B}_{\mathrm{tot}}(\mathbf{r}, t) = \mathbf{B}_{\mathrm{xc}}(\mathbf{r}, t) + \mathbf{B}_{\mathrm{local}}(\mathbf{r}, t). \tag{5.176}$$

We use this field to define a local Stoner vector $\mathbf{I}(\mathbf{r}, t)$ parallel to $\mathbf{B}_{\mathrm{tot}}(\mathbf{r}, t)$ and normalized with respect to the amplitude of the magnetization at each spatial point

$$\mathbf{B}_{\mathrm{tot}}(\mathbf{r}, t) = \mathbf{I}(\mathbf{r}, t) \cdot |\mathbf{m}(\mathbf{r}, t)|. \tag{5.177}$$

Hence, similarly to Eq. (5.176), $\mathbf{I}(\mathbf{r}, t)$ can be identified with the sum of the two separated contributions coming from the local and the exchange-correlation fields,

$$\mathbf{I}(\mathbf{r}, t) = \mathbf{I}_{\mathrm{xc}}(\mathbf{r}, t) + \mathbf{I}_{\mathrm{loc.}}(\mathbf{r}, t). \tag{5.178}$$

In Fig. 5.11(c) we plot the module of the vector field $|\mathbf{I}(\mathbf{r}, t)|$ integrated in a sphere centered on the Fe site. Its real time evolution within the first 20 fs shows some oscillations activated by the action of the laser pulse. However the overall change in the Stoner parameter during the evolution is not appreciable and $I(t)$ remains approximately constant throughout the entire dynamics and close to its initial value. This behavior suggests that the initial dynamical change in the on-site z component of the magnetization due to a transfer of spin density among the two atomic sites is mainly driven by the contribution $\nabla \cdot \mathcal{D}(\mathbf{r}, t)$ to the spin continuity equation (5.174) and not due to a collapse of $\mathbf{I}(t)$ that, instead, describes the resistance opposed by the band structure to the inter-band transitions.

Apparently, there is no relevant modification of the band structure during the application of the laser pulse. The laser field drives the system into a new magnetic configuration characterized by different local values of the spin vectors with respect to the ground state configuration.

Fig. 5.11(d) shows the dynamical evolution of the function $F(t)$, which represents a measure of the normalized scalar product between the spin vector computed over the Fe site and the spin vector over the Mn site (solid line). This curve

is a measure of the alignment of the two spins. During the action of the laser pulse $F(t)$ changes from an almost anti-ferromagnetic configuration (slightly non collinear) to a ferromagnetic one, with the amount of spin misalignment that is preserved in the process.

Such an effect is determined, as we have already discussed, by the Stoner excitations activated in the anti-ferromagnet by the action of the laser pulse. This initial phase of the evolution characterizes approximately the first 5 fs. At longer times $F(t)$ starts to oscillate around its new value and eventually approaches 1, with the spin misalignment that is lifted out during the process.

The dashed curve, instead, represents the evolution of $F[\Xi](t)$ when $\Xi(t)$ represents the Fe on-site kinetic field. As we have already seen, this object is not necessarily parallel to the local magnetization and it could, in principle, generate a torque. Within the first 5 fs of dynamical evolution $F(t)$ is characterized by a strong fluctuation induced by the internal currents activated by the laser and its behaviour is similar to that described by the solid curve. However, after this initial phase, the dynamics of $F(t)$ in the two cases appears quite different. The dashed curve strongly oscillates also after the action of the pulse inducing a torque on the magnetization vector.

We can therefore summarize the previous findings as follows

- During the initial phase of the evolution the laser field activates inter-band transitions, with consequent enhanced electronic hopping between the two atomic sites. The hopping is spin conserving and it leads to a decrease of the local magnetic moments of the two atomic sites.
- After the action of the pulse it starts a second phase of the dynamical evolution, where the inter-band transitions are not allowed and the hopping is suppressed. Each Kohn-Sham state evolves, then, separately. The role played by the out-of-equilibrium kinetic field becomes more important, inducing intra-band transitions and considerably modifying the spin dynamics over the two atomic sites with respect to the previous dynamical phase.

A further confirmation of these conclusions is provided in Fig. 5.12(d), where we show a comparison between the local z component of the magnetization $S_z^{Fe}(t)$ and its module $|\mathbf{S}^{Fe}(t)|$. During the action of the laser both the quantities decrease even if at different rates. After this first phase the $S_z^{Fe}(t)$ component starts to oscillate around its new average value, while the module remains approximately constant. This difference in the dynamical behaviour may be clearly explained in terms of initial inter-band transitions and a successive intra-band dynamical relaxation where the spin is exchanged among its different components while its module remains constant.

Similarly we find in Fig. 5.12(b) that the module of the exchange component $|\mathbf{B}_x^{Fe}(t)|$ after the initial decay due to the action of the pulse and the consequent change in electronic and spin densities remains approximately constant, on the

other hand the module of the local component of the kinetic field $|\mathbf{B}_{\text{loc}}(t)|$ introduced in Eq. (5.165) appears after the initial excitation more oscillatory resembling the long time dynamics of the $S_z^{\text{Fe}}(t)$ component. In Fig. 5.12(a) we

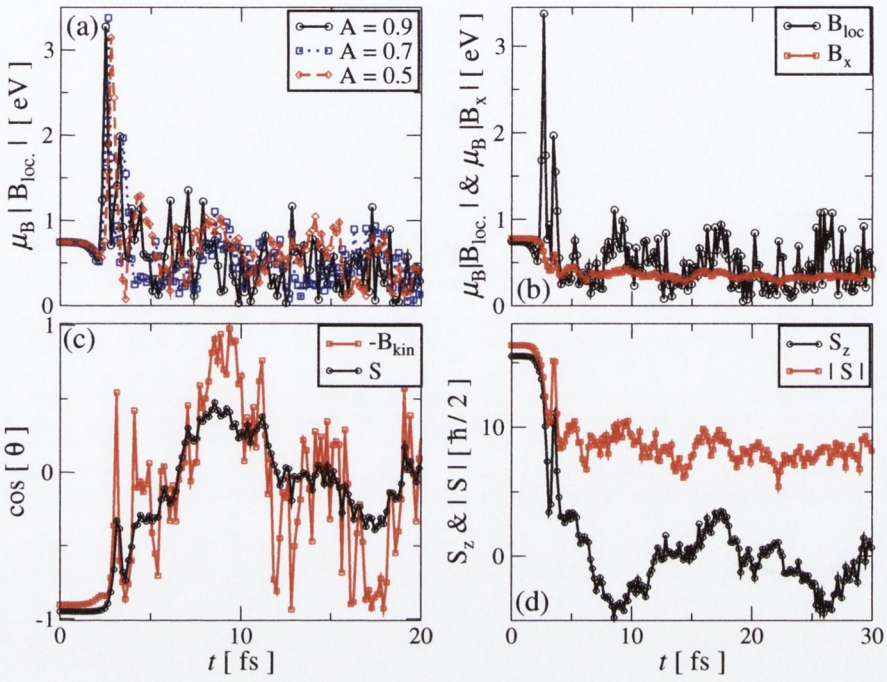


FIGURE 5.12: Plots of the time-averaged observables evaluated in spheres of radius 1.4 Å around the atomic sites. (a) The averaged temporal evolution of $\left|\mathbf{B}_{\text{loc}}^{\text{Fe}}(t)\right|$ under different pulse amplitudes ($A = 0.5\,\text{eV/Å}, 0.7\,\text{eV/Å}, 0.9\,\text{eV/Å}$); (b) comparison of $\left|\mathbf{B}_{\text{loc}}^{\text{Fe}}(t)\right|$ and $\left|\mathbf{B}_{\text{x}}^{\text{Fe}}(t)\right|$ under the pulse with amplitude ($A = 0.7\,\text{eV/Å}$); (c) average value of $\cos\theta$ during the time evolution, with θ angle formed with the z axis by the $\mathbf{S}^{\text{Fe}}(t)$ vector (black curve) and by the $\mathbf{B}_{\text{kin}}^{\text{Fe}}$ vector (red curve), same pulse of panel (b); (d) comparison between $\left|\mathbf{S}^{\text{Fe}}(t)\right|$ and $S_z^{\text{Fe}}(t)$ during the temporal evolution with the same pulse of panel (b).

compare $|\mathbf{B}_{\text{loc}}^{\text{Fe}}(t)|$ under the application of the pulses shown in Fig. 5.10(b). In all the three cases this quantity is excited during the application of the pulse, but in the second phase of the dynamical evolution it collapses to a lower value and it starts to oscillate around it. The application of different laser amplitudes does not seem to be reflected in a clear trend of the dynamical evolution of the local field. Finally we look at panel (c) where we plot the value of $\cos\theta$, with θ being the angle formed by the magnetization vector $\mathbf{S}^{\text{Fe}}(t)$ (black curve), or the kinetic field $-\mathbf{B}_{\text{kin}}^{\text{Fe}}(t)$ with the z axis. This clearly shows, as we have already seen in Fig. 5.11(d), that after the application of the pulse the two vectors are highly non parallel with $\mathbf{B}_{\text{kin}}$ that plays a major role in the local dynamics of the magnetization vector.

We can now focus our attention on the effective mean field term introduced in Eq. (5.168) having the form of an effective spin-spin interaction. This object,

a non-local function of the magnetization vector density, can effectively be the source of spin waves in the dynamical evolution of the system. The temporal evolution of the dynamical exchange parameter $\mathcal{J}_{\mathrm{mf}}(t)$ is presented in Fig. 5.13 panels (a) and (b), and it appears to be strongly dependent on the laser-pulse excitation. In panel (b) it is shown that $\mathcal{J}_{\mathrm{mf}}(t)$ follows the shape of the pulse. The value of the field is integrated within a sphere with small radius (0.5 Å) around the Fe site, therefore, higher pulse amplitudes excite more the electronic system with consequent higher modification of $\mathcal{J}_{\mathrm{mf}}$. The quantity sharply increases from its initial value and then returns close to its ground state value on the timescale of the pulse disappearance. The maximum amplitude of $\mathcal{J}_{\mathrm{mf}}$ also scales systematically with the amplitude of the laser pulse, i.e. it increases for the more intensive pulses. The trend of $\mathcal{J}_{\mathrm{mf}}(t)$ shown in panel (a) is very similar, the quantity is

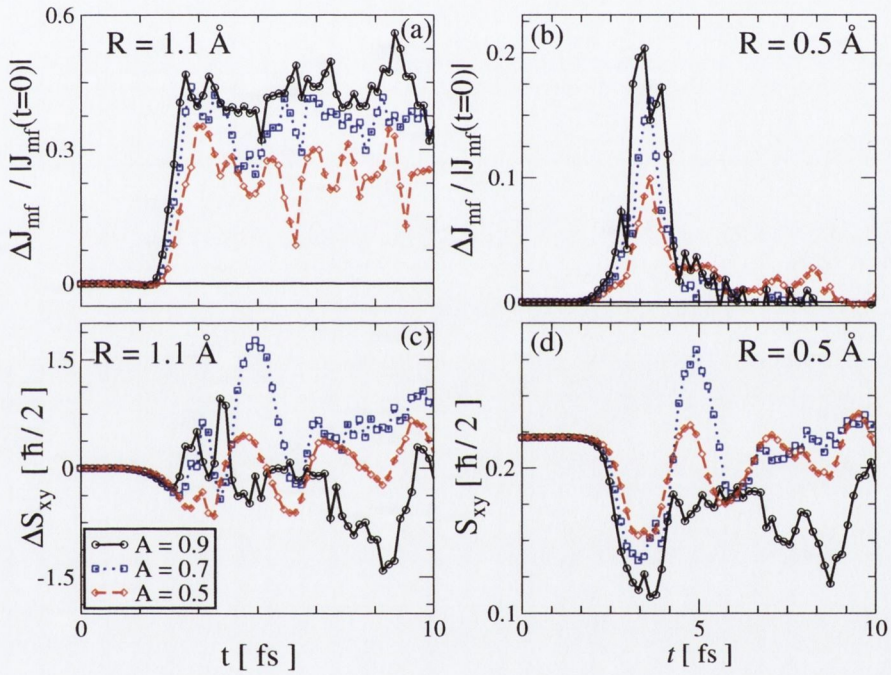


FIGURE 5.13: Plots of the exchange coupling evaluated inside a spheres of different radii centered on the Fe atomic site and of $S^{\mathrm{Fe}}_{\mathrm{xy}}(t)$ calculated inside the same spatial regions using three different type of pulses ($A = 0.7$, $A = 0.9$, $A = 0.5$) in $eV/Å$, the dynamical exchange coupling here corresponds to the expression (5.168): (a) the averaged temporal variation of $\frac{\Delta\mathcal{J}_{\mathrm{mf}}(t)}{|\mathcal{J}_{\mathrm{mf}}(t=0)|} = \frac{\mathcal{J}_{\mathrm{mf}}(t)}{|\mathcal{J}_{\mathrm{mf}}(t=0)|} - 1$ in the first 10 fs, the quantity is integrated within a sphere of radius $R = 1.1$ Å; (b) the same averaged temporal variation $\frac{\Delta\mathcal{J}_{\mathrm{mf}}(t)}{|\mathcal{J}_{\mathrm{mf}}(t=0)|}$ inside a smaller sphere; (c) the averaged temporal variation of $\Delta S^{\mathrm{Fe}}_{\mathrm{xy}}(t)$ obtained by spatial integration inside sphere of radius $R = 1.1$ Å; (d) the averaged temporal evolution of the same quantity $S^{\mathrm{Fe}}_{\mathrm{xy}}(t)$.

computed within a sphere of larger radius. While during the application of the pulse $\mathcal{J}_{\mathrm{mf}}(t)$ looks strongly affected and its growth rate scales proportionally to

the pulse amplitude. After that the exchange coupling stabilizes around an average value, different in the three cases. Such behaviour reflects the different amount of energy injected into the system by the three pulses. In comparison, Fig. 5.13 panels (c) and (d) show the evolution of the non-collinear spin function $S^{\mathrm{Fe}}_{xy}(t)$ for the same set of simulations with increasing laser-pulse intensity. We find clear similarities during the pulse-coherent stage of the dynamics. Both $\mathcal{J}_{\mathrm{mf}}$ and $S^{\mathrm{I}}_{xy}(t)$ follow the pulse, their amplitudes vary with the pulse intensity. At times longer than the pulse duration the dynamics of the two objects is completely different. This difference stems from the fact that the non-collinear spin component $S^{\mathrm{I}}_{xy}(t)$ is driven by two torques, as described by Eq. (5.166), and only a part of the second torque is related to $\mathcal{J}_{\mathrm{mf}}$. The dynamical exchange coupling shown in Fig. 5.13(a) is characterized by a large variation during the action of the laser pulse and it could, at least in principle, activate an out-of-equilibrium dynamics involving the non collinear components of the two atomic spins dependent on the amplitude of the applied laser field. We will see now that this is indeed the case. Further evidence of the validity of this argument for the spin-

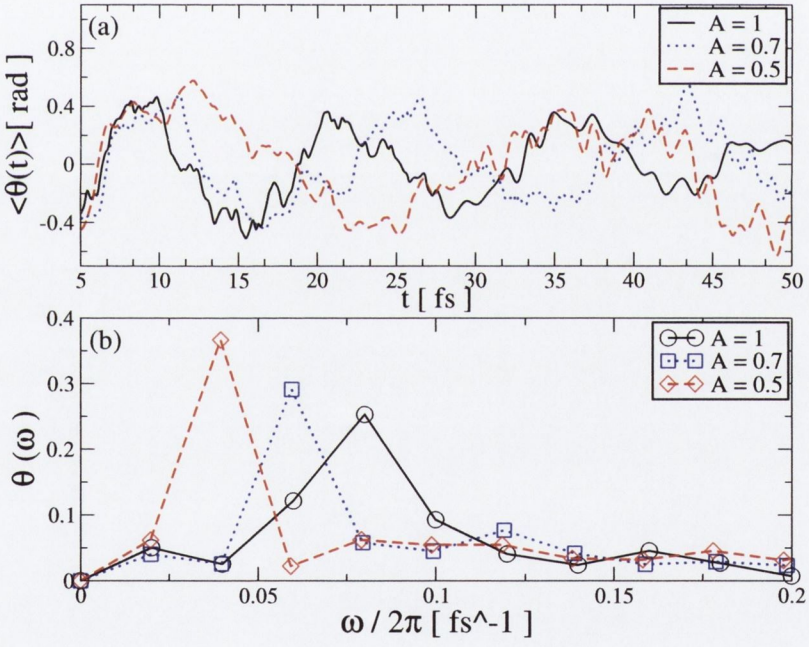


FIGURE 5.14: Plots of the time-averaged observables evaluated in spheres of radius $R = 0.5$ Å around the Fe atomic site with three different type of pulses ($A = 1.0$, $A = 0.7$, $A = 0.5$): (a) the temporal variation of the angle $\theta(t) = \arccos\left(S^{\mathrm{Fe}}_{z}(t)/|\mathbf{S}^{\mathrm{Fe}}(t)|\right)$ with respect to its temporal averaged value $\langle\theta(t)\rangle = \frac{\sum_{n=1}^{N}\theta(t_n)}{N}$; (b) the Fourier transform $\mathfrak{F}(\theta)(\omega)$ where $\theta(t)$ is the angle previously defined.

spin exchange are provided in Fig. 5.14(b), where we present the Fourier transform of the angle $\theta(t)$ formed by the spin $\mathbf{S}^{\mathrm{Fe}}(t)$ on the Fe site [see Eq. (5.169)] with the z axis. In panel (a) we present the corresponding temporal evolution

of $\theta(t)$. As before we compare the results from the three different simulations with increasing pulse amplitudes. Focusing on the lowest part of the spectrum, we observe that the lowest frequency peak in the spectrum blue-shifts with the increase of the pulse amplitude. Although our resolution is limited by the length of numerically-stable time integration and we only observe one or two periods of the lowest frequency mode, it is clear that the laser pulse amplitude affects directly the energy of that spin-wave mode. This correlates with our previous observation of strongly pulse-intensity dependent effective exchange interaction $\mathcal{J}_{\mathrm{mf}}(t)$.

In a summary, it is clear that the laser excites directly only the electronic system and this is propagated to the spin system through the consequent formation of Stoner excitations and transfer of magnetization between the two sites. However, at the same time the excitations in the electronic sub-system contribute also to the ultrafast modification of the effective intersite exchange interaction $\mathcal{J}_{\mathrm{mf}}(t)$ depicted in Fig. 5.13(a). Certainly, the degree of laser-induced modification of this quantity is proportional to the amount of energy injected into the system by the pulse, i.e. to the amplitude of the applied external field. The physical interpretation of $\mathcal{J}_{\mathrm{mf}}(t)$ as a Heisenberg-like exchange parameter is further validated by the observation that the lower energy spin-wave modes follow an analogous dependence on the excitation magnitude.

CHAPTER 6

THE TIME EVOLUTION OF THE ORBITAL MOMENT

In this chapter we will look at the ultrafast dynamics of the angular momentum in ferromagnetic metals. This is a topic that we have not considered in the previous chapters where we focused on the analysis of the ultrafast spin dynamics in transition metals. We will use as a prototype system the same Fe_6 cluster that we have considered before.

Our purpose here is to develop an equation of motion for the orbital moment similar to the one we have introduced in Chapter 1 for the isolated semi-relativistic spinning particle. In the case of periodic systems, the standard definition of orbital moment is ambiguous due to the fact that the position vector is not well defined and it changes according to the choice of the origin of the reference system. The standard procedure of computing the orbital magnetization $\mathbf{M}$ is by integrating currents inside atom centered spheres and requires the introduction of a cut-off radius with the consequence that interstitial contributions are usually neglected. A rigorous theory for the computation of the orbital magnetization in periodic crystals free from such approximation was introduced only quite recently [178–180]. In the case of a non-interacting particles the orbital magnetization has the form

$$\mathbf{M} = \frac{e}{2\hbar}\mathrm{Im}\sum_{n}\int \frac{d^3k}{(2\pi)^3} f_{n\mathbf{k}} \langle \partial_{\mathbf{k}} u_{n\mathbf{k}} | \hat{H}_{\mathbf{k}} + \varepsilon_{n\mathbf{k}} - 2\varepsilon_{\mathrm{F}} | \partial_{\mathbf{k}} u_{n\mathbf{k}} \rangle \,, \tag{6.1}$$

where the integration is performed over all the vectors in the Brillouin zone, and the Bloch Hamiltonian, $\hat{H}_{\mathbf{k}} = e^{-i\mathbf{k}\cdot\mathbf{r}} \mathscr{H} e^{i\mathbf{k}\cdot\mathbf{r}}$, has eigenstates $|u_{n\mathbf{k}}\rangle$, eigenvalues $\varepsilon_{n\mathbf{k}}$, Fermi distribution $f_{n\mathbf{k}}$ and Fermi energy ε_{F}. The last term in the previous expression is zero in the case of insulators, while for metals it cannot be neglected.

The orbital moment of a finite system can be always calculated without employing such a complicated expression because the ambiguity related to the definition of the position vector disappears. This allows us to employ the usual quantum

mechanical definition of the orbital moment operator

$$\hat{\mathbf{L}} = \mathbf{r} \times \hat{\mathbf{p}}, \tag{6.2}$$

as we have already seen in Chapter 2, where we have discussed the differences between the density functional theory (DFT) and the current-density functional theory (CDFT). In fact we have noted that the paramagnetic current calculated through the non interacting Kohn-Sham system $\mathbf{j}_{\mathrm{p}}^{\mathrm{KS}}(\mathbf{r})$ does not correspond to the paramagnetic current of the equivalent many-body system $\mathbf{j}_{\mathrm{p}}(\mathbf{r})$. This result also affects the calculation of the orbital moment, within DFT we have only access to the non interacting Kohn-Sham orbital moment defined as

$$\langle \hat{\mathbf{L}} \rangle = \left\langle \Psi^{\mathrm{KS}} \middle| \hat{\mathbf{L}} \middle| \Psi^{\mathrm{KS}} \right\rangle, \tag{6.3}$$

where $|\Psi^{\mathrm{KS}}\rangle$ is the Kohn-Sham Slater determinant. We then obtain

$$\mathbf{L}^{\mathrm{KS}}(\mathbf{r}) = \mathbf{r} \times \mathbf{j}_{\mathrm{p}}^{\mathrm{KS}}(\mathbf{r}), \tag{6.4}$$

i.e. the paramagnetic Kohn-Sham current enters in the definition of $\langle \hat{L} \rangle$. From this relation we conclude that the fully interacting orbital moment can only be obtained from CDFT, where the paramagnetic current is related to the Kohn-Sham current through

$$\mathbf{j}_{\mathrm{p}}(\mathbf{r}) = \mathbf{j}_{\mathrm{p}}^{\mathrm{KS}}(\mathbf{r}) + en(\mathbf{r})\mathbf{A}_{\mathrm{xc}}(\mathbf{r}), \tag{6.5}$$

and the orbital moment of the fully interacting system may be rewritten as

$$\mathbf{L}(\mathbf{r}) = \mathbf{r} \times [\mathbf{j}_{\mathrm{p}}^{\mathrm{KS}}(\mathbf{r}) + en(\mathbf{r})\mathbf{A}_{\mathrm{xc}}(\mathbf{r})], \tag{6.6}$$

$$\mathbf{L}(\mathbf{r}) = \mathbf{L}^{\mathrm{KS}}(\mathbf{r}) + en(\mathbf{r})\mathbf{r} \times \mathbf{A}_{\mathrm{xc}}(\mathbf{r}). \tag{6.7}$$

Where in the equation above $\mathbf{A}_{\mathrm{xc}}$ is the exchange-correlation vector potential. Analogous arguments are valid in the case of the time-dependent theory. In TD-CDFT we have seen that the fundamental variable is the gauge invariant current density $\mathbf{j}(\mathbf{r}, t)$ related to the Kohn-Sham one through the relation

$$\mathbf{j}(\mathbf{r}, t) = \mathbf{j}^{\mathrm{KS}}(\mathbf{r}, t) + en(\mathbf{r}, t)\mathbf{A}_{\mathrm{xc}}(\mathbf{r}, t). \tag{6.8}$$

The time dependent expression of the orbital moment then becomes

$$\mathbf{L}(\mathbf{r}, t) = \mathbf{L}^{\mathrm{KS}}(\mathbf{r}, t) + en(\mathbf{r}, t)\mathbf{r} \times [\mathbf{A}_{\mathrm{xc}}(\mathbf{r}, t) + \mathbf{A}_{\mathrm{ext}}(\mathbf{r}, t)], \tag{6.9}$$

where we have used the definition (6.4) for the Kohn-Sham orbital moment obtained from the time-dependent non-interacting paramagnetic current.

Since we are employing TD-DFT for our real time calculations, we will simply use the non interacting Kohn-Sham expression of the orbital moment to study its

temporal evolution, namely

$$\mathbf{L}(\mathbf{r},t) = \mathbf{L}^{\mathrm{KS}}(\mathbf{r},t) + en(\mathbf{r},t)\mathbf{r} \times \mathbf{A}_{\mathrm{ext}}(\mathbf{r},t). \tag{6.10}$$

The choice to neglect the many-body corrections to the current density may seem very crude at a first sight. In practice, several CDFT based calculations have shown [102, 181, 182] that while the level of accuracy of this approximation is questionable in the case of open-shell atomic configurations with orbital current carrying states, in general corrections to the orbital current are pretty small. Then, in first approximation, we can consider $\mathbf{L}^{\mathrm{KS}}(\mathbf{r},t)$ as a good approximation of the true many-body orbital moment of the system. However, at the same time, in the final part of this chapter we will also explore the role played by orbital polarization terms in the ultrafast dynamics of the orbital moment. This terms can enter into the description only through the exchange-correlation vector potential $\mathbf{A}_{\mathrm{xc}}$ and an update to CDFT is necessary in order to properly describe these effects.

In the following sections we will separate $\mathbf{L}^{\mathrm{KS}}(\mathbf{r},t)$ in two components, the first one describing the evolution of the angular momentum of the center of mass, and the second one describing the orbital moment due to the motion of the charges with respect to the center of mass. For both these quantities we will obtain an equation of motion. Finally we will develop a model providing a simplified account of all the most important contributions to the ultrafast dynamics of the orbital moment in transition metals. We will see that this separation can help also in disentangling the different contribution to the orbital moment dynamics, with the component describing the motion with respect to the center of mass that is essential for the understanding of the difference in the spin dynamics observed in Fe_6 between in-plane and out-of-plane atoms.

6.1 Center of mass and internal orbital moment

We start by considering a single spinning particle in an external scalar potential $\varphi(\mathbf{r})$ and a time-dependent magnetic field $\mathbf{B}(\mathbf{r},t)$ that simply couples with the spin of the particle. The Hamiltonian $\mathscr{H}(\mathbf{r},\mathbf{p},t)$ can be simply written as

$$\mathscr{H}(\mathbf{r},\mathbf{p},t) = \frac{\mathbf{p}^2}{2m} + q\varphi(\mathbf{r}) - \mathbf{s}\cdot\mathbf{B}(\mathbf{r},t), \tag{6.11}$$

with $\mathbf{s}$ being the particle spin.

The corresponding Lagrangian is

$$\mathscr{L}(\mathbf{r},\mathbf{v},t) = \frac{\mathbf{p}^2}{2m} - q\varphi(\mathbf{r}) + \mathbf{s}\cdot\mathbf{B}(\mathbf{r},t), \tag{6.12}$$

with the particle momentum $\mathbf{p} = m\mathbf{v}$. The Lagrangian function for a system of N non-interacting particles in an external vector potential $\mathbf{A}(t)$ can be immediately

expressed as

$$\mathscr{L}(\{\mathbf{r}_i\},\{\mathbf{v}_i\},t) = \sum_{i=1}^{N}\frac{m}{2}\mathbf{v}_i^2 - q\sum_{i=1}^{N}\Big(\varphi(\mathbf{r}_i) - \mathbf{v}_i\cdot\mathbf{A}(t)\Big) + \sum_{i=1}^{N}\mathbf{s}_i\cdot\mathbf{B}(\mathbf{r}_i,t), \tag{6.13}$$

where we have introduced the physical particle velocity $\mathbf{v}_i$. We could now switch to a new coordinate system in which the particle coordinates in phase-space are taken with respect to the center of mass of the many-particles system. The Particle velocity and position become then

$$\mathbf{v}_i = \Delta\mathbf{v}_i + \mathbf{V}_{\mathrm{CM}}, \qquad i = 1,\ldots,N. \tag{6.14}$$

$$\mathbf{r}_i = \Delta\mathbf{r}_i + \mathbf{R}_{\mathrm{CM}}, \qquad i = 1,\ldots,N. \tag{6.15}$$

Here $\mathbf{R}_{\mathrm{CM}}$ and $\mathbf{V}_{\mathrm{CM}}$ are respectively the center of mass position and velocity of the system of particles. By substituting $\mathbf{v}_i^2$ with

$$\mathbf{v}_i^2 = \Delta\mathbf{v}_i^2 + 2\Delta\mathbf{v}_i\cdot\mathbf{V}_{\mathrm{CM}} + \mathbf{V}_{\mathrm{CM}}^2, \tag{6.16}$$

the Lagrangian then becomes

$$\begin{aligned}\mathscr{L}(\{\mathbf{r}_i\},\{\mathbf{v}_i\},t) = &\sum_{i=1}^{N}\frac{m}{2}\Delta\mathbf{v}_i^2 + m\mathbf{V}_{\mathrm{CM}}\cdot\sum_{i=1}^{N}\Delta\mathbf{v}_i + \frac{m}{2}\sum_{i=1}^{N}\mathbf{V}_{\mathrm{CM}}^2 - \\ &- q\sum_{i=1}^{N}\Big[\varphi(\mathbf{r}_i+\mathbf{R}_{\mathrm{CM}}) - \mathbf{V}_{\mathrm{CM}}\cdot\mathbf{A}(t) - \Delta\mathbf{v}_i\cdot\mathbf{A}(t)\Big] + \\ &+ \sum_{i=1}^{N}\mathbf{s}(\Delta\mathbf{r}_i+\mathbf{R}_{\mathrm{CM}})\cdot\mathbf{B}(\Delta\mathbf{r}_i+\mathbf{R}_{\mathrm{CM}}),\end{aligned} \tag{6.17}$$

which after some simplifications gives

$$\begin{aligned}\mathscr{L}(\{\mathbf{r}_i\},\{\mathbf{v}_i\},t) = &\sum_{i=1}^{N}\frac{m}{2}\Delta\mathbf{v}_i^2 + m\mathbf{V}_{\mathrm{CM}}\cdot\sum_{i=1}^{N}\Delta\mathbf{v}_i + \frac{Nm}{2}\mathbf{V}_{\mathrm{CM}}^2 - \\ &- q\sum_{i=1}^{N}\Big[\varphi(\Delta\mathbf{r}_i+\mathbf{R}_{\mathrm{CM}}) - \Delta\mathbf{v}_i\cdot\mathbf{A}(t)\Big] + qN\mathbf{V}_{\mathrm{CM}}\cdot\mathbf{A}(t) + \\ &+ \sum_{i=1}^{N}\mathbf{s}(\Delta\mathbf{r}_i+\mathbf{R}_{\mathrm{CM}})\cdot\mathbf{B}(\Delta\mathbf{r}_i+\mathbf{R}_{\mathrm{CM}}).\end{aligned} \tag{6.18}$$

We can now define the conjugate momenta of the variables $\mathbf{R}_{\mathrm{CM}}$ and $\{\Delta\mathbf{r}_i\}_{i=1}^N$ as

$$\Delta\mathbf{p}_i = \frac{\partial\mathscr{L}}{\partial\Delta\mathbf{v}_i}, \tag{6.19}$$

$$\Delta\mathbf{p}_i = m\Delta\mathbf{v}_i + m\mathbf{V}_{\mathrm{CM}} + q\mathbf{A}(t), \tag{6.20}$$

$$\Delta \mathbf{v}_i = \frac{\Delta \mathbf{p}_i}{m} - \mathbf{V}_{\mathrm{CM}} - \frac{q}{m}\mathbf{A}(t). \tag{6.21}$$

The conjugate center of mass momentum is defined as

$$\mathbf{P}_{\mathrm{CM}} = \frac{\partial \mathscr{L}}{\partial \mathbf{V}_{\mathrm{CM}}}, \tag{6.22}$$

$$\mathbf{P}_{\mathrm{CM}} = m\sum_{i=1}^{N} \Delta \mathbf{v}_i + mN\mathbf{V}_{\mathrm{CM}} + qN\mathbf{A}(t), \tag{6.23}$$

which leads to the center of mass velocity

$$\mathbf{V}_{\mathrm{CM}} = \frac{\mathbf{P}_{\mathrm{CM}}}{Nm} - \frac{1}{N}\sum_{i=1}^{N} \Delta \mathbf{v}_i - \frac{q}{m}\mathbf{A}(t). \tag{6.24}$$

By substituting Eq. (6.21) into the expression for $\mathbf{P}_{\mathrm{CM}}$ we find

$$\mathbf{P}_{\mathrm{CM}} = mN\mathbf{V}_{\mathrm{CM}} + \sum_{i=1}^{N} \Delta \mathbf{p}_i - mN\mathbf{V}_{\mathrm{CM}} + qN\mathbf{A}(t) - qN\mathbf{A}(t), \tag{6.25}$$

with the result

$$\mathbf{P}_{\mathrm{CM}} = \sum_{i=1}^{N} \Delta \mathbf{p}_i. \tag{6.26}$$

We rewrite the Lagrangian, $\mathscr{L}$, in terms of the new variables $\Delta \mathbf{p}_i$ and $\mathbf{P}_{\mathrm{CM}}$

$$\begin{aligned}\mathscr{L}(\{\Delta \mathbf{r}_i\}, \mathbf{R}_{\mathrm{CM}}, \{\Delta \mathbf{p}_i\}, \mathbf{P}_{\mathrm{CM}}, t) = &\sum_{i=1}^{N} \frac{m}{2}\left[\frac{\Delta \mathbf{p}_i}{m} - \mathbf{V}_{\mathrm{CM}} - \frac{q}{m}\mathbf{A}(t)\right]^2 + \frac{Nm}{2}\mathbf{V}_{\mathrm{CM}}^2 + \\ &+ m\mathbf{V}_{\mathrm{CM}} \cdot \sum_{i=1}^{N}\left[\frac{\Delta \mathbf{p}_i}{m} - \mathbf{V}_{\mathrm{CM}} - \frac{q}{m}\mathbf{A}(t)\right] + qN\mathbf{V}_{\mathrm{CM}} \cdot \mathbf{A}(t) - \\ &- q\sum_{i=1}^{N} \varphi(\Delta \mathbf{r}_i + \mathbf{R}_{\mathrm{CM}}) + \sum_{i=1}^{N} \mathbf{s}(\Delta \mathbf{r}_i + \mathbf{R}_{\mathrm{CM}}) \cdot \mathbf{B}(\Delta \mathbf{r}_i + \mathbf{R}_{\mathrm{CM}}),\end{aligned} \tag{6.27}$$

which after some simplifications becomes

$$\begin{aligned}\mathscr{L}(\{\Delta \mathbf{r}_i\}, \mathbf{R}_{\mathrm{CM}}, \{\Delta \mathbf{p}_i\}, \mathbf{P}_{\mathrm{CM}}, t) = &\sum_{i=1}^{N} \frac{\Delta \mathbf{p}_i^2}{2m} - q\sum_{i=1}^{N} \varphi(\Delta \mathbf{r}_i + \mathbf{R}_{\mathrm{CM}}) - \frac{q^2}{2m}N\mathbf{A}(t)^2 + \\ &+ \sum_{i=1}^{N} \mathbf{s}(\Delta \mathbf{r}_i + \mathbf{R}_{\mathrm{CM}}) \cdot \mathbf{B}(\Delta \mathbf{r}_i + \mathbf{R}_{\mathrm{CM}}).\end{aligned} \tag{6.28}$$

The definition of the corresponding Hamiltonian is

$$H(\{\Delta\mathbf{r}_i\}, \mathbf{R}_{CM}, \{\Delta\mathbf{p}_i\}, \mathbf{P}_{CM}, t) = \\ = \sum_{i=1}^{N} \Delta\mathbf{p}_i \cdot \Delta\mathbf{v}_i + \mathbf{P}_{CM} \cdot \mathbf{V}_{CM} - \mathscr{L}(\{\Delta\mathbf{r}_i\}, \mathbf{R}_{CM}, \{\Delta\mathbf{p}_i\}, \mathbf{P}_{CM}, t). \tag{6.29}$$

By substituting $\Delta\mathbf{v}_i$ with Eq. (6.21) we obtain

$$H(\{\Delta\mathbf{r}_i\}, \mathbf{R}_{CM}, \{\Delta\mathbf{p}_i\}, \mathbf{P}_{CM}, t) = \sum_{i=1}^{N} \Delta\mathbf{p}_i \cdot \left[\frac{\Delta\mathbf{p}_i}{m} - \mathbf{V}_{CM} - \frac{q}{m}\mathbf{A}(t)\right] + \mathbf{P}_{CM} \cdot \mathbf{V}_{CM} - \\ - \sum_{i=1}^{N} \frac{\Delta\mathbf{p}_i^2}{2m} + q\sum_{i=1}^{N} \varphi(\Delta\mathbf{r}_i + \mathbf{R}_{CM}) + \frac{q^2}{2m} N\mathbf{A}^2(t) - \\ - \sum_{i=1}^{N} \mathbf{s}(\Delta\mathbf{r}_i + \mathbf{R}_{CM}) \cdot \mathbf{B}(\Delta\mathbf{r}_i + \mathbf{R}_{CM}), \tag{6.30}$$

$$H(\{\Delta\mathbf{r}_i\}, \mathbf{R}_{CM}, \{\Delta\mathbf{p}_i\}, \mathbf{P}_{CM}, t) = \sum_{i=1}^{N} \frac{\Delta\mathbf{p}_i^2}{2m} - \frac{q}{m}\mathbf{A}(t) \cdot \mathbf{P}_{CM} + q\sum_{i=1}^{N} \varphi(\Delta\mathbf{r}_i + \mathbf{R}_{CM}) + \\ + \frac{q^2}{2m} N\mathbf{A}^2(t) - \sum_{i=1}^{N} \mathbf{s}(\Delta\mathbf{r}_i + \mathbf{R}_{CM}) \cdot \mathbf{B}(\Delta\mathbf{r}_i + \mathbf{R}_{CM}). \tag{6.31}$$

The orbital moment of a system of N independent particles can be then written as

$$\mathbf{L} = \sum_{i=1}^{N} \mathbf{r}_i \times [\mathbf{p}_i - q\mathbf{A}(t)], \tag{6.32}$$

where $\mathbf{p}_i$ is the single particle conjugate momentum, $\mathbf{p}_i = m\mathbf{v}_i + q\mathbf{A}(t)$

$$\mathbf{p}_i = m\mathbf{V}_{CM} + m\Delta\mathbf{v}_i + q\mathbf{A}(t), \tag{6.33}$$

from which we conclude that $\mathbf{p}_i = \Delta\mathbf{p}_i$. Then, in terms of the new set of variables $\mathbf{R}_{CM}$, $\{\Delta\mathbf{r}_i\}$, $\mathbf{P}_{CM}$ and $\{\Delta\mathbf{p}_i\}$ the orbital moment $\mathbf{L}$ becomes

$$\mathbf{L} = \sum_{i=1}^{N} [\mathbf{R}_{CM} + \Delta\mathbf{r}_i] \times [\Delta\mathbf{p}_i - q\mathbf{A}(t)], \tag{6.34}$$

$$\mathbf{L} = -qN\mathbf{R}_{CM} \times \mathbf{A}(t) + \mathbf{R}_{CM} \times \sum_{i=1}^{N} \Delta\mathbf{p}_i - q\sum_{i=1}^{N} \Delta\mathbf{r}_i \times \mathbf{A}(t) + \sum_{i=1}^{N} \Delta\mathbf{r}_i \times \Delta\mathbf{p}_i. \tag{6.35}$$

By using Eq. (6.26) we finally write

$$\mathbf{L} = -qN\mathbf{R}_{\mathrm{CM}} \times \mathbf{A}(t) + \mathbf{R}_{\mathrm{CM}} \times \mathbf{P}_{\mathrm{CM}} - q\sum_{i=1}^{N} \Delta\mathbf{r}_i \times \mathbf{A}(t) + \sum_{i=1}^{N} \Delta\mathbf{r}_i \times \Delta\mathbf{p}_i, \quad (6.36)$$

that defines the gauge invariant orbital moment of the system of particles expressed in the center of mass coordinates. The quantization of the Hamiltonian in Eq. (6.31) proceeds by expressing the variables $\{\Delta\mathbf{r}_i\}$, $\mathbf{R}_{\mathrm{CM}}$ together with the conjugate momenta $\{\Delta\mathbf{p}_i\}$ and $\mathbf{P}_{\mathrm{CM}}$ as operators over an Hilbert space $\mathscr{H}$

$$\hat{H}(t) = \sum_{i=1}^{N} \frac{\Delta\hat{\mathbf{p}}_i^{\,2}}{2m} - \frac{q}{m}\mathbf{A}(t) \cdot \hat{\mathbf{P}}_{\mathrm{CM}} + q\sum_{i=1}^{N} \varphi(\Delta\hat{\mathbf{r}}_i + \hat{\mathbf{R}}_{\mathrm{CM}}) + \frac{q^2}{2m}N\mathbf{A}^2(t) -$$
$$- \mu_{\mathrm{B}} \sum_{i=1}^{N} \hat{\boldsymbol{\sigma}}_i \cdot \mathbf{B}(\Delta\hat{\mathbf{r}}_i + \hat{\mathbf{R}}_{\mathrm{CM}}). \quad (6.37)$$

The scalar potential $\varphi(\mathbf{r})$ and the magnetic field $\mathbf{B}(\mathbf{r})$ are simple scalar and vector functions of the position operator in Hilbert space, while the conjugate momentum operator $\Delta\hat{\mathbf{p}}_i$ is expressed as

$$\Delta\hat{\mathbf{p}}_i = \hat{\mathbf{p}}_i, \quad (6.38)$$
$$\Delta\hat{\mathbf{p}}_i = -i\hbar\nabla_{\mathbf{r}_i}, \quad (6.39)$$

and the center of mass momentum becomes

$$\hat{\mathbf{P}}_{\mathrm{CM}} = -i\hbar\nabla_{\mathrm{CM}}. \quad (6.40)$$

Given that $\mathbf{A}(t)$ commutes with the center of mass momentum operator $\hat{\mathbf{P}}_{\mathrm{CM}}$, and we have $[\nabla_{\mathrm{C.M.}}, \mathbf{A}(t)] = 0$. The Hamiltonian may be rewritten in the form

$$\hat{H}(t) = -\frac{\hbar^2}{2m}\sum_{i=1}^{N} \nabla_{\mathbf{r}_i}^2 + i\hbar\frac{q}{m}\mathbf{A}(t) \cdot \nabla_{\mathrm{CM}} + q\sum_{i=1}^{N} \varphi(\Delta\hat{\mathbf{r}}_i + \hat{\mathbf{R}}_{\mathrm{CM}}) + \frac{q^2}{2m}N\mathbf{A}^2(t) -$$
$$- \mu_{\mathrm{B}} \sum_{i=1}^{N} \hat{\boldsymbol{\sigma}}_i \cdot \mathbf{B}(\Delta\hat{\mathbf{r}}_i + \hat{\mathbf{R}}_{\mathrm{CM}}). \quad (6.41)$$

The orbital moment operator then becomes

$$\hat{\mathbf{L}} = \hat{\mathbf{R}}_{\mathrm{CM}} \times [\hat{\mathbf{P}}_{\mathrm{CM}} - Nq\mathbf{A}(t)] - q\sum_{i=1}^{N} \Delta\hat{\mathbf{r}}_i \times \mathbf{A}(t) + \sum_{i=1}^{N} \Delta\hat{\mathbf{r}}_i \times \Delta\hat{\mathbf{p}}_i. \quad (6.42)$$

Thus the orbital moment operator can be splitted in two parts, the first related to the center of mass, while the second one arises due to the motion of the charges in the reference frame of the center of mass

$$\hat{\mathbf{L}} = \hat{\mathbf{L}}_{\mathrm{CM}} + \Delta\hat{\mathbf{L}}, \quad (6.43)$$

with

$$\hat{\mathbf{L}}_{\mathrm{CM}} = \hat{\mathbf{R}}_{\mathrm{CM}} \times [\hat{\mathbf{P}}_{\mathrm{CM}} - Nq\mathbf{A}(t)], \tag{6.44}$$

and the internal contribution

$$\Delta\hat{\mathbf{L}} = q\mathbf{A}(t) \times \sum_{i=1}^{N} \Delta\hat{\mathbf{r}}_i + \sum_{i=1}^{N} \Delta\hat{\mathbf{r}}_i \times \Delta\hat{\mathbf{p}}_i. \tag{6.45}$$

The expectation value of the center of mass contribution becomes

$$\langle\hat{\mathbf{L}}_{\mathrm{CM}}\rangle = \langle\hat{\mathbf{R}}_{\mathrm{CM}} \times \hat{\mathbf{P}}_{\mathrm{CM}}\rangle - Nq\,\langle\hat{\mathbf{R}}_{\mathrm{CM}}\rangle \times \mathbf{A}(t). \tag{6.46}$$

The center of mass position may be expressed as an operator in the Hilbert space as

$$\hat{\mathbf{R}}_{\mathrm{CM}} = \int \mathrm{d}^3 r\, \hat{n}(\mathbf{r})\mathbf{r}, \tag{6.47}$$

where the operator $\hat{n}(\mathbf{r})$ is

$$\hat{n}(\mathbf{r}) = \frac{\hat{\rho}(\mathbf{r})}{\|\langle\hat{\rho}(\mathbf{r})\rangle\|_1}. \tag{6.48}$$

Here $\hat{\rho(\mathbf{r})}$ is the single particle density operator. $\|\langle\hat{\rho}(\mathbf{r})\rangle\|_1$ is the L_1-norm of the single-particle electron density, that is equal to the total number of electrons in the system. As such $\hat{n}(\mathbf{r})$ represents some form of normalized single-particle density operator, and the expectation value of the center of mass position becomes equivalent to its classical mechanics definition

$$\langle\hat{\mathbf{R}}_{\mathrm{CM}}\rangle = \frac{\int \mathrm{d}^3 r\, n(\mathbf{r})\mathbf{r}}{N}. \tag{6.49}$$

In order to evaluate the expectation value $\langle\hat{\mathbf{R}}_{\mathrm{CM}} \times \hat{\mathbf{P}}_{\mathrm{CM}}\rangle$, we need to rewrite the gradient with respect to the center of mass position ∇_{CM} in a form that allows us to compute gradients of quantities of the form $f(\mathbf{r})$, i.e. as a function of the ordinary spatial coordinates.

By subdividing the entire space in a set of M equivalent subregions and by assuming that these regions are small enough to label them with a single position vector $\mathbf{r}_k$, we can rewrite the center of mass position in the following way

$$\mathbf{R}_{\mathrm{CM}} = \sum_{k=1}^{M} \mathbf{r}_k \frac{\int_{\Omega_k} \mathrm{d}^3 r\, n(\mathbf{r})}{N}. \tag{6.50}$$

The quantity $f_k = \frac{\int_{\Omega_k} \mathrm{d}^3 r n(\mathbf{r})}{N}$ represents the frequency of finding an electron in the region Ω_k. The center of mass position becomes

$$\mathbf{R}_{\mathrm{CM}} = \sum_{k=1}^{M} \mathbf{r}_k f_k, \tag{6.51}$$

or

$$\mathbf{R}_{\mathrm{CM}} = \sum_{k=1}^{M} \frac{n_k}{N} \mathbf{r}_k, \tag{6.52}$$

with n_k representing the number of electrons contained within the spatial region, Ω_k. Finally

$$\nabla_{\mathrm{CM}} = \sum_{k=1}^{M} \frac{N}{n_k} \nabla_{\mathbf{r}_k}, \tag{6.53}$$

and the expectation value becomes (by making use of the set of single particle states $\{\phi_i(\mathbf{r})\}_{i=1}^{N}$),

$$\langle \hat{\mathbf{R}}_{\mathrm{CM}} \times \hat{\mathbf{P}}_{\mathrm{CM}} \rangle = m\mathbf{R}_{\mathrm{CM}} \times \sum_{k=1}^{M} \frac{N}{n_k} \sum_{i \in \mathrm{occ.}} \int \mathrm{d}^3 r \left(-\frac{i\hbar}{2m} \right) \left[\phi_i(\mathbf{r})^* \nabla_k \phi_i(\mathbf{r}) - \nabla_k \phi_i(\mathbf{r})^* \phi_i(\mathbf{r}) \right]. \tag{6.54}$$

The current obtained over a particular region Ω_k is then

$$\mathbf{j}_k = -\frac{i\hbar}{2m} \sum_{i \in \mathrm{occ.}} \int_{\Omega_k} d^3 r \left[\phi_i(\mathbf{r})^* \nabla_k \phi_i(\mathbf{r}) - \nabla_k \phi_i(\mathbf{r})^* \phi_i(\mathbf{r}) \right], \tag{6.55}$$

and we can introduce a velocity field with a value $\mathbf{v}_k$ in correspondence of every spatial region Ω_k as

$$\mathbf{v}_k = \frac{\mathbf{j}_k}{n_k}, \tag{6.56}$$

with the final result that

$$\langle \hat{\mathbf{R}}_{\mathrm{CM}} \times \hat{\mathbf{P}}_{\mathrm{CM}} \rangle = Nm\mathbf{R}_{\mathrm{CM}} \times \sum_{k=1}^{M} \mathbf{v}_k. \tag{6.57}$$

The expectation value of the center of mass component of the orbital moment may be finally expressed as

$$\langle \hat{\mathbf{L}}_{\mathrm{CM}} \rangle = N\mathbf{R}_{\mathrm{CM}} \times \left[m \sum_{k=1}^{M} \mathbf{v}_k - q\mathbf{A}(t) \right], \tag{6.58}$$

and the contribution per electron (angular momentum density) is

$$\frac{\langle \hat{\mathbf{L}}_{\mathrm{CM}} \rangle}{N} = \mathbf{R}_{\mathrm{CM}} \times \left[m \sum_{k=1}^{M} \mathbf{v}_k - q\mathbf{A}(t) \right]. \tag{6.59}$$

The expectation value of the contribution of the electronic motion with respect to the center of mass (6.45) becomes

$$\langle \Delta \hat{\mathbf{L}} \rangle = q\mathbf{A}(t) \times \sum_{i \in \mathrm{occ.}} \int \mathrm{d}^3 r \, \Delta\mathbf{r} |\phi_i(\mathbf{r})|^2 + \sum_{i \in \mathrm{occ.}} \int \mathrm{d}^3 r \, \phi_i(\mathbf{r})^* \Delta\mathbf{r} \times [-i\hbar \nabla \phi(\mathbf{r})], \tag{6.60}$$

$$\langle \Delta\hat{\mathbf{L}} \rangle = q\mathbf{A}(t) \times \int \mathrm{d}^3 r \, \Delta\mathbf{r} n(\mathbf{r}) + m \int \mathrm{d}^3 r \, \Delta\mathbf{r} \times \mathbf{j}_{\mathrm{p}}(\mathbf{r}). \tag{6.61}$$

The first term in the previous expression may be rewritten as

$$\int \mathrm{d}^3 r \, \Delta\mathbf{r} n(\mathbf{r}) = -\mathbf{R}_{\mathrm{CM}} \int \mathrm{d}^3 r \, n(\mathbf{r}) + \int \mathrm{d}^3 r \, \mathbf{r} n(\mathbf{r}), \tag{6.62}$$

giving

$$\int \mathrm{d}^3 r \, \Delta\mathbf{r} \, n(\mathbf{r}) = 0. \tag{6.63}$$

By inserting this into the expression for $\langle \Delta\hat{\mathbf{L}} \rangle$, we obtain

$$\langle \Delta\hat{\mathbf{L}} \rangle = m \int \mathrm{d}^3 r \, \Delta\mathbf{r} \times \mathbf{j}_{\mathrm{p}}(\mathbf{r}), \tag{6.64}$$

where $\mathbf{j}_{\mathrm{p}}(\mathbf{r})$ is the usual paramagnetic current density.

In order to derive the equations of motion for the angular momentum we need to use the following commutators between position and momentum operators

$$\begin{aligned}
[\Delta\hat{r}_i^k, \Delta\hat{p}_j^l] &= i\hbar\delta_{i,j}\delta_{k,l}, && (6.65)\\
[\Delta\hat{r}_i^k, \hat{P}_{\mathrm{CM}}^l] &= i\hbar\delta_{k,l}, && (6.66)\\
[\Delta\hat{p}_i^k, \hat{P}_{\mathrm{CM}}^l] &= 0, && (6.67)\\
[\Delta\hat{p}_i^k, \hat{R}_{\mathrm{CM}}^l] &= -i\hbar\delta_{k,l}, && (6.68)\\
[\hat{R}_{\mathrm{CM}}^k, \Delta\hat{r}_i^l] &= 0, && (6.69)\\
[\hat{R}_{\mathrm{CM}}^k, \hat{P}_{\mathrm{CM}}^l] &= N \cdot i\hbar\delta_{k,l}. && (6.70)
\end{aligned}$$

We look now at the equations of motion for the two different components of the orbital moment separately, starting from $\hat{\mathbf{L}}_{\mathrm{CM}}$. In the Heisenberg representation the equation of motion is

$$i\hbar\frac{d}{dt}\hat{\mathbf{L}}_{\mathrm{CM}} = [\hat{\mathbf{L}}_{\mathrm{CM}}, \hat{H}(t)], \tag{6.71}$$

$$\begin{aligned}
i\hbar\frac{d}{dt}\hat{\mathbf{L}}_{\mathrm{CM}} = \sum_{i=1}^{N}\left(\frac{1}{2m}[\Delta\hat{p}_i^2, \hat{\mathbf{R}}_{\mathrm{CM}}] - \frac{q}{m}\sum_{k=1}^{3} A^k(t)[\hat{P}_{\mathrm{CM}}^k, \hat{\mathbf{R}}_{\mathrm{CM}}]\right) \times [\hat{\mathbf{P}}_{\mathrm{CM}} - Nq\mathbf{A}(t)] -\\
+ q\hat{\mathbf{R}}_{\mathrm{CM}} \times \sum_{i=1}^{N}[\varphi(\mathbf{r}_i), \hat{\mathbf{P}}_{\mathrm{CM}}] - \mu_{\mathrm{B}} \sum_{i=1}^{N}\sum_{k=1}^{3} \hat{\sigma}_i^k \cdot \hat{\mathbf{R}}_{\mathrm{CM}} \times [B^k(\mathbf{r}_i), \hat{\mathbf{P}}_{\mathrm{CM}}].
\end{aligned} \tag{6.72}$$

By making use of the commutation relations we have

$$[\Delta\hat{p}_i^2, \hat{\mathbf{R}}_{\mathrm{CM}}] = -2i\hbar\Delta\hat{\mathbf{p}}_i, \tag{6.73}$$

and by considering the first term in the orbital moment time derivative expression

$$\sum_{i=1}^{N} \frac{1}{2m}[\Delta\hat{p}_i^2, \hat{\mathbf{R}}_{\mathrm{CM}}]\times[\hat{\mathbf{P}}_{\mathrm{CM}}-Nq\mathbf{A}(t)] = \sum_{i=1}^{N} \frac{1}{2m} \sum_{l,m} \epsilon_{nlm}[\Delta\hat{p}_i^2, \hat{R}_{\mathrm{CM}}^l][\hat{P}_{\mathrm{CM}}-NqA(t)]_m, \tag{6.74}$$

$$\sum_{i=1}^{N} \frac{1}{2m}[\Delta\hat{p}_i^2, \hat{\mathbf{R}}_{\mathrm{CM}}] \times [\hat{\mathbf{P}}_{\mathrm{CM}} - Nq\mathbf{A}(t)] = -\frac{i\hbar}{m} \sum_{i=1}^{N} \sum_{l,m} \epsilon_{nlm}\Delta\hat{p}_i^l[\hat{P}_{\mathrm{CM}} - NqA(t)]_m. \tag{6.75}$$

Finally by using Eq. (6.38), we have that $\sum_{i=1}^{N} \Delta\hat{p}_i^l = \hat{P}_{\mathrm{CM}}^l$

$$\sum_{i=1}^{N} \frac{1}{2m}[\Delta\hat{p}_i^2, \hat{\mathbf{R}}_{\mathrm{CM}}] \times [\hat{\mathbf{P}}_{\mathrm{CM}} - Nq\mathbf{A}(t)] = -\frac{i\hbar}{m}\hat{\mathbf{P}}_{\mathrm{CM}} \times [\hat{\mathbf{P}}_{\mathrm{CM}} - Nq\mathbf{A}(t)], \tag{6.76}$$

with the result

$$\sum_{i=1}^{N} \frac{1}{2m}[\Delta\hat{p}_i^2, \hat{\mathbf{R}}_{\mathrm{CM}}] \times [\hat{\mathbf{P}}_{\mathrm{CM}} - Nq\mathbf{A}(t)] = -i\hbar\frac{Nq}{m}\mathbf{A}(t) \times \hat{\mathbf{P}}_{\mathrm{CM}}. \tag{6.77}$$

The second term in Eq. (6.72) may be expressed as

$$\frac{q}{m} \sum_{k=1}^{3} A^k(t)[\hat{P}_{\mathrm{CM}}^k, \hat{\mathbf{R}}_{\mathrm{CM}}]\times[\hat{\mathbf{P}}_{\mathrm{CM}}-Nq\mathbf{A}(t)] = \frac{q}{m} \sum_{l,m} \epsilon_{nlm}A^l(t)(-i\hbar N)[\hat{P}_{\mathrm{CM}}-NqA(t)]_m, \tag{6.78}$$

$$\frac{q}{m} \sum_{k=1}^{3} A^k(t)[\hat{P}_{\mathrm{CM}}^k, \hat{\mathbf{R}}_{\mathrm{CM}}] \times [\hat{\mathbf{P}}_{\mathrm{CM}} - Nq\mathbf{A}(t)] = -i\hbar\frac{q}{m}N\mathbf{A}(t) \times \hat{\mathbf{P}}_{\mathrm{CM}}. \tag{6.79}$$

By using this result into Eq. (6.72) the sum of the first two terms gives exactly 0. Hence the time derivative of the orbital moment center of mass can then be finally written as

$$-i\hbar\frac{d}{dt}\hat{\mathbf{L}}_{\mathrm{CM}} = i\hbar q \sum_{i=1}^{N} \hat{\mathbf{R}}_{\mathrm{CM}}\times\nabla_{\mathrm{CM}}\varphi(\mathbf{r}_i) - i\hbar\mu_{\mathrm{B}} \sum_{i=1}^{N} \sum_{k=1}^{3} \hat{\sigma}_i^k \cdot \hat{\mathbf{R}}_{\mathrm{CM}}\times\nabla_{\mathrm{CM}}B^k(\mathbf{r}_i), \tag{6.80}$$

that is the final equation for the center of mass component of the orbital moment operator. By considering only the component $\hat{\mathbf{R}}_{\mathrm{CM}} \times \hat{\mathbf{P}}_{\mathrm{CM}}$ of the center of mass

orbital moment, we have

$$-i\hbar\frac{d}{dt}(\hat{\mathbf{R}}_{\mathrm{CM}}\times\hat{\mathbf{P}}_{\mathrm{CM}}) = i\hbar\frac{qN}{m}\mathbf{A}(t)\times\hat{\mathbf{P}}_{\mathrm{CM}} + i\hbar q\sum_{i=1}^{N}\hat{\mathbf{R}}_{\mathrm{CM}}\times\nabla_{\mathrm{CM}}\varphi(\mathbf{r}_i) - \\ - i\hbar\mu_{\mathrm{B}}\sum_{i=1}^{N}\sum_{k=1}^{3}\hat{\sigma}_i^k\cdot\hat{\mathbf{R}}_{\mathrm{CM}}\times\nabla_{\mathrm{CM}}B^k(\mathbf{r}_i). \tag{6.81}$$

We can now evaluate the expectation value of this time derivative, which returns the variation rate of the center of mass component of the orbital moment in the case of a system of independent particles under a set of external scalar and vector potentials $\{\varphi, \mathbf{B}, \mathbf{A}(t)\}$. Explicitly we have

$$-\frac{d}{dt}\langle\hat{\mathbf{R}}_{\mathrm{CM}}\times\hat{\mathbf{P}}_{\mathrm{CM}}\rangle = Nq\mathbf{A}(t)\times\sum_{k=1}^{M}\mathbf{v}_k + q\mathbf{R}_{\mathrm{CM}}\times\nabla_{\mathrm{CM}}\varphi - \mu_B\sum_k m_k\cdot(\mathbf{R}_{\mathrm{CM}}\times\nabla_{\mathrm{CM}})B_k(\mathbf{r}), \tag{6.82}$$

where using the definition of ∇_{CM} given by Eq. (6.53) we obtain

$$-\frac{d}{dt}\langle\hat{\mathbf{R}}_{\mathrm{CM}}\times\hat{\mathbf{P}}_{\mathrm{CM}}\rangle = Nq\mathbf{A}(t)\times\sum_{k=1}^{M}\mathbf{v}_k + Nq\sum_{k=1}^{M}\frac{(\mathbf{R}_{\mathrm{CM}}\times\nabla_k)\varphi}{n_k} - \\ - N\mu_B\sum_j m_j\cdot\sum_{k=1}^{M}\frac{(\mathbf{R}_{\mathrm{CM}}\times\nabla_k)B_j}{n_k}. \tag{6.83}$$

Eq. (6.82) shows that the only sources of change for the center of mass orbital moment come from the set of external fields $\mathbf{A}(t)$, $\varphi(\mathbf{r})$ and $\mathbf{B}(\mathbf{r})$. In the absence of these fields the center of mass orbital moment is conserved during the evolution.

Considering now the equation of motion for the internal orbital moment component $\Delta\hat{\mathbf{L}}$. From the Eq. (6.45) we have that

$$-i\hbar\frac{d}{dt}\Delta\hat{\mathbf{L}} = [\hat{H}(t), \Delta\hat{\mathbf{L}}], \tag{6.84}$$

where the Hamiltonian $\hat{H}(t)$ was defined in Eq. (6.41). The evaluation of the commutator leads to the following expression

$$-i\hbar\frac{d}{dt}\Delta\hat{\mathbf{L}} = \sum_{i,j}\left[\frac{\Delta\hat{\mathbf{p}}_i^{\,2}}{2m}, \Delta\hat{\mathbf{r}}_j\right]\times(\Delta\hat{\mathbf{p}}_j - q\mathbf{A}(t)) + q\sum_{i,j}[\varphi(\mathbf{r}_i), \Delta\hat{\mathbf{r}}_j\times(\Delta\hat{\mathbf{p}}_j - q\mathbf{A}(t))] - \\ - \frac{q}{m}\sum_j[\mathbf{A}(t)\cdot\hat{\mathbf{P}}_{\mathrm{CM}}, \Delta\hat{\mathbf{r}}_j\times(\Delta\hat{\mathbf{p}}_j - q\mathbf{A}(t))] - \\ - \mu_B\sum_{i,j}[\hat{\sigma}_i\cdot\mathbf{B}(\mathbf{r}_i), \Delta\hat{\mathbf{r}}_j\times(\Delta\hat{\mathbf{p}}_j - q\mathbf{A}(t))]. \tag{6.85}$$

The first term on the right hand side can be written

$$\sum_{i,j}\left[\frac{\Delta\hat{\mathbf{p}}_i^{\,2}}{2m},\Delta\hat{\mathbf{r}}_j\right]\times(\Delta\hat{\mathbf{p}}_j-q\mathbf{A}(t))=-\frac{i\hbar}{m}\sum_i\Delta\hat{\mathbf{p}}_i\times(\Delta\hat{\mathbf{p}}_i-q\mathbf{A}(t)),\tag{6.86}$$

which becomes

$$\sum_{i,j}\left[\frac{\Delta\hat{\mathbf{p}}_i^{\,2}}{2m},\Delta\hat{\mathbf{r}}_j\right]\times(\Delta\hat{\mathbf{p}}_j-q\mathbf{A}(t))=\frac{i\hbar}{m}\sum_i\Delta\hat{\mathbf{p}}_i\times q\mathbf{A}(t).\tag{6.87}$$

At the same time the third term in Eq. (6.85) may be rewritten as follows

$$-\frac{q}{m}\sum_j[\mathbf{A}(t)\cdot\hat{\mathbf{P}}_{\mathrm{CM}},\Delta\hat{\mathbf{r}}_j\times(\Delta\hat{\mathbf{p}}_j-q\mathbf{A}(t))]=\mathbf{T}_1+\mathbf{T}_2,\tag{6.88}$$

where,

$$\mathbf{T}_1=-\frac{q}{m}\sum_j\sum_k A^k(t)\cdot[P^k_{\mathrm{CM}},\Delta\hat{\mathbf{r}}_j]\times(\Delta\hat{\mathbf{p}}_j-q\mathbf{A}(t)),\tag{6.89}$$

$$\mathbf{T}_2=-\frac{q}{m}\sum_j\sum_k A^k(t)\Delta\hat{\mathbf{r}}_j\times[\hat{P}^k{}_{\mathrm{CM}},(\Delta\hat{\mathbf{p}}_j-q\mathbf{A}(t))].\tag{6.90}$$

The second term $\mathbf{T}_2$ is exactly zero and, by employing the commutation rule (6.66), we obtain

$$-\frac{q}{m}\sum_j[\mathbf{A}(t)\cdot\hat{\mathbf{P}}_{\mathrm{CM}},\Delta\hat{\mathbf{r}}_j\times(\Delta\hat{\mathbf{p}}_j-q\mathbf{A}(t))]=i\hbar\frac{q}{m}\sum_j\mathbf{A}(t)\times(\Delta\hat{\mathbf{p}}_j-q\mathbf{A}(t)),\tag{6.91}$$

and finally

$$-\frac{q}{m}\sum_j[\mathbf{A}(t)\cdot\hat{\mathbf{P}}_{\mathrm{CM}},\Delta\hat{\mathbf{r}}_j\times(\Delta\hat{\mathbf{p}}_j-q\mathbf{A}(t))]=i\hbar\frac{q}{m}\sum_j\mathbf{A}(t)\times\Delta\hat{\mathbf{p}}_j.\tag{6.92}$$

The sum of the first and third terms on the right-hand side of Eq. (6.85) gives exactly zero and we finally have

$$\frac{d}{dt}\Delta\hat{\mathbf{L}}=-q\sum_i\Delta\hat{\mathbf{r}}_i\times\nabla_i\varphi(\mathbf{r}_i)+\mu_B\sum_i\sum_k\hat{\sigma^k}_i\cdot(\Delta\hat{\mathbf{r}}_i\times\nabla_i)B^k(\mathbf{r}_i)\tag{6.93}$$

with the expectation value that becomes

$$\frac{d}{dt}\langle\Delta\hat{\mathbf{L}}\rangle=-q\int\mathrm{d}^3r\,\rho(\mathbf{r},t)\Delta\mathbf{r}\times\nabla_{\mathbf{r}}\varphi+\mu_B\sum_k\int\mathrm{d}^3r\,m^k(\mathbf{r},t)\cdot(\Delta\mathbf{r}\times\nabla_{\mathbf{r}})B^k(\mathbf{r}).\tag{6.94}$$

Eq. (6.94) shows that the time derivative of the internal component of the orbital moment is not affected, globally, by the interaction of the electronic system with the external pulse, which is spatially homogeneous, but it only scatters with the spatial gradients of the scalar potential φ and the magnetic field $\mathbf{B}(\mathbf{r})$.

In Chapter 1 we have derived the equation of motion for the orbital moment in the case of a single semi-relativistic particle. The same expression may be employed here, with no relevant differences, to the case of many non-interacting particles. We need still to distinguish the motion of the internal orbital moment component from the motion of the center of mass component. In order to do this we need to subtract the time derivative of the center of mass part from the time derivative of the global orbital moment $\langle \hat{\mathbf{L}} \rangle$.

The equation of motion for the non-gauge-invariant, or canonical momentum, may be expressed as from Eq. (6.82), i.e.

$$\frac{d}{dt}\langle \hat{\mathbf{R}}_{\mathrm{CM}} \times \hat{\mathbf{P}}_{\mathrm{CM}} \rangle = -Nq\mathbf{A}(t) \times \sum_{k=1}^{M} \mathbf{v}_k - q\mathbf{R}_{\mathrm{CM}} \times \nabla_{\mathrm{CM}}\varphi + \mu_B \sum_k m_k \cdot (\mathbf{R}_{\mathrm{CM}} \times \nabla_{\mathrm{CM}}) B_k(\mathbf{r}). \tag{6.95}$$

Where we can distinguish essentially two type of contributions.

External vector potential of the laser field: The application of the external time-dependent and spatially homogeneous laser field described by the vector potential, $\mathbf{A}(t)$, leads to a global excitation of the electronic system through the term

$$-Nq\mathbf{A}(t) \times \sum_{k=1}^{M} \mathbf{v}_k.$$

This is equivalent to a torque exerted over the global current of the system. (In absence of spin-orbit coupling, as we have seen in Chapter 4, there is no global orbital moment, or current, in the ground-state and this term does not affect the dynamics.

External scalar potential and magnetic field: The last two terms on the right hand side of Eq. (6.95) can also extert a torque on

$$\langle \hat{\mathbf{R}}_{\mathrm{CM}} \times \hat{\mathbf{P}}_{\mathrm{CM}} \rangle .$$

However, if we start the evolution from the ground-state of the Hamiltonian with potentials $(\varphi, \mathbf{B})$ these objects cannot torque the center of mass momentum in the ground-state configuration. Only after the action of the laser, when the system is described by a new out-of-equilibrium charge distribution, there can be a contribution to the modification of the orbital moment due to the scattering of the electronic cloud with the scalar potentials.

We can now focus our discussion on the equation of motion for the internal component of the orbital moment, $\langle \Delta\hat{\mathbf{L}} \rangle$, from Eq. (6.64). Now, in addition to the terms on the right hand side of Eq. (6.94) we need to include also the orbital current and the spin-orbit coupling contributions derived in Chapter 1 in the case of a single particle with spin. We obtain in the case of a generalization to a many-particle system, by subtracting Eq. (6.95) to the equation for $\frac{d}{dt}\langle \hat{\mathbf{L}} \rangle$, the

following expression

$$\frac{d}{dt}\Delta\mathbf{L} = \frac{i\hbar}{2m}\sum_{r\in\text{occ.}}\sum_{k}\nabla_k\Big[(\mathbf{r}\times(-i\hbar\nabla\psi_r^\dagger))\nabla_k\psi_r - (\mathbf{r}\times(-i\hbar\nabla\psi_r))\nabla_k\psi_r^\dagger\Big]+$$
$$+\sum_{r\in\text{occ.}}\sum_{k} j^k_{\text{p},r}(\mathbf{r},t)\nabla_k\mathbf{l}_r(\mathbf{r},t) + \mu_B\sum_k(\Delta\mathbf{r}\times\nabla)B_k(\mathbf{r},t)m_k(\mathbf{r},t)-$$
$$-\rho(\mathbf{r},t)[\Delta\mathbf{r}\times\nabla\varphi(\mathbf{r})] - \mathbf{T}_{\text{SO}}(\mathbf{r},t) + \rho(\mathbf{r},t)[\Delta\mathbf{r}\times q\mathbf{E}(t)], \tag{6.96}$$

where $\mathbf{j}_{\text{p},r}(\mathbf{r},t)$ is the single-state paramagnetic current defined as

$$\mathbf{j}_{\text{p},r}(\mathbf{r},t) = \frac{i\hbar}{2m}[\nabla\psi_r^\dagger\psi_r - \psi_r^\dagger\nabla\psi_r], \tag{6.97}$$

with ψ_r single orbital state, while the single-state orbital moment density is

$$\mathbf{l}_r(\mathbf{r},t) = \frac{\psi_r^\dagger\hat{\mathbf{L}}\psi_r}{\psi_r^\dagger\psi_r}. \tag{6.98}$$

We can, now, distinguish several terms from the previous expression (6.96)

Orbital currents: The first term on the right hand side of the expression (6.96) represents the so-called orbital currents,

$$\frac{i\hbar}{2m}\sum_{r\in\text{occ.}}\sum_{k}\nabla_k\Big[(\mathbf{r}\times(-i\hbar\nabla\psi_r^\dagger))\nabla_k\psi_r - (\mathbf{r}\times(-i\hbar\nabla\psi_r))\nabla_k\psi_r^\dagger\Big].$$

This object originates from the local non conservation of the orbital moment due to the charge fluxes activated during the temporal evolution. The second object in the equation of motion,

$$\sum_{r\in\text{occ.}}\sum_{k} j^k_{\text{p},r}(\mathbf{r},t)\nabla_k\mathbf{l}_r(\mathbf{r},t),$$

defines a second contribution to the orbital moment change due to the charge currents.

External potential torques: As in the case of the center of mass component, also the internal part of the orbital moment undergoes a torque due to the presence of spatially localized scalar potentials and magnetic fields

$$\mu_B\sum_k(\Delta\mathbf{r}\times\nabla)B_k(\mathbf{r},t)m_k(\mathbf{r},t) - \rho(\mathbf{r},t)[\Delta\mathbf{r}\times\nabla v(\mathbf{r})].$$

Electro-magnetic potential torque: The torque exterted by the homogeneous electric field $\mathbf{E}(t)$ is given by

$$\rho(\mathbf{r},t)[\Delta\mathbf{r}\times q\mathbf{E}(t)].$$

It is interesting to observe that this quantity automatically disappears if we

integrate over the entire simulation region. This demonstrates that globally the electric field acts only on the center of mass leaving unchanged the internal angular momentum.

Spin orbit torque: Finally, in analogy with the spin continuity equation the spin-orbit torque is expressed as

$$-\mathbf{T}_{\mathrm{SO}}(\mathbf{r},t).$$

In conclusion the expression for the time derivative of the internal orbital moment of the non-interacting Kohn-Sham system, in TDSDFT, may be written as

$$\begin{aligned}\frac{d}{dt}\Delta\mathbf{L}^{\mathrm{KS}}(\mathbf{r},t) = &\sum_{r\in\mathrm{occ.}}(\mathbf{j}^{\mathrm{KS}}_{\mathrm{p},r}(\mathbf{r},t)\cdot\nabla)\mathbf{l}^{\mathrm{KS}}_{r}(\mathbf{r},t)+\mu_B\sum_{k}(\Delta\mathbf{r}\times\nabla B^{k}_{s}(\mathbf{r},t))m^{k}(\mathbf{r},t)+\\
&+\frac{i\hbar}{2m}\sum_{r\in\mathrm{occ.}}\sum_{k}\nabla_k\Big[(\mathbf{r}\times(-i\hbar\nabla\psi^{\mathrm{KS}\dagger}_{r}))\nabla_k\psi^{\mathrm{KS}}_{r}-(\mathbf{r}\times(-i\hbar\nabla\psi^{\mathrm{KS}}_{r}))\nabla_k\psi^{\mathrm{KS}\dagger}_{r}\Big]-\\
&-\rho(\mathbf{r},t)[\Delta\mathbf{r}\times\nabla v_s(\mathbf{r},t)]-\mathbf{T}_{\mathrm{SO}}(\mathbf{r},t)+\rho(\mathbf{r},t)[\Delta\mathbf{r}\times q\mathbf{E}(t)],\end{aligned}\tag{6.99}$$

with $v_s(\mathbf{r},t)$ being the scalar potential and $\mathbf{B}_s(\mathbf{r},t)$ the magnetic field of the non-interacting system.

6.2 Analysis of the orbital moment evolution in Fe_6

We start this section by looking at the center of mass motion of the Fe_6 cluster. The system is excited with the same laser that we have used to discuss the spin dynamics in Chapter 5. In Fig. 6.1(a) we show the evolution of the different components of the center of mass position vector. While, along y and z, $\Delta R^{i}_{\mathrm{CM}}$ is zero during the entire evolution, R^{x}_{CM} oscillates around its initial value, during the action of the laser pulse (that is polarized along x). The amplitude of the oscillations increases, while at longer times the oscillations become damped. The laser field pushes the system out of equilibrium. In this new configuration huge currents are still driving charge motion inside the system with consequent oscillations of the center of mass momentum.

In Fig. 6.1(b) we plot, instead, the evolution of the center of mass velocity that corresponds quite accurately to the time derivative of the center of mass position. In panel (c), we show the evolution of the component $\langle\hat{\mathbf{R}}_{\mathrm{CM}}\times\hat{\mathbf{P}}_{\mathrm{CM}}\rangle$ of the orbital moment. This clearly undergoes a huge modification during the application of the laser pulse, according to Eq.(6.95). The long oscillation tail is, instead, related to the presence of internal currents, that (as we have already seen in Chapter 4 in the case of Fe_2 and Fe_6) persist during the entire simulation and do not conserve the orbital moment in presence of the spin orbit coupling. These oscillations may be in practice directly related to the oscillation of the center of

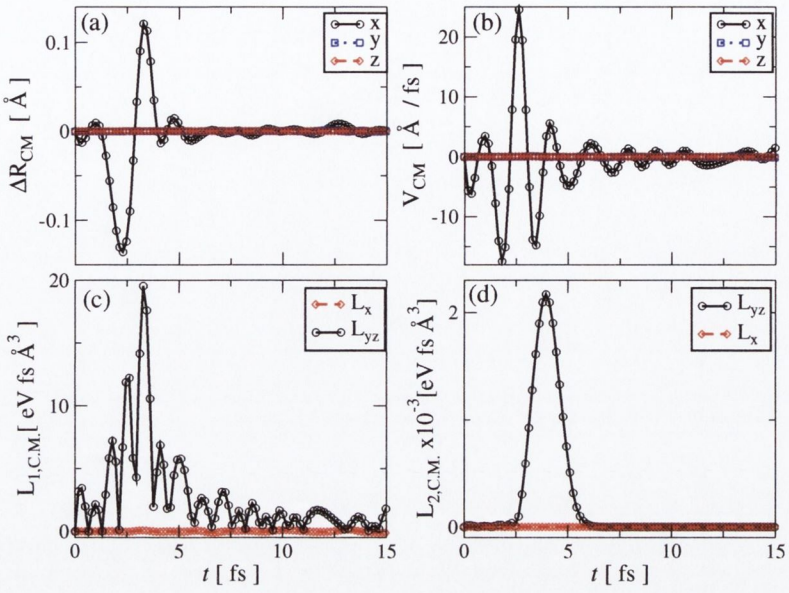


FIGURE 6.1: Dynamics of the Fe_6 cluster center of mass momentum (a) Measure of the variation of the center of mass position $\Delta\mathbf{R}_{CM}(t)$ during the evolution; (b) Center of mass velocity $\mathbf{V}_{CM}(t) = \int d^3r\, \mathbf{j}_p(\mathbf{r},t)/N$; (c) Evolution of the orbital moment center of mass component $\langle \hat{\mathbf{R}_{CM}} \times \hat{\mathbf{P}_{CM}} \rangle$ along x (red curve) and in the yz plane (black curve); (d) orbital moment $-qN\mathbf{R}_{CM} \times \mathbf{A}(t)$ evolution.

mass position around its average value. Finally panel (d) shows the last component of the center of mass momentum $-qN\mathbf{R}_{CM} \times \mathbf{A}(t)$ reflecting the amount of orbital moment injected into the system by the application of the laser pulse. We can now focus on the second component of the orbital moment appearing in Eq. (6.64). In Fig. 6.2 we plot the value of the function integrated around different atomic sites I according to

$$\Delta\mathbf{L}^{\mathrm{I}}(t) = \int_{\mathcal{S}_{\mathrm{I}}^{\mathrm{R}}} d^3r\, \Delta\mathbf{L}(\mathbf{r},t), \tag{6.100}$$

where $\mathcal{S}_{\mathrm{I}}^{\mathrm{R}}$ defines the integration sphere of radius R.

The first observation is that, while this component appears to be much smaller with respect to the center of mass component of Fig. 6.1, the dynamics of the internal orbital moment in correspondence of the in plane atomic sites appears completely different with respect to that observed for the out-of-plane sites 5 and 6 (for the numbering of the atoms see Fig. 6.3). This is intimately connected to the geometrical structure of the Fe_6 cluster, and, at the same time to the polarization direction of the applied electric field that has a clear influence on the particular component of the orbital moment that becomes excited after the application of the pulse. The electronic charge of the atoms forming the central square of the cluster moves only inside the xy plane, as it can be also seen from the change in the center of mass position in Fig. 6.1(a). The consequence is that

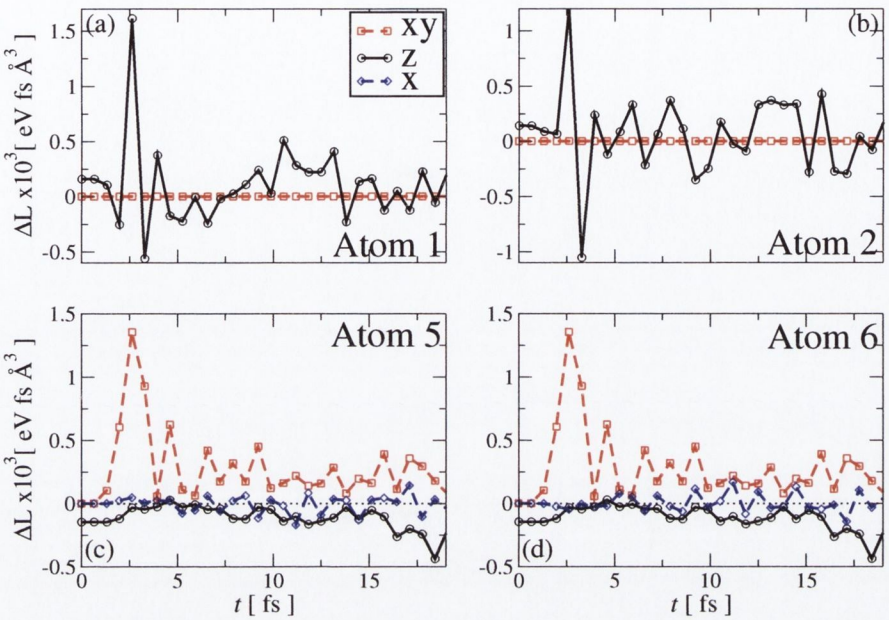


FIGURE 6.2: Dynamics of the Fe_6 cluster internal orbital moment component $\Delta \mathbf{L}_I(t)$ centered over different atomic sites and integrated within a radius $R = 1.2$ Å (a) Site 1; (b) Site 2; (c) Site 5; (d) Site 6.

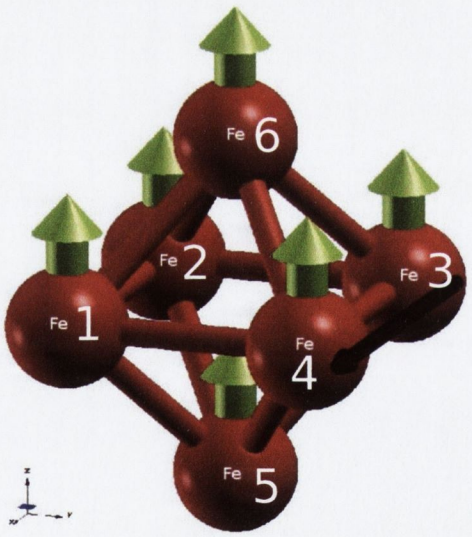


FIGURE 6.3: Picture of the Fe_6 with the black arrow indicating the electric field polarization direction.

the variation of the internal orbital moment component is approximately along z. In panel (a) and (b) of Fig. 6.2 we measure $\Delta\mathbf{L}^{\mathrm{I}}(t)$ in correspondence of sites 1 and 2. While the non collinear component of the orbital moment is almost zero throughout the entire evolution (even if, as we will see later, the intra site non-collinear component is not exactly zero, but it is averaged out by the integral over the atom-centered sphere), the z component undergoes a sudden modification during the application of the laser pulse, and after this initial phase it starts to oscillate around zero. This suggests that the center of mass component of the orbital moment is the dominant one, at least for the in plane electrons, during the dynamical evolution.

The situation is completely different in the case of the out of plane atoms 5 and 6. In panel (c) and (d) we do not see the huge oscillations of $\Delta L^{\mathrm{I}}_z(t)$ observed, instead, in the case of atoms 1 and 2. The out-of-plane z component of the orbital moment appears unaffected by the action of the laser. The same is not true for the xy non-collinear component, $\Delta L^{\mathrm{I}}_{xy}(t) = \sqrt{\Delta L^{\mathrm{I}}_x(t)^2 + \Delta L^{\mathrm{I}}_y(t)^2}$, that instead grows during the application of the laser and then collapses around a new average value different from zero. In both the panels we show also the x component alone of the internal orbital moment (blue line). $\Delta L^{\mathrm{I}}_x(t)$ almost vanishes during the application of the laser pulse, but it is characterized by a slow growth after the pulse that contributes to the effective value of $\Delta L^{\mathrm{I}}_{xy}(t)$.

This completely different behaviour of the local component of the orbital moment $\Delta\mathbf{L}^{\mathrm{I}}(t)$, depending if we are considering in-plane or out-of-plane electrons has also consequences on the spin dynamics of the cluster as we will see in the following sections. But, first, we need to shed more light on the mechanism driving the oscillations in the orbital moment expectation value after the action of the laser pulse. In particular we want to explain in more detail the connection between these oscillations and the single-particle scalar DFT potential.

6.3 A new model for the dynamics of the orbital moment

In this section we look for an explanation of the orbital moment dynamics, already discussed in Chapter 4 for Fe_2 and Fe_6. In particular we want to explain the strong oscillations that follow the action of the external laser pulse. We will see that the scattering of the excited electrons with the external ionic potential plays a fundamental role in the phenomenon, and this will help us also to understand why the spin loss through the spin-orbit coupling is not reflected in a consequent increase of the orbital moment expectation value.

In the previous section we have discovered that the huge oscillations of the orbital moment after the application of the laser pulse may be attributed to the

variation of the position of the center of mass of the electronic cloud with respect to its ground state value. These oscillations in the value of $\Delta\mathbf{R}_{\mathrm{CM}}(t)$ may be directly associated to the temporal evolution of those Kohn-Sham states that are not localized around a certain atomic site (see Fig. 6.3 and Fig. 6.3). During the action of the laser pulse these states contribute to the formation of an electric dipole among different atomic sites. After this initial excitation the system tries to compensate such charge inbalance through oscillations of the center of mass position. The question is, then: How does this effect contribute to the dynamics of the orbital moment ? In order to answer to this question we extend the model for the out-of-equilibrium spin dynamics introduced in Chapter 4 by including a set of on-site scattering potentials. An important aspect that we need to mention is that the quantum state we evolve under this new time-dependent Hamiltonian is not localized on any of the ionic scattering centers. In this way we want to simulate the behaviour of one of these delocalized Kohn-Sham states that contribute to the oscillations of the system orbital moment.

The on-site potentials at the DFT-level are described by the non-interacting Kohn-Sham potential $v_s(\mathbf{r}, t)$,

$$v_s(\mathbf{r}, t) = \int \mathrm{d}^3 r' \, \frac{n(\mathbf{r}', t)}{|\mathbf{r} - \mathbf{r}'|} + V_{\mathrm{ion}}^{\mathrm{PS}}(\mathbf{r}) + v_{\mathrm{xc}}(\mathbf{r}, t). \tag{6.101}$$

From the fact that the Hartree and the exchange-correlation potential cannot exert a global torque on the orbital moment, we will focus on the ionic pseudopotential part

$$\hat{V}_{\mathrm{ion}}^{\mathrm{PS}}(\mathbf{r}) = \sum_{\mathrm{I}} \sum_{l} \sum_{m=-l}^{l} \bar{V}_{\mathrm{I},l}(\mathbf{r} - \mathbf{R}_{\mathrm{I}}) \, |I, l, m\rangle \langle I, l, m| \, . \tag{6.102}$$

The general form of the Hamiltonian we are going to solve is

$$\hat{H}(t) = -\frac{\hat{\mathbf{L}}^2}{2R^2} + \lambda \hat{\mathbf{L}} \cdot \hat{\mathbf{S}} + \mathbf{B}(t) \cdot \hat{\mathbf{S}} + \mathbf{E}(t) \cdot \hat{\mathbf{D}} + \hat{V}, \tag{6.103}$$

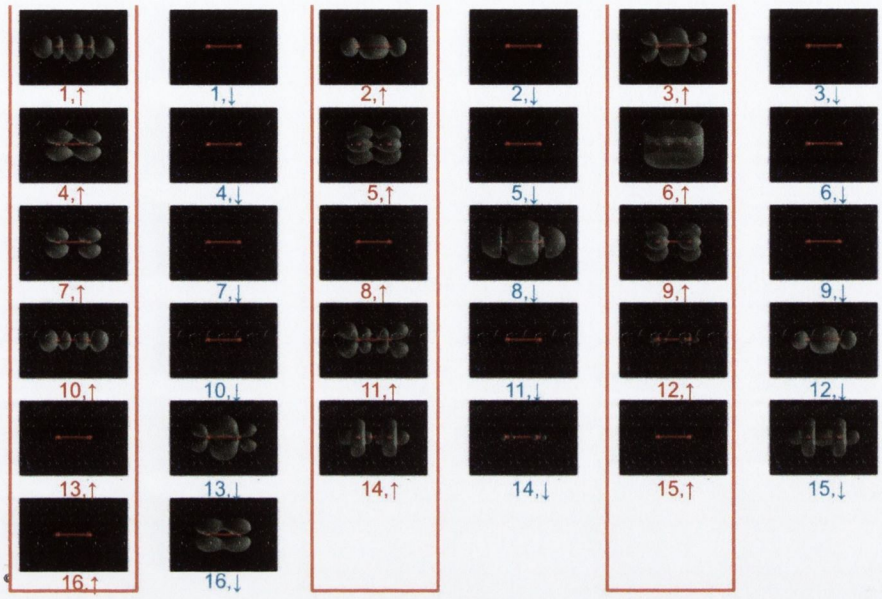
with R being free parameter. Here $\mathbf{B}(t)$ defines the external applied magnetic field, $\mathbf{E}(t)$ the external electric field and $\hat{V}$ is the sum of the internal ionic potentials

$$\hat{V} = \sum_{\mathrm{I}} \sum_{l} \sum_{m=-l}^{l} \bar{V}_{\mathrm{I},l} \, |I, l, m\rangle \langle I, l, m| \, . \tag{6.104}$$

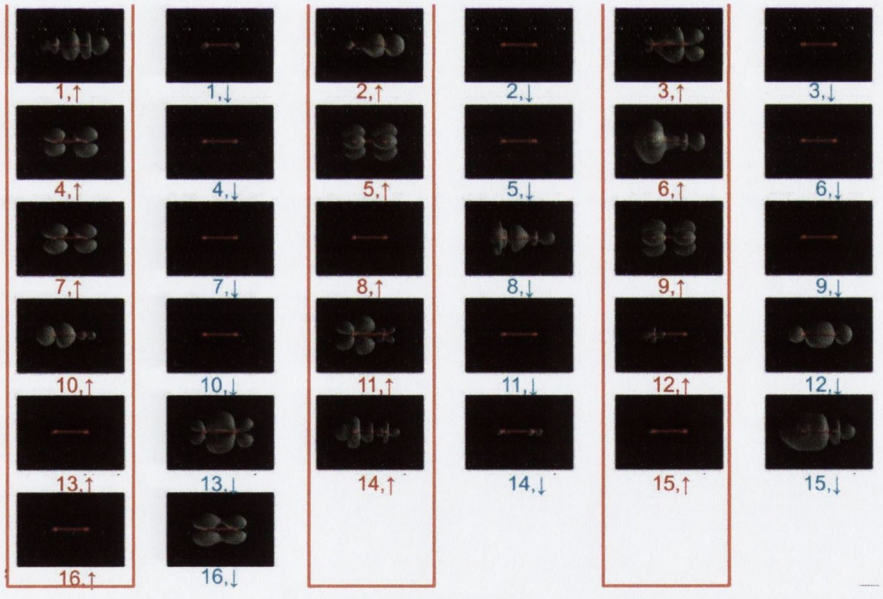
The wave function solution of the time-dependent Schrödinger equation

$$i \frac{d}{dt} |\Psi(t)\rangle = \hat{H}(t) \, |\Psi(t)\rangle \, , \tag{6.105}$$

with $\hbar = 1$, will be expanded over a set of eigenstates of $\hat{L}_z$ and $\hat{S}_z$. The basis set is thus given by $\{|l, l_z, s_z\rangle\}$, where the spherical harmonics, eigenfunctions of $\hat{L}_z$ are not centered on a particular site, but defined with respect to the origin of

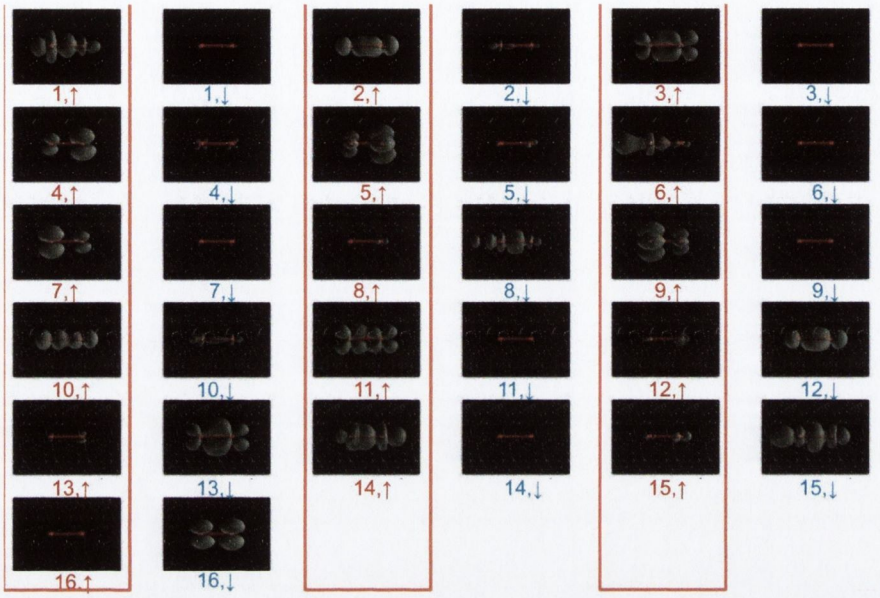


(A) $t = 0$ fs.

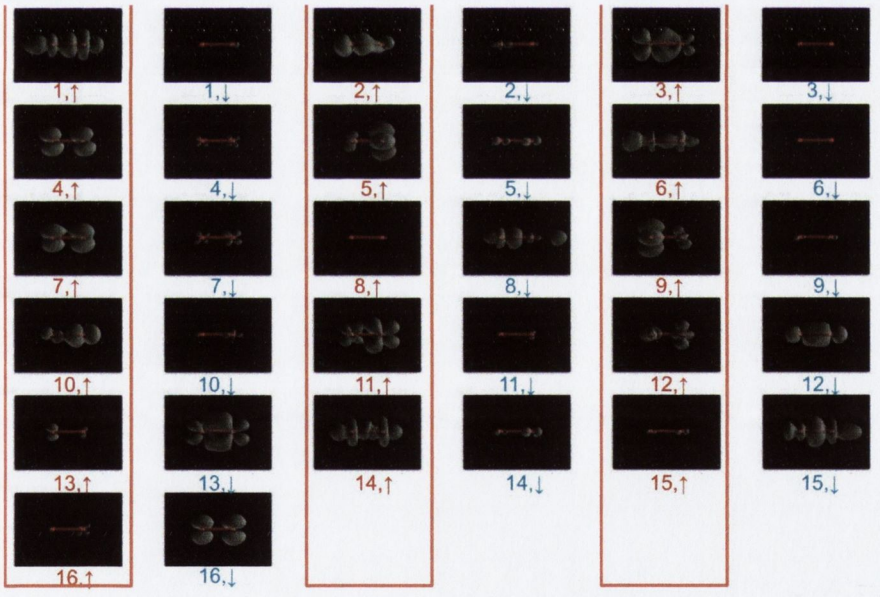


(B) $t = 4$ fs.

FIGURE 6.4: Collection of the 16 different Kohn-Sham states up and down for the Fe_2 cluster at $t = 0$ and after 4 fs. Certain states like $1\uparrow$ and $2\uparrow$ are delocalized and have the tendency to oscillate between the two atomic sites during the evolution.



(A) $t = 9$ fs.



(B) $t = 18$ fs.

FIGURE 6.5: Collection of the 16 different Kohn-Sham states up and down for the Fe_2 cluster at $t = 9$ fs and $t = 18$ fs. Certain states like $1\uparrow$ and $2\uparrow$ are delocalized and have the tendency to oscillate between the two atomic sites during the evolution.

the reference system. This means that the elements of the basis set $\{|l, l_z, s_z\rangle\}$ are, in general, not orthogonal to the spherical harmonics $\{|I, l, m\rangle\}$ centered on the atomic site I.

By projecting the Schrödinger equation over such basis set we obtain the following matrix equation

$$i\frac{d}{dt}\langle l, l_z, s_z|\Psi(t)\rangle = \sum_{l', l'_z, s'_z} \langle l, l_z, s_z|\hat{H}(t)|l', l'_z, s'_z\rangle \langle l', l'_z, s'_z|\Psi(t)\rangle . \tag{6.106}$$

The matrix elements of the Hamiltonian operator may be expressed as

$$\begin{aligned}\langle l, l_z, s_z|\hat{H}(t)|l', l'_z, s'_z\rangle = &-\frac{l(l+1)}{2R^2}\delta_{l,l'}\delta_{l_z,l'_z}\delta_{s_z,s'_z} + \lambda\langle l, l_z, s_z|\hat{\mathbf{L}}\cdot\hat{\mathbf{S}}|l', l'_z, s'_z\rangle + \\ &+ \mathbf{B}(t)\cdot\langle l, l_z, s_z|\hat{\mathbf{S}}|l', l'_z, s'_z\rangle + \mathbf{E}(t)\cdot\langle l, l_z, s_z|\hat{\mathbf{D}}|l', l'_z, s'_z\rangle + \\ &+ \langle l, l_z, s_z|\hat{V}|l', l'_z, s'_z\rangle ,\end{aligned} \tag{6.107}$$

where we need to consider the different matrix elements separately. For the spin orbit coupling we have the following result

$$\langle l, l_z, s_z|\hat{\mathbf{L}}\cdot\hat{\mathbf{S}}|l', l'_z, s'_z\rangle = C_1^{\mathrm{SO}} + C_2^{\mathrm{SO}} + C_3^{\mathrm{SO}}, \tag{6.108}$$

with

$$\begin{aligned}C_1^{\mathrm{SO}} &= \frac{1}{2}\sqrt{\left(\frac{3}{4} - s'_z - s'^2_z\right)\cdot(l(l+1) + l'_z - l'^2_z)}\delta(l_z - l'_z + 1)\delta(s_z - s'_z - 1)\delta_{l,l'},\\ C_2^{\mathrm{SO}} &= \frac{1}{2}\sqrt{\left(\frac{3}{4} + s'_z - s'^2_z\right)\cdot(l(l+1) - l'_z - l'^2_z)}\delta(l_z - l'_z - 1)\delta(s_z - s'_z + 1)\delta_{l,l'},\\ C_3^{\mathrm{SO}} &= l'_z s'_z\delta(l_z - l'_z)\delta(s_z - s'_z)\delta_{l,l'}.\end{aligned}$$

For the Zeeman coupling term we have instead

$$\mathbf{B}(t)\cdot\langle l, l_z, s_z|\hat{\mathbf{S}}|l', l'_z, s'_z\rangle = C_1^{\mathrm{Z}} + C_2^{\mathrm{Z}} + C_3^{\mathrm{Z}}, \tag{6.109}$$

where

$$\begin{aligned}C_1^{\mathrm{Z}} &= \frac{1}{2}\sqrt{\left(\frac{1}{2} - s'_z\right)\cdot\left(\frac{1}{2} + s'_z + 1\right)}\delta(s_z - s'_z - 1)\delta(l_z - l'_z)\delta_{l,l'}B_-(t),\\ C_2^{\mathrm{Z}} &= \frac{1}{2}\sqrt{\left(\frac{1}{2} + s'_z\right)\cdot\left(\frac{1}{2} - s'_z + 1\right)}\delta(s_z - s'_z + 1)\delta(l_z - l'_z)\delta_{l,l'}B_+(t),\\ C_3^{\mathrm{Z}} &= s'_z\delta(s_z - s'_z)\delta(l_z - l'_z)\delta_{l,l'}B_z(t).\end{aligned}$$

Here, in order to simplify the notation, we have introduced $B_\pm(t) = B_x(t) \pm iB_y(t)$. The last two terms representing respectively the dipole coupling with the external electric field and the scattering of the wave function to the localized ionic potentials are more involved. The computation of the matrix elements of the dipole operator $\hat{\mathbf{D}}$ requires the use of the Wigner-Eckart theorem (see Ref. [183]

Chapter 2).

According to this theorem, the matrix elements of a spherical tensor operator of rank k, $\hat{T}^{(k)}$, can be computed over the basis of the spherical harmonics through the following general relation

$$\langle \alpha', j', m' | \hat{T}^{(k)}_q | \alpha, j, m \rangle = \langle j, k; m, q | j, k; j', m' \rangle \frac{\langle \alpha', j' \| T^{(k)} \| \alpha, j \rangle}{\sqrt{2j+1}}, \tag{6.110}$$

where α and α' represent two set of quantum numbers not related to the rotational properties of the tensor, $\langle \alpha', j' \| T^{(k)} \| \alpha, j \rangle$ is known as the reduced tensor matrix element and it is independent from the set of magnetic quantum numbers m, m' and q. In our case this object will represent only a multiplicative coefficient that defines the dipole strength and the coupling with the external electric field $\mathbf{E}(t)$.

The term $\langle j, k; m, q | j, k; j', m' \rangle$ on the right hand side of the expression implies the following two selection rules $m' = m + q$ and $|j - k| \leq j'$, due to the Glebsch-Gordan coefficients (see Ref. [183], Chapter 3). In our case the three components of the rank 1 spherical tensor are

$$\hat{T}^{(1)}_1 = -\frac{1}{\sqrt{2}}(\hat{x} + i\hat{y}), \tag{6.111}$$

$$\hat{T}^{(1)}_{-1} = \frac{1}{\sqrt{2}}(\hat{x} - i\hat{y}), \tag{6.112}$$

$$\hat{T}^{(1)}_0 = \hat{z}. \tag{6.113}$$

From this the matrix elements for the position operators it follows straightforwardly

$$\begin{aligned} &\langle l, l_z, s_z | \hat{x} | l', l'_z, s'_z \rangle = \\ &= \frac{\langle l \| \hat{T}^{(1)} \| l' \rangle}{\sqrt{2(2l'+1)}} [- \langle l', 1; l'_z, 1 | l', 1; l, l_z \rangle + \langle l', 1; l'_z, -1 | l', 1; l, l_z \rangle] \delta_{s_z, s'_z}, \end{aligned} \tag{6.114}$$

$$\begin{aligned} &\langle l, l_z, s_z | \hat{y} | l', l'_z, s'_z \rangle = \\ &= i \frac{\langle l \| \hat{T}^{(1)} \| l' \rangle}{\sqrt{2(2l'+1)}} [\langle l', 1; l'_z, 1 | l', 1; l, l_z \rangle + \langle l', 1; l'_z, -1 | l', 1; l, l_z \rangle] \delta_{s_z, s'_z}, \end{aligned} \tag{6.115}$$

$$\langle l, l_z, s_z | \hat{z} | l', l'_z, s'_z \rangle = \frac{\langle l \| \hat{T}^{(1)} \| l' \rangle}{\sqrt{2l'+1}} \langle l', 1; l'_z, 0 | l', 1; l, l_z \rangle \delta_{s_z, s'_z}. \tag{6.116}$$

By assuming unitary electronic charge $e = 1$, and the reduced matrix element $\langle l \| \hat{T}^{(1)} \| l' \rangle = 1$, the expressions (6.114), (6.115) and (6.116) may be immediately used into the matrix element of the electric dipole operator to give

$$\mathbf{E}(t) \cdot \langle l, l_z, s_z | \hat{\mathbf{D}} | l', l'_z, s'_z \rangle = C^{\mathrm{D}}_1 + C^{\mathrm{D}}_2 + C^{\mathrm{D}}_3, \tag{6.117}$$

where

$$
\begin{aligned}
C_1^{\mathrm{D}} &= E_x(t)\left[\frac{-\langle l',1;l'_z,1|l',1;l,l_z\rangle}{\sqrt{2(2l'+1)}}+\frac{\langle l',1;l'_z,-1|l',1;l,l_z\rangle}{\sqrt{2(2l'+1)}}\right]\delta_{s_z,s'_z},\\
C_2^{\mathrm{D}} &= iE_y(t)\left[\frac{\langle l',1;l'_z,1|l',1;l,l_z\rangle}{\sqrt{2(2l'+1)}}+\frac{\langle l',1;l'_z,-1|l',1;l,l_z\rangle}{\sqrt{2(2l'+1)}}\right]\delta_{s_z,s'_z},\\
C_3^{\mathrm{D}} &= E_z(t)\frac{\langle l',1;l'_z,0|l',1;l,l_z\rangle}{\sqrt{2l'+1}}\delta_{s_z,s'_z}.
\end{aligned}
\tag{6.118}
$$

Finally we define the matrix elements of the ionic potential $\hat{V}$. By making use of the definition of Eq. (6.104) we have

$$
\langle l,l_z,s_z|\hat{V}|l',l'_z,s'_z\rangle=\sum_{\mathrm{I}}\sum_{L}\sum_{M=-L}^{L}\bar{V}_{\mathrm{I,L}}\,\langle l,l_z|I,L,M\rangle\,\langle I,L,M|l',l'_z\rangle\,, \tag{6.119}
$$

and the problem is reduced to the computation of the set of matrix elements $\langle l,l_z|I,L,M\rangle$ among different spherical harmonics. By expanding over the solid angle we can write

$$
\langle l,l_z|I,L,M\rangle=\int_{\Omega}d\Omega\,\langle l,l_z|\theta,\phi\rangle\,\langle\theta,\phi|I,L,M\rangle\,. \tag{6.120}
$$

According to Fig. 6.7 we see that the spherical harmonics centered at the origin and at $\mathbf{R}_{\mathrm{I}}$ will not associate to a generic point P the same pair of angles (θ,ϕ). From this observation the equation (6.120) may be rewritten as

$$
\langle l,l_z|I,L,M\rangle=\int_{\Omega}d\Omega\Upsilon^{l}_{l_z}(\theta,\phi)^{*}\Upsilon^{L}_{M}(\theta',\phi'), \tag{6.121}
$$

where $\Upsilon^{l}_{l_z}$ is the spherical harmonics corresponding to the orbital state $|l,l_z\rangle$. The integral in Eq. (6.121) may be then computed by making use of the so-called Slater-Koster rules for the calculation of the overlap integrals between orbitals localized over different atomic sites in the tight-binding formalism [184,185]. In practice, at a fixed distance $\mathbf{d}$ between the two atomic centers, it can be shown that only 10 Slater-Koster integrals (in the case of s, p and d states) labeled $dd\sigma$, $dd\pi$, $dd\delta$, $pd\sigma$, $pd\pi$, $pp\sigma$, $pp\pi$, $sd\sigma$, $sd\pi$ and $ss\sigma$ are needed in order to obtain all the other matrix elements. The symbols σ, π and δ refer to the angular momentum projected along the bond axis. Starting from the knowledge of these 10 fundamental integrals and from the orientation of the bond axis all the other integrals may be obtained through the set of exact Slater-Koster transformations (see Fig. 6.6).

$$
S_{\mu\nu}(\mathbf{d})=\int \mathrm{d}^3r\,\phi_{\mu}(\mathbf{r})^{*}\phi_{\nu}(\mathbf{r}+\mathbf{d}). \tag{6.122}
$$

TABLE I. Energy integrals for crystal in terms of two-center integrals.

$E_{s,s}$	$(ss\sigma)$
$E_{s,x}$	$l(sp\sigma)$
$E_{x,x}$	$l^2(pp\sigma)+(1-l^2)(pp\pi)$
$E_{x,y}$	$lm(pp\sigma)-lm(pp\pi)$
$E_{x,z}$	$ln(pp\sigma)-ln(pp\pi)$
$E_{s,xy}$	$\sqrt{3}lm(sd\sigma)$
E_{s,x^2-y^2}	$\frac{1}{2}\sqrt{3}(l^2-m^2)(sd\sigma)$
$E_{s,3z^2-r^2}$	$[n^2-\frac{1}{2}(l^2+m^2)](sd\sigma)$
$E_{x,xy}$	$\sqrt{3}l^2m(pd\sigma)+m(1-2l^2)(pd\pi)$
$E_{x,yz}$	$\sqrt{3}lmn(pd\sigma)-2lmn(pd\pi)$
$E_{x,xz}$	$\sqrt{3}l^2n(pd\sigma)+n(1-2l^2)(pd\pi)$
E_{x,x^2-y^2}	$\frac{1}{2}\sqrt{3}l(l^2-m^2)(pd\sigma)+l(1-l^2+m^2)(pd\pi)$
E_{y,x^2-y^2}	$\frac{1}{2}\sqrt{3}m(l^2-m^2)(pd\sigma)-m(1+l^2-m^2)(pd\pi)$
E_{z,x^2-y^2}	$\frac{1}{2}\sqrt{3}n(l^2-m^2)(pd\sigma)-n(l^2-m^2)(pd\pi)$
$E_{x,3z^2-r^2}$	$l[n^2-\frac{1}{2}(l^2+m^2)](pd\sigma)-\sqrt{3}ln^2(pd\pi)$
$E_{y,3z^2-r^2}$	$m[n^2-\frac{1}{2}(l^2+m^2)](pd\sigma)-\sqrt{3}mn^2(pd\pi)$
$E_{z,3z^2-r^2}$	$n[n^2-\frac{1}{2}(l^2+m^2)](pd\sigma)+\sqrt{3}n(l^2+m^2)(pd\pi)$
$E_{xy,xy}$	$3l^2m^2(dd\sigma)+(l^2+m^2-4l^2m^2)(dd\pi)+(n^2+l^2m^2)(dd\delta)$
$E_{xy,yz}$	$3lm^2n(dd\sigma)+ln(1-4m^2)(dd\pi)+ln(m^2-1)(dd\delta)$
$E_{xy,xz}$	$3l^2mn(dd\sigma)+mn(1-4l^2)(dd\pi)+mn(l^2-1)(dd\delta)$
E_{xy,x^2-y^2}	$\frac{3}{2}lm(l^2-m^2)(dd\sigma)+2lm(m^2-l^2)(dd\pi)+\frac{1}{2}lm(l^2-m^2)(dd\delta)$
E_{yz,x^2-y^2}	$\frac{3}{2}mn(l^2-m^2)(dd\sigma)-mn[1+2(l^2-m^2)](dd\pi)+mn[1+\frac{1}{2}(l^2-m^2)](dd\delta)$
E_{xz,x^2-y^2}	$\frac{3}{2}nl(l^2-m^2)(dd\sigma)+nl[1-2(l^2-m^2)](dd\pi)-nl[1-\frac{1}{2}(l^2-m^2)](dd\delta)$
$E_{xy,3z^2-r^2}$	$\sqrt{3}lm[n^2-\frac{1}{2}(l^2+m^2)](dd\sigma)-2\sqrt{3}lmn^2(dd\pi)+\frac{1}{2}\sqrt{3}lm(1+n^2)(dd\delta)$
$E_{yz,3z^2-r^2}$	$\sqrt{3}mn[n^2-\frac{1}{2}(l^2+m^2)](dd\sigma)+\sqrt{3}mn(l^2+m^2-n^2)(dd\pi)-\frac{1}{2}\sqrt{3}mn(l^2+m^2)(dd\delta)$
$E_{xz,3z^2-r^2}$	$\sqrt{3}ln[n^2-\frac{1}{2}(l^2+m^2)](dd\sigma)+\sqrt{3}ln(l^2+m^2-n^2)(dd\pi)-\frac{1}{2}\sqrt{3}ln(l^2+m^2)(dd\delta)$
$E_{x^2-y^2,x^2-y^2}$	$\frac{1}{4}(l^2-m^2)^2(dd\sigma)+[l^2+m^2-(l^2-m^2)^2](dd\pi)+[n^2+\frac{1}{4}(l^2-m^2)^2](dd\delta)$
$E_{x^2-y^2,3z^2-r^2}$	$\frac{1}{4}\sqrt{3}(l^2-m^2)[n^2-\frac{1}{2}(l^2+m^2)](dd\sigma)+\sqrt{3}n^2(m^2-l^2)(dd\pi)+\frac{1}{4}\sqrt{3}(1+n^2)(l^2-m^2)(dd\delta)$
$E_{3z^2-r^2,3z^2-r^2}$	$[n^2-\frac{1}{2}(l^2+m^2)]^2(dd\sigma)+3n^2(l^2+m^2)(dd\pi)+\frac{3}{4}(l^2+m^2)^2(dd\delta)$

FIGURE 6.6: Table of Slater-Koster transformations for s, p and d orbitals, with $l = d_x/|\mathbf{d}|$, $m = d_y/|\mathbf{d}|$ and $n = d_z/|\mathbf{d}|$. Here $\mathbf{d}$ is the vector distance between the two atomic centers, $(ss\sigma)$ is the irreducible integral between the s orbitals of the two sites with σ indicating the value of m_l along the bond axis (from Ref. [185]).

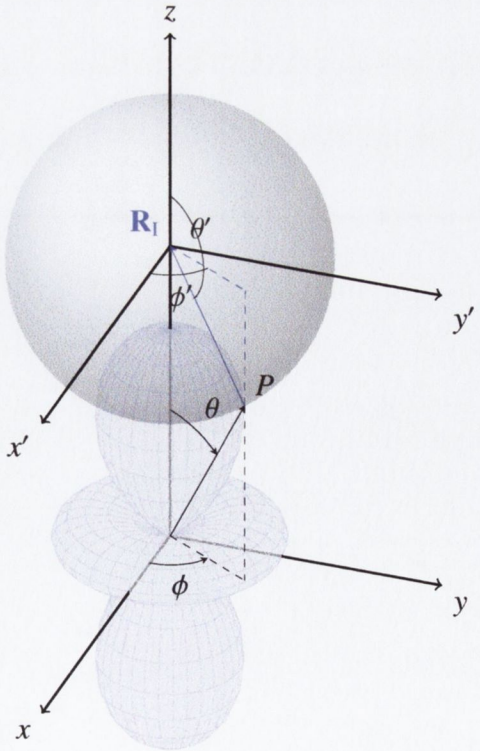


FIGURE 6.7: Graphical representation of one of the integrals in Eq. (6.120), with $|I, L, M\rangle$ s type orbital and $|l, l_z\rangle$ corresponding to a Υ_0^2 spherical harmonics.

6.4 The role of the ionic potential scattering in the ultrafast dynamics of the orbital moment

In this section we solve the model previously defined paying particular attention to the effect of the ionic potential $\hat{V}$ on the orbital moment dynamics. In order to

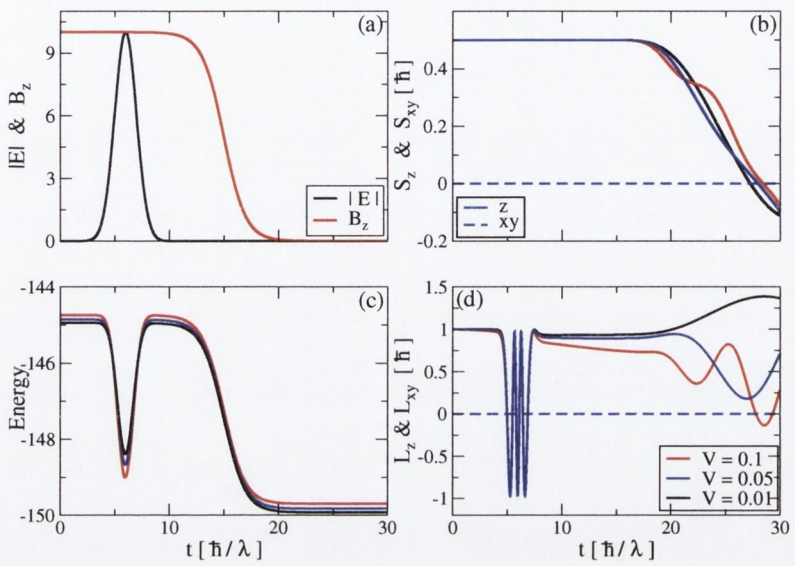


FIGURE 6.8: Dynamical evolution of the model with Hamiltonian $\hat{H}(t)$ (from Eq. 6.103) and initial quantum state $|\Psi(0)\rangle = |l = 2, l_z = 1, s_z = 0.5\rangle$. (a) Amplitude of the external electric field $\mathbf{E}(t)$ and magnetic field $B_z(t)$ directed along z; (b) Evolution of the collinear $S_z(t)$ and non-collinear $S_{xy}(t)$ component of the spin vector under different ionic potentials $\hat{V}$; (c) Evolution of the total energy $E(t) = \langle \hat{H}(t) \rangle$ under different potentials $\hat{V}$; (d) Evolution of the collinear $L_z(t)$ and non-collinear component of the orbital moment $L_{xy}(t)$.

understand this effect we evolve a quantum state $|\Psi(t)\rangle$ under the Hamiltonian of Eq. (6.103), with external electric and magnetic fields represented in Fig. 6.8(a). The electric field employed in the dynamical evolution is $\mathbf{E}(t) = \frac{|\mathbf{E}(t)|}{\sqrt{2}}\mathbf{e}_1 + \frac{|\mathbf{E}(t)|}{\sqrt{2}}\mathbf{e}_2$ (black curve), while the magnetic field has only z component along the quantization axis. Here $\mathbf{e}_1$ and $\mathbf{e}_2$ are the unit vectors along x and y respectively.

In panel (c) of Fig. 6.8, instead, we plot the time-dependent energy function of the system $E(t) = \langle \hat{H}(t) \rangle$ in three cases characterized by different ionic potentials $\hat{V}$ [see Eq. (6.104)]. In the simulations we use two indistinguishable scattering centers with potential amplitude V for every orbital channel l and every atomic site. In this way we can rewrite $\hat{V}$ as

$$\hat{V} = V \sum_{\mathbf{R}_I} \sum_{L} \sum_{M=-L}^{L} |I, L, M\rangle \langle I, L, M| . \tag{6.123}$$

The black, the blue and the red lines in Fig. 6.8(b, c, d) refer to different value of the multiplicative factor V. The energy expectation value shows in these three cases the same behaviour during the evolution with the curves being only shifted due to the different values of the amplitude V.

In Fig. 6.8(b) we plot, instead, the time-dependent expectation value of the spin operator $\langle \hat{S}_z(t) \rangle$ with different values of V. In all three cases after the application of the external magnetic field $B_z(t)$ the spin expectation value collapses with the value of the non-collinear component $\langle \hat{S}_{xy}(t) \rangle$ remaining exactly constant during the temporal evolution. The application of different potential operators $\hat{V}$ does not contribute with a clear trend to the spin dynamics that is only slightly affected during the application of the external magnetic pulse.

We already know that the spin transfer into the spin down component, shown in panel (c) of Fig. 6.8, is due to the spin-orbit coupling term. However, when we look to panel (d) of the same figure we observe that the $\langle \hat{L}_z \rangle$ component of the orbital moment grows concurrently with the spin loss only in the case of the smallest potential amplitude $V = 0.01$. In the other two cases the transfer is not so evident and the growth in the orbital moment component following the spin decay is hidden by a second contribution to the motion of the orbital moment due to the scattering potential $\hat{V}$. The $\langle \hat{L}_z \rangle$ evolution is due to a combination of two types of oscillation with different amplitudes and frequency. The scattering with the potential $\hat{V}$ mixes the initial state $|\Psi(0)\rangle$ with the $l_z = -1$ state, while the frequency of the oscillations are directly proportional to the amplitude V of the scalar potential.

In Fig. 6.9 we repeat the same calculations, but for a different set of ionic potentials. The potentials employed in this case have higher amplitudes, while the Hamiltonian is perturbed with the same type of external fields $\mathbf{E}(t)$ and $B_z(t)$. The results in panel (b) show a much clearer trend in the spin decay after the application of the field $B_z(t)$ with respect to that observed in Fig. 6.8(b). Higher is the value of the potential V used in the Hamiltonian (6.103) and higher is the loss observed in the z component of the spin vector, $\langle \hat{S}_z \rangle$, suggesting a similar law to that derived in Chapter 4 which related the spin decay rate with the spin-orbit coefficient λ.

In Fig. 6.9(d), after the strong dynamics induced by the application of the external electric field $\mathbf{E}(t)$, the frequency of the oscillations of the $\langle \hat{L}_z \rangle$ expectation value is directly proportional to the amplitude V of the potential. At the same time we clearly see that after the application of the external magnetic field, $B_z(t)$, the dynamics of $\langle \hat{L}_z \rangle$ is influenced by a second type of higher frequency oscillations that interfere with the ones driven by the scattering with the potential $\hat{V}$. These second oscillations are connected to the action of the spin-orbit coupling and their interference with the higher amplitude oscillations generate an orbital moment dynamics that is closely related to that observed in Chapter 4 for the Fe_2 cluster.

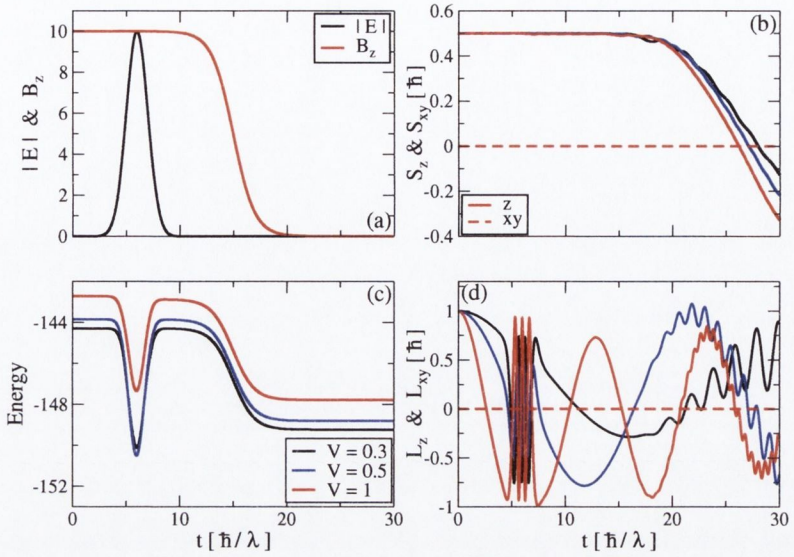


FIGURE 6.9: Dynamical evolution of the model with Hamiltonian $\hat{H}(t)$ (from Eq. 6.103) and initial quantum state $|\Psi(0)\rangle = |l = 2, l_z = 1, s_z = 0.5\rangle$. (a) Amplitude of the external electric field $\mathbf{E}(t)$ and magnetic field $B_z(t)$ directed along z; (b) Evolution of the collinear $S_z(t)$ and non-collinear $S_{xy}(t)$ component of the spin vector under different ionic potentials $\hat{V}$; (c) Evolution of the total energy $E(t) = \langle \hat{H}(t) \rangle$ under different potentials $\hat{V}$; (d) Evolution of the collinear $L_z(t)$ and non-collinear component of the orbital moment $L_{xy}(t)$.

In conclusion, the dynamics of the global angular momentum of the system that corresponds, in good approximation, to the center of mass component, is driven, after the application of the laser pulse, by the scattering with the ionic potential. This effect is much stronger with respect to the effect due to the spin-orbit coupling. The consequence is that the total angular momentum of the system, $J_z = L_z + S_z$, as a cause of the effective torque generated by the atomic nuclei on the electronic orbital moment, is not conserved dynamically.

6.5 The role of the orbital currents in the spin loss process

Until now we have discussed only the effect of the ionic scalar potential on the orbital moment dynamics, and how this effect, together with the spin-orbit coupling, can explain the global orbital moment dynamics observed in Fe clusters.

We have also observed (see Fig. 6.8 and Fig. 6.9) that the scattering with the ionic potential alone does not produce non-collinearity in both the orbital moment and in the spin vector. At the same time by looking at Fig. 6.2 it is clear that, while the amount of orbital moment non-collinearity around the atomic sites is

approximately zero in the ground-state configuration, after the application of the laser pulse it remains zero in correspondence of the in-plane atoms, while it grows for the out-of-plane atoms (in the case of x-polarized field).

From the results of Chapter 5 we also learned that the degree of spin loss and the amount of spin non-collinearity is considerably higher in correspondence of the out-of-plane atoms. Spin and orbital moment are coupled through the spin-orbit interaction, so, a dynamical modification of the orbital moment driven by the application of the laser pulse should affect also the dynamics of the spin vector. The aim of this section is to understand the mechanism through which such an effect takes place.

We start from the continuity equation for the internal component of the orbital moment (6.99). During the action of the laser the electric dipole term will be the most important source of orbital moment variation. Moreover, from the fact that in these simulations the electric field polarization direction is assumed to be along x we can write

$$\rho(\mathbf{r},t)[\Delta\mathbf{r}\times q\mathbf{E}(t)] = \rho(\mathbf{r},t)\Delta z E_x(t)\mathbf{e}_2 - \rho(\mathbf{r},t)\Delta y E_x(t)\mathbf{e}_3, \tag{6.124}$$

with $\mathbf{e}_3$ being the unit vector along z. The center of mass of the system is approximately located at the center of the cluster, so that in correspondence of the out-of-plane atoms 5 and 6 we have $\Delta z \gg \Delta y$ and we can neglect the second term on the right hand side with the result

$$\rho(\mathbf{r},t)[\Delta\mathbf{r}\times q\mathbf{E}(t)] = \rho(\mathbf{r},t)\Delta z E_x(t)\mathbf{e}_2. \tag{6.125}$$

This means that during the application of the laser the internal orbital moment in correspondence of the apex atoms will mainly acquire a contribution along the y direction. This is clear also from Fig. 6.2 where in panels (c) and (d) the non collinear component of the orbital moment ΔL_{xy} for the apex atoms is explicitly shown together with the component ΔL_z. However, what is not clear from the previous discussion is the origin of the growth of the ΔL_x component after the application of the laser pulse, that in principle cannot act on this particular component of the orbital moment. In order to understand this feature of the dynamics we need to look in more detail at the continuity equation (6.99) and in particular at the first term on the right-hand side describing the orbital currents flux within the system. Analogously to what we have done in Chapter 5 for the spin current we obtain, by making use of the following definition[1]

$$\mathbf{l}^{\mathrm{KS}}(\mathbf{r},t) = \frac{\sum_{j\in\mathrm{occ.}} \psi_j^{\mathrm{KS}\dagger}\hat{\mathbf{L}}\psi_j^{\mathrm{KS}}}{2n(\mathbf{r},t)} + \mathrm{c.c}, \tag{6.126}$$

[1]The term $\psi^\dagger\hat{\mathbf{L}}\psi$ is complex. Its real part is $m\mathbf{r}\times\mathrm{Re}(\psi^\dagger(-i\hbar\nabla\psi))/m = m\mathbf{r}\times\mathbf{j}(\mathbf{r},t)$ where we have used the standard definition of the probability current $\mathbf{j}(\mathbf{r},t) = \mathrm{Re}(\psi^\dagger(-i\hbar\nabla\psi))/m$.

where c.c means that we are taking the complex conjugate of the expression on the right-hand side. We can now evaluate the following product

$$l_i^{\mathrm{KS}} \cdot \nabla l_k^{\mathrm{KS}} = \frac{l_i^{\mathrm{KS}}}{2n} \sum_{j\in \mathrm{occ.}} \nabla \psi_j^{\mathrm{KS}\dagger} (\mathbf{r} \times (-i\hbar \nabla \psi_j^{\mathrm{KS}}))_k + \frac{l_i^{\mathrm{KS}}}{2n} \sum_{j\in \mathrm{occ.}} \psi_j^{\mathrm{KS}\dagger} \nabla (\mathbf{r} \times (-i\hbar \nabla \psi_j^{\mathrm{KS}}))_k -$$
$$- \frac{\nabla n}{n(\mathbf{r},t)} l_i^{\mathrm{KS}} \cdot l_k^{\mathrm{KS}} + \mathrm{c.c}, \tag{6.127}$$

where ψ_j^{KS} indicates the single-particle j-th Kohn-Sham state. We need now to modify the first and the second term on the right-hand side of Eq. (6.127). For the first one we find

$$\frac{l_i^{\mathrm{KS}}}{2n(\mathbf{r},t)} \sum_{j\in \mathrm{occ.}} \nabla \psi_j^{\mathrm{KS}\dagger} (\mathbf{r} \times (-i\hbar \nabla \psi_j^{\mathrm{KS}}))_k =$$
$$= \frac{1}{4n^2} \sum_{j,r\in \mathrm{occ.}} \sum_{\alpha,\alpha',\beta,\beta'} \nabla \psi_{j\alpha}^{\mathrm{KS}*} \psi_{r\beta}^{\mathrm{KS}*} L^i_{\beta,\beta'} \psi_{r,\beta'}^{\mathrm{KS}} L^k_{\alpha,\alpha'} \psi_{j\alpha'}^{\mathrm{KS}} + \mathrm{c.c.}, \tag{6.128}$$

we can subtract to Eq. (6.128) the same expression obtained by inverting the indices i and k. We then obtain

$$\frac{l_i^{\mathrm{KS}}}{2n} \sum_{j\in \mathrm{occ.}} \nabla \psi_j^{\mathrm{KS}\dagger} (\mathbf{r} \times (-i\hbar \nabla \psi_j^{\mathrm{KS}}))_k - (i \leftrightarrow k) =$$
$$= \sum_{j,r\in \mathrm{occ.}} \sum_{\alpha,\alpha',\beta,\beta'} \frac{\nabla \psi_{j,\alpha}^{\mathrm{KS}*} \psi_{r,\beta}^{\mathrm{KS}*} L^{[i,}_{\beta,\beta'} L^{k]}_{\alpha,\alpha'} \psi_{r\beta'}^{\mathrm{KS}} \psi_{j\alpha'}^{\mathrm{KS}}}{4n^2} + \mathrm{c.c.}. \tag{6.129}$$

Given the fact that the orbital moment operators obey to the same Lie algebra of the spin operators we can use the relation

$$L^{[i,}_{\beta,\beta'} L^{k]}_{\alpha,\alpha'} = i \sum_s \epsilon_{iks} [L^s_{\beta\alpha'} \delta_{\alpha,\beta'} - \delta_{\beta,\alpha'} L^s_{\alpha\beta'}], \tag{6.130}$$

so that Eq. (6.129) becomes

$$\frac{l_i^{\mathrm{KS}}}{2n} \sum_{j\in \mathrm{occ.}} \nabla \psi_j^{\mathrm{KS}\dagger} (\mathbf{r} \times (-i\hbar \nabla \psi_j^{\mathrm{KS}}))_k - (i \leftrightarrow k) =$$
$$= \frac{i}{4n} \sum_{j,r\in \mathrm{occ.}} \sum_s \epsilon_{iks} \frac{\nabla \psi_j^{\mathrm{KS}\dagger} \psi_r^{\mathrm{KS}}}{n(\mathbf{r},t)} \psi_r^{\mathrm{KS}\dagger} \hat{L}^s \psi_j^{\mathrm{KS}} - \frac{i}{4n} \sum_{j,r\in \mathrm{occ.}} \sum_s \epsilon_{iks} \nabla \psi_j^{\mathrm{KS}\dagger} \hat{L}^s \psi_r^{\mathrm{KS}} \frac{\psi_r^{\mathrm{KS}\dagger} \psi_j^{\mathrm{KS}}}{n(\mathbf{r},t)} +$$
$$+ \mathrm{c.c.}. \tag{6.131}$$

We can now examine the second term on the right-hand side of Eq. (6.127)

$$\frac{l_i^{\mathrm{KS}}}{2n}\sum_{j\in\mathrm{occ.}}\psi_j^{\mathrm{KS}\dagger}\nabla_l(\mathbf{r}\times(-i\hbar\nabla\psi_j^{\mathrm{KS}}))_k = \\ = \frac{l_i^{\mathrm{KS}}}{2n}\sum_q\sum_j\epsilon_{klq}\psi_j^{\mathrm{KS}\dagger}(-i\hbar\nabla_q\psi_j^{\mathrm{KS}}) + \frac{l_i^{\mathrm{KS}}}{2n}\sum_{j\in\mathrm{occ.}}\psi_j^{\mathrm{KS}\dagger}\hat{L}_k\nabla_l\psi_j^{\mathrm{KS}}. \tag{6.132}$$

By proceeding as before we have then

$$\frac{l_i^{\mathrm{KS}}}{2n}\sum_{j\in\mathrm{occ.}}\psi_j^{\mathrm{KS}\dagger}\nabla_l(\mathbf{r}\times(-i\hbar\nabla\psi_j^{\mathrm{KS}}))_k - (i\leftrightarrow k) = \\ = \frac{l_i^{\mathrm{KS}}}{2n}\sum_{j\in\mathrm{occ.}}\sum_q\epsilon_{klq}\psi_j^{\mathrm{KS}\dagger}(-i\hbar\nabla_q\psi_j^{\mathrm{KS}}) - \frac{l_k^{\mathrm{KS}}}{2n}\sum_{j\in\mathrm{occ.}}\sum_q\epsilon_{ilq}\psi_j^{\mathrm{KS}\dagger}(-i\hbar\nabla_q\psi_j^{\mathrm{KS}}) + \\ + \frac{1}{4n^2}\left[\sum_{j,r\in\mathrm{occ.}}\sum_{\alpha,\beta,\alpha',\beta'}\psi_{r\alpha}^{\mathrm{KS}*}\psi_{j\alpha'}^{\mathrm{KS}*}L^{[i,}_{\alpha\beta}L^{k]}_{\alpha'\beta'}\psi_{r\beta}^{\mathrm{KS}}\nabla_l\psi_{j\beta'}^{\mathrm{KS}} + \mathrm{c.c.}\right]. \tag{6.133}$$

Considering only the last term on the right hand-side of Eq. (6.133) we find

$$\frac{1}{4n^2}\sum_{j,r\in\mathrm{occ.}}\sum_{\alpha,\beta,\alpha',\beta'}\psi_{r\alpha}^{\mathrm{KS}*}\psi_{j\alpha'}^{\mathrm{KS}*}L^{[i,}_{\alpha\beta}L^{k]}_{\alpha'\beta'}\psi_{r\beta}^{\mathrm{KS}}\nabla\psi_{j\beta'}^{\mathrm{KS}} = \\ = \frac{i}{4n^2}\sum_s\epsilon_{iks}\sum_{j,r\in\mathrm{occ.}}\psi_r^{\mathrm{KS}\dagger}\hat{L}^s\nabla\psi_j^{\mathrm{KS}}\psi_j^{\mathrm{KS}\dagger}\psi_r^{\mathrm{KS}} - \frac{i}{4n^2}\sum_s\epsilon_{iks}\sum_{j,r\in\mathrm{occ.}}\psi_j^{\mathrm{KS}\dagger}\hat{L}^s\psi_r^{\mathrm{KS}}\psi_r^{\mathrm{KS}\dagger}\nabla\psi_j^{\mathrm{KS}}. \tag{6.134}$$

and by substituting this into Eq. (6.133)

$$\frac{l_i^{\mathrm{KS}}}{2n}\sum_{j\in\mathrm{occ.}}\psi_j^{\mathrm{KS}\dagger}\nabla_l(\mathbf{r}\times(-i\hbar\nabla\psi_j^{\mathrm{KS}}))_k - (i\leftrightarrow k) = \\ = \frac{i}{4n}\sum_s\epsilon_{iks}\sum_{j,r\in\mathrm{occ.}}\left[\psi_r^{\mathrm{KS}\dagger}\hat{L}^s\nabla_l\psi_j^{\mathrm{KS}}\frac{\psi_j^{\mathrm{KS}\dagger}\psi_r^{\mathrm{KS}}}{n(\mathbf{r},t)} - \psi_j^{\mathrm{KS}\dagger}\hat{L}^s\psi_r^{\mathrm{KS}}\frac{\psi_r^{\mathrm{KS}\dagger}\nabla_l\psi_j^{\mathrm{KS}}}{n(\mathbf{r},t)} + \mathrm{c.c.}\right] + \\ + \frac{l_i^{\mathrm{KS}}}{2n}\sum_{j\in\mathrm{occ.}}\sum_q\epsilon_{klq}\psi_j^{\mathrm{KS}\dagger}(-i\hbar\nabla_q\psi_j^{\mathrm{KS}}) - \frac{l_k^{\mathrm{KS}}}{2n}\sum_{j\in\mathrm{occ.}}\sum_q\epsilon_{ilq}\psi_j^{\mathrm{KS}\dagger}(-i\hbar\nabla_q\psi_j^{\mathrm{KS}}). \tag{6.135}$$

By using Eq. (6.135) together with Eq. (6.131) we obtain

$$l_i^{\mathrm{KS}}\nabla_l l_k^{\mathrm{KS}} - l_k^{\mathrm{KS}}\nabla_l l_i^{\mathrm{KS}} = \frac{i}{4n}\sum_s \epsilon_{iks}\sum_{j,r\in\mathrm{occ.}} \psi_r^{\mathrm{KS}\dagger}\hat{L}^s\psi_j^{\mathrm{KS}}\left[\frac{\nabla_l\psi_j^{\mathrm{KS}\dagger}\psi_r^{\mathrm{KS}} - \psi_j^{\mathrm{KS}\dagger}\nabla_l\psi_r^{\mathrm{KS}}}{n(\mathbf{r},t)}\right] -$$
$$- \frac{i}{4n}\sum_s \epsilon_{iks}\sum_{j,r\in\mathrm{occ.}}\left[\nabla_l\psi_j^{\mathrm{KS}\dagger}\hat{L}^s\psi_r^{\mathrm{KS}}\frac{\psi_r^{\mathrm{KS}\dagger}\psi_j^{\mathrm{KS}}}{n(\mathbf{r},t)} - \psi_r^{\mathrm{KS}\dagger}\hat{L}^s\nabla_l\psi_j^{\mathrm{KS}}\frac{\psi_j^{\mathrm{KS}\dagger}\psi_r^{\mathrm{KS}}}{n(\mathbf{r},t)}\right]+$$
$$+ \frac{l_i^{\mathrm{KS}}}{2n}\sum_q \epsilon_{klq}\sum_{j\in\mathrm{occ.}}\psi_j^{\mathrm{KS}\dagger}(-i\hbar\nabla_q\psi_j^{\mathrm{KS}}) - \frac{l_k^{\mathrm{KS}}}{2n}\sum_q \epsilon_{ilq}\sum_{j\in\mathrm{occ.}}\psi_j^{\mathrm{KS}\dagger}(-i\hbar\nabla_q\psi_j^{\mathrm{KS}})+$$
$$+ \mathrm{c.c.}. \tag{6.136}$$

The previous expression after some rearrangements becomes

$$\sum_{ik}\epsilon_{ikn}[l_i^{\mathrm{KS}}\nabla_l l_k^{\mathrm{KS}} - l_k^{\mathrm{KS}}\nabla_l l_i^{\mathrm{KS}}] = i\sum_{j,r\in\mathrm{occ.}}\frac{\psi_r^{\mathrm{KS}\dagger}\hat{L}^n\psi_j^{\mathrm{KS}}}{2n(\mathbf{r},t)}\left[\frac{\nabla_l\psi_j^{\mathrm{KS}\dagger}\psi_r^{\mathrm{KS}} - \psi_j^{\mathrm{KS}\dagger}\nabla_l\psi_r^{\mathrm{KS}}}{n(\mathbf{r},t)}\right] -$$
$$- \frac{i}{2n(\mathbf{r},t)}\sum_{j,r\in\mathrm{occ.}}\left[\nabla_l\psi_j^{\mathrm{KS}\dagger}\hat{L}^n\psi_r^{\mathrm{KS}}\frac{\psi_r^{\mathrm{KS}\dagger}\psi_j^{\mathrm{KS}}}{n(\mathbf{r},t)} - \psi_r^{\mathrm{KS}\dagger}\hat{L}^n\nabla_l\psi_j^{\mathrm{KS}}\frac{\psi_j^{\mathrm{KS}\dagger}\psi_r^{\mathrm{KS}}}{n(\mathbf{r},t)}\right]-$$
$$- \frac{l_l^{\mathrm{KS}}}{n(\mathbf{r},t)}\sum_{j\in\mathrm{occ.}}\psi_j^{\mathrm{KS}\dagger}(-i\hbar\nabla_n\psi_j^{\mathrm{KS}}) + \sum_k\frac{l_k^{\mathrm{KS}}}{n(\mathbf{r},t)}\sum_{j\in\mathrm{occ.}}\psi_j^{\mathrm{KS}\dagger}(-i\hbar\nabla_k\psi_j^{\mathrm{KS}})\delta_{n,l}+$$
$$+ \mathrm{c.c.}. \tag{6.137}$$

As we have done in Chapter 5, we can introduce, in order to simplify the previous expression, the following velocity field

$$\mathbf{v}^{(j,r)}(\mathbf{r},t) = \frac{\hbar}{2mi}\frac{\psi_j^{\mathrm{KS}\dagger}\nabla\psi_r^{\mathrm{KS}} - \nabla\psi_j^{\mathrm{KS}\dagger}\psi_r}{\psi_j^{\mathrm{KS}\dagger}\psi_r^{\mathrm{KS}}}, \tag{6.138}$$

together with the term $\mathscr{F}_{jr} = \frac{\psi_j^{\mathrm{KS}\dagger}\psi_r^{\mathrm{KS}}}{n}$, already introduced in Chapter 5 and $\mathbf{L}^{(jr)}(\mathbf{r},t) = \psi_j^{\mathrm{KS}\dagger}\hat{\mathbf{L}}\psi_r^{\mathrm{KS}}$. Then Eq. (6.137) becomes

$$2(n\mathbf{l}^{\mathrm{KS}}\times\nabla_l\mathbf{l}^{\mathrm{KS}})_n = -l_l^{\mathrm{KS}}\sum_{j\in\mathrm{occ.}}\psi_j^{\mathrm{KS}\dagger}(-i\hbar\nabla_n\psi_j^{\mathrm{KS}}) + \delta_{nl}\sum_k l_k^{\mathrm{KS}}\sum_{j\in\mathrm{occ.}}\psi_j^{\mathrm{KS}\dagger}(-i\hbar\nabla_k\psi_j^{\mathrm{KS}})+$$
$$+ \frac{m}{\hbar}\sum_{j,r\in\mathrm{occ.}}\mathscr{F}_{jr}L_n^{(rj)}(\mathbf{r},t)v_l^{(jr)}(\mathbf{r},t) - \frac{i}{2}\sum_{j,r\in\mathrm{occ.}}\mathscr{F}_{jr}\left[\nabla_l\psi_j^{\mathrm{KS}\dagger}\hat{L}_n\psi_r^{\mathrm{KS}} - \psi_r^{\mathrm{KS}\dagger}\hat{L}_n\nabla_l\psi_j^{\mathrm{KS}}\right]+$$
$$+ \mathrm{c.c.}. \tag{6.139}$$

It is convenient now to separate the term on the right-hand side in a single-particle and a many-particle contribute (in order to simplify the expression $\tilde{\mathscr{F}} = \frac{\langle\psi_j^{\mathrm{KS}\dagger}\psi_j^{\mathrm{KS}}\rangle_j}{n(\mathbf{r},t)}$ is considered homogeneous, given that it is also small compared to the

other components)

$$\frac{\hbar}{m\bar{\mathscr{F}}}(n\mathbf{l}^{\mathrm{KS}}\times\nabla_l\mathbf{l}^{\mathrm{KS}})_n=-\frac{i\hbar}{2m}\sum_{j\in\mathrm{occ.}}\left[\nabla_l\psi_j^{\mathrm{KS}\dagger}\hat{L}_n\psi_j^{\mathrm{KS}}-\psi_j^{\mathrm{KS}\dagger}\hat{L}_n\nabla_l\psi_j^{\mathrm{KS}}\right]-$$
$$-\frac{\hbar l_l^{\mathrm{KS}}}{m\bar{\mathscr{F}}}\sum_{j\in\mathrm{occ.}}\mathrm{Re}\left[\psi_j^{\mathrm{KS}\dagger}(-i\hbar\nabla_n\psi_j^{\mathrm{KS}})\right]+\frac{\hbar}{m\bar{\mathscr{F}}}\sum_k l_k^{\mathrm{KS}}\sum_{j\in\mathrm{occ.}}\mathrm{Re}\left[\psi_j^{\mathrm{KS}\dagger}(-i\hbar\nabla_k\psi_j^{\mathrm{KS}})\right]\delta_{n,l}+$$
$$+\bar{\mathscr{F}}^{-1}\mathscr{P}_{ln}(\mathbf{r},t)+\sum_{j\in\mathrm{occ.}}\mathrm{Re}(L_j^n(\mathbf{r},t))v_j^l(\mathbf{r},t),\tag{6.140}$$

where the tensor $\mathscr{P}_{ln}(\mathbf{r},t)$ is defined as

$$\mathscr{P}_{ln}(\mathbf{r},t)=\sum_{j,r\in\mathrm{occ.}}\left[\mathscr{F}_{jr}L_n^{(rj)}(\mathbf{r},t)v_l^{(jr)}(\mathbf{r},t)-\frac{i\hbar\mathscr{F}_{jr}}{2m}\left(\nabla_l\psi_j^{\mathrm{KS}\dagger}\hat{L}_n\psi_r^{\mathrm{KS}}-\psi_r^{\mathrm{KS}\dagger}\hat{L}_n\nabla_l\psi_j^{\mathrm{KS}}\right)\right].\tag{6.141}$$

We can now express the orbital current term as follows

$$-\frac{i\hbar}{2m}\sum_{j\in\mathrm{occ.}}\left[\nabla_l\psi_j^{\mathrm{KS}\dagger}\hat{L}^n\psi_j^{\mathrm{KS}}-\psi_j^{\mathrm{KS}\dagger}\hat{L}^n\nabla_l\psi_j^{\mathrm{KS}}\right]=\frac{\hbar}{m\bar{\mathscr{F}}}(n\mathbf{l}^{\mathrm{KS}}\times\nabla_l\mathbf{l}^{\mathrm{KS}})_n+$$
$$+\frac{\hbar}{\bar{\mathscr{F}}}l_l^{\mathrm{KS}}(\mathbf{r},t)j_{\mathrm{p}}^{\mathrm{KS},n}(\mathbf{r},t)-\frac{\hbar}{\bar{\mathscr{F}}}\mathbf{l}^{\mathrm{KS}}(\mathbf{r},t)\cdot\mathbf{j}_{\mathrm{p}}^{\mathrm{KS}}(\mathbf{r},t)\delta_{n,l}-\bar{\mathscr{F}}^{-1}\mathscr{P}_{ln}(\mathbf{r},t)-$$
$$-\sum_{j\in\mathrm{occ.}}\mathrm{Re}(L_j^n(\mathbf{r},t))v_j^l(\mathbf{r},t).\tag{6.142}$$

By evaluating the spatial divergence of the previous expression and considering that the functions $\mathbf{l}^{\mathrm{KS}}(\mathbf{r},t)$ and $\mathbf{j}^{\mathrm{KS}}(\mathbf{r},t)$ are orthogonal we find

$$-\frac{i\hbar}{2m}\sum_l\nabla_l\cdot\sum_{j\in\mathrm{occ.}}\left[\nabla_l\psi_j^{\mathrm{KS}\dagger}\hat{L}^n\psi_j^{\mathrm{KS}}-\psi_j^{\mathrm{KS}\dagger}\hat{L}^n\nabla_l\psi_j^{\mathrm{KS}}\right]=\frac{\hbar}{m\bar{\mathscr{F}}}\sum_l\nabla_l\cdot(n\mathbf{l}^{\mathrm{KS}}\times\nabla_l\mathbf{l}^{\mathrm{KS}})_n-$$
$$-\sum_{r\in\mathrm{occ.}}[(\mathbf{j}_{\mathrm{p},r}^{\mathrm{KS}}\cdot\nabla)l_r^{\mathrm{KS},n}+\nabla\cdot\mathbf{j}_{\mathrm{p},r}^{\mathrm{KS}}l_r^{\mathrm{KS}}]+\frac{\hbar}{\bar{\mathscr{F}}}\sum_l\nabla_l\cdot(l_l^{\mathrm{KS}}(\mathbf{r},t)j_{\mathrm{p},n}^{\mathrm{KS}}(\mathbf{r},t))-$$
$$-\bar{\mathscr{F}}^{-1}\sum_l\nabla_l\cdot\mathscr{P}_{ln}(\mathbf{r},t),\tag{6.143}$$

that inserted into Eq. (6.99) gives rise to the following equation of motion

$$\frac{d}{dt}\Delta\mathbf{L}^{\mathrm{KS}}(\mathbf{r},t)+\sum_{r\in\mathrm{occ.}}(\nabla\cdot\mathbf{j}_{\mathrm{p},r}^{\mathrm{KS}})\mathbf{l}_r^{\mathrm{KS}}(\mathbf{r},t)=\frac{\hbar}{m\bar{\mathscr{F}}}\sum_l\nabla_l\cdot[n\mathbf{l}^{\mathrm{KS}}\times\nabla_l\mathbf{l}^{\mathrm{KS}}]+$$
$$+\frac{\hbar}{\bar{\mathscr{F}}}\sum_l\nabla_l[l_l^{\mathrm{KS}}(\mathbf{r},t)\mathbf{j}_{\mathrm{p}}^{\mathrm{KS}}(\mathbf{r},t)]-\mathbf{T}_{\mathrm{SO}}(\mathbf{r},t)+\rho(\mathbf{r},t)[\Delta\mathbf{r}\times q\mathbf{E}(t)]+$$
$$+\mu_B\sum_k(\Delta\mathbf{r}\times\nabla)B_k(\mathbf{r},t)m_k(\mathbf{r},t)-\rho(\mathbf{r},t)[\Delta\mathbf{r}\times\nabla\varphi(\mathbf{r})]-$$
$$-\bar{\mathscr{F}}^{-1}\nabla\cdot\mathscr{P}(\mathbf{r},t).\tag{6.144}$$

The previous expression represents our final version of the internal orbital moment continuity equation. The term on the left-hand side of Eq. (6.144) represents a sort of material derivative for the internal orbital moment component $\Delta\mathbf{L}^{\mathrm{KS}}(\mathbf{r},t)$, while on the right-hand side we can distinguish three terms in addition to the spin-orbit coupling torque, to the external electric dipole component and to the scalar potential and magnetic field terms.

Rotational component $\frac{\hbar}{m\bar{\mathscr{F}}}\sum_l \nabla_l \cdot (n\mathbf{l}^{\mathrm{KS}} \times \nabla_l \mathbf{l}^{\mathrm{KS}})$**:** This object is the analogous of $\mathbf{B}_{\mathrm{kin}}$ in the orbital moment continuity equation. It may be considered as the main source of orbital moment non-collinearity.

Dissipative term $-\nabla \cdot \mathscr{P}(\mathbf{r},t)$**:** This object represents the flux of orbital currents between different Kohn-Sham states. These transitions are relevant in particular in presence of the external laser pulse when the difference in energy between the different Kohn-Sham states is lowered and the transitions are allowed. Nevertheless, this term cannot induce a global modification of the orbital moment vector.

Orbital flux $\frac{\hbar}{\bar{\mathscr{F}}}\sum_l \nabla_l (l_l^{\mathrm{KS}}(\mathbf{r},t)\mathbf{j}_{\mathrm{p}}^{\mathrm{KS}}(\mathbf{r},t))$**:** This last term instead regulates the amount of orbital momentm lost in a particular spatial region due to the flow of currents and the inhomogeneities of the orbital moment vector field.

During the remaining of this section we will focus on the nature of the orbital moment kinetic field $\mathbf{L}_{\mathrm{kin}}(\mathbf{r},t)$ defined as

$$\mathbf{L}_{\mathrm{kin}}(\mathbf{r},t) = \frac{\hbar}{m\bar{\mathscr{F}}}\left[\frac{\nabla n}{n}\cdot\nabla\mathbf{l}^{\mathrm{KS}} + \nabla^2\mathbf{l}^{\mathrm{KS}}\right], \tag{6.145}$$

that couples in the continuity equation with the orbital moment as

$$\begin{aligned}\frac{d}{dt}\Delta\mathbf{L}^{\mathrm{KS}}(\mathbf{r},t) + \sum_{r\in\mathrm{occ.}}(\nabla\cdot\mathbf{j}_{\mathrm{p},r}^{\mathrm{KS}})\mathbf{l}_r^{\mathrm{KS}}(\mathbf{r},t) &= -\bar{\mathscr{F}}^{-1}\nabla\cdot\mathscr{P}(\mathbf{r},t) + \Delta\mathbf{L}^{\mathrm{KS}}(\mathbf{r},t)\times\mathbf{L}_{\mathrm{kin}}(\mathbf{r},t) + \\ &+ \frac{\hbar}{\bar{\mathscr{F}}}\sum_l \nabla_l[l_l^{\mathrm{KS}}(\mathbf{r},t)\mathbf{j}_{\mathrm{p}}^{\mathrm{KS}}(\mathbf{r},t)] - \mathbf{T}_{\mathrm{SO}}(\mathbf{r},t) + \rho(\mathbf{r},t)[\Delta\mathbf{r}\times q\mathbf{E}(t)] + \\ &+ \mu_B\sum_k(\Delta\mathbf{r}\times\nabla)B_k(\mathbf{r},t)m_k(\mathbf{r},t) - \rho(\mathbf{r},t)[\Delta\mathbf{r}\times\nabla\varphi(\mathbf{r})].\end{aligned} \tag{6.146}$$

This object represents a direct source of torque for the internal component of the orbital moment and it will be used to explain the different dynamics, observed at the in-plane and the out-of-plane regions, for both spin and angular momentum. In particular, we can measure the angle formed between the internal component of the orbital moment and this new kinetic field $\mathbf{L}_{\mathrm{kin}}$ in correspondence of the two groups of atoms of the Fe_6 cluster. The quantities are measured, as usual, by integrating over spheres centered on the atoms,

$$\Delta\mathbf{L}_{\mathrm{I}}^{\mathrm{KS}}(t) = \int_{\mathcal{S}_{\mathrm{I}}^{\mathrm{R}}} \mathrm{d}^3r\,\Delta\mathbf{L}^{\mathrm{KS}}(\mathbf{r},t), \qquad \Delta\mathbf{L}_{\mathrm{kin}}^{\mathrm{I}}(t) = \int_{\mathcal{S}_{\mathrm{I}}^{\mathrm{R}}} \mathrm{d}^3r\,\Delta\mathbf{L}_{\mathrm{kin}}(\mathbf{r},t). \tag{6.147}$$

In Fig. 6.10 we show the cosine of the angles $\theta_{\rm kin}(t)$ and $\phi_{\rm kin}(t)$ formed, in spherical coordinates, by the vector $\Delta\mathbf{L}^{\rm I}_{\rm kin}(t)$, measured with respect to its center of mass component.

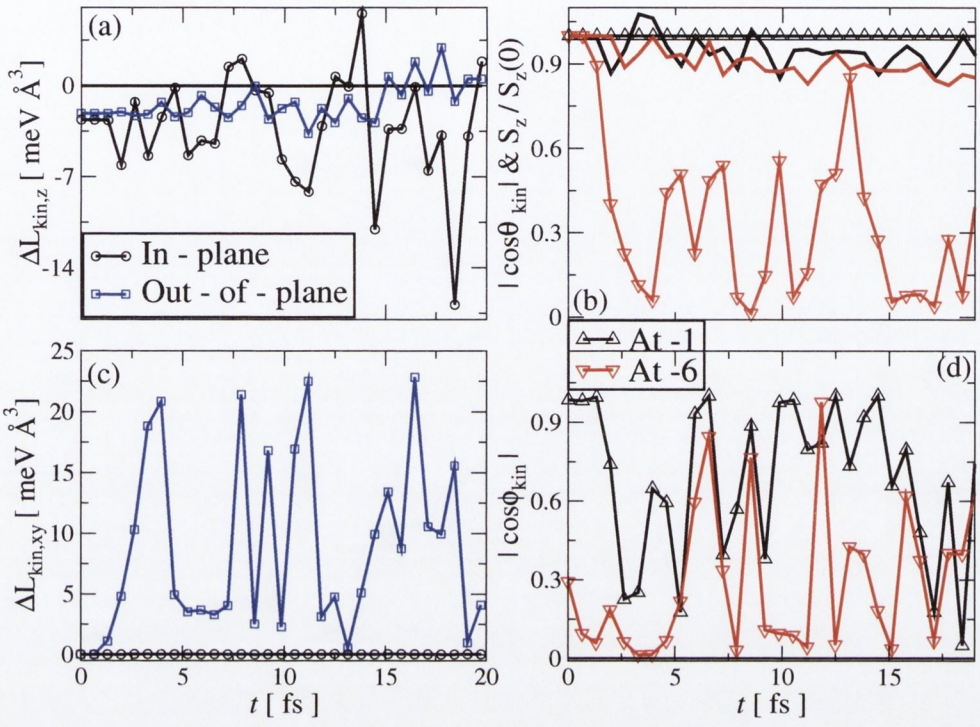


FIGURE 6.10: Dynamics of the two angles $\theta_{\rm kin}(t) = \text{acos}\left(\langle\Delta\mathbf{L}^{\rm I}_{\rm kin}(t), \hat{z}\rangle / |\Delta\mathbf{L}^{\rm I}_{\rm kin}(t)|\right)$ and $\phi_{\rm kin}(t) = \text{atan}\left(\Delta L^{\rm I}_{{\rm kin},y}(t) / \Delta L^{\rm I}_{{\rm kin},x}(t)\right)$ obtained by integrating inside a radius $R = 1.4$ Å around the atoms (the sphere includes also part of the interstitial region). (a) temporal evolution of $\Delta L^{\rm I}_{{\rm kin},z}(t)$ for the in plane atoms (black curve) and the out-of-plane atoms (blue curve); (b) Evolution of $|\cos\theta_{\rm kin}(t)|$ (thin line) together with $S^{\rm I}_z / S^{\rm I}_z(0)$ (thick line) for the in-plane and the out-of-plane atoms; (c) temporal evolution of $\Delta L^{\rm I}_{{\rm kin},xy}(t)$ for the in plane atoms (black curve) and the out-of-plane atoms (blue curve); (d) Evolution of $|\cos\phi_{\rm kin}(t)|$ for in-plane (black line) and out-of-plane atoms (red line).

In Fig. 6.10(a) we plot the temporal evolution of the z component of $\Delta\mathbf{L}^{\rm I}_{\rm kin}(t)$ for the in-plane and the out-of-plane atoms. It is clear that for the amplitude of the oscillations of the in-plane atoms is much larger than that of those observed in correspondence of the out-of-plane atoms. Therefore, $\Delta L_{{\rm kin},z}(t)$ appears to be larger in correspondence to the atoms 1 and 2 of the cluster with respect to its value close to atoms 5 and 6. In Fig. 6.10(c) we show, instead, the local values of $\Delta L^{\rm I}_{{\rm kin},xy}(t)$ defined as

$$\Delta L^{\rm I}_{{\rm kin},xy}(t) = \sqrt{\Delta L^{\rm I}_{{\rm kin},x}(t)^2 + \Delta L^{\rm I}_{{\rm kin},y}(t)^2}. \tag{6.148}$$

The dynamical behaviour of this quantity appears to be completely different with respect to that observed for $\Delta L^{\mathrm{I}}_{\mathrm{kin},z}(t)$ in panel (a). Now it is the out-of-plane quantity to be dominant during the evolution, while the value of $\Delta L^{\mathrm{I}}_{\mathrm{kin},xy}(t)$ measured in correspondence of the in-plane atoms is substantially negligible. This fact suggests a possible explanation for the growth, in correspondence of the apex atoms of the cluster, of the $\Delta L^{\mathrm{I}}_{x}(t)$ component. The huge value of $\Delta L^{\mathrm{I}}_{\mathrm{kin},xy}(t)$ obtained at the out-of-plane spatial region can be, in fact, a source of local torque for the orbital moment of the system, if the two vectors are not perfectly aligned.

These conclusions are confirmed also in Fig. 6.10(b,d) where we analyze the dynamics of the two angles $\theta_{\mathrm{kin}}(t)$ and $\phi_{\mathrm{kin}}(t)$ formed by the vector $\Delta\mathbf{L}^{\mathrm{I}}_{\mathrm{kin}}(t)$ with the coordination axis in correspondence of various atomic sites. In panel (b) together with $\cos\theta_{\mathrm{kin}}(t)$ we plot also the ratio $S^z(t)/S^z(0)$ for the in-plane (black curve) and out-of-plane (red curve) atoms. While, for in plane atoms $\cos\theta_{\mathrm{kin}}(t) = 1$ throughout the entire evolution the same is not true for the out-of-plane atoms, where the amount of non-collinearity is considerably higher. At the same time we observe also that the spin loss characterizing the out-of-plane region and the huge oscillations in the value of $\cos\theta_{\mathrm{kin}}(t)$ are to some degree correlated suggesting a direct relation between $\mathbf{L}_{\mathrm{kin}}$ and the rise of local non-collinearity in the spin vector field.

In panel (d), instead, we plot the temporal evolution of the variable $\cos\phi_{\mathrm{kin}}(t)$. This is characterized, in the same way as $\cos\theta_{\mathrm{kin}}(t)$, by huge out-of-plane oscillations, indicating a contribution from both the x and the y components of the field. The same quantity, for the in-plane atoms, follows a similar behaviour, but the fact that the non-collinear component in this particular region of space is very small makes this contribution not relevant. This confirms, in conclusion, that the origin of the orbital moment dynamics in the two spatial regions needs to be associated to different sources. Apparently, while in the in-plane region the non-collinear component of $\mathbf{L}_{\mathrm{kin}}$ appears very small, in the out-of-plane region its contribution to the dynamics could be more relevant.

In practice, according to our discussion at the beginning of the section, the laser polarization direction can strongly influence the local dynamics of the orbital moment vector field. We expect, for instance, that by applying a z-polarized electric field to the Fe_6 cluster, the change in the internal component of the orbital moment will be given by

$$\rho(\mathbf{r},t)[\Delta\mathbf{r}\times q\mathbf{E}(t)] = \rho(\mathbf{r},t)[\Delta y E_z(t)\mathbf{e}_1 - \Delta x E_z(t)\mathbf{e}_2]. \tag{6.149}$$

The previous quantity evaluated at the apex atoms is much smaller than that obtained in the case of an x-polarized electric field with the same amplitude (6.125). The reason is that in this case we have $\Delta x, \Delta y \ll \Delta z$ and, as a consequence, the excitation of the orbital moment x and y components will be smaller. In addition, the torque mechanism acting on the orbital moment driven by $\mathbf{L}_{\mathrm{kin}}$ appears particularly important, in the case of x-polarized electric field, in the interstitial regions where after the application of the pulse the gradient $\nabla\mathbf{l}^{\mathrm{KS}}(\mathbf{r},t)$ will be

characterized by strong modifications in direction and intensity due to the fact that the orbital moment vector in-plane and out-of-plane has different direction [see Fig. 6.2]. In Fig. 6.11 we relate this discussion on the orbital moment dynamics to the spin dynamics by observing that the interstitial regions, in the case of x-polarized laser field, are characterized by a much higher non-collinearity with respect to the case of the z-polarized field (the level of non-collinearity is measured in terms of the time averaged angle between $\mathbf{m}$ and $\mathbf{B}_{\text{kin}}$). This suggests a direct relation between the spin non-collinearity and the orbital torque $\mathbf{L}_{\text{kin}}(\mathbf{r}, t)$ that will be explored in the next section. In Fig. 6.11 the two simulations dif-

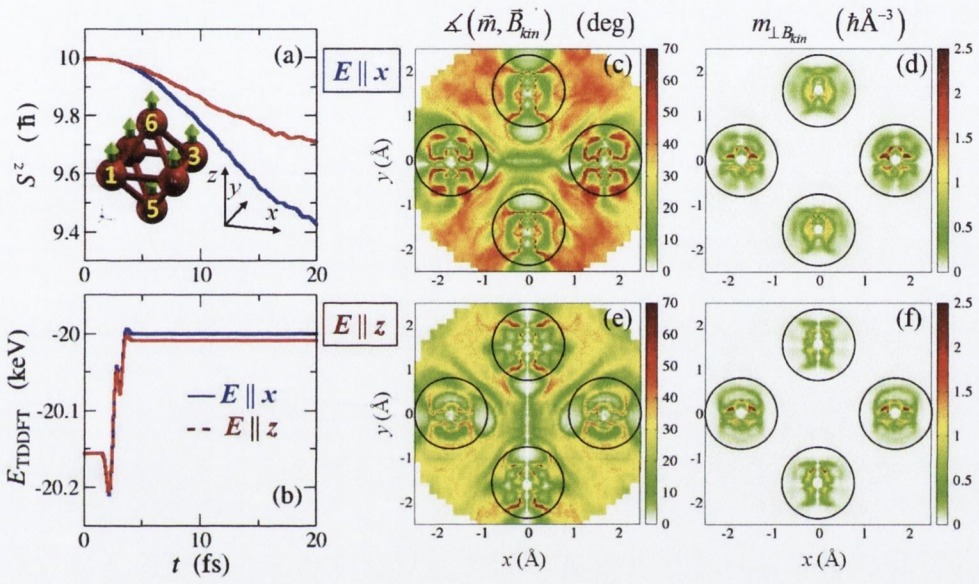


FIGURE 6.11: Global (a) spin and (b) energy variation in Fe_6 for two excitations differing only by the direction of polarization vector of the electric field pulse. Cartoon of the cluster with labels of the relevant atoms and the reference frame are depicted as insets. The contour plots represent the distribution of the angle (c, e) between $\mathbf{m}$ and $\mathbf{B}_{\text{kin}}$ in a plane through atoms 1, 3, 5 and 6 and the perpendicular component of $\mathbf{m}$ with respect to $\mathbf{B}_{\text{kin}}$ (d, f) averaged over the time of the simulation, for the two different excitations **E||x** and **E||z**, respectively, the top and bottom panels.

fer only by the direction (but notably not the magnitude) of the applied electric field. The x-polarization direction is oriented along the slightly longer side of the base of the bi-pyramid of the Fe_6 cluster, while in the other simulation the field is polarized along z, the direction connecting the two apex atoms 5 and 6. The case **E||x** shows nearly 3 times faster demagnetization compared to the **E||z** one. Evidently, in the former situation more energy is absorbed by the cluster (an excess of about 8.6 eV), we show a comparison of the total energy shift due to the pulse in Fig. 6.11(b).

From panel (c) we observe that the amount of non-collinearity enclosed in a relatively small radius around the apex atoms does not significatively change in the two cases, suggesting that the intra-site non-collinear component of the spin vector is already present in the ground-state configuration. What really differs is the amount of inter-sites non-collinearity concentrated in the out-of-plane region. In the $\mathbf{E}||\mathbf{x}$ case, if we examine the angle between $\mathbf{B}_{\text{kin}}(\mathbf{r}, t)$ and $\mathbf{m}(\mathbf{r}, t)$ averaged in time over the entire simulation along one particular cross-section plane (vertical through the base diagonal of the cluster as depicted in the inset), one can observe, in particular in the out-of-plane interstitial regions, a significant larger amount of non-collinearity, of the spin vector density, accumulating in the case of the faster demagnetization.

Notably there is a change in the symmetry between panels (c) and (e) in Fig. 6.11 – in both cases no significant spin non-collinearity arises in the plane parallel to the field connecting the atomic centers. It is, however, important to observe that the amount of intra-site spin non-collinearity for the in-plane atoms is strongly dependent on the polarization direction of the applied laser field. In fact, in the case of $\mathbf{E}||\mathbf{x}$ the temporal averaged angle between $\mathbf{s}$ and $\mathbf{B}_{\text{kin}}$ appears much higher with respect to the one computed in the $\mathbf{E}||\mathbf{z}$ case. This quantity is mostly averaged out by the integration procedure but it is clearly visible in the panel (c) of the figure.

As a representative quantity the component of $\mathbf{m}$ transverse to $\mathbf{B}_{\text{kin}}$ is depicted for the two simulations in panels (d) and (f). Although $\mathbf{B}_{\text{kin}}$ is not the only torque generator and the SO contribution is significant too, the former plays a rôle in deflecting the spins in the system in a manner that correlates with the rate of global demagnetization. The demagnetization process looks, in conclusion, very anisotropic and particular directions of the exciting electric field may enhance its rate.

Now we want to add more details to the comparison of the demagnetization of Fe_6 cluster under the two perpendicularly polarized electric field pulses. Fig. 6.12 shows the distributions of spin-density components in a plane through atoms 1, 3, 5 and 6, as in Fig. 6.11. Depicted are the $\mathbf{m}$ components both before the excitation (i.e. in the ground-state, top panels) and the averaged variations of those three components over the entire time-dependent simulation of 20 fs with respect to the ground-state values from the top panels.

Evident from these graphs is the intricate inherent symmetry of the transverse spin and its cancellation (with respect to the quantization axis z) for the whole plane both in the ground-state and over the two time-dependent simulations, which in both examples results in global demagnetization. Note that color code bars in all panels from the the two left-most columns are ideally centered around zero and there are identical areas with positive and negative contrast. It is interesting that there are qualitative differences in the excited spin variations which do not necessarily adhere to the ground-state symmetries and depend on the orientation of the $\mathbf{E}$-field. Since we have already discussed the dynamics of the

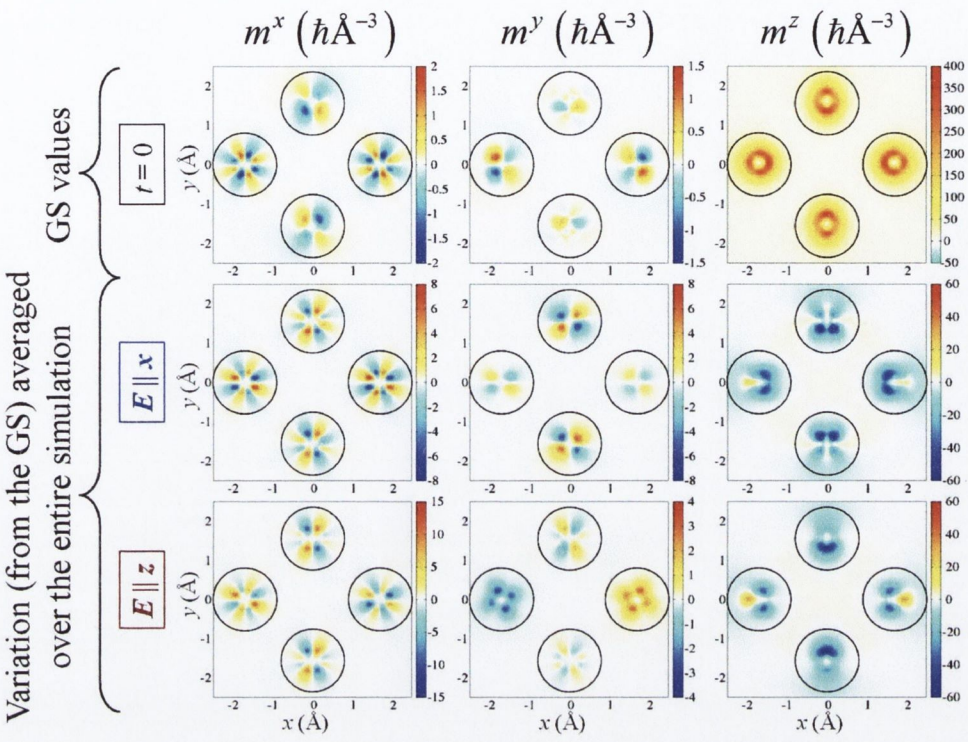


FIGURE 6.12: The three columns represent the three Cartesian components of the spin-density distribution in the plane used in Fig. 6.11. Black circles are centered on all atomic sites and have a radius of 0.8 Å. The top row correspond to the ground-state properties. The next two rows show the averaged over the entire time-dependent simulation variation of the corresponding quantities with respect to their ground-state values for the two simulations only differing by the direction of the electric field of the excitation pulse.

apex atoms and of the interstitial region, now we focus on the dynamics of the in-plane atoms. By making use of the two expressions (6.125) and (6.149) we observe that the z-polarized field should produce, as a consequence of the fact that atoms 1 and 3 are located at approximately opposite values of Δx and Δy, opposite in plane orbital moment vectors (while the z component remaining instead constant). This determines, through the spin-orbit coupling, an opposite polarization direction of the non-collinear spin component at the two atomic sites (particularly evident for the S_y term). In the $\mathbf{E} \| x$ case this cannot happen due to the fact that only Δy is involved in the expression for the orbital moment variation and the in-plane symmetry is broken.

Quantitatively the transverse spin variations appear substantially smaller than the variations in the z-component. Interestingly, simulations resulting in just a few percent of global demagnetization along z excite variations in the x and y spin components several times larger in magnitude than their ground-state values.

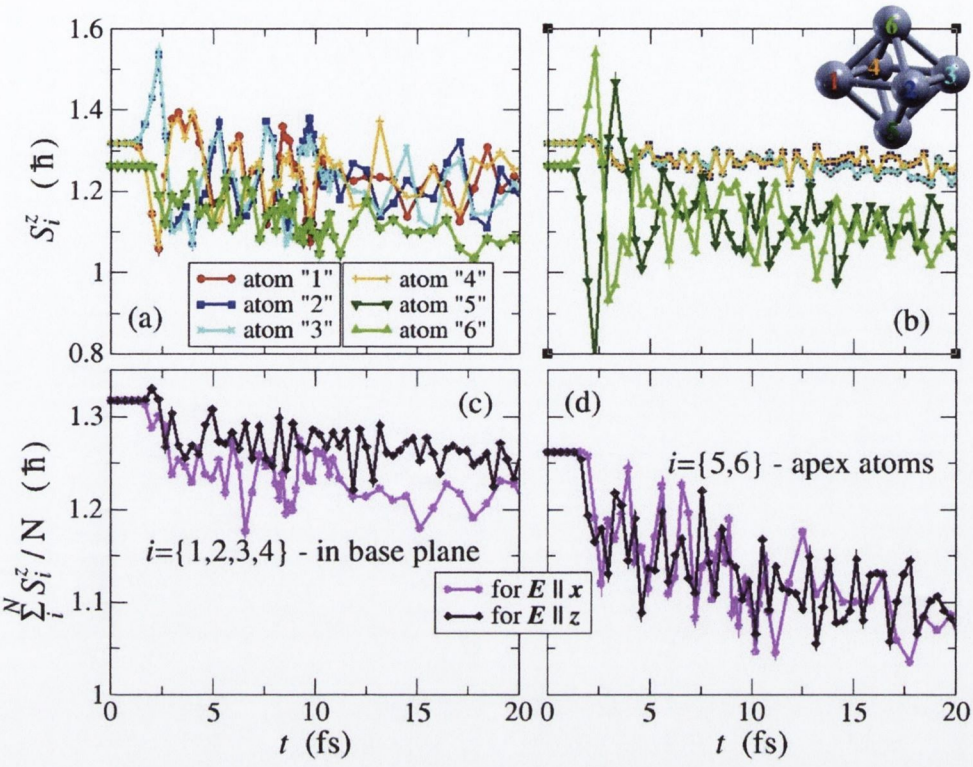


FIGURE 6.13: Evolutions of the spin around the individual atoms, defined as $S_{\mathrm{I}}^z = \frac{1}{|\mathcal{S}_{\mathrm{I}}^{\mathrm{R}}|}\int_{\mathcal{S}_{\mathrm{I}}^{\mathrm{R}}} \mathrm{d}^3 r\, s_z(\mathbf{r},t)$, where $\mathcal{S}_{\mathrm{I}}^{\mathrm{R}}$ is a spherical volume of radius 0.8 Å centered at atom I, for each of the two excitations: (a) **E**||**x** and (b) **E**||**z**. Comparison of the evolution of the base plane (c) and apex atoms (d) averaged spins (as in the top panels) for the two simulations. The lines are only guides to the eye connecting the data corresponding to snapshots of the TD-SDFT simulations.

This is confirmed also in Fig. 6.13(d) where the value of the local S_z component of the spin is computed within the same spherical region shown in Fig. 6.12 centered on the apex atoms. Only the intra-site non collinearity is enclosed in this sphere while the interstitial component lies outside. The amount of spin loss in the two cases is comparable and it cannot be directly associated to the polarization direction of the applied laser field and to the consequent orbital moment excitation as we have done for the other atoms. The demagnetization inside these atom-centered spheres is, therefore, only due to the intrinsic intra-site non-collinearity of the spin vector.

The actual loss of spin is clearly localized close to the atomic centers. The two simulations show somewhat different distributions of the average spin lost (averaged S^z variation is depicted in the bottom two panels of the right-most column in Fig. 6.12). The corresponding local variation of S^z integrated around each of the atomic sites is presented in Fig. 6.13. We find significant differences in the response of the atoms in the base plane of the bi-pyramid (1, 2, 3 and 4) and those

at the apexes (atoms 5 and 6) between the two simulations. While the individual local spins behavior depends on their particular position, the averaged values in the two groups show clearly a decrease with time. It appears that the for the **E**||**x** case the in-plane loss is more pronounced compared to the one developed in the case of the **E**||**z** excitation. This difference may be attributed to the fact that while in the first case the electric field can excite the local z component of the orbital moment, this cannot happen in the second case. Through the spin-orbit coupling this effect has some consequences on the spin dynamics as we will see in the next section.

6.6 The origin of the spin non-collinearity

In this section we will discuss how the the torque field $\mathbf{L}_{\text{kin}}$, or even the electric field that effectively acts as a source of modification of the orbital moment, can contribute to the local formation of non-collinear components of the spin vector field or to a change in the S_z component. To this goal we start from a simplified model analogous to the one employed in Chapter 4.

We consider a Hamiltonian of the form

$$\hat{H}(t) = \lambda \hat{\mathbf{L}} \cdot \hat{\mathbf{S}} + \mathbf{B}(t) \cdot \hat{\mathbf{S}} + \mathbf{B}_{\text{L}}(t) \cdot \hat{\mathbf{L}}, \tag{6.150}$$

where the first term on the right-hand side defines, as usual, the spin-orbit coupling. $\mathbf{B}(t) \cdot \hat{\mathbf{S}}$ is the Zeeman coupling of the spin vector with the external magnetic field, $\mathbf{B}(t)$, and the last term describes the coupling of the orbital moment operator $\hat{\mathbf{L}}$ with an external, time-dependent classical field $\mathbf{B}_{\text{L}}(t)$. This plays the role of the kinetic torque field $\mathbf{L}_{\text{kin}}(\mathbf{r}, t)$, or of a generic pre-factor that describes the effect of the laser on the dynamical modification of the orbital moment.

The solution of the time-dependent Schrödinger equation

$$i\frac{d}{dt}|\Psi(t)\rangle = \hat{H}(t)\,|\Psi(t)\rangle\,, \tag{6.151}$$

for a $\mathbf{B}_{\text{L}}(t)$ directed along z are shown in Fig. 6.14. We choose an initial spin-up state and zero orbital moment $|\Psi(0)\rangle = |l = 2, l_z = 0, s_z = 1/2\rangle$. The magnetic field $\mathbf{B}(t)$ is chosen constant in one case [see Fig. 6.14(a)] (in order to isolate the effect of $\mathbf{B}_{\text{L}}(t)$) and it is taken time-dependent in the second case [see Fig. 6.14(c)], but both are directed along z. while the temporal evolution of $B_{\text{L},z}(t)$ is chosen to reproduce the excitation following the action of the laser field. The situation is analogous to that experienced by the in-plane atoms in the **E**||**x** case, when the application of the laser should lead to a change in the L_z component of the orbital moment (see Eq. 6.125). $\mathbf{B}_{\text{L}}$ is introduced in order to simulate this laser induced modification. In Fig. 6.14(b, d) we plot the dynamical evolution of the spin expectation value along the quantization axis, $\langle \hat{S}_z(t) \rangle$, and the orbital moment $\langle \hat{L}_z(t) \rangle$ together with the respective non-collinear components

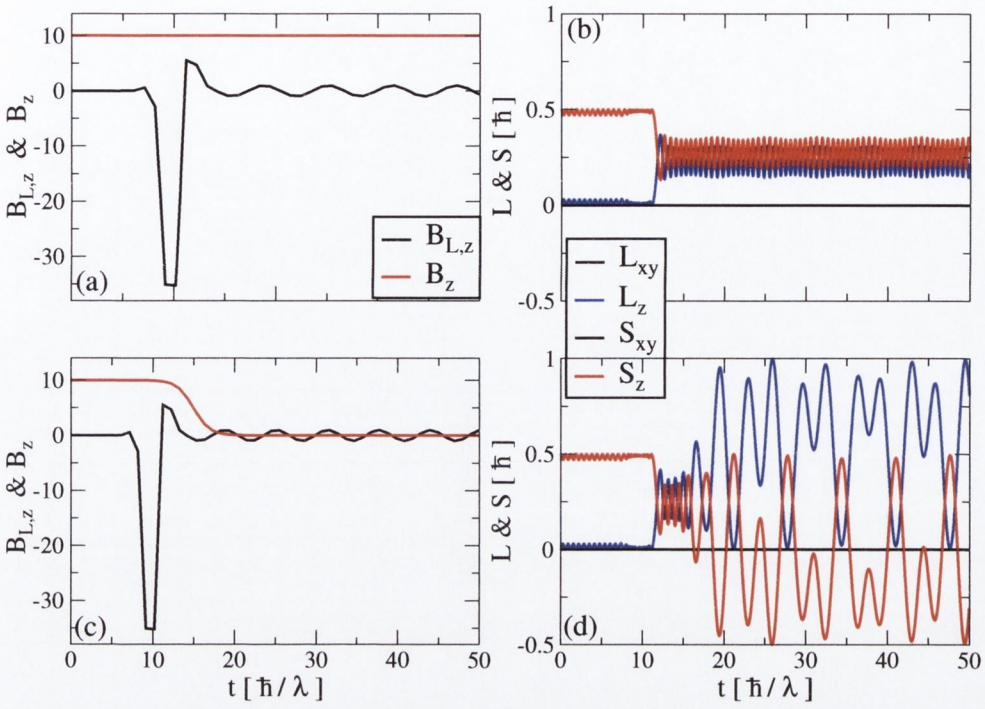


FIGURE 6.14: Dynamics of the spin $\langle \hat{\mathbf{S}} \rangle$ and orbital moment $\langle \hat{\mathbf{L}} \rangle$ expectation values evolving under the time-dependent Hamiltonian (6.150) with $\mathbf{B}_L$ directed along z and two different $\mathbf{B}(t)$. (a) and (c) temporal evolution of $B_z(t)$ (red curve) and of $B_{L,z}(t)$ (black curve); (b) evolution of the expectation values $\langle \hat{S}_z(t) \rangle$, $\langle S_{xy}(t) \rangle = \sqrt{\langle \hat{S}_x \rangle^2 + \langle \hat{S}_y \rangle^2}$, $\langle \hat{L}_z \rangle$ and $\langle \hat{L}_{xy} \rangle$ evolved under the fields of panel (a); (d) same quantities of panel (b) evolved under the fields of panel (c).

$\langle S_{xy}(t) \rangle$ and $\langle L_{xy}(t) \rangle$. While the two non collinear terms remain zero throughout the entire evolution, in panel (b) $\langle \hat{S}_z(t) \rangle$ undergoes a sudden change during the application of the external field $B_{L,z}(t)$ with part of the spin being transfered into the orbital moment through the spin-orbit coupling. After this initial dynamical phase the two expectation values remain approximately constant for the rest of the evolution. In panel (d) we evolve the time-dependent Schrödinger equation (6.151) under the effect of the pulses shown in panel (c), in this case in addition to the field $B_{L,z}(t)$ we have also a time dependent external magnetic field $B_z(t)$. The transfer of spin into the orbital moment is even larger with respect to that observed in panel (b), this suggests that the combination of the exchange field modification, described in Chapter 4, with the orbital moment excitation due to the laser may enhance the transfer of spin into the orbital moment and can explain the different behaviour of the in-plane spin density under the two fields $\mathbf{E}\|\mathbf{x}$ and $\mathbf{E}\|\mathbf{z}$ [see Fig. 6.13]. In practice, when $\mathbf{E}\|\mathbf{x}$ we have that $B_{L,z}(t) = -\rho \Delta y E_x(t)$ according to Eq. (6.125), while for $\mathbf{E}\|\mathbf{z}$ we have $B_{L,z}(t) = 0$. The consequence is that in the first case the in-plane demagnetization will be higher, as it is clearly shown in Fig. 6.13(c).

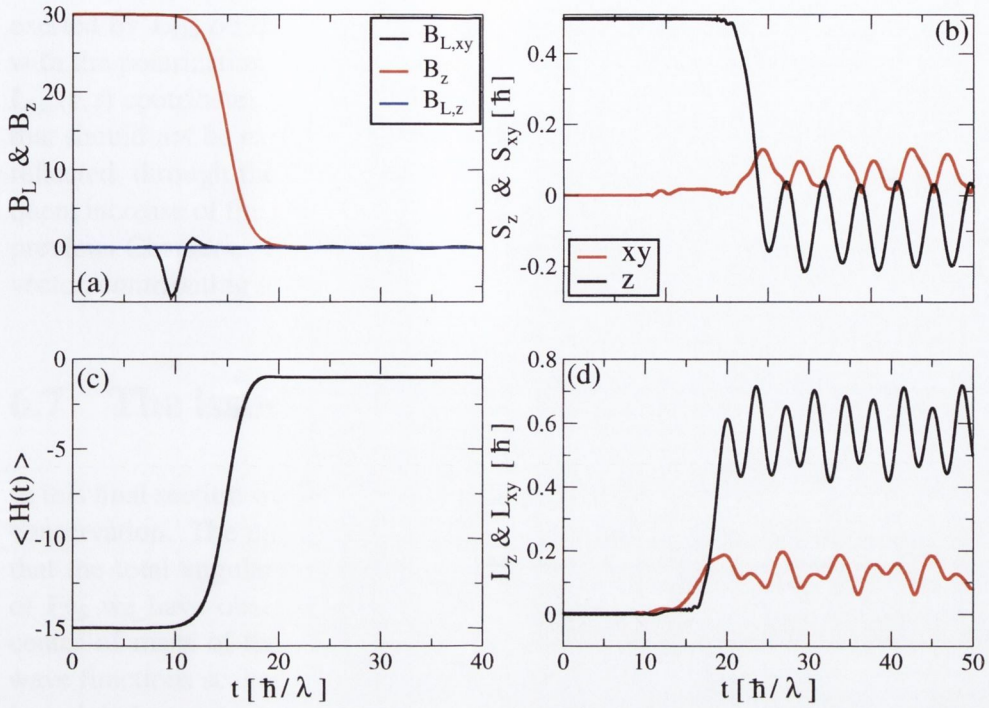


FIGURE 6.15: Dynamics of the spin $\langle \hat{\mathbf{S}} \rangle$ and orbital moment $\langle \hat{\mathbf{L}} \rangle$ expectation values with $\mathbf{B}_L$ lying in the $x - y$ plane. (a) temporal evolution of $B_z(t)$ (red curve), $B_{L,z}(t)$ (blue curve) and $B_{L,xy}(t)$ (black curve); (b) evolution of the expectation values $\langle \hat{S}_z(t) \rangle$ and $\langle S_{xy}(t) \rangle = \sqrt{\langle \hat{S}_x \rangle^2 + \langle \hat{S}_y \rangle^2}$; (c) temporal evolution of the Hamiltonian expectation value $\langle \hat{H}(t) \rangle$; (d) evolution of the orbital moment expectation values $\langle \hat{L}_z \rangle$ and $\langle L_{xy} \rangle$.

In Fig. 6.15 we evolve the quantum state under the same Hamiltonian (6.150) with the difference that in this case $\mathbf{B}_L(t)$ is not directed along the z-axis, but it lies in the xy-plane [see Fig. 6.15(a)]. This is used to simulate the effect of $\mathbf{L}_{kin}$ in the out-of-plane interstitial region of the Fe_6 cluster where, as we have already discussed in the previous section, its effect should be dominant in the case of $\mathbf{E}\|\mathbf{x}$. Now the dynamics of the system appears very different with respect to that of Fig. 6.14. From panel (b) and (d) it can be observed that the non collinearity in the spin vector and in the orbital moment starts growing after the application of the field $\mathbf{B}_L(t)$ that now can act as a torque on the angular momentum vector. As a consequence $S_{xy}(t)$, that is now not collinear to $B_z(t)$, can further increase while the $S_z(t)$ component collapses.

In conclusion, in this section we have made an attempt at explaining the origin of the different orbital moment and spin dynamics observed in the in-plane and the out-of-plane regions of the Fe_6 cluster with respect to the center of mass. The in-plane decay of $S_z(t)$ is strongly affected by the direction of polarization of the applied electric field and this may be explained in terms of the laser induced excitation of the orbital moment component L_z. The rise of the non-collinearity in the out-of-plane region may be explained, instead, in terms of the strong torque

exerted by $\mathbf{L}_{\text{kin}}$ on the local orbital moment vector that also change massively with the polarization direction of the applied field (see Fig. 6.11). We find that $\mathbf{L}_{\text{kin}}(\mathbf{r}, t)$ contributes to the torque of the orbital moment, even along directions that should not be excited by the application of the laser. These effects are then reflected, through the spin-orbit coupling, into the spin dynamics with a consequent increase of the non-collinear component, $S_{xy}(t)$, as widely discussed in the previous Chapters. The kinetic field, $\mathbf{B}_{\text{kin}}(\mathbf{r}, t)$, can act as a torque on the spin vector, contributing to the long tail of spin variation observed in the Fe_6 cluster.

6.7 The issue of the orbital moment conservation

In this final section we want to briefly discuss the problem of the orbital moment conservation. The numerical results of section 6.2 and also of Chapter 4 show that the total angular momentum of the system is not conserved. In the case of Fe_6 we have observed that this can be attributed to the oscillations of the center of mass of the electronic system. In fact, the delocalized Kohn-Sham wave functions scatter to the potential generated by the atomic centers resulting in a global non-conservation of the orbital moment.

Here, we seek to understand the meaning of the center of mass dynamics subsisting at longer times in the previously studied magnetic clusters. In order to achieve this we have developed a time-dependent *tight-binding* model [187], where we have included coupled to the electronic dynamics in an external field also the dynamics of the classical nuclei [189, 190]. This approximation describing the dynamics of the full system, electrons + nuclei, as a combination of a quantum mechanical equation of motion for the electrons with a set of classical Newtonian equations for the nuclei is known as the Ehrenfest approximation [191, 192]. This method adds some non-adiabatic feature to the standard molecular dynamics description, it is, however, a form of mean-field electron-ion dynamics that cannot describe electrons relaxing into the nuclear motion, but describes nuclei thermalizing into an electron bath.

In the Ehrenfest method the electrons interact with the nuclei through a classical field generated by the electronic charge distribution, which represents the mean-field approximation. This allows us to write the full density matrix operator as a tensor product of the electronic and the nuclear parts

$$\hat{\rho} = \hat{\rho}_{\text{e}} \otimes \hat{\rho}_{\text{N}}. \tag{6.152}$$

The quantum Liouville equation for the full system is written as

$$\frac{d}{dt}\hat{\rho} = \frac{1}{i\hbar}[\hat{H}(t), \hat{\rho}]. \tag{6.153}$$

By tracing out respectively the nuclear and the electronic degrees of freedom we obtain two separate equations respectively for $\hat{\rho}_e$ and $\hat{\rho}_N$

$$\frac{d}{dt}\hat{\rho}_e = \frac{1}{i\hbar}[\hat{H}_e(t), \hat{\rho}_e], \tag{6.154}$$

$$\frac{d}{dt}\hat{\rho}_N = \frac{1}{i\hbar}[\hat{H}_N(t), \hat{\rho}_N], \tag{6.155}$$

where $\hat{H}_e(t) = \mathrm{Tr}_N[\hat{H}(t)\hat{\rho}_N]$ and $\hat{H}_N(t) = \mathrm{Tr}_e[\hat{H}(t)\hat{\rho}_e]$ are the reduced Hamiltonians for, respectively, the electronic and the nuclear system. The second fundamental assumption of the Ehrenfest approximation is that the nuclei may be treated as classical point particles. By considering the following nuclear density function

$$\rho_N(\{\mathbf{R}_I\}, \{\mathbf{P}_I\}) = \prod_I \delta(\mathbf{R}_I - \mathbf{R}_I(t))\delta(\mathbf{P}_I - M_I\dot{\mathbf{R}}_I(t)), \tag{6.156}$$

the set of classical equations of motion for the nuclei become

$$\dot{\mathbf{R}}_I = \frac{\mathbf{P}_I}{M_I}, \tag{6.157}$$

$$\dot{\mathbf{P}}_I = -\frac{\partial H_N(\{\mathbf{R}_I\})}{\partial \mathbf{R}_I}. \tag{6.158}$$

Equations (6.154), (6.157) and (6.158) constitute the fundamental equations of the Ehrenfest approximation. This approximation, in general, fails either when the nuclei needs to be treated as quantum particles or when they need to respond to the fluctuations of the electron density. However, despite these limitations, we will employ the Ehrenfest approximation to describe the ultrafast dynamics of the system in the first few 10 fs after the application of the laser pulse. This can be justified also by the fact that the dynamics of the nuclei is very slow compared to that of the electrons.

Here, we focus on some paradigmatic cases with the objective of achieving a clearer understanding of the ultrafast dynamics of spin and orbital moment in systems with a more accurate description of the Coulomb repulsion between electrons. In practice, until now, we have explored the dynamics of these quantities in the case of transition metal systems described at the level of the local density approximation. This approach lacks accuracy in describing both the correlation effects and the Coulomb exchange interaction, treated only partially through the $\mathbf{B}_{xc}$ field, while the exchange between orbitals with different quantum number l_z is not considered.

We have already seen that in the LDA the electrons move in a mean-field potential created by all the other particles including themselves. Such unphysical self-iteraction is partially taken into account by the exchange-correlation functional. This also means that in the LDA the localization of the electrons in a particular spatial region is not driven by the Coulomb repulsion U, like in the Hubbard model, but by the Stoner exchange I. The exchange splitting potential

between the spin-up and the spin-down bands is given by

$$B_{\mathrm{xc}}(\mathbf{r}) = \frac{\delta E_{\mathrm{xc}}}{\delta \rho_{\uparrow}(\mathbf{r})} - \frac{\delta E_{\mathrm{xc}}}{\delta \rho_{\downarrow}(\mathbf{r})}, \tag{6.159}$$

and the Stoner exchange parameter $I(\mathbf{r})$ becomes

$$I(\mathbf{r}) = \frac{B_{\mathrm{xc}}(\mathbf{r})}{m(\mathbf{r})}, \tag{6.160}$$

with $m(\mathbf{r}) = \rho_{\uparrow}(\mathbf{r}) - \rho_{\downarrow}(\mathbf{r})$ being magnetization of the system. The gap between up and down states will be therefore completely specified by the parameter I that in transition metal compounds is determined by the on-site Hund exchange interaction J. This is in general much smaller than the Coulomb repulsion U explaining the difference in the prediction of the magnetic properties between the LDA and the Hubbard model.

In conclusion, the description of the magnetization and orbital moment dynamics in transition metals requires to go beyond LDA with a proper treatment of the Coulomb interaction that needs to be included into the electronic Hamiltonian $\hat{H}_{\mathrm{e}}$ of Eq. (6.154). The model Hamiltonian for the electronic system will have, therefore, the following final form

$$\hat{H}_{\mathrm{e}}(t) = \hat{H}_0 + \hat{H}_{\mathrm{C}} + \hat{V}_{\mathrm{SO}} + \hat{U}_{\mathrm{pen}} + \mu_B \mathbf{B}_{\mathrm{L}}(t) \cdot [\hat{\mathbf{S}} + 2\hat{\mathbf{L}}] + \hat{\mathbf{D}} \cdot \mathbf{E}(t), \tag{6.161}$$

where we distinguish six different terms

Crystal field term $\hat{H}_0$: this component represents the part of the electronic Hamiltonian that includes only the kinetic energy and the external ionic potential,

$$\hat{H}_0 = \hat{T} + \sum_{\mathrm{I}} \hat{V}_{\mathrm{I}}, \tag{6.162}$$

where $\hat{V}_{\mathrm{I}}$ represents the single ion potential from atom I experienced by the electrons. By employing a localized basis set $\{|I, n, l, m_l, m_s\rangle\}$ the matrix element of the operator $\hat{H}_0$ become

$$\begin{aligned} &\langle I_1, n', l', m'_l, m'_s | \hat{H}_0 | I_2, n, l, m_l, m_s \rangle = \\ &= \int \mathrm{d}^3\mathbf{r}\, \psi_{n',l',m'_l}(\mathbf{r} - \mathbf{R}_{\mathrm{I}_1})^* H_0(\mathbf{r}) \psi_{n,l,m_l}(\mathbf{r} - \mathbf{R}_{\mathrm{I}_2}) \delta_{m_s,m'_s}. \end{aligned} \tag{6.163}$$

Given that the basis of localized orbitals constitute the solution of the eigenvalue problem,

$$\left[-\frac{\nabla^2}{2} + V_{\mathrm{I}}(\mathbf{r}) \right] \psi_{n,l,m_l}(\mathbf{r} - \mathbf{R}_{\mathrm{I}}) = \epsilon_{n,l} \psi_{n,l,m_l}(\mathbf{r} - \mathbf{R}_{\mathrm{I}}), \tag{6.164}$$

where $\epsilon_{n,l}$ defines the on-site energy eigenvalue, Eq. 6.163 may be rewritten as

$$\langle I_1, n', l', m'_l, m'_s | \hat{H}_0 | I_2, n, l, m_l, m_s \rangle = \epsilon_{n,l} \langle I_1, n', l', m'_l, m'_s | I_2, n, l, m_l, m_s \rangle + \\ + \sum_{I' \neq I_2} \int \mathrm{d}^3\mathbf{r}\, \psi_{n',l',m'_l}(\mathbf{r} - \mathbf{R}_{\mathrm{I}_1})^* V(\mathbf{r} - \mathbf{R}_{\mathrm{I}'}) \psi_{n,l,m_l}(\mathbf{r} - \mathbf{R}_{\mathrm{I}_2}) \delta_{m_s,m'_s}, \tag{6.165}$$

where $\langle I_1, n', l', m'_l, m'_s | I_2, n, l, m_l, m_s \rangle = S_{n',l',m'_l;n,l,m_l}(\mathbf{R}_{\mathrm{I}_1} - \mathbf{R}_{\mathrm{I}_2}) \delta_{m_s,m'_s}$ is the overlap matrix between the two orbitals [determined according to the Slater-Koster transformation rules introduced in 6.3]. The overlap matrix is assumed to be different from zero only if the two atomic sites I_1 and I_2 are nearest neighbors, longer range terms are usually neglected. The second term on the right-hand side is more complex. It contains in fact the atomic potential on a third atom besides the sites upon which the orbitals are centered. This means that the general form of the matrix element contains three-center integrals. In order to simplify the notation, in Ref. [185] the authors introduced the so-called two-center approximation (2CA) in which all the three center contributions are neglected. Given that, in the majority of the cases this can be considered a reasonably good approximation, we will employ the 2CA in our calculations [188].

The matrix element (6.165) in the case of $I_1 = I_2$ becomes a single site term and may be reduced to

$$\langle I, n', l', m'_l, m'_s | \hat{H}_0 | I, n, l, m_l, m_s \rangle = \epsilon_{n,l} \delta_{n,n'} \delta_{l,l'} \delta_{m_l,m'_l} \delta_{m_s,m'_s}, \tag{6.166}$$

that corresponds just to the atomic eigenvalue. Instead, in the most general situation we will have

$$\langle I_1, n', l', m'_l, m'_s | \hat{H}_0 | I_2, n, l, m_l, m_s \rangle = [\epsilon_{n,l} S_{n',l',m'_l;n,l,m_l}(\mathbf{R}_{\mathrm{I}_1} - \mathbf{R}_{\mathrm{I}_2}) + \Delta V] \delta_{m_s,m'_s}, \tag{6.167}$$

where ΔV is the so-called crystal field. This obeys the Slater-Koster transformation rules (a detailed explanation of these rules applied to f orbitals may be found in [186]) and represents the non spherical potential that arises because of the presence of the other ions. In practice it corresponds to the ionic scalar potential that we have already introduced as a contribution to the equation of motion (6.96) for the internal momentum $\Delta\mathbf{L}$. This matrix element defines the probability amplitude for the electron to hop from the orbital $|I_2, n, l, m_l, m_s\rangle$ localized on the site I_2, to the orbital $|I_1, n', l', m'_l, m'_s\rangle$ localized on the site I_1.

Coulomb interaction $\hat{H}_{\mathrm{C}}$: The Coulomb interaction between electrons that scatter from orbitals α, β to orbitals α', β' has the following form

$$U_{\alpha'\beta'\beta\alpha} = \int \mathrm{d}^3\mathbf{r}\mathrm{d}^3\mathbf{r}'\, \psi_{\alpha'}(\mathbf{r})^* \psi_{\beta'}(\mathbf{r}')^* V(|\mathbf{r}' - \mathbf{r}|) \psi_{\beta}(\mathbf{r}') \psi_{\alpha}(\mathbf{r}). \tag{6.168}$$

The previous expression is usually simplified in the following standard form [193, 194],

$$\hat{H}_{\mathrm{C}} = \sum_{\mathrm{I},\alpha} U^{\mathrm{I}}_{\alpha\alpha} \hat{n}_{\mathrm{I}\alpha\uparrow} \hat{n}_{\mathrm{I}\alpha\downarrow} + \sum_{\mathrm{I},\alpha<\beta} \left[U'_{\alpha\beta\mathrm{I}} - \frac{J^{\mathrm{I}}_{\alpha\beta}}{2} \right] \hat{n}_{\mathrm{I}\alpha} \hat{n}_{\mathrm{I}\beta} - 2 \sum_{\mathrm{I},\alpha<\beta} J^{\mathrm{I}}_{\alpha\beta} \hat{\mathbf{S}}_{\mathrm{I}\alpha} \cdot \hat{\mathbf{S}}_{\mathrm{I}\beta} + \\ + \sum_{\mathrm{I}} J^{\mathrm{I}}_{\mathrm{dd}} \sum_{\alpha<\beta} (\hat{d}^{\dagger}_{\mathrm{I}\alpha\uparrow} \hat{d}^{\dagger}_{\mathrm{I}\alpha\downarrow} \hat{d}_{\mathrm{I}\beta\downarrow} \hat{d}_{\mathrm{I}\beta\uparrow} + \mathrm{h.c.}), \tag{6.169}$$

that includes all the spin-spin interaction terms. Here α, β denote all the orbitals used to describe the system (s, p, d and f). The parameters U and J describing respectively the Coulomb repulsion and the Hund coupling are assumed, in order to simplify the notation, to depend only on the orbital quantum number l and not on m_l. At the same time, the Coulomb repulsion U_{ss} and U_{pp} is negligible with respect to that experienced by d and f orbitals and the same argument is valid also for the Hund coupling.

$\hat{\mathbf{S}}_{\mathrm{I}\alpha}$ and $\hat{n}_{\mathrm{I}\alpha}$ are respectively the spin density and the electronic density for the orbital α localized on the atomic site I. The relation $U = U' - 2J$ between the different Kanamori parameters has been used. The first term in Eq. (6.169) describes the energy cost of having two electrons in the same orbital α, while the second term introduces the energy cost of having two electrons on different orbitals but on the same orbital channel. The third term is the Hund coupling that favours the ferromagnetic alignment of two spins on the same orbital. As we have already discussed, this is the equivalent to $\mathbf{B}_{\mathrm{xc}}$ in the multi-orbital Hubbard model. The fourth term is the pair-hopping term that involves only d orbitals with coupling J_{dd}, but it will be neglected in the calculations.

In performing our calculations we have added to $\hat{H}_{\mathrm{C}}$ an additional term that needs to be used in order to describe the correct orbital ordering of the single atom. This term allows us to verify the second Hund rule according to which, for a given spin multiplicity, the configuration with the largest value of the total orbital angular momentum, L, is the lowest in energy. We, therefore, rewrite the Coulomb interaction as

$$\hat{H}_{\mathrm{C}} = \sum_{\mathrm{I},\alpha} U_{\alpha\alpha} \hat{n}_{\mathrm{I}\alpha\uparrow} \hat{n}_{\mathrm{I}\alpha\downarrow} + \sum_{\mathrm{I},\alpha<\beta} \left[U'_{\alpha\beta} - \frac{J_{\alpha\beta}}{2} \right] \hat{n}_{\mathrm{I}\alpha} \hat{n}_{\mathrm{I}\beta} - 2 \sum_{\mathrm{I},\alpha<\beta} \hat{\mathbf{S}}_{\mathrm{I}\alpha} \cdot \hat{\mathbf{S}}_{\mathrm{I}\beta} - \sum_{\mathrm{I},\alpha,\beta} E_{\mathrm{I}\alpha\beta} \hat{L}^{z}_{\mathrm{I}\alpha} \hat{L}^{z}_{\mathrm{I}\beta}. \tag{6.170}$$

The last term on the right-hand side is generally known as the orbital polarization term, and $E_{\mathrm{I}\alpha\beta}$ is a orbital dependent parameter defining the strength of the coupling. This object has no equivalent within the LDA formalism. SDFT within LDA can, in fact, accounts for the first Hund's rule and can be extended in order to properly describe the third Hund's rule for the spin orbit coupling, but it cannot keep track of Hund's second rule given that that exchange correlation functional does not include orbital angular momentum dependent terms [195, 196]. In this case we just

employ an orbital polarization term analogous to the original proposal for $4f$ electrons [197] and successively considered also for d electrons [198]

$$\Delta E = -\frac{1}{2}EL^2. \tag{6.171}$$

Here E is the Racah parameter defined in terms of Slater integrals [199] and $L = \sum_i \langle \hat{l}_{z,i} \rangle$ corresponds to the orbital moment of the open shell. This orbital polarization term should allow us to reproduce, in addition to the spin and the charge densities, also the localized orbital moments of the system.

Spin orbit coupling V_{SO}: This represents the usual spin-orbit coupling term, where in addition we have included a term that accounts for the changes in the atomic positions

$$\hat{V}_{\mathrm{SO}} = \sum_{\mathrm{I},\alpha} (\lambda_{\mathrm{I}\alpha} + f_\alpha(\Delta\mathbf{R}_\mathrm{I}))\hat{\mathbf{L}}_{\alpha\mathrm{I}} \cdot \hat{\mathbf{S}}_{\alpha\mathrm{I}}. \tag{6.172}$$

In Eq. (6.172) the sum extends over all the atoms of the system. While the first term on the right-hand side represents the ordinary orbital dependent spin-orbit coupling

$$\lambda_{\mathrm{I}\alpha} = \int dr R_\alpha(r)^* V^\alpha_{\mathrm{SO}}(r) R_\alpha(r), \tag{6.173}$$

with $V^\alpha_{\mathrm{SO}}(r)$ spin orbit potential for the orbital channel α, the second term appears from the first order expansion of the potential of the atom at the new position $\mathbf{R}_\mathrm{I} + \boldsymbol{\delta}$. The effective coupling becomes

$$\lambda'_{\mathrm{I}\alpha} = \lambda_{\mathrm{I}\alpha} + \boldsymbol{\delta} \cdot \int dr R_\alpha(r)^* \boldsymbol{\nabla} V^\alpha_{\mathrm{SO}}(r) R_\alpha(r). \tag{6.174}$$

This object introduces an effective spin-phonon coupling into the dynamical equations.

Penalization potential U_{pen}: The penalization potential is defined as

$$\langle \mathrm{I}, l, m_l, m_s | \hat{U}_{\mathrm{pen}} | \mathrm{I}', l', m'_l, m'_s \rangle = \frac{1}{2} S_{l,m_l;l',m'_l}(|\mathbf{R}_I - \mathbf{R}_{I'}|)\, \delta_{m_s,m'_s} \sum_{\xi=1}^{N} (\gamma_{\mathrm{I}\xi} + \gamma_{\mathrm{I}'\xi}) \Delta q_\xi, \tag{6.175}$$

where N is the total number of sites. Here Δq_ξ defines the excess or reduction of charge on the site and $\gamma_{\mathrm{I}_1\mathrm{I}_2}$ is a short-range function of the form

$$\gamma_{\mathrm{I}_1\mathrm{I}_2} = \frac{1}{|\mathbf{R}_{I_1} - \mathbf{R}_{I_2}|} - s(\tau_1, \tau_2, |\mathbf{R}_{I_1} - \mathbf{R}_{I_2}|), \tag{6.176}$$

with τ parameter describing the on-site spherical electron density

$$\rho_0(\mathbf{r}) = \frac{\tau^3}{8\pi} e^{-\tau|\mathbf{r}|}. \tag{6.177}$$

The function $s(\tau_1, \tau_2, |\mathbf{R}_{I_1} - \mathbf{R}_{I_2}|)$ must also satisfy the following exact condition [200]

$$\lim_{R\to 0} s(\tau_1, \tau_2, R) = \frac{5}{16}\tau_1 + \frac{1}{R}. \tag{6.178}$$

$\hat{U}_{\text{pen}}$ describes the energetic cost of loosing of charge neutrality at a given atomic site.

Laser field induced transitions: The first component

$$\hat{\mathbf{D}} \cdot \mathbf{E}(t),$$

has been already discussed in section 5.8. Here we use the same on-site transition matrix elements (6.114), (6.115) and (6.116) and neglect the inter-site electric-field-induced transitions.

The second term,

$$\mu_B \mathbf{B}_{\text{L}}(t) \cdot [\hat{\mathbf{S}} + 2\hat{\mathbf{L}}],$$

defines the coupling between the laser magnetic field and the total orbital moment operator. It arises only in presence of circularly polarized light and compared to the electric field term its effect is negligible.

Now that we have introduced all the different components of the electronic Hamiltonian $\hat{H}_{\text{e}}$, we can generalize the set of equations described in Ref. [189] to the many orbitals case by starting from the following Lagrangian function

$$\mathscr{L}(\{\psi_i\}, \{\psi_i^*\}, \{\mathbf{R}_n\}) = i\hbar \sum_i p_{it} \langle \psi_i | \partial_t \psi_i \rangle - \sum_i p_{it} \text{Tr}(\hat{\rho}_i \hat{H}_{\text{e}}) + \frac{1}{2} \sum_n M_n \dot{\mathbf{R}}_n^2 - \varphi(\{\mathbf{R}_n\}). \tag{6.179}$$

In the previous expression we have introduced the set of single particle states $\{\psi_i\}$ that we are evolving dynamically with occupation probability $\{p_{it}\}$. As usual $\hat{\rho}_i$ is the density operator of the single particle state ψ_i. The set $\{\mathbf{R}_n\}$ defines the position of all the atoms of the system, while $\varphi(\{\mathbf{R}_n\})$ is the interaction energy between the different atoms. By expanding the expression (6.179) over the basis set of localized orbitals $\{|\alpha(\{\mathbf{R}_n\})\rangle\}$ which in turn depends on the set of atomic positions we obtain

$$\begin{aligned}\mathscr{L}(\{\psi_i\}, \{\psi_i^*\}, \{\mathbf{R}_n\}) = i\hbar \sum_i p_{it} \sum_{\alpha\beta} \psi_{i\alpha}^* \psi_{i\beta} \sum_n \dot{\mathbf{R}}_n \cdot \boldsymbol{\nabla}_n S_{\alpha\beta} + i\hbar \sum_i p_{it} \sum_{\alpha\beta} \psi_{i\alpha}^* S_{\alpha\beta} \dot{\psi}_{i\beta} - \\ - \sum_i p_{it} \sum_{\alpha\beta} \psi_{i\alpha}^* H_{\alpha\beta} \psi_{i\beta} + \frac{1}{2} \sum_n M_n \dot{\mathbf{R}}_n^2 - \varphi(\{\mathbf{R}_n\}),\end{aligned} \tag{6.180}$$

where the overlap matrix $S_{\alpha\beta}$ depends on the given set of atomic positions $\{\mathbf{R}_n\}$. We can now use the Euler-Lagrange equation

$$\frac{d}{dt}\frac{\partial \mathscr{L}}{\partial \dot{\psi}^*_{i\alpha}} = \frac{\partial \mathscr{L}}{\partial \psi^*_{i\alpha}}, \tag{6.181}$$

leading to

$$\dot{\psi}_{i\alpha'} + \sum_{\alpha,\beta}\psi_{i\beta}\sum_n \mathbf{R}_n \cdot \boldsymbol{\nabla}_n S_{\alpha\beta} S^{-1}_{\alpha'\alpha} = \frac{1}{i\hbar}\sum_{\beta,\alpha}\psi_{i\beta} S^{-1}_{\alpha'\alpha} H^{\alpha\beta}_{\mathrm{e}}. \tag{6.182}$$

The complex conjugate equation is

$$\dot{\psi}^*_{i\alpha'} + \sum_{\alpha,\beta}\psi^*_{i\beta}\sum_n \mathbf{R}_n \cdot \boldsymbol{\nabla}_n S^*_{\alpha\beta} (S^*_{\alpha'\alpha})^{-1} = -\frac{1}{i\hbar}\sum_{\beta,\alpha}\psi^*_{i\beta}(S^*_{\alpha'\alpha})^{-1} H^{\beta\alpha}_{\mathrm{e}}, \tag{6.183}$$

and by combining the two we obtain

$$\psi_{i\alpha}\dot{\psi}^*_{i\beta} + \sum_n \dot{\mathbf{R}}_n \cdot \sum_{\gamma,\delta}\rho^i_{\alpha\delta}\boldsymbol{\nabla}_n S_{\delta\gamma} S^{-1}_{\gamma\beta} = -\frac{1}{i\hbar}\sum_{\gamma\delta}\rho^i_{\alpha\gamma} H^{\gamma\delta}_{\mathrm{e}} S^{-1}_{\delta\beta}, \tag{6.184}$$

$$\dot{\psi}_{i\alpha}\psi^*_{i\beta} + \sum_n \dot{\mathbf{R}}_n \cdot \sum_{\gamma,\delta} S^{-1}_{\alpha\gamma}\boldsymbol{\nabla}_n S_{\gamma\delta}\rho^i_{\delta\beta} = \frac{1}{i\hbar}\sum_{\gamma,\delta} S^{-1}_{\alpha\gamma} H^{\gamma\delta}_{\mathrm{e}}\rho^i_{\delta\beta}. \tag{6.185}$$

This finally leads to the following equation of motion for the single state density matrix $\boldsymbol{\rho}^i$

$$\frac{d}{dt}\boldsymbol{\rho}^i = -\sum_n \dot{\mathbf{R}}_n \cdot \left[\boldsymbol{\rho}^i \boldsymbol{\nabla}_n \bullet \bullet^{-1} + \bullet^{-1}\boldsymbol{\nabla}_n \bullet \boldsymbol{\rho}^i\right] - \frac{1}{i\hbar}\left[\boldsymbol{\rho}^i \bullet {}_{\mathrm{e}}\bullet^{-1} - \bullet^{-1}\bullet {}_{\mathrm{e}}\boldsymbol{\rho}^i\right]. \tag{6.186}$$

The Euler-Lagrange equation for the atomic positions

$$\frac{d}{dt}\frac{\partial \mathscr{L}}{\partial \dot{\mathbf{R}}_n} - \frac{\partial \mathscr{L}}{\partial \mathbf{R}_n} = 0, \tag{6.187}$$

gives

$$M_n\ddot{\mathbf{R}}_n + i\hbar\sum_i p_{it}\sum_{\alpha,\beta}\psi_{i\beta}\dot{\psi}^*_{i\alpha}\boldsymbol{\nabla}_n S_{\alpha\beta} + \sum_{\alpha,\beta}\rho_{\beta\alpha}\boldsymbol{\nabla}_n H_{\alpha\beta} + \boldsymbol{\nabla}_n\varphi = 0, \tag{6.188}$$

where by making use of Eq. (6.183) we obtain

$$\dot{\psi}^*_{i\alpha} = -\frac{1}{i\hbar}\sum_{\gamma,\delta}\psi^*_{i\gamma} S^{-1}_{\delta\alpha} H^{\gamma\delta}_{\mathrm{e}} - \sum_{n'}\dot{\mathbf{R}}_{n'} \cdot \sum_{\gamma,\delta}\psi^*_{i\delta}\boldsymbol{\nabla}_{n'} S_{\delta\gamma} S^{-1}_{\gamma\alpha}. \tag{6.189}$$

The equation of motion for the atomic positions then becomes

$$M_n\ddot{\mathbf{R}}_n - \sum_{\alpha,\beta,\gamma,\delta} \rho_{\beta\gamma} H_{\mathrm{e}}^{\gamma\delta} S^{-1}_{\delta\alpha} \boldsymbol{\nabla}_n S_{\alpha\beta} - i\hbar \sum_{\alpha,\beta,\gamma,\delta} \sum_{n'} \rho_{\beta\delta} (\dot{\mathbf{R}}_{n'} \cdot \boldsymbol{\nabla}_{n'} S_{\delta\gamma}) S^{-1}_{\gamma\alpha} \boldsymbol{\nabla}_n S_{\alpha\beta} +$$
$$+ \sum_{\alpha,\beta} \rho_{\beta\alpha} \boldsymbol{\nabla}_n H_{\mathrm{e}}^{\alpha\beta} + \boldsymbol{\nabla}_n \varphi = 0. \tag{6.190}$$

By considering only the real part we finally have

$$M_n\ddot{\mathbf{R}}_n - \sum_{\alpha,\beta,\gamma,\delta} \rho_{\beta\gamma} H_{\mathrm{e}}^{\gamma\delta} S^{-1}_{\delta\alpha} \boldsymbol{\nabla}_n S_{\alpha\beta} + \sum_{\alpha,\beta} \rho_{\beta\alpha} \boldsymbol{\nabla}_n H_{\mathrm{e}}^{\alpha\beta} + \boldsymbol{\nabla}_n \varphi = 0, \tag{6.191}$$

that in matrix form gives,

$$M_n\ddot{\mathbf{R}}_n = \mathrm{Tr}\left[\boldsymbol{\rho}\bullet\ {}_{\mathrm{e}}\bullet^{-1} \boldsymbol{\nabla}_n \bullet\right] - \mathrm{Tr}\left[\boldsymbol{\rho}\boldsymbol{\nabla}_n \bullet\ {}_{\mathrm{e}}\right] - \boldsymbol{\nabla}_n \varphi, \tag{6.192}$$

with $\boldsymbol{\rho} = \sum_i p_{it}\, \boldsymbol{\rho}^i$ being density matrix of the electronic system. We now solve numerically the set of coupled equations (6.186) and (6.192). In order to simplify the description we will assume that in first approximation the Pulay forces can be neglected from the description leading to the simplified forms

$$\frac{d}{dt}\boldsymbol{\rho}^i = -\frac{1}{i\hbar}\left[\boldsymbol{\rho}^i \bullet\ {}_{\mathrm{e}}\bullet^{-1} - \bullet^{-1} \bullet\ {}_{\mathrm{e}}\boldsymbol{\rho}^i\right], \tag{6.193}$$

and

$$M_n\ddot{\mathbf{R}}_n = -\mathrm{Tr}\left[\boldsymbol{\rho}\boldsymbol{\nabla}_n \bullet\ {}_{\mathrm{e}}\right] - \boldsymbol{\nabla}_n \varphi. \tag{6.194}$$

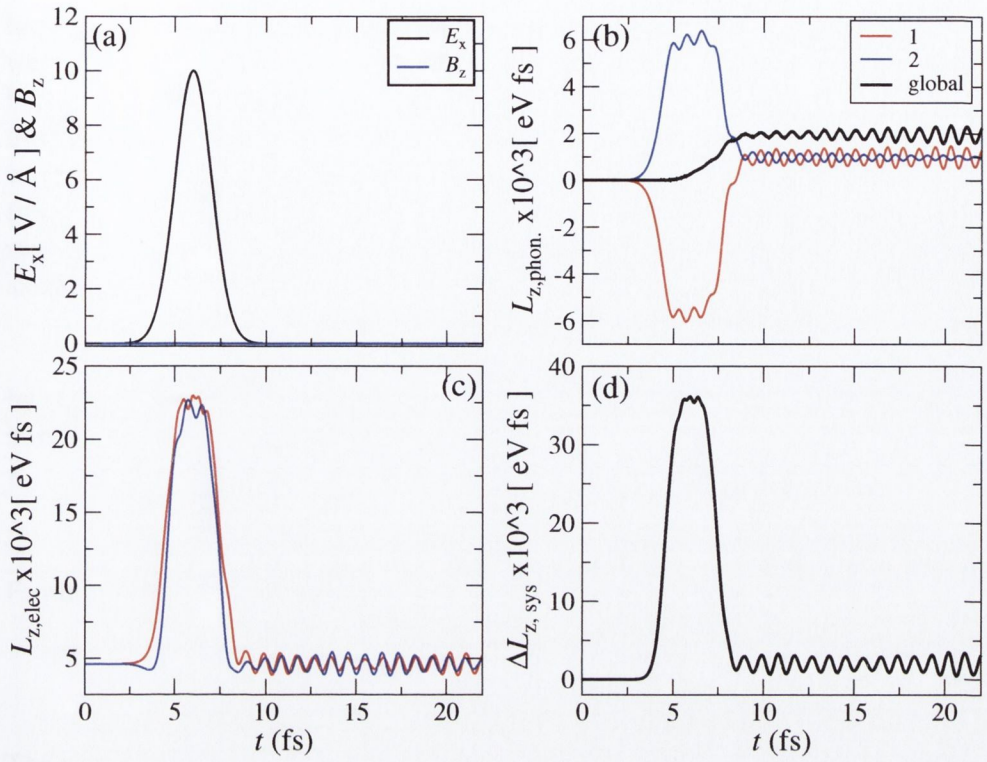
In the presence of an external magnetic and electric field we need to include also the Lorentz force leading to the following final set of equations for the atomic positions

$$M_n\ddot{\mathbf{R}}_n = -\mathrm{Tr}\left[\boldsymbol{\rho}\boldsymbol{\nabla}_n \bullet\ {}_{\mathrm{e}}\right] - \boldsymbol{\nabla}_n \varphi + Z_{\mathrm{eff}} e(\mathbf{E}(t) + \dot{\mathbf{R}}_n \times \mathbf{B}_{\mathrm{L}}(t)), \tag{6.195}$$

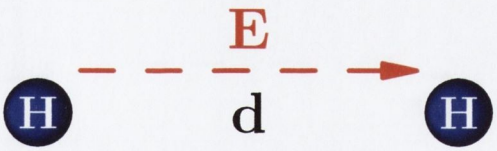
where Z_{eff} is the effective atomic number given by $Z - n_{\mathrm{core}}$, and n_{core} is the number of core electrons in the atom.

We apply the formalism developed in this section to the study of the case of the H-H dimer. At this level we want to solve a simplified model, that, at the same time, already includes some realistic features. We decide to use different values for the spin orbit coupling λ, Hund exchange and Hubbard repulsion, given that our purpose, here, is not that of obtaining completely accurate results for the dynamics of the spin and the orbital moment, but rather to achieve a more qualitative understanding of the ultrafast dynamics in these systems that does not change significatively within a reasonable range of values of these parameters.

The Coulomb part of the Hamiltonian, being a two-body interaction must be evaluated at the mean-field level. This requires only the knowledge of the orbital occupations $n_{\mathrm{I}\alpha}$ at each time step of the dynamical evolution. In Fig. 6.16a we show the time-dependent evolution of the H-H dimer in an external laser with



(A) Dynamics of the phononic orbital moment $\mathbf{L}_{\text{phonons}}$ and of the electronic orbital moment $\langle \hat{\mathbf{L}}_{\text{elec}} \rangle$ expectation values in the H-H cluster (the spin orbit coupling λ is set to zero). The onsite ground-state value of the electronic orbital moment is close to $9eVfs$ obtained by shifting the onsite energy levels. (a) temporal evolution of $B_z(t)$ (blue curve) and $E_x(t)$ (black curve); (b) evolution of the phononic contribution to the orbital moment $L_{\text{z,phonons}} = \sum_{\text{I}} M_{\text{I}} \mathbf{R}_{\text{I}} \times \dot{\mathbf{R}}_{\text{I}}$; (c) temporal evolution of the on-site electronic orbital moment $\langle \hat{L}^{\text{I}}_{\text{elec,z}} \rangle$; (d) global evolution of the summation of the electronic and phononic contribution to the orbital moment $\sum_{\text{I}} \left(\langle \hat{L}^{\text{I}}_{\text{elec,z}} \rangle + L^{\text{I}}_{\text{z,phonons}} \right)$.



(B) Picture of the H-H dimer oriented along the x axis, the two atoms are at a distance of 0.75 Å, the red arrow defines the orientation of the electric field applied to the cluster.

FIGURE 6.16: Temporal evolution of the H-H dimer.

electric and magnetic fields plotted in panel (a) (the magnetic field generated by the external pulse is always negligible in these calculations), the orientation of the dimer with respect to the electric field is shown in Fig. 6.16b. The electronic forces contributing to the nuclear motion come from the term $\text{Tr}\left[\boldsymbol{\rho} \boldsymbol{\nabla}_n \bullet_{\text{e}}\right]$ in Eq. (6.195). This term, namely the electron-phonon coupling, induces both a translational and a rotational component on the motion of the nuclei. Given that

here we are interested in the study of the system angular momentum evolution, we focus only on the rotational component of the electronic induced dynamics. From panel (d) of Fig. 6.16a it is clear that even on a global scale the orbital moment is not conserved at the level of the Ehrenfest approximation. The electronic orbital momentum is not entirely transfered into the phononic degrees of freedom. Within the tight-binding formalism it is customary to define the current operator through the introduction of the projector operator at a given atomic site [190],

$$\hat{P}_{\mathrm{I}} = \sum_{\alpha} |\psi_{\mathrm{I}\alpha}\rangle\langle\psi_{\mathrm{I}\alpha}|\,, \tag{6.196}$$

by defining the current J_{I} as a measure of the rate of change of the occupation number of the atomic site I we can write

$$\hat{J}_{\mathrm{I}} = \frac{1}{i\hbar}[\hat{P}_{\mathrm{I}}, \hat{H}]. \tag{6.197}$$

From the completeness condition $\sum_{\mathrm{I}} \hat{P}_{\mathrm{I}} = \bullet$ we can also write

$$\hat{J}_{\mathrm{I}} = \frac{1}{i\hbar} \sum_{\mathrm{I}' \neq \mathrm{I}} [\hat{P}_{\mathrm{I}} \hat{H} \hat{P}_{\mathrm{I}'} - \hat{P}_{\mathrm{I}'} \hat{H} \hat{P}_{\mathrm{I}}]. \tag{6.198}$$

The previous expression can be rewritten also in a matrix form. The non-orthogonality of the basis of localized atomic orbitals makes the expression for the current expectation value dependent also on the overlap matrix $\bullet$ [201]. Given that the matrix element of the product of two operators becomes,

$$\langle m|\hat{A}\hat{B}|n\rangle = \sum_{ij} A_{mi} S^{-1}_{ij} B_{jn}, \tag{6.199}$$

the matrix elements of the current operator (6.198) are written as

$$J_{\mathrm{I}} = \frac{2}{\hbar} \mathrm{Im}\Big\{\mathrm{Tr}_{\mathrm{I}}\big[\bullet\ {}_{\mathrm{e}}\bullet^{-1}\boldsymbol{\rho}\big]\Big\}. \tag{6.200}$$

An analogous expression may be found for the current of orbital moment through a given site. The orbital current in correspondence of the atomic site I is

$$J^{\mathrm{orb}}_{\mathrm{I},z}(t) = -\frac{i}{\hbar}\mathrm{Tr}_{\mathrm{I}}\big(\hat{\rho}[\hat{H}_0, \hat{L}_z]\big). \tag{6.201}$$

The object $\boldsymbol{J}^{\mathrm{orb}}_{\mathrm{I}}(t)$ may be thought as the flux of orbital moment from the electronic system to the atom I, and defines the amount of orbital moment accumulated by the atom. In the system composed by electrons and atoms this term represents only an internal transfer of orbital moment between the two subsystems. However, the variation of orbital moment of the phononic modes at site I do not in general coincide with $\boldsymbol{J}^{\mathrm{orb}}_{\mathrm{I}}(t)$.

In Fig. 6.16a(b) we measure the phononic orbital moment at the two sites (red

and blue curves). $L^{I}_{z,\text{phonons}}(t)$ is excited during the initial phase of the dynamical evolution in opposite directions, while after the application of the pulse the two quantities tend to oscillate around the same average value but with opposite phases. The black line, instead, represents the sum of the two components $\sum_I M_I \mathbf{R}_I \times \dot{\mathbf{R}}_I$. In Fig. 6.16a(c) we show instead the behaviour of the quantity $\langle \hat{L}^{I}_{z,\text{elec}}(t) \rangle$ during the dynamical evolution computed in correspondence of both the two atomic sites. The quantity changes during the application of the external laser pulse because the electric field acts directly on the orbital moment through the electric-dipole interaction term.

In conclusion, the atoms can, locally, accumulate orbital moment. In Fig. 6.16a(b) we show this accumulation along z due to the scattering of the electrons with the crystal field. The ion-ion interactions also contribute to the change of the orbital moment, however, this effect is more important at longer times, after the application of the laser we may assume, in fact, that a large fraction of energy is directly absorbed by the electronic subsystem.

In Fig. 6.16b we study the evolution of the cluster 6.16b activated by the same type of pulse. In this case, with respect to Fig. 6.16a we increase both the hopping parameters and the spin orbit coupling ($\lambda = 2\ eV$), while the Hubbard terms are still neglected in the calculation. In panel (a) of the figure the L_z component of the phononic orbital moment of the system is characterized after the application of the laser pulse by huge oscillations which increase in time. The strength of the oscillations is certainly affected by the value of the hopping coefficients, much higher with respect to the case depicted in Fig. 6.16a. The panel (b) of the figure instead describes the electronic orbital moment evolution which resembles the phononic one with an initial excitation due to the application of the laser and a successive evolution due to the scattering of the electrons with the crystal field potential of the cluster. In panel (c) it is represented the evolution of the spin system, it appears not comparable to the evolution of the orbital moment of the system. The ground state spin in correspondence of the two atomic sites is different from zero due to a spin dependent shift of the onsite energy, the application of the laser pulse leads to a slight transfer of spin between the two atomic sites and it is followed by small oscillation of the two S_z components around their average values. Finally in panel (d) it is depicted the summation of all the different global orbital components with the result that the total orbital moment of the system is not conserved during the dynamical evolution.

In conclusion, after the application of the external laser pulse the dynamics of the on-site atomic orbital moment is driven by the scattering with the crystal field potential, at the level of the Ehrenfest approximation the sum of the electronic and phononic orbital moment is not conserved neither during nor after the application of the laser pulse. This has been shown in the case of the H-H dimer in figures 6.16a and 6.17, but it keeps absolute general validity even in the case of more complex systems and by including the Hubbard repulsion that has the function to promote the formation of localized spin and orbital moment. When the effect of the Coulomb repulsion is important the change in the orbital

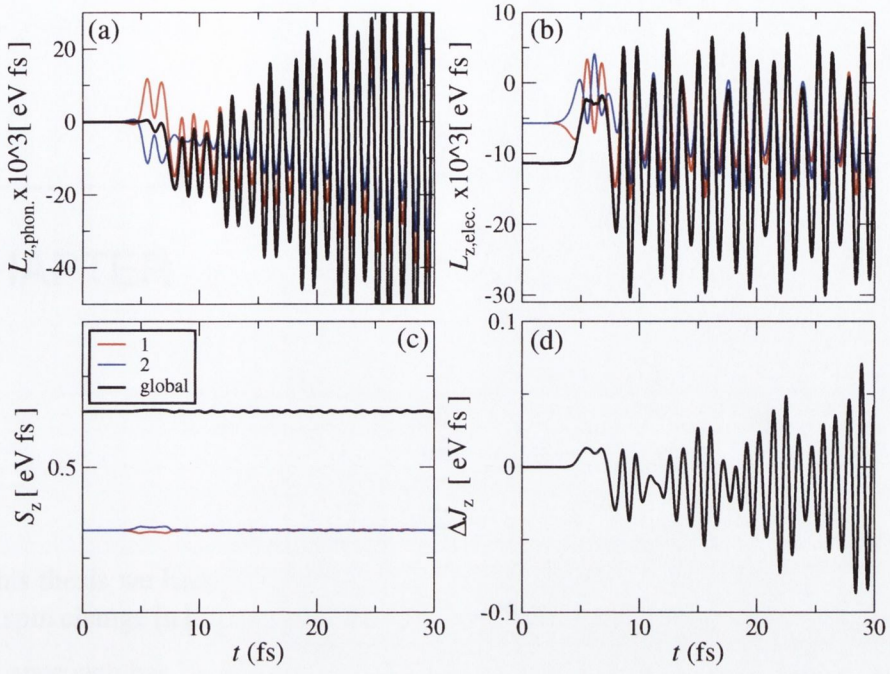


FIGURE 6.17: Dynamics of the H-H dimer under the same field of Fig. 6.16a and same dimer orientation. (a) z component of the phononic orbital moment $L^{\mathrm{I}}_{\mathrm{z,phon}}(t)$; (b) z component of the electronic orbital moment $\langle \hat{L}^{\mathrm{I}}_{\mathrm{z,elec}}(t) \rangle$; (c) evolution of the spin expectation value at the two atomic sites $\langle \hat{S}^{\mathrm{I}}_{\mathrm{z}}(t) \rangle$; (d) global evolution of the variation of the system orbital moment with respect to its ground state value $\sum_{\mathrm{I}} (\Delta \langle \hat{L}^{\mathrm{I}}_{\mathrm{z,elec}}(t) \rangle + \Delta L^{\mathrm{I}}_{\mathrm{z,phon}}(t) + \Delta S^{\mathrm{I}}_{\mathrm{z}}(t))$.

moment due to the scattering of the electrons with the ionic potential will be, instead, less important allowing the formation of local moments in correspondence of the atomic sites.

In the TD-DFT simulations we have observed that not only $\langle \hat{L}_{z,\mathrm{tot}} \rangle$ (see Fig. 6.1), but also $\int_{\Omega} \mathrm{d}^3 r \, (L_x^2 + L_y^2 + L_z^2)$ are not conserved during the evolution suggesting that the scattering of the electronic wave functions with the crystal field can give rise, globally, to a current that contributes to a modification of the center of mass moment even in absence of the external electric field. This effect is in practice equivalent to an effective rotation, with respect to the center of mass, of the entire system, that is not represented in our simulations because the box containing the system is maintained fixed by construction. In this view the long time center of mass dynamics may be thought as an impossibility for the system to relax into a new global equilibrium configuration because of the fixed spatial orientation of the simulation box.

CHAPTER 7

CONCLUSIONS

In this thesis we have investigated the fundamental mechanism that drives ultrafast spin change in transition metal systems, both bulk and in the form of clusters.

Our approach has been two-folds. On the one side, we have employed ab-initio methods, namely ground-state DFT based on the local density approximation and its adiabatic time-dependent equivalent (TD-SDFT), to study the dynamical evolution of both ferromagnetic and anti-ferromagnetic structures. On the other side, we have interpreted the results obtained by means of a more simplified description in terms of models. In particular in the case of the ultrafast spin dynamics we have used the so-called hydro-dynamical interpretation of Quantum Mechanics. We are conscious that these methods are limited and cannot describe the femto-second pump-probe experiments in their full complexity. The limitations can be ascribed mainly to the inability of the local density approximation to provide a complete description of the electronic structure of the transition metals, where correlation effects play an important role. We have attempted to overcome this difficulty in Chapter 6 even if the analysis cannot be certainly considered complete.

Our most important result, shown in Chapter 5, is that the ultrafast demagnetization process may be ultimately considered a pure single-particle effect. This conclusion arises in particular from the discussion carried out in Chapter 5 about the kinetic field $\mathbf{B}_{\text{kin}}$. Following the hydrodynamical interpretation of Quantum Mechanics we have expressed the spin continuity equation in a form that does not directly involve the spinor wave functions but only spin and electron densities

$$\frac{D}{Dt}\mathbf{m}(\mathbf{r},t) = -\nabla\cdot\mathcal{D}(\mathbf{r},t) - \sum_j \mathbf{m}_j(\mathbf{r},t)\nabla\cdot\mathbf{v}_j + \mu_B\mathbf{m}(\mathbf{r},t)\times\mathbf{B}_{\text{eff}}(\mathbf{r},t) + \mathbf{T}_{\text{SO}}(\mathbf{r},t). \quad (7.1)$$

This can be done only partially in the case of a many-particles system. The reason is that the term $-\nabla\cdot\mathcal{D}(\mathbf{r},t)$, that disappears in the single-particle case, is characterized by a non trivial dependence on the many-particle wave functions that does not allow one to express the magnetization time derivative in a simple

form involving only the many particle densities,

$$\mathcal{D}(\mathbf{r},t) = \sum_{j\in\text{occ.}}\sum_{r\neq j\text{occ.}} \mathscr{F}_{jr}\mathbf{m}^{(r,j)}(\mathbf{r},t)\otimes\left[\mathbf{v}^{(j,r)}(\mathbf{r},t)+\frac{e}{mc}\mathbf{A}(\mathbf{r},t)\right]- \\ -\sum_{j\in\text{occ.}}\sum_{r\neq j\in\text{occ.}} \mathscr{F}_{rj}\mathcal{J}^{(j,r)}(\mathbf{r},t). \tag{7.2}$$

We have established that the previous spin loss term plays an important role in the initial phase of the ultrafast magnetization dynamics by inducing inter-band transitions that do not locally conserve spin, while they cannot produce a global torque of the spin vector. The term on which, however, we have mainly focused our attention is the effective magnetic field, $\mathbf{B}_{\text{eff}}(\mathbf{r},t)$, that in absence of external magnetic field writes

$$\mathbf{B}_{\text{eff}}(\mathbf{r},t) = \mathbf{B}_{\text{xc}}(\mathbf{r},t) + \frac{1}{\mathscr{F}e}\left[\frac{\nabla n(\mathbf{r},t)\cdot\nabla\mathbf{s}(\mathbf{r},t)}{n(\mathbf{r},t)} + \nabla^2\mathbf{s}(\mathbf{r},t)\right]. \tag{7.3}$$

In $\mathbf{B}_{\text{eff}}$ we distinguish two components, the first one, $\mathbf{B}_{\text{xc}}$, includes all the many-body corrections, while the second term on the right-hand side, that we call $\mathbf{B}_{\text{kin}}$, is single-particle in origin and it is the equivalent for spin system of the quantum potentials appearing in the hydro-dynamical formalism. Both the terms are important in order to explain the spin dynamics in many particle systems, but we have seen throughout this thesis that the kinetic field is not negligible compared to $\mathbf{B}_{\text{xc}}$ and plays a dominant role in the dynamical evolution.

We have seen that in absence of the spin-orbit coupling there cannot be dynamical modification of the magnetization during the evolution. In fact while spin-flip mechanisms are forbidden, the spin vector cannot even rotate around its quantization axis. Since, both the spin-orbit coupling in its lowest order approximation and the kinetic field are single-particle terms the ultrafast demagnetization process may be, as a consequence, considered a single-particle phenomenon. In this view $\mathbf{B}_{\text{xc}}$ can contribute to the process but it does not constitute the fundamental source of magnetization variation.

In practice, by changing our view from the standard quantum mechanical formulation to the new hydro-dynamical one, where the basic variable of the problem is the probability density evolving dynamically under the influence of a quantum potential, we can explain the demagnetization process in terms of the deterministic torque exerted by this quantum potential, namely $\mathbf{B}_{\text{kin}}$, on the spin vector density. At the same time the dependence of $\mathbf{B}_{\text{kin}}$ from the gradients of the probability and spin densities save the non locality of the quantum mechanical description.

In Chapter 6 we have put aside the issue of the magnetization dynamics in transition metals and we have considered the orbital moment dynamics. We have shown, by means also of various models, that the most important source of the ultrafast dynamics of the orbital moment is the scattering with the crystal field,

that can in principle cover also the temporal variation due to the spin-orbit coupling. The polarization direction of the applied laser field can also induce strong differences in the local orbital moment dynamics and, consequently, also in the spin dynamics. These effects are explained in terms of excitation of different orbital moment components that, through the spin-orbit coupling, leads to a different dynamics of the spin vector.

In the final part of the Chapter we have identified two main issues in the description of the ultrafast orbital moment dynamics. The first one is related to a limitation of the LDA functional that strongly underestimates the formation of localized orbital moments. Formally, the introduction of the hybrid exchange-correlation functionals that include in addition to the exact exchange (EXX) also a portion of LDA-correlation would allow a proper treatment of this issue through a correct description of the second Hund's rule for the orbital ordering. This effect is substantially the source of the non-conservation of the orbital moment in the TD-SDFT simulation for the isolated Fe atom, where the amount of energy injected into the system by the laser is such that the different m_l states appear almost degenerate and the electrons do not distinguish between these different states.

An alternative path towards the solution of the problem requires to switch to TD-CDFT with the introduction of the $\mathbf{A}_{\mathrm{xc}}$ vector potential. As we have seen in Chapter 3 the currents, and consequently also the orbital moment, are formally exact variables of this theory. Here $\mathbf{A}_{\mathrm{xc}}$ plays a role analogous to that of $\mathbf{B}_{\mathrm{xc}}$ in TD-SDFT, inducing the formation of localized orbital moments in the system. Our approach, much simpler, is based on the introduction in the Coulomb interaction part of the Hamiltonian of orbital polarization terms that contribute to the formation of localized orbital moments, as can be clearly seen for the FeGd dimer.

The second issue that we have addressed is related to the problem of the orbital moment conservation. The simulations show that in the case of the H_4 cluster is $\langle \hat{L}^2_{\mathrm{tot}} \rangle$ to be conserved for the electronic subsystem, while $\langle \hat{L}_{\mathrm{z,tot}} \rangle$ is not due to the fact that, as we have already explained, in a many electrons system also the exact exchange interaction needs to be properly taken into account. In addition, we have also shown that locally each orbital moment component can be transfered from the electronic to the atomic system through the scattering of the electrons with the crystal field potential.

In general a global non-conservation of the orbital moment L_z would induce a rotation of the entire system with respect to its center, that is not allowed in our TD-SDFT simulations. In the case of finite systems this would imply a rotation of the entire cluster in empty space, but in the case of bulk systems this is connected to a direct transfer of angular momentum from the electrons to the lattice, with possible excitation of collective modes. In conclusion a proper treatment of the angular momentum dynamics requires the analysis of not only electrons but also

of the entire lattice as sources of orbital moment.

$$\Delta \mathbf{S} + \Delta \mathbf{L}_{\text{electrons}} + \Delta \mathbf{L}_{\text{laser}} + \Delta \mathbf{L}_{\text{lattice}} = 0. \tag{7.4}$$

Before concluding, we would mention also that it is known that the exchange-correlation approximation based on the homogeneous electron gas (LDA) does not provide a completely adequate description of systems with narrow bands. In these cases the electrons preserve their atomic orbital nature and DFT can give quantitative wrong results. It is, therefore, important to understand to which degree these deficiencies can affect the LDA description of the ultrafast magnetization dynamics in transition metals. The most important issue is related to the fact that the LDA exchange-correlation potential $\mathbf{B}_{\text{xc}}^{\text{LDA}}(\mathbf{r}, t)$ is adiabatic and it is by construction collinear to the local value of the magnetization density. The true exchange-correlation field $\mathbf{B}_{\text{xc}}$ should relax this constraint contributing to the local spin dynamics of the system. However, despite this aspect needs to be taken into account for future improvement of the exchange-correlation functional (some of these are already available and were described in Chapter 3 in the context of the introduction of the SDFT method), we believe that the fundamental aspects of the spin dynamics are already described at this level of the TD-SDFT implementation, given that all the fundamental ingredients of the ultrafast demagnetization process have a single-particle nature and do not arise from many-body considerations.

BIBLIOGRAPHY

[1] M. Jammer, *The philosophy of Quantum Mechanics*, by John Wiley & Sons, Inc. (1974).

[2] M. Fähnle and C. Illg, J. Phys.: Condens. Matter **23**, 493201 (2011).

[3] A. Kirilyuk, A.V. Kimel and Th. Rasing, Rev. Mod. Phys. **82**, 2731 (2010).

[4] T.L. Gilbert, Phys. Rev. **100**, 1243 (1955).

[5] L.D. Landau and E. Lifshitz, Phys. Z. Sowjet. **8**, 153 (1935).

[6] L.D. Landau, *Collected Papers* (Nauka, Moscow) (1969).

[7] C. Tannous and J. Gieraltowski, Eur. J. Phys. **29**, 475 (2008).

[8] I. Tudosa et Al., Nature **428**, 831 (2004).

[9] E. Beaurepaire, J.-C. Merle, A. Daunois and J.Y. Bigot, Phys. Rev. Lett. **76**, 4250 (1996).

[10] G. Ju, A.V. Nurmikko et Al., Phys. Rev. B **58**, R11857 (1998).

[11] M. van Kampen, C. Jozsa et Al., Phys. Rev. Lett. **88**, 227201 (2002).

[12] A.V. Kimel, A. Kirilyuk, A. Tsvetkov, R.V. Pisarev and Th. Rasing, Nature **429**, 850 (2004).

[13] J.-Y. Bigot, M. Vomir et Al., Chem. Phys. **318**, 137 (2005).

[14] G. Ju, J. Hohlfeld, B. Bergman et Al., Phys. Rev. Lett. **93**, 197403 (2004).

[15] C. Cohen-Tannoudji, J. Dupont-Roc and G. Grynberg, *Atom - Photon Interactions: Basic Processes and Applications*, Wiley-WCH Verlag GmbH & Co. (2004).

[16] P. Strange, *Relativistic Quantum Mechanics*, Cambridge University Press (1998).

[17] J.M. Jauch and F. Rohrlich, *The Theory of Photons and Electrons*, Springer-Verlag (1980).

[18] D.H. Kobe and E.C.T. Wen, Phys. Rev. D **26**, 1927 (1982).

[19] E.P. Wigner, Progress of Theoretical Physics **11**, 437 (1954).

[20] Qing-feng Sun and X.C. Xie, Phys.Rev.B **72**, 245305 (2005).

[21] Z. An, F.Q. Liu, Y. Lin and C. Liu, Scientific Reports **2**: 388 (2012).

[22] J. Shi, P. Zhang, D. Xiao and Q. Niu, Phys.Rev.Lett. **96**, 076604 (2006).

[23] E. Beaurepaire, J.-C. Merle, A. Daunois and J.Y. Bigot, Phys.Rev.Lett. **76**, 4250 (1996).

[24] M. Van Kampen, C. Josza, J.T. Kohlhepp et Al., Phys.Rev.Lett. **88**, 227201 (2002).

[25] I. Radu, K. Vahaplar, C. Stamm, T. Kachel et Al., Nature **472**, 205 (2011).

[26] G. Ju, A.V. Nurmikko, R.F.C Farrow et Al., Phys. Rev. B **58**, 857 (1998).

[27] J. Shah, *Ultrafast spectroscopy of semiconductors and semiconductor nanostructures*, Springer Series in Solid-State Sciences **115**, (Springer, Berlin) (1996).

[28] http://www3.ntu.edu.sg/home/howesiang/new/research.htm .

[29] M. Dressel and G.Grüner, *Electrodynamics of Solids*, Cambridge University Press (2002).

[30] Z. Qiu and S. Bader, J. Magn. Magn. Mater. **200**, 664 (1999).

[31] P.N. Argyres, Phys.Rev. **97**, 334 (1955).

[32] G.P. Zhang, W. Hübner, G. Lefkidis et Al., Nature **5**, 499 (2009).

[33] F. Mandl and G. Shaw, *Quantum field theory*, Wiley - Interscience publication (1984).

[34] L.L. Foldy and S.A. Wouthuysen, Phys.Rev. **78**, 29 (1950).

[35] L.L. Foldy, Phys.Rev. **87**, 688 (1952).

[36] G.P. Zhang, Phys.Rev.Lett. **101**, 187203 (2008).

[37] H. Vonesch and J.-Y. Bigot, Phys.Rev.B **85**, 180407 (2012).

[38] Y. Hinschberger and P.-A. Hervieux, Phys.Rev.B **88**, 134413 (2013).

[39] Y. Hinschberger and P.-A. Hervieux, Phys.Lett.A **376**, 813 (2012).

[40] G. Lefkidis and W. Hübner, Phys.Rev.B **87**, 014404 (2013).

[41] M. Battiato, G. Barbalinardo and P.M. Oppeneer, Phys.Rev.B **89**, 014413 (2014).

[42] J.-Y. Bigot, M. Vomir and E. Beaurepaire, Nat. Phys. **5**, 515 (2009).

[43] P.S. Pershan, J.P. van der Ziel and L.D. Malmstrom, Phys.Rev. **143**, 574 (1966).

[44] A.V. Kimel, A. Kirilyuk and Th. Rasing, Laser & Photon. Rev. **1**, 275 (2007).

[45] M.S. Si and G.P. Zhang, J.Phys.:Condens.Matter **22** 076005 (2010).

[46] L. Guidoni, E. Beaurepaire and J.-Y. Bigot, Phys.Rev.Lett. **89**, 017401 (2002).

[47] W. Nolting and A. Ramakanth, *Quantum Theory of Magnetism*, (Springer) (2009).

[48] J. Hubbard, Proc.R.Soc. **A276**, 238 (1963).

[49] J. Kanamori, Progr.Theor.Phys. **A30**, 275 (1963).

[50] M.C. Gutzwiller, Phys.Rev.Lett. **A10**, 59 (1963).

[51] F.H.L. Hessler, V.E. Korepin and K. Schoutens, Phys.Rev.Lett. **67**, 3848 (1991).

[52] G.P. Zhang, M.S. Si, Y.H. Bai and T.F. George, J.Phys.: Condens. Matter **27**, 206003 (2015).

[53] N.W. Ashcroft and N.D. Mermin, *Solid State Physics*, (London: Harcourt Brace) (1976).

[54] I. Žutić, J. Fabian and S.D. Sarma, Rev.Mod.Phys. **76**, 323 (2004).

[55] W. Töws and G.M. Pastor, Phys.Rev.Lett. **115**, 217204 (2015).

[56] R.J. Elliott, Phys.Rev. **96**, 266 (1954).

[57] M. Krauß, T. Roth, S. Alebrand et Al., Phys.Rev.B **80**, 180407 (2009).

[58] M. Haag, C. Illg and M. Fähnle, Phys.Rev.B **87**, 214427 (2013).

[59] M. Haag, C. Illg and M. Fähnle, Phys.Rev.B **90**, 014417 (2014).

[60] A.B. Schmidt, M. Pickel, M. Donath et Al., Phys.Rev.Lett. **105**, 197401 (2010).

[61] G. Grimvall, *The Electron - Phonon interaction in metals*, (North-Holland Publishing Co.) (1981).

[62] D. Steiauf and M. Fähnle, Phys.Rev.B **79**, 140401 (2009).

[63] B. Koopmans, G. Malinowski, F. Dalla Longa et Al., Nat.Mater. **9**, 259 (2010).

[64] K. Carva, M. Battiato and P.M. Oppeneer, Phys.Rev.Lett. **107**, 207201 (2011).

[65] M. Battiato, K. Carva and P.M. Oppeneer, Phys.Rev.Lett. **105**, 027203 (2010).

[66] M. Battiato, K. Carva and P.M. Oppeneer, Phys.Rev.B **86**, 024404 (2012).

[67] A. Kirilyuk, A.V. Kimel and Th. Rasing, Rep.Prog.Phys. **76**, 026501 (2013).

[68] B. Koopmans, H.H.J.E. Kicken, M. v. Kampen and W.J.M. De Jonge, J.Magn.Magn.Mater. **286**, 271 (2005).

[69] M. Lakshmanan, Phil.Trans.R.Soc.A **369**, 1280 (2011).

[70] J. Seib, D. Steiauf and M. Fähnle, Phys.Rev.B **79**, 064419 (2009).

[71] D. Steiauf and M. Fähnle, Phys.Rev.B **72**, 064450 (2005).

[72] K. Gilmore, M.D. Stiles et Al., Phys.Rev.B **81**, 174414 (2010).

[73] B. Koopmans, J.J.M. Ruigrok, F. Dalla Longa and W.J.M. De Jonge, Phys.Rev.Lett. **95**, 267207 (2005).

[74] M. Fähnle, J. Seib and C. Illg, Phys.Rev.B **82**, 144405 (2010).

[75] K. Krieger, J.K. Dewhurst, P. Elliott, S. Sharma and E.K.U. Gross, J.Chem. Theory Comput. **11**, 4870 (2015).

[76] M. Stamenova, J. Simoni and S. Sanvito, Phys. Rev. B **94**, 014423 (2016).

[77] R.M. Martin *Electronic Structure Basic Theory and Practical Methods*, Cambridge University press (2004).

[78] V. Anisimov and Y. Izyumov, *Electronic Structure of Strongly Correlated Materials*, Springer Series in Solid-State Sciences (2010).

[79] C.J. Cramer *Essentials of Computational Chemistry*, Chichester: John Wiley & Sons (2002).

[80] I.N. Levine, *Quantum Chemistry* (4th ed.). Englewood Cliffs, New Jersey: Prentice Hall. (1991). pp. 455544.

[81] M. Kaku, *Quantum field theory a modern introduction*, Oxford University press (1993).

[82] R.G. Parr, W. Yang, *Density functional theory of atoms and molecules*, Oxford University press, Inc., (1989).

[83] S.H. Vosko, L. Wilk, M. Nusair, Can. J. Phys. **58**, 1200, (1980).

[84] K. Burke, L. Wagner, Int. J. Quantum Chem. **113**, 96, (2013).

[85] E. Engel, R.M. Dreizler, *Density functional theory*, Springer Verlag Berlin, Inc., (1990).

[86] W. Kohn, P. Hohenberg, Phys. Rev. B **136**, 864, (1964).

[87] A.D. Becke, Phys. Rev. A **38**, 3098 (1988).

[88] C. Lee, W. Yang and R.G. Parr, Phys. Rev. B **37**, 785 (1988).

[89] F. Zahariev, S.S. Leang and M.S. Gordon, J. Chem. Phys. **138**, 244108 (2013).

[90] R. Van Leeuwen, Adv. Quantum Chem.,**43**, 25, (2003).

[91] E.H. Lieb, Int. J. Quantum Chem., **24**, 243, (1983).

[92] J.P. Perdew, A. Zunger, Phys. Rev. B, **23**, 5048, (1981).

[93] D.M. Ceperley, B.J. Alder, Phys. Rev. Lett.**45**, 566, (1980).

[94] J.P. Perdew, K. Burke, M. Ernzerhof, Phys. Rev. Lett.**77**, 3865, (1996).

[95] K. Capelle, G. Vignale, Phys. Rev. Lett.**86**, 5546, (2001).

[96] N.I. Gidopoulos, Phys. Rev. B **75**, 134408, (2007).

[97] K. Capelle, G. Vignale and B.L. Györffy, Phys.Rev.Lett. **87**, 206403, (2001).

[98] G. Vignale and M. Rasolt, Phys.Rev.B **37**, 10685 (1988).

[99] S. Rohra and A. Görling, Phys. Rev. Lett. **97**, 013005, (2006).

[100] G. Vignale, M. Rasolt, Phys. Rev. Lett.**59**, 2360, (1987).

[101] S. Sharma, J.K. Dewhurst, C. Ambrosch-Draxl, et Al., Phys. Rev. Lett.**98**, 196405, (2007).

[102] S. Sharma, S. Pittalis, S. Kurth, S. Shallcross, J.K. Dewhurst and E.K.U. Gross, Phys.Rev.B **76**, 100401, (2007).

[103] F.G. Eich and E.K.U. Gross, Phys.Rev.Lett. **111**, 156401 (2013).

[104] X.Y. Pan, V. Sahni, Int. J. Quantum Chem. **110**, 2833, (2010).

[105] G. Vignale, C.A. Ullrich, K. Capelle, Int. J. Quantum Chem. **113**, 1422, (2013).

[106] K. Capelle and E.K.U. Gross, Phys. Rev. Lett. **78**, 1872, (2002).

[107] E.K.U. Gross and R.M. Dreizler, *Density Functional Theory*, Plenum, New York (1995).

[108] K. Bencheikh, J.Phys.A:Math.Gen. **36**, 11929, (2003).

[109] L. Kleinman, D.M. Bylander, Phys.Rev.Lett. **48**, 1425, (1982).

[110] D.D. Koelling and B.N. Harmon, J. Phys. C: Solid State Phys. **10**, 3107 (1977).

[111] E. Engel, A.Höck and S. Varga, Phys.Rev.B **63**, 125121, (2001).

[112] E. Runge and E.K.U. Gross, Phys.Rev.Lett. **52**, 997, (1984).

[113] G. Vignale, Phys.Rev.Lett. **74**, 3233, (1995).

[114] G. Vignale, Phys.Lett.A **209**, 206, (1995).

[115] R. D'Agosta and G. Vignale, Phys.Rev.B **71**, 245103, (2005).

[116] I. Žutić, J. Fabian and S. Das Sarma, Rev.Mod.Phys. **76**, (323), (2004).

[117] S.K. Ghosh and A.K. Dhara, Phys.Rev.A **38**, 1149, (1988).

[118] J.P. Perdew and Y. Wang, Phys. Rev. B **45**, 13244 (1992).

[119] M.A.L. Marques, A. Castro, G.F. Bertsch and A. Rubio, Comp. Phys. Comm. **151**, 60 (2003).

[120] O. Dieguez, M.M.G. Alemany, C. Rey, P. Ordejon and L.J. Gallego, Phys. Rev. B **63**, 205407 (2001).

[121] G.L. Gutsev and C.W. Beuschlicher, J. Phys. Chem. **107**, 7013 (2003).

[122] S. Chrétien and D.R. Salahub, Phys. Rev. B **66**, 155425 (2002).

[123] M.J.T. Oliveira and F. Nogueira, Comp. Phys. Comm. **178**, 524 (2008).

[124] S.C. Watson and E.A. Carter, Phys. Rev. B **58**, 309 (1998).

[125] C.L. Reis, J.M. Pacheco and J.L. Martins, Phys. Rev. B **68**, 155111 (2003).

[126] J. Zhu, X.W. Wang and S.G. Louie, Phys. Rev. B **45**, 8887 (1992).

[127] N. Troullier and J.L. Martins, Phys. Rev. B **43**, 1993 (1991).

[128] J.C. Slater, Phys. Rev. **81**, 385 (1951).

[129] J.P. Perdew and A. Zunger, Phys. Rev. B **23**, 5048 (1981).

[130] D.A. Garanin and E.M. Chudnovsky, Phys. Rev. B **92**, 024421 (2015).

[131] A.R. Mackintosh and O.K. Andersen, *Electrons at Fermi surface* p.149, edited by M. Springford, Cambridge University Press, Cambridge (1980).

[132] B. Judd, *Operator techniques in atomic spectroscopy* McGraw-Hill, New York (1963).

[133] V. Anisimov and O. Gunnarsson, Phys. Rev. B **43**, 7570 (1991).

[134] W.E. Pickett, S.C. Erwin and E.C. Ethridge, Phys. Rev. B **58**, 1201 (1998).

[135] M.I. Katsnelson and A.I. Lichtenstein, Phys. Rev. B **61**, 8906 (2000).

[136] M.I. Katsnelson and A.I. Lichtenstein, J. Phys.: Condens. Matter **16**, 7439 (2004).

[137] S. Lounis and P.H. Dederichs, Phys. Rev. B **82**, 180404(R) (2010).

[138] L. Noodleman, J. Chem. Phys. **74**, 5737 (1981).

[139] A.I. Liechtenstein, M.I. Katsnelson, V.P. Antropov and V.A. Gubanov, J. Magn. Magn. Mat. **54-57**, 965 (1986).

[140] A.I. Liechtenstein, M.I. Katsnelson, V.P. Antropov and V.A. Gubanov, J. Magn. Magn. Mat. **67**, 65 (1987).

[141] A.R. Machintosh and O.K. Andersen, *Electrons at the Fermi Surface*, ed. M. Springford (Cambridge University Press, London 1980) p. 149.

[142] D.A. Rowlands, J.B. Staunton and B.L. Györffy, Phys. Rev. B **67**, 115109 (2003).

[143] H. Ebert, D. Ködderitzsch and J. Minár, Rep. Prog. Phys. **74**, 096501 (2011).

[144] P. Lloyd and P.V. Smith, Advan. Phys. **21**, 69 (1972).

[145] A. Jacobsson, B. Sanyal, M, Ležaić and S. Blügel, Phys. Rev. B **88**, 134427 (2013).

[146] P. Bruno, Phys. Rev. Lett. **90**, 087205 (2003).

[147] K.L. Liu and S.H. Vosko, Can. J. Phys. **67**, 1015 (1989).

[148] M. Stamenova and S. Sanvito, Phys. Rev. B **88**, 104423 (2013).

[149] E. Carpene, H. Hedayat, F. Boschini and C. Dallera, Phys. Rev. B **91**, 174414 (2015).

[150] S. Mathias, C. La-O-Vorakiat, P. Grychtol et Al., Proceeding of the National Academy of Sciences of the U.S.A **109**, 4792 (2012).

[151] G.P. Zhang, M. Gu and X.S. Wu, J. Phys.: Condens. Matter **26**, 376001 (2014).

[152] A. Secchi et Al., Annals of Physics **333**, 221 (2013).

[153] R.V. Mikhaylovskiy, E. Hendry, A. Secchi, J.H. Mentink et Al., arXiv:1412.7094 [cond-mat.str-el].

[154] I.E. Dzyaloshinskii, J. Phys. Chem. Solids **4**, 241 (1958).

[155] T. Moriya, Phys. Rev. **120**, 91 (1960).

[156] M. Bode, M. Heide, K. von Bergmann et Al., Nature **447**, 190 (2007).

[157] U.K. Rößler, A.N. Bogdanov and C. Pfleiderer, Nature **442**, 797 (2006).

[158] J.H. Mentink, K. Balzer and M. Eckstein, Nat. Commun. **6**, 6708 (2015).

[159] G.P. Zhang, Y.H. Bai and T.F. George, J. Phys.: Condens. Matter **28**, 236004 (2016).

[160] B.Y. Mueller, A. Baral, S. Vollmar et Al., Phys. Rev. Lett. **111**, 167204 (2013).

[161] D. Bohm, Phys. Rev. **85**, 166 (1952).

[162] D. Bohm, Phys. Rev. **85**, 180 (1952).

[163] D. Bohm and J.P. Vigier, Phys. Rev. **96**, 208 (1954).

[164] N. Bohr, Phys. Rev. **48**, 696 (1935).

[165] A. Einstein, B. Podolsky and N. Rosen, Phys. Rev. **47**, 777 (1935).

[166] T. Takabayasi, Prog. Theor. Phys. **14**, 283 (1955).

[167] M. Schönberg, Il Nuovo Cimento Vol. **XII**, N.1 (1954).

[168] P.R. Holland, *The Quantum Theory of Motion*, (Cambridge: Cambridge University Press), (1993).

[169] T. Koide, Phys. Rev. C **87**, 034902 (2013).

[170] M. Marklund and G. Brodin, Phys. Rev. Lett. **98**, 025001 (2007).

[171] G. Brodin, M. Marklund, J. Zamanian and M. Stefan, Plasma Phys. Control. Fusion **53**, 074013 (2011).

[172] V.P. Antropov, J. Appl. Phys. **97**, 10A704 (2005).

[173] M.I. Katsnelson and V.P. Antropov, Phys. Rev. B **67**, 140406(R), (2003).

[174] S. Weinberg, *Gravitation and Cosmology: Principles and Applications of the General Theory of Relativity*, John Wiley and Sons, Inc. (1972).

[175] https://en.wikipedia.org/wiki/Connection_(mathematics)

[176] M. Ekholm and I.A. Abrikosov, Phys. Rev. B **84**, 104423 (2011).

[177] C. Grazioli, D. Alfé, S.R. Krishnakumar, S.S. Gupta et Al., Phys. Rev. Lett. **95**, 117201 (2005).

[178] R. Resta, Rev. Mod. Phys. **66**, 899 (1994).

[179] T. Thonhauser, D. Ceresoli, D. Vanderbilt and R. Resta, Phys. Rev. Lett. **95**, 137205 (2005).

[180] D. Ceresoli, T. Thonhauser, D. Vanderbilt and R. Resta, Phys. Rev. B **74**, 024408 (2006).

[181] K. Capelle, Phys. Rev. A **60**, 733 (1999).

[182] E. Orestes, T. Marcasso and K. Capelle, Phys. Rev. A **68**, 022105 (2003).

[183] J.J. Sakurai, S.F. Tuan editor, *Modern Quantum Mechanics Revised Edition*, Addison-Wesley Publishing Company (1994).

[184] P. Koskinen and V. Mäkinen, Comp. Mater. Sci. **47**, 237 (2009).

[185] J.C. Slater and G.F. Koster, Phys. Rev. **94**, 1498 (1954).

[186] K. Lendi, Phys. Rev. B **9**, 2433 (1974).

[187] A.P. Sutton, M.W. Finnis, D.G. Pettifor and Y. Ohta, J. Phys. C: Solid State Phys. **21**, 35 (1988).

[188] W.A. Harrison, Phys. Rev. B **27**, 3592 (1983).

[189] T.N. Todorov, J. Phys.: Condens. Matter **13**, 10125 (2001).

[190] T.N. Todorov, J. Phys.: Condens. Matter **14**, 3049 (2002).

[191] A.P. Horsfield, D.R. Bowler, H. Ness et Al., Rep. Prog. Phys. **69**, 1195 (2006).

[192] E.J. McEniry, D.R. Bowler, D. Dundas et Al., J. Phys.: Condens. Matter **19**, 196201 (2007).

[193] Q. Luo and E. Dagotto, Phys. Rev. B **89**, 045115 (2014).

[194] T. Ribic, E. Assmann, A. Tóth and K. Held, Phys. Rev. B **90**, 165105 (2014).

[195] J.M. Morbec and K. Capelle, Int. J. Quantum Chem. **108**, 2433 (2008).

[196] T. Huhne, C. Zecha, H. Ebert et Al., Phys. Rev. B **58**, 10236 (1998).

[197] M.S.S. Brooks, Physica **130B**, 6 (1985).

[198] M.R. Norman, Phys. Rev. Lett. **64**, 1162 (1990).

[199] G. Racah, Phys. Rev. **62**, 438 (1942).

[200] A.F. Oliveira, G. Seifert, T. Heine and H.A. Duarte, J. Braz. Chem. Soc. **20**, 1193 (2009).

[201] M. Soriano and J.J. Palacios, Phys. Rev. B **90**, 075128 (2014).